Final Report on RES0040661 to Petroleum Technology Alliance Canada

Identifying Regional Variation in the Source Depths of Migrating Gas from Conventional and Unconventional Wells in the Western Canadian Sedimentary Basin

Prof. Karlis Muehlenbachs

Department of Earth and Atmospheric Sciences

University of Alberta

Gabriela Gonzalez Arismendi

Department of Earth and Atmospheric Sciences

University of Alberta

March 17, 2020

Contents

Executive Summary

This report consists of a set of maps contouring the carbon isotope values of production, surface casing vent flow (SCVF) and ground migration gases (GM) in the Western Canada Sedimentary Basin. From regional to mesoscale, these maps document the isotopic composition of n-alkane and carbon dioxide from the whole Western Canada Sedimentary Basin to part of one oil field. Mapped isotopic variability was reported, broadly discussed, and explained, even though a full understanding of such response requires considering other variables suggested as part of future work. These maps are useful tools for Regulators, Industry and the Public to anticipate or predict the source of fugitive gases at any given location. Our results show that most SCVF and GM originates somewhere along the wellbore above the target formation.

In compiling the maps, we made two important discoveries. (1) We observed that contours continuity on the mapped SCVF and GM isotopic values from multiple nearby wells have the same or similar isotope fingerprints, even though the wells are of differing age and drilled by different operators. (2) The maps and current modelled isotopic response can be used by service companies and regulators faced with remediating wells. Their problem well can be placed on these maps and used to predict the source, depth of putative SCVF and GM, thereby improving budgeting and scheduling. Drillers can use the maps to predict likely zones that need special attention or cementing, implementing techniques to prevent future SCVF and GM problems, which in the long term will save monetary resources.

Perhaps a more surprising observation is that the uniformity of failure depths in adjacent wells changes at topographic breaks. The isotope contours tend to follow topography. In most cases, isotope fingerprints of SCVF and GM of wells in valleys are more depleted of ^{13}C, indicating a shallower source for SCVF than in nearby wells on higher ground. The reservoir gas isotopic

fingerprint also constrains such a response. Documentation of the influence of surface topography on the source depth of SCVF has clear economic and engineering implications. Knowing that in any one region, the SCVF in valley wells originates from a different zone than wells on topographic highs will lower the cost of remediation of clusters of wells and should challenge drillers and cementers to avoid SCVF and GM problems in future wells.

1. Introduction

In 1999 the then Alberta Regulator recognized carbon isotope fingerprinting (EUB, GB 99-6) as a valid tool, developed in Muehlenbachs' laboratory, to identify source depths of migrating gases. Since then, many thousands of migrating and surface casing vent flow gases have been analyzed at the University of Alberta. Isotope fingerprinting is a relatively inexpensive test (about $400 ea). It can lower the cost of wells' beset abandonment with GM and SCVF substantially, thus likely reducing the number of wells left standing and/or transferred to the Orphan Well Association. Success in gas isotope fingerprinting of migrating gases is contingent on knowing granular, related background data of known production gases and isotope mud logs/profiles. Here we provide industry and regulators with easily accessible detailed maps of the variation of carbon isotope values in natural gases across the Western Canada Sedimentary Basin (WCSB). Components in this initiative are the known carbon isotope fingerprints of production gases as well as of thousands of fugitive gases isotopic values, from ground migrating (GM) and surface casing vent flow (SCVF) gases. Value-added components are maps of GM and SCVF isotope data draped over topography. Experience has shown that most GM and SCVF gases entering the environment do not originate from the production target but emanate from shallower formations along the wellbore. Identifying the source depth of migrating gas is necessary to plug any well before abandonment successfully. The maps provide better knowledge of the depths from which gas

typically migrates by showing that in any one area of the WCSB their source depth is controlled by both regional geology and topography. The maps will be useful to operators when planning to plug and abandon wells, and for regulators to better predict future liability and target monitoring.

The science behind these maps is relatively simple and well known. Physical, chemical and biological processes fractionate the ratio of the stable carbon isotopes, ^{13}C and ^{12}C. The size of the partitioning depends on temperature. Larges effects occur at the lowest temperatures, the smallest at the higher temperature. Gases show the most significant effects, solids and liquids relatively small effects. Among gases, the largest effect is with the lowest molecular weight entity and the smallest, with the heaviest molecule. Thus one can predict in a classic "oil window" scenario, when the source kerogen is more or less uniform, that gases formed at lower maturities or by biogenesis will reflect the largest isotope fractionations, whereas the deepest most mature gases the least fractionation. Simultaneously, the scale of isotopic differences between methane, ethane and propane will decrease with maturity in proportion to their molecular weights. But, always methane should contain the least ^{13}C, butane the most. Biogenic gas has only methane and possibly only traces of ethane. However, such an ideal distribution of ^{13}C is very rarely seen in nature.

Microbiological or abiological alteration can selectively alter the carbon isotope ratio of the hydrocarbon gases, as well as mixing from different sources. The net result in the real world is that the carbon isotope ratio of natural gases varies across a petroliferous basin in a complicated but understandable way (see Fig. 1 from Tilley and Muehlenabchs, 2006). Local quirks in the isotope composition of gas lead to the possibility of using gas isotope fingerprints of problem gases to identify their source. Therefore, here we used maps as a tool, and pre-existing knowledge to understand the fate and distribution of hydrocarbon and carbon dioxide, fugitive gases isotopic

composition from surface casing vent and ground migration in the WCSB to track and predict their occurrence.

2. Methodology

2.1. Data compilation, analysis, and mapping

The carbon isotope data of gases from the Western Canada Sedimentary Basin, measured at the University of Alberta since 1994, have been organized, formatted and mapped. Samples were obtained from Industry of production, surface casing vent (SCV) and ground migration (GM) gases. We rely on the sample labels written on the sample containers for classification and location. The data on methane ($\delta^{13}C_1$, ‰, VPDB), ethane ($\delta^{13}C_2$, ‰, VPDB), propane ($\delta^{13}C_3$, ‰, VPDB), *n*-butane ($\delta^{13}nC_4$, ‰, VPDB), iso-butane ($\delta^{13}iC_4$, ‰, VPDB), as well as carbon dioxide ($\delta^{13}CO_2$, ‰, VPDB), were acquired using a Finnigan-MAT 252 GC-CF-IR MS at the University of Alberta (see for details Tilley and Muehlenbachs, 2006). The data were calibrated against internationally recognized standards NGS-1, NGS-2, NGS-3, NBS18 and NBS 19.

The descriptive statistical treatment has been performed for the measurements to understand the variables' general distribution (boxplot, mean values, and histograms). A kriging model was used to map the gas isotope data (Pyrcz and Deutsch, 2014). Interpolation via simple kriging produces maps that are too smooth by their very nature: best estimates will never reproduce values at the tail ends of the input distributions (extreme highs and lows), however, such isoscapes aid at predicting potential isotopic response. The following maps were generated on a regional (basin data display) to mesoscale (zoom-ins): (1) sampling site locations; (2) colour contoured isotopic variation of n-alkanes and carbon dioxide (3) topographic maps overplayed by n-alkane and carbon

dioxide isotopic contouring. These maps were generated for production, ground migration (GM), and surface casing vent (SCV).

3. Results and discussion

Our sample locations are shown for production gas Fig 2A, SCVF Fig. 2B and GM, Fig. 2C. It is important to note that in this report, we call gases "production" if they are associated with the production, thus we lump commercially produced natural gases with oil associated or solution gas from oil wells.

3.1. Regional variations

Figs. 3 shows the boxplots diagram illustrating the averages, minimum/maximum of the cleaned carbon isotope data for production gases (Fig. 3A), SCVF (Fig. 3B) and GM (Fig. 3 C). The isotope values of the gases vary significantly across the WCSB, and it is more instructive to examine them with a narrower focus.

Fig. 4A are histograms of production and oil associated gases from W3 in the WCSB. Immediate inspection reveals a bimodal distribution for methane, ethane and propane that is easily explainable. Production W3 gases are mostly from either the Mannville oil associated gases that have relatively $\delta^{13}C$ enriched components vs the Colorado dry gases that are extraordinarily depleted of $\delta^{13}C$ (see Rowe and A Muehlenbachs, 1999 for discussion). The SCVF gases from W3 (Fig. 4B) do not show pronounced bimodal distribution of $\delta^{13}C$. Yet, the values for ethane and propane are more negative than for the production gases indicating that for the most part, the SCVF source is in the Colorado, even for wells finished in the Mannville. Ground migration gases W3 (Fig. 4C) are similar to the SCVF gases (Fig. 4C), but $\delta^{13}C$ methane and CO_2 are much more variable than in the production or SCVF gases. The $\delta^{13}C$ variation in methane simply reflects that

methane in the ground can be destroyed or created by microbial activity that also is reflected in the $\delta^{13}C$ of CO_2.

Production $\delta^{13}C$ values from W4 also show bimodal behaviour (Fig. 5A) again, reflecting shallow gas production to the east and deeper production to the west. SCVF gases W4 do not show the bimodal distribution (Fig. 5B), and as in the case of W3 discussed above, their ethane and propane $\delta^{13}C$ values indicate shallower sources than the production targets. Ground migration gases W4 are similar to the SCVF gases implying both have the same geological sources (Fig. 5C).

W5 production gases (Fig. 6A) show more bell-shaped distribution of hydrocarbon $\delta^{13}C$ than in W4 and W3. The tighter distribution of $\delta^{13}C$ values likely reflects that most of the production W5 is of mature thermogenic oil and gas. The modes of $\delta^{13}C$ of methane, ethane and propane would fall in the "ideal" predict world wide range of mature gas at the peak of the "oil window". The SCVF distributions (Fig. 6B) are very different from the production gases. The SCVF methane $\delta^{13}C$ values are much broader, and the ethane and propane $\delta^{13}C$ values are both broader and bimodal. Clearly, most SCVF gases are not from the production horizon. The bimodal distribution of ethane and propane $\delta^{13}C$ values is intriguing. The inference is that across W5, there are formations that preferentially source SCVF irrespective of the target formation. The ground migration $\delta^{13}C$ distributions (Fig. 6C) W5 are compatible with the SCVF data.

The $\delta^{13}C$ distribution of production gases W6 (Fig. 7A) is more complicated, reflecting production from shallow, mature and overmature deeper sources. The $\delta^{13}C$ distribution of W6 SCVF (Fig 7B) shows similarity to SCVF W5 in that the ethane distribution is bimodal, as is the methane. The inference can again be drawn that the origin SCVF is not random but is sourced regionally from

select horizons. Unfortunately, only a few ground migration samples from W 6 have been analyzed (Fig. 7C).

Production gases from NE BC show the tightest $\delta^{13}C$, and ^{13}C richest, distribution (Fig. 8A). For the most part, they are from the very deep and overmature Horn River Basin Shale play. Gases from the Horn River and a few from the Montney, show the very unexpected isotope feature of reversals where methane has less ^{13}C than ethane or propane. An explanation for such reversed isotope behaviour can be found in Tilley et al., (2011). SCVF from NE BC have a much wider $\delta^{13}C$ distribution (Fig. 8B) than the production gases with methane showing bimodal distribution. The conclusion is that some deep gases do migrate to the SCV, but most have shallower sources. Ground migration in NE BC (Fig. 8C) is coming from both deep and shallow sources. The isotope geochemistry of all these gases will be discussed in more detail later in this report.

3.2. Contour maps of *n*-alkanes and carbon dioxide isotopic response

Carbon isotope data of production, SCVF and GM gases from wells identified on Figs. 2A, 2B and 2C have been mapped and contoured across the WCSB and at greater detail at select locations. The color scheme is such that blue, cooler, colors represent more negative carbon isotope values that, as discussed above, indicate relatively shallower sources of the gases. In contrast, warmer colors represent less negative $\delta^{13}C$ values indicating deeper sources. The contour maps have also been draped over topographic maps for additional insights on the distribution of gas isotope $\delta^{13}C$ values.

Figures 9A, 9B and 9C are maps of $\delta^{13}C$ of methane across the WCSB from production, SCVF and GM, respectively. Contours of methane $\delta^{13}C$ values of production gases (Fig. 9A) show the geographic pattern one expects given the geology of the various oil and gas fields. Shallow gases

are to the SE, deeper gases W and NW. Methane $\delta^{13}C$ of SCVF (Fig. 9B) follows to some extent the trends visible in the production methane but the SCVF $\delta^{13}C$ values of methane are more dispersed. Contours of methane $\delta^{13}C$ of the GM gases (Fig. 9C) shows little correlation with the production map showing shallow methane even in areas of deep production. GM, in some cases, may simply be shallow biogenic "swamp gas".

Figures 10A, 10B and 10C are maps of $\delta^{13}C$ of ethane across the WCSB from production, SCVF and GM respectively. Contours of ethane $\delta^{13}C$ values of production gases (Fig. 10A) show more clearly than did the methane map, the geographic pattern one expects from the geology of the various oil and gas fields. Shallow gases are confined to the SE, deeper gases W and NW reflecting the known regional burial depths. Again, ethane $\delta^{13}C$ of SCVF (Fig. 10B) follows to some extent the trends visible in the production ethane, but the SCVF $\delta^{13}C$ contours of ethane are less continuous and have patches of shallower SCVF gas than in production gases. Significantly, these colder colored, more superficial patches of SCVF can extend over several townships. The contours of ethane $\delta^{13}C$ of the GM gases (Fig. 10C) shows little correlation with the production map. However, some GM gases are clearly thermogenic.

Figures 11A, 11B and 11C are maps of $\delta^{13}C$ of propane across the WCSB from production, SCVF and GM, respectively. Contours of propane $\delta^{13}C$ values of production gases (Fig. 11A) show the geographic pattern one expects from the geology of the various oil and gas fields. Shallow gases are confined to the SE, deeper gases W and NW reflecting the known regional burial depths. Again, propane $\delta^{13}C$ of SCVF (Fig. 11B) follows to some extent, the trend visible in the production propane. Still, the SCVF $\delta^{13}C$ contours of propane are less continuous and have patches of shallower SCVF gas than in production gases. Conversely, these cooler colored, shallower patches

of SCVF can extend over several townships. Contours of propane $\delta^{13}C$ of the GM gases (Fig. 11C) show less correlation with the production map. However, some GM gases are thermogenic.

As explained above, the isotopic fractionations in a gas and the resulting $\delta^{13}C$ values will always vary less among larger molecules like butanes and pentanes. Figures 12A, B and C are maps of $\delta^{13}C$ of *n*-butane across the WCSB from production, SCVF and GM, respectively. Figures 13A, B and C are maps of $\delta^{13}C$ of *i*-butane across the WCSB from production, SCVF and GM, respectively. The reader is warned that when comparing the color patterns seen on these figures, color scale is calibrated according to maximum and minimum measured values. This was done to accentuate the contoured $\delta^{13}C$ differences on each individual map per analyte. None of these maps of *n* and *i*-butane $\delta^{13}C$ values contradict observations made on the methane, ethane and propane maps. Bear in mind also that butanes were absent in some of the sampled gases.

Figs. 14A, B and C are maps of $\delta^{13}C$ of carbon dioxide across the WCSB from production, SCVF and GM. Carbon dioxide in these systems has a complicated history. It can be formed directly from kerogen during the thermogenic generation of oil and gas. Carbon dioxide also forms directly from dolomite and limestone in reservoirs. Microbiological and abiological oxidation of gas, kerogen or soil organic matter also produces carbon dioxide. Also, CO_2 in the surface environment can be reduced to methane microbiologically or produced by fermentation. Each of these separate processes impacts $\delta^{13}C$ of CO_2 differently, and more than one process can affect any given gas sample. Thus the CO_2 contour maps are complicated. Carbonate reservoirs can be identified on the production CO_2 map (Fig. 14A) within the 0 +/4‰ contours. Also evident is the production of CO_2 enriched in ^{13}C from the Bluesky and Gething in N Alberta as well as some Mannville gases in the Lloydminster area. The $\delta^{13}C$ of SCVF and GM CO_2 varies much more than the

production gases (Figs. 14B and C), reflecting a variety of the processes mentioned at the beginning of this paragraph.

Much more information can be gleaned from our data set by draping the isotope contour maps over topography. Figures 15A, B and C are maps of $\delta^{13}C$ of methane across the WCSB from production, SCVF and GM, respectively, but now overlying topographic base maps. Contours of methane $\delta^{13}C$ values of production gases show the same geographic pattern one saw on (Fig. 9A) reflecting the geology of the various oil and gas fields. Production of shallow low maturity gases to the SE, deeper, maturer gases W and NW.

More in-depth insight is gained by examining methane $\delta^{13}C$ of SCVF (Fig. 15B) about topography. As noted in Fig. 9B, SCVF contours follow to some extent the trends visible in the production methane, but the SCVF $\delta^{13}C$ values of methane are more dispersed. Inspection of Fig. 15B suggests that those deviations, which are expressed by cooler colors follow topographic contours. This suggestion will be followed up in the following discussion. Contours of methane $\delta^{13}C$ of the GM gases (Fig. 15C) shows little correlation with the production map showing shallow methane even in areas of deep production. GM, in such cases, may simply be shallow biogenic "swamp gas".

Figures 16A, B and C are maps of $\delta^{13}C$ of ethane across the WCSB from production, SCVF and GM respectively draped over topography. Contours of ethane $\delta^{13}C$ values of production gases (Fig. 16A) show more clearly than did the methane maps, the geographic pattern one expects from the geology of the various oil and gas fields. Shallow gases are confined to the SE, (cool colored, low $\delta^{13}C$), deeper gases (warmer colors less negative $\delta^{13}C$ values) W and NW reflecting the known regional burial depths.

Ethane $\delta^{13}C$ of SCVF (Fig. 16B) contours follows to some extent the trends notable in the production ethane contours, but the SCVF $\delta^{13}C$ contours of ethane are less continuous and have patches of shallower SCVF gas than in production gases. Inspection of Fig. 16B clearly shows a relationship of the SCVF isotope contours with topography. Generally, lower topographic features appear to have cooler, lower $\delta^{13}C$, shallower SCVF than on adjacent topographic highs. Significantly, these colder colored, shallower patches of SCVF can extend over several townships.

Contours of ethane $\delta^{13}C$ of the GM gases on topography (Fig. 16C) show little consistency with the production or SCVF maps. The lack of regional consistency of $\delta^{13}C$ GM gases will be addressed in our discussion of the local regions later in this report.

Figures 17A, B and C are maps of $\delta^{13}C$ of propane across the WCSB from production, SCVF and GM respectively draped over topography. Contours of propane $\delta^{13}C$ values of production gases (Fig. 17A) show the geographic pattern one expects from the geology and maturity of the various oil and gas fields. Shallow gases are confined to the SE, deeper gases W and NW reflecting the known regional burial depths.

Again, propane $\delta^{13}C$ contours of SCVF (Fig. 17B) follow to some extent the trend visible in the production propane's, but the SCVF $\delta^{13}C$ contours of propane are less continuous and have patches of shallower SCVF gas than in production gases. Colder colored display shallower patches of SCVF that extend over several townships. Note that cooler SCVF propane contours also tend to follow topography with the lower $\delta^{13}C$ values, indicative of SCVF of shallower origin found at lower topography. This discussion will be expanded when we present geographically more local maps.

Inspection of contours of propane $\delta^{13}C$ GM gases (Fig. 17C) over topography reveals regional geomorphological controls over ethane and propane values. Thus, one may conclude that the $\delta^{13}C$ of GM propane is controlled in some regions by soil type.

As explained above, the isotopic fractionations in a gas and the resulting $\delta^{13}C$ values will vary less with larger molecules like butanes and pentanes. Figures 18A, B and C are maps of $\delta^{13}C$ of *n*-butane across the WCSB from production, SCVF and GM. Figures 19A, B and C are maps of $\delta^{13}C$ of *i*-butane across the WCSB from production, SCVF and GM, respectively. Inspection of the GM butanes, figs. 18C and 19C confirm the inference drawn from GM propane that geomorphology and type of soil influences the isotope fingerprint of GM gas.

Figs. 20A, B and C are maps of $\delta^{13}C$ of carbon dioxide across the WCSB from production, SCVF and GM respectively draped over topography. As already mentioned above, carbon dioxide in these systems has a complicated history. In addition, CO_2 in the surface environment can be reduced to methane microbiologically or produced by fermentation. Each of these separate processes impacts $\delta^{13}C$ of CO_2 differently, and more than one process can affect any given gas sample. Thus the CO_2 contour maps are expected to be complicated. Carbonate reservoirs can be identified on the production CO_2 map (Fig. 20A) within the 0 +/4‰ contours. Also evident is the production of CO_2 enriched in ^{13}C from the Bluesky and Gething in N Alberta as well as some Mannville gases in the Lloydminster area.

The $\delta^{13}C$ of CO_2 from SCVF and GM varies much more than the production gases (Figs. 20B and 20C), reflecting a variety of the processes mentioned earlier. However, a closer examination of the $\delta^{13}C$ contours with geomorphology reveals enigmatic relationships that will be explored later in this report.

3.2.1. Local areas – zoom-ins

The WCSB isotope contour maps SCVF and GM gases not only suggest that the source depths of gas migrating from production wells is generally shallower than the production targets, but also that the source depth may be controlled to some extent by geography and topography. Of special note is that smooth contours of the isotope data imply that on a smaller, township scale, multiple adjacent wells have the same source of problem gas. To investigate further these observations, we present a series of maps detailing areas where we have the highest well density data. We will present contour maps of east central Alberta and adjacent Saskatchewan, then zoom into oilfields of Lloydminster area, specifically Lindbergh, Wildmere and Beaver Dam (Fig. 21D) as well as Pembina.

Fig. 21 A shows the locations of SCVF sampled in east central Alberta and adjacent Saskatchewan. Figs. 21 B, C, D, E, F and G are color contour maps with well locations of SCVF methane, ethane, propane, *n- & i*-butane and CO_2. A cursory inspection of all these maps indicates spotty contours but with multiple wells within a given contour interval or "spot". The multiple wells within one contour all have the same carbon isotope fingerprint indicating the same or similar source depth. The same isotope contours are draped over topography in Figs. 21H, I, J, K, L and M. Inspection of all the maps, especially Fig. 21I for ethane and Fig. 21J for propane clearly shows that most valleys, topographic lows have SCVF with cooler contours, lower $\delta^{13}C$ values, in contrast to topographic highs that are contoured in warmer colors, less negative $\delta^{13}C$ values. The lower $\delta^{13}C$ values in the valleys indicate SCVF in valleys is from shallower formations than SCVF in wells spudded on the topographic highs. However, the target for most of the wells in this region are Mannville heavy oil zones.

Fig. 22 A shows the locations of GM sampled in east central Alberta and adjacent Saskatchewan. Figs. 22 B, C, D, E, F and G are color contour maps with well locations of GM methane, ethane, propane, *n*- & i-butane and CO_2, respectively. As with SCVF, cursory inspection of all the GM maps indicates spotty contours but with multiple wells within a given contour interval or "spot". The multiple wells within one contour all have the same carbon isotope fingerprint indicating the same or similar source depths. The same isotope contours are draped over topography in Figs, 22H, I, J, K, L and M. Inspection of all the maps, especially Fig. 22I for ethane and Fig. 21J for propane clearly shows that most valleys and topographic lows have GM with cooler contours, lower $\delta^{13}C$ values, in contrast to topographic highs that are contoured in warmer colors, less negative $\delta^{13}C$ values. The lower $\delta^{13}C$ values in the valleys indicate GM in valleys mostly is from shallower formations than GM in wells spudded on the topographic highs, although the target for most of the wells in this region are Mannville heavy oil zones. Comparing the SCVF and GM reveals subtle differences, most obvious in the maps of CO_2 $\delta^{13}C$ values (Figs. 22G & M). GM gases are subjected to bioalteration in soil, raising the $\delta^{13}C$ values of the hydrocarbons but because of mass balance, lowering the $\delta^{13}C$ values of CO_2. Thus geomorphology, near-surface hydrology and soil type will control the evolution of the GM $\delta^{13}C$ values.

We now zoom in to the Lloydminster area, a region of high-density wells per area that all target the Mannville heavy oils. Fig. 23A shows the locations of SCVF sampled in Alberta and adjacent Saskatchewan. Figs. 23 B, C, D, E, F and G are color contour maps with well locations of SCVF methane, ethane, propane, *n*- & i-butane and CO_2, respectively. All the maps indicate plumes contours with multiple wells within a given contour interval or "spot". The multiple wells within one contour all have the same carbon isotope fingerprint showing same or similar source depth. These well groups are draped over topography in Figs, 23H, I, J, K, L and M. Inspection of all the

maps, especially Fig. 23I for ethane and Fig. 23J for propane suggests that valleys in topographic lows have SCVF with cooler contours, lower $\delta^{13}C$ values, in contrast to topographic highs that are contoured in warmer colors, less negative $\delta^{13}C$ values. The lower $\delta^{13}C$ values in the valleys indicate SCVF in valleys is from shallower formations than SCVF in wells spudded on the topographic highs, although the target for most of the wells in this region are Mannville heavy oil zones.

Fig. 24A shows the locations of GM sampled in the Lloydminster region. Figs. 24B, C, D, E, F and G are color contour maps with well locations of GM methane, ethane, propane, *n*- & i-butane and CO_2 respectively. As with SCVF map, cursory inspection of all the GM maps indicates spotty contours but with multiple wells within a given contour interval or "spot". The multiple wells within one contour all have the same carbon isotope fingerprint indicating the same or similar source depths. The same isotope contours are draped over topography in Figs, 24H, I, J, K, L and M. Inspection of all the maps, especially Fig. 24I for ethane and Fig. 24J for propane clearly shows that valleys in topographic lows have GM with cooler contours, lower $\delta^{13}C$ values, in contrast to topographic highs that are contoured in warmer colors, less negative $\delta^{13}C$ values. The lower $\delta^{13}C$ values in the valleys indicate GM in valleys is from shallower formations than GM in wells spudded on the topographic highs, although the target for most of the wells in this region are Mannville heavy oil zones. Comparing the SCVF and GM reveals subtle differences, most obvious in the maps of CO_2 $\delta^{13}C$ values (Figs. 24G & M). GM gases are subjected to bioalteration in soil raising the $\delta^{13}C$ values of the hydrocarbons but because of mass balance, lowering the $\delta^{13}C$ values of CO_2. Thus geomorphology, near surface hydrology and soil type will control the evolution of the GM $\delta^{13}C$ values.

The sampled well density in some oilfields is so great we can further zoom in on the maps. Fig. 25A shows the locations of SCVF sampled at Lindbergh. Figs. 25 B, C, D, E, F and G are color contour maps with well locations of SCVF methane, ethane, propane, *n*- & i-butane and CO_2 respectively. Cursory inspection of all the maps indicates spotty contours with multiple wells within a given contour interval or "spot". The multiple wells within one contour all have the same carbon isotope fingerprint indicating same or similar source depth. The same isotope contours are draped over topography in Figs. 25H, I, J, K, L and M. Inspection of all the maps, especially Fig. 25I for ethane and Fig. 25J for suggests that valleys in topographic lows have SCVF with cooler contours, lower $\delta^{13}C$ values, in contrast to topographic highs that are contoured in warmer colors, less negative $\delta^{13}C$ values. The lower $\delta^{13}C$ values in the valleys indicate SCVF in valleys is from shallower formations than SCVF in wells spudded on the topographic highs although the target of all wells are Mannville heavy oil zones. It is remarkable how within one topographic zone, next nearest wells have the same isotope fingerprint implying the same source depth.

Fig. 26A shows the locations of GM sampled at Lindbergh. Figs. 26 B, C, D, E, F and G are color contour maps with well locations of GM methane, ethane, propane, *n*- & i-butane and CO_2, respectively. As with SCVF map, cursory inspection of all the GM maps indicates spotty contours but with multiple wells within a given contour interval or "spot". The multiple wells within one contour all have the same carbon isotope fingerprint indicating the same or similar source depths. The same isotope contours are draped over topography in Figs. 26H, I, J, K, L and M. Inspection of all the maps, especially Fig. 26I for ethane and Fig. 26J for propane suggests that valleys in topographic lows have GM with cooler contours, lower $\delta^{13}C$ values, in contrast to topographic highs that are contoured in warmer colors, less negative $\delta^{13}C$ values. The lower $\delta^{13}C$ values in the valleys indicate GM in valleys is often from shallower formations than GM in wells spudded on

the topographic highs although the target for most of the wells in this region are Mannville heavy oil zones. Comparing the SCVF and GM reveals subtle differences, most obvious in the maps of CO_2 $\delta^{13}C$ values (Figs. 26G & M). GM gases are subjected to bioalteration in soil raising the $\delta^{13}C$ values of the hydrocarbons but because of mass balance, lowering the $\delta^{13}C$ values of CO_2. Thus geomorphology, near surface hydrology and soil type will control the evolution of the GM $\delta^{13}C$ values.

The sampled well density of SCVF is also high at Wildmere. Fig. 27A shows the locations of SCVF sampled at Wildmere. Figs. 27 B, C, D, E, F and G are color contour maps with well locations of SCVF methane, ethane, propane, *i & n* butane and CO_2 respectively. Cursory inspection of all the maps indicates contours with multiple wells within a given contour interval or "spot". The multiple wells within one contour all have the same carbon isotope fingerprint indicating same or similar source depth. The same isotope contours are draped over topography in Figs. 27H, I, J, K, L and M. Inspection of all the maps, especially Fig. 27I for ethane and Fig. 27J for propane suggest that valleys and topographic lows have SCVF with cooler contours, lower $\delta^{13}C$ values, in contrast to topographic highs that are contoured in warmer colors, less negative $\delta^{13}C$ values. The lower $\delta^{13}C$ values in the valleys indicate SCVF in valleys is from shallower formations than SCVF in wells spudded on the topographic highs although the target of all wells are Mannville heavy oil zones. It is remarkable how within one topographic zone, SCVF of next nearest wells have the same isotope fingerprint implying the same source depth for the near adjacent wells.

There are fewer GM samples at Wildmere (Fig. 28A) but they are spaced such that we can see trends. Figs. 28 B, C, D, E, F and G are color contour maps with well locations of GM methane, ethane, propane, *n- &* i-butane and CO_2 respectively. The same isotope contours are draped over

topography in Figs, 28H, I, J, K, L and M. The lower $\delta^{13}C$ values in the valleys indicate GM in valleys is from shallower formations than GM in wells spudded on the topographic highs although the target for most of the wells in this region are Mannville heavy oil zones. Comparing the SCVF and GM reveals subtle differences, most obvious in the maps of CO_2 $\delta^{13}C$ values (Figs. 28G & M). GM gases are subjected to bioalteration in soil raising the $\delta^{13}C$ values of the hydrocarbons but because of mass balance, lowering the $\delta^{13}C$ values of CO_2. Thus geomorphology, near surface hydrology and soil type will control the evolution of the GM $\delta^{13}C$ values.

The Beaver Dam oil field also produces Mannville heavy oil but there the reservoir is much shallower than at Lindbergh or Wildmere. Fig. 29A shows the locations of SCVF sampled at Beaver Dam. Figs. 29 B, C, D, E, F and G are color contour maps with well locations of SCVF methane, ethane, propane, *n- &* i-butane and CO_2, respectively. Cursory inspection of all the maps indicates contours with multiple wells within a given contour interval or "spot". The multiple wells within one contour all have the same carbon isotope fingerprint indicating same or similar source depth. The same isotope contours are draped over topography in Figs, 29H, I, J, K, L and M. Inspection of all the maps, especially Fig. 29I for ethane and Fig. 29J for propane clearly show that valleys in topographic lows have SCVF with cooler contours, lower $\delta^{13}C$ values, in contrast to topographic highs that are contoured in warmer colors, less negative $\delta^{13}C$ values. The trends noted above in the discussions on $\delta^{13}C$ of SCVF at Lindbergh and Wildmere also hold at Beaver Dam, but here they are muted because the reservoir is so much closer to surface.

The location of GM samples from Beaver Dam are shown in Fig. 30A. Figs. 30 B, C, D, E, F and G are color contour maps with well locations of GM methane, ethane, propane, *i & n* butane and CO_2, respectively. The same isotope contours are draped over topography in Figs, 30H, I, J, K, L and M. Comparing the SCVF and GM reveals subtle differences, most evident in the maps of CO_2

$\delta^{13}C$ values (Figs. 30G & M). GM gases are subjected to bioalteration in soil, raising the $\delta^{13}C$ values of the hydrocarbons but because of mass balance, lowering the $\delta^{13}C$ values of CO_2. Thus geomorphology, near-surface hydrology and soil type will control the evolution of the GM $\delta^{13}C$ values.

To contrast the detailed look at the relatively shallow heavy oil fields, we now take a closer look at SCVF and GM in the Pembina region, where we also have high sample density (Fig. 31A). Figs. 31 B, C, D, E, F and G are color contour maps with well locations of SCVF methane, ethane, propane, *n- &* i-butane and CO_2, respectively. Cursory inspection of all the maps indicates spotty contours but with multiple wells within a given contour interval or "spot" as was noted on other maps. The multiple wells within one contour all have the same carbon isotope fingerprint indicating same or similar source depths. The same isotope contours are draped over topography in Figs. 31H, I, J, K, L and M. Inspection of all the maps, especially Fig. 31I for ethane and Fig. 31J for propane suggests that valleys in topographic lows have SCVF with cooler contours, lower $\delta^{13}C$ values, in contrast to topographic highs that are contoured in warmer colors, less negative $\delta^{13}C$ values. Matching the topography and geomorphology to the of $\delta^{13}C$ contours of SCVF suggests that perhaps underlying tectonics also influences the source depth of SCVF.

We do not have many GM samples from the Pembina area relatively evenly spaced (Fig. 32 A). Figs. 32 B, C, D, E, F and G are color contour maps with well locations of GM methane, ethane, propane, *i & n* butane and CO_2 respectively. As with SCVF, cursory inspection of all the GM maps indicates spotty contours but with multiple wells within a given contour interval or "spot". The multiple wells within one contour all have the same carbon isotope fingerprint indicating same or similar source depths. The same isotope contours are draped over topography in Figs. 22H, I, J, K, L and M. Inspection of all the maps reveals the isotope fingerprint of GM gases are clustered

and as deduced from other maps may reflect sources controlled by topography and geology but modified in the soil horizon.

3.2.2. Topography and source of SCVF and GM

Maps show a visual relationship between topography and the source depth of SCVF and GM, as discussed above $\delta^{13}C$. Theresa Watson (personal communication) suggested that the additional weight of cement in a well at higher topography would tend to seal better the lower parts of the well, compared to a well set at lower topography where both target the same horizon. This statement agrees with our observations, but exceptions should be considered. The Lindbergh field shows an inverse relationship between topography and the source of SCVF. Fig. 33Ai illustrates the colored contour map of $\delta^{13}C$ of ethane, identifying a sub-region both with strongly contrasting colors (ethane $\delta^{13}C$ values) and topography (Fig.33Aii). That sub-region has a plethora of wells through which a 43 well cross-section (Fig. 33Aiii, line A to A') shows landforms characteristic of a valley in the prairie. This landform and location was selected and studied because it also indicates an isotope transition characteristic in the zoomed-in area.

Fig. 33B shows the topographic height above sea level (Fig. 33Bi) and $\delta^{13}C$ values of SCVF along with the 70 km profile A to A'. Please note for illustrative purposes, the isotope scale in Fig 33B has been reversed. The $\delta^{13}C$ values of the methane (Fig. 33Bii), ethane (Fig. 33Biii), propane (Fig. 33Biv) and butanes (Fig. 33Bv & vi) follow a smooth trend from 0 to 50 km but then become less negative as we approach the valley and then become more negative on the other side of the valley. The source depths of the SCVF along the profile can be identified by comparing their $\delta^{13}C$ fingerprint with an isotope mudlog.

Fig. 34 shows two mudlogs, very near profile A-A'. Comparison of the SCVF $\delta^{13}C$ fingerprint to the mudlogs reveals that along the first 50 km of the profile on the prairie, the SCVF fugitive gas comes from failures at the Second White Speckled Shale level. In contrast, failures in wells at the bottom of the valley are in the Mannville. Wells on the flanks of the valley failed at intermediate depths, the Viking and Joli Fu. Therefore, the isotopic response can be correlated with

3.3. Overview of gas isotope geochemistry of the WCSB

To effectively use the above maps for gas isotope fingerprinting of problem gases, one needs to understand what causes the variations of $\delta^{13}C$ within and between gases. This is not the place for an extensive discussion, but it is useful to look in detail at production, SCVF and GM gases from across the WCSB. These vary extensively as per changes in maturity range, or formation's temperature across the basin and the myriad of processes that alter and mix them. We will discuss isotope systematics among gases shown as histograms in Figs. 4, 5, 6, 7 and 8.

Cross plots of $\delta^{13}C$ values of the different components in natural gas are standard tools for understanding the origin and history of natural gases. In theory, set of gases in the basin generated at different maturities from uniform kerogen, $\delta^{13}C$ values of methane, ethane propane and n-butane should be systematically correlated and fall on straight lines on isotope cross plots with low maturity gases starting low in $\delta^{13}C$, but increasing with maturity. Fig. 35A shows $\delta^{13}C$ cross plots of production gas methane vs ethane, ethane vs propane and propane vs. *n*-butane from W3. The cross plots suggest the existence of two types of gases. The W3 gases are mostly from either the Mannville oil associated gases that have relatively $\delta^{13}C$ enriched ethane and propane vs the dry Colorado gases in SE Alberta and SW Saskatchewan that are extraordinarily depleted of $\delta^{13}C$ and may be incipient thermogenic (see Rowe and A Muehlenbachs, 1999 for discussion). Note the comparatively greater scatter in the $\delta^{13}C$ methane vs $\delta^{13}C$ ethane plot than plots of $\delta^{13}C$ ethane vs

$\delta^{13}C$ propane or $\delta^{13}C$ propane vs. $\delta^{13}C$ *n*-butane. The greater scatter in methane $\delta^{13}C$ is a universal feature, because methane has more than one mechanism of generation, whereas the higher hydrocarbons can only be formed by thermogenesis.

Fig. 35B shows $\delta^{13}C$ cross plots of production gas methane vs ethane, ethane vs propane and propane vs. *n*-butane from W4. Several gas types can be recognized in addition to the low maturity, biogenic gases of SE Alberta and the altered gases of the heavy oil fields already seen W3. Conventional thermogenic gases are found to the west and thus show a better correlation among the hydrocarbons.

Fig. 35C shows $\delta^{13}C$ cross plots of production gas methane vs ethane, ethane vs propane and propane vs. *n*-butane from W5. The $\delta^{13}C$ cross plots of ethane vs propane and propane vs. *n*-butane are relatively well correlated, indicating that most of the production is from unaltered thermogenic reservoirs. $\delta^{13}C$ cross plot methane vs ethane shows the poorer correlation for the reasons already given.

Fig. 35D shows $\delta^{13}C$ cross plots of production gas methane vs ethane, ethane vs propane and propane vs. *n*-butane from W6. Indications are that most of the production W6 is from normal thermogenic reservoirs, but $\delta^{13}C$ cross plots of ethane vs propane and propane vs. n-butane show an unexpected deviation from the expected trend at the least negative $\delta^{13}C$ values. The deviating samples have reversals of their expected $\delta^{13}C$ of coexisting ethane and propane and will be discussed next.

Fig. 35E shows $\delta^{13}C$ cross plots of production gas methane vs ethane, ethane vs propane and propane vs. *n*-butane from NE BC. The $\delta^{13}C$ methane vs ethane plot shows two very unexpected populations. One population is characteristic of all the other production gases that methane $\delta^{13}C$

is always less than ethane $\delta^{13}C$. In contrast, the non-normal cluster has the opposite $\delta^{13}C$ relationship between methane and ethane. That isotopic bifurcation was observed in the $\delta^{13}C$ ethane vs propane and propane vs. *n*-butane plots. This isotope reversal anomaly are common in over mature shale gases and the Horn River Basin, as well in a few Montney wells. Tilley et al., (2011) explained the origin of the isotope reversals in overmature, tight shale gases.

Fig. 36A, B, C, D, and E show $\delta^{13}C$ cross plots of SCVF methane vs ethane, ethane vs propane and propane vs. *n*-butane from W3, W4, W5, W6 and NE BC respectively. The patterns seen on the graphs can be explained by all the mechanisms discussed above but with a bit more scatter. Important to note in general, the SCVF gas isotope geochemistry is similar to that of production gases, but at any one location, the SCVF gases would likely plot differently than the production gases. Combining information from the maps and the isotope cross plots of SCVF we suggest that SCVF in the WCSB can be grouped into five gas families, as shown in Fig. 37.

Fig. 38A, B, C, D, and E show $\delta^{13}C$ cross plots of GM methane vs ethane, ethane vs propane, propane vs. n-butane and methane vs CO_2 from W3, W4, W5, W6 and NE BC respectively. The correlations seen between the hydrocarbons show that most GM gases had a thermogenic origin, but some GM gas is purely biogenic. $\delta^{13}C$ methane vs CO_2 plots show huge variations, the cause of which has been discussed above. As with SCVF, it is crucial to note the GM gas isotope geochemistry may indicate a thermogenic origin but not likely from the well's target.

4. Conclusions

Various components, methane, ethane, propane, *i & n*-butane and CO_2 constituting carbon isotope fingerprints of fugitive gases from oil and gas wells across the whole of the Western Canada Sedimentary Basin have been mapped and contoured and overlain on topography. The maps reveal

regional variations in $\delta^{13}C$ of fugitive methane, ethane, propane, *i & n* butane and CO_2 that can be understood and explained in terms of differing burial depth of reservoirs, alteration history and mixing both in the original source region, as well as along the migration pathway. The maps confirm that most SCVF and GM originates somewhere along the wellbore above the target formation. Contouring of the $\delta^{13}C$ values of methane, ethane, propane and butane of SCVF and GM yields smooth contours that are coherent with topography when so overlain. The mapping and contouring of the $\delta^{13}C$ data revealed novel and useful insights into the origin of SCVF and GM, which should facilitate remediation of existing problematic wells, but also may improve well planning, integrity and completion in the future. The maps also show that many locations multiple nearby SCV wells have the same or similar isotope fingerprint even though the wells are of differing age and drilled by different operators. Service companies and regulators can use these maps to predict the source depth of putative SCVF and GM, thereby improving budgeting and scheduling.

Yet, such response and correlation with geomorphological units, left outstanding questions, such as -why nearby wells tend to have cementing failures at similar depths?. Relic tectonic stresses, as well as rheology of formations and geomorphological units, may play a role. This must be tested and identified to improve future drilling and cementing. Uniformity of failure depths in adjacent wells is an outstanding observation. Hence, the source depth of SCVF and GM in regions tapping into the same reservoir is related to surface topography sometimes in a counterintuitive way. Bachu and Watson (2006) have noted wells in river valleys have more frequent SCVF and GM than wells on topographic highs. Our mapped isotope fingerprints reveal that in the valleys, SCVF frequently comes from shallower depths than on the heights. Documentation of the influence of surface topography on the source depth of SCVF has clear economic and engineering implications.

Knowing that topography and geomorphology may influence the SCVF and GM in valley wells will lower the cost of remediation of such wells as well should challenge cementers to avoid the problem in future wells.

5. Future work

Two relevant tasks still need to be accomplished with the carbon isotope database and maps. New contour maps need to be prepared to translate the isotope fingerprint of the SCVF and GM into the name of the source formation or approximate depth in meters. This would perhaps require machine learning and 3D modelling. An added benefit of such 3D maps may be that the geographic and geomorphological distribution of the subset of GM and SCVF originating from the production horizon may reveal as of yet unknown factors controlling stresses in the subsurface.

The other unfinished task was the subject of the proposal for the second phase of this project that digitizing the information and making it accessible online to Industry, Regulators and the Public.

6. References

Pyrcz, M.J. and Deutsch, C.V., (2014). Geostatistical reservoir modelling; Oxford University Press, 433 p.

Tilley, B., and Muehlenbachs, K., (2006). Gas maturity and alteration systematics across the Western Canada Sedimentary Basin from four mud gas isotope depth profiles. *Organic Geochemistry*, 37(12), 1857–1868.

Tilley, B., McLellan, S., Hiebert, S., Quartero, B., Veilleux, B., and Muehlenbachs, K., (2011). Gas isotope reversals in fractured gas reservoirs of the western Canadian Foothills: Mature shale gases in disguise. *AAPG bulletin*, 95(8), 1399–1422.

Rowe, D., and Muehlenbachs, K., (1999). Low-temperature thermal generation of hydrocarbon gases in shallow shales. Nature, 398(6722), 61–63.

Watson, T. L., and Bachu, S., (2009). Evaluation of the potential for gas and CO2 leakage along wellbores. *SPE Drilling & Completion*, 24(01), 115–126.

List of figures

Figure 1. Isotope depth profiles for four mudlogs across the Western Canada Sedimentary Basin showing. Variables display in each profile includes: lithology; isotope profiles for n-alkanes (methane, ethane and propane); percent methane; and total hydrocarbon gas recovered at each depth (please see for details Tilley and Muehlenbachs, 2006).

Figure 2. Map of production (a), surface casing vent (SCV)(b), and ground migration (GM)(c) wells locations in the Western Canada Sedimentary Basin (WCSB).

Figure 3. Boxplots of n-alkanes (methane, ethane, propane, i-butane, n-butane) and carbon dioxide isotopic values for production (a), surface casing vent (SCV) (b), and ground migration (GM)(c) gases for the Western Canada Sedimentary Basin (WCSB).

Figure 4. Histogram showing the methane (i), ethane (ii), propane (iii) and carbon dioxide (iv) isotopic values for production (a), surface casing vent (b), and ground migration (c) in W3.

Figure 5. Histogram showing the methane, ethane, propane and carbon dioxide isotopic values for production (a), surface casing vents (b), and ground migration (GM) gases from W4.

Figure 6. Histogram showing the methane, ethane, propane and carbon dioxide isotopic values for production (a), surface casing vents (b), and ground migration (GM) gases from W5.

Figure 7. Histogram showing the methane, ethane, propane and carbon dioxide isotopic values for production (a), surface casing vents (b), and ground migration (GM) gases from W6.

Figure 8. Histogram showing the methane, ethane, propane and carbon dioxide isotopic values for production (a), surface casing vents (b), and ground migration (GM) gases from British Columbia (BC).

Figure 9. Contour map of methane carbon isotope values of production (a), surface casing vent (SCV)(b), and ground migration (GM)(c) gases.

Figure 10. Contour map of ethane carbon isotope values of production (a), surface casing vent (SCV)(b), and ground migration (GM)(c) gases.

Figure 11. Contour map of propane carbon isotope values of production (a), surface casing vent (SCV)(b), and ground migration (GM)(c) gases.

Figure 12. Contour map of n-butane carbon isotope values of production (a), surface casing vent (SCV)(b), and ground migration (GM)(c) gases.

Figure 13. Contour map of i-butane carbon isotope values of production (a), surface casing vent (SCV)(b), and ground migration (GM)(c) gases.

Figure 14. Contour map of carbon dioxide carbon isotope values of production (a), surface casing vent (SCV)(b), and ground migration (GM)(c) gases.

Figure 15. Topography under contour map of methane carbon isotope values of production (a), surface casing vent (SCV)(b), and ground migration (GM)(c) gases.

Figure 16. Topography under contour map of ethane carbon isotope values of production (a), surface casing vent (SCV)(b), and ground migration (GM)(c) gases.

Figure 17. Topography under contour map of propane carbon isotope values of production (a), surface casing vent (SCV)(b), and ground migration (GM)(c) gases.

Figure 18. Topography under contour map of n-butane carbon isotope values of production (a), surface casing vent (SCV)(b), and ground migration (GM)(c) gases.

Figure 19. Topography under contour map of i-butane carbon isotope values of production (a), surface casing vent (SCV)(b), and ground migration (GM)(c) gases.

Figure 20. Topography under contour map of carbon dioxide carbon isotope values of production (a), surface casing vent (SCV)(b), ground migration (GM)(c) gases. Location map of zoom-in areas in the region (d).

Figure 21. Location, isotope values contour maps and topography under contour maps for surface casing vent (SCV) gases in the Easter Alberta zoom-in area. The maps include: location maps of samples (a), methane contour map (b), ethane contour map (c), propane contour map (d), n-butane contour map (e), i-butane contour map (f), carbon dioxide contour map (g), topography under methane contoured isotopic values (h), topography under ethane contoured isotopic values (i), topography under propane contoured isotopic values (j), topography under n-butane contoured isotopic values (k), topography under i-butane contoured isotopic values (l), and topography under i-butane contoured isotopic values (m).

Figure 22. Location, isotope values contour maps and topography under contour maps for ground migration (GM) gases in the Easter Alberta zoom-in area. The maps include: location maps of

samples (a), methane contour map (b), ethane contour map (c), propane contour map (d), n-butane contour map (e), i-butane contour map (f), carbon dioxide contour map (g), topography under methane contoured isotopic values (h), topography under ethane contoured isotopic values (i), topography under propane contoured isotopic values (j), topography under n-butane contoured isotopic values (k), topography under i-butane contoured isotopic values (l), and topography under i-butane contoured isotopic values (m).

Figure 23. Location, isotope values contour maps and topography under contour maps for surface casing vent (SCV) gases in the Lloydminster zoom-in area. The maps include: location maps of samples (a), methane contour map (b), ethane contour map (c), propane contour map (d), n-butane contour map (e), i-butane contour map (f), carbon dioxide contour map (g), topography under methane contoured isotopic values (h), topography under ethane contoured isotopic values (i), topography under propane contoured isotopic values (j), topography under n-butane contoured isotopic values (k), topography under i-butane contoured isotopic values (l), and topography under i-butane contoured isotopic values (m).

Figure 24. Location, isotope values contour maps and topography under contour maps for ground migration (GM) gases in the Lloydminster zoom-in area. The maps include: location maps of samples (a), methane contour map (b), ethane contour map (c), propane contour map (d), n-butane contour map (e), i-butane contour map (f), carbon dioxide contour map (g), topography under methane contoured isotopic values (h), topography under ethane contoured isotopic values (i), topography under propane contoured isotopic values (j), topography under n-butane contoured isotopic values (k), topography under i-butane contoured isotopic values (l), and topography under i-butane contoured isotopic values (m).

Figure 25. Location, isotope values contour maps and topography under contour maps for surface casing vent (SCV) gases in the Lindbergh zoom-in area. The maps include: location maps of samples (a), methane contour map (b), ethane contour map (c), propane contour map (d), n-butane contour map (e), i-butane contour map (f), carbon dioxide contour map (g), topography under methane contoured isotopic values (h), topography under ethane contoured isotopic values (i), topography under propane contoured isotopic values (j), topography under n-butane contoured isotopic values (k), topography under i-butane contoured isotopic values (l), and topography under i-butane contoured isotopic values (m).

Figure 26. Location, isotope values contour maps and topography under contour maps for ground migration (GM) gases in the Lindbergh zoom-in area. The maps include: location maps of samples (a), methane contour map (b), ethane contour map (c), propane contour map (d), n-butane contour map (e), i-butane contour map (f), carbon dioxide contour map (g), topography under methane contoured isotopic values (h), topography under ethane contoured isotopic values (i), topography under propane contoured isotopic values (j), topography under n-butane contoured isotopic values (k), topography under i-butane contoured isotopic values (l), and topography under i-butane contoured isotopic values (m).

Figure 27. Location, isotope values contour maps and topography under contour maps for surface casing vent (SCV) gases in the Wildmere zoom-in area. The maps include: location maps of samples (a), methane contour map (b), ethane contour map (c), propane contour map (d), n-butane contour map (e), i-butane contour map (f), carbon dioxide contour map (g), topography under methane contoured isotopic values (h), topography under ethane contoured isotopic values (i), topography under propane contoured isotopic values (j), topography under n-butane contoured

isotopic values (k), topography under i-butane contoured isotopic values (l), and topography under i-butane contoured isotopic values (m).

Figure 28. Location, isotope values contour maps and topography under contour maps for ground migration (GM) gases in the Wildmere zoom-in area. The maps include: location maps of samples (a), methane contour map (b), ethane contour map (c), propane contour map (d), n-butane contour map (e), i-butane contour map (f), carbon dioxide contour map (g), topography under methane contoured isotopic values (h), topography under ethane contoured isotopic values (i), topography under propane contoured isotopic values (j), topography under n-butane contoured isotopic values (k), topography under i-butane contoured isotopic values (l), and topography under i-butane contoured isotopic values (m).

Figure 29. Location, isotope values contour maps and topography under contour maps for surface casing vent (SCV) gases in the Beaver Dam zoom-in area. The maps include: location maps of samples (a), methane contour map (b), ethane contour map (c), propane contour map (d), n-butane contour map (e), i-butane contour map (f), carbon dioxide contour map (g), topography under methane contoured isotopic values (h), topography under ethane contoured isotopic values (i), topography under propane contoured isotopic values (j), topography under n-butane contoured isotopic values (k), topography under i-butane contoured isotopic values (l), and topography under i-butane contoured isotopic values (m).

Figure 30. Location, isotope values contour maps and topography under contour maps for ground migration (GM) gases in the Beaver Dam zoom-in area. The maps include: location maps of samples (a), methane contour map (b), ethane contour map (c), propane contour map (d), n-butane contour map (e), i-butane contour map (f), carbon dioxide contour map (g), topography under

methane contoured isotopic values (h), topography under ethane contoured isotopic values (i), topography under propane contoured isotopic values (j), topography under n-butane contoured isotopic values (k), topography under i-butane contoured isotopic values (l), and topography under i-butane contoured isotopic values (m).

Figure 31. Location, isotope values contour maps and topography under contour maps for surface casing vent (SCV) gases in the Pembina zoom-in area. The maps include: location maps of samples (a), methane contour map (b), ethane contour map (c), propane contour map (d), n-butane contour map (e), i-butane contour map (f), carbon dioxide contour map (g), topography under methane contoured isotopic values (h), topography under ethane contoured isotopic values (i), topography under propane contoured isotopic values (j), topography under n-butane contoured isotopic values (k), topography under i-butane contoured isotopic values (l), and topography under i-butane contoured isotopic values (m).

Figure 32. Location, isotope values contour maps and topography under contour maps for ground migration (GM) gases in the Pembina zoom-in area. The maps include: location maps of samples (a), methane contour map (b), ethane contour map (c), propane contour map (d), n-butane contour map (e), i-butane contour map (f), carbon dioxide contour map (g), topography under methane contoured isotopic values (h), topography under ethane contoured isotopic values (i), topography under propane contoured isotopic values (j), topography under n-butane contoured isotopic values (k), topography under i-butane contoured isotopic values (l), and topography under i-butane contoured isotopic values (m).

Figure 33. Zoomed-in map showing a high sample density area of the heavy oil field at Lloydminster, eastern Alberta (a), and a and a cross-section from A to A’ (b). Contour map of

Easter Alberta zoomed-in area of ethane carbon isotope composition (i). Overlaid ethane isotopic composition highlight the geomorphological features in the area (ii), whereas a contoured map clearly displays energy wells' sampling location, ethane isotopic composition contouring, and a cross-section from A to A' (iii). Cross-section from A to A' showing: topographic variation, red rhombus indicate actual well measurements (i), methane (ii), ethane (iii), propane (iv), n-butane (v), and i-butane (iv) isotopic values.

Figure 34. Correlation of isotope mud-logs of two wells from the Lindberg heavy oil field. Wells are from high (a) and low (b) elevation areas.

Figure 35. Cross-plot of n-alkane production gases isotopic composition from W3 (a), W4 (b), W5 (c), W6 (d), and BC (e).

Figure 36. Cross-plot of n-alkane surface casing vent (SCV) gases isotopic composition from W3 (a), W4 (b), W5 (c), W6 (d), and BC (e).

Figure 37. Contour map of ethane carbon isotope values of SCV over topography showing potential gas families in the region. Isoscape map showing topographic base map overlaid by ethane isotopic composition contours. Color scale match mean isotopic values, which also correlates with depth (cold colors: depleted ethane isotope values, shallow leaks. Warm colors: enrich ethane values, deep-mature fingerprinting). Five groups are spatially distinctive and can be identified in the WCSB. Such distribution seems to be constrain by geological factors. Importantly, we observed that shallow leak are predominant in the southeastern region, and correlates with Quaternary geomorphological features, such as paleo-ice stream tracks.

Figure 38. Cross-plot of n-alkane ground migration (GM) gases isotopic composition from W3 (a), W4 (b), W5 (c), W6 (d), and BC (e).

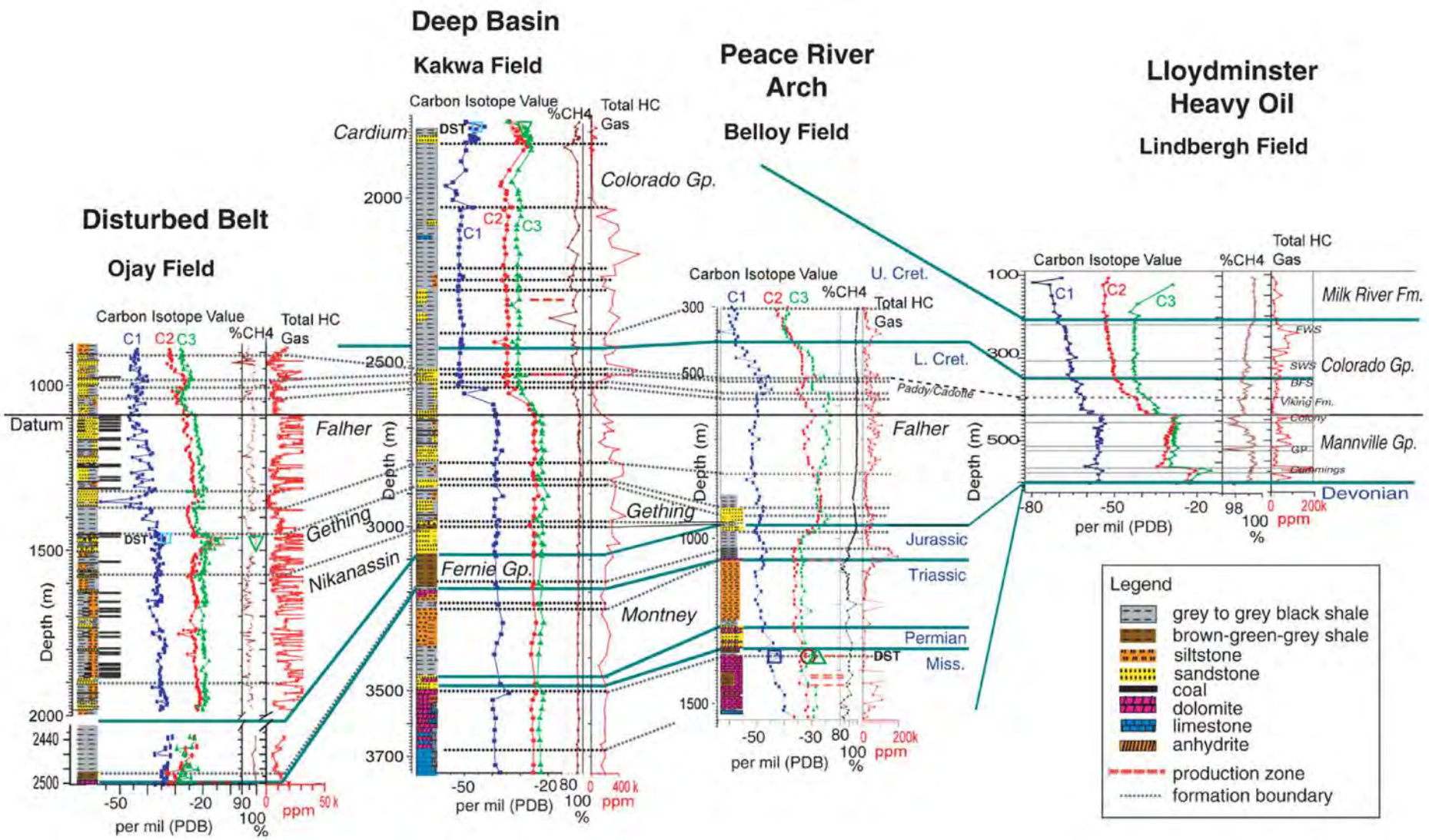

Fig. 1. Isotope depth profiles for four mudlogs across the Western Canada Sedimentary Basin showing (modified from Tilley and Muehlenbachs, 2006)

Fig. 2A. Map of Production wells Locations in the Western Canada Sedimentary Basin (WCSB)

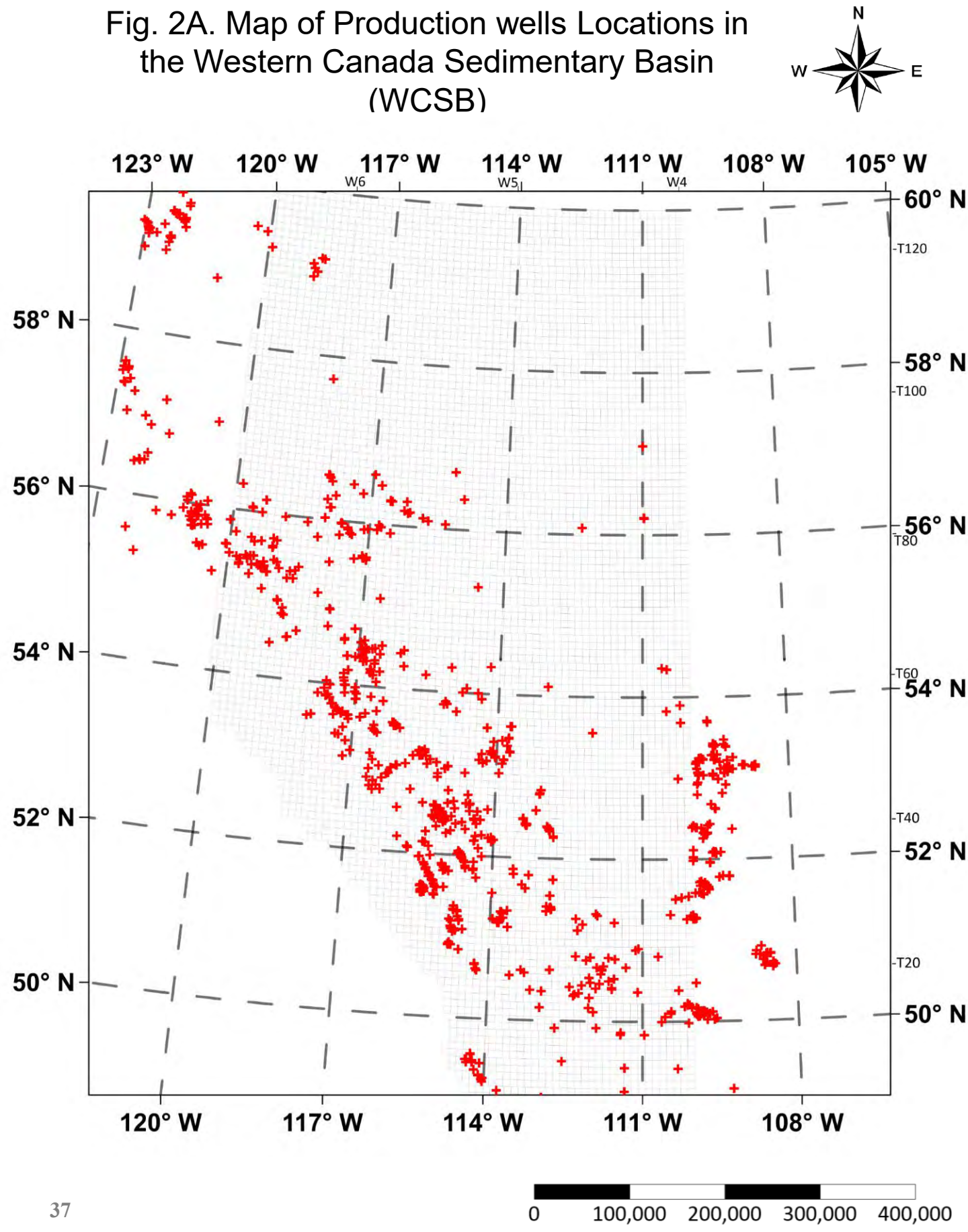

Fig. 2B. Map of Surface Casing Vent (SCV) Locations in the Western Canada Sedimentary Basin (WCSB)

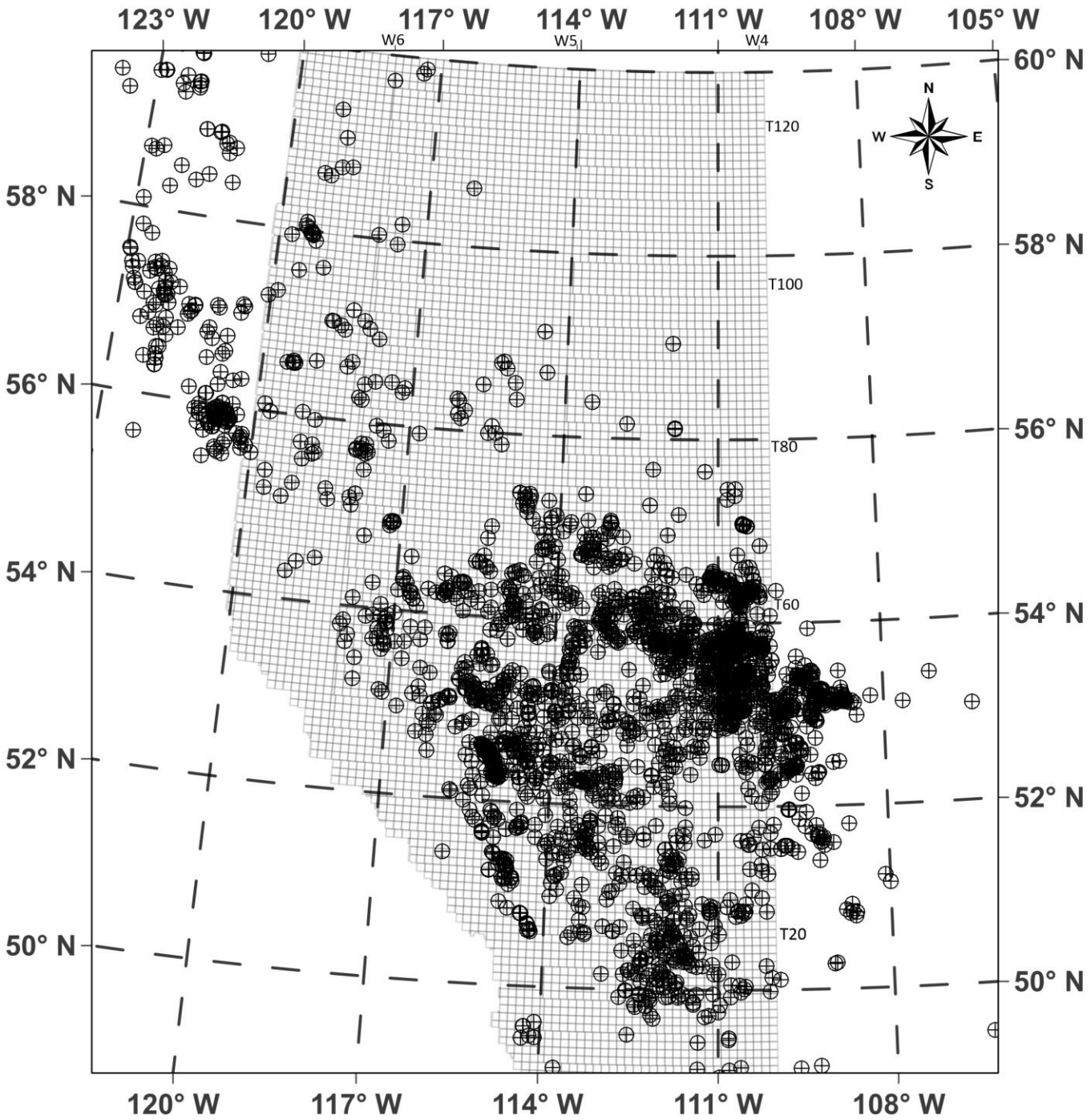

Fig. 2C. Map of Ground Migration Locations in the Western Canada Sedimentary Basin (WCSB)

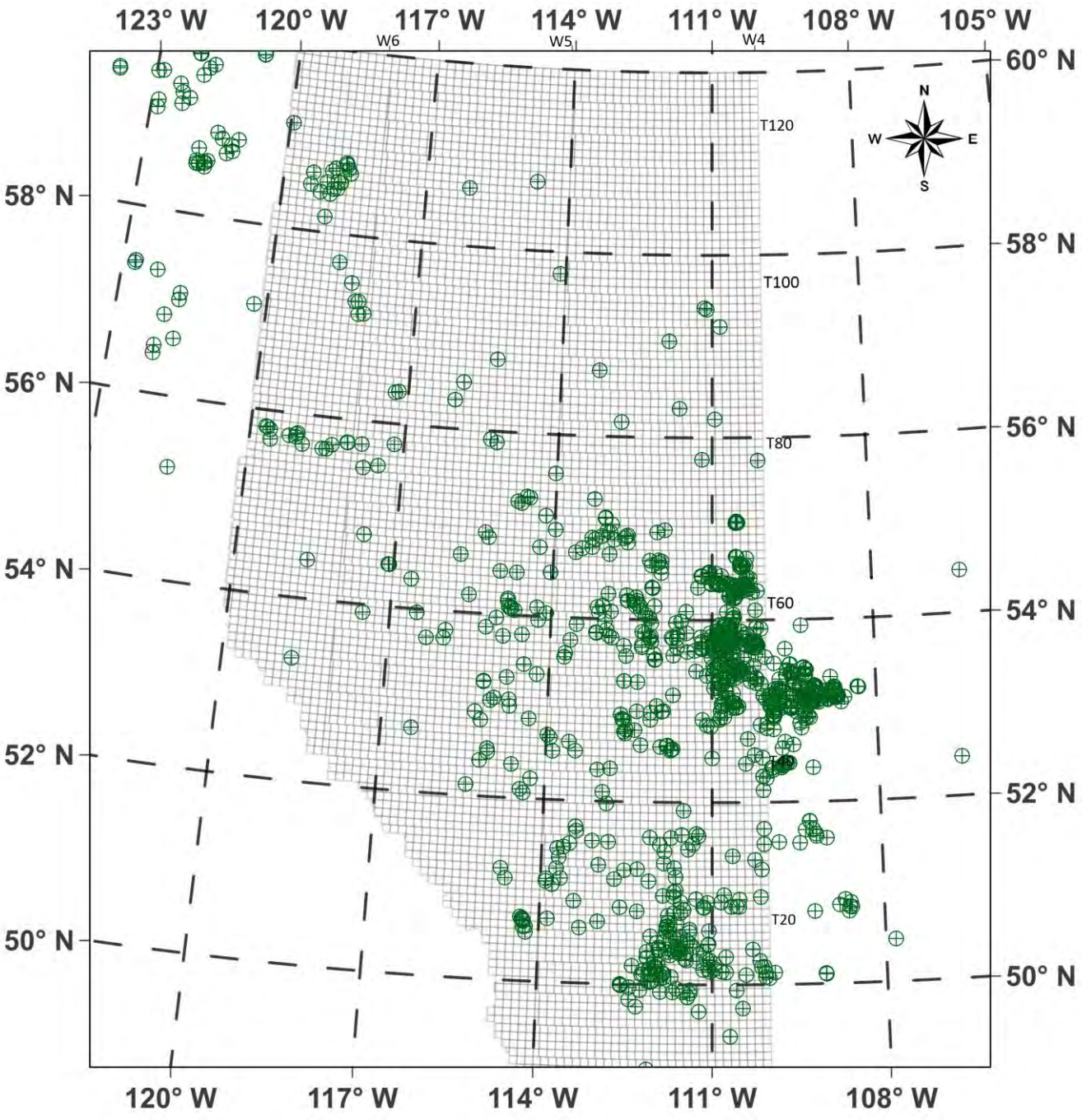

Fig. 3. WCSB statistical analyses for Production, SCV and GM regional data

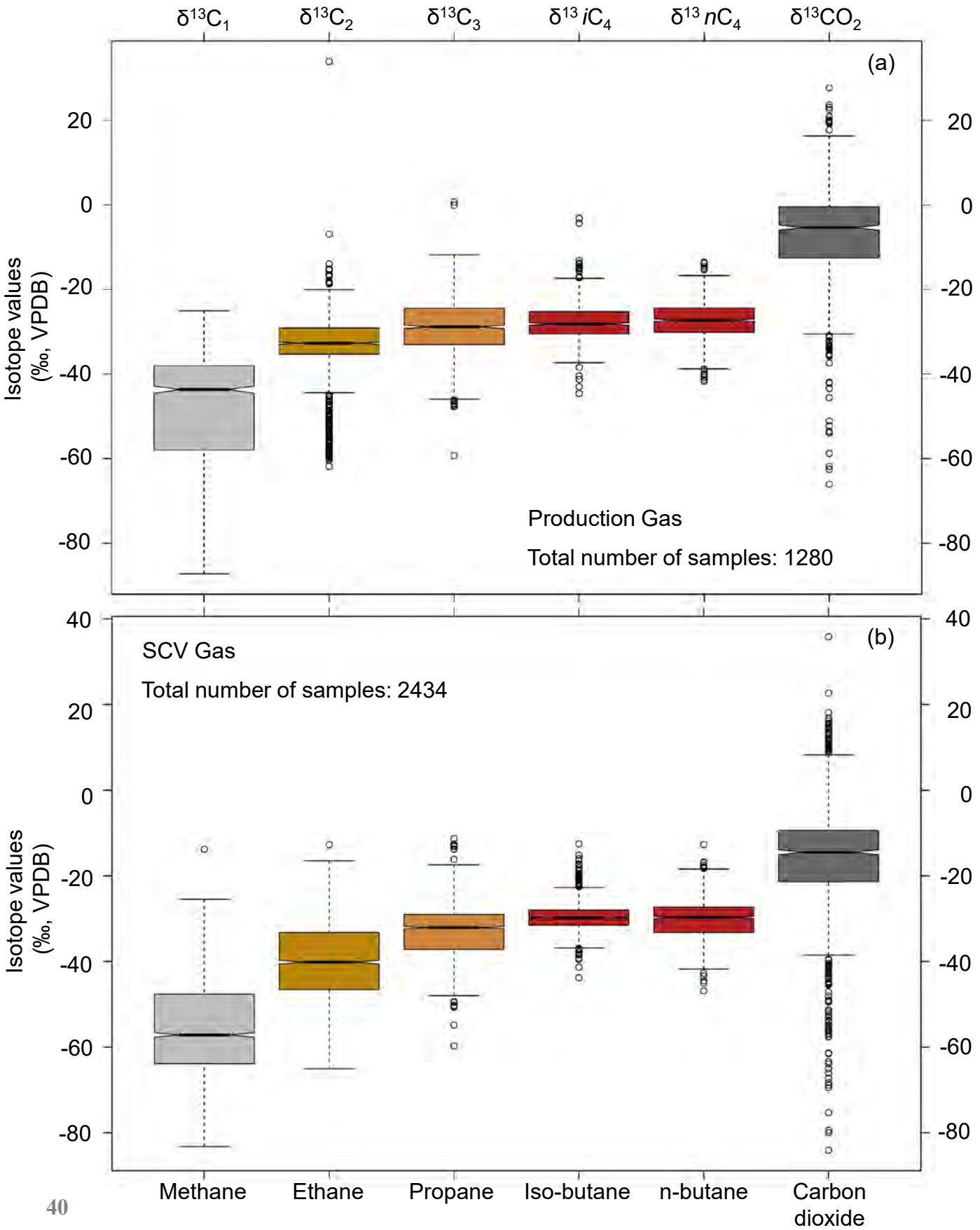

Fig. 3. WCSB boxplots for Production, SCV and GM regional data

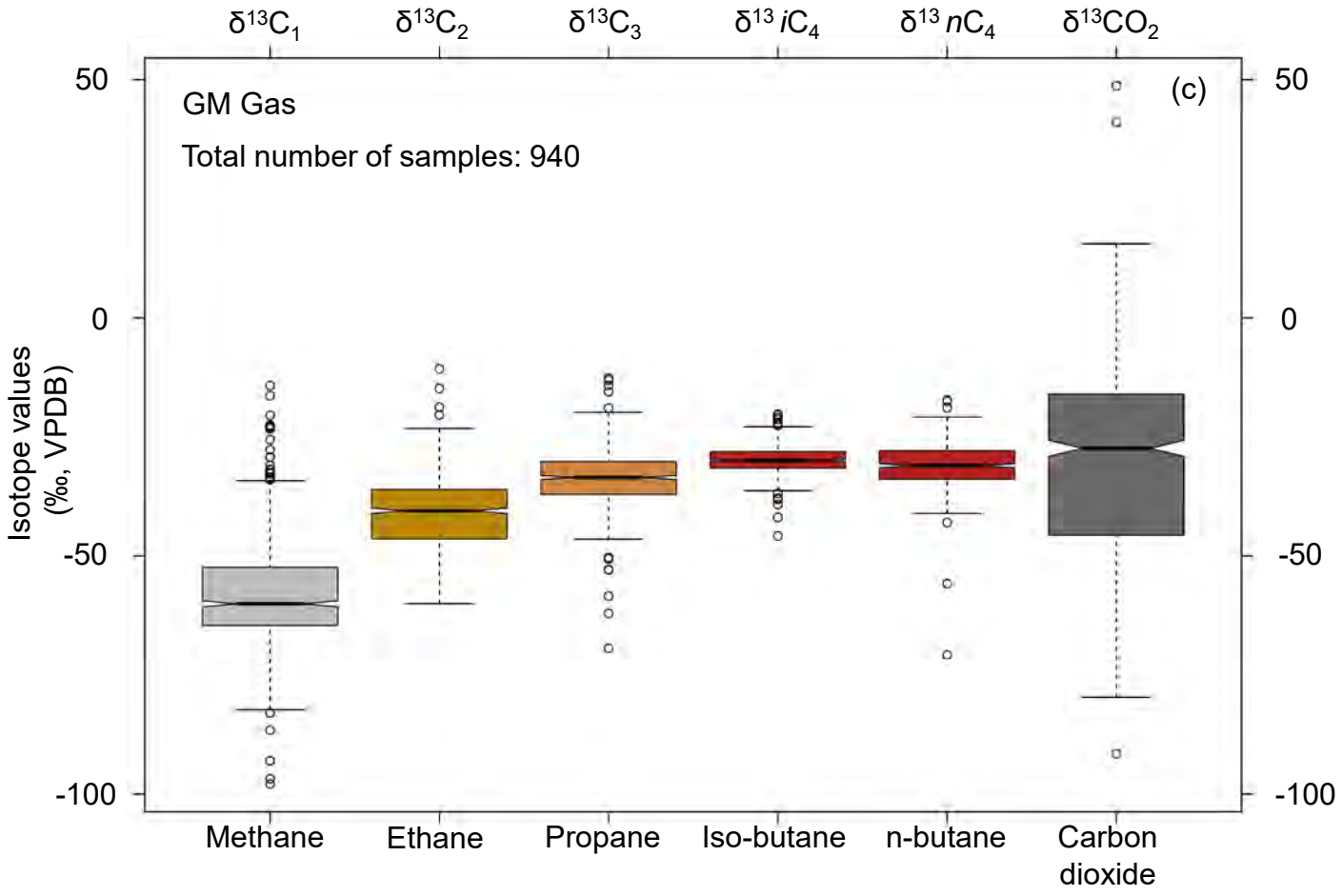

Fig. 4A. Histogram showing the methane, ethane, propane and carbon dioxide isotopic values for production gases from W3

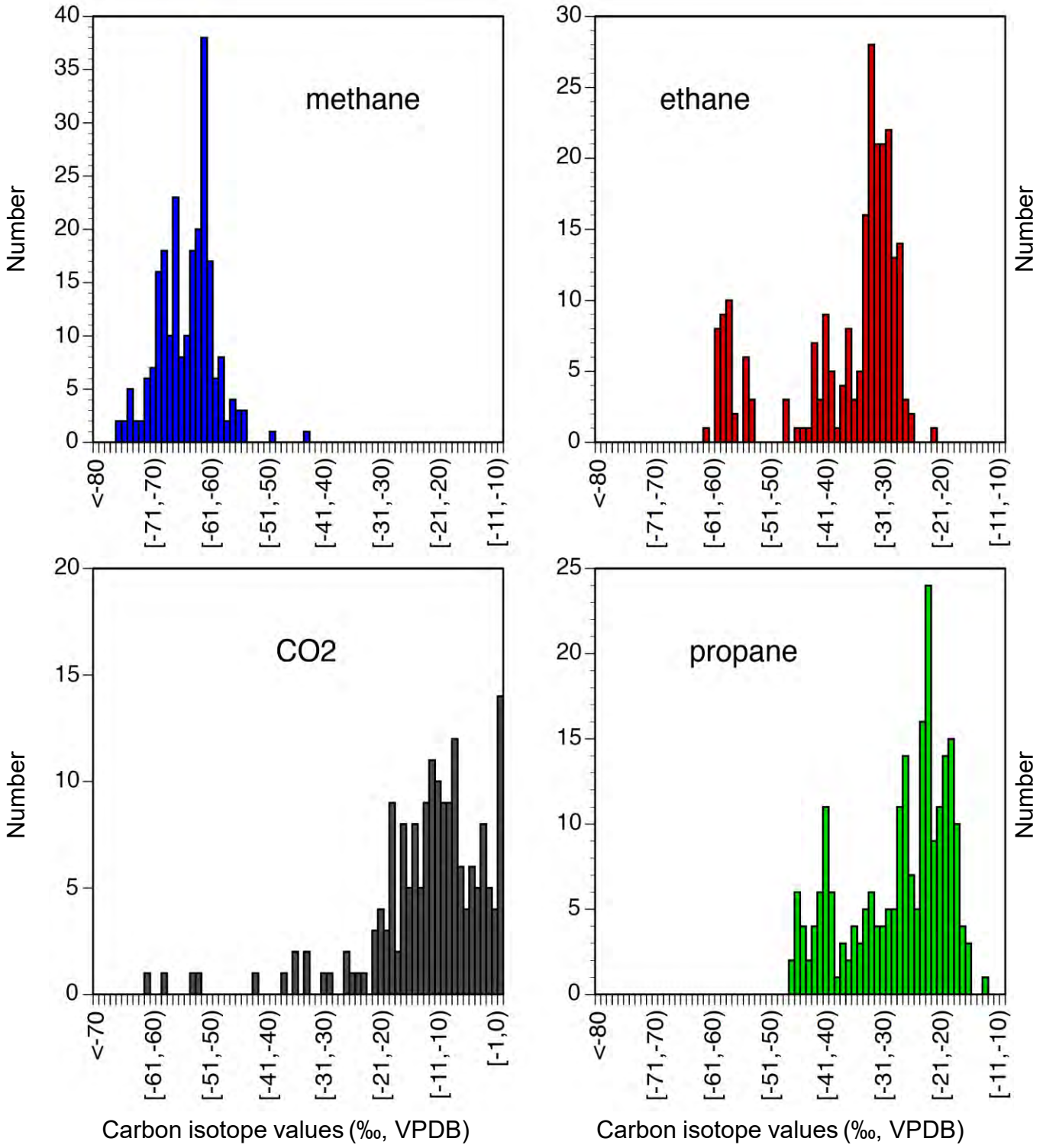

Fig. 4B. Histogram showing the methane, ethane, propane and carbon dioxide isotopic values for surface casing vent (SCV) gases from W3

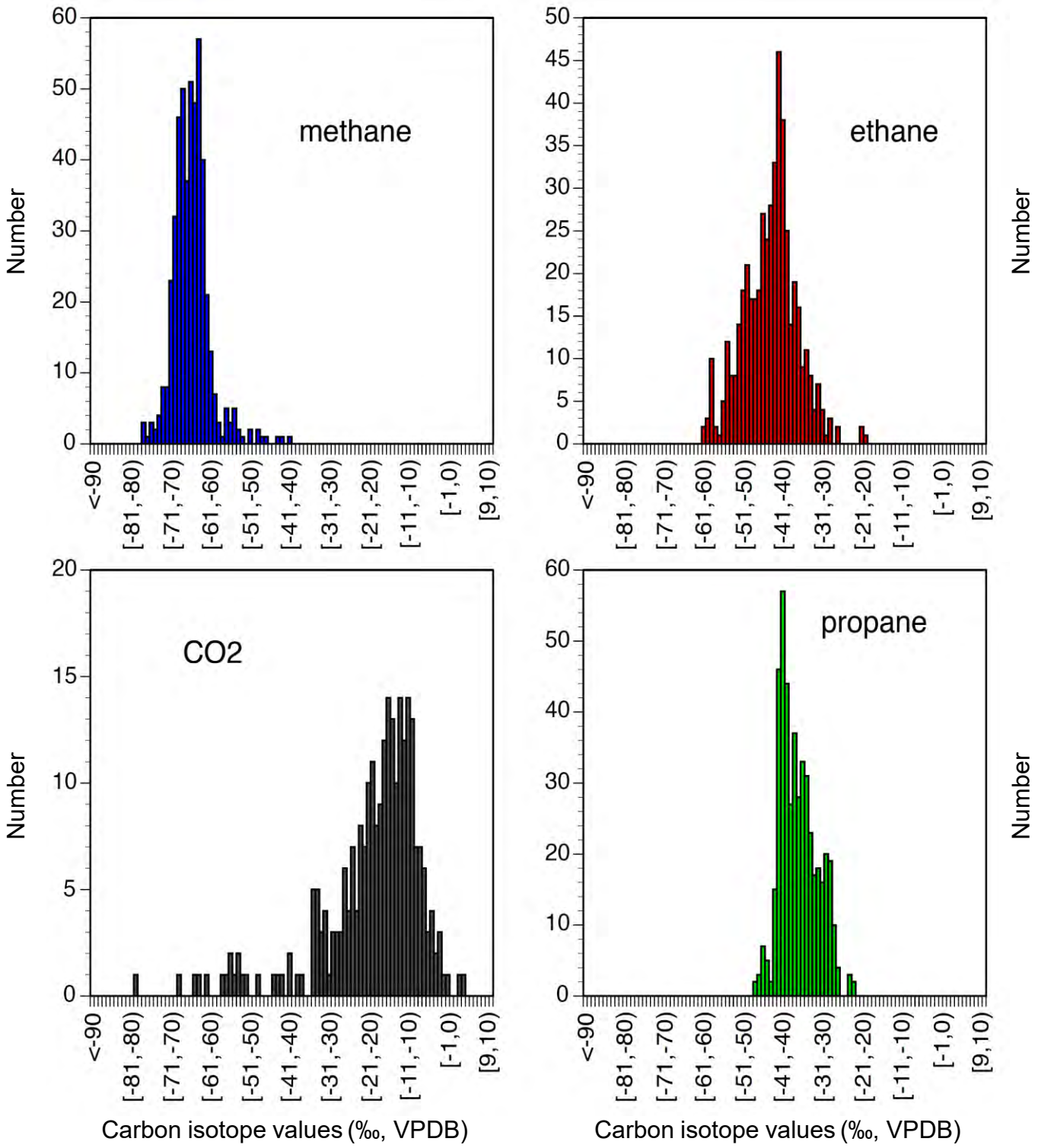

Fig. 4C. Histogram showing the methane, ethane, propane and carbon dioxide isotopic values for ground migration (GM) gases from W3

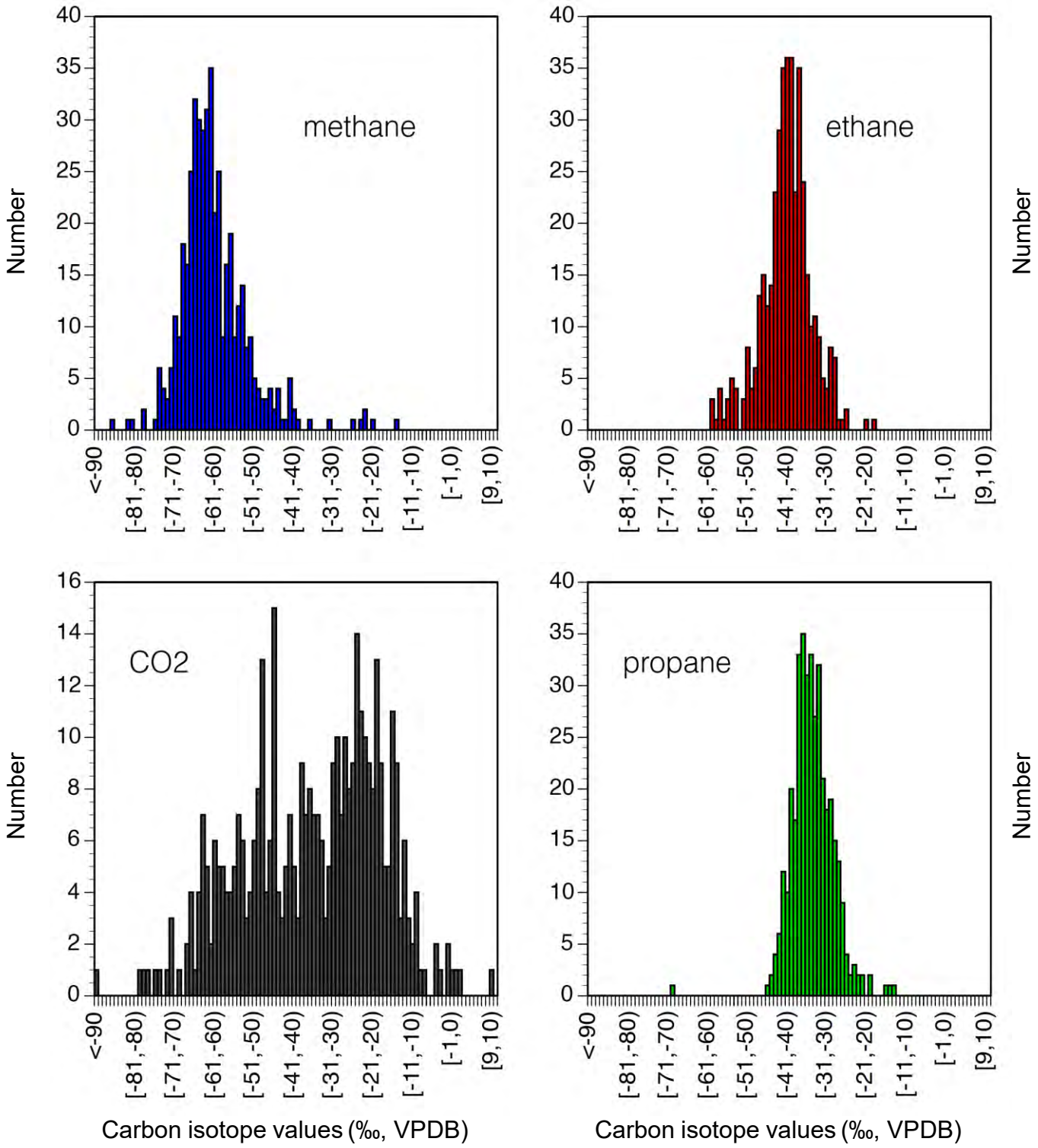

Fig. 5A. Histogram showing the methane, ethane, propane and carbon dioxide isotopic values for production gases from W4

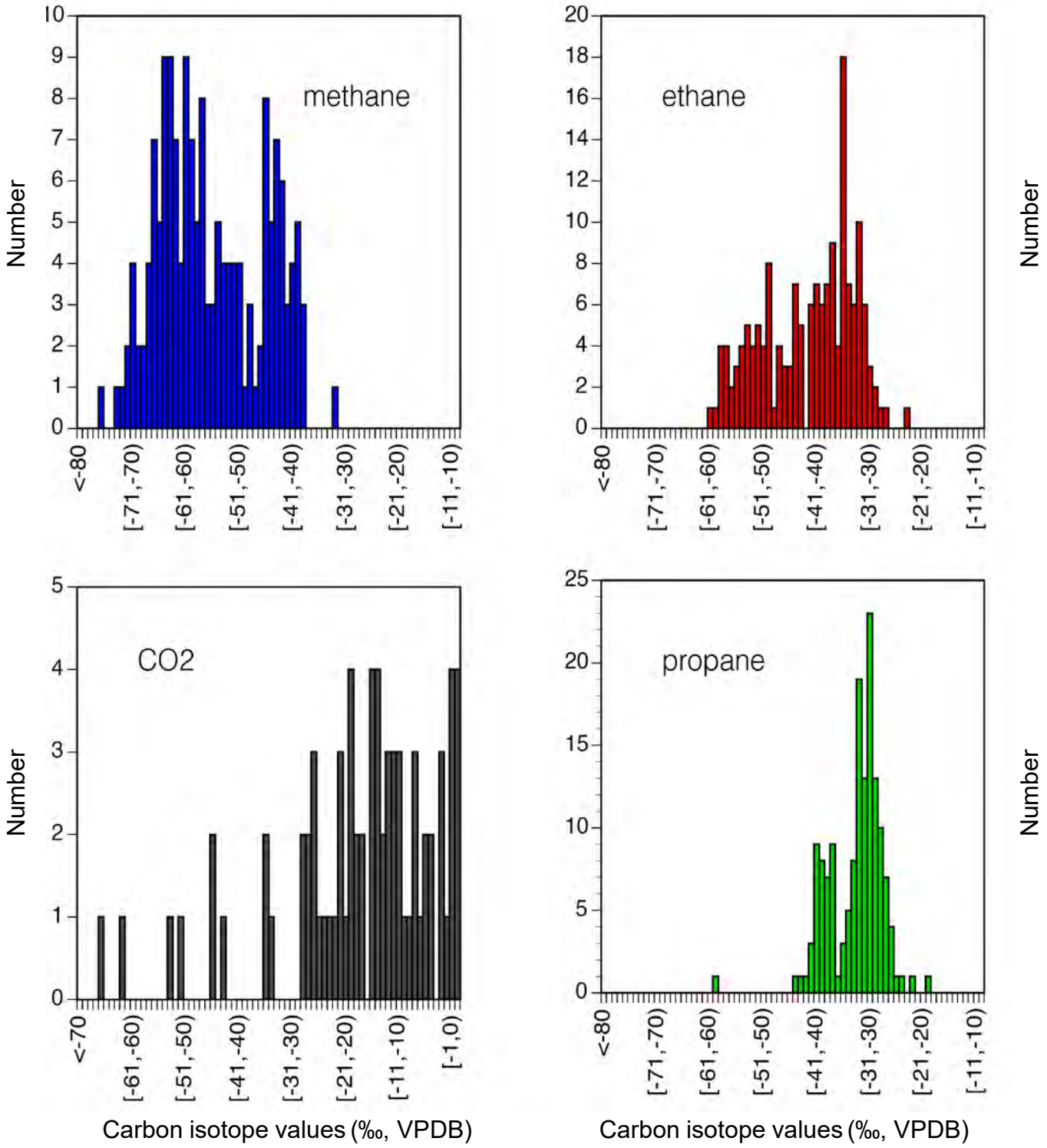

Fig. 5B. Histogram showing the methane, ethane, propane and carbon dioxide isotopic values for SCV gases from W4

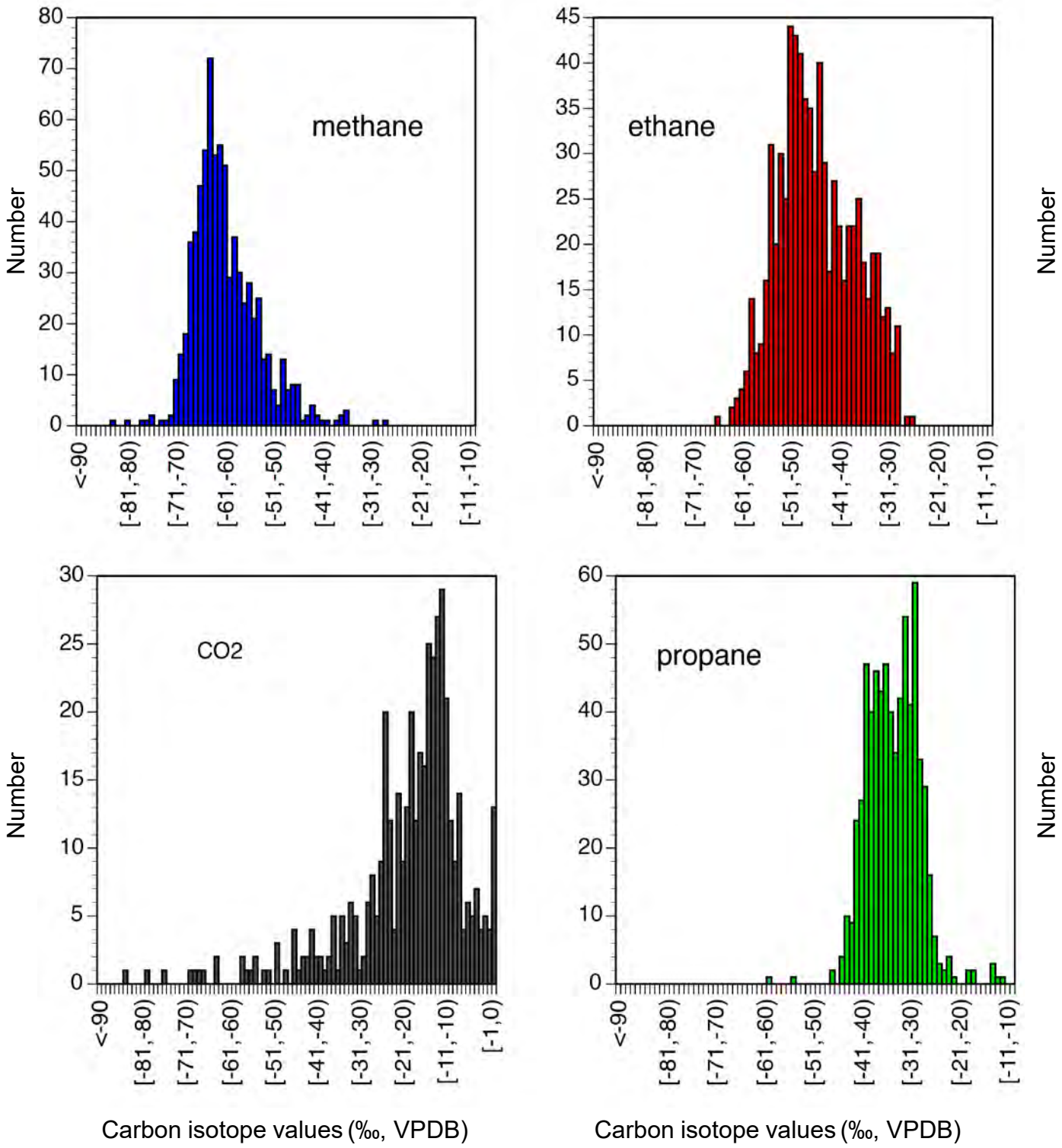

Fig. 5C. Histogram showing the methane, ethane, propane and carbon dioxide isotopic values for GM gases from W4

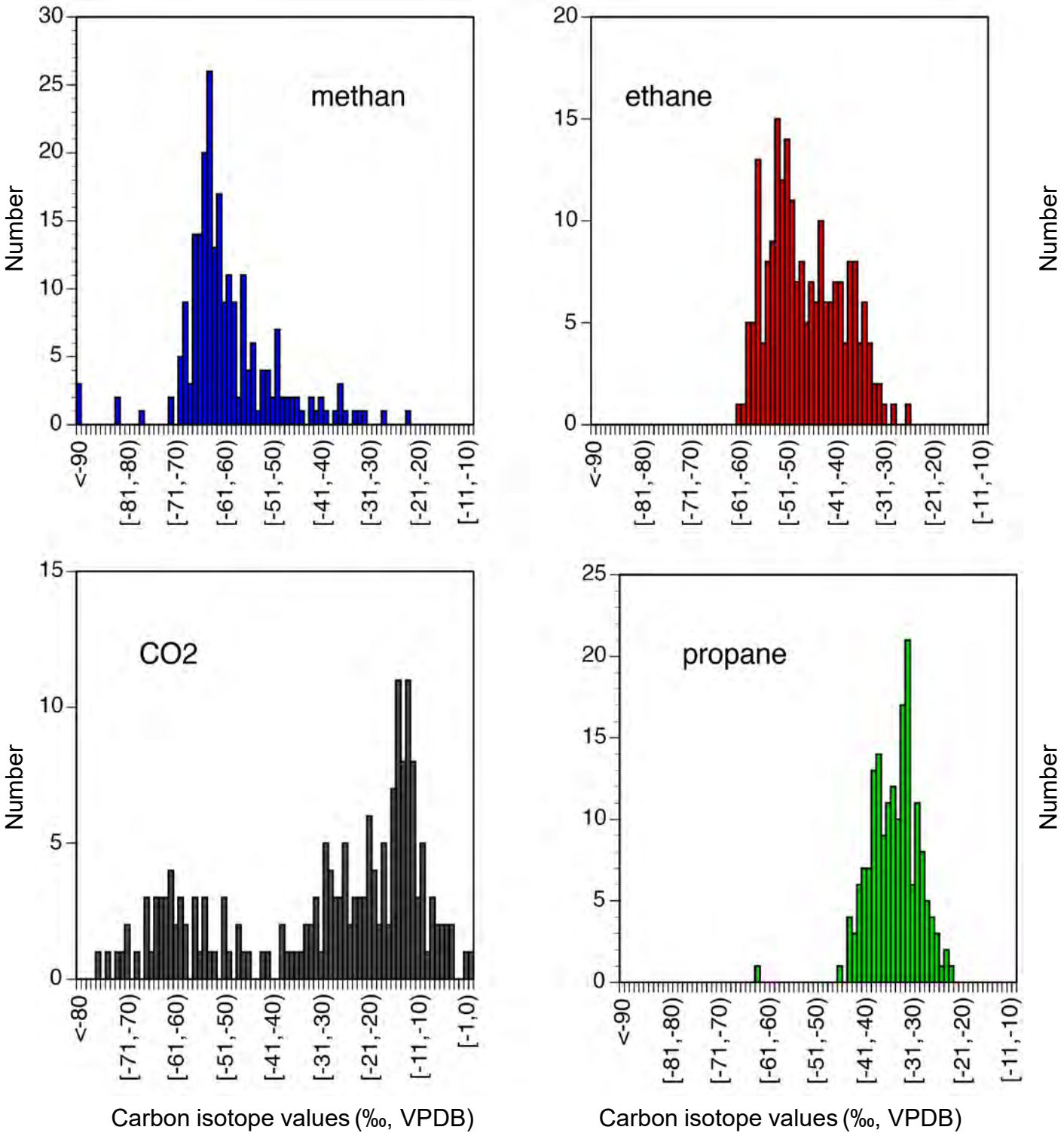

Fig. 6A. Histogram showing the methane, ethane, propane and carbon dioxide isotopic values for production gases from W5

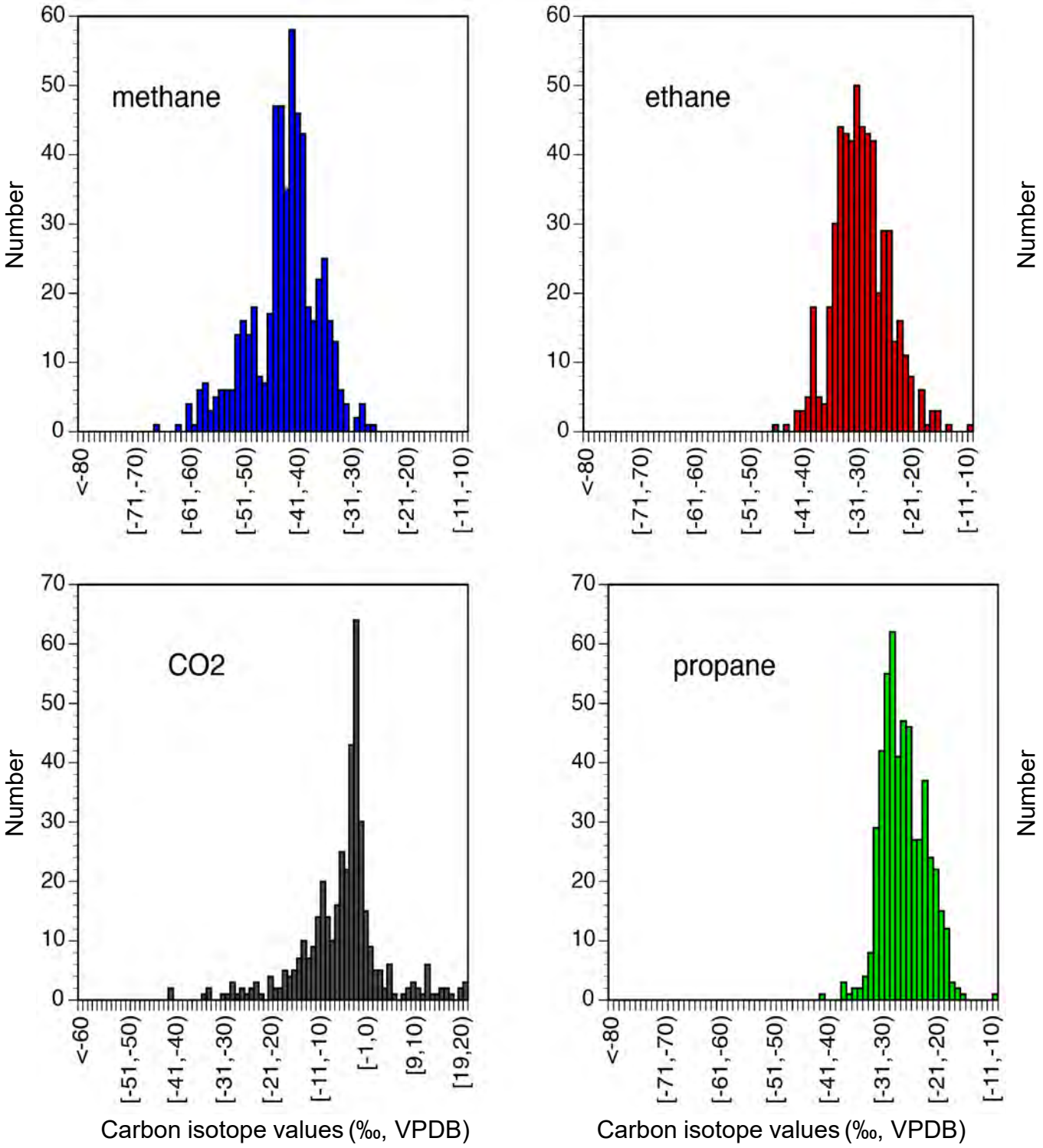

Fig. 6B. Histogram showing the methane, ethane, propane and carbon dioxide isotopic values for SCV gases from W5

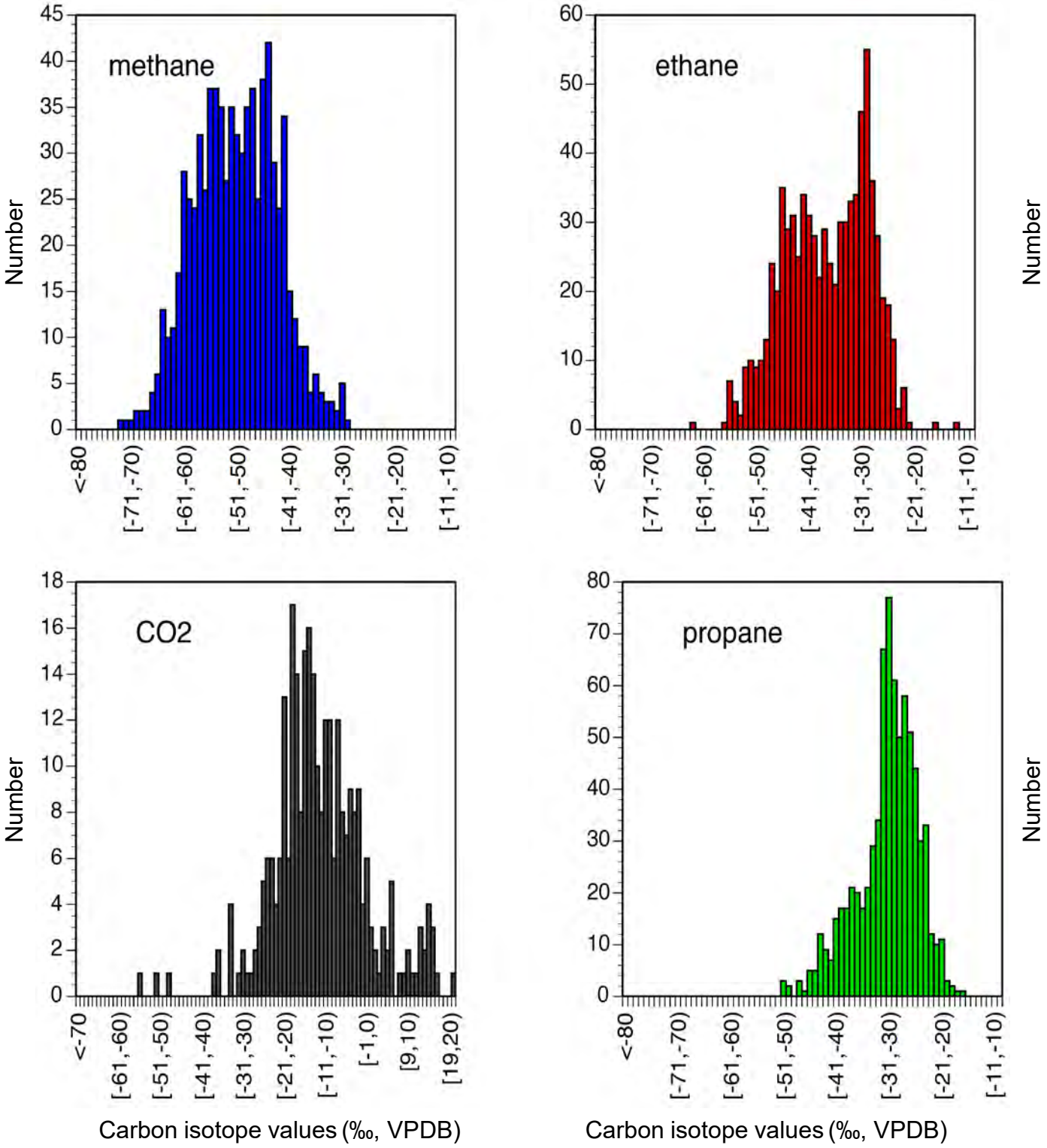

Fig. 6C. Histogram showing the methane, ethane, propane and carbon dioxide isotopic values for GM gases from W5

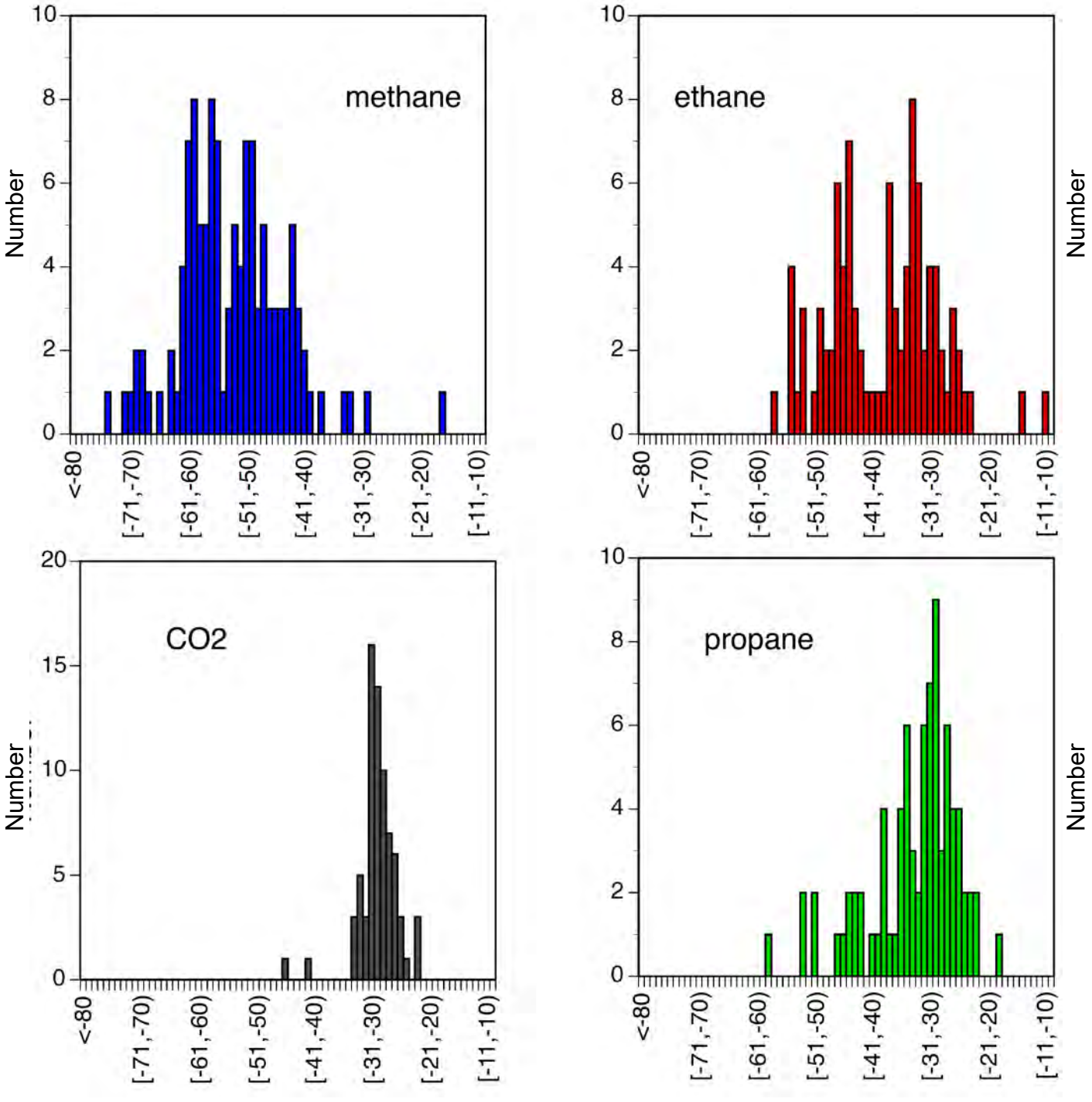

Fig. 7A. Histogram showing the methane, ethane, propane and carbon dioxide isotopic values for production gases from W6

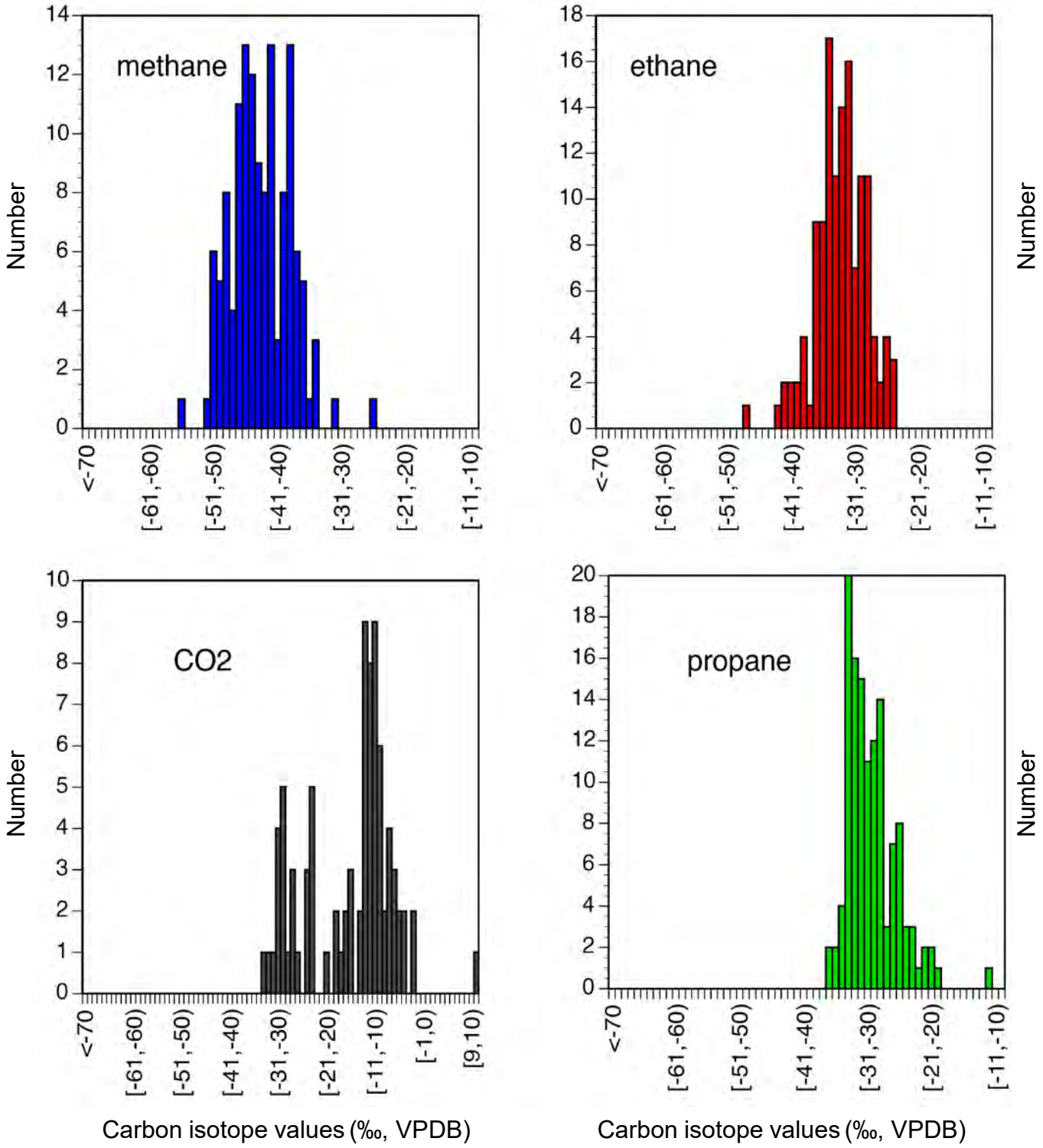

Fig. 7B. Histogram showing the methane, ethane, propane and carbon dioxide isotopic values for production gases from W6

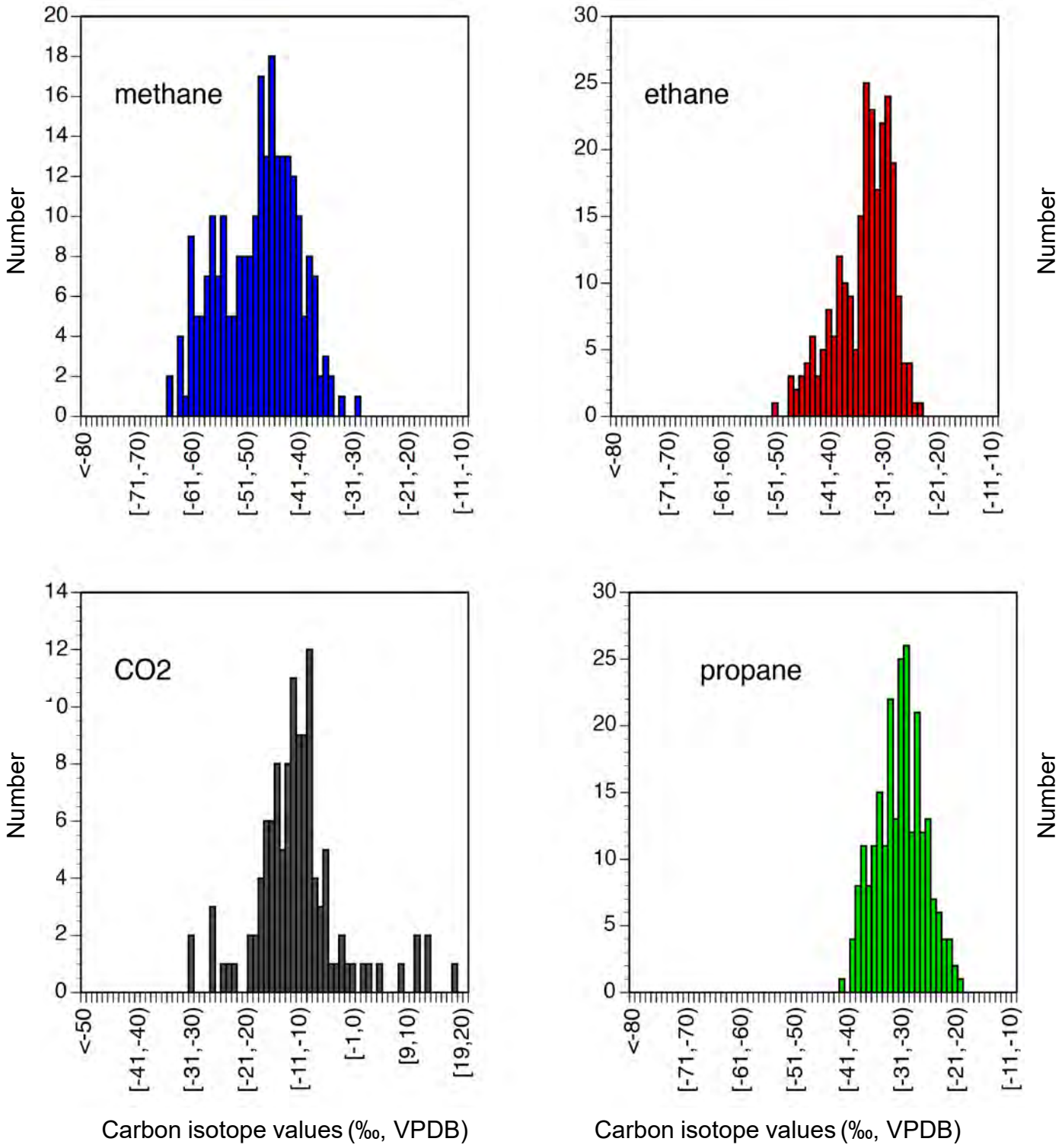

Fig. 7C. Histogram showing the methane, ethane, propane and carbon dioxide isotopic values for production gases from W6

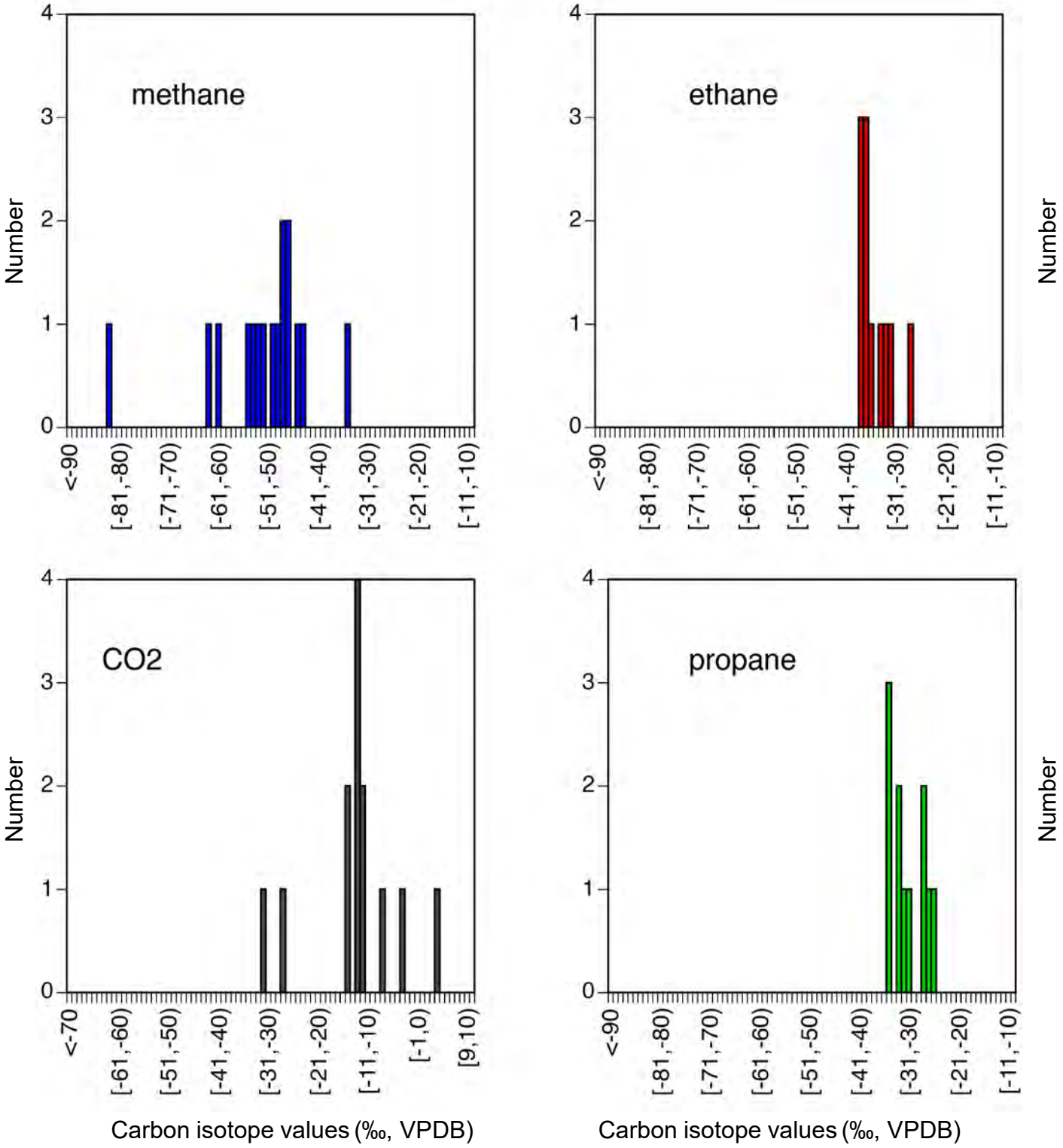

Fig. 8A. Histogram showing the methane (i), ethane (ii), propane (iv) and carbon dioxide (v) isotopic values for production gases from British Columbia

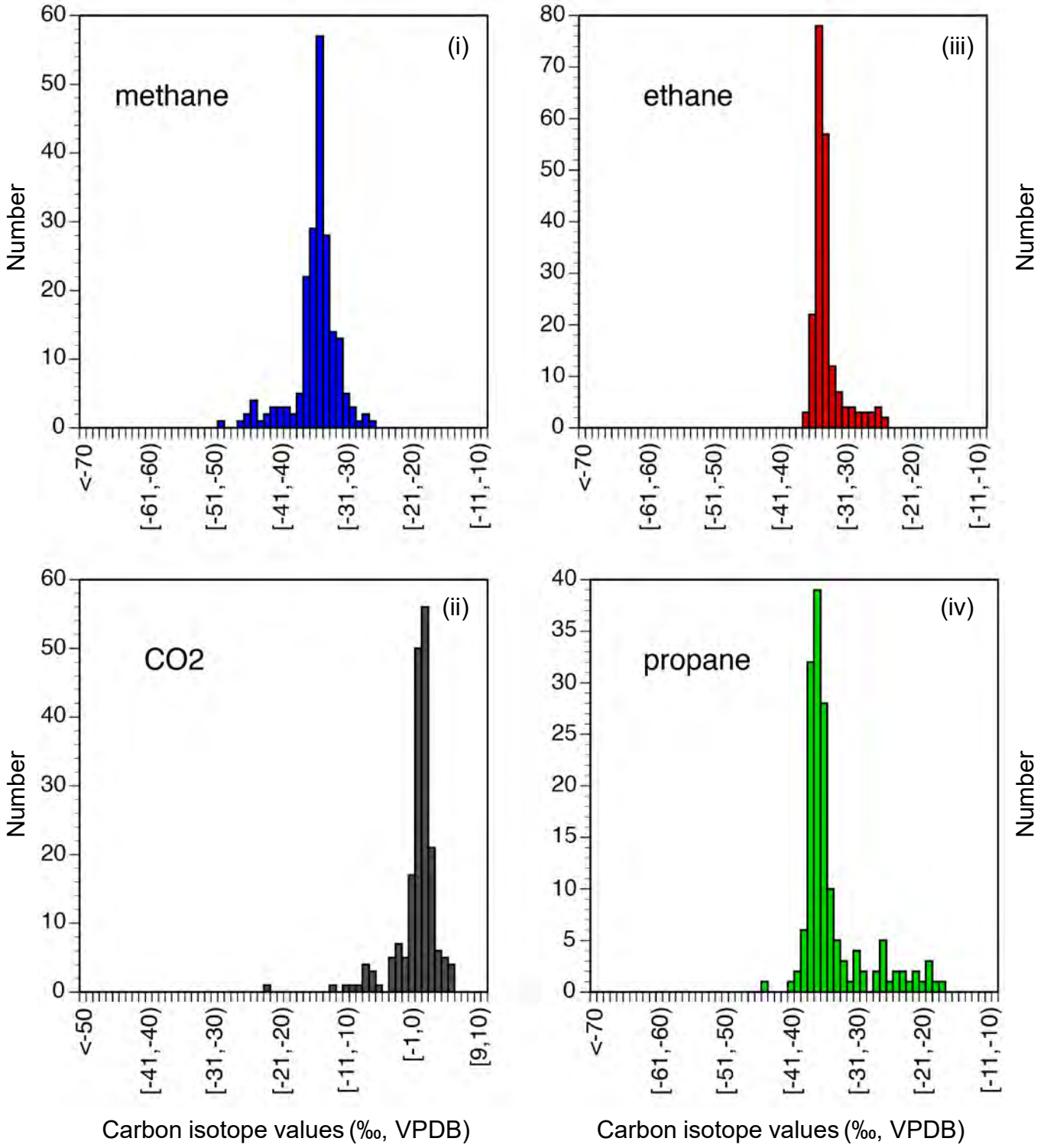

Fig. 8B. Histogram showing the methane (i), ethane (ii), propane (iv) and carbon dioxide (v) isotopic values for surface casing vent (SCV) gases from British Columbia

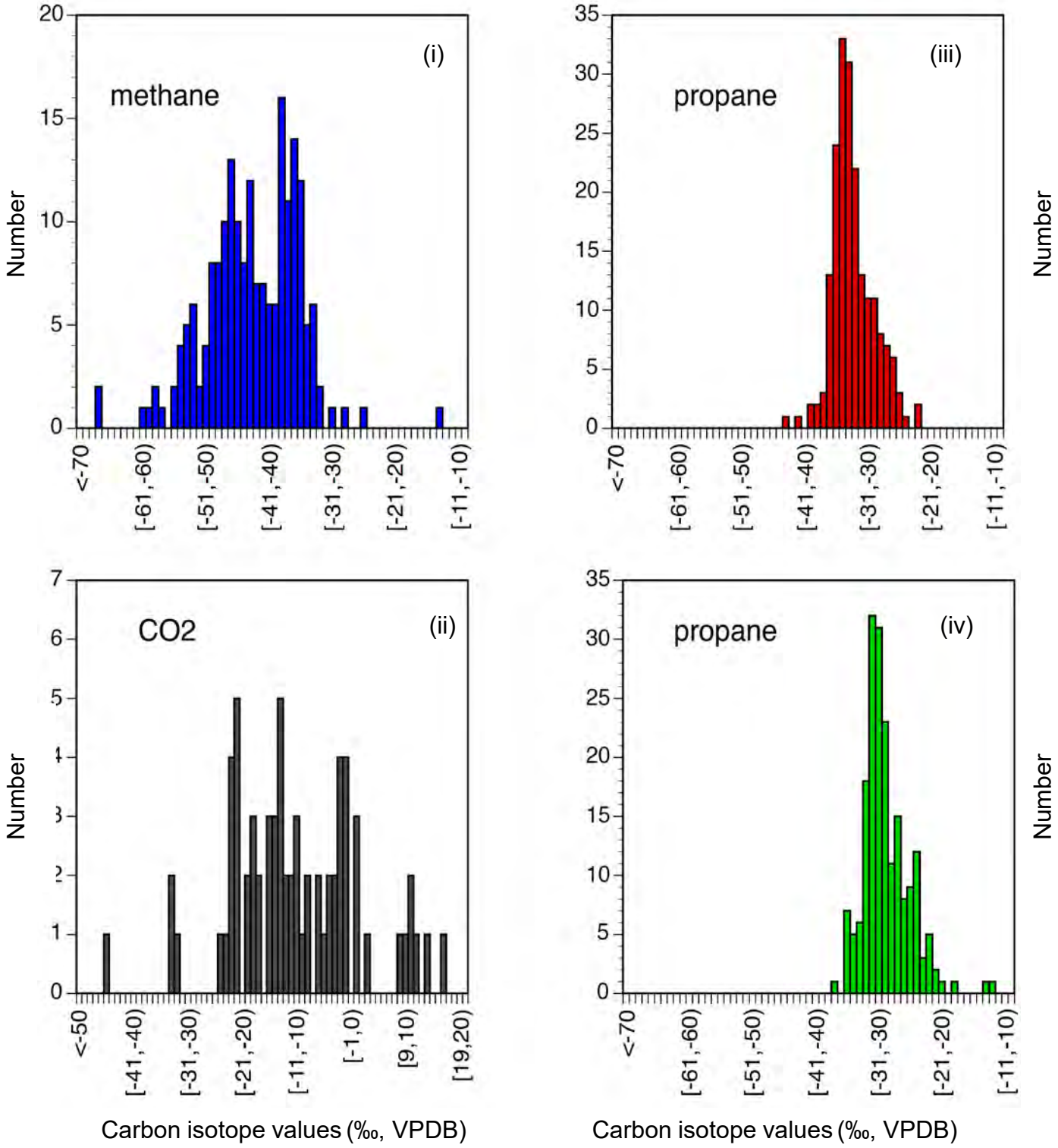

Fig. 8C. Histogram showing the methane (i), ethane (ii), propane (iv) and carbon dioxide (v) isotopic values for ground migration (GM) gases from British Columbia

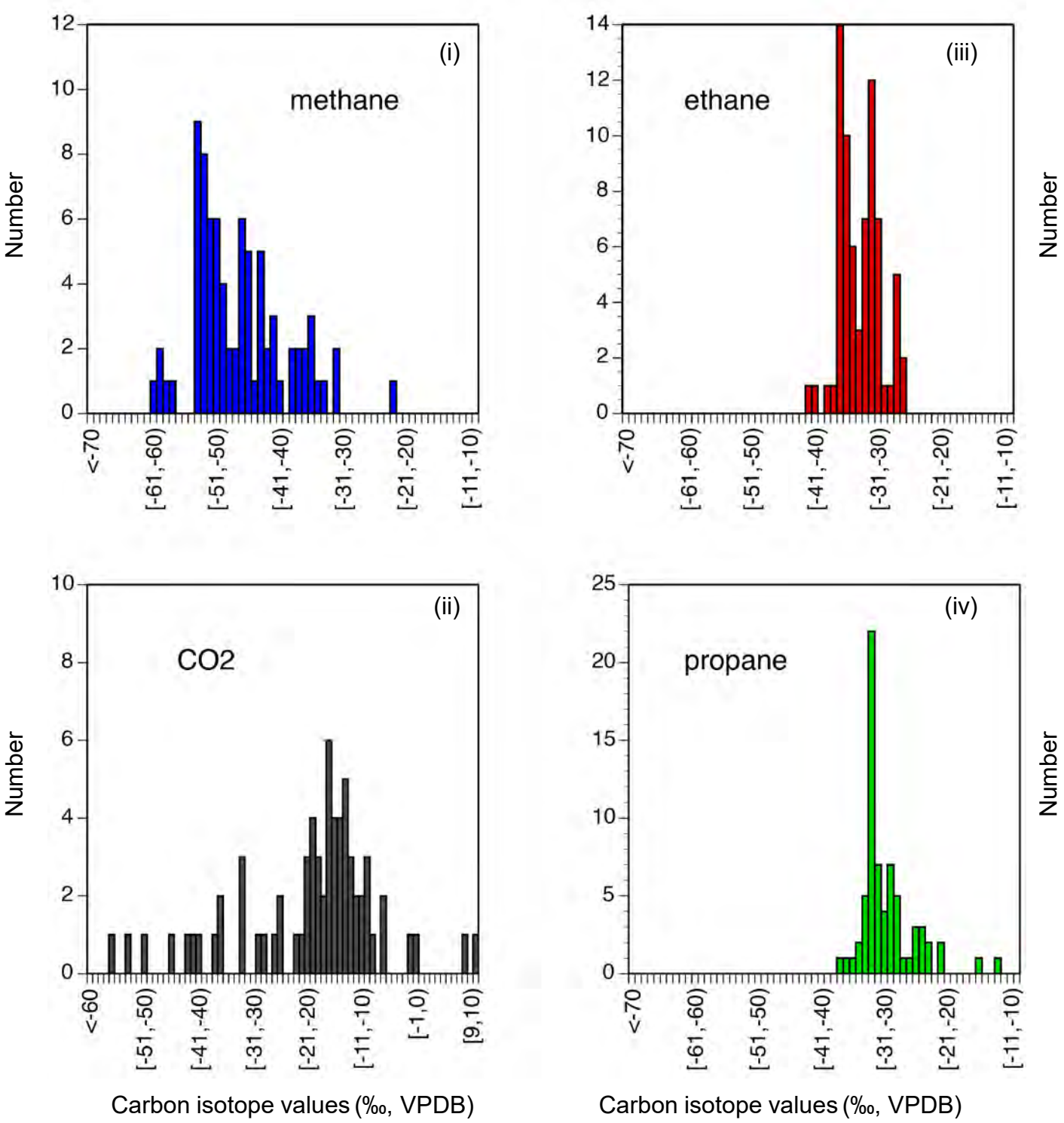

Fig. 9A. Contour Map of Methane Carbon Isotope Values of Production Wells

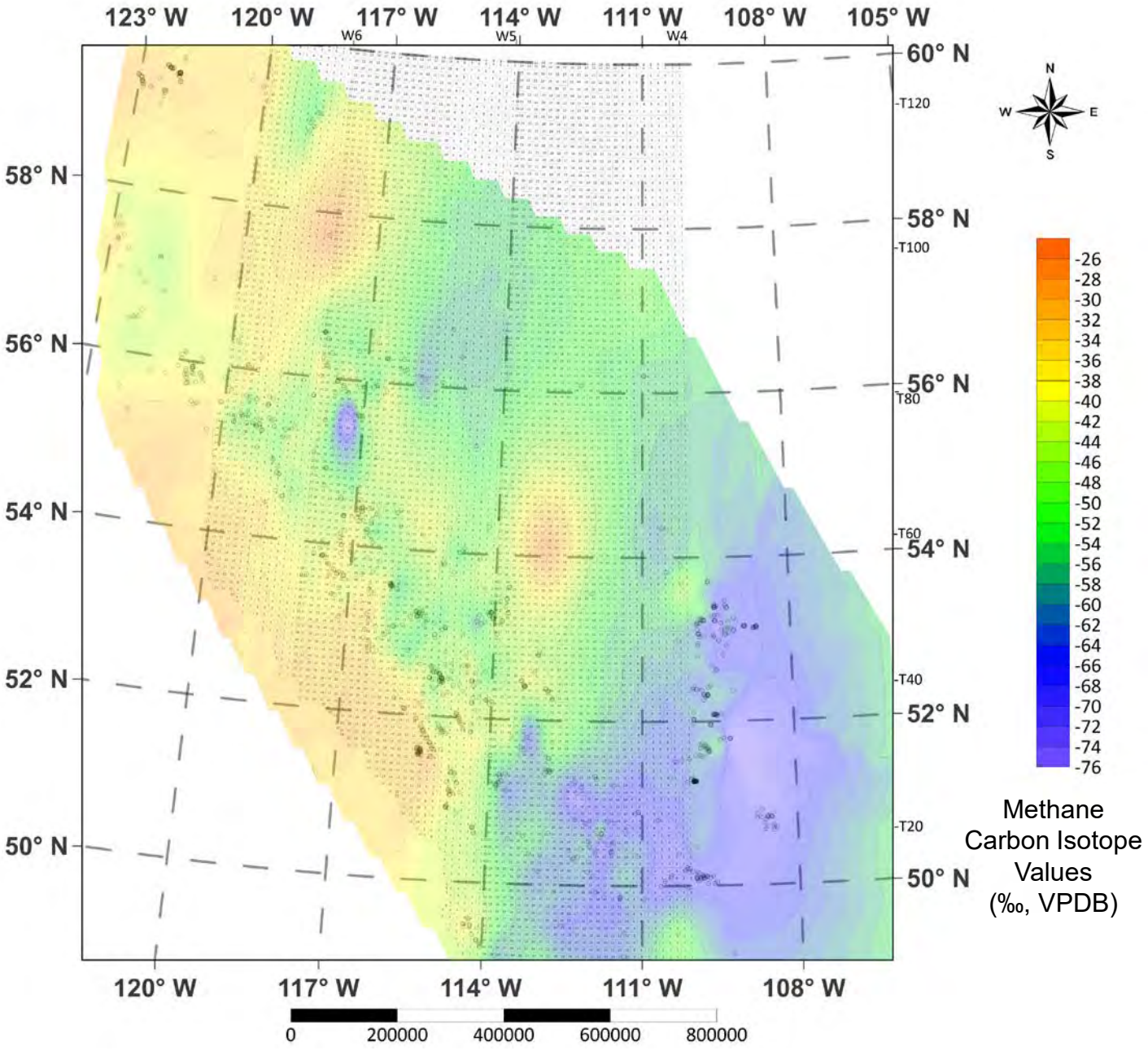

Fig. 9B. Contour Map of Methane Carbon Isotope Values of SCV

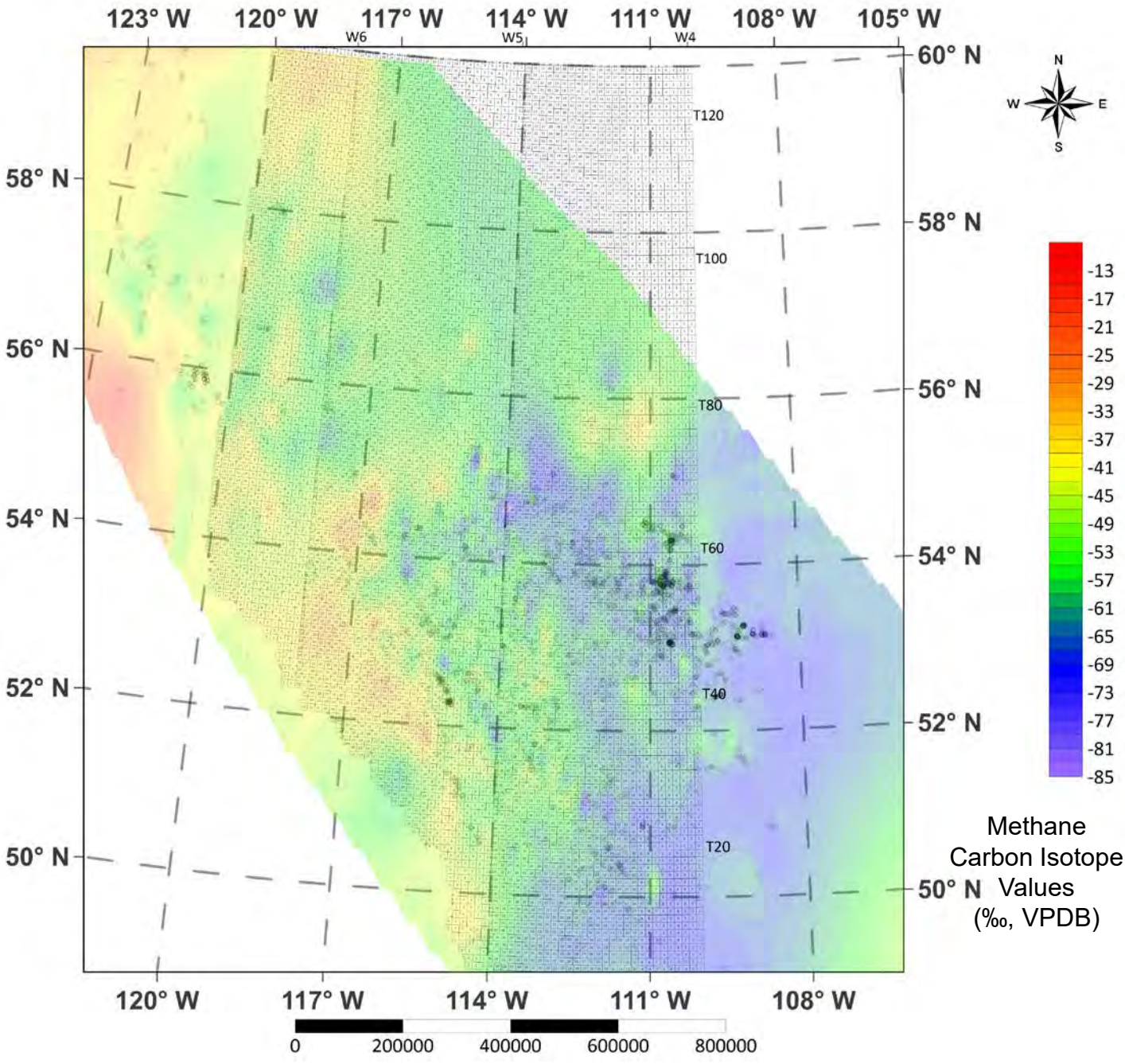

Fig. 9C. Contour Map of Methane Carbon Isotope Values of GM

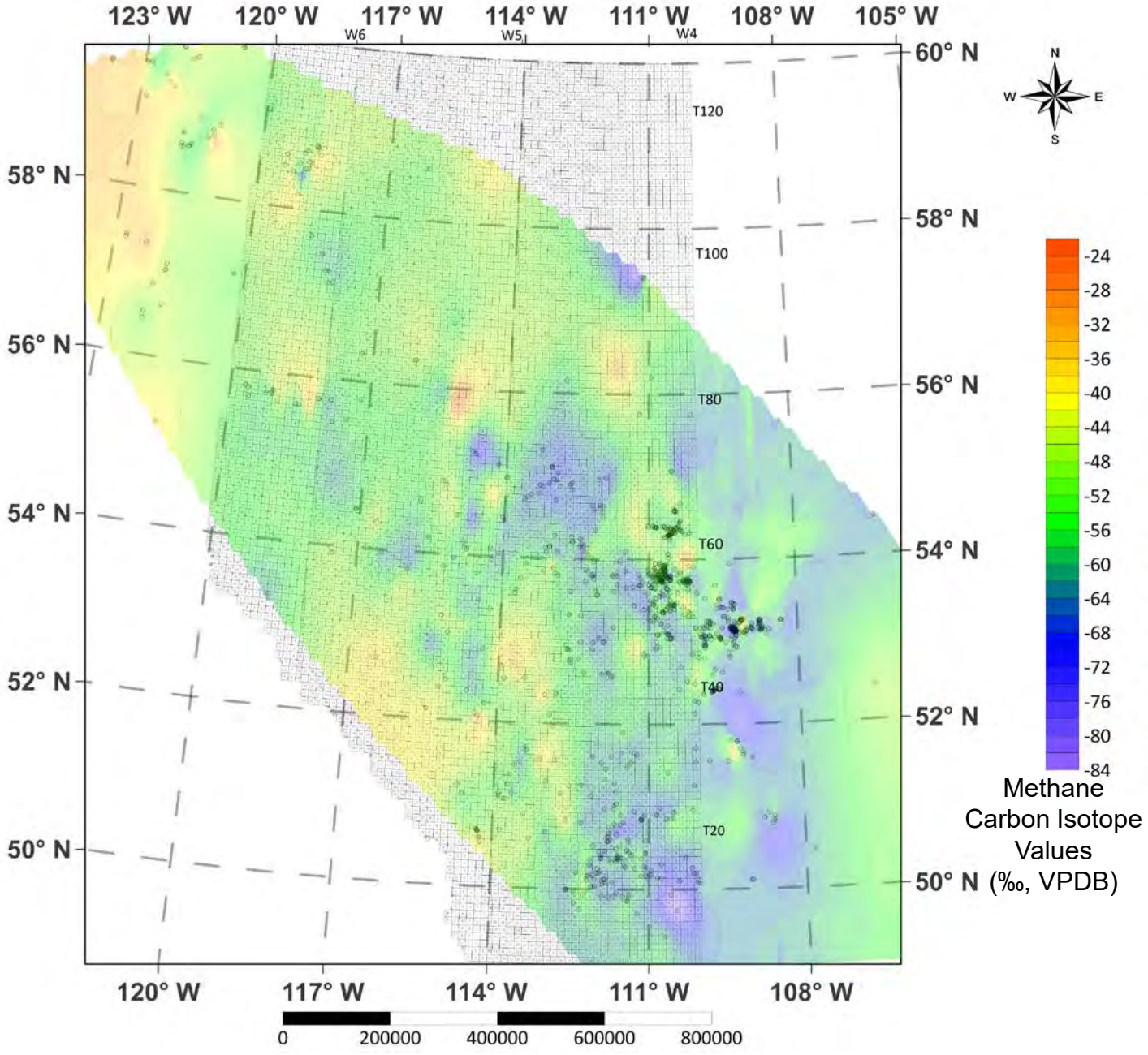

Fig. 10A. Contour Map of Ethane Carbon Isotope Values of Production Wells

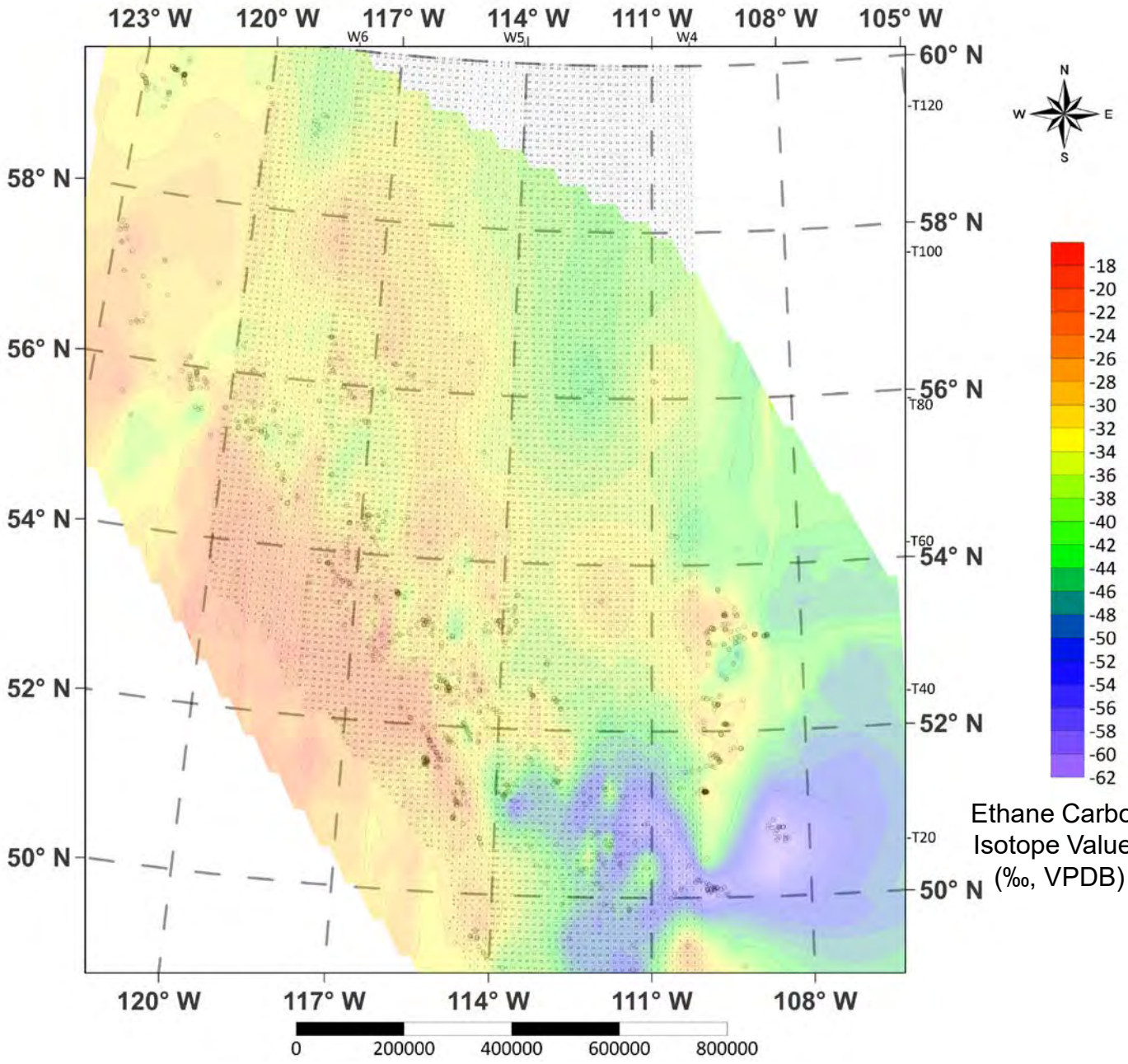

Fig. 10B. Contour Map of Ethane Carbon Isotope Values of SCV

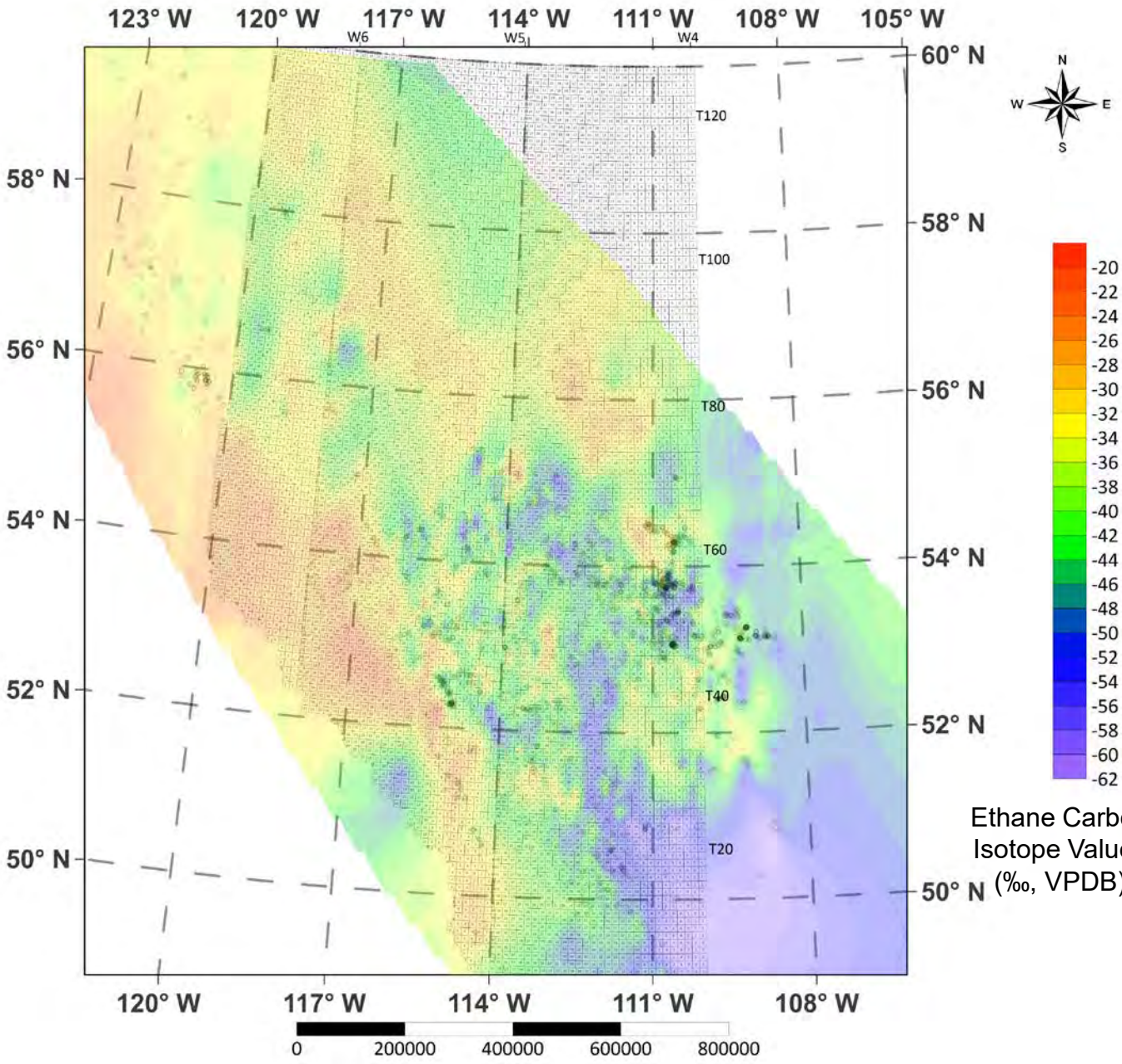

Fig. 10C. Contour Map of Ethane Carbon Isotope Values of GM

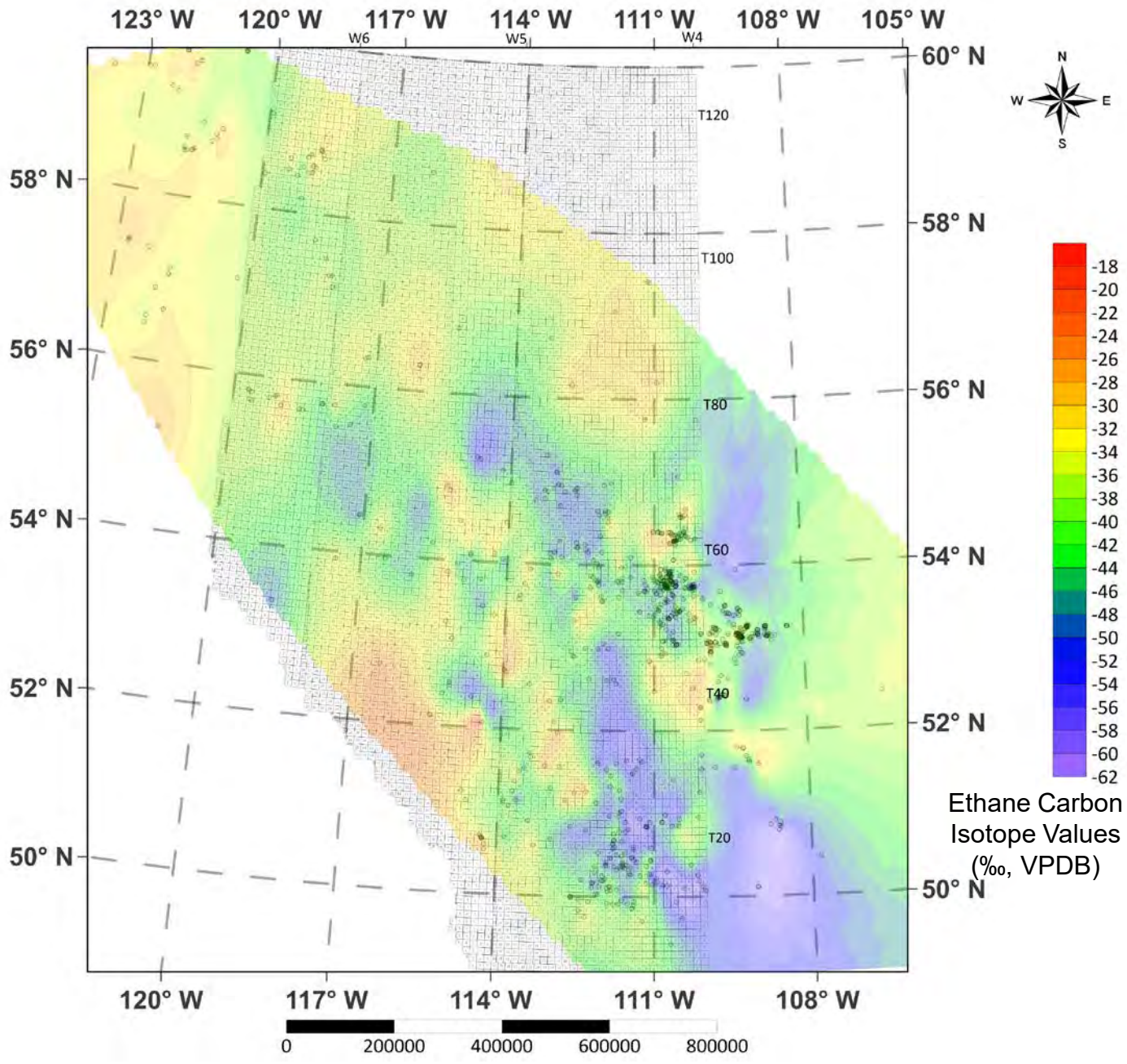

Fig. 11A. Contour Map of Propane Carbon Isotope Values of Production Wells

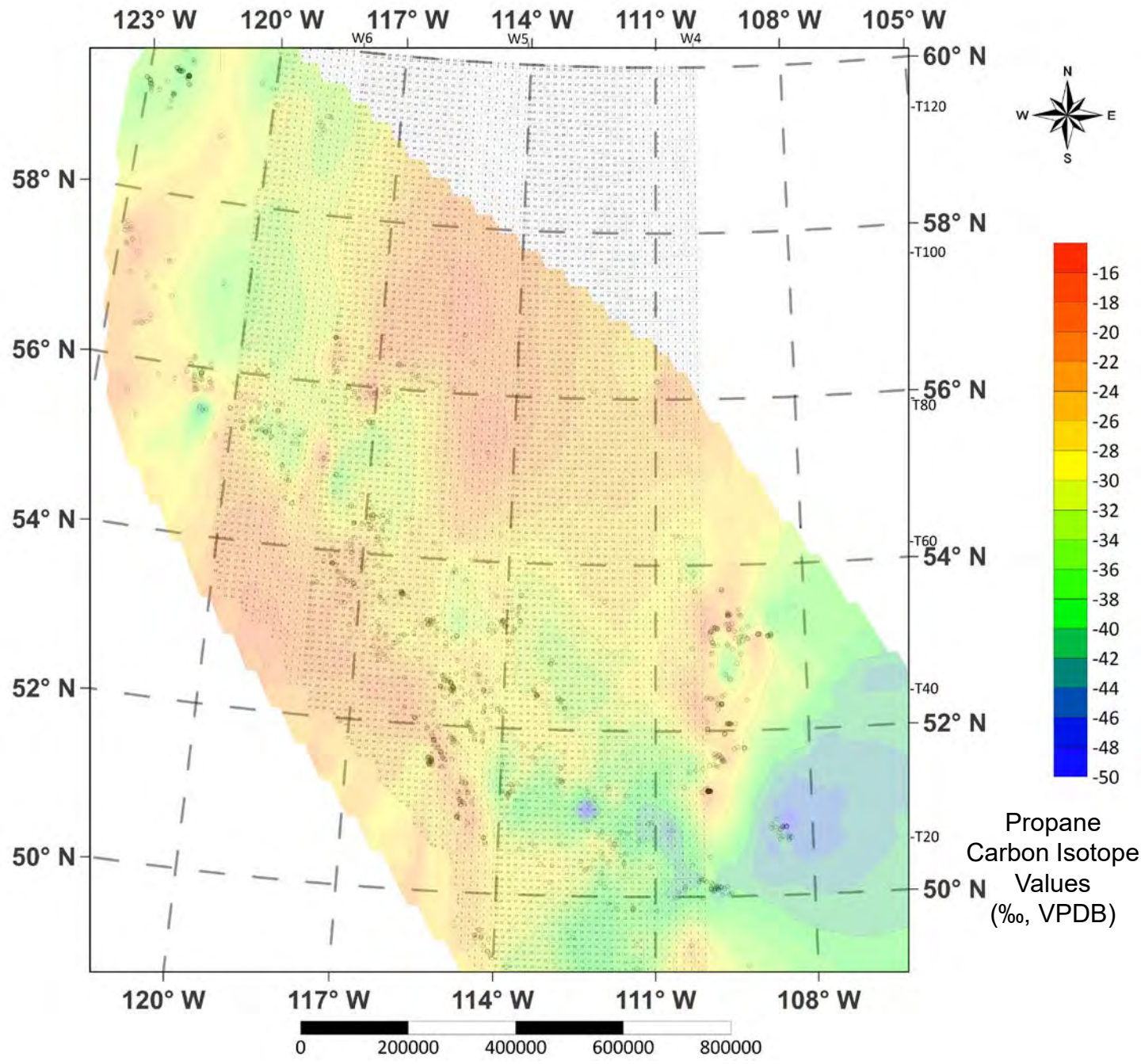

Fig. 11B. Contour Map of Propane Carbon Isotope Values of SCV

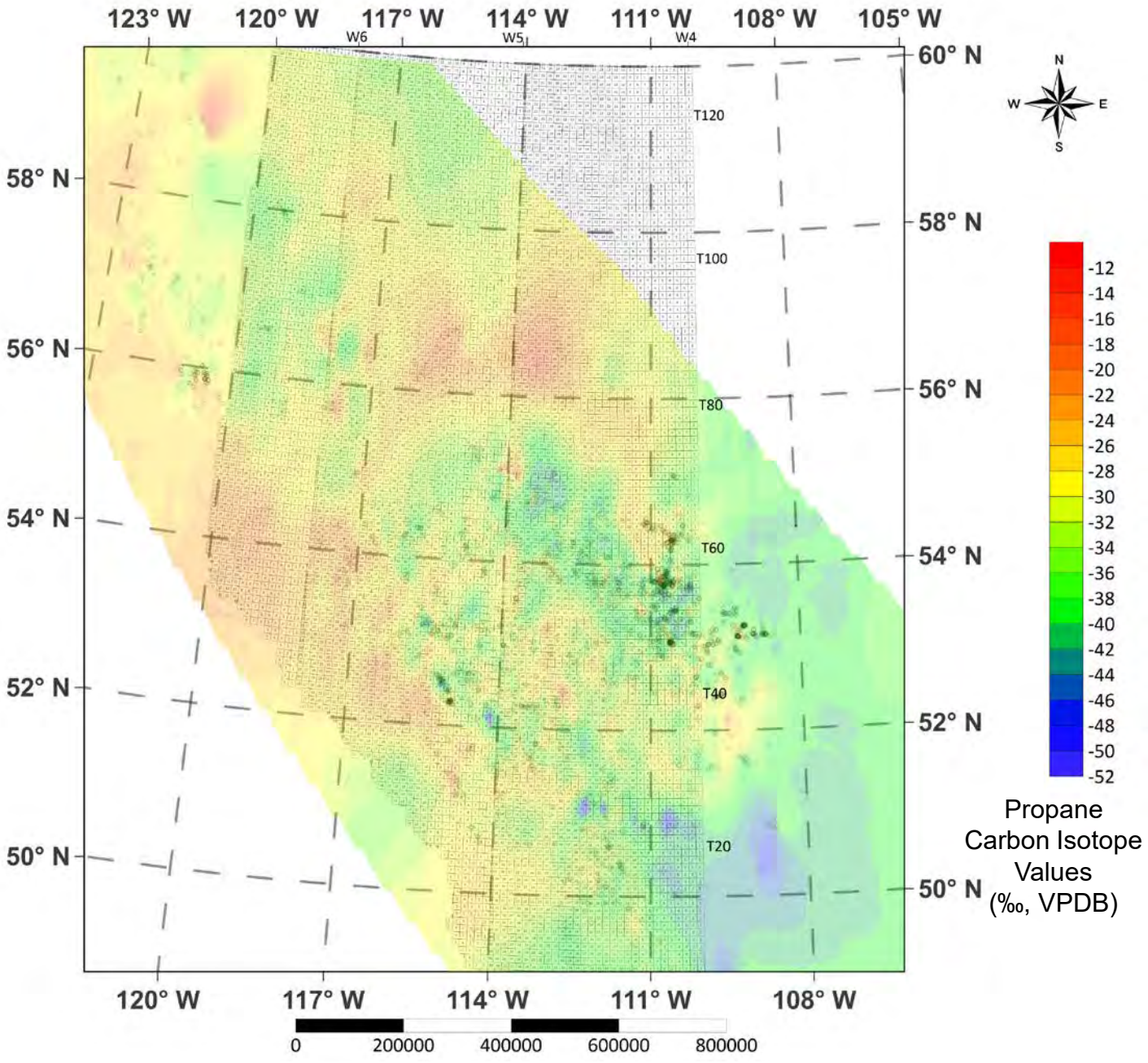

Fig. 11C. Contour Map of Propane Carbon Isotope Values of GM

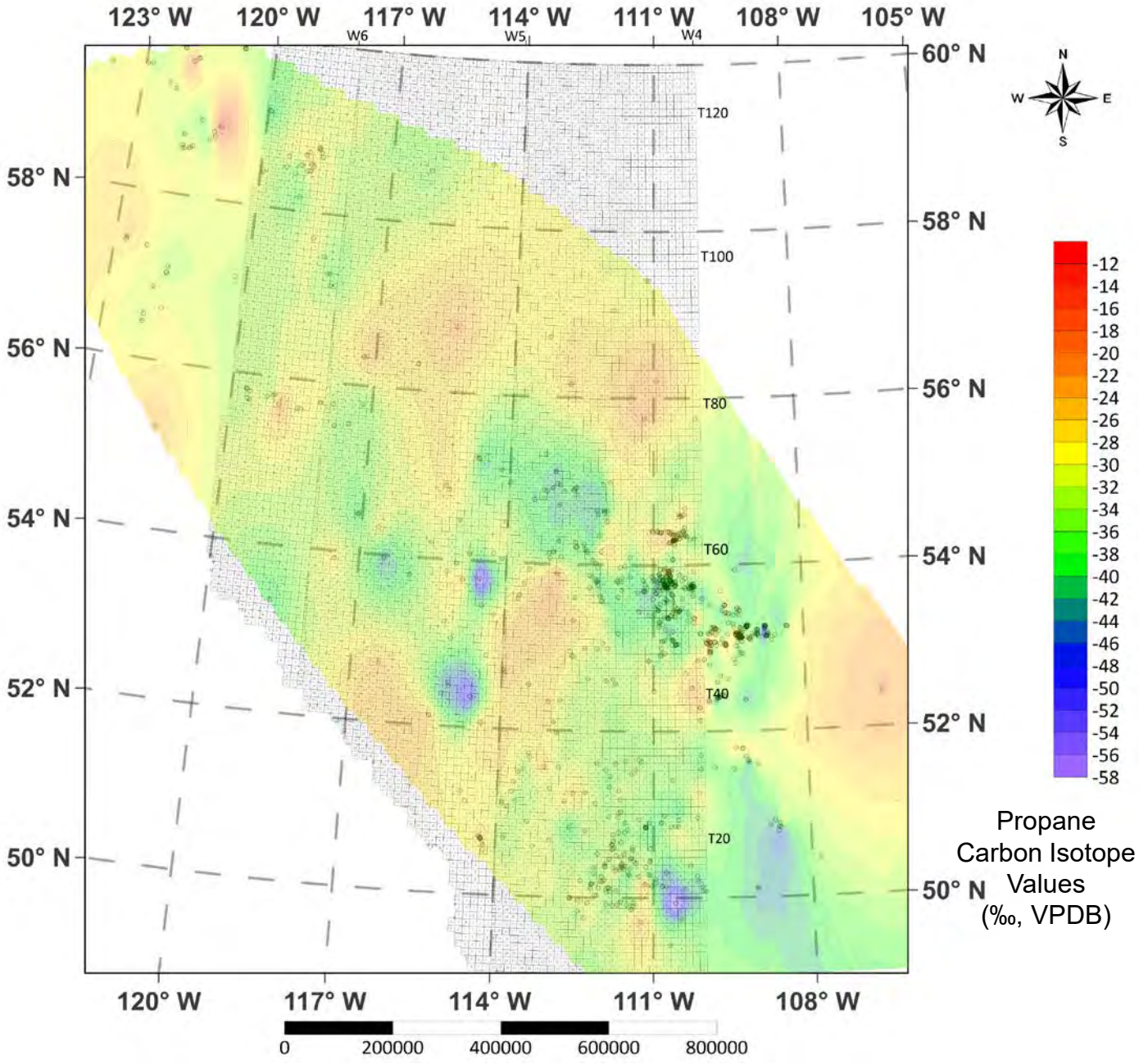

Fig. 12A. Contour Map of *n*-Butane Carbon Isotope Values of Production Wells

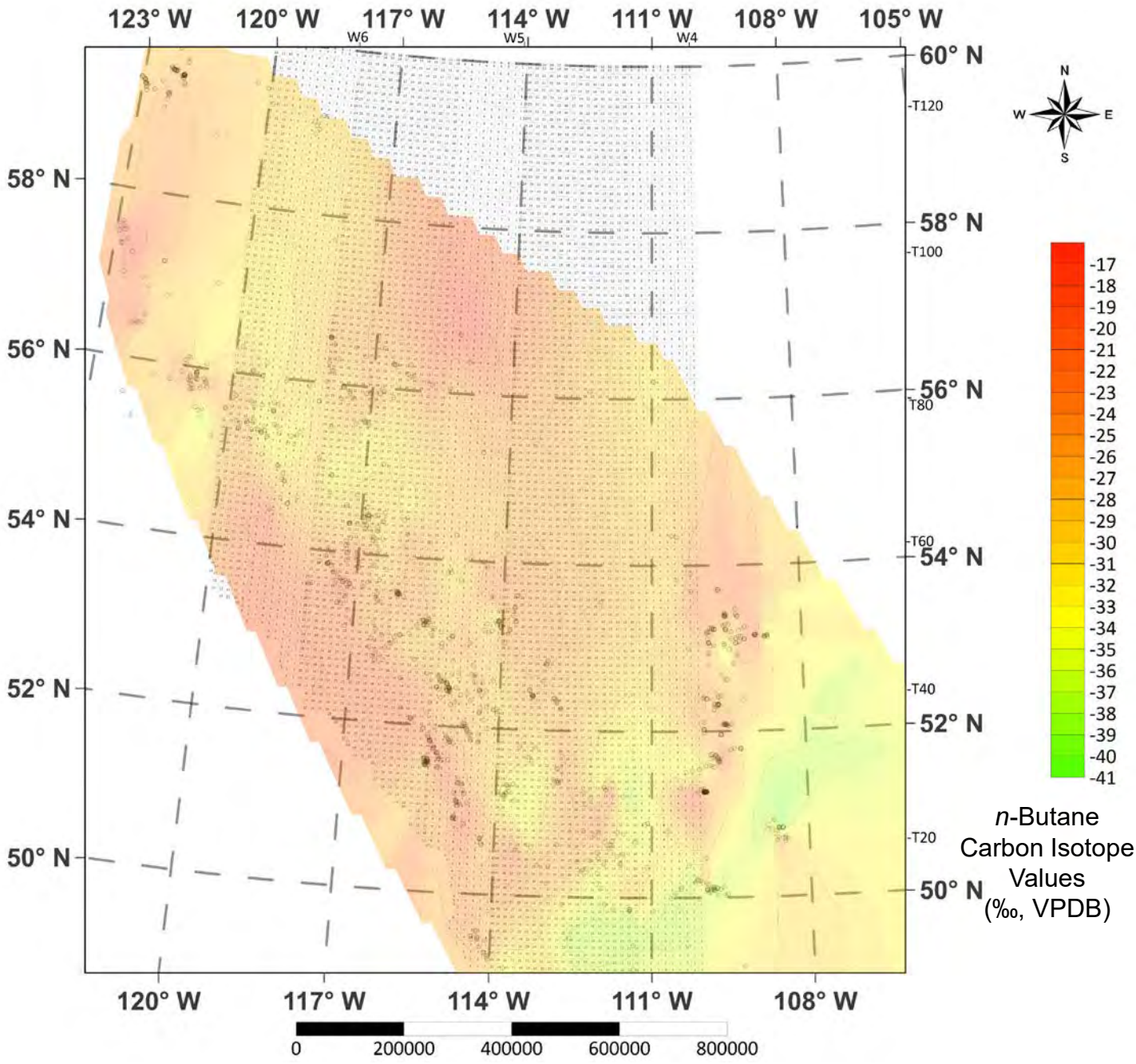

Fig. 12B. Contour Map of *n*-Butane Carbon Isotope Values of SCV

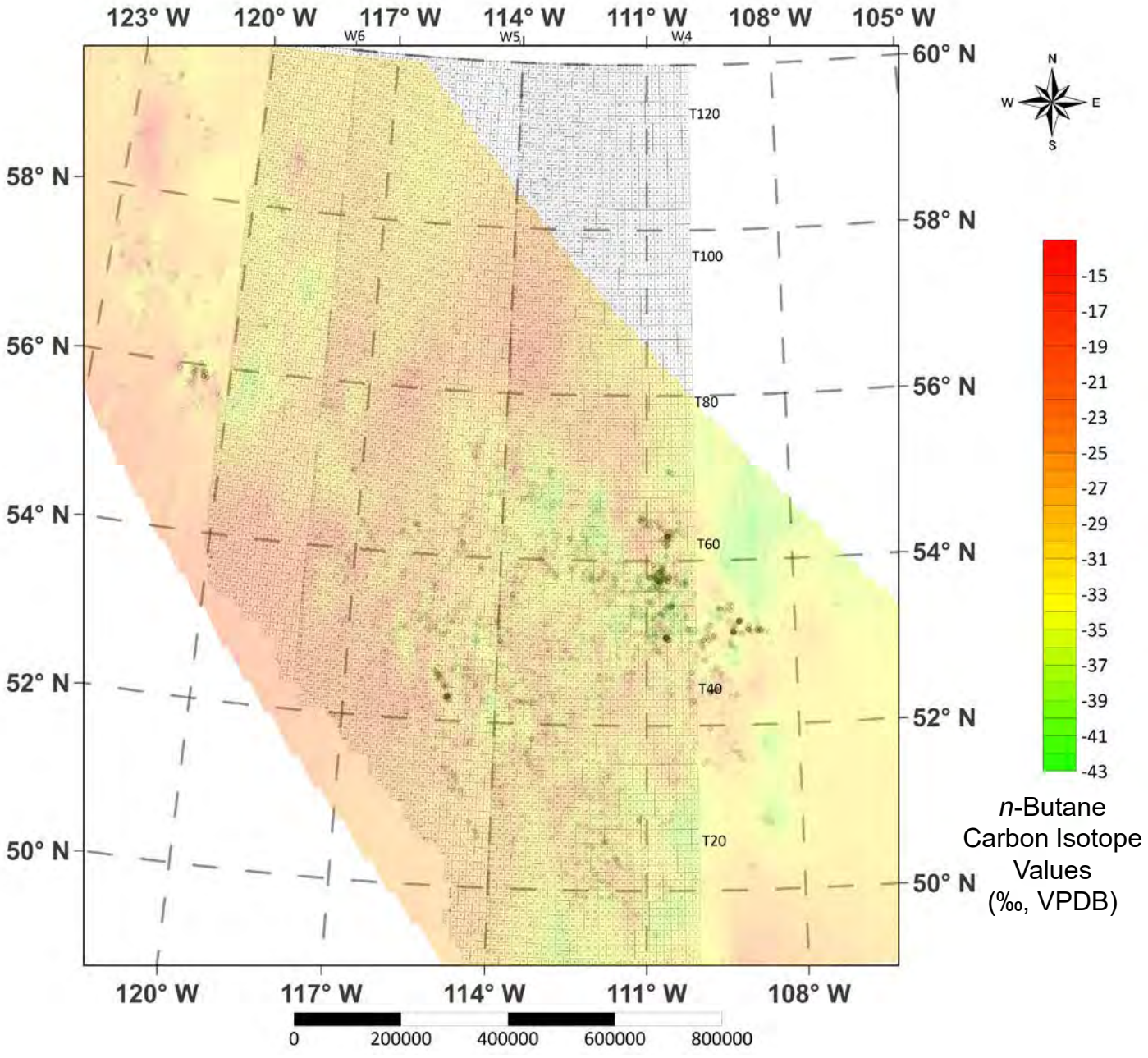

Fig. 12C. Contour Map of *n*-Butane Carbon Isotope Values of GM

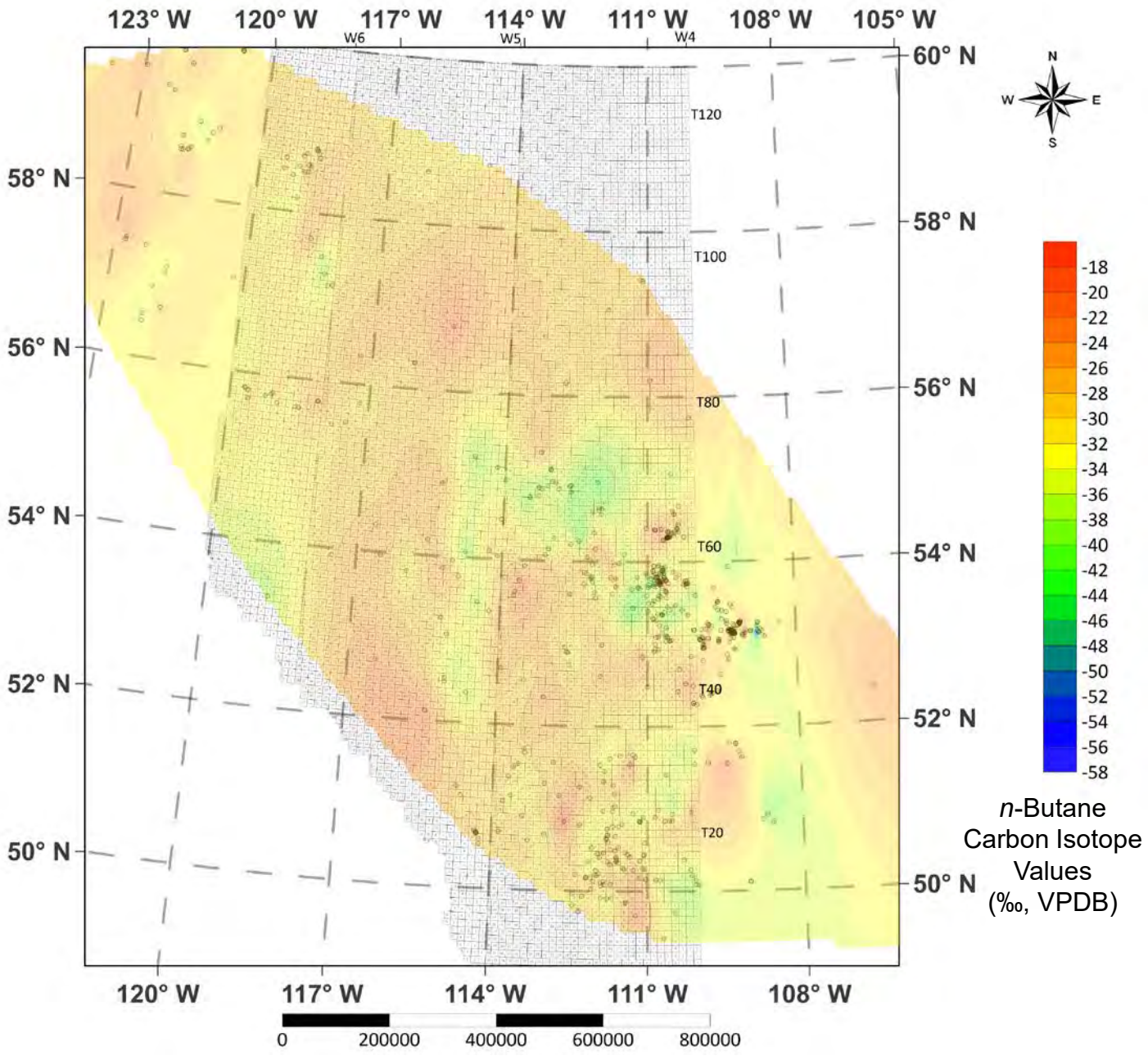

Fig. 13A. Contour Map of *i*-Butane Carbon Isotope Values of Production Wells

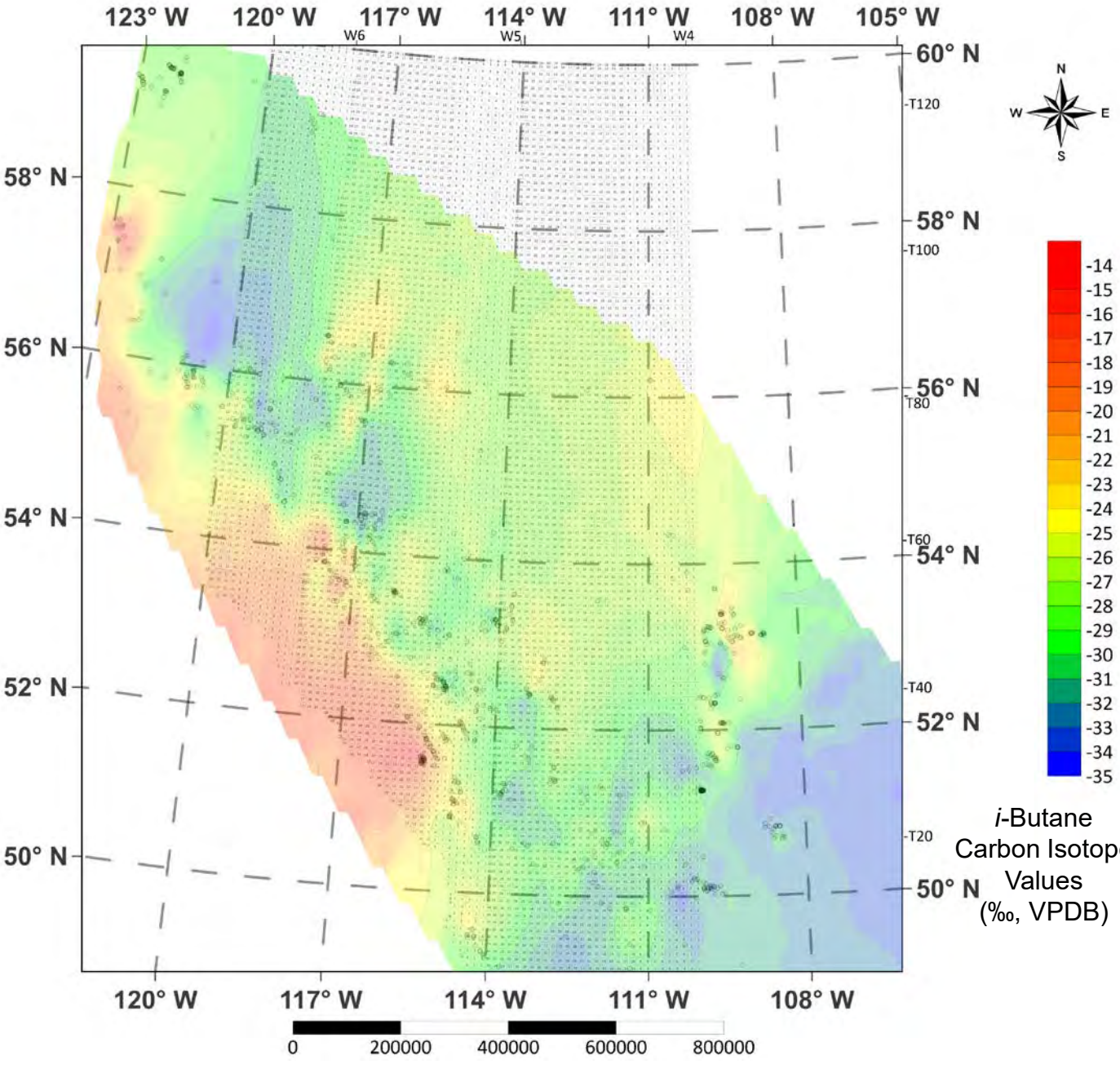

Fig. 13B. Contour Map of *i*-Butane Carbon Isotope Values of SCV

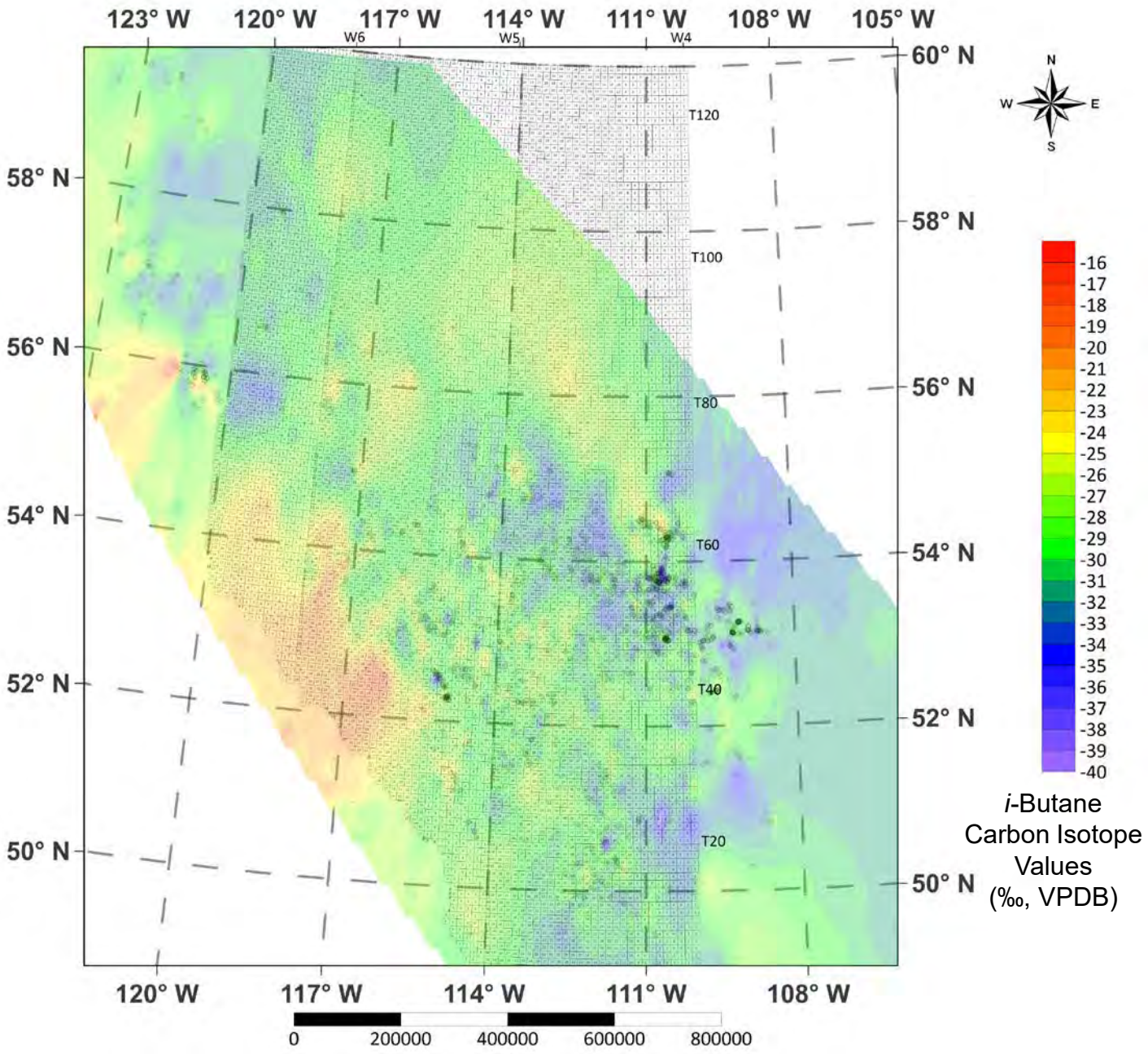

Fig. 13C. Contour Map of *i*-Butane Carbon Isotope Values of GM

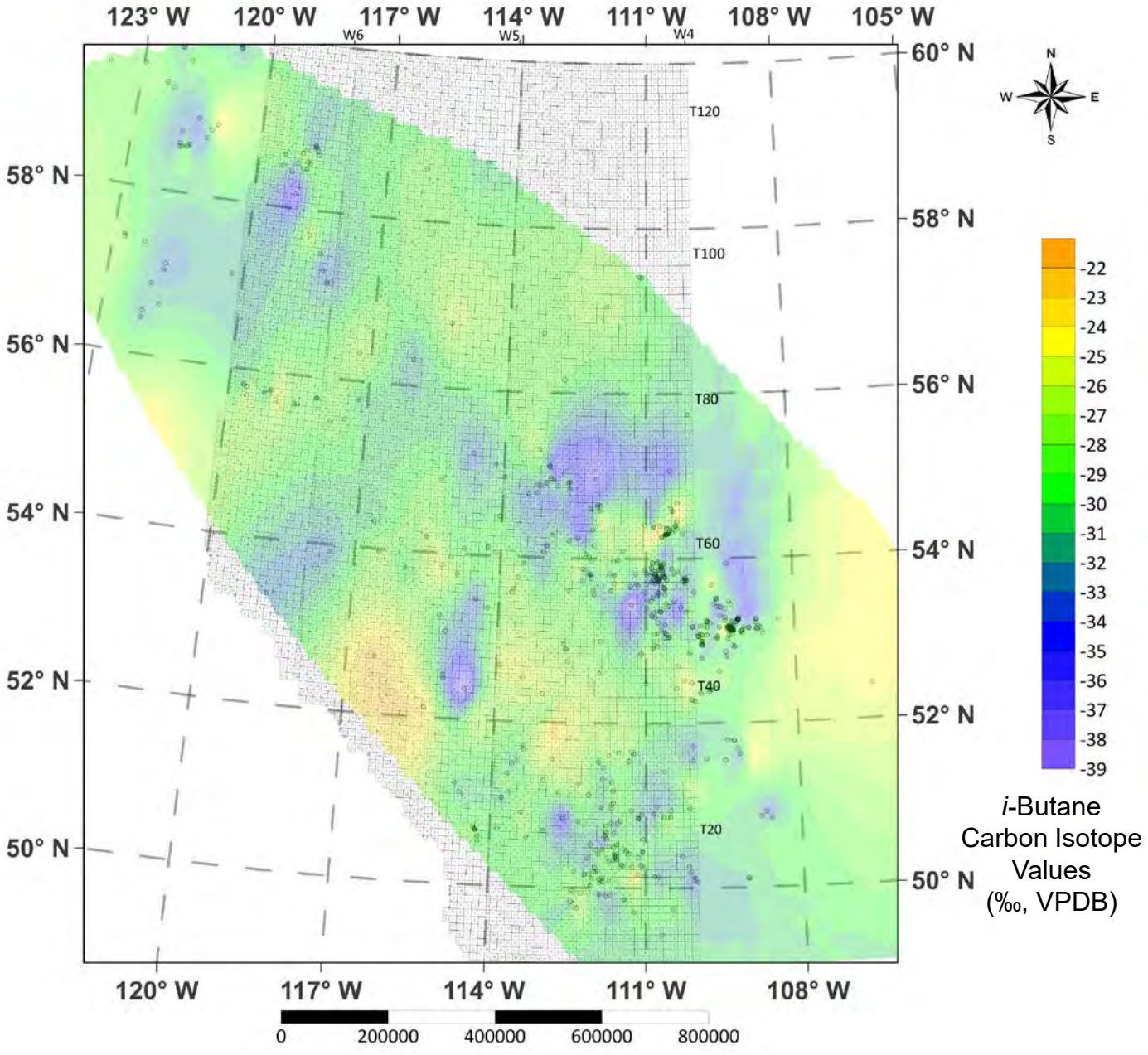

Fig. 14A. Contour Map of Carbon Dioxide Carbon Isotope Values of Production Wells

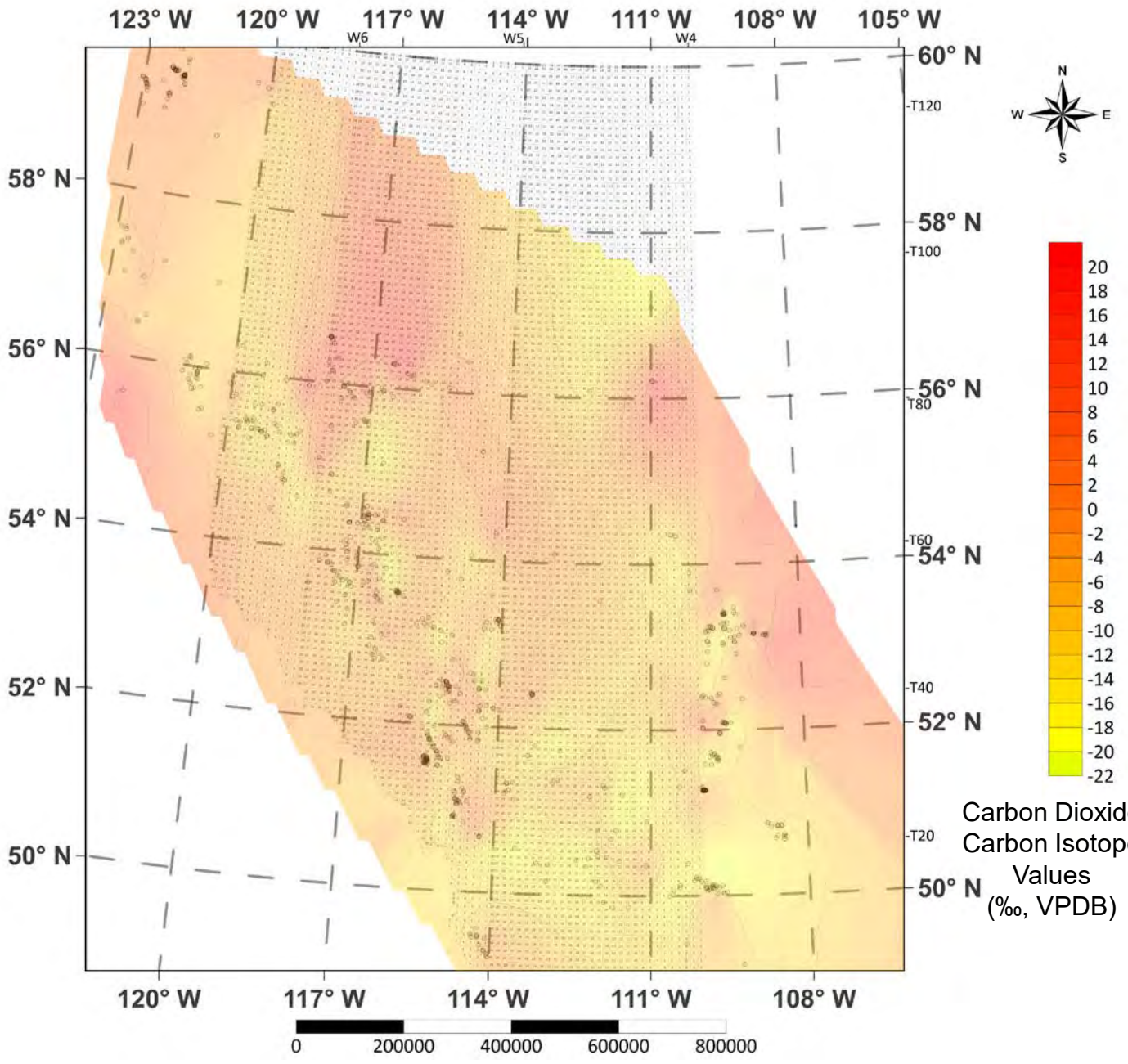

Fig. 14B. Contour Map of Carbon Dioxide Carbon Isotope Values of SCV

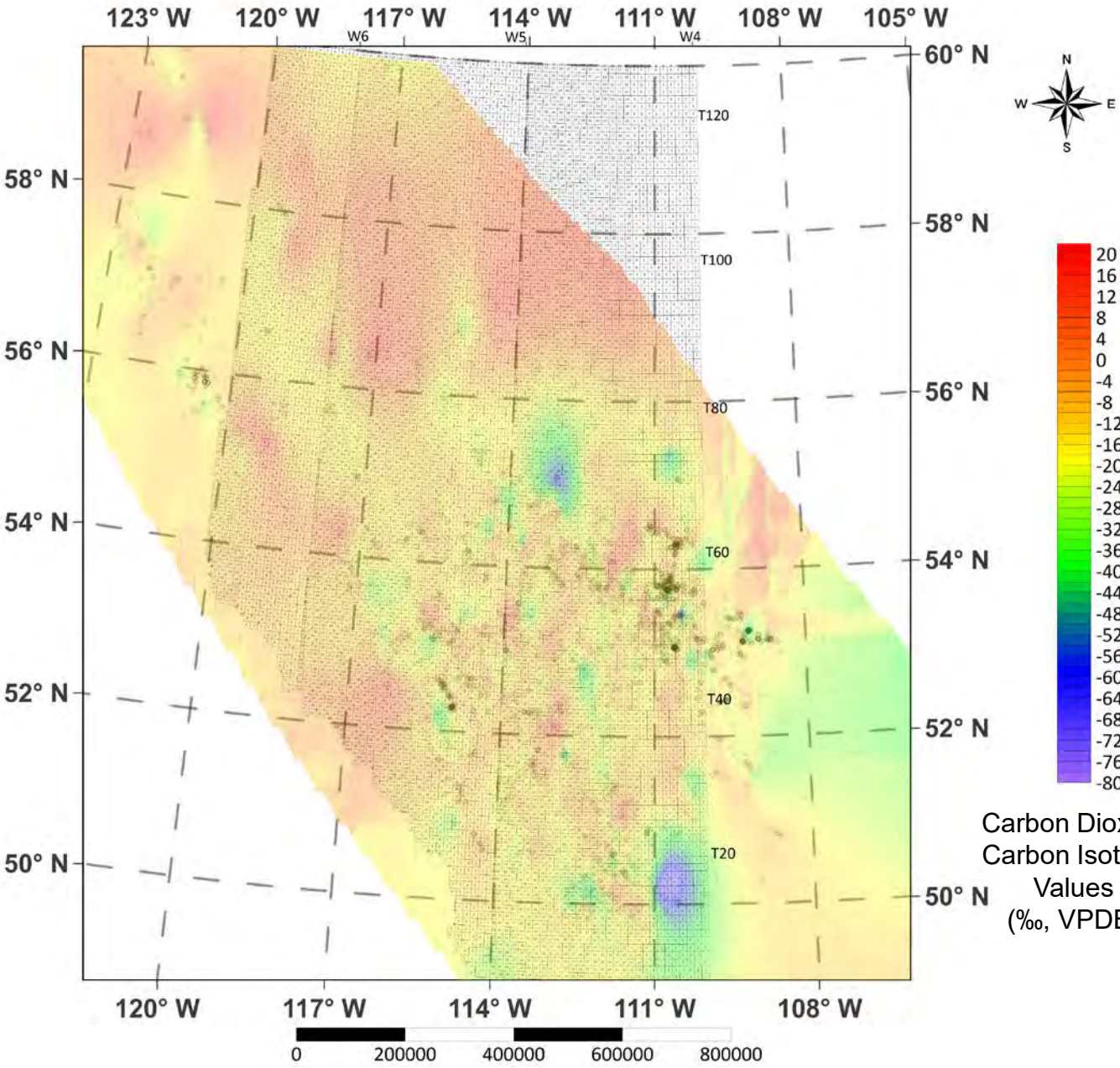

Fig. 14C. Contour Map of Carbon Dioxide Carbon Isotope Values of GM

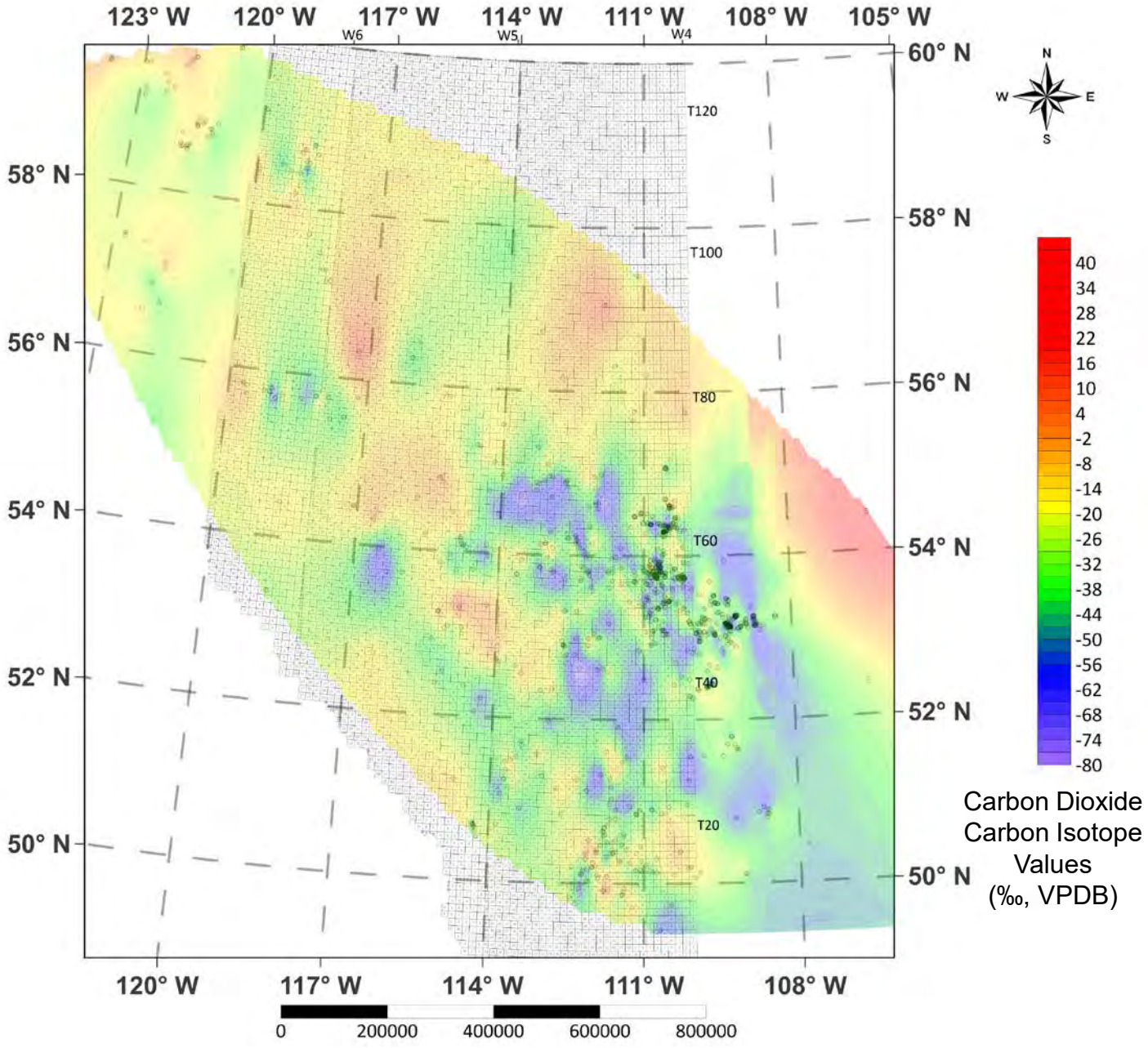

Fig. 15A. Contour Map of Methane Carbon Isotope Values of Production Wells over Topographic Map

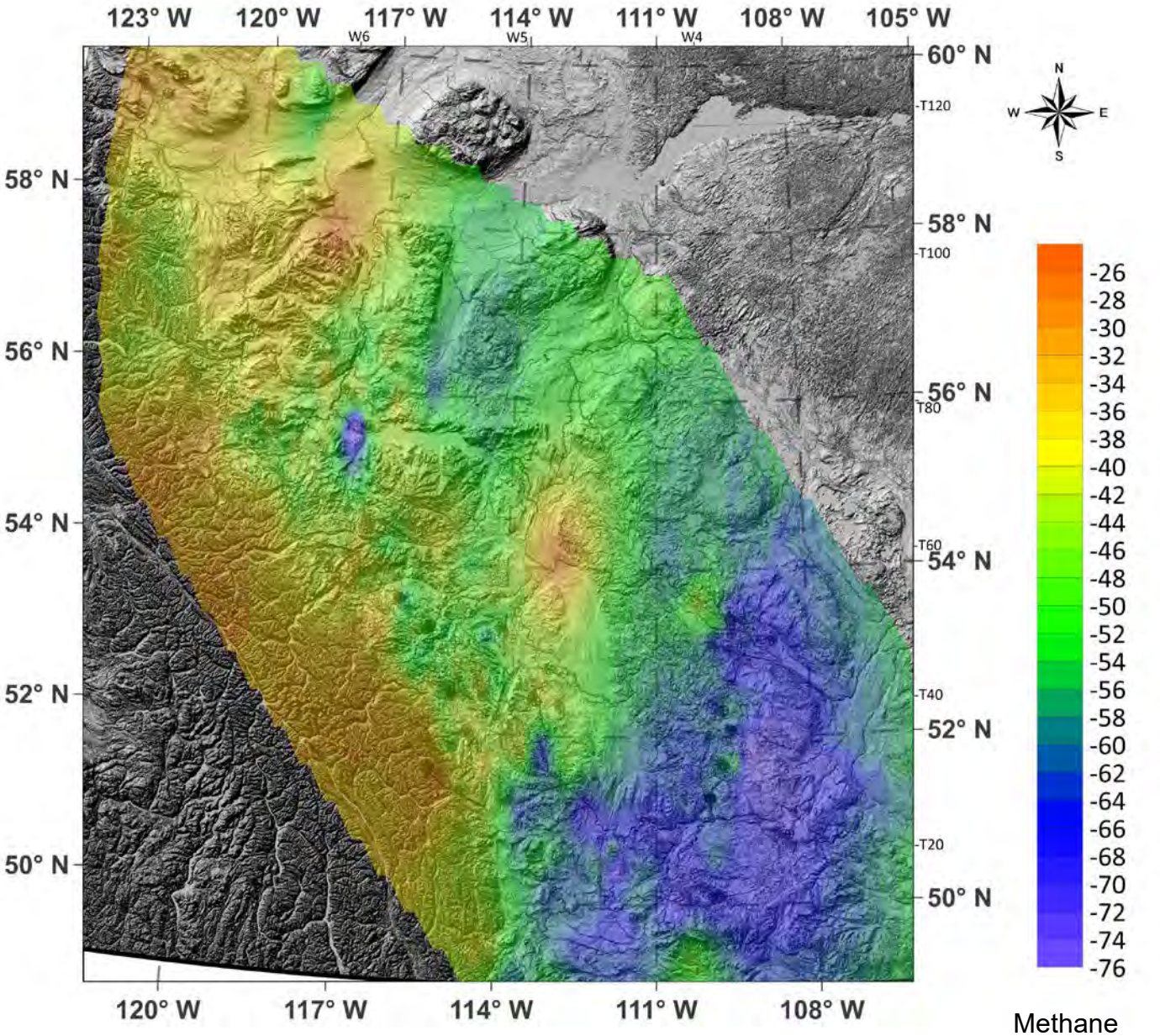

Fig. 15B. Contour Map of Methane Carbon Isotope Values of SCV over Topographic Map

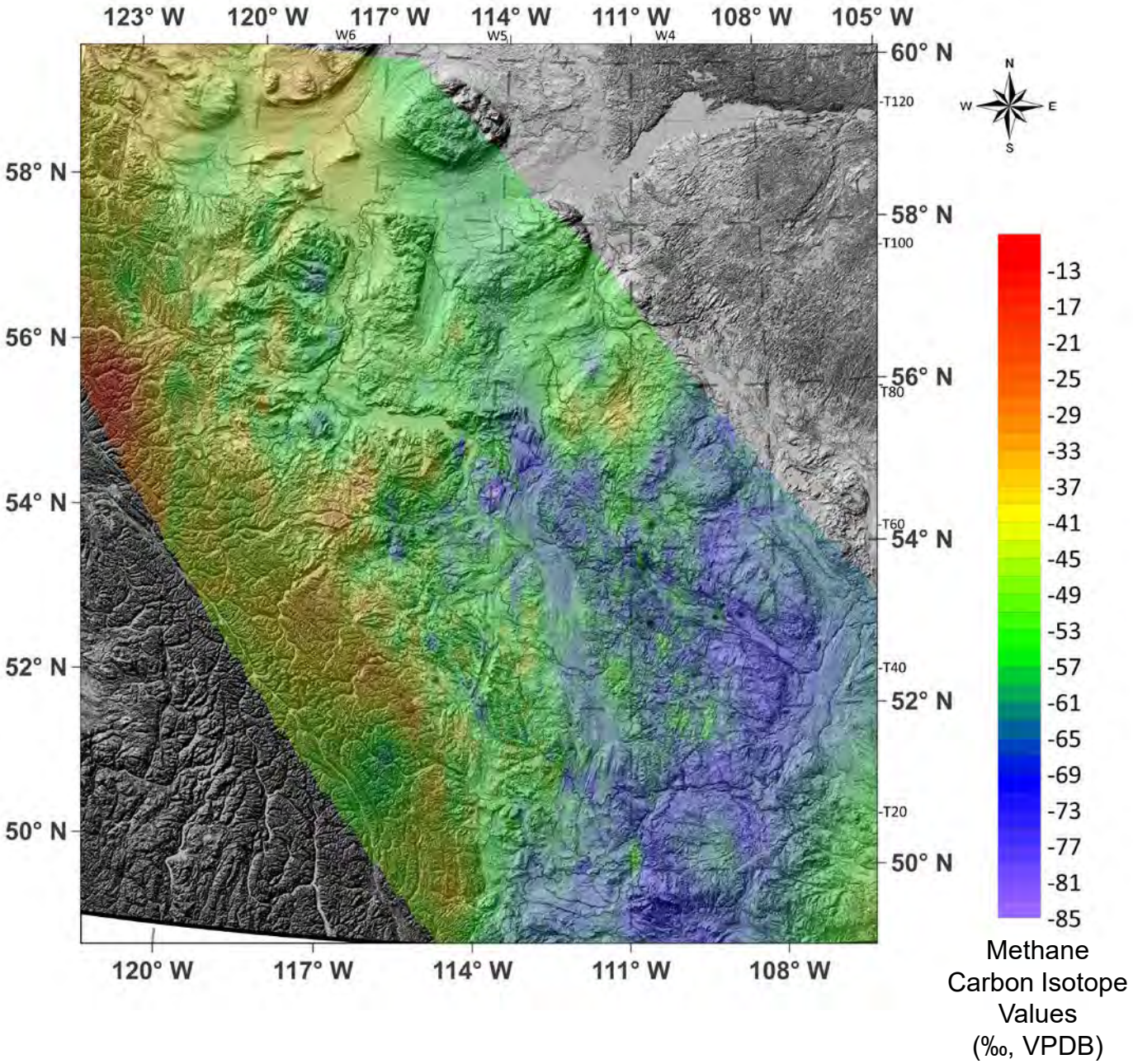

Fig. 15C. Contour Map of Methane Carbon Isotope Values of GM over Topographic Map

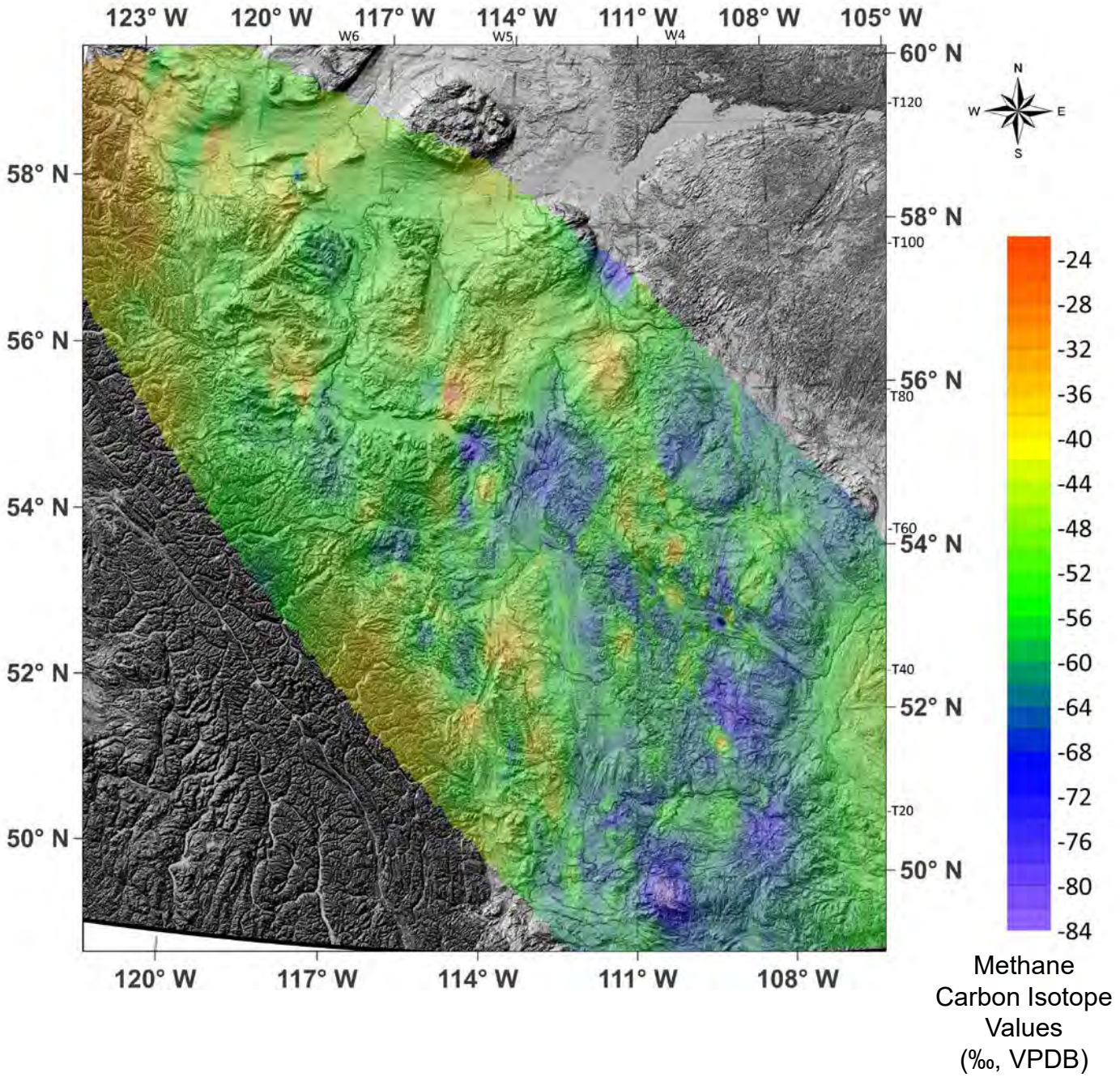

Fig. 16A. Contour Map of Ethane Carbon Isotope Values of Production Wells over Topographic Map

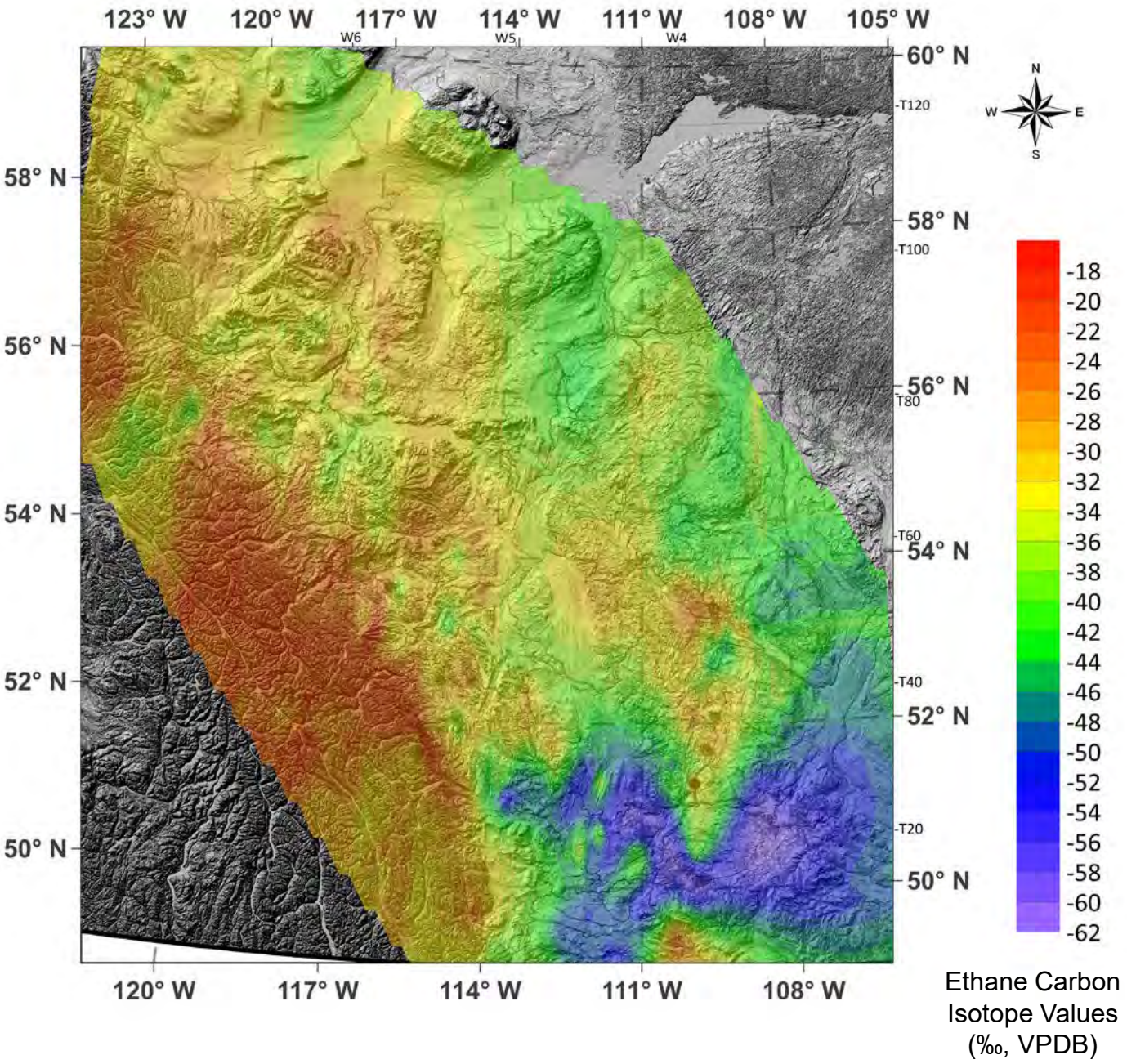

Fig. 16B. Contour Map of Ethane Carbon Isotope Values of SCV over Topographic Map

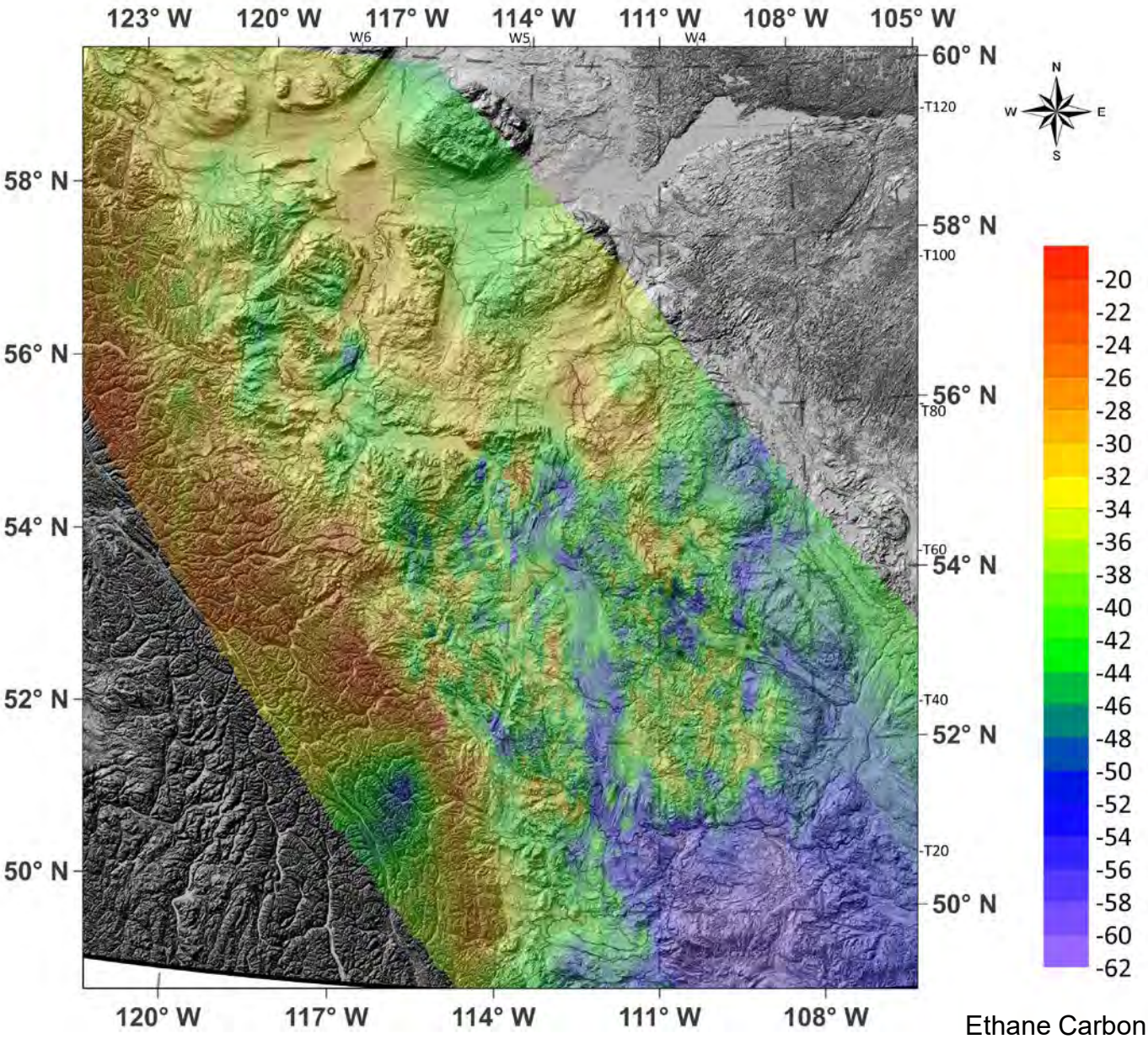

Fig. 16C. Contour Map of Ethane Carbon Isotope Values of GM over Topographic Map

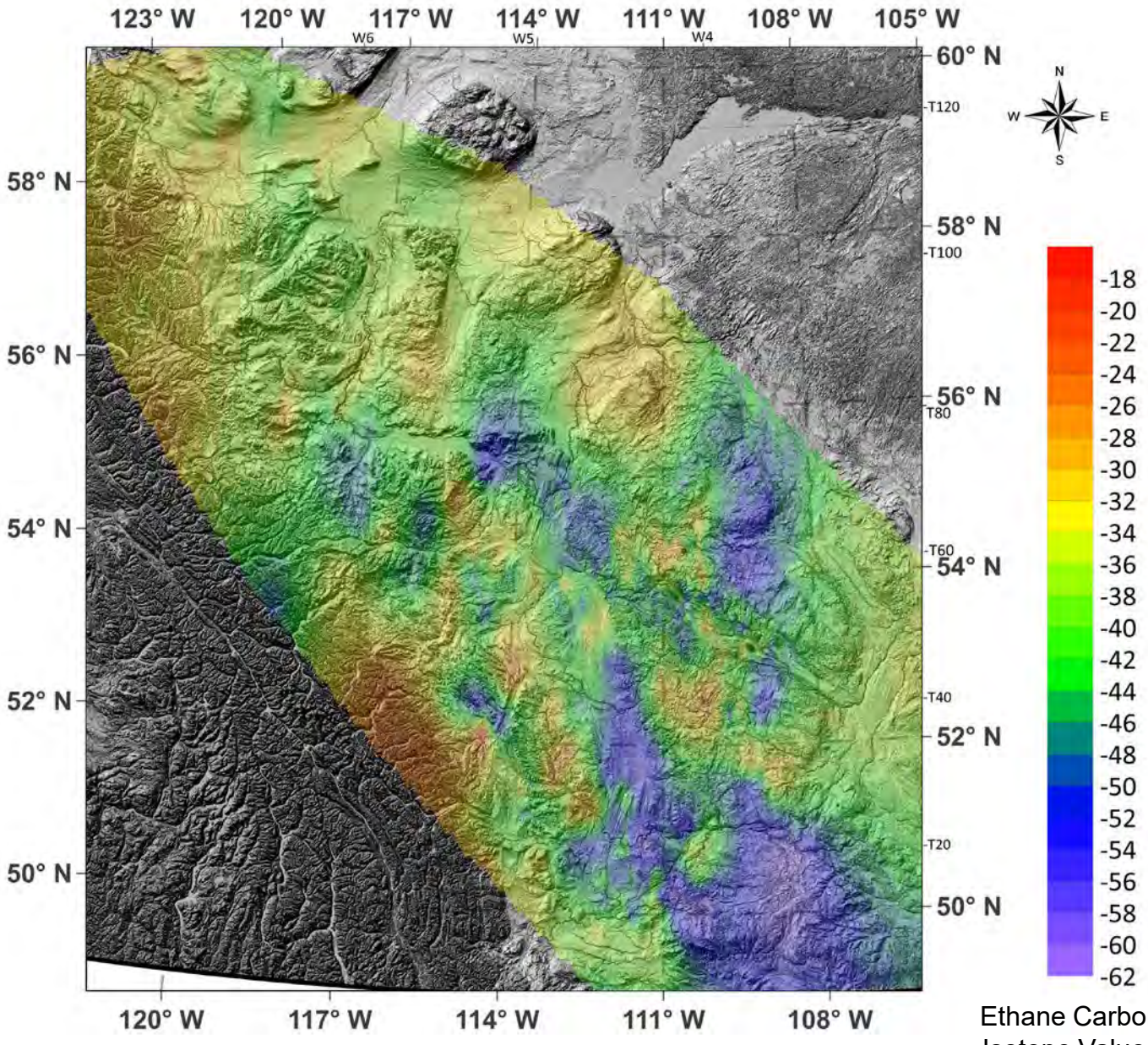

Fig. 17A. Contour Map of Propane Carbon Isotope Values of Production Wells over Topographic Map

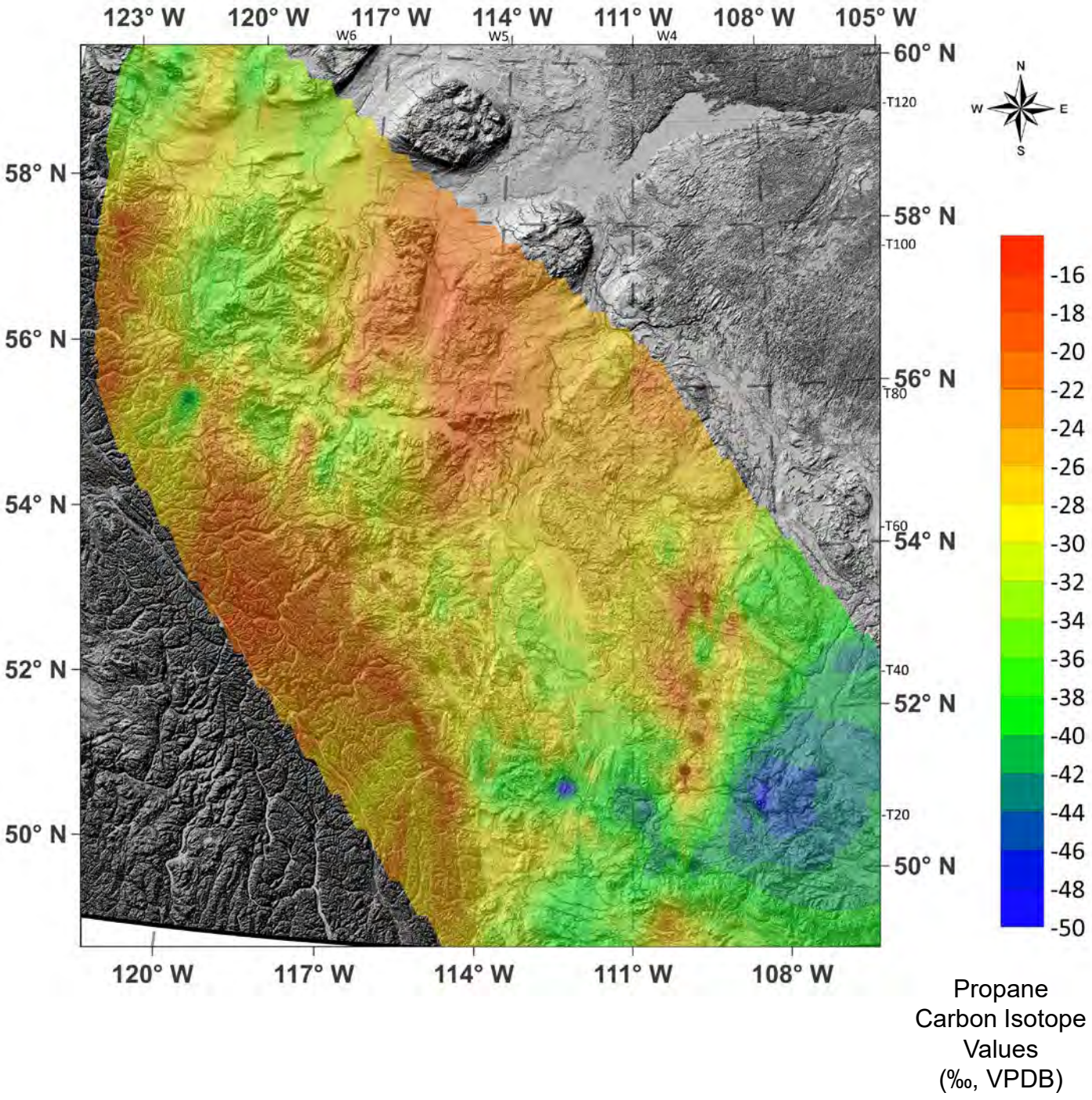

Fig. 17B. Contour Map of Propane Carbon Isotope Values of SCV over Topographic Map

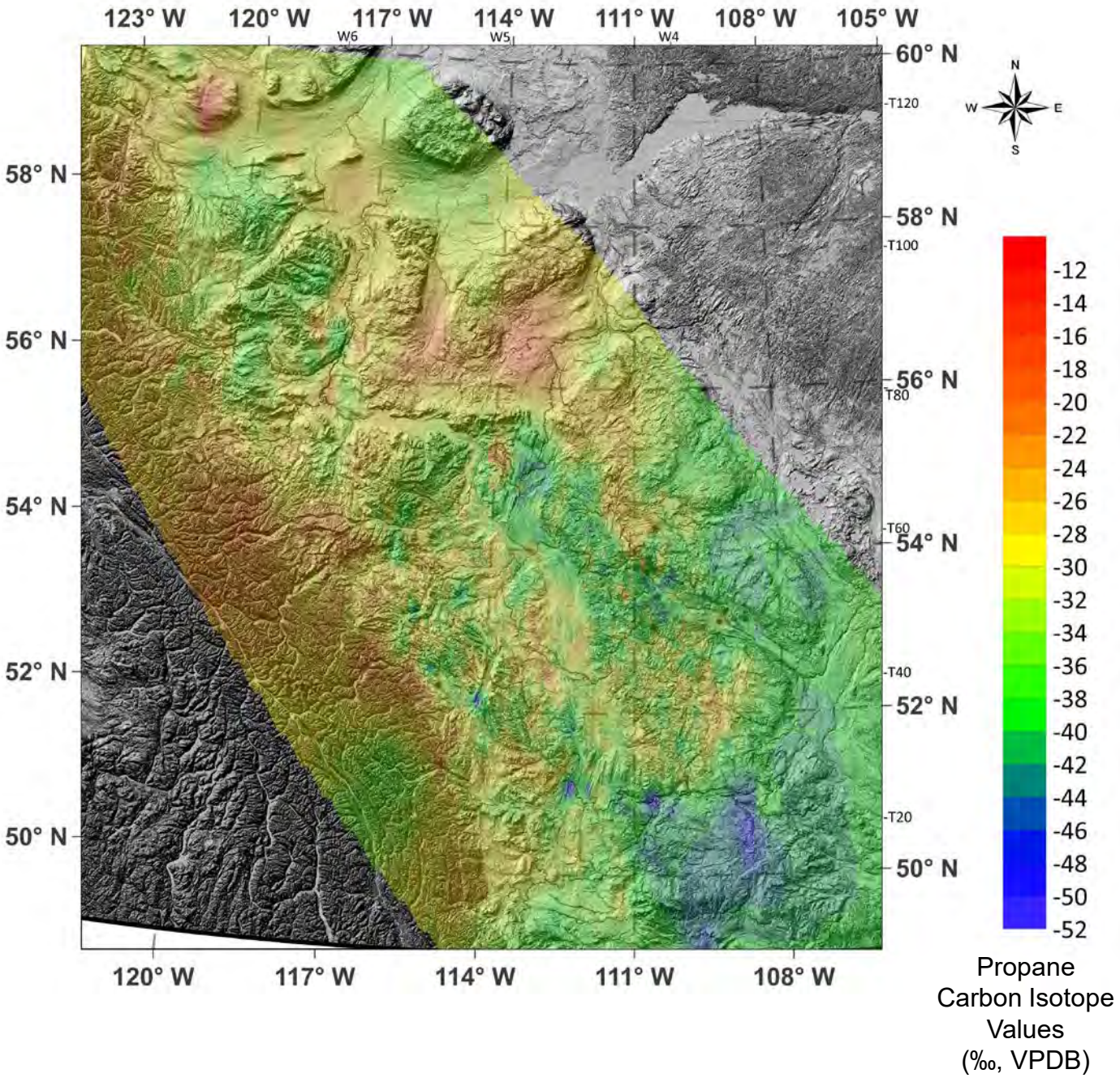

Fig. 17C. Contour Map of Propane Carbon Isotope Values of GM over Topographic Map

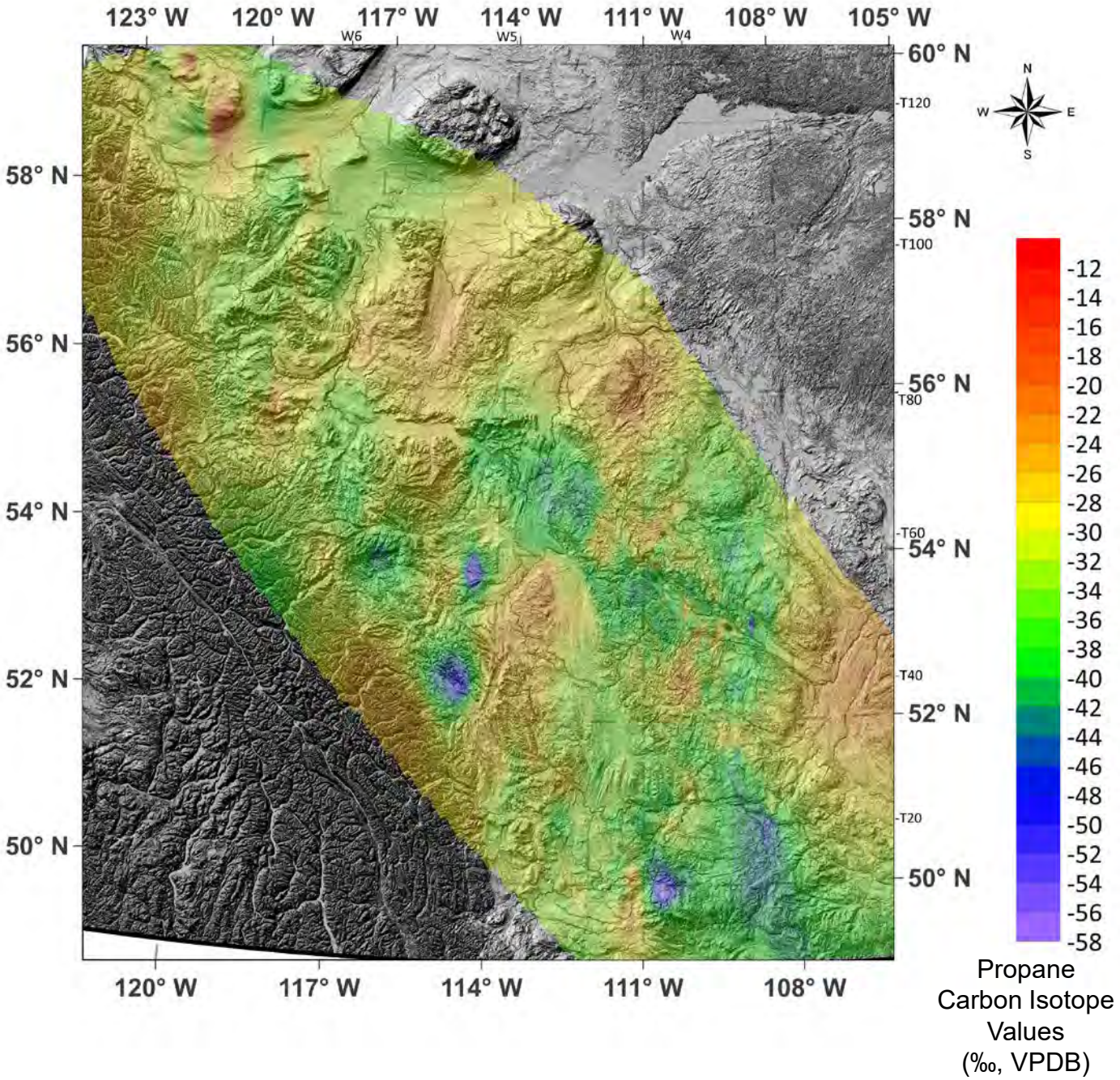

Fig. 18A. Contour Map of *n*-Butane Carbon Isotope Values of Production Wells over Topographic Map

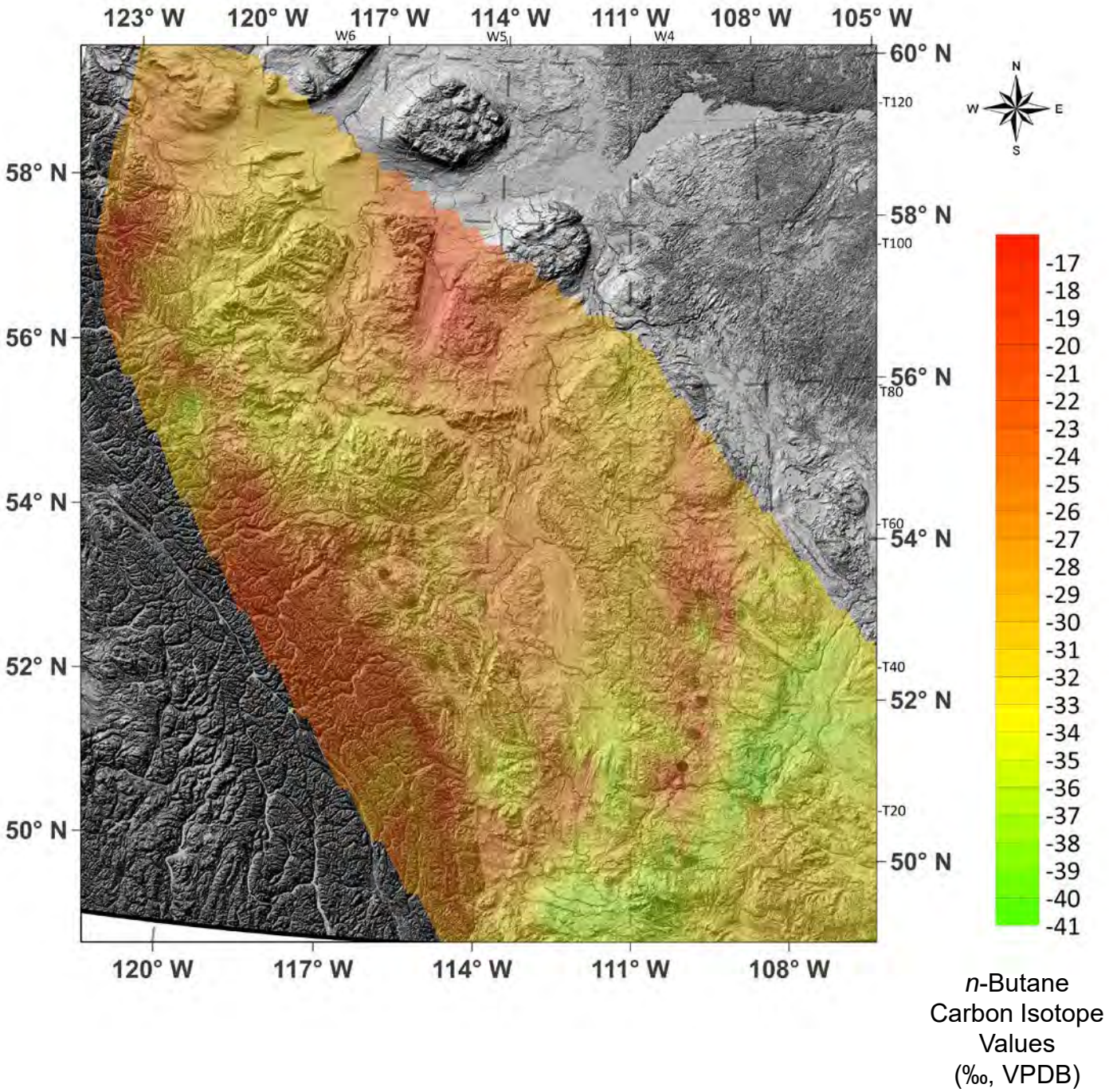

Fig. 18B. Contour Map of *n*-Butane Carbon Isotope Values of SCV over Topographic Map

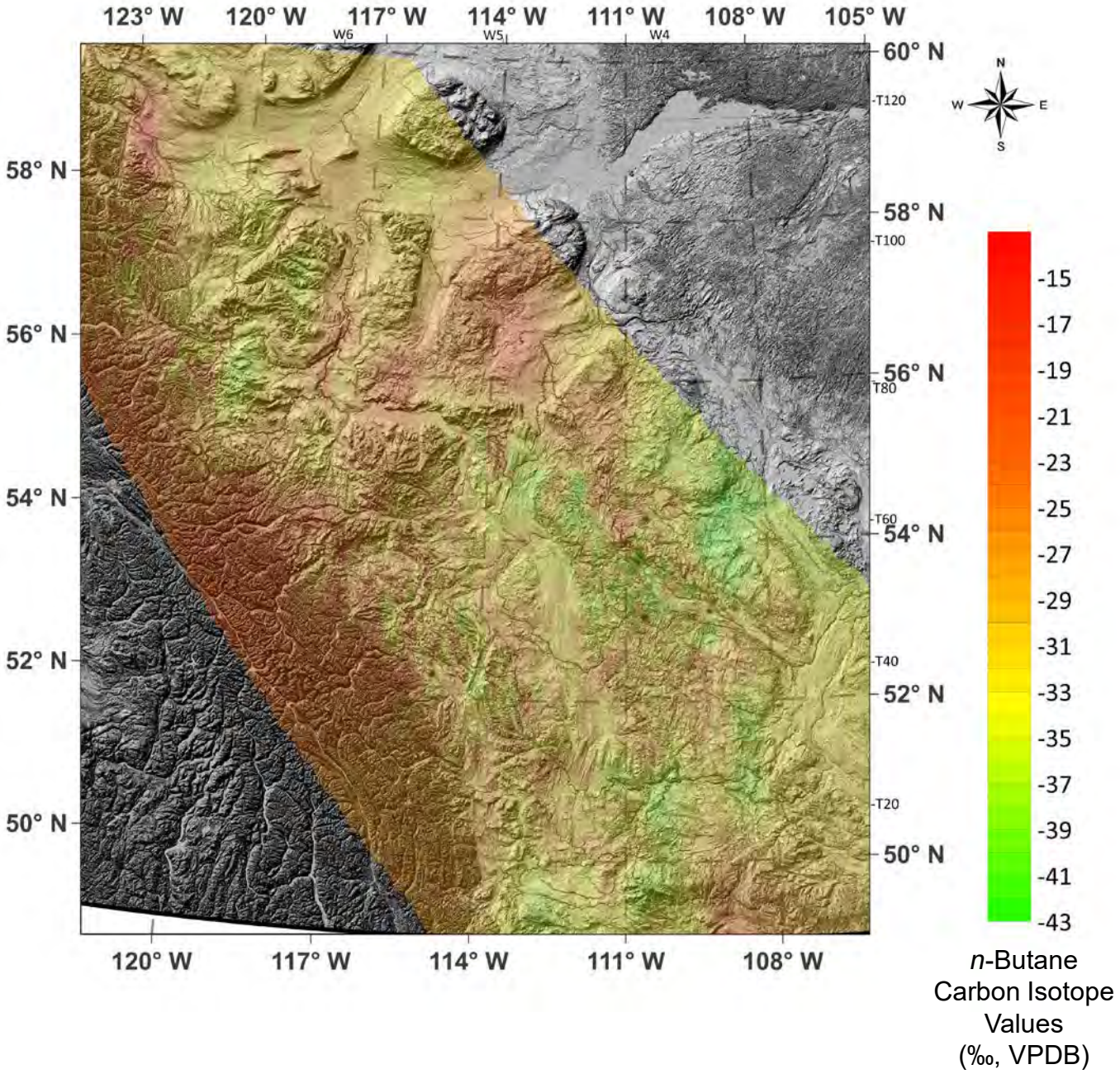

Fig. 18C. Contour Map of *n*-Butane Carbon Isotope Values of GM over Topographic Map

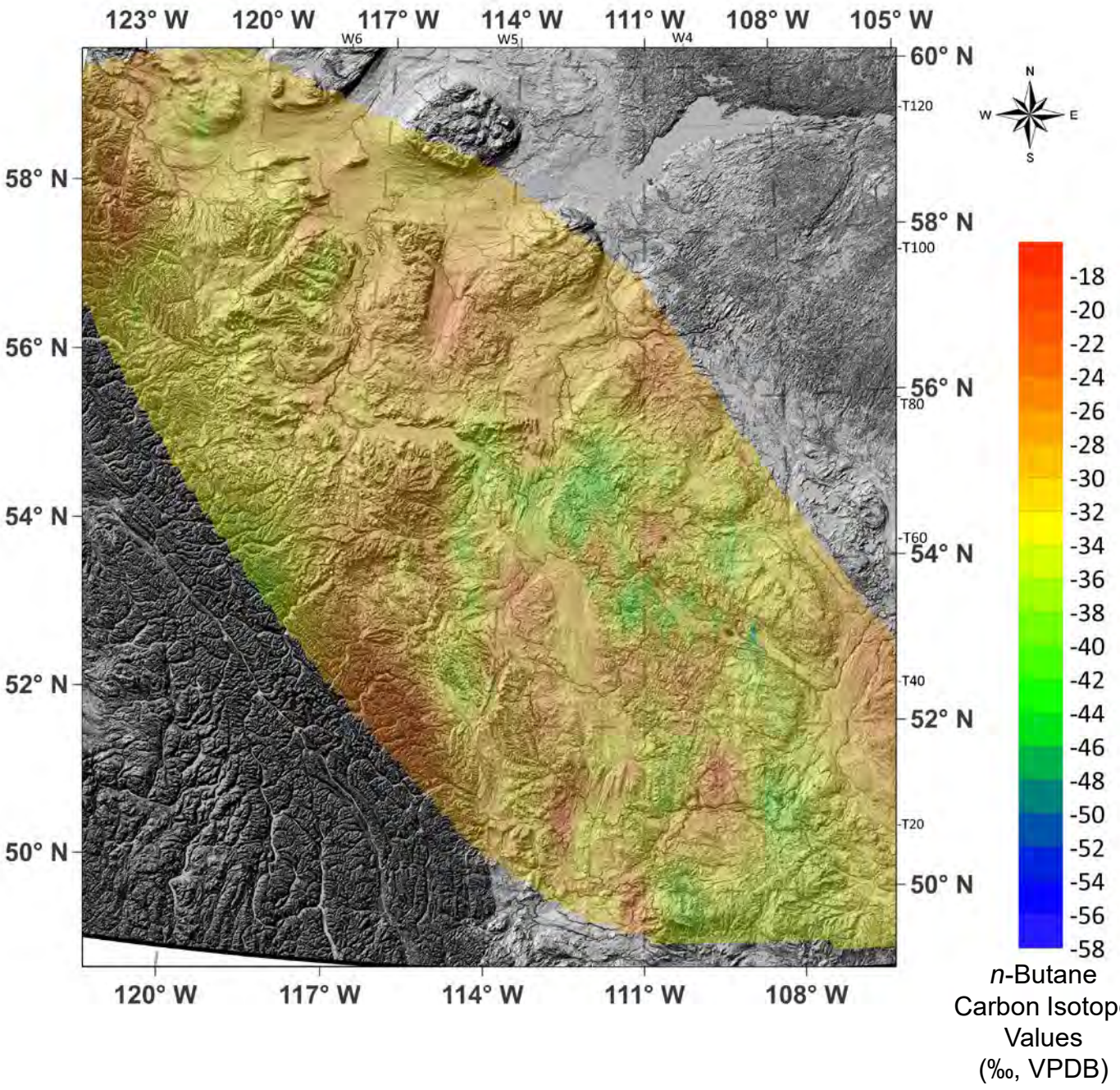

Fig. 20A. Contour Map of Carbon Dioxide Carbon Isotope Values of Production Wells over Topographic Map

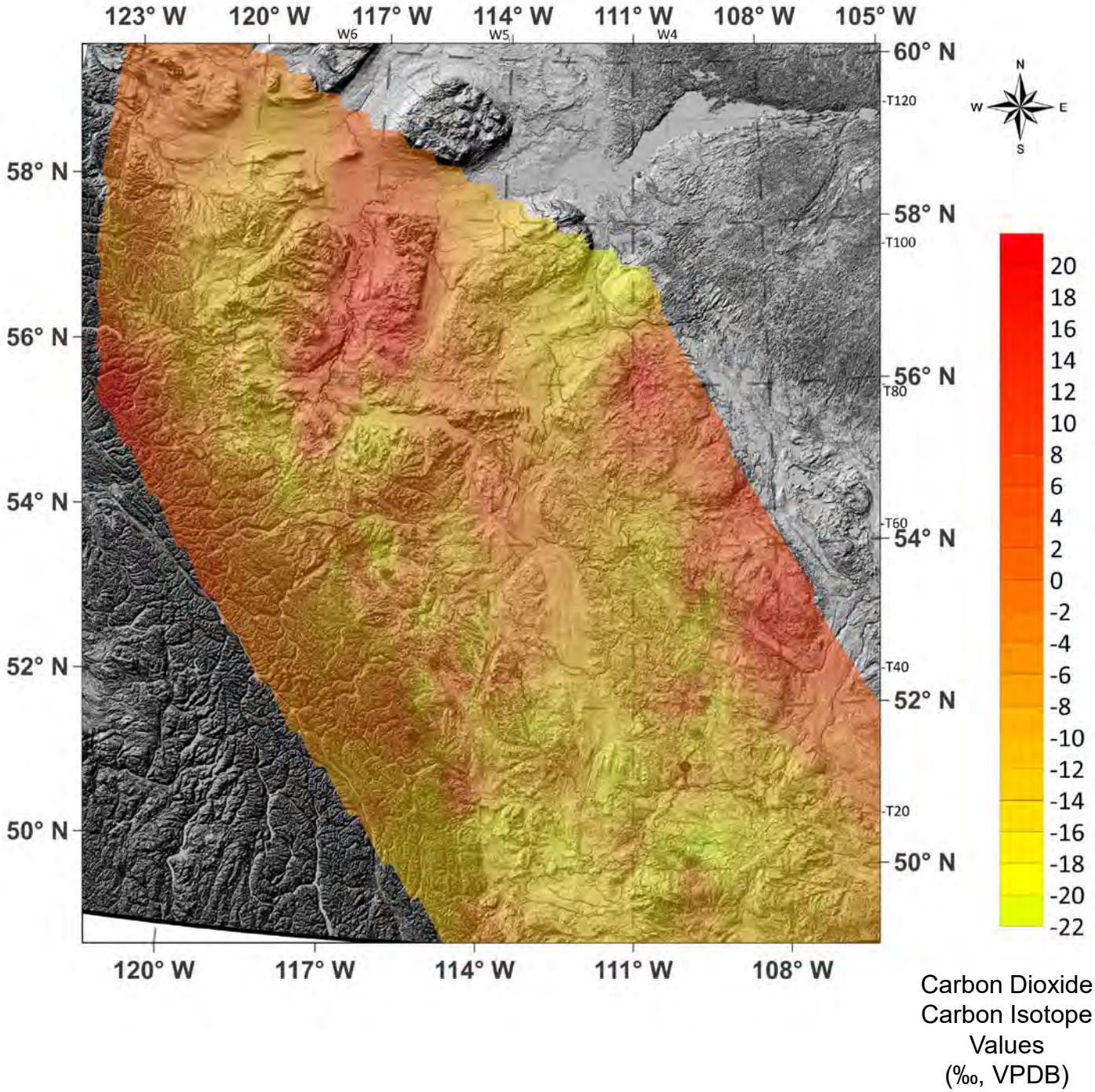

Fig. 20B. Contour Map of Carbon Dioxide Carbon Isotope Values of SCV over Topographic Map

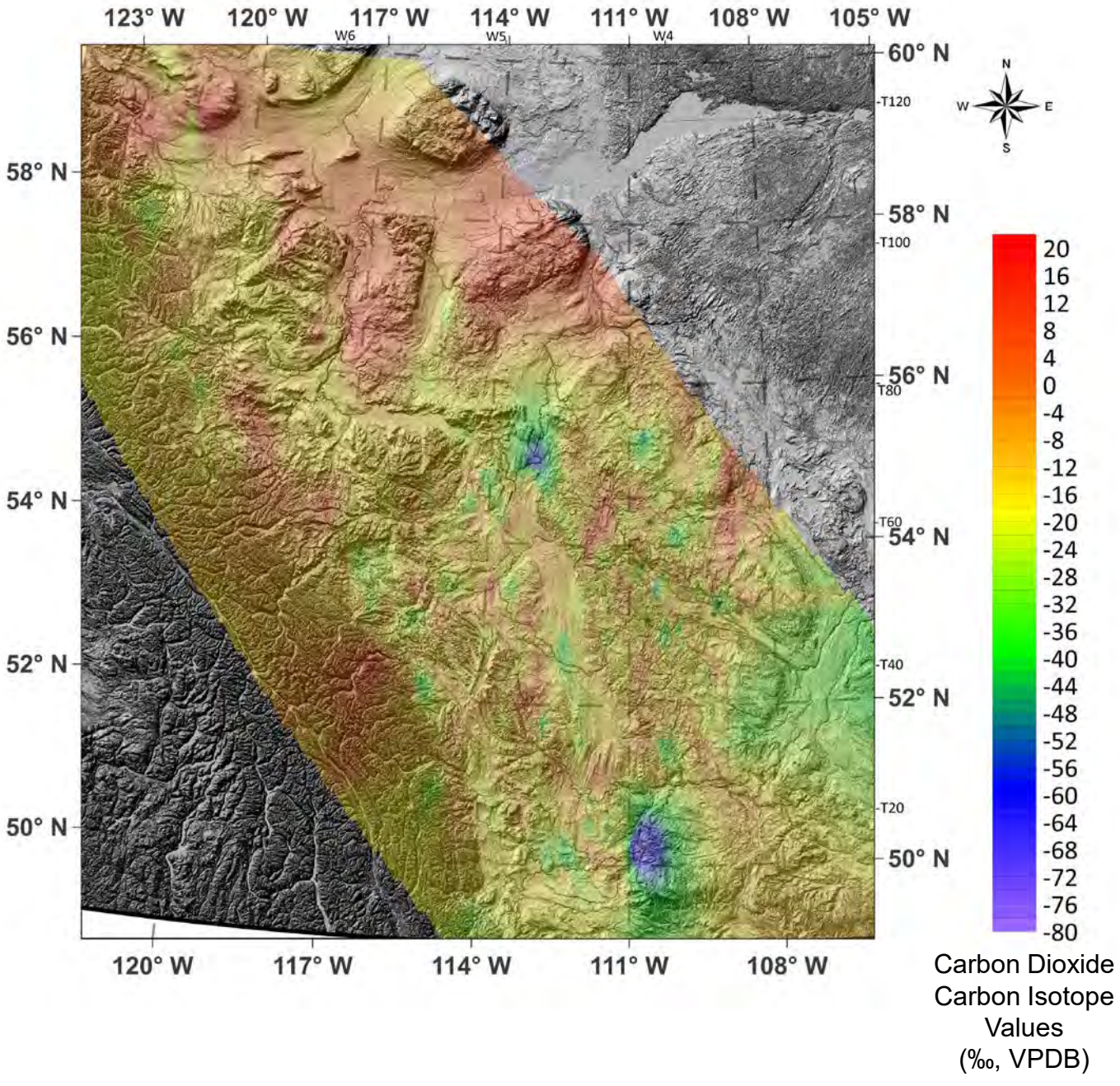

Fig. 20C. Contour Map of Carbon Dioxide Carbon Isotope Values of GM over Topographic Map

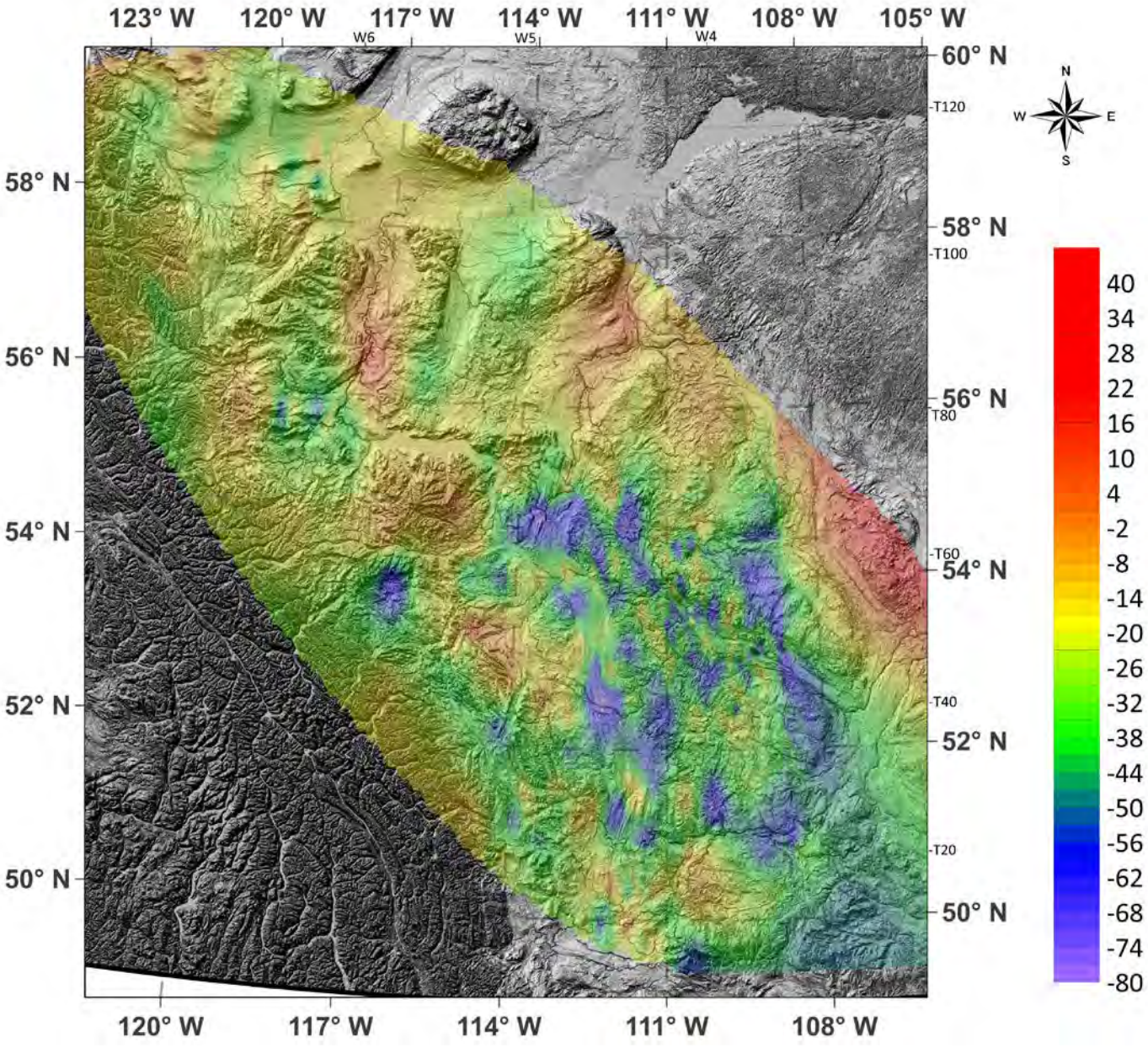

Fig. 20A. Contour Map of Carbon Dioxide Carbon Isotope Values of Production Wells over Topographic Map

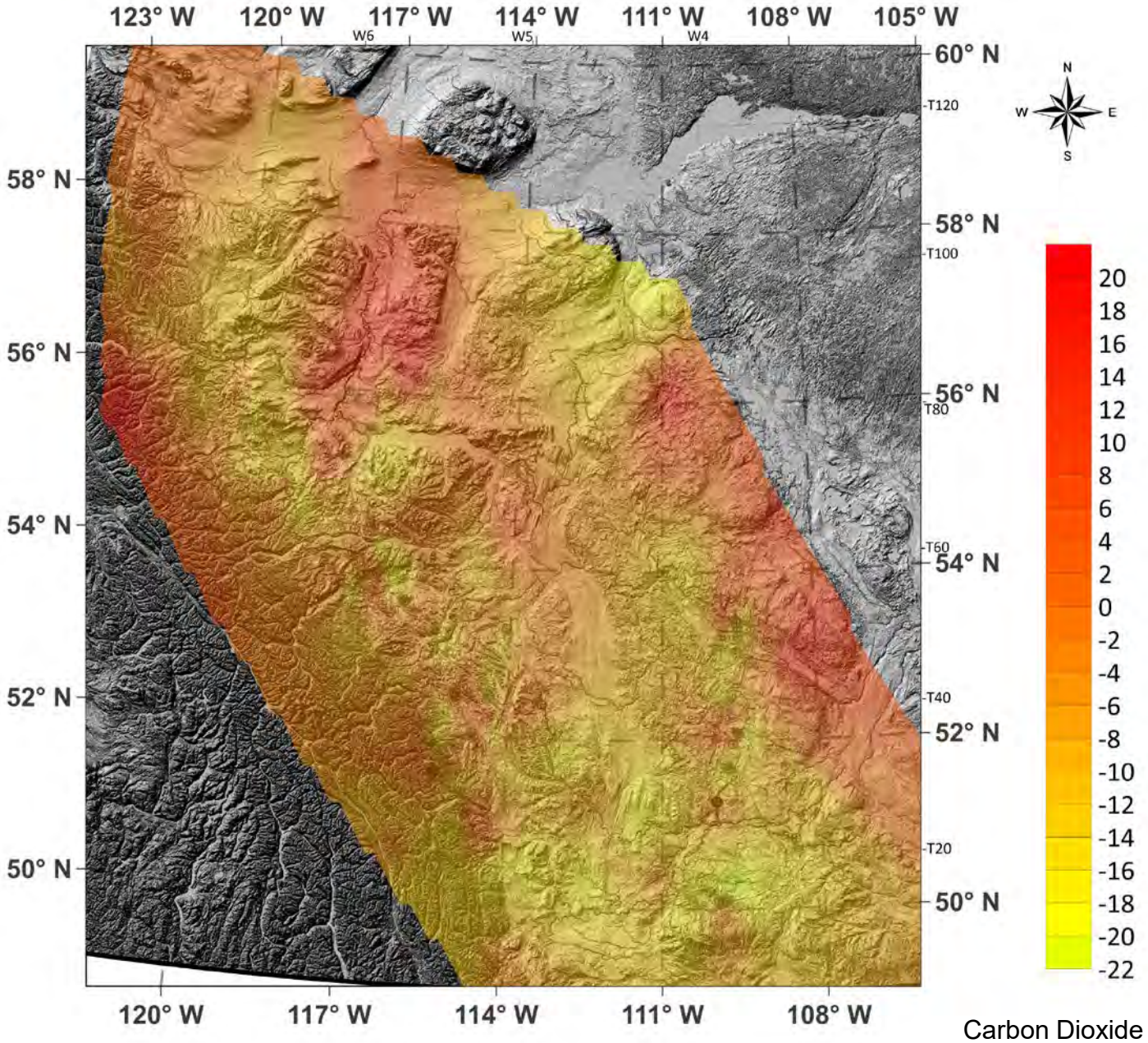

Fig. 20B. Contour Map of Carbon Dioxide Carbon Isotope Values of SCV over Topographic Map

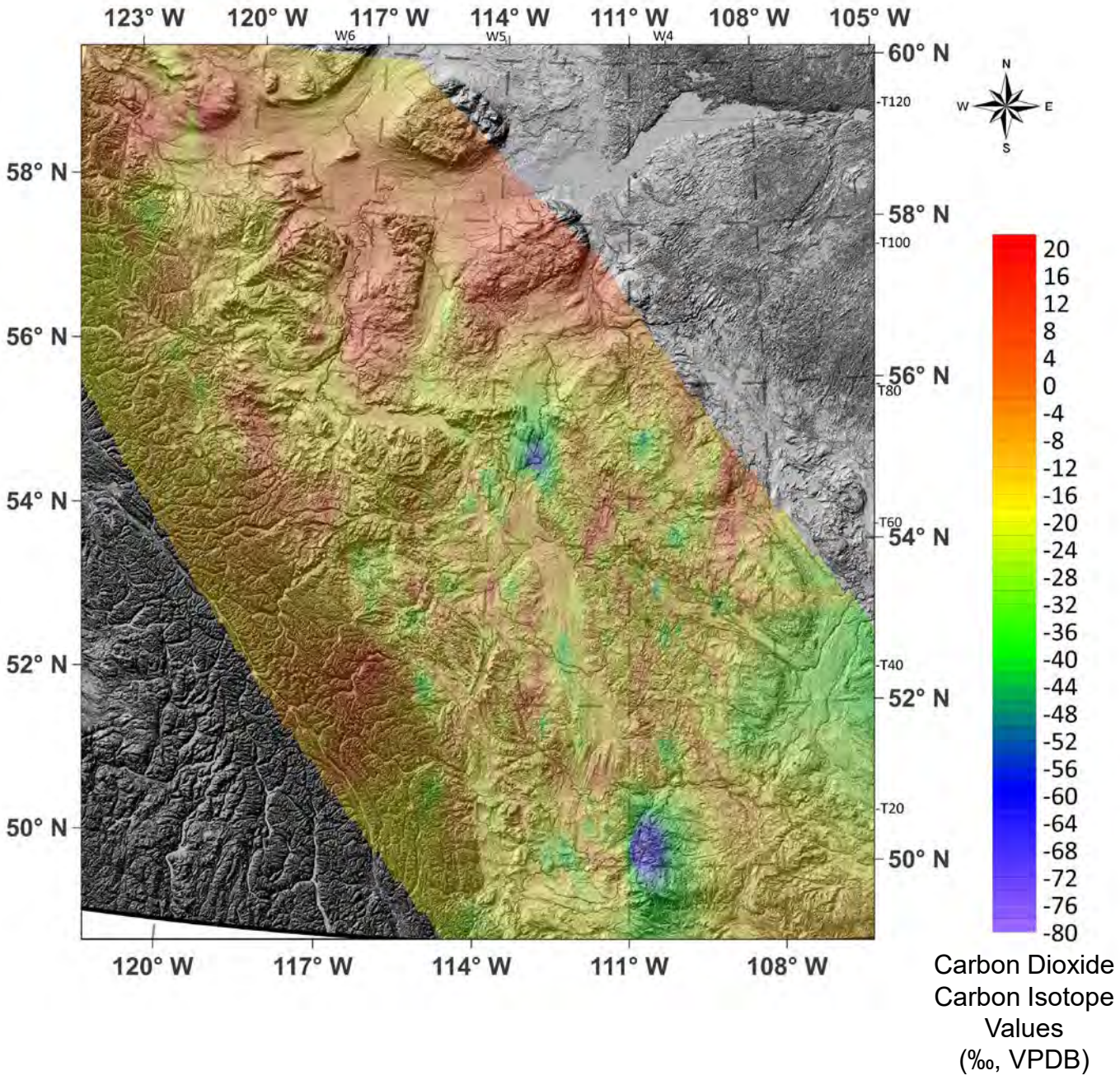

Fig. 20C. Contour Map of Carbon Dioxide Carbon Isotope Values of GM over Topographic Map

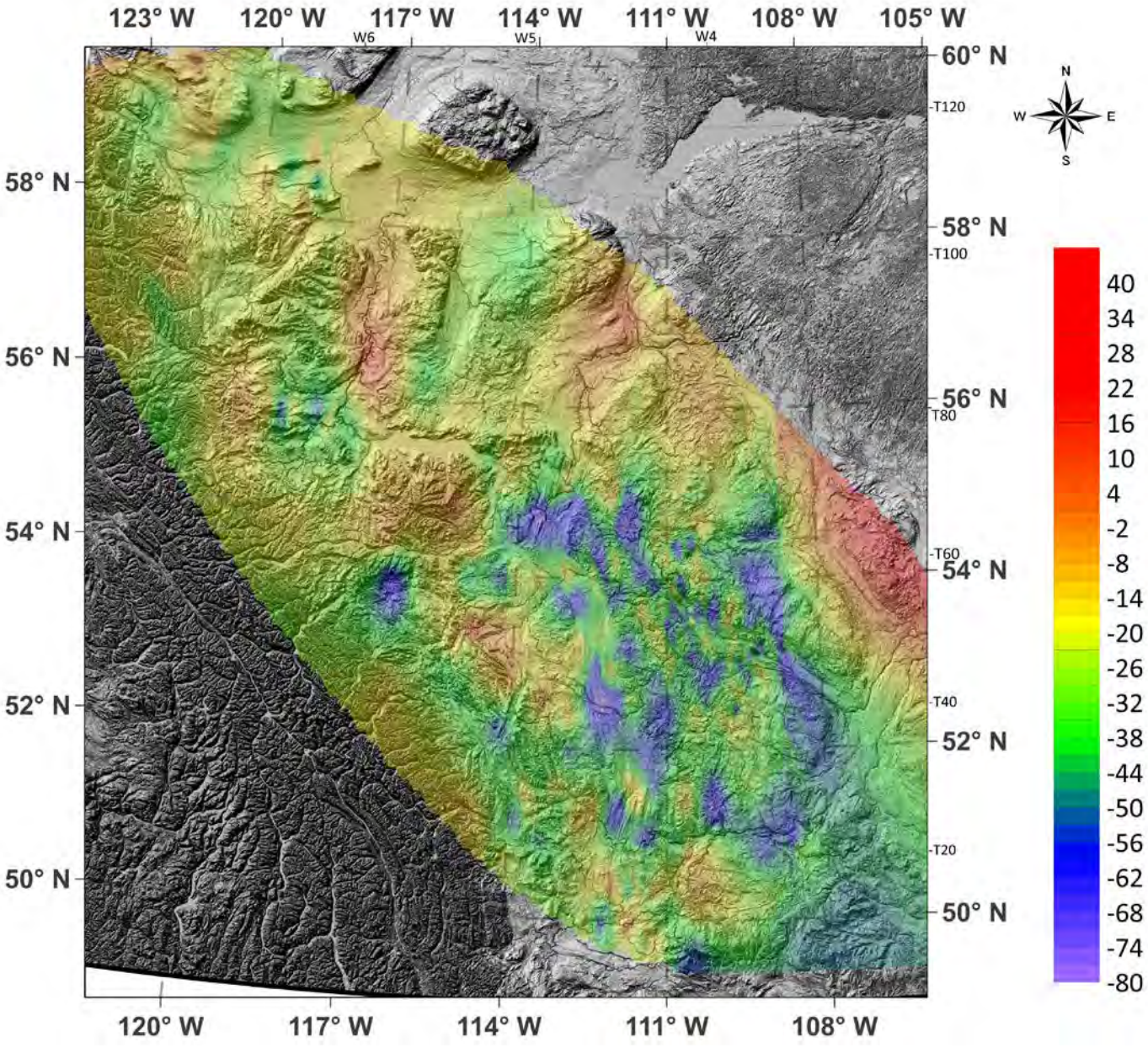

Fig. 21A. Map of Surface Casing Vent (SCV) Locations in the Eastern Alberta Zoom-in

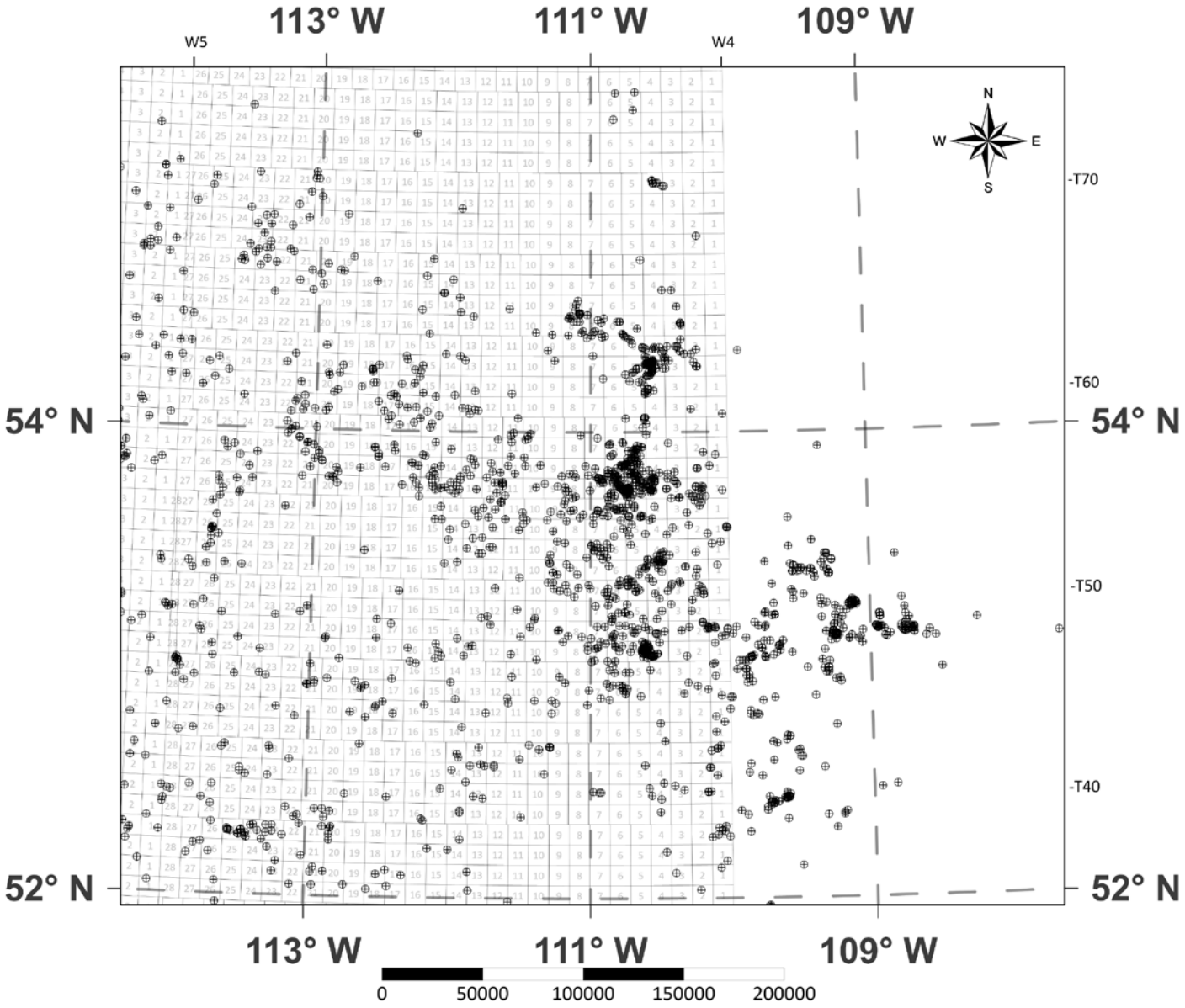

Fig. 21B. Contour Map of Methane Carbon Isotope Values of SCV Eastern Alberta Zoom-in

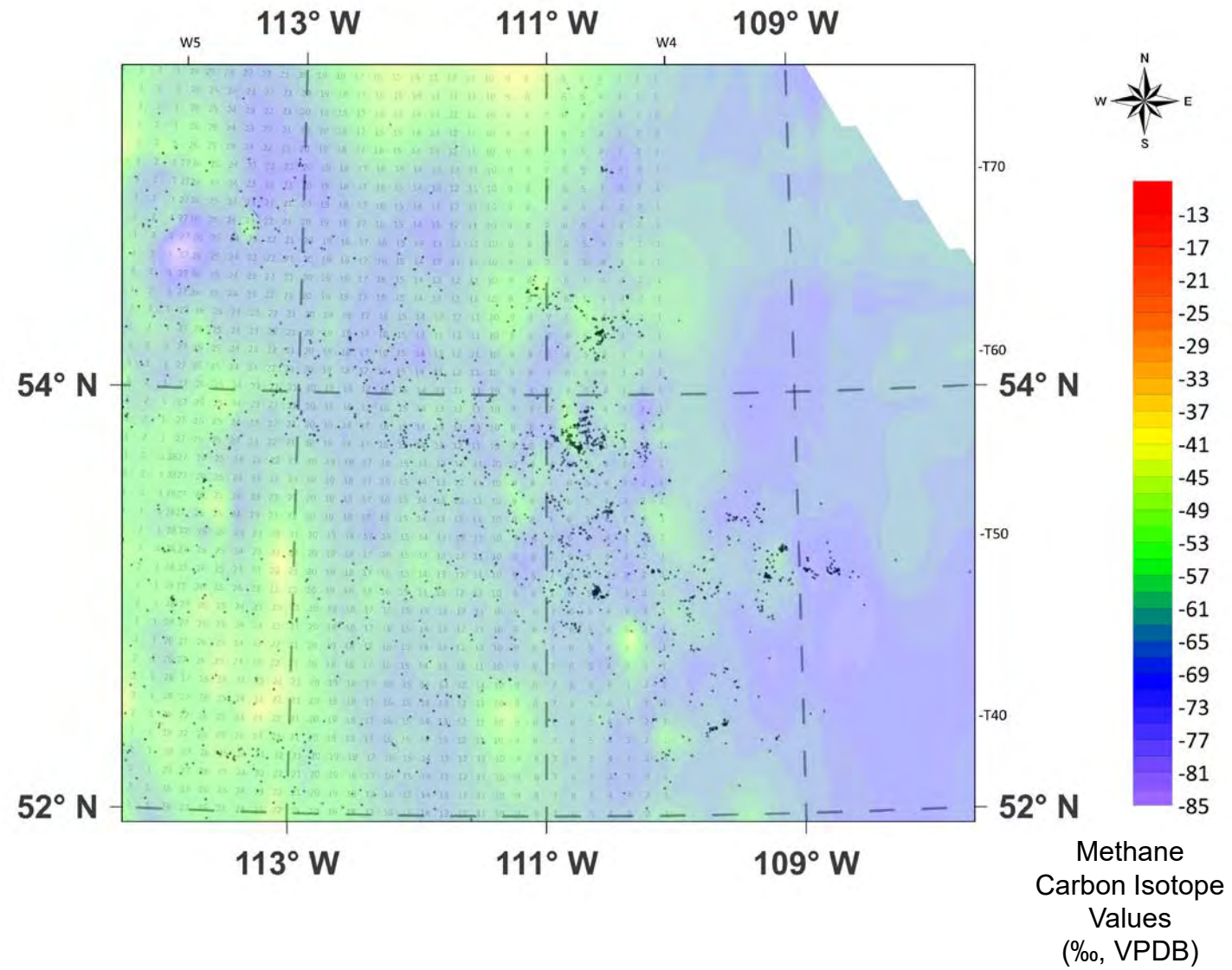

Fig. 21C. Contour Map of Ethane Carbon Isotope Values of SCV Eastern Alberta Zoom-in

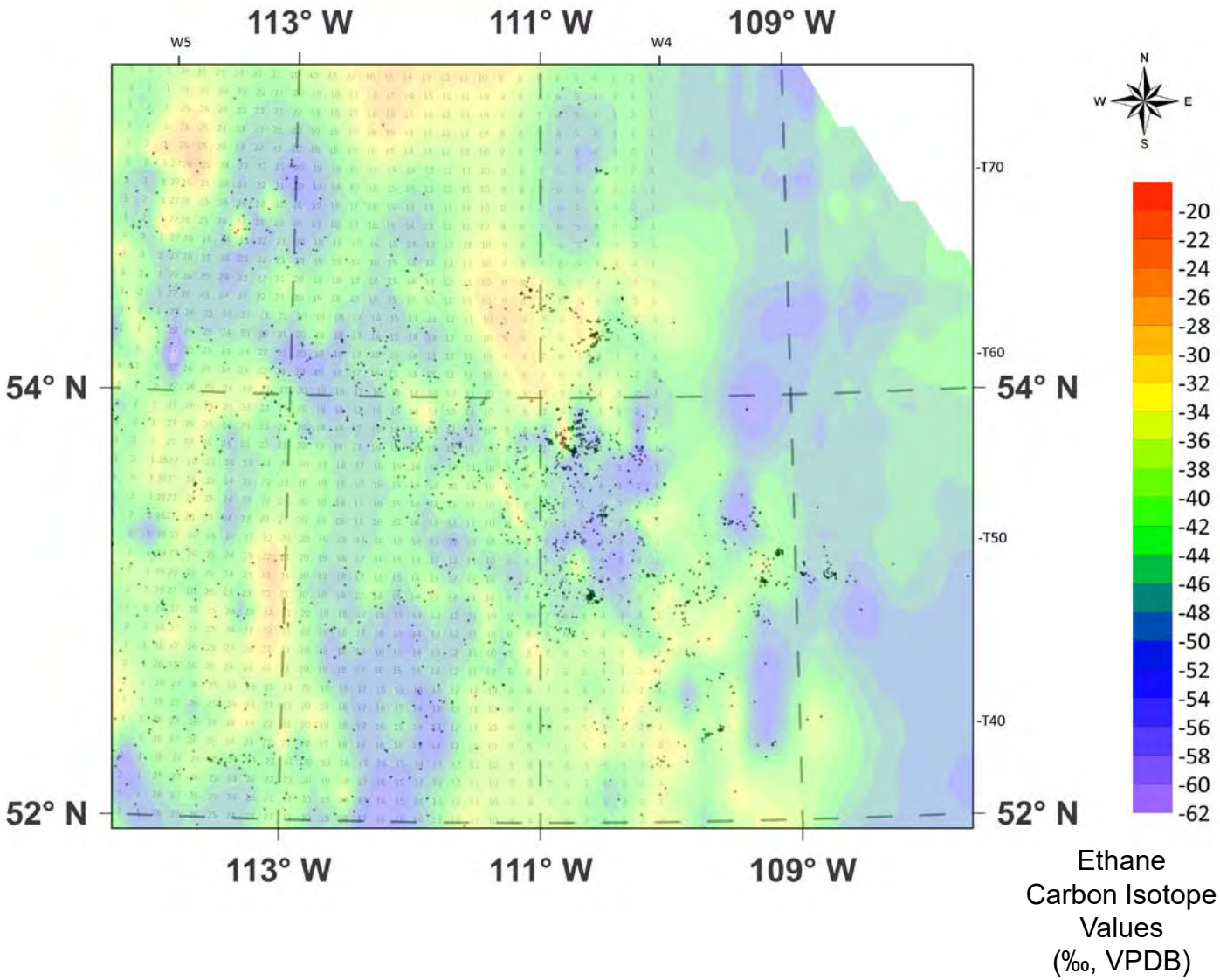

Fig. 21D. Contour Map of Propane Carbon Isotope Values of SCV Eastern Alberta Zoom-in

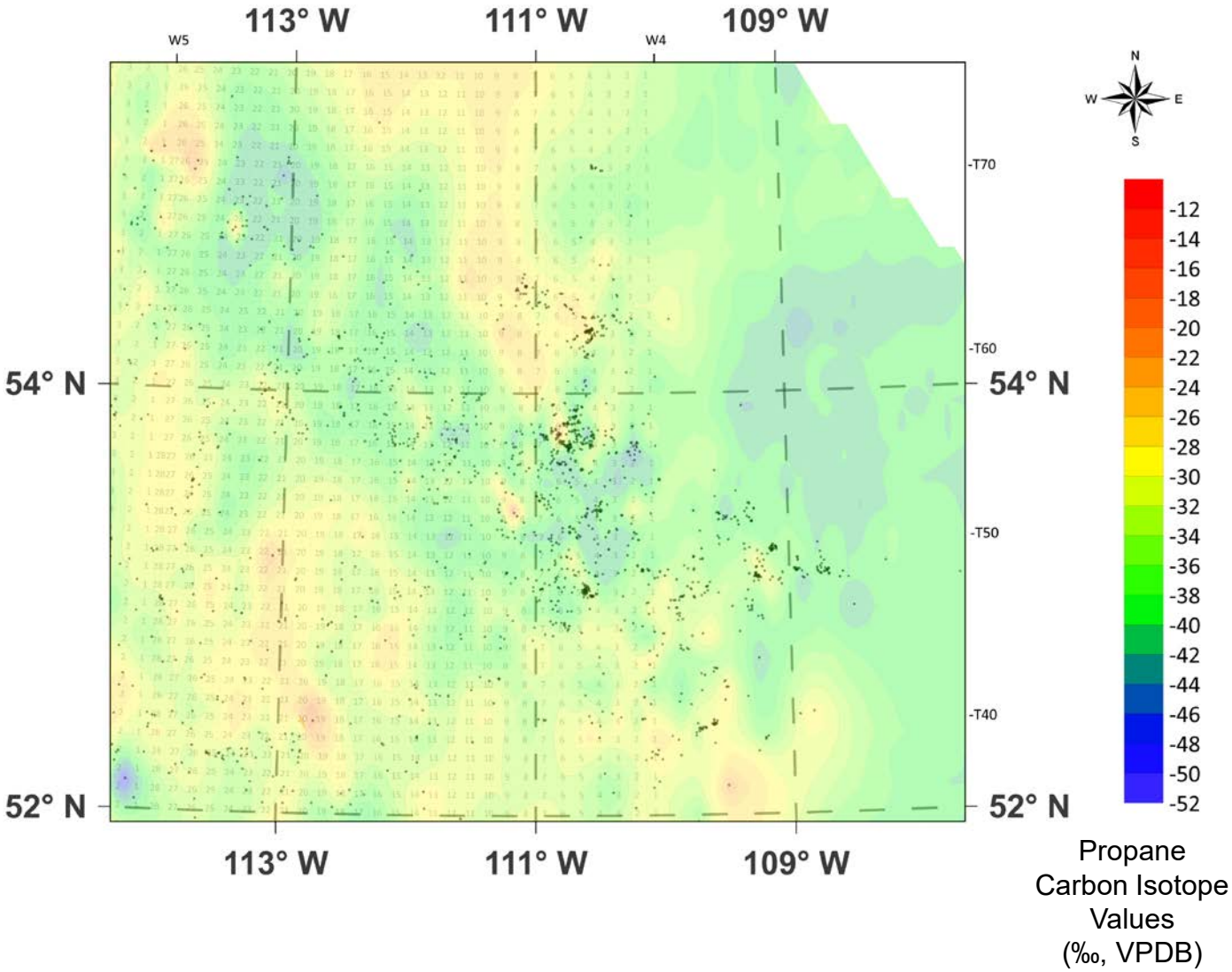

Fig. 21E. Contour Map of *n*-Butane Carbon Isotope Values of SCV Eastern Alberta Zoom-in

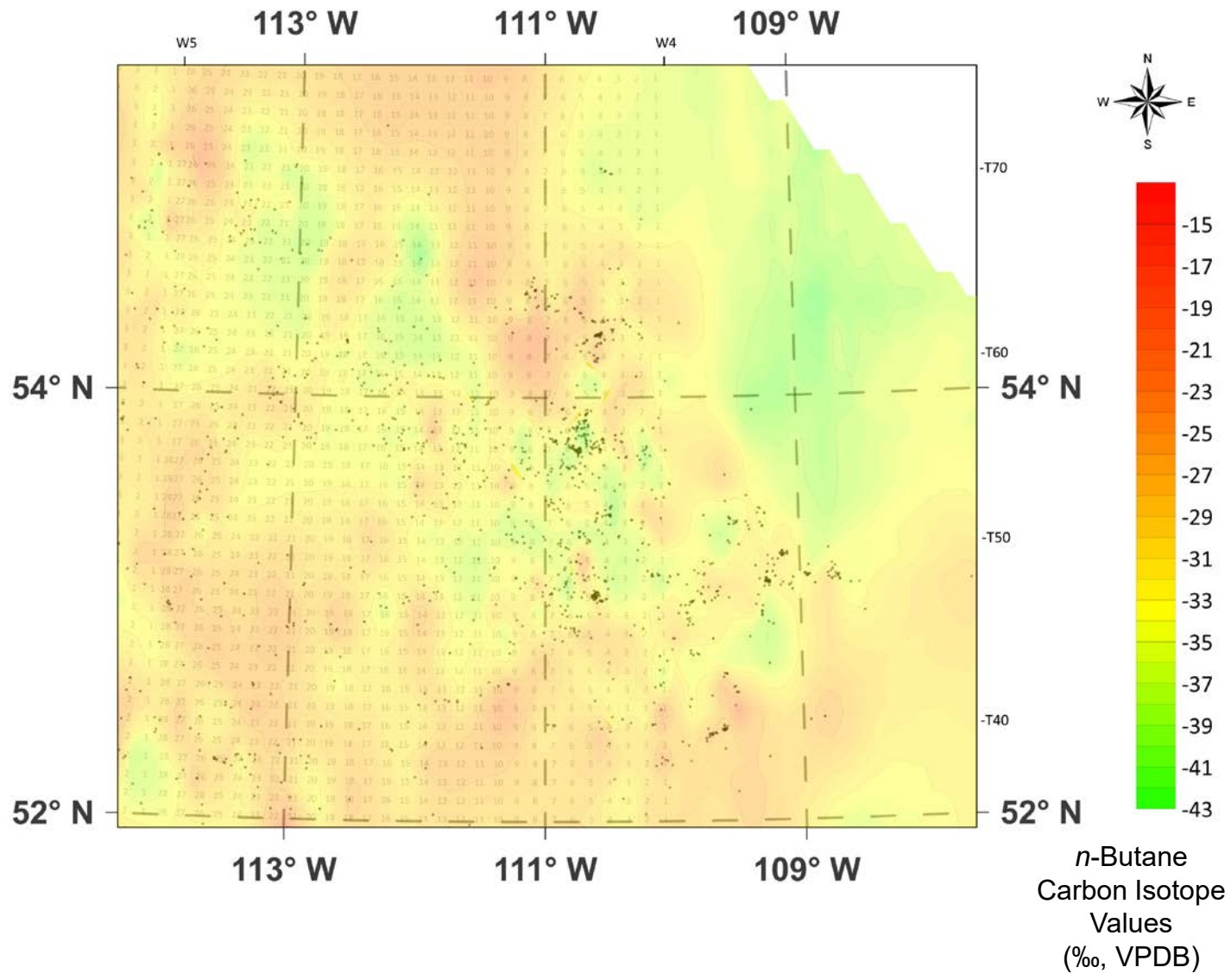

Fig. 21F. Contour Map of *i*-Butane Carbon Isotope Values of SCV Eastern Alberta Zoom-in

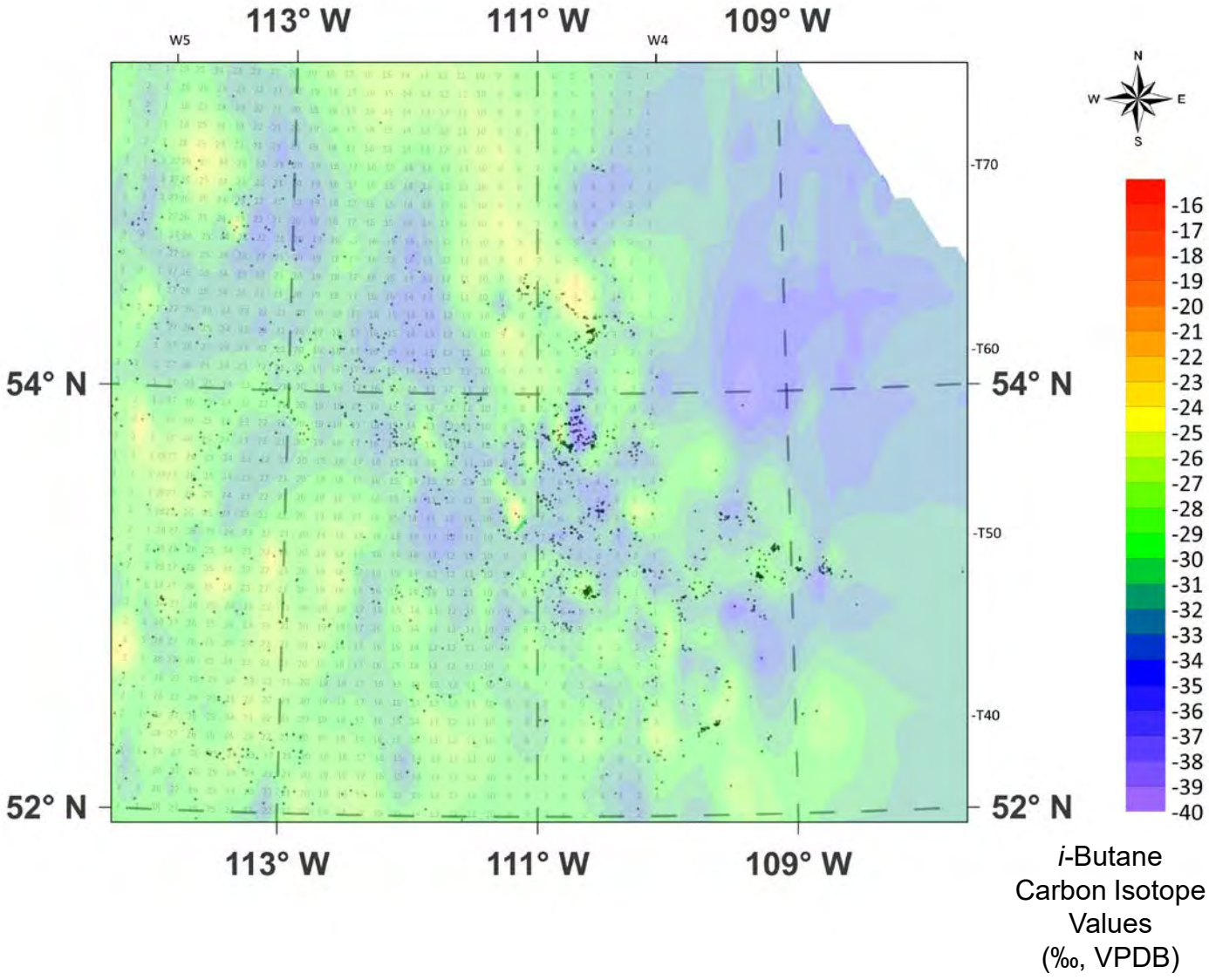

Fig. 21G. Contour Map of Carbon Dioxide Carbon Isotope Values of SCV Eastern Alberta Zoom-in

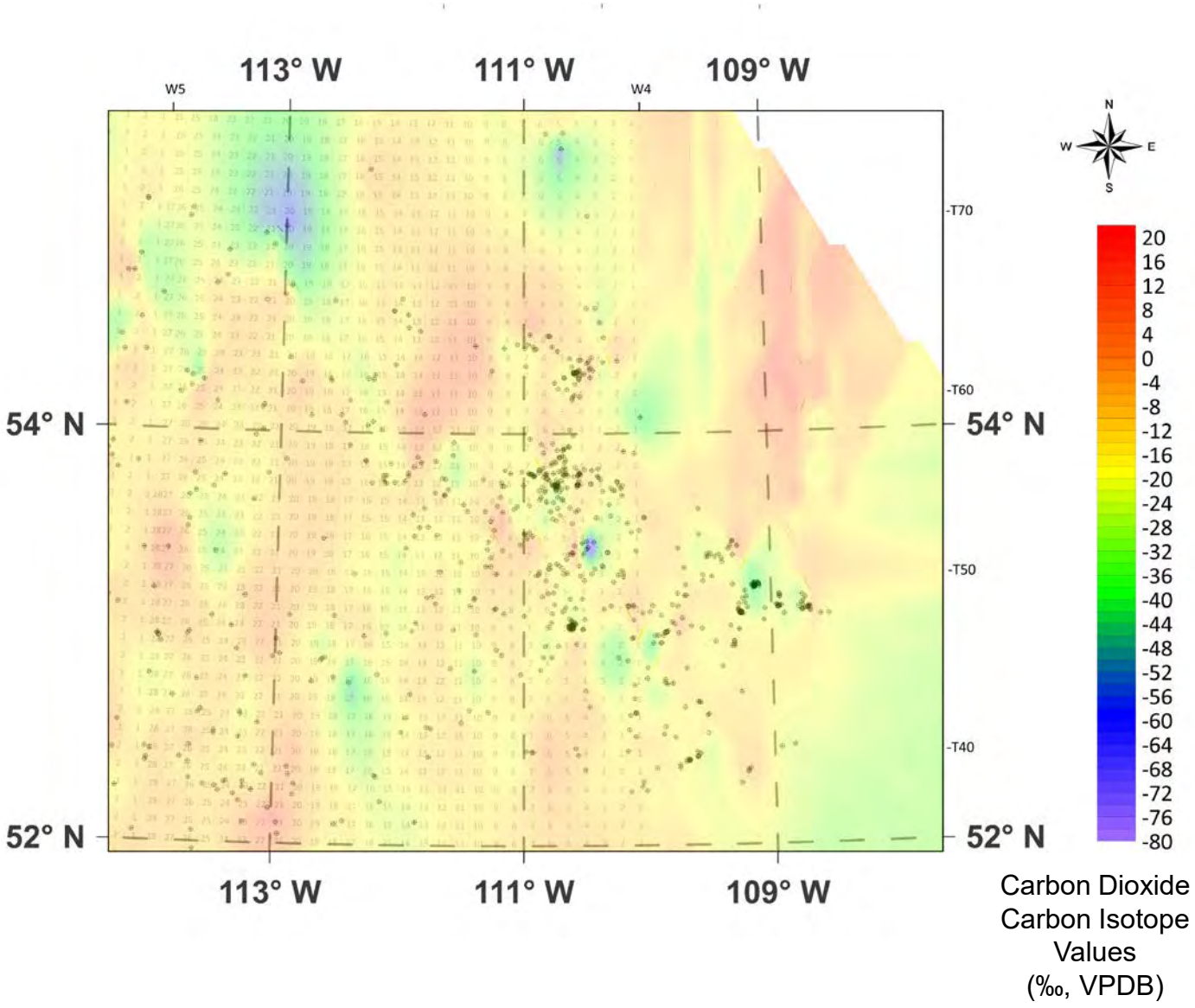

Fig. 21H. Contour Map of Methane Carbon Isotope Values of SCV Eastern Alberta Zoom-in over Topographic Map

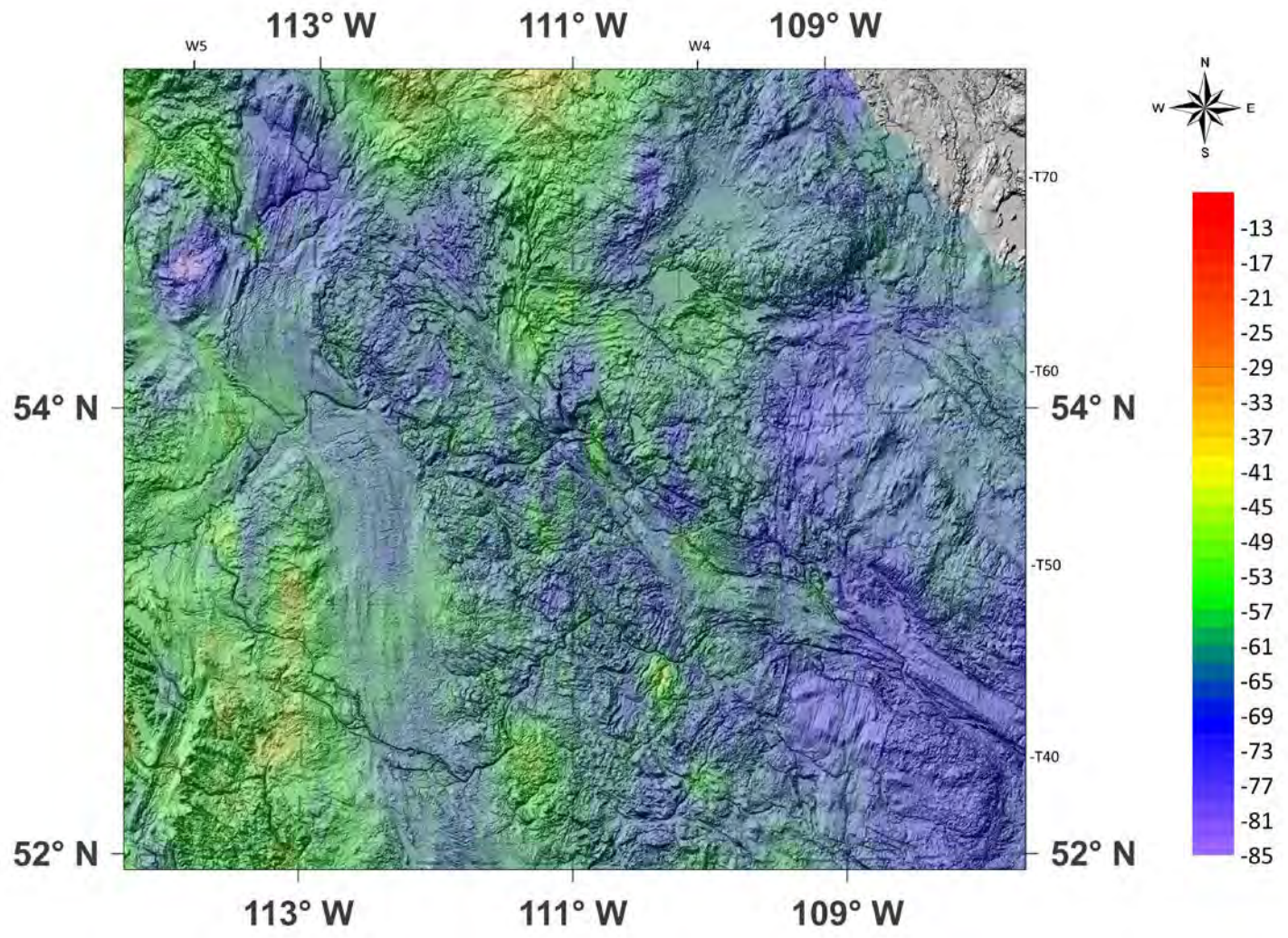

Methane Carbon Isotope Values (‰, VPDB)

Fig. 21I. Contour Map of Ethane Carbon Isotope Values of SCV Eastern Alberta Zoom-in over Topographic Map

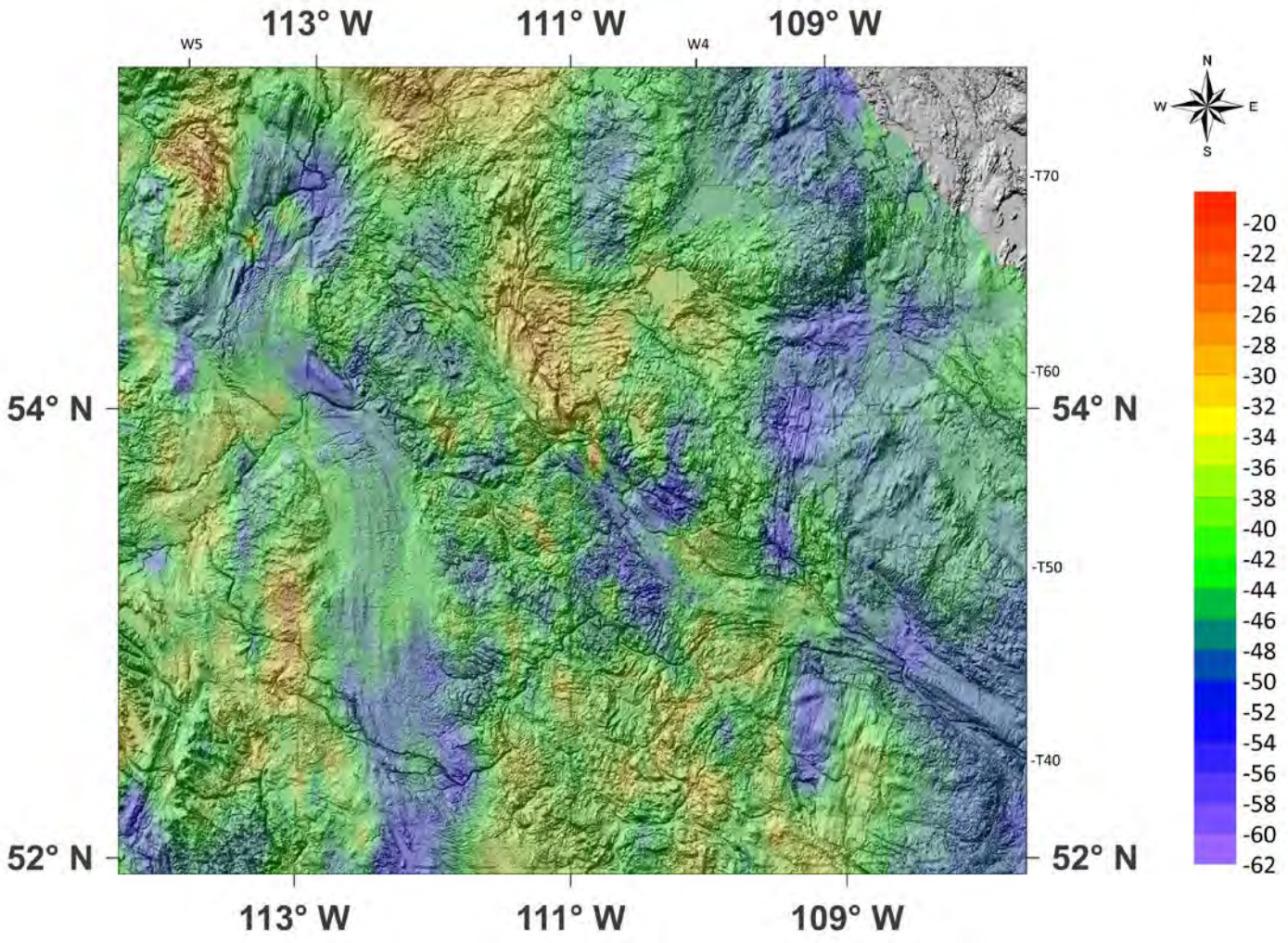

Ethane Carbon Isotope Values (‰, VPDB)

Fig. 21J. Contour Map of Propane Carbon Isotope Values of SCV Eastern Alberta Zoom-in over Topographic Map

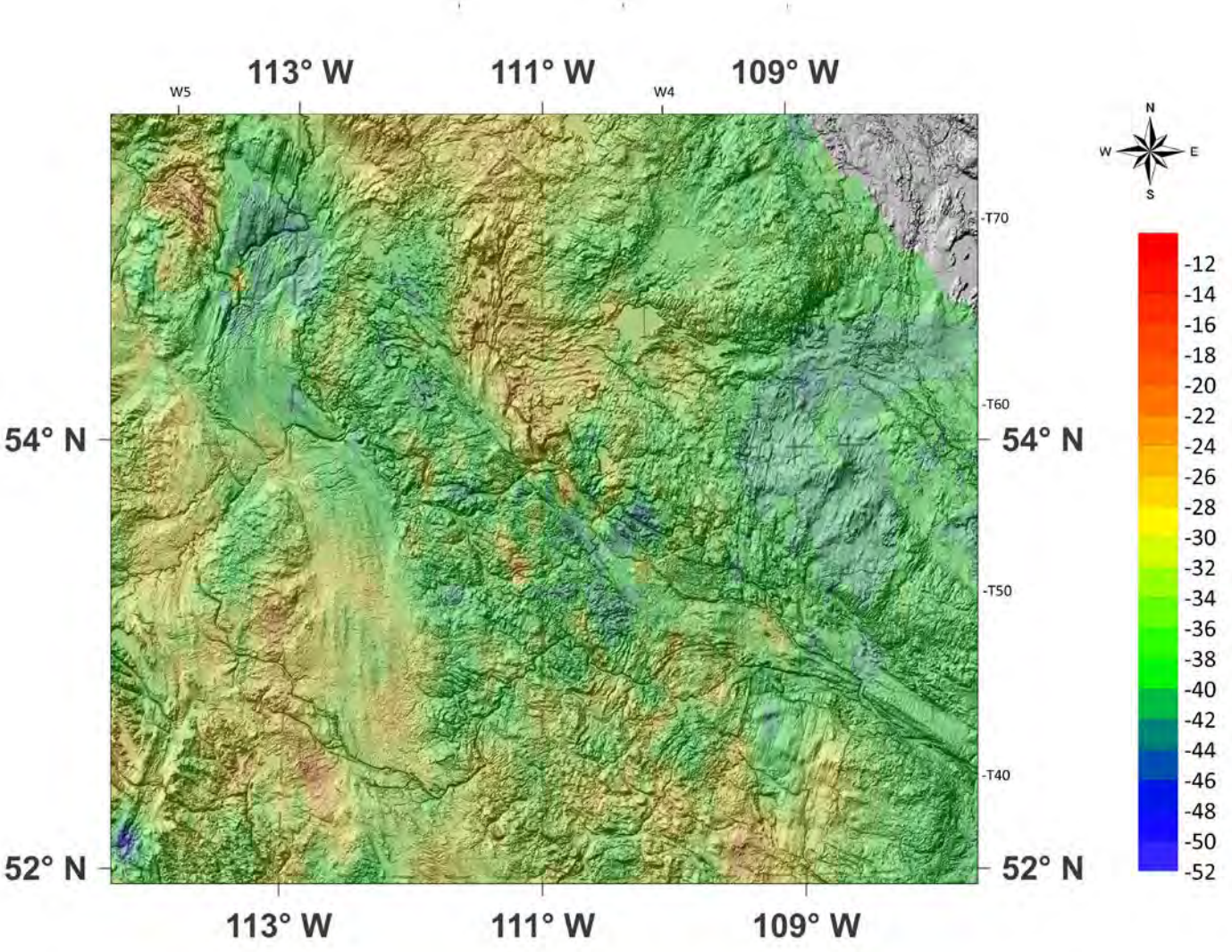

Propane Carbon Isotope Values (‰, VPDB)

Fig. 21K. Contour Map of *n*-Butane Carbon Isotope Values of SCV Eastern Alberta Zoom-in over Topographic Map

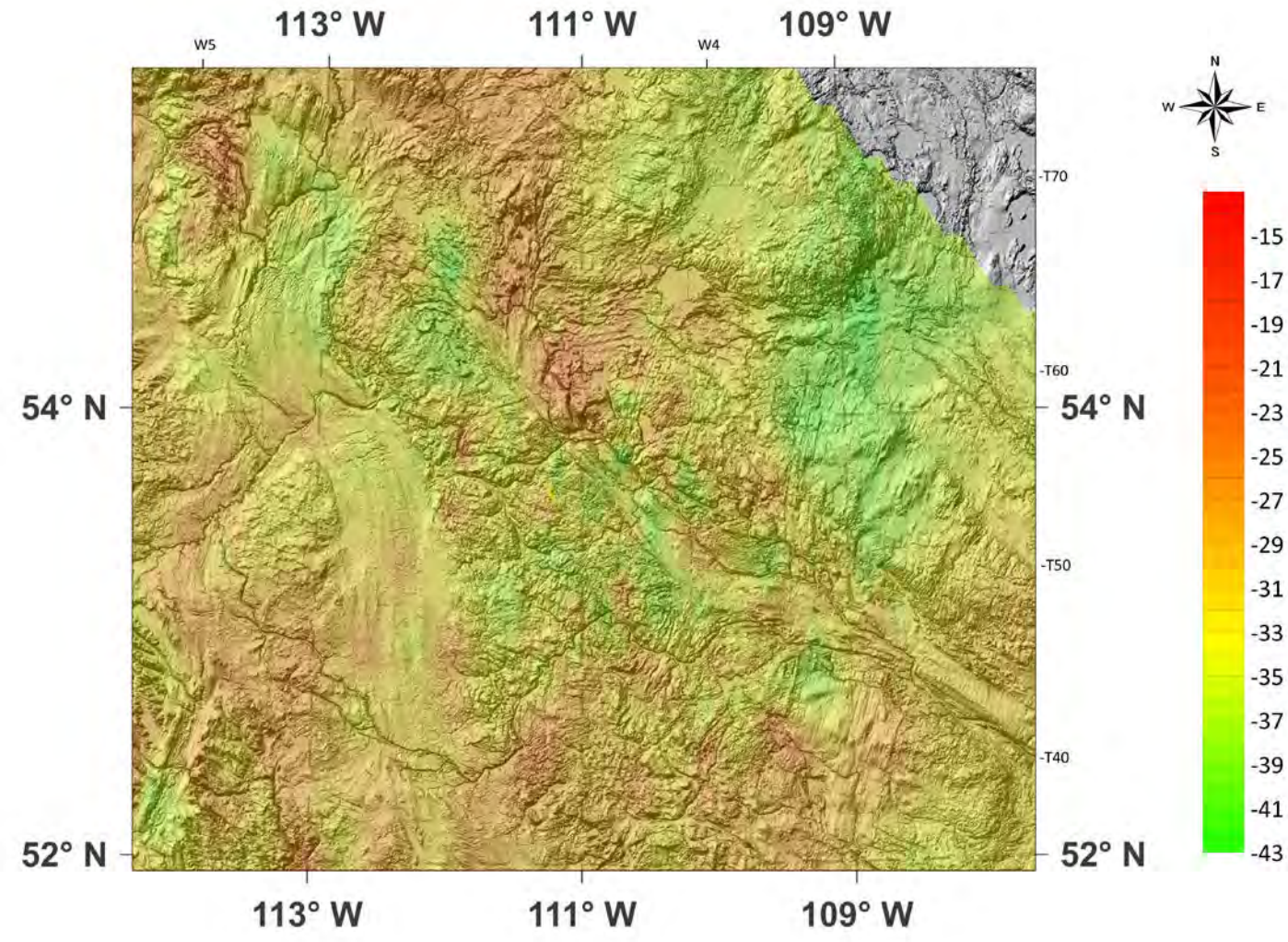

n-Butane Carbon Isotope Values (‰, VPDB)

Fig. 21L. Contour Map of *i*-Butane Carbon Isotope Values of SCV Eastern Alberta Zoom-in over Topographic Map

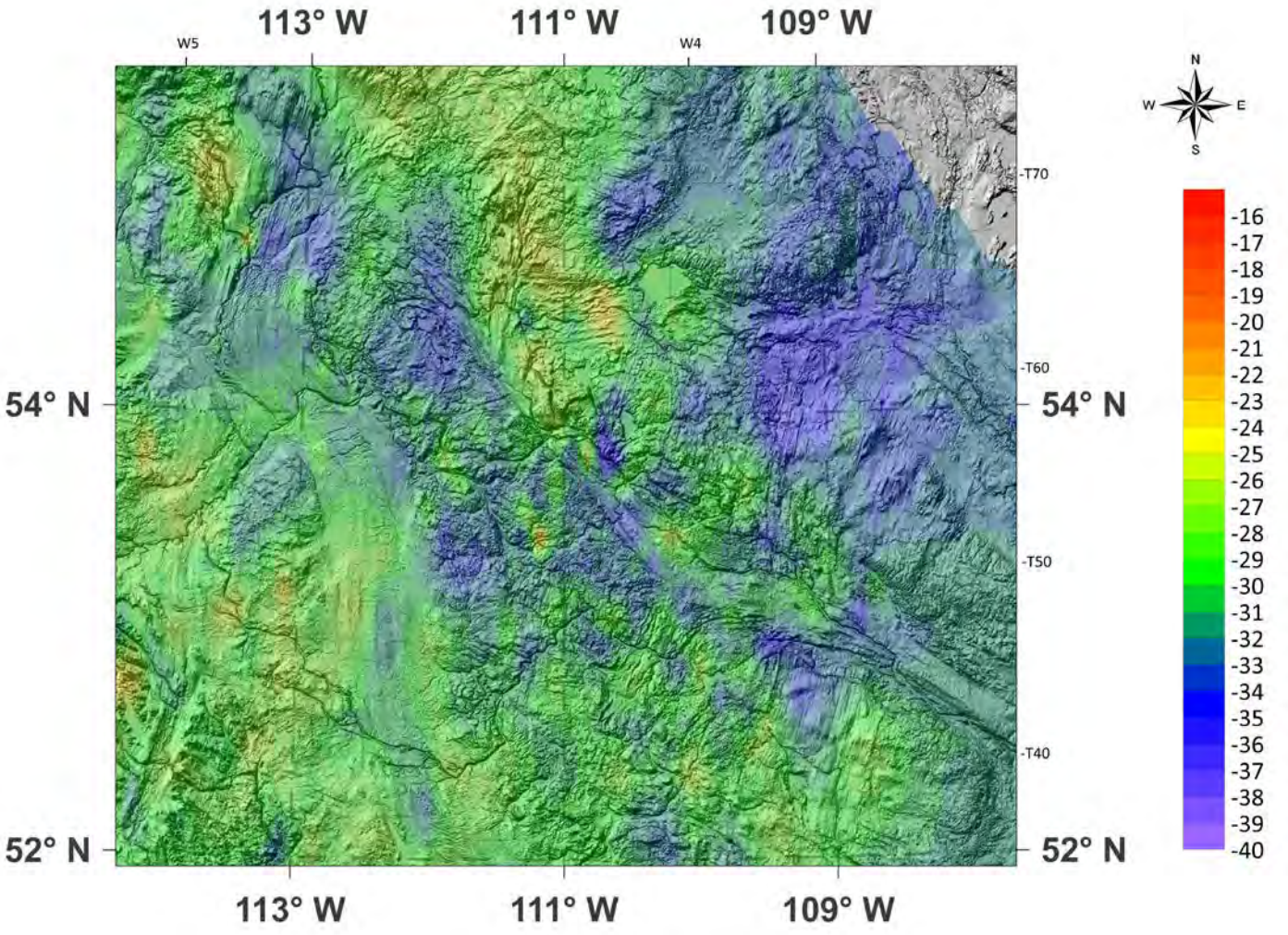

i-Butane Carbon Isotope Values (‰, VPDB)

Fig. 21M. Contour Map of Carbon Dioxide Carbon Isotope Values of SCV Eastern Alberta Zoom-in over Topographic Map

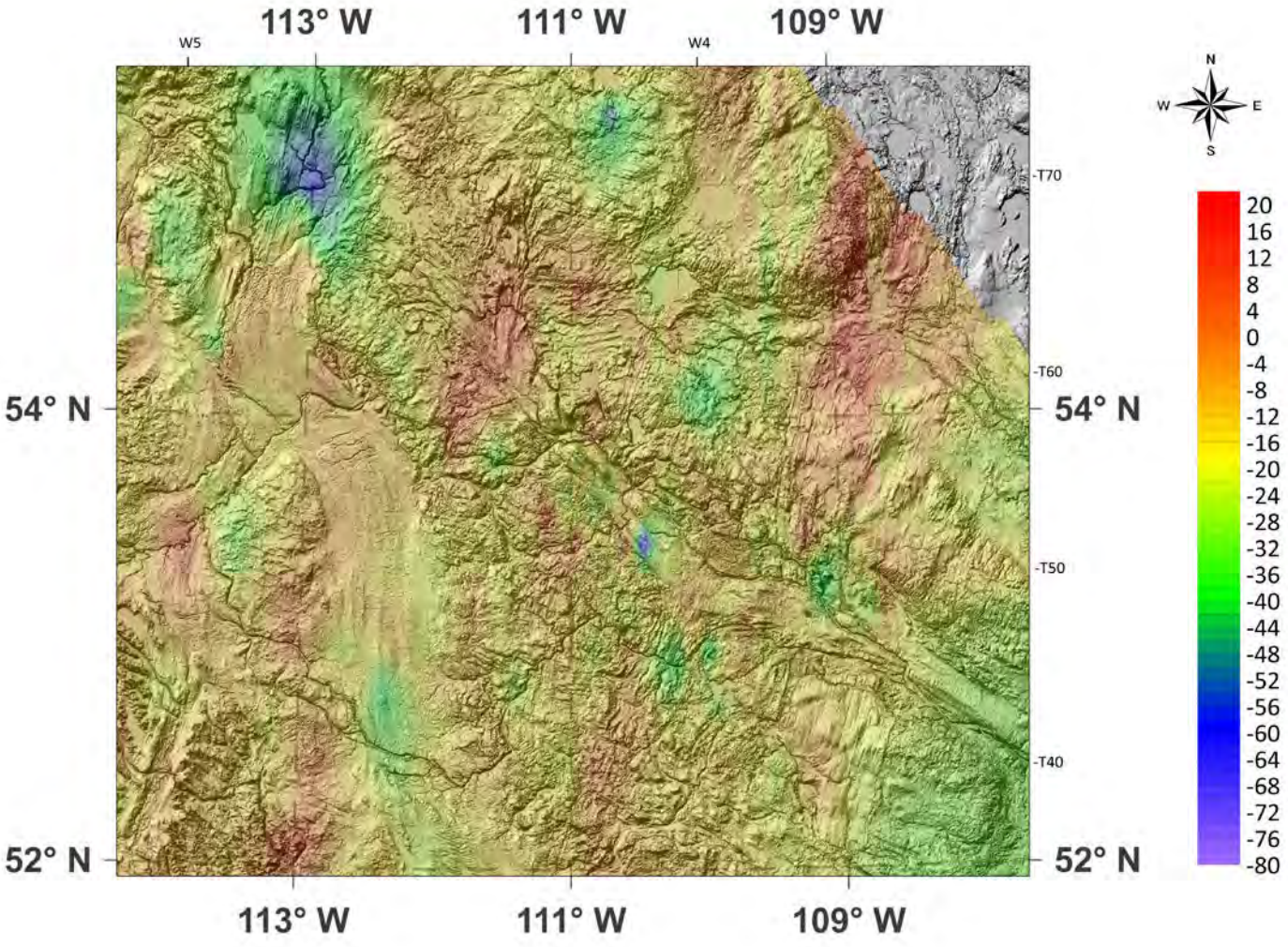

Carbon Dioxide Carbon Isotope Values (‰, VPDB)

Fig. 22A. Map of Ground Migration (GM) Locations in the Eastern Alberta Zoom-in

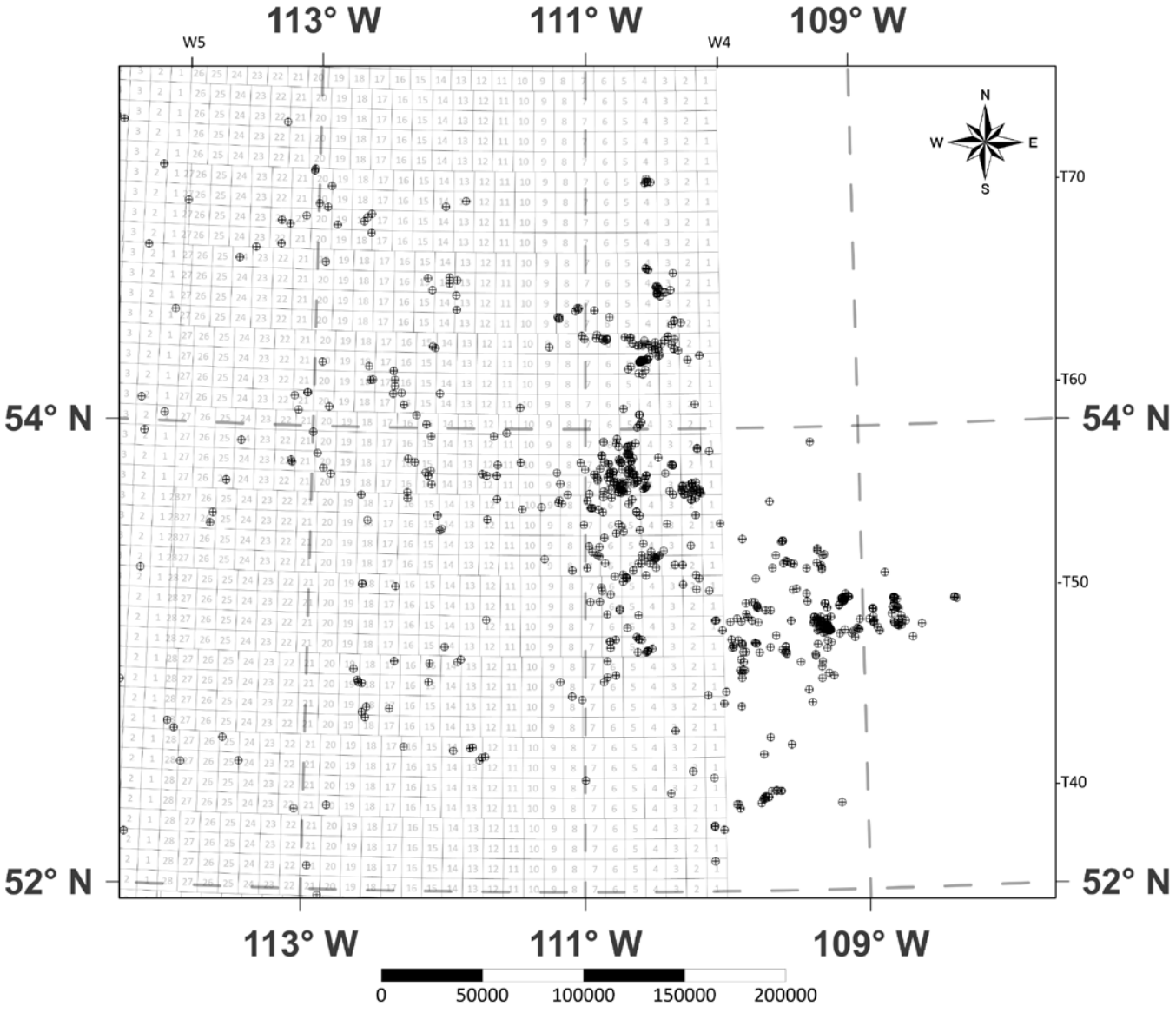

Fig. 22B. Contour Map of Methane Carbon Isotope Values of GM Eastern Alberta Zoom-in

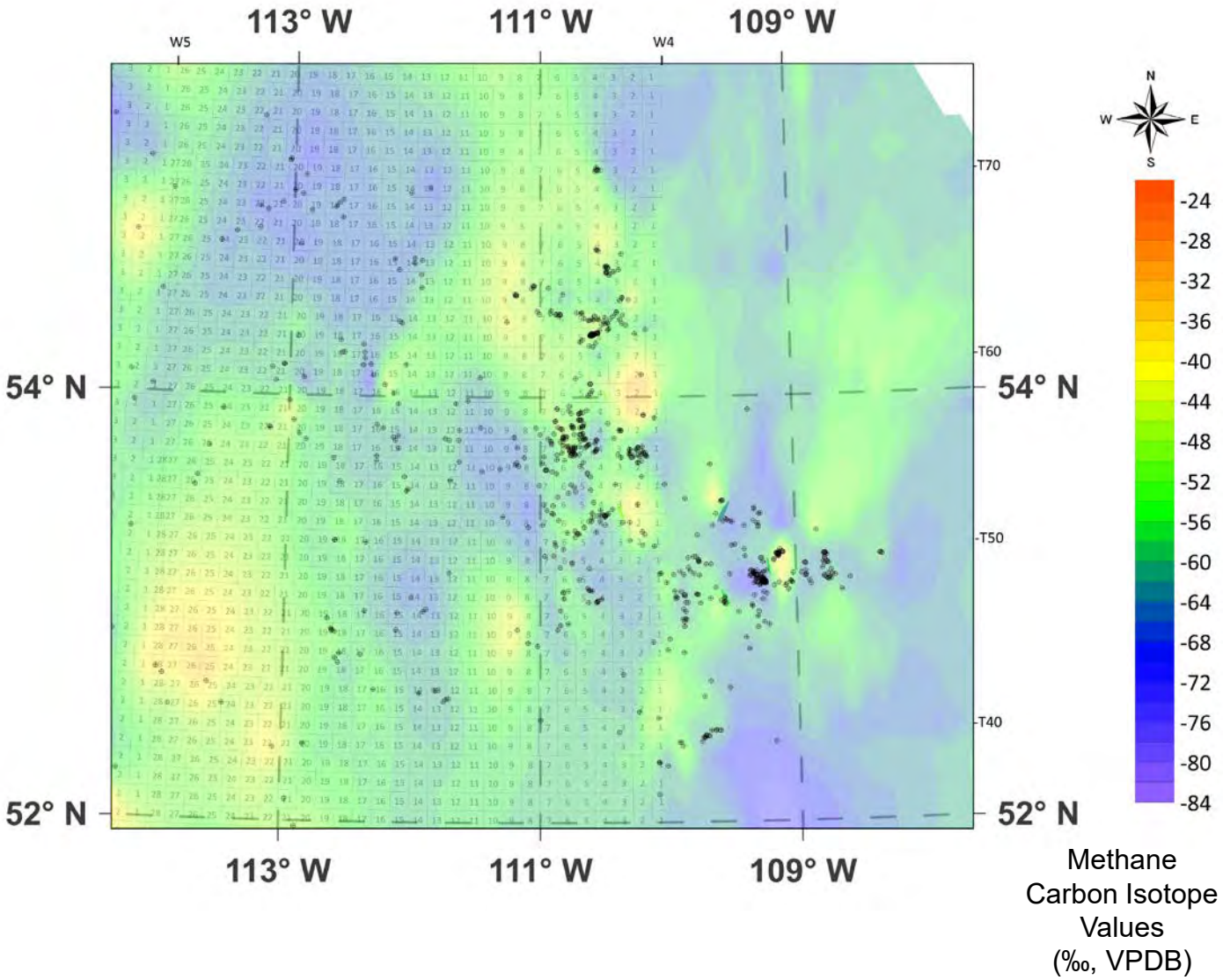

Fig. 22C. Contour Map of Ethane Carbon Isotope Values of GM Eastern Alberta Zoom-in

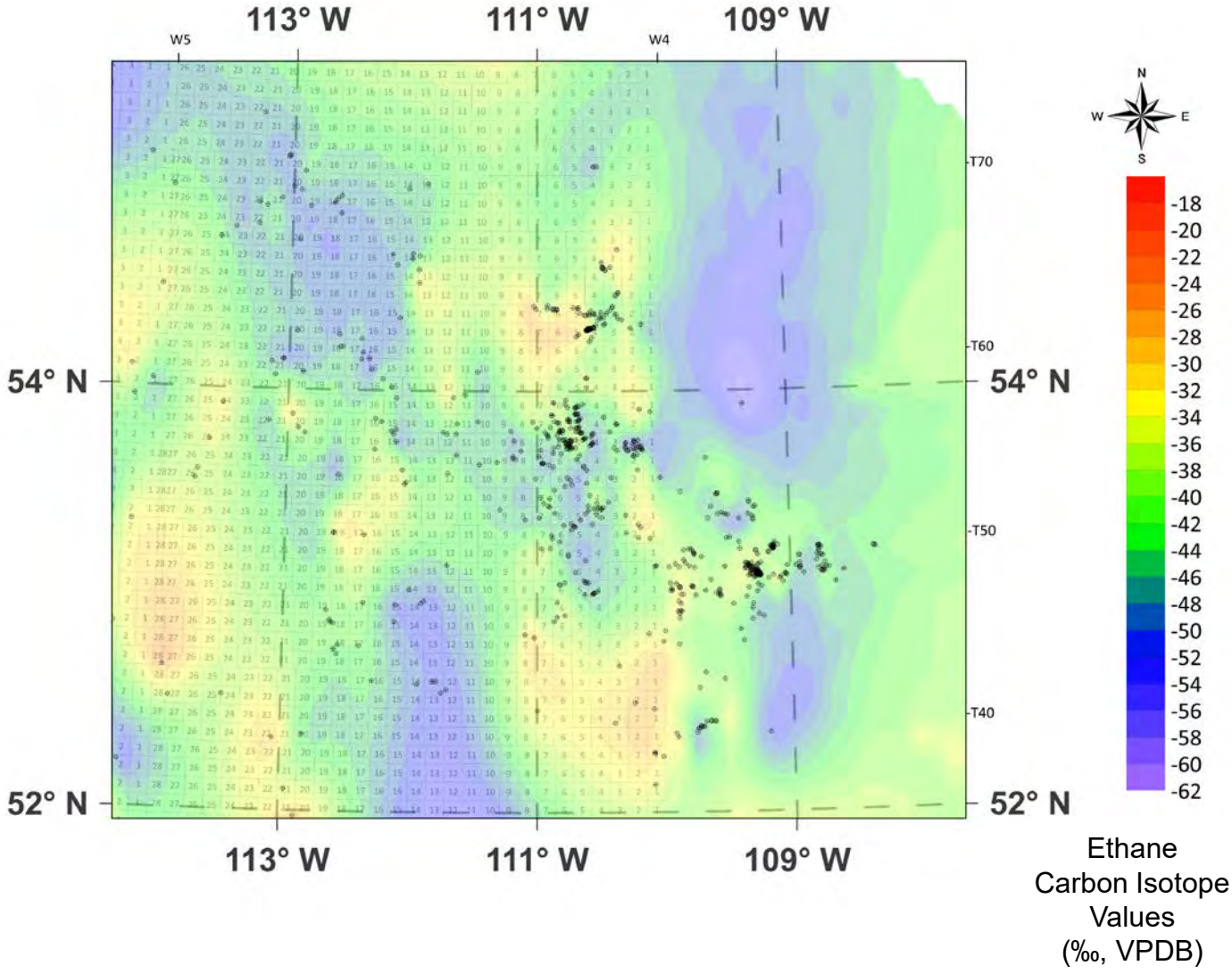

Fig. 22D. Contour Map of Propane Carbon Isotope Values of GM Eastern Alberta Zoom-in

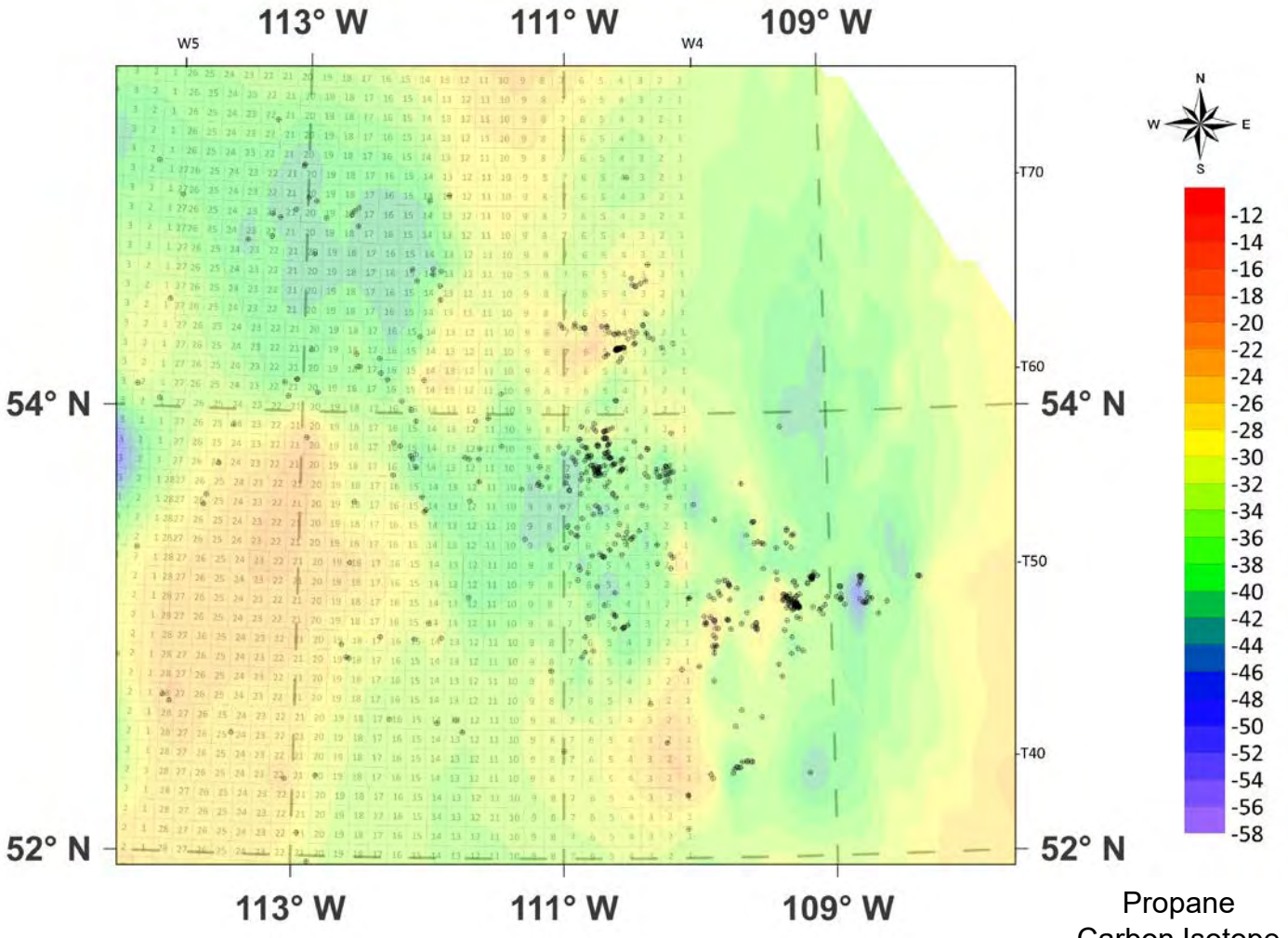

Fig. 22E. Contour Map of *n*-Butane Carbon Isotope Values of GM Eastern Alberta Zoom-in

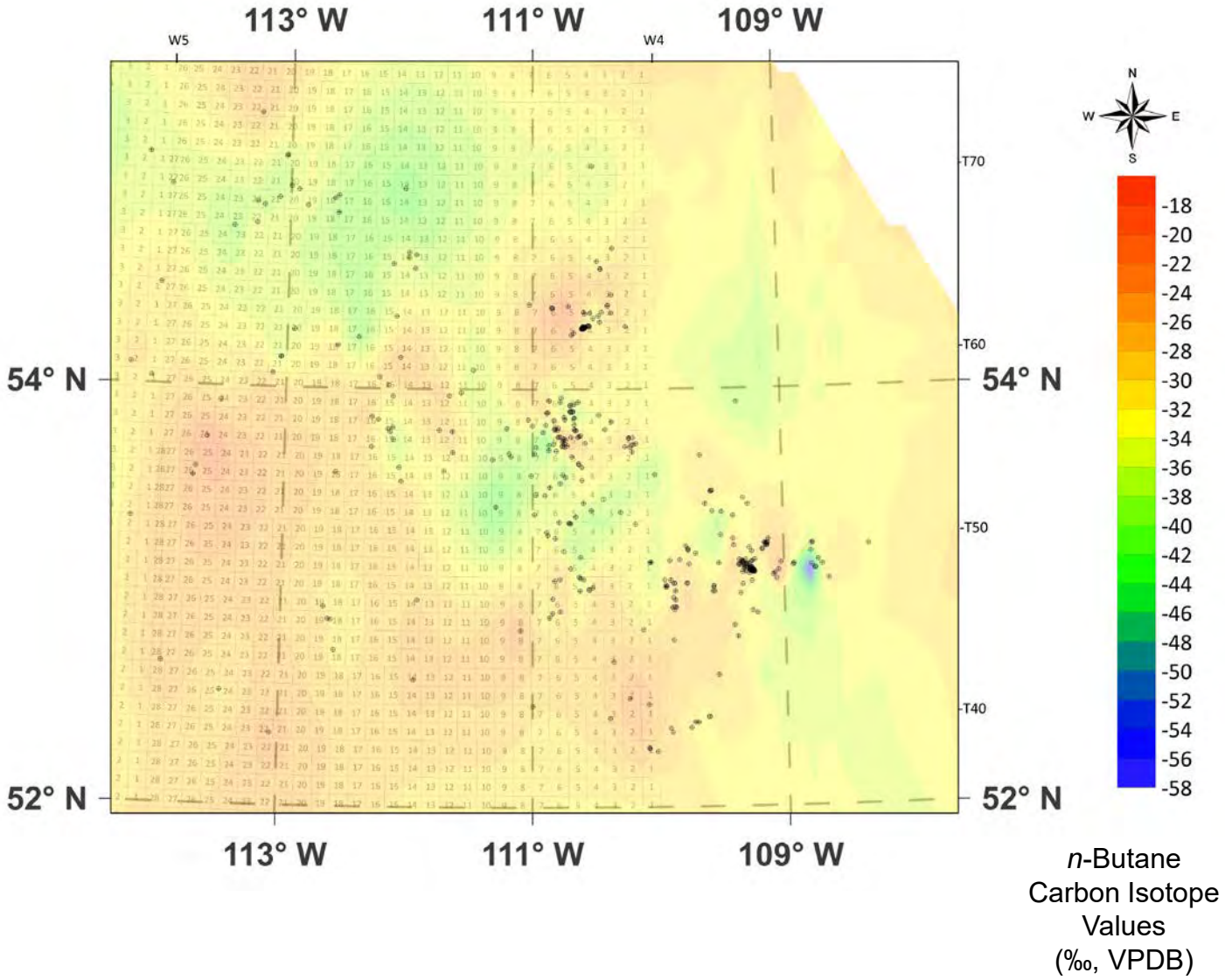

Fig. 22F. Contour Map of *i*-Butane Carbon Isotope Values of GM Eastern Alberta Zoom-in

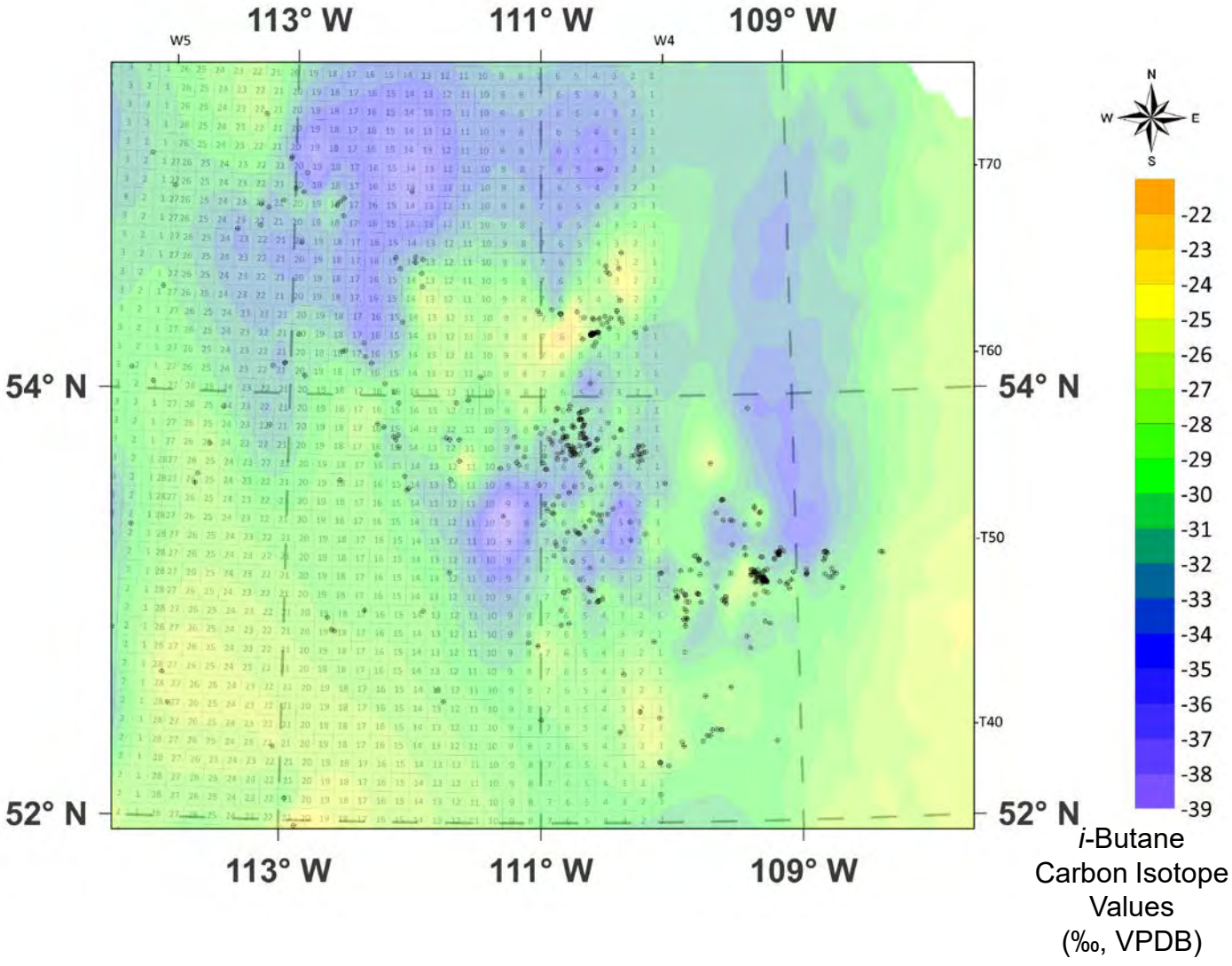

Fig. 22G. Contour Map of Carbon Dioxide Carbon Isotope Values of GM Eastern Alberta Zoom-in

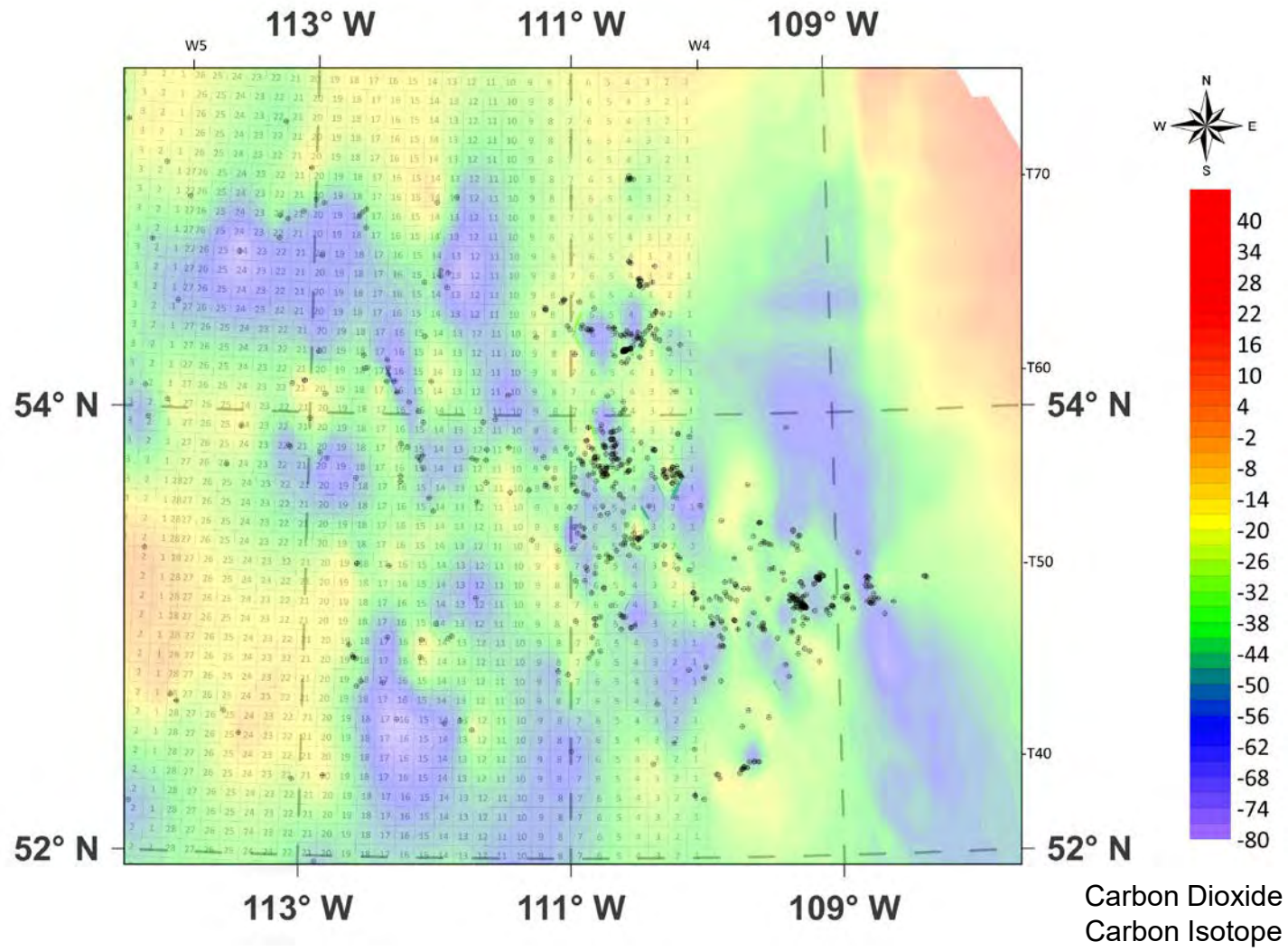

Fig. 22H. Contour Map of Methane Carbon Isotope Values of GM Eastern Alberta Zoom-in over Topographic Map

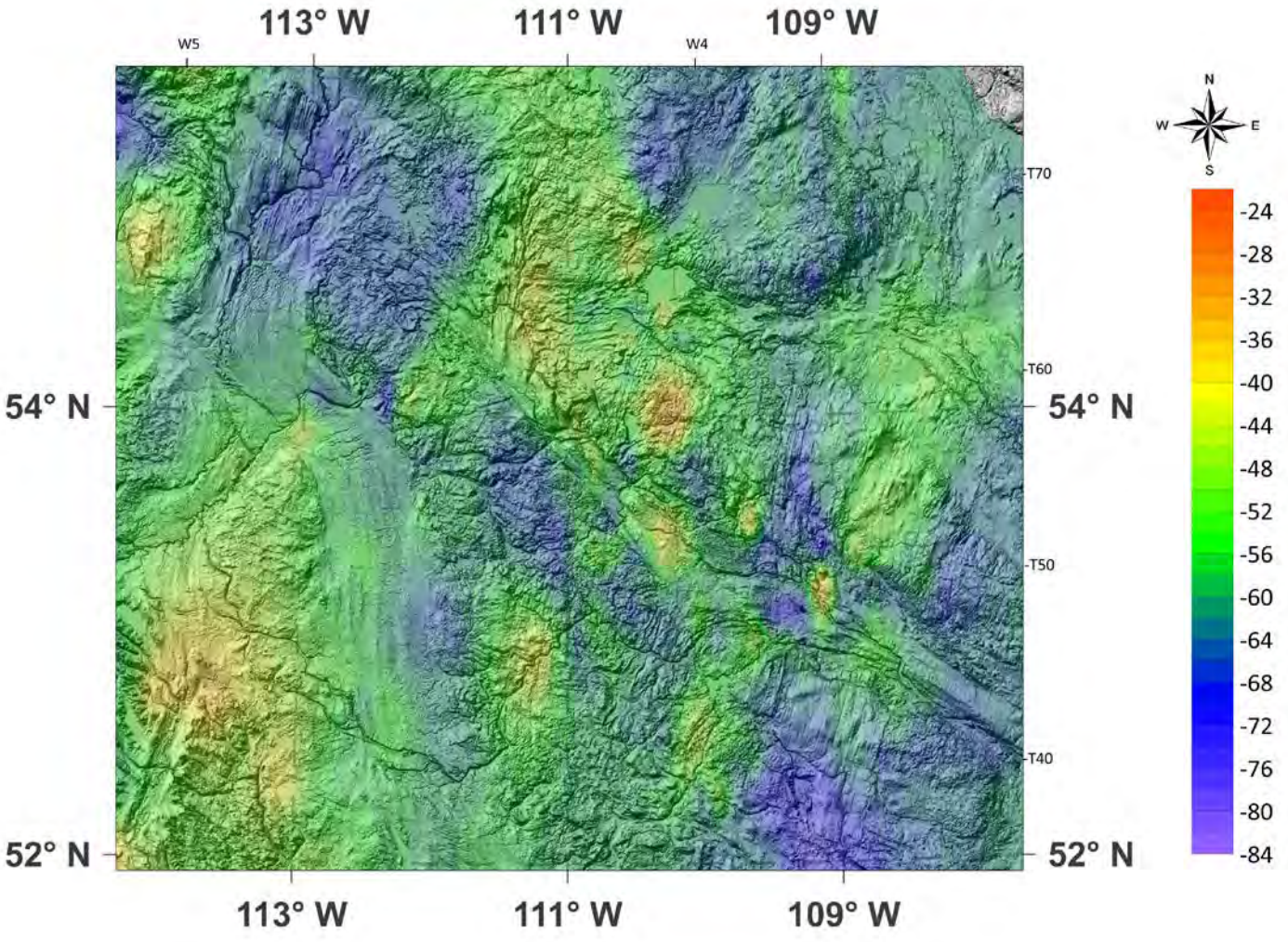

Methane Carbon Isotope Values (‰, VPDB)

Fig. 22I. Contour Map of Ethane Carbon Isotope Values of GM Eastern Alberta Zoom-in over Topographic Map

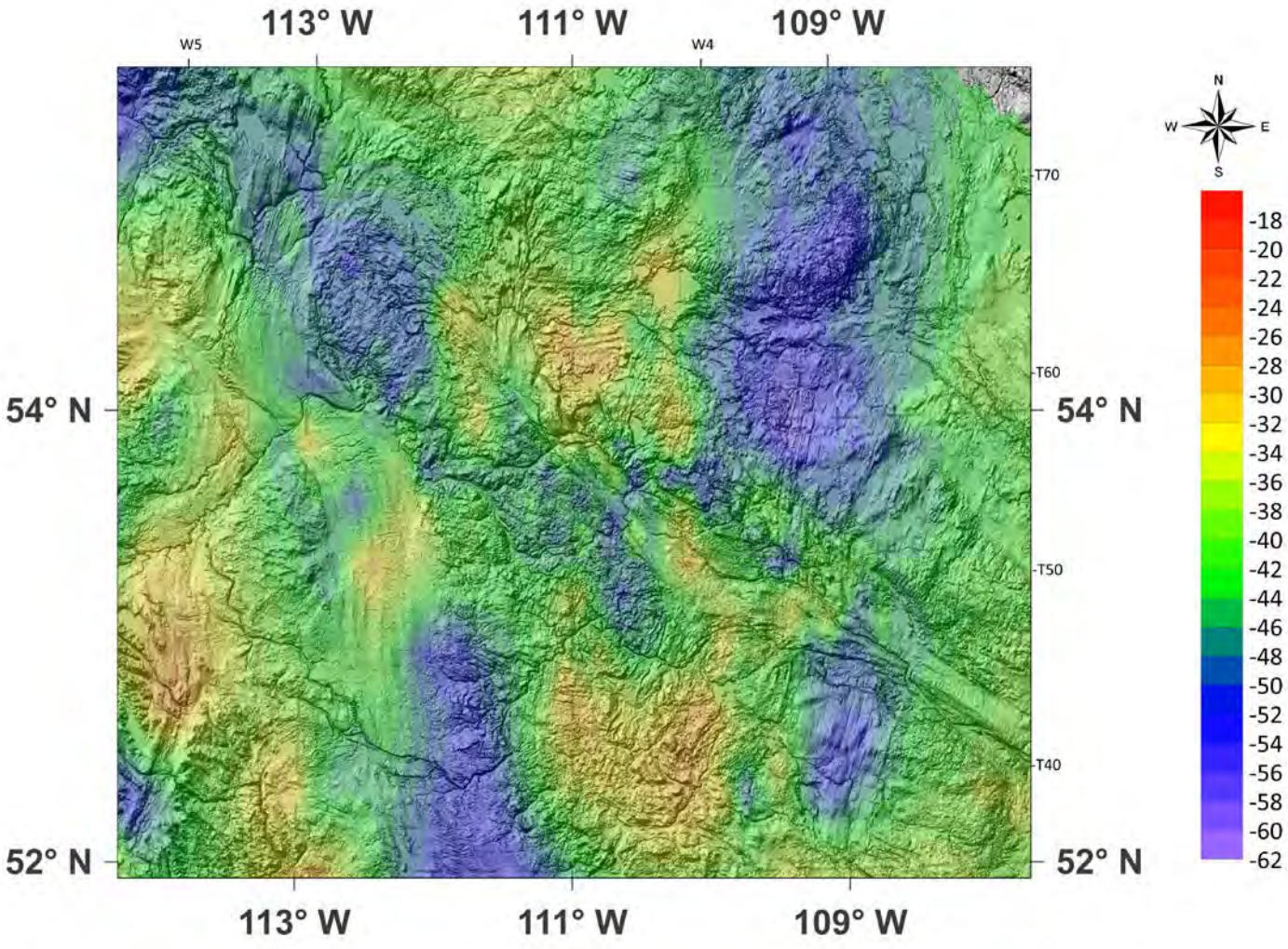

Ethane Carbon Isotope Values (‰, VPDB)

Fig. 22J. Contour Map of Propane Carbon Isotope Values of GM Eastern Alberta Zoom-in over Topographic Map

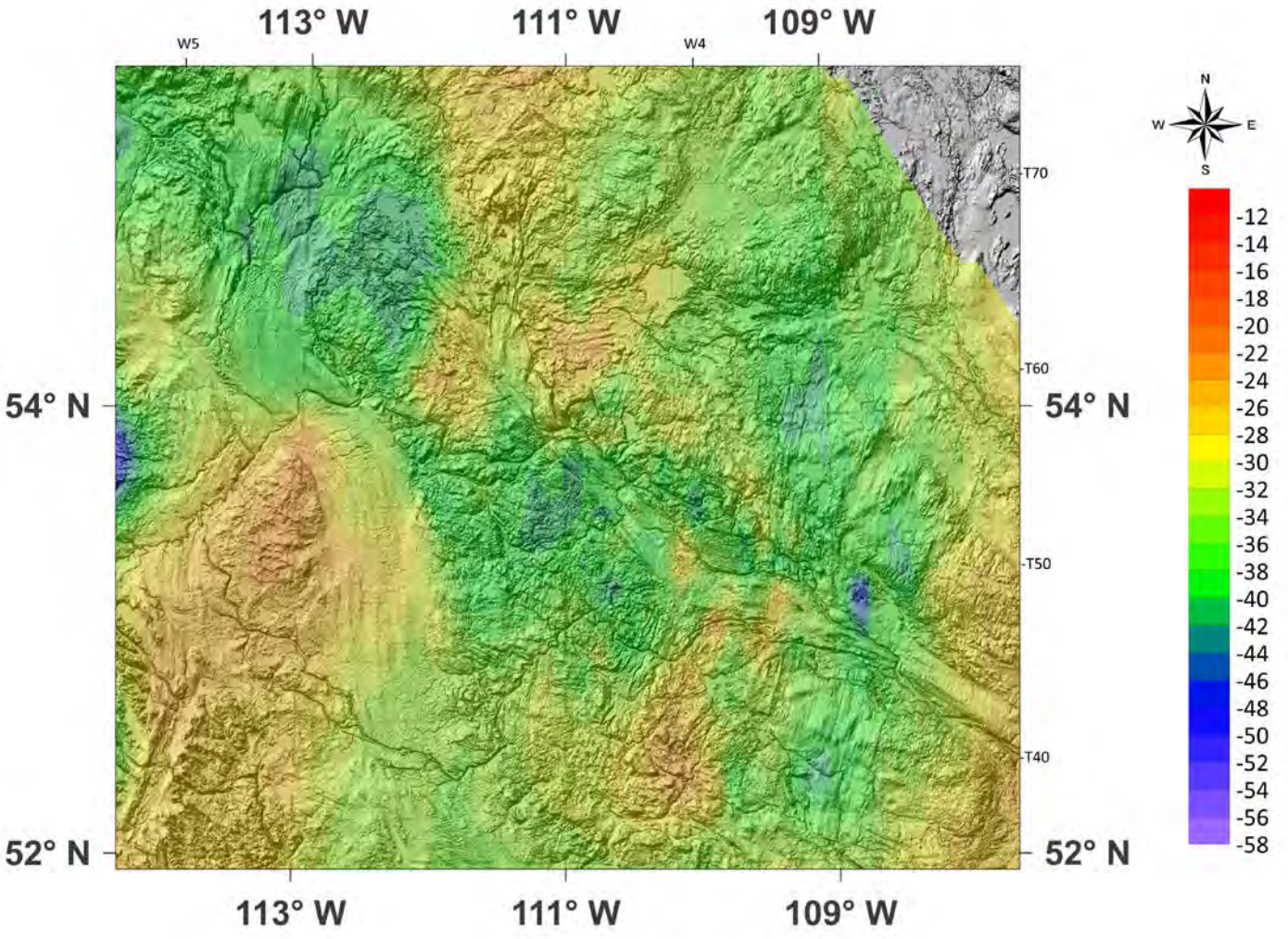

Propane Carbon Isotope Values (‰, VPDB)

Fig. 22K. Contour Map of *n*-Butane Carbon Isotope Values of GM Eastern Alberta Zoom-in over Topographic Map

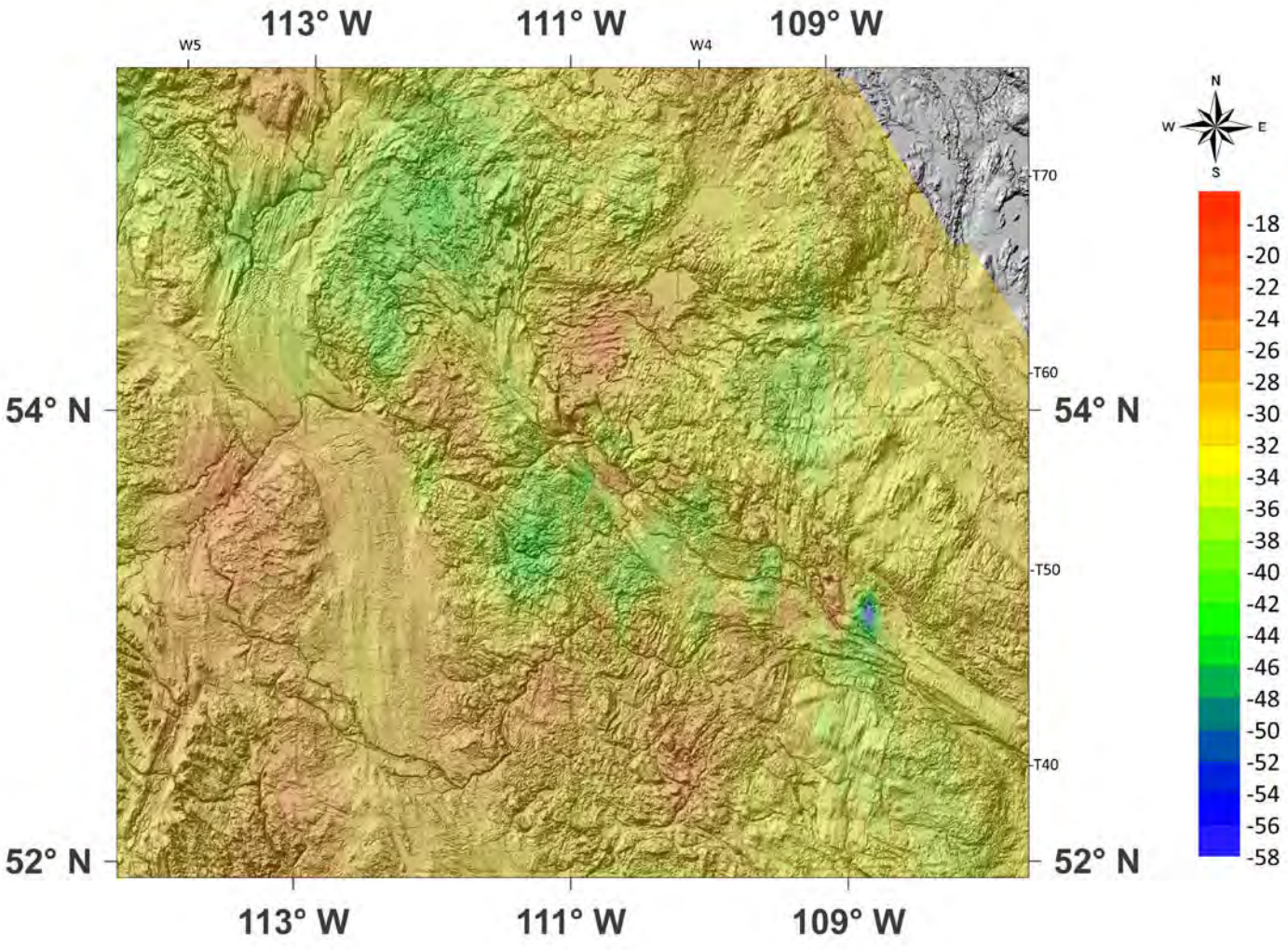

n-Butane Carbon Isotope Values (‰, VPDB)

Fig. 22L. Contour Map of *i*-Butane Carbon Isotope Values of GM Eastern Alberta Zoom-in over Topographic Map

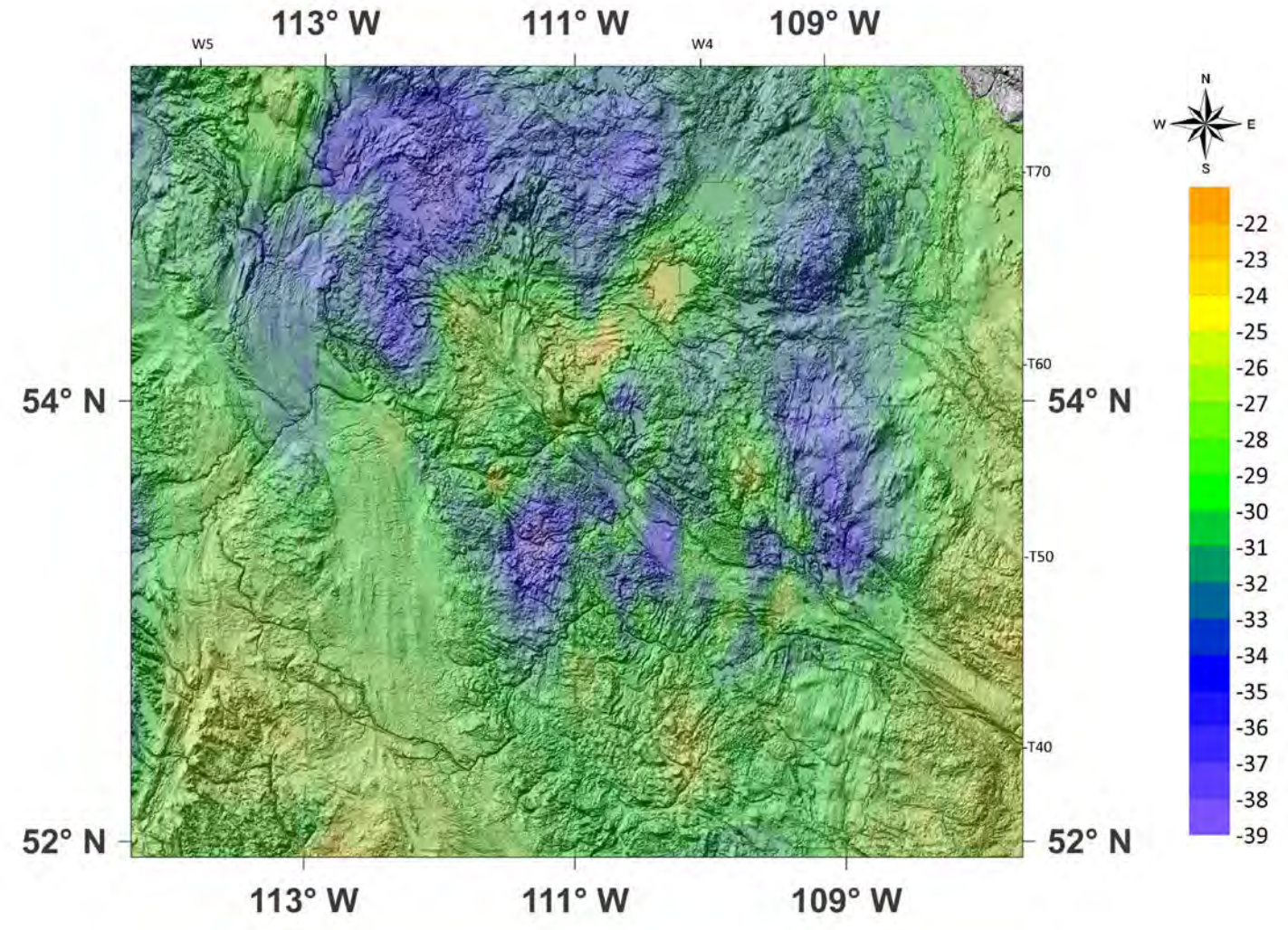

i-Butane Carbon Isotope Values (‰, VPDB)

Fig. 22M. Contour Map of Carbon Dioxide Carbon Isotope Values of GM Eastern Alberta Zoom-in over Topographic Map

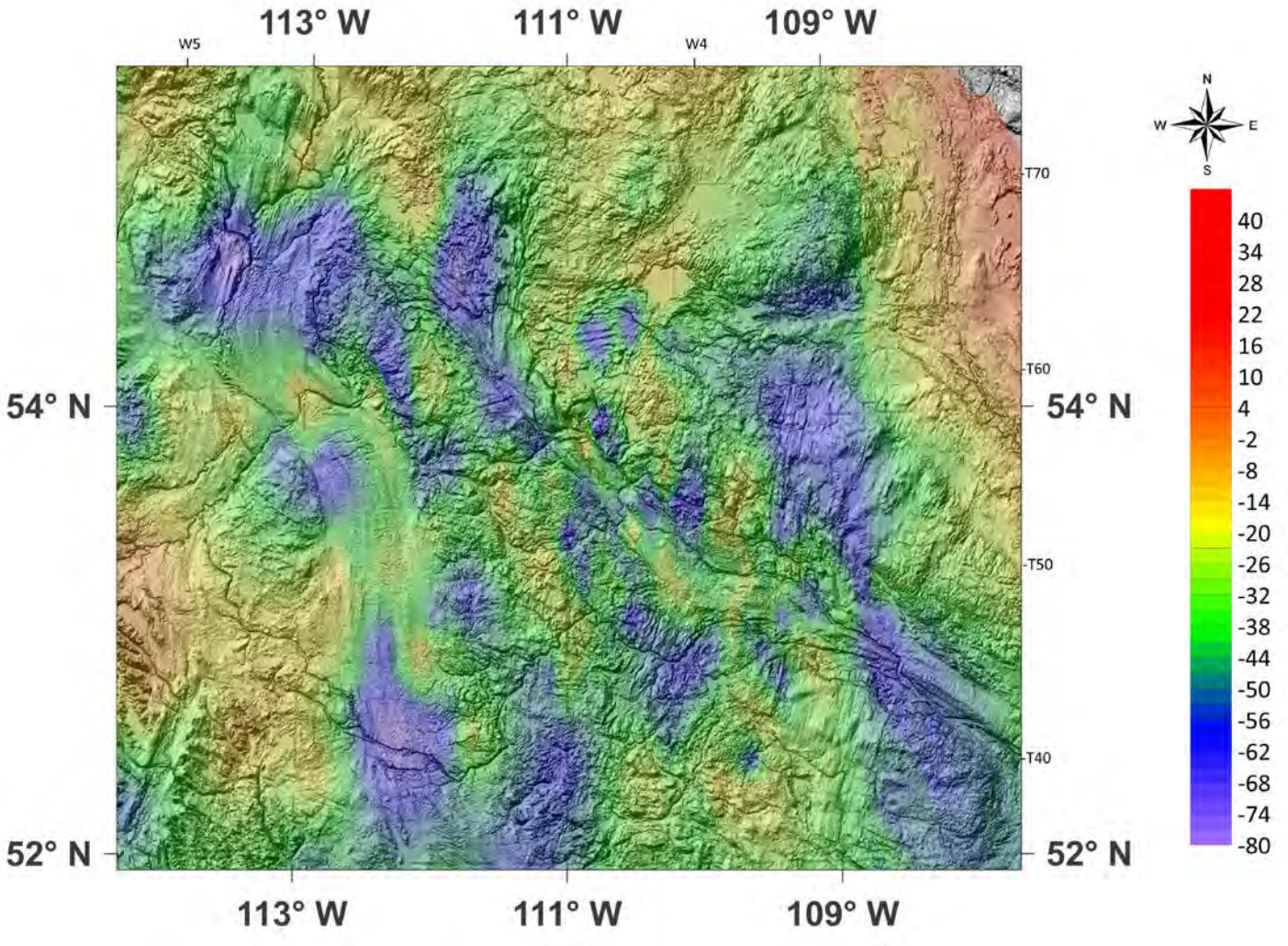

Carbon Dioxide Carbon Isotope Values (‰, VPDB)

Fig. 23A. Map of Surface Casing Vent (SCV) Locations in the Lloydminster Zoom-in

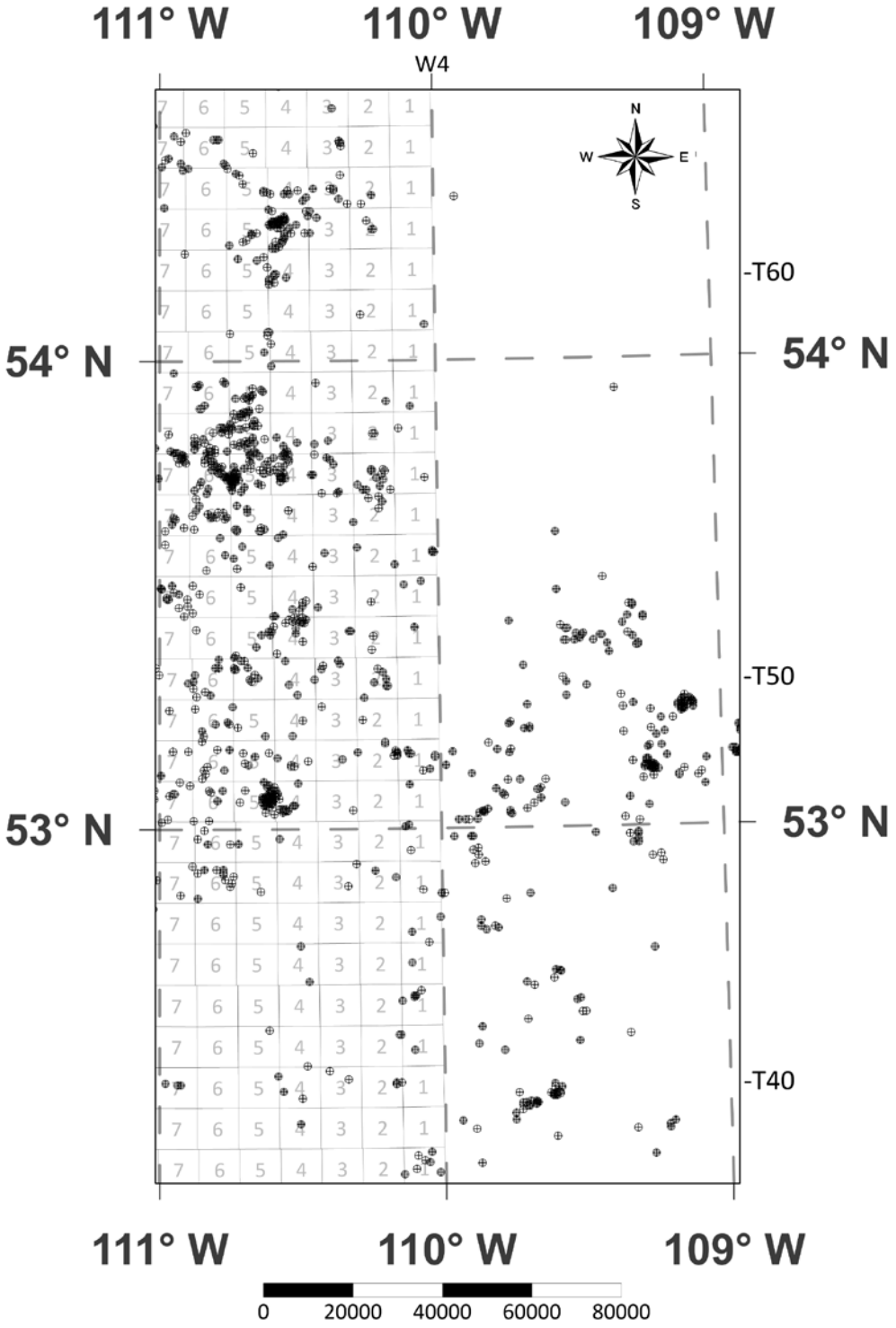

Fig. 23B. Contour Map of Methane Carbon Isotope Values of SCV Lloydminster Zoom-in

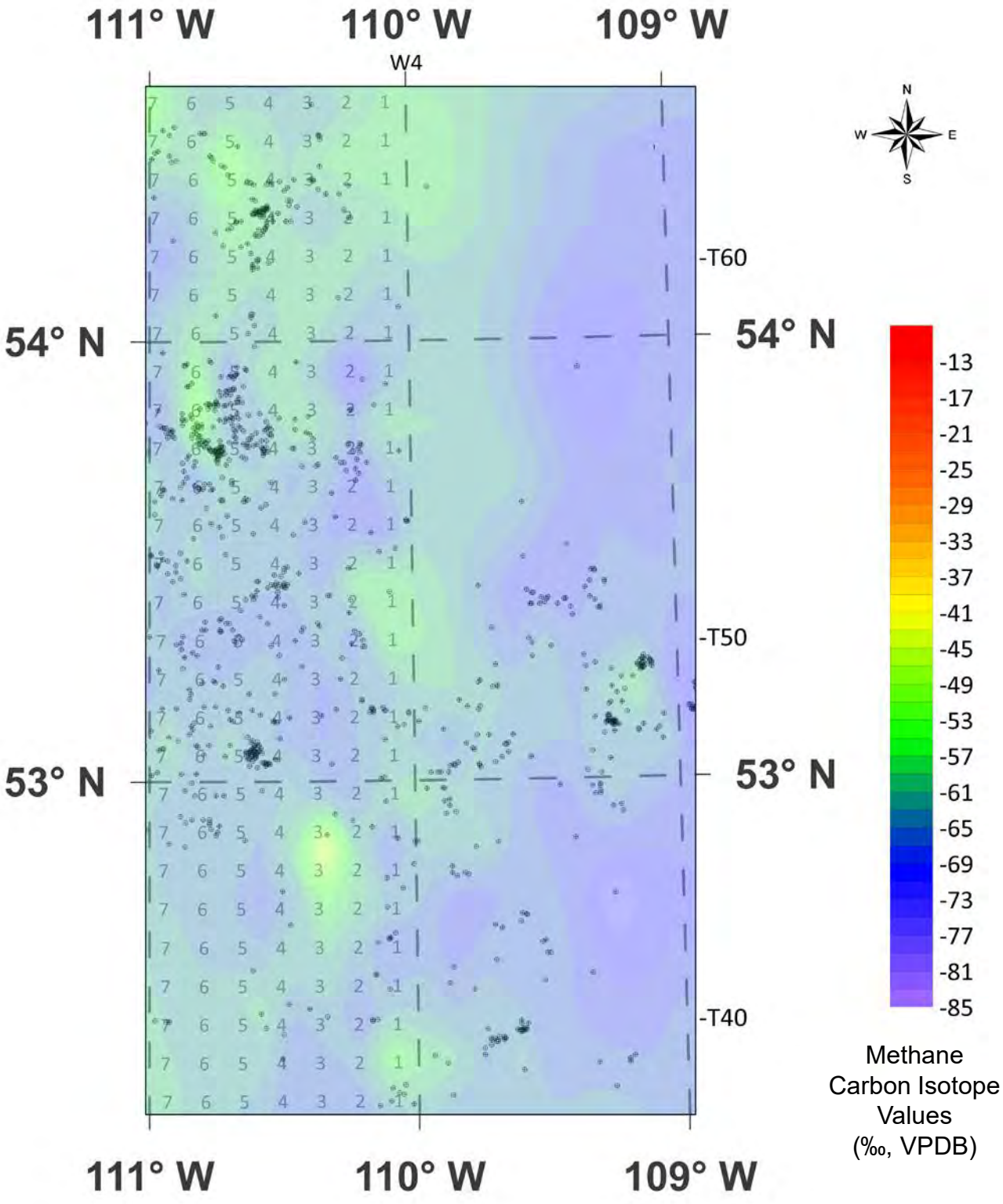

Fig. 23C. Contour Map of Ethane Carbon Isotope Values of SCV Lloydminster Zoom-in

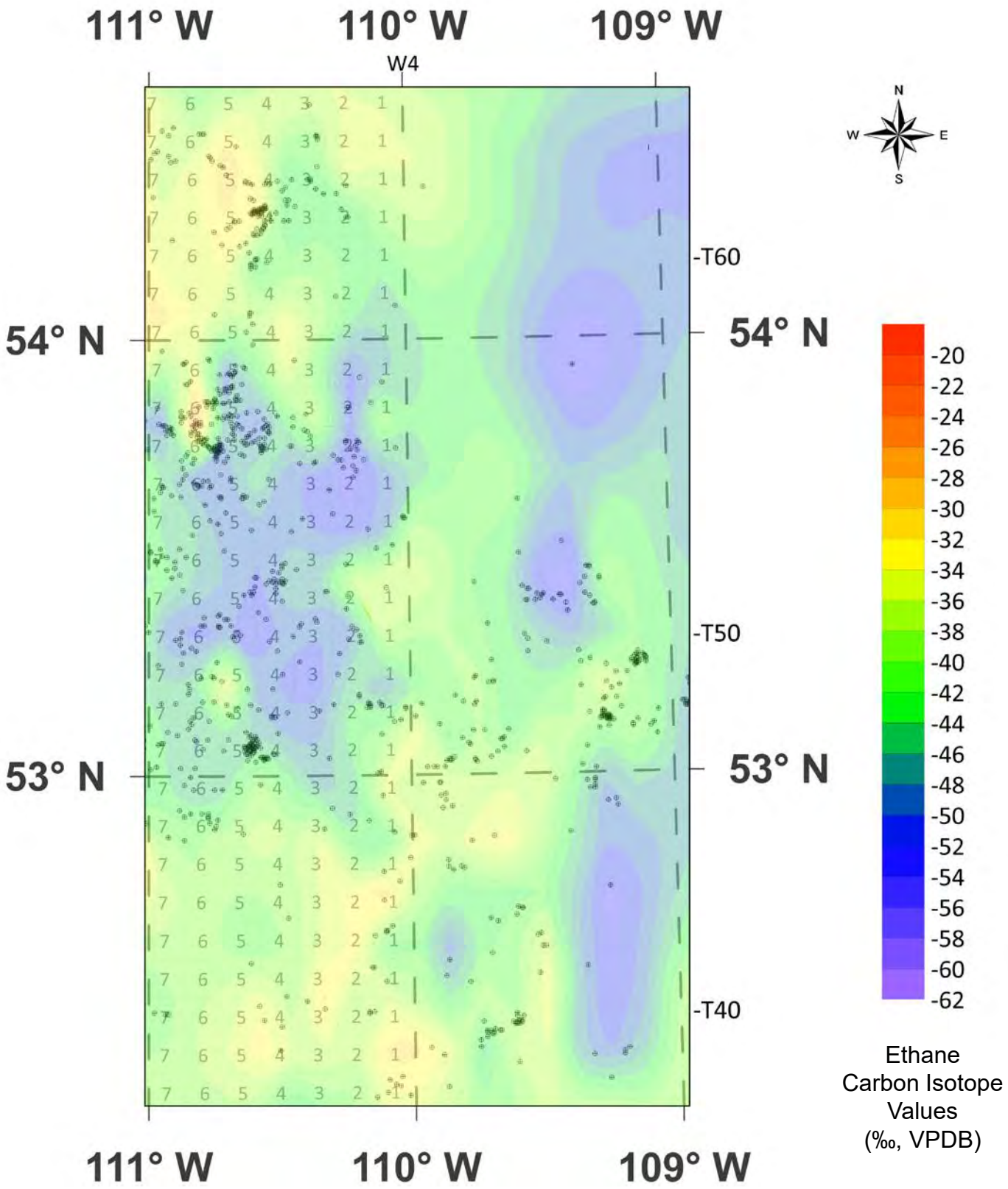

Fig. 23D. Contour Map of Propane Carbon Isotope Values of SCV Lloydminster Zoom-in

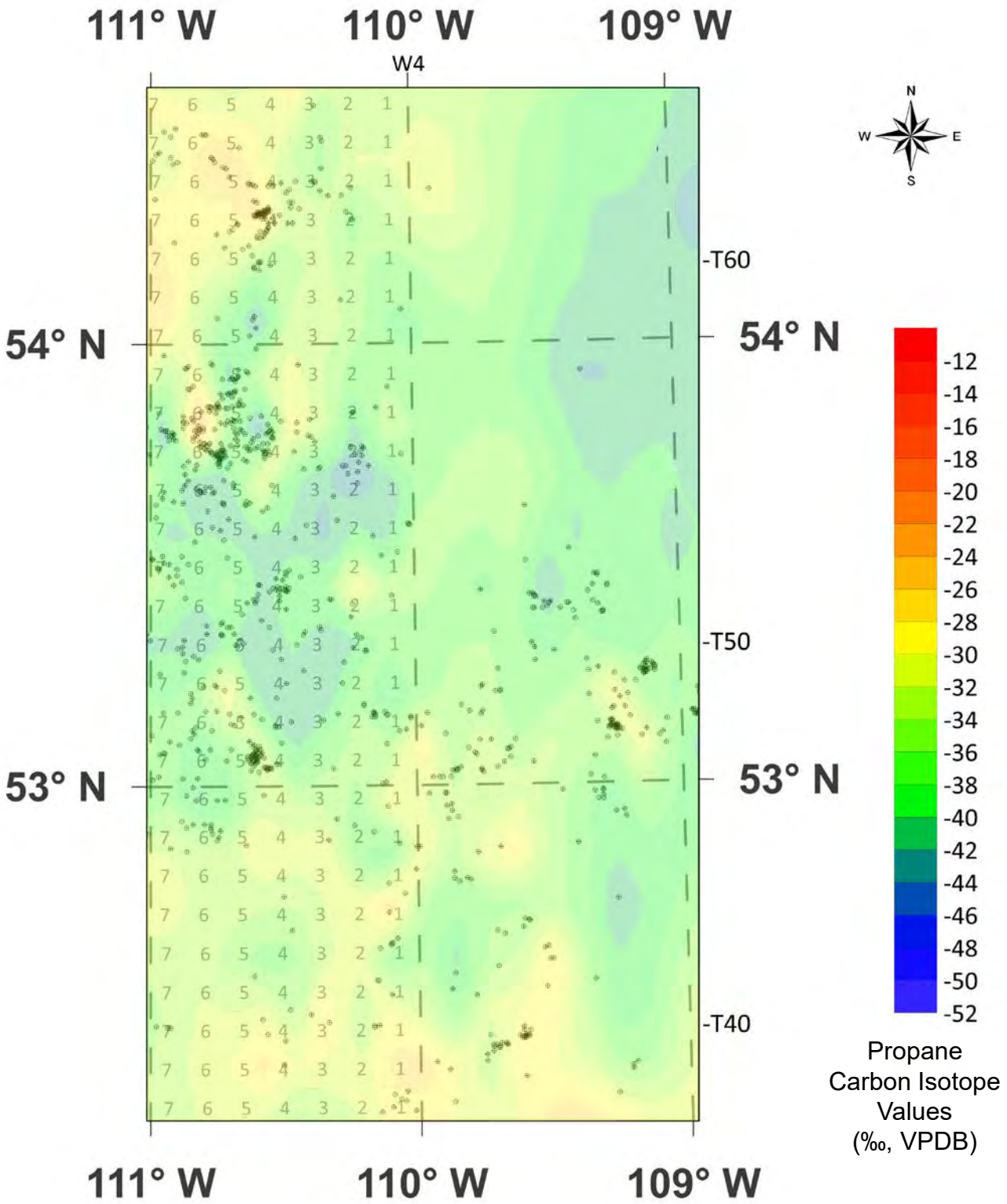

Fig. 23E. Contour Map of *n*-Butane Carbon Isotope Values of SCV Lloydminster Zoom-in

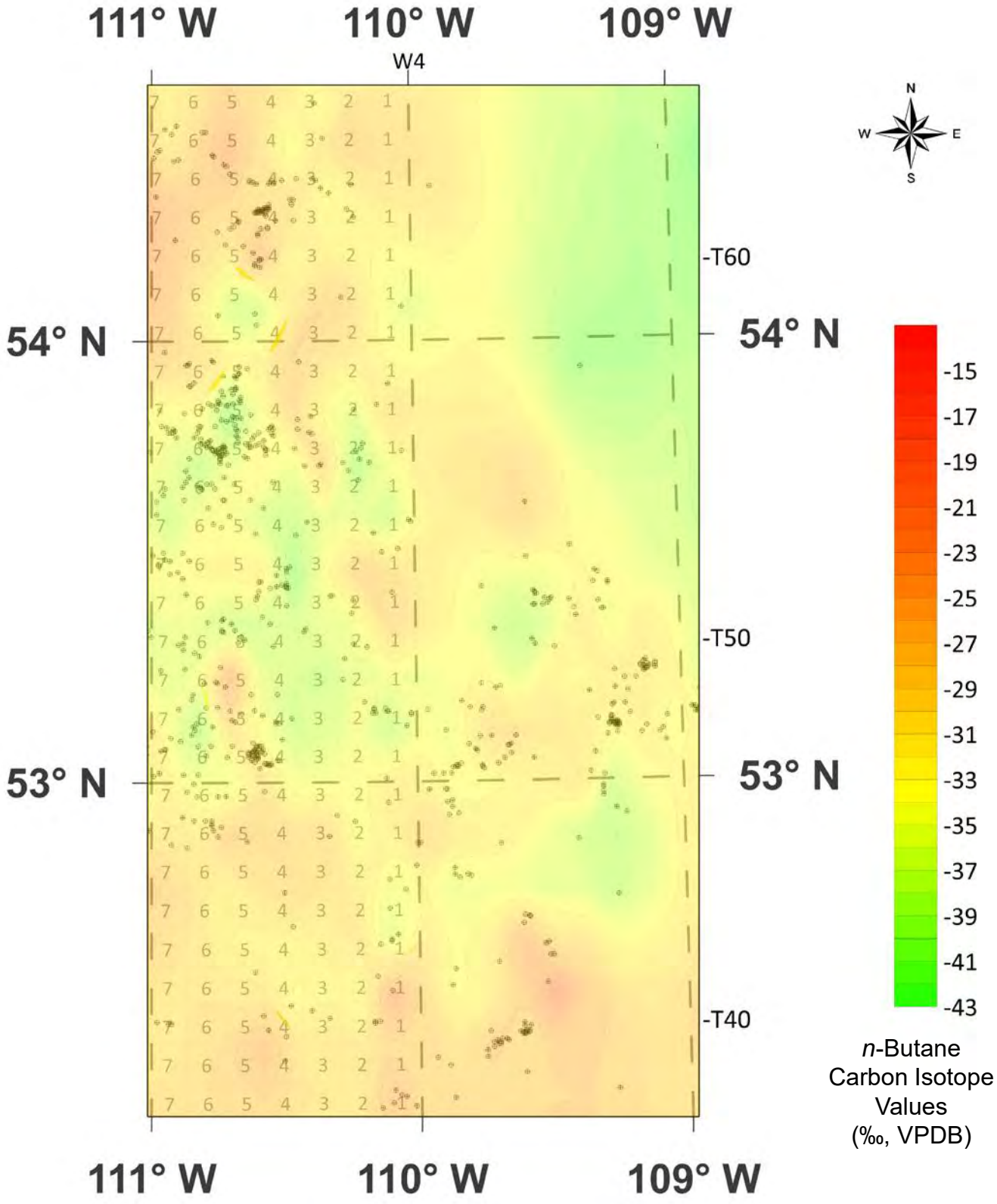

Fig. 23F. Contour Map of *i*-Butane Carbon Isotope Values of SCV Lloydminster Zoom-in

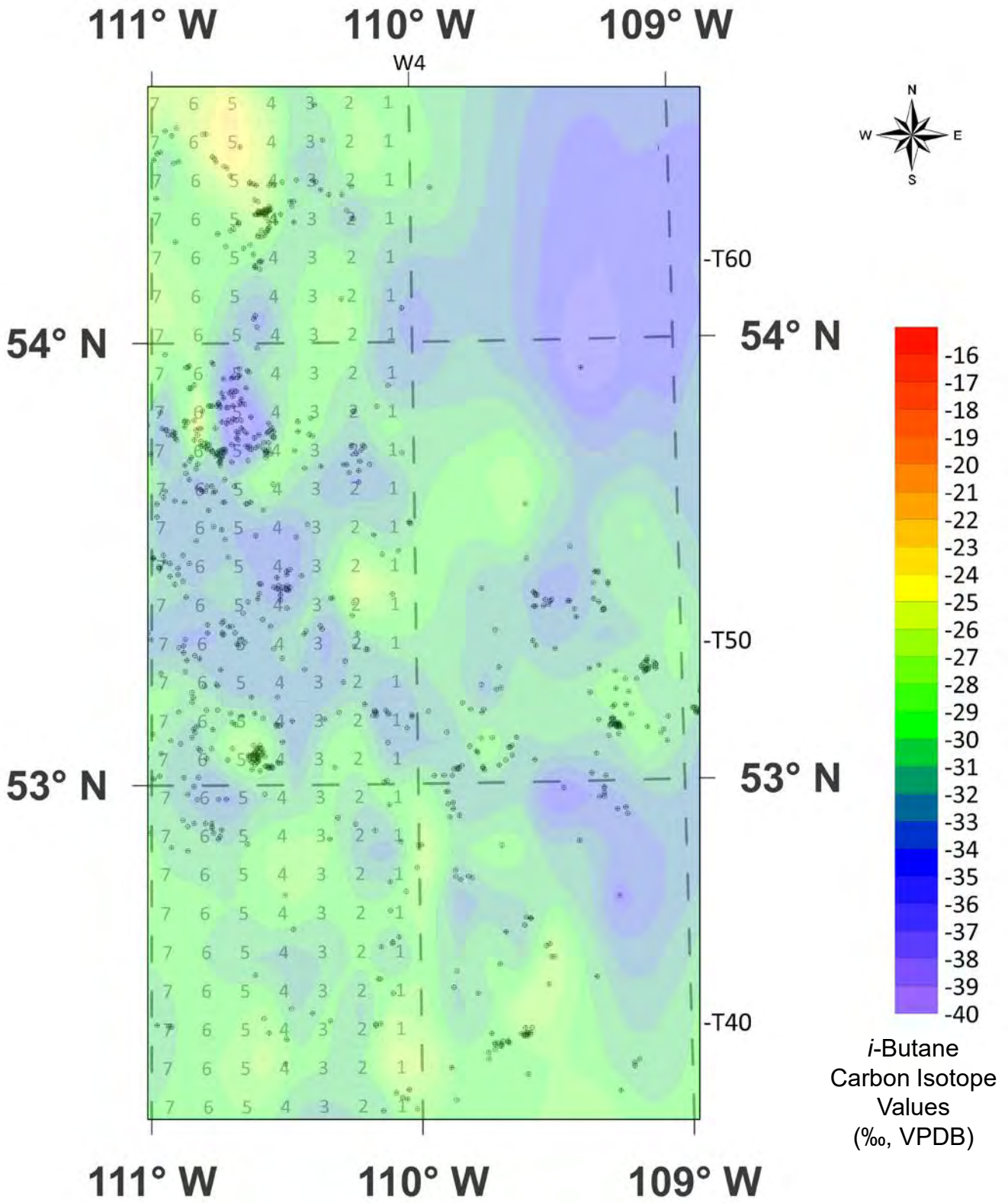

Fig. 23G. Contour Map of Carbon Dioxide Carbon Isotope Values of SCV Lloydminster Zoom-in

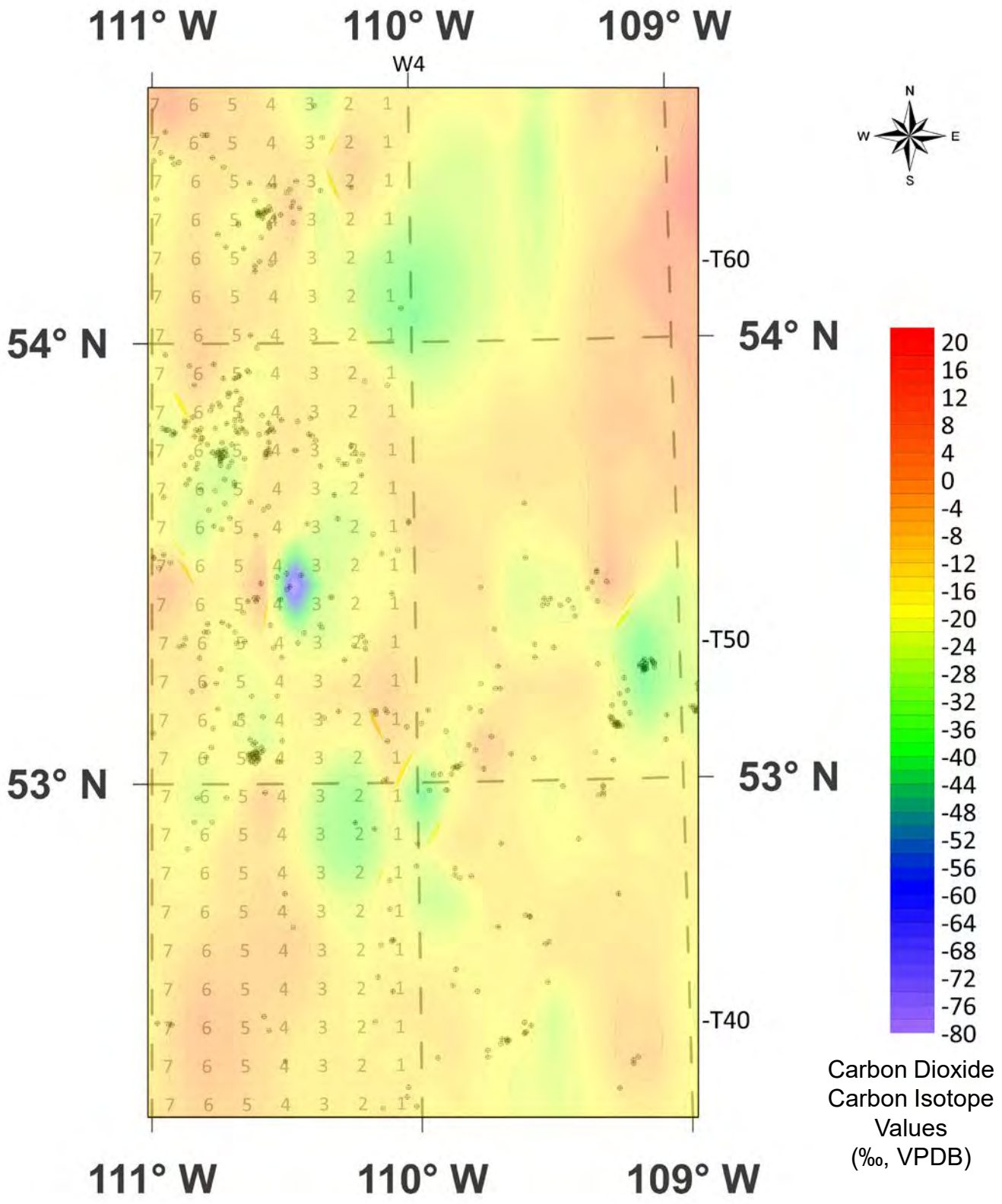

Fig. 23H. Contour Map of Methane Carbon Isotope Values of SCV Lloydminster Zoom-in over Topographic Map

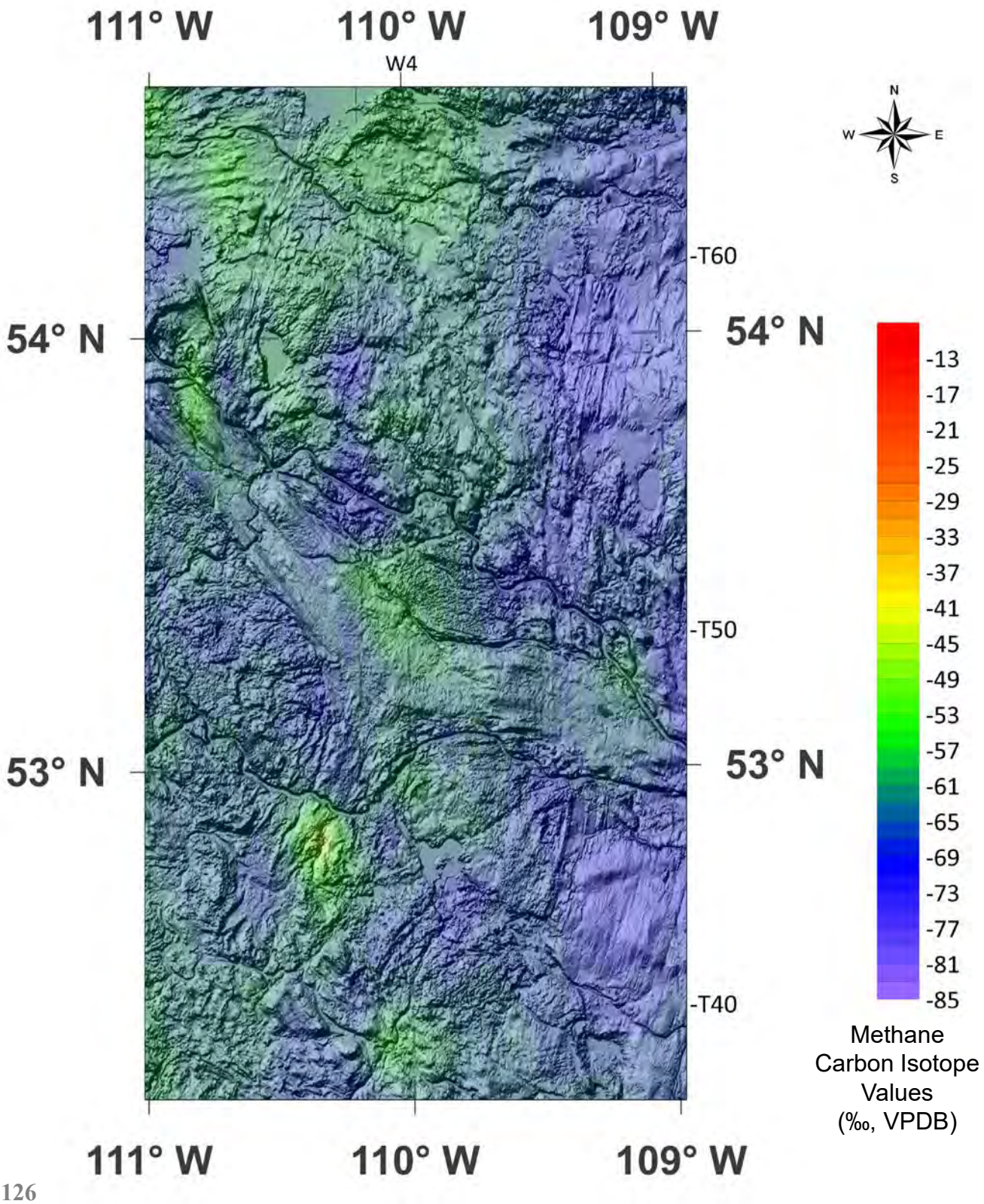

Fig. 23I. Contour Map of Ethane Carbon Isotope Values of SCV Lloydminster Zoom-in over Topographic Map

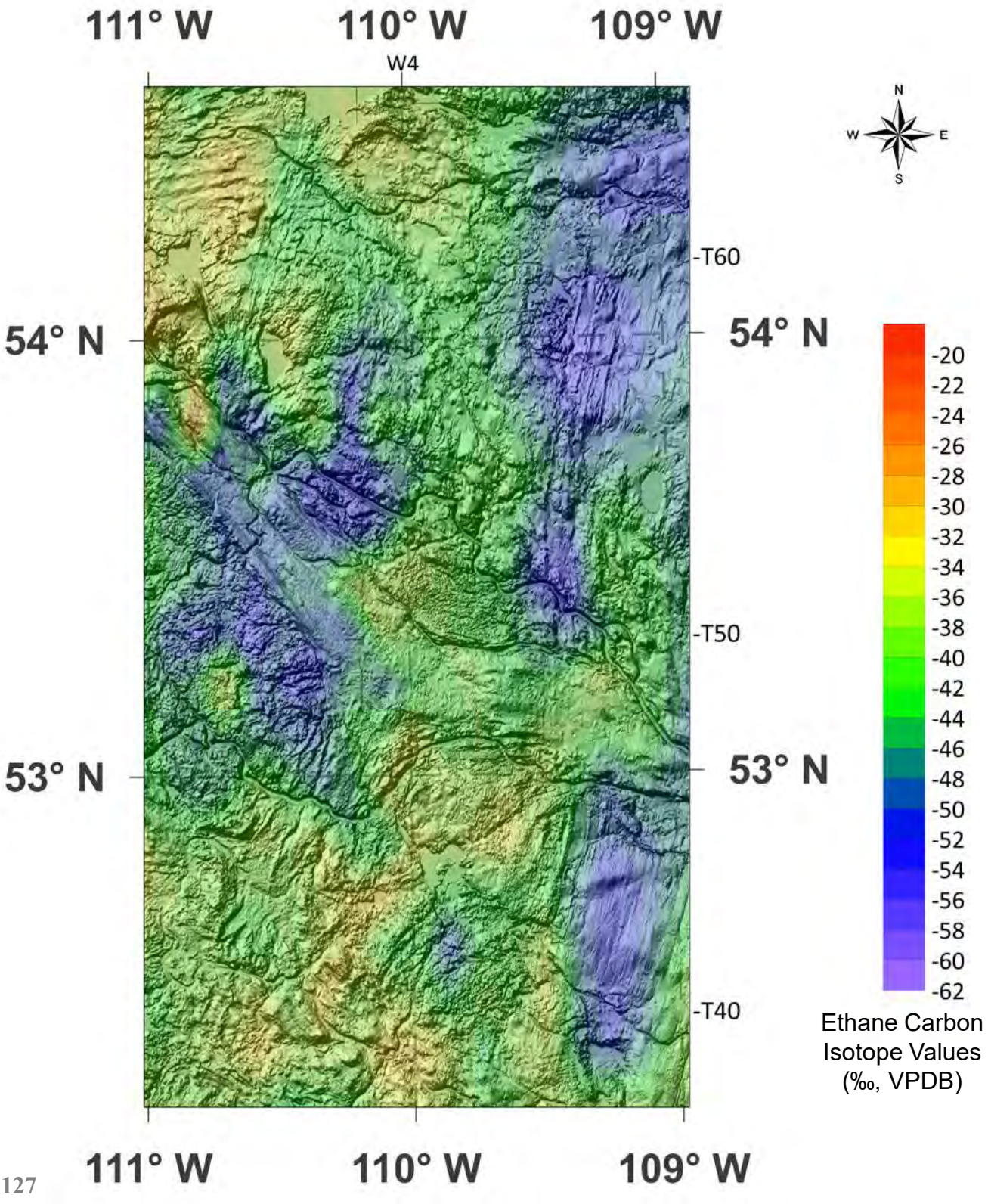

Fig. 23J. Contour Map of Propane Carbon Isotope Values of SCV Lloydminster Zoom-in over Topographic Map

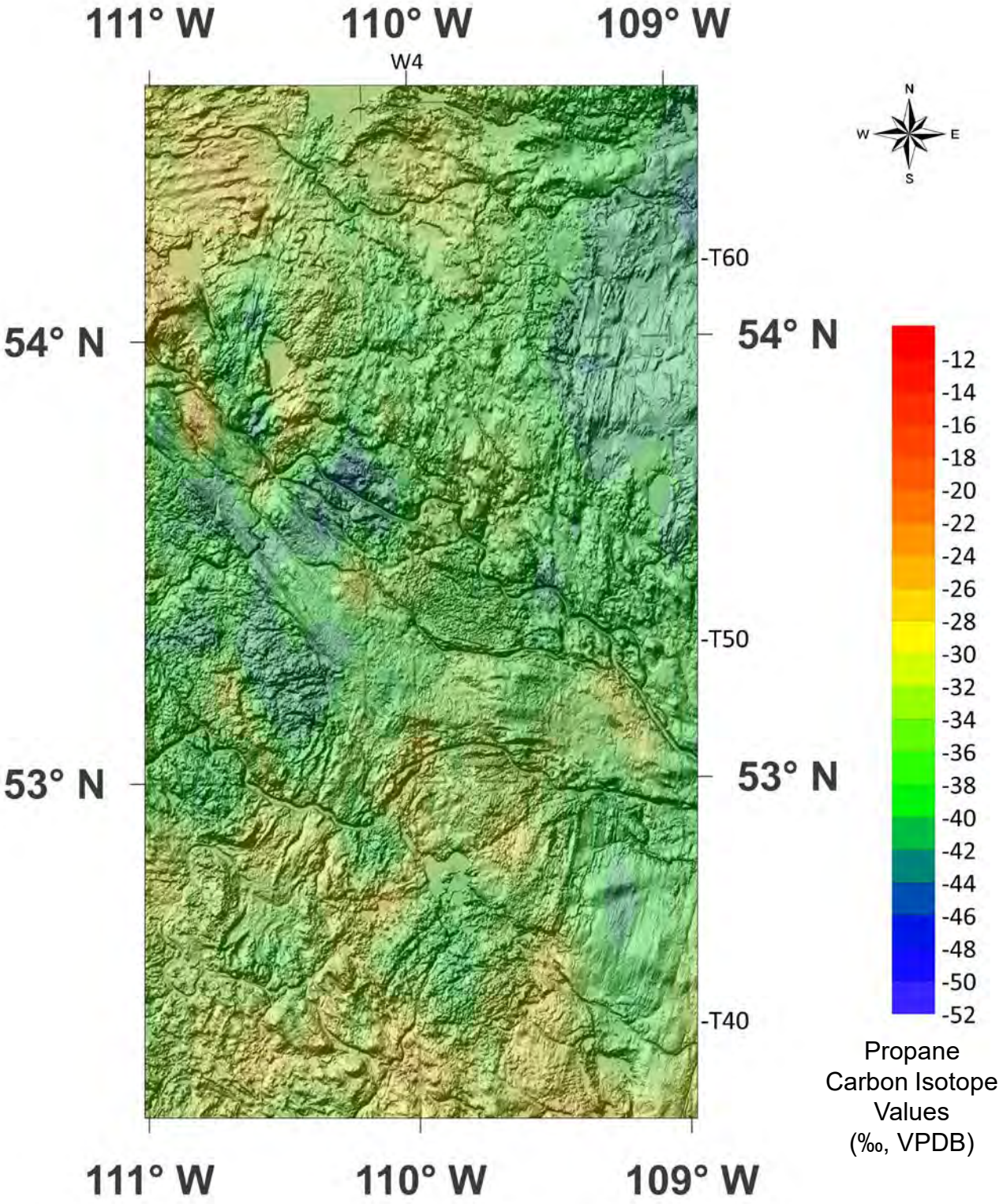

Fig. 23K. Contour Map of *n*-Butane Carbon Isotope Values of SCV Lloydminster Zoom-in over Topographic Map

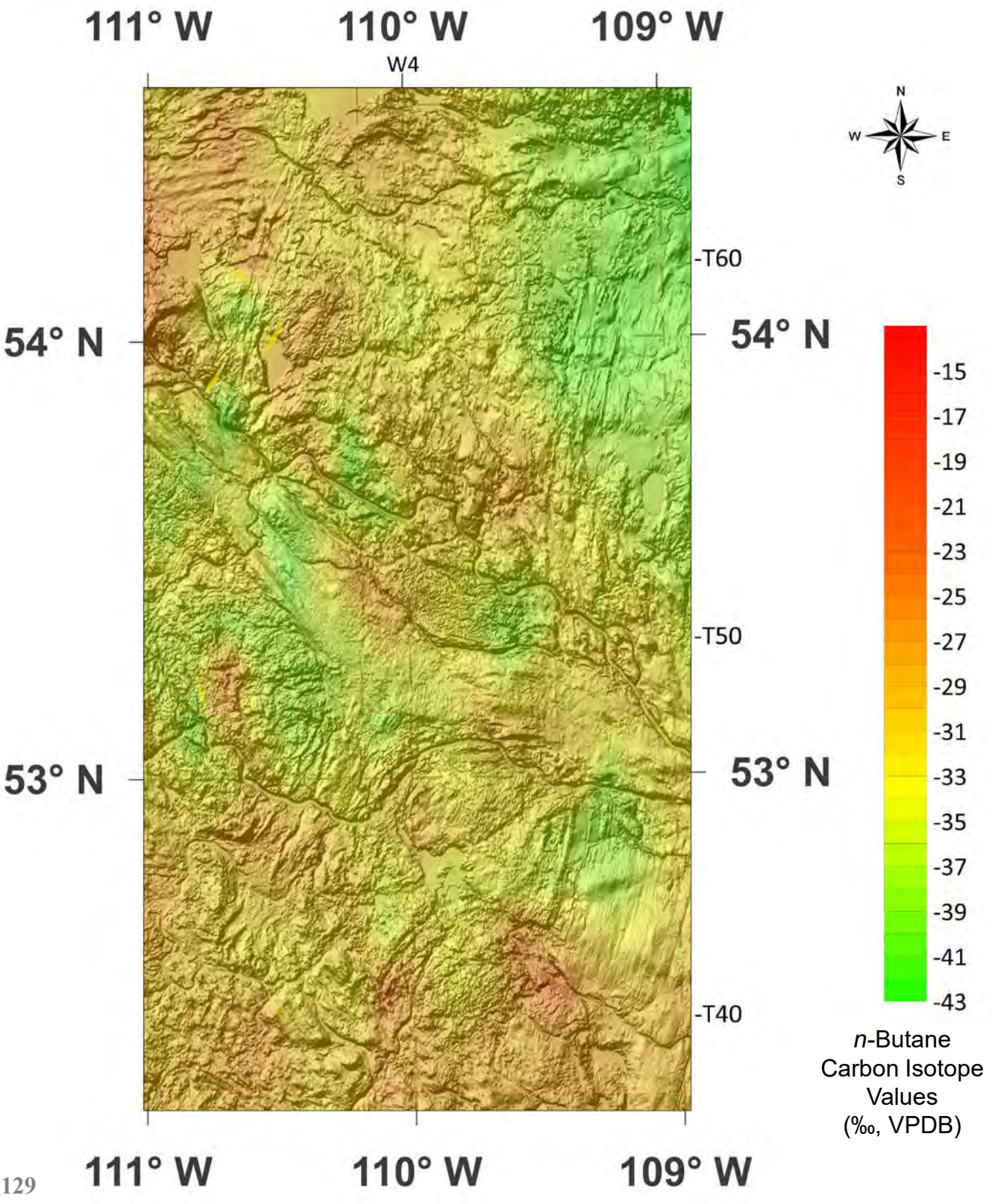

Fig. 23K. Contour Map of *i*-Butane Carbon Isotope Values of SCV Lloydminster Zoom-in over Topographic Map

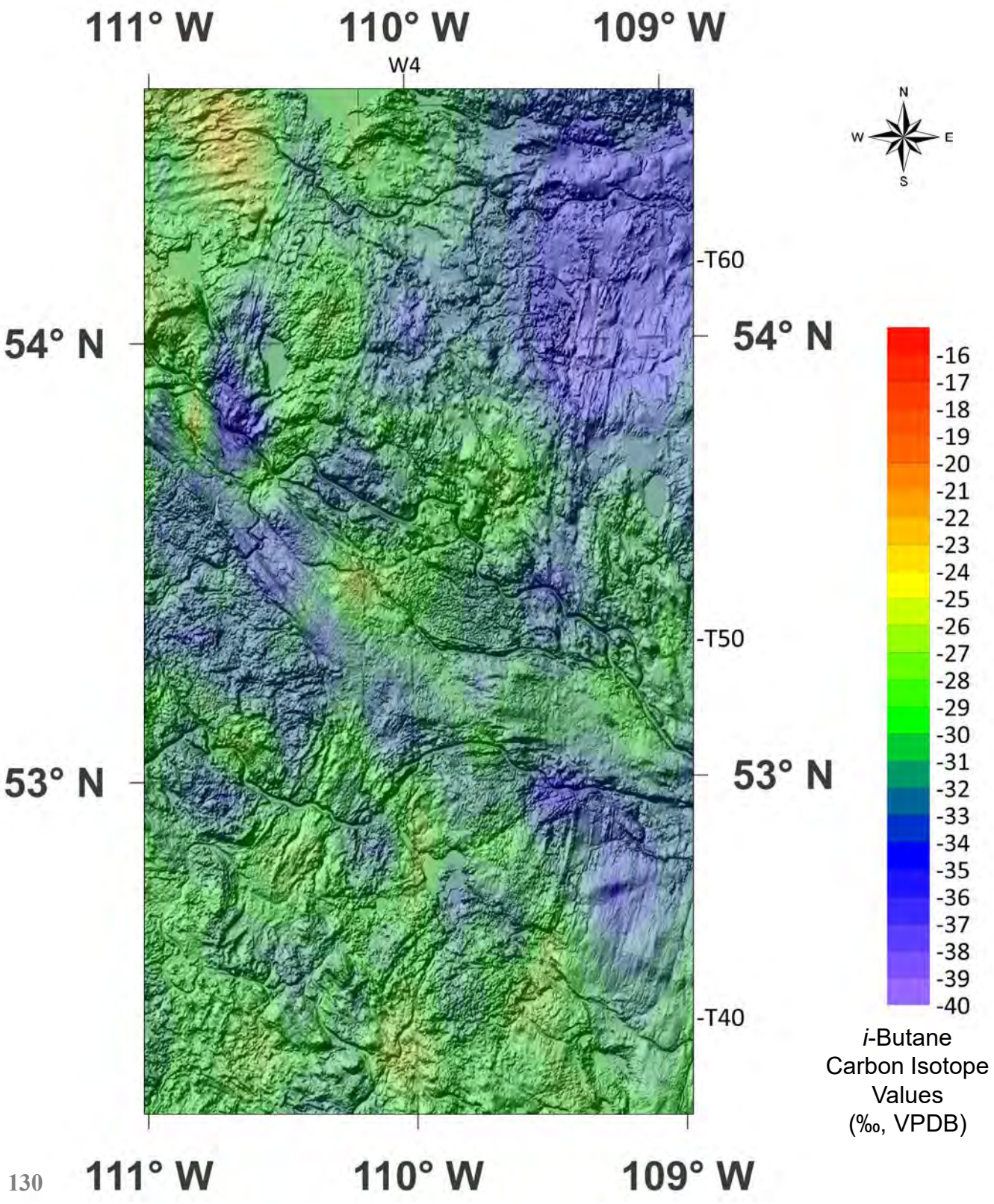

Fig. 23M. Contour Map of Carbon Dioxide Carbon Isotope Values of SCV Lloydminster Zoom-in over Topographic Map

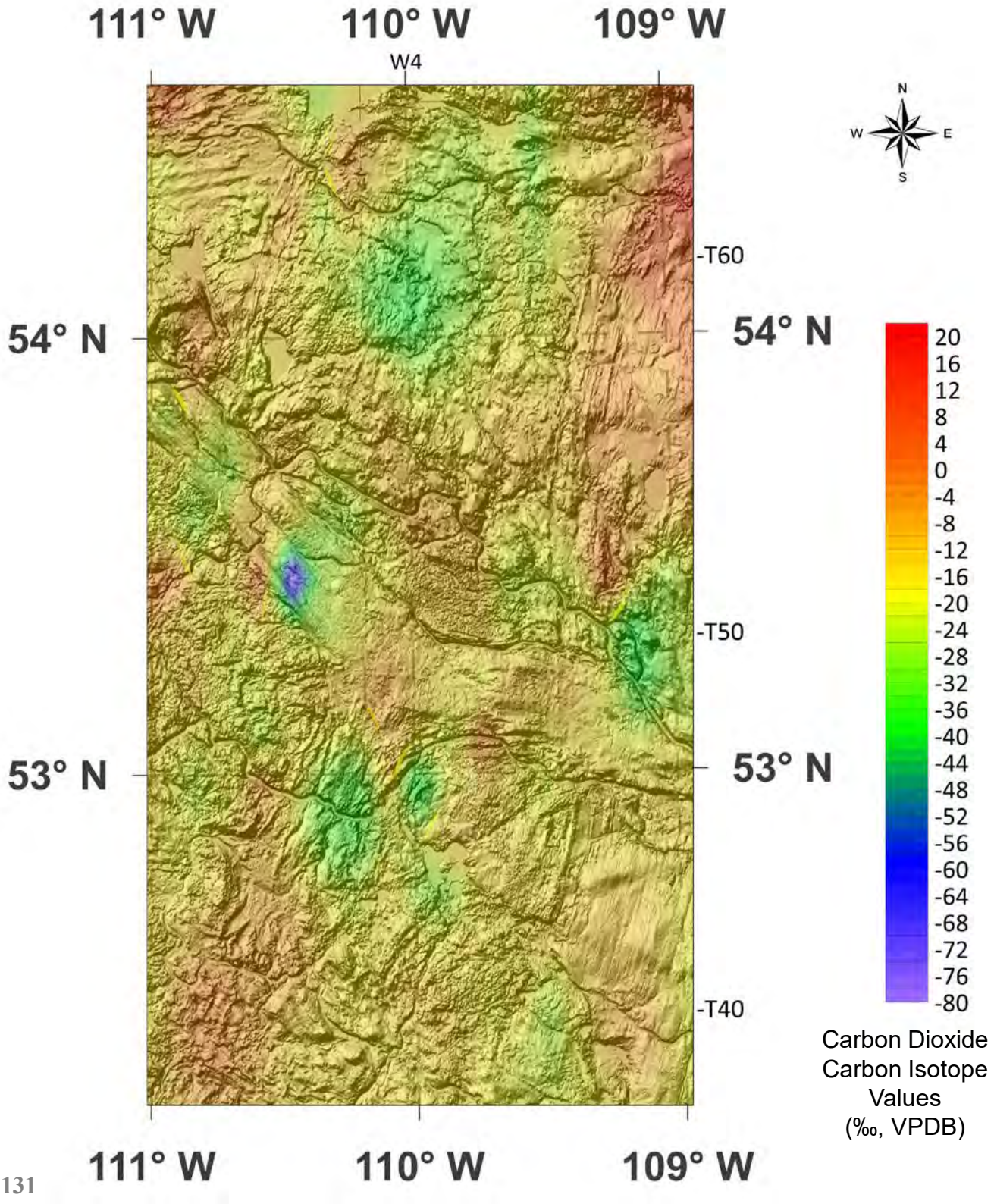

Fig. 24A. Map of Ground Migration (GM) Locations in the Lloydminster Zoom-in

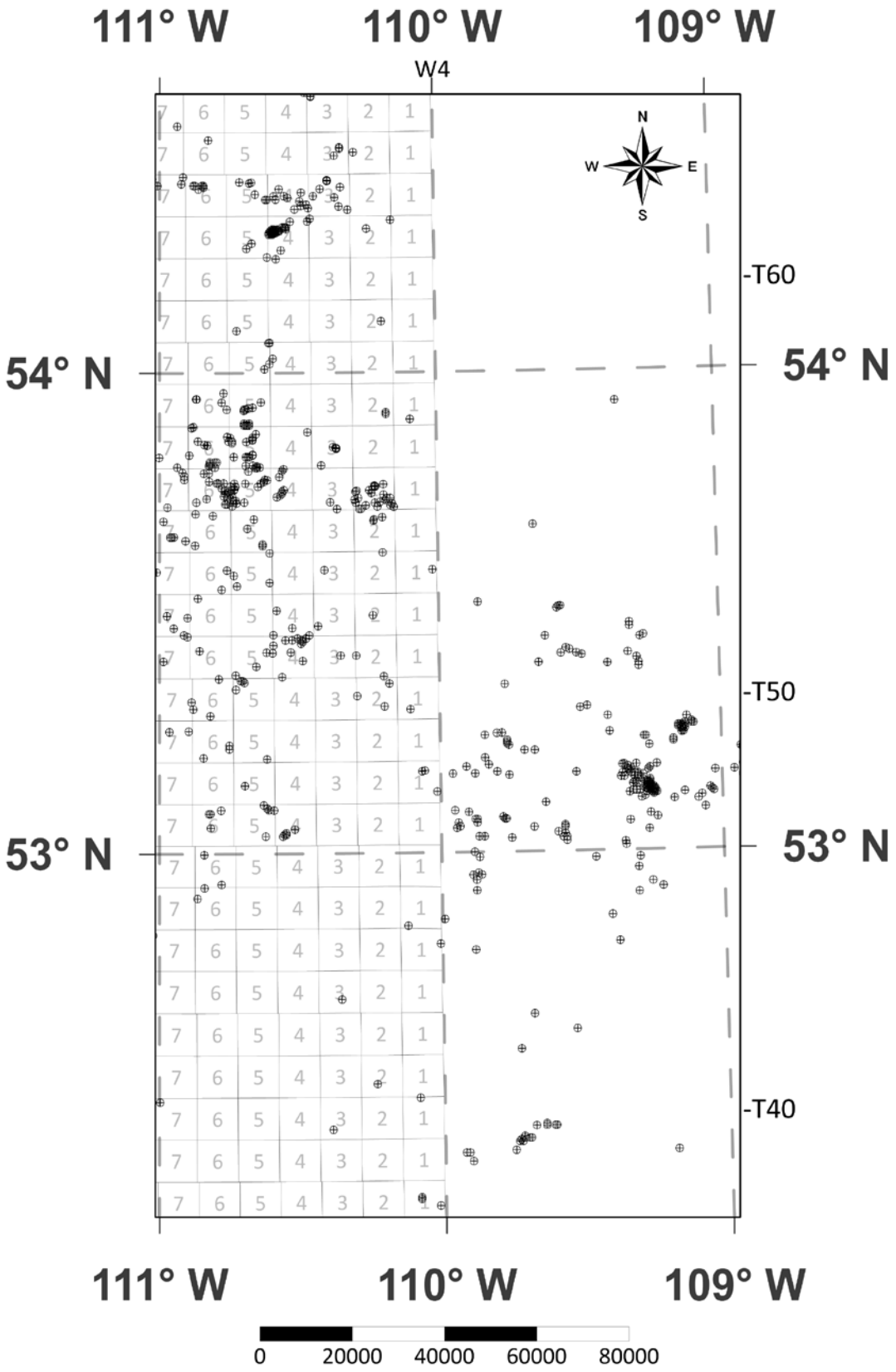

Fig. 24B. Contour Map of Methane Carbon Isotope Values of GM Lloydminster Zoom-in

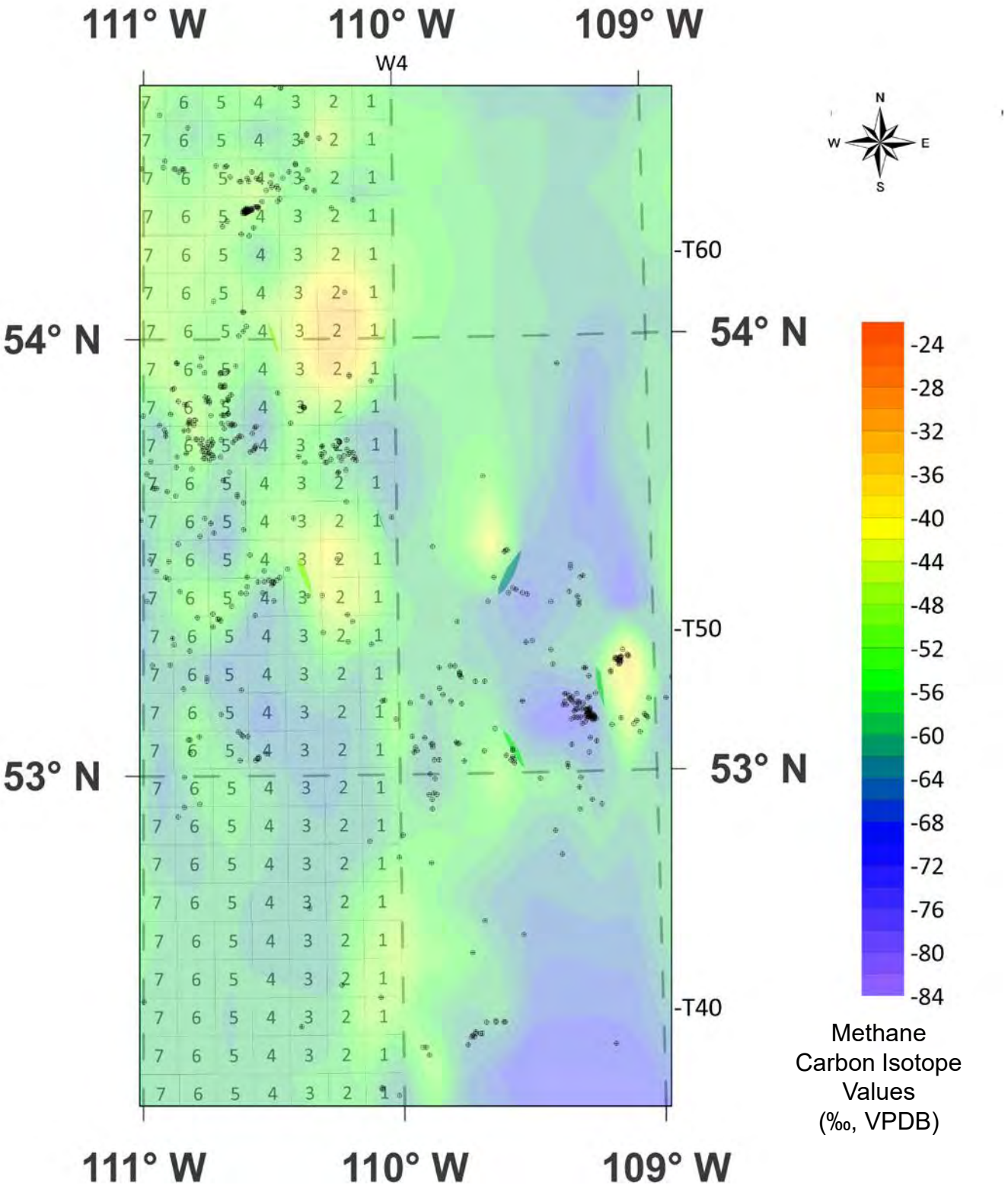

Fig. 24C. Contour Map of Ethane Carbon Isotope Values of GM Lloydminster Zoom-in

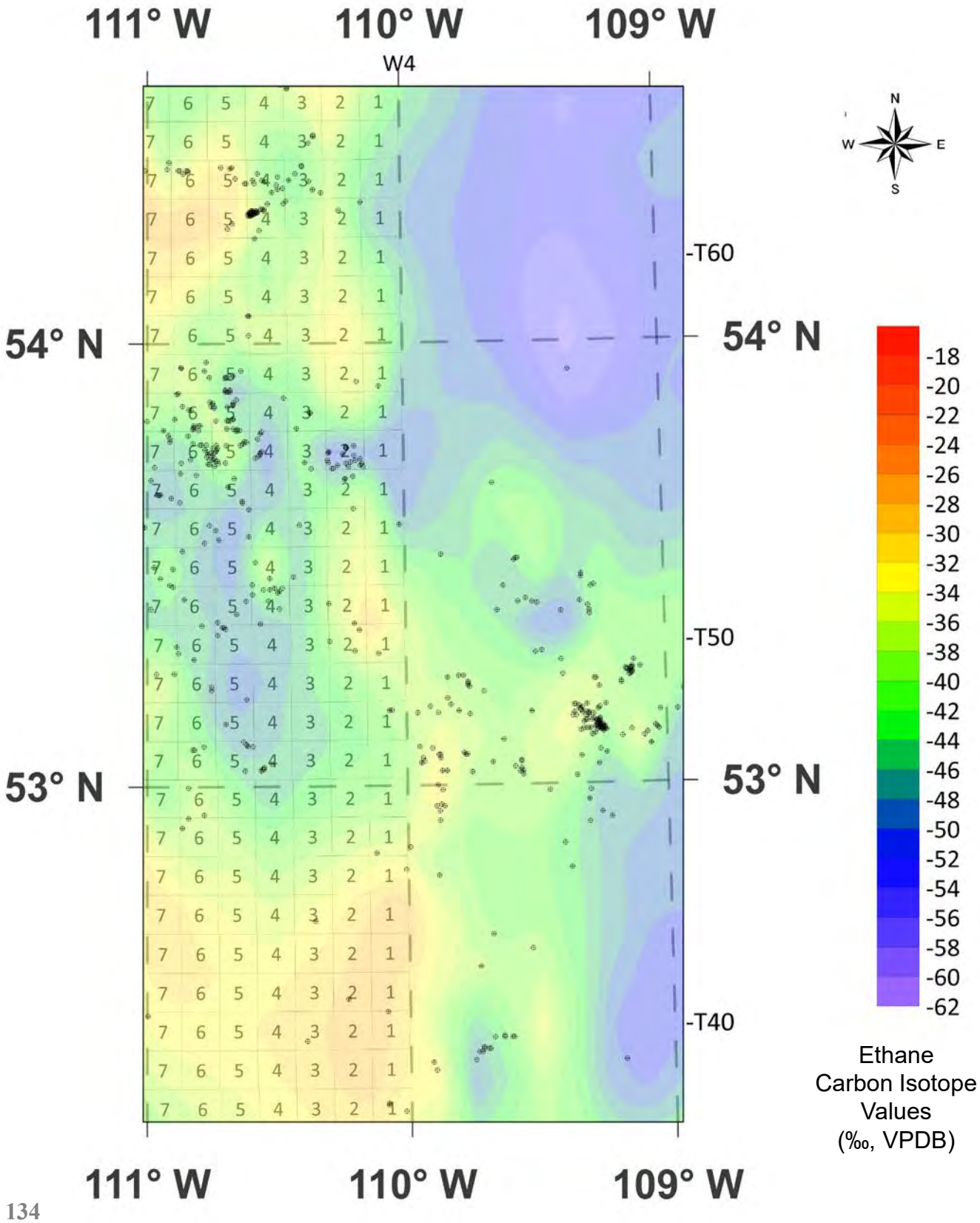

Fig. 24D. Contour Map of Propane Carbon Isotope Values of GM Lloydminster Zoom-in

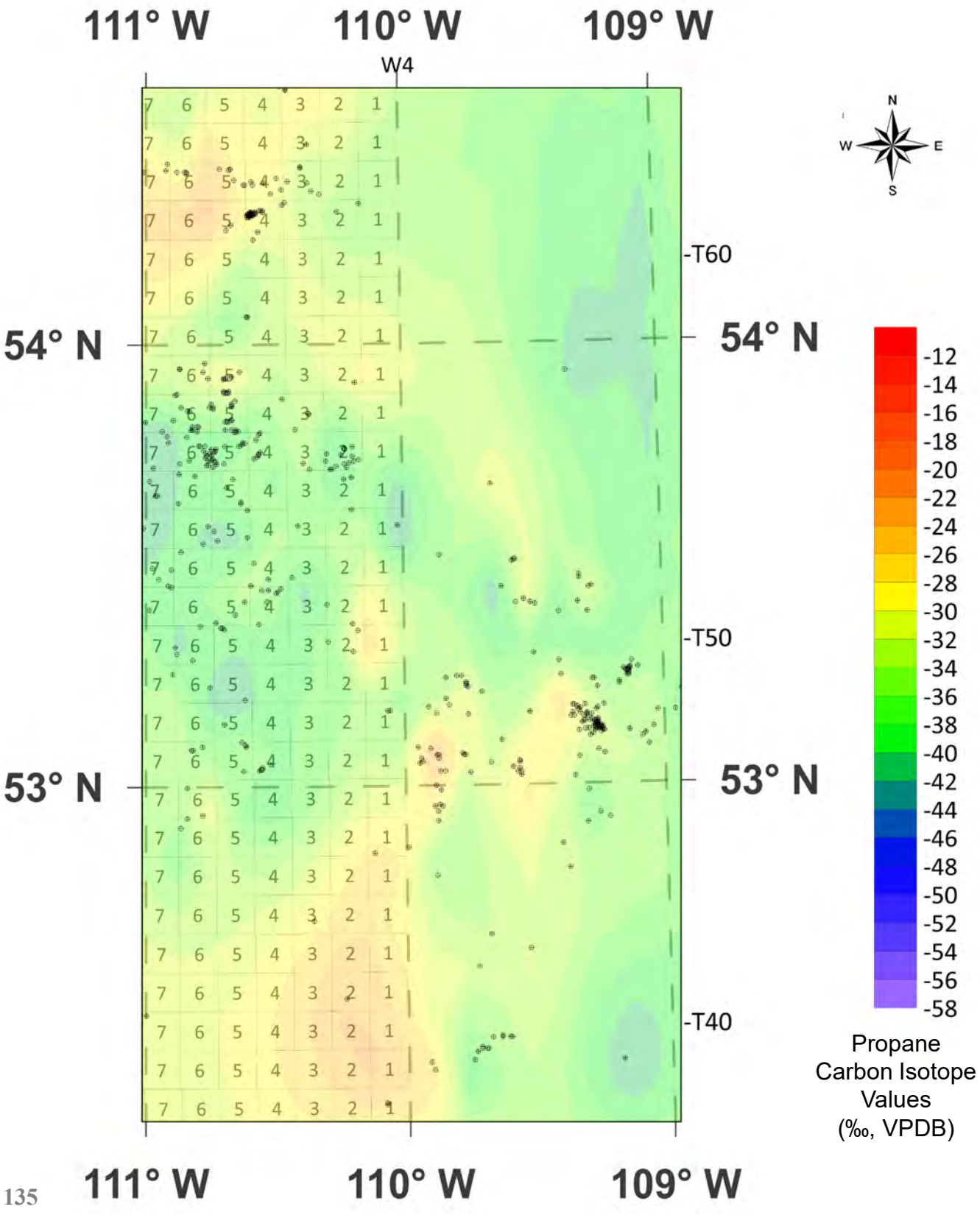

Fig. 24E. Contour Map of *n*-Butane Carbon Isotope Values of GM Lloydminster Zoom-in

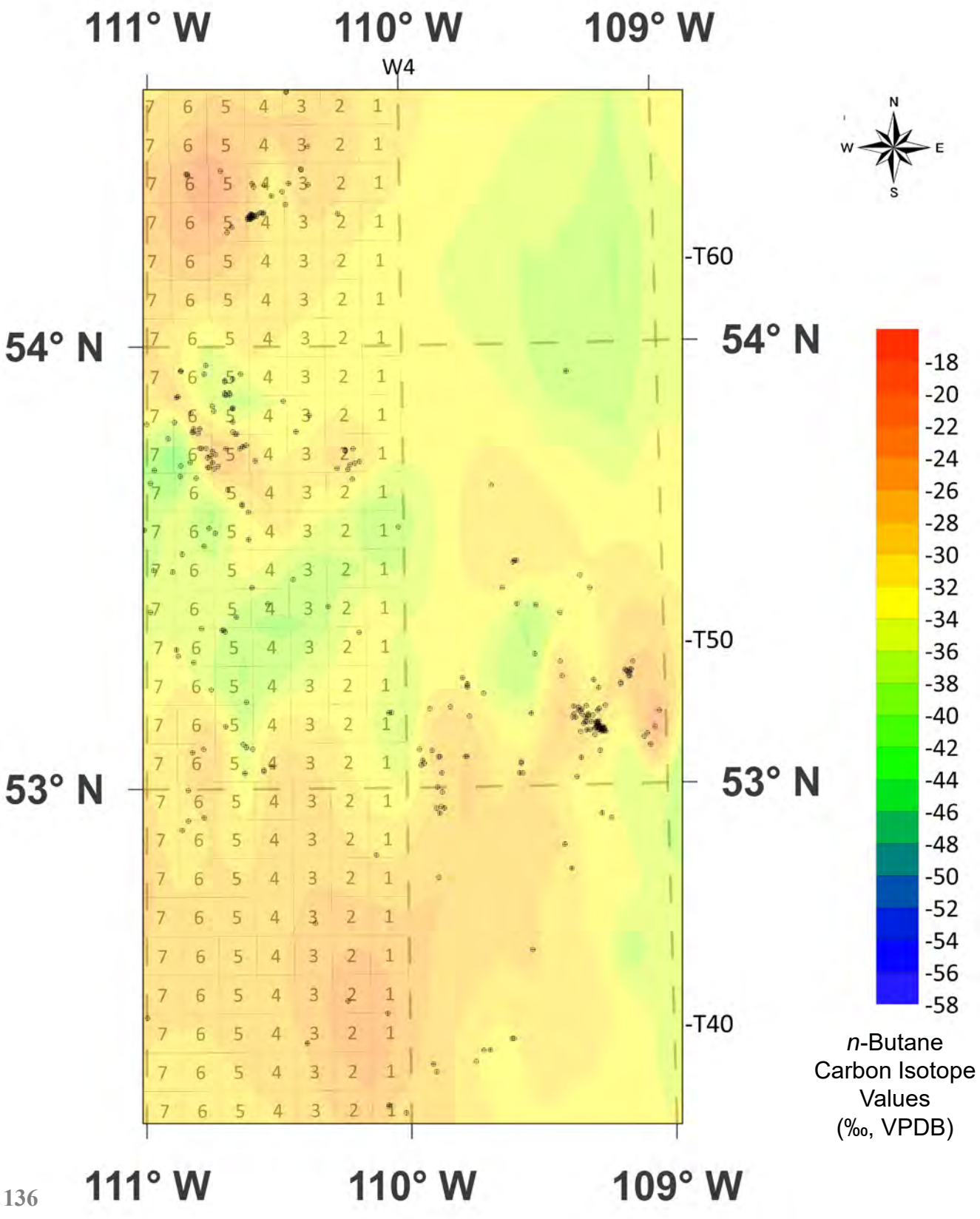

Fig. 24F. Contour Map of *i*-Butane Carbon Isotope Values of GM Lloydminster Zoom-in

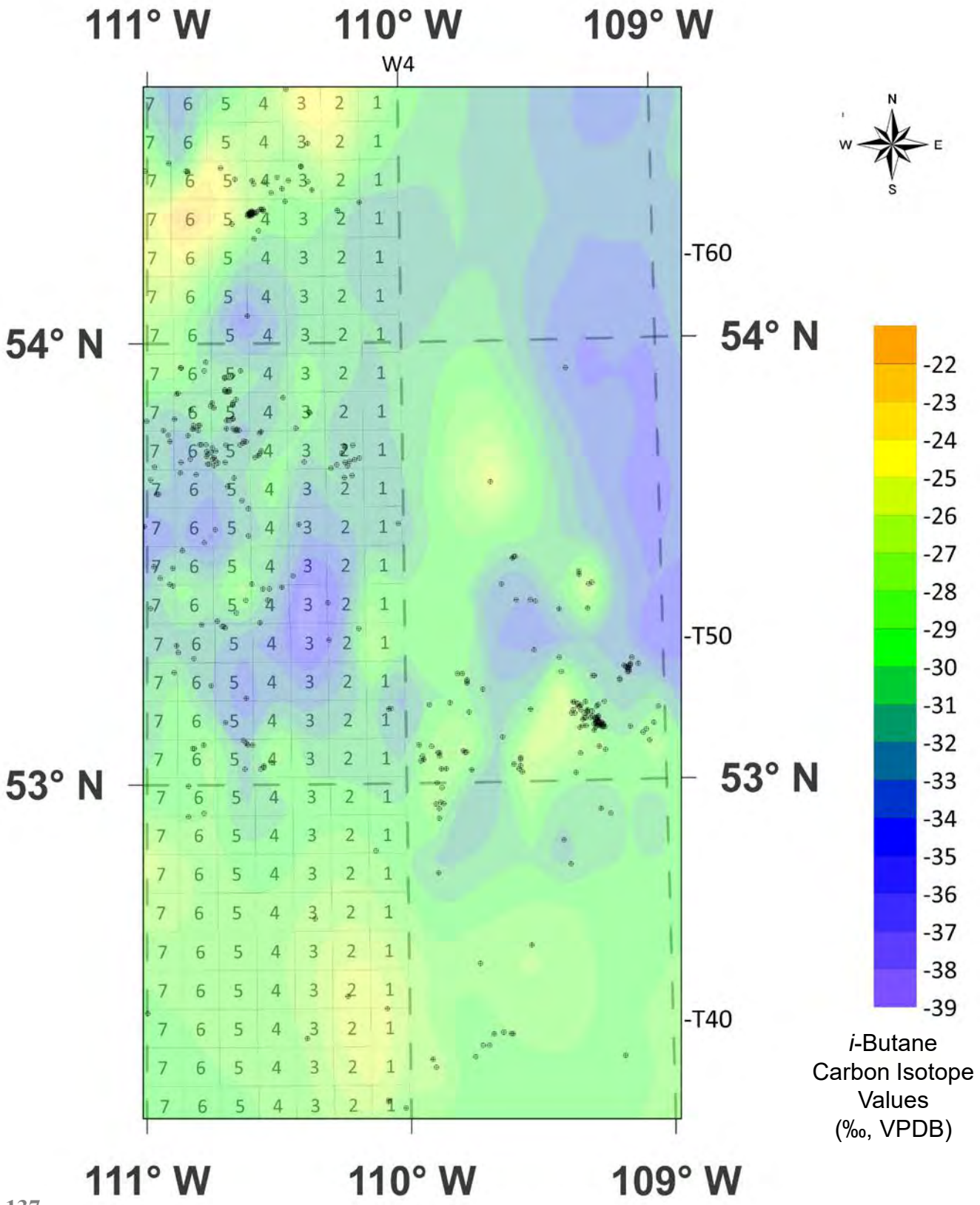

Fig. 24G. Contour Map of Carbon Dioxide Carbon Isotope Values of GM Lloydminster Zoom-in

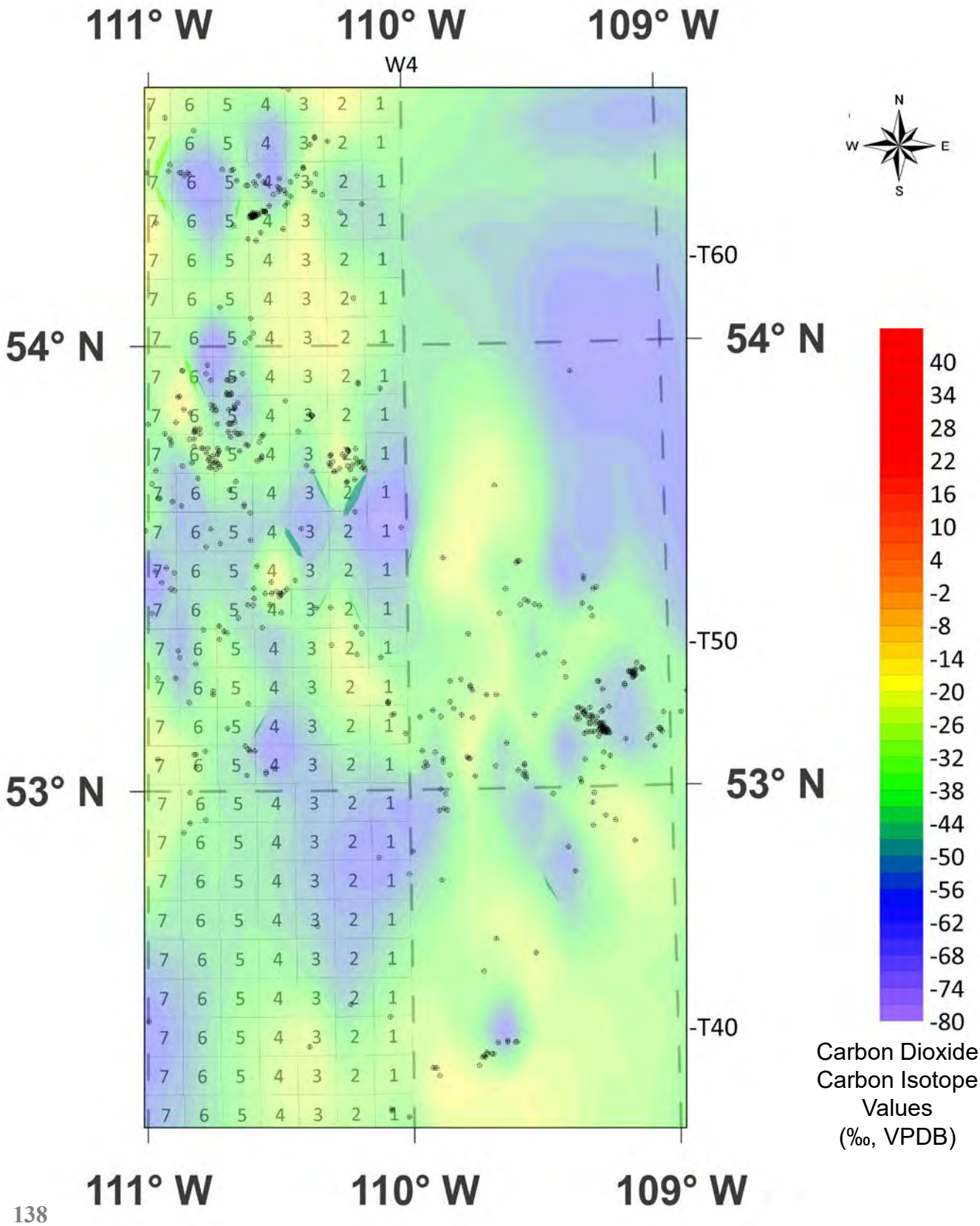

Fig. 24H. Contour Map of Methane Carbon Isotope Values of GM Lloydminster Zoom-in over Topographic Map

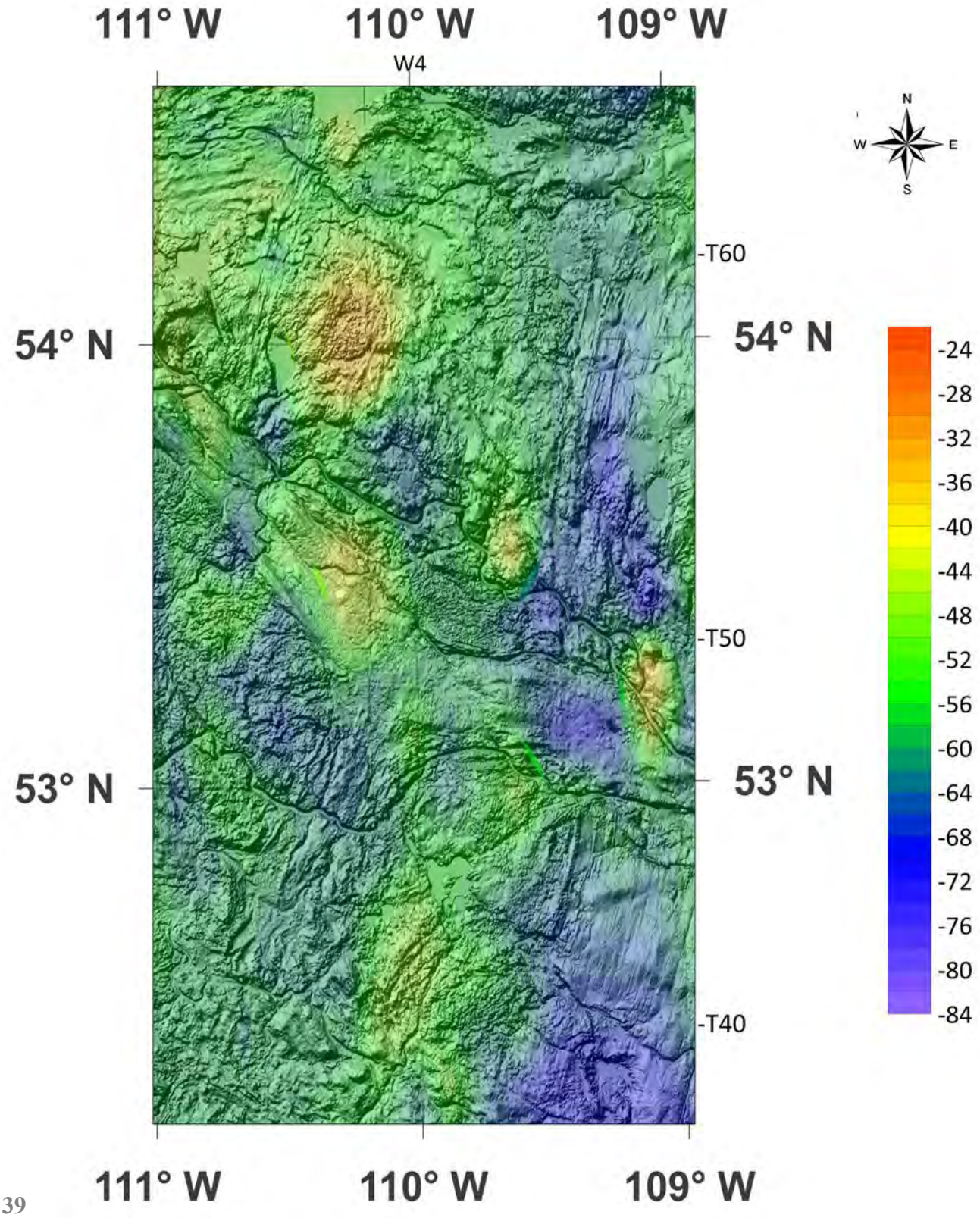

Fig. 24I. Contour Map of Ethane Carbon Isotope Values of GM Lloydminster Zoom-in over Topographic Map

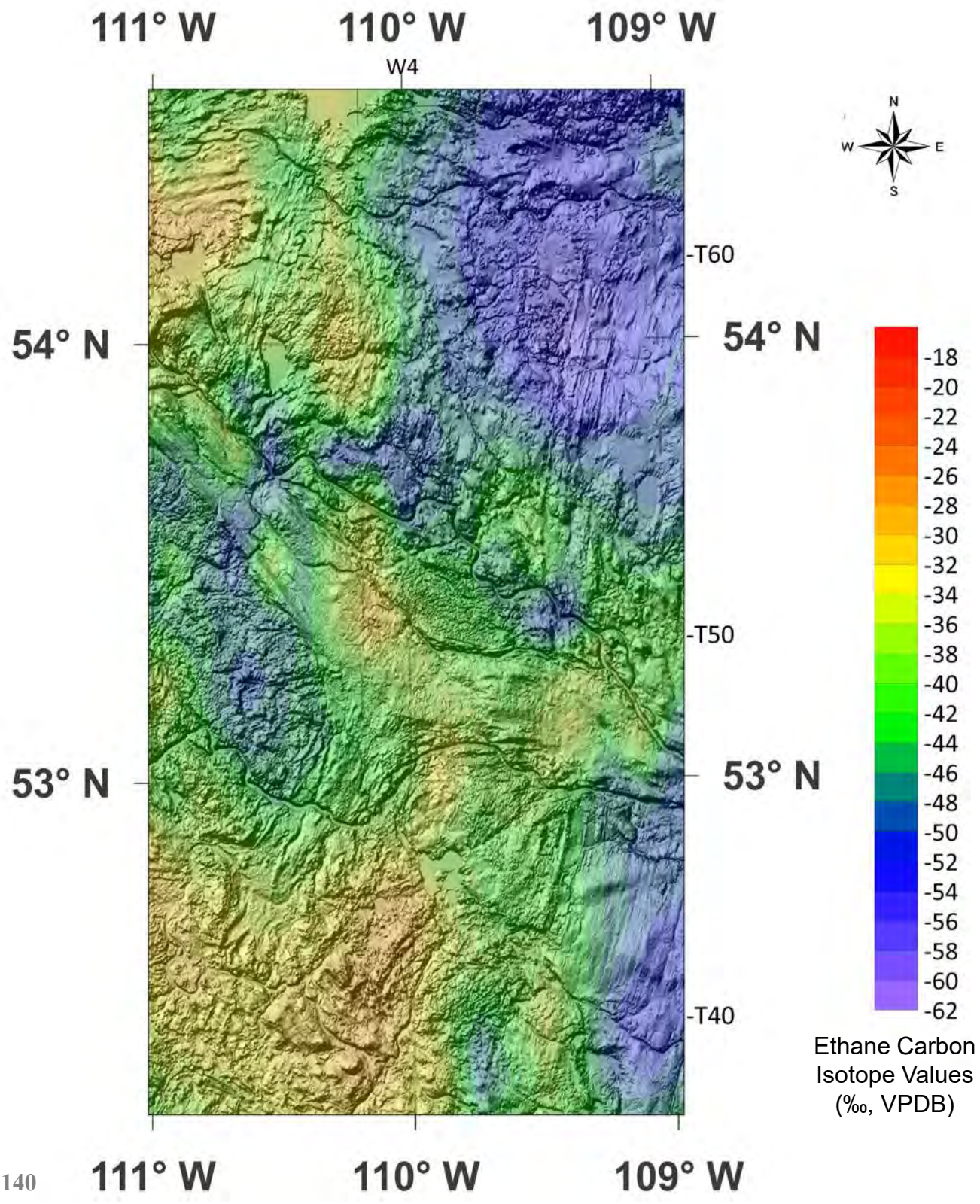

Fig. 24J. Contour Map of Propane Carbon Isotope Values of GM Lloydminster Zoom-in over Topographic Map

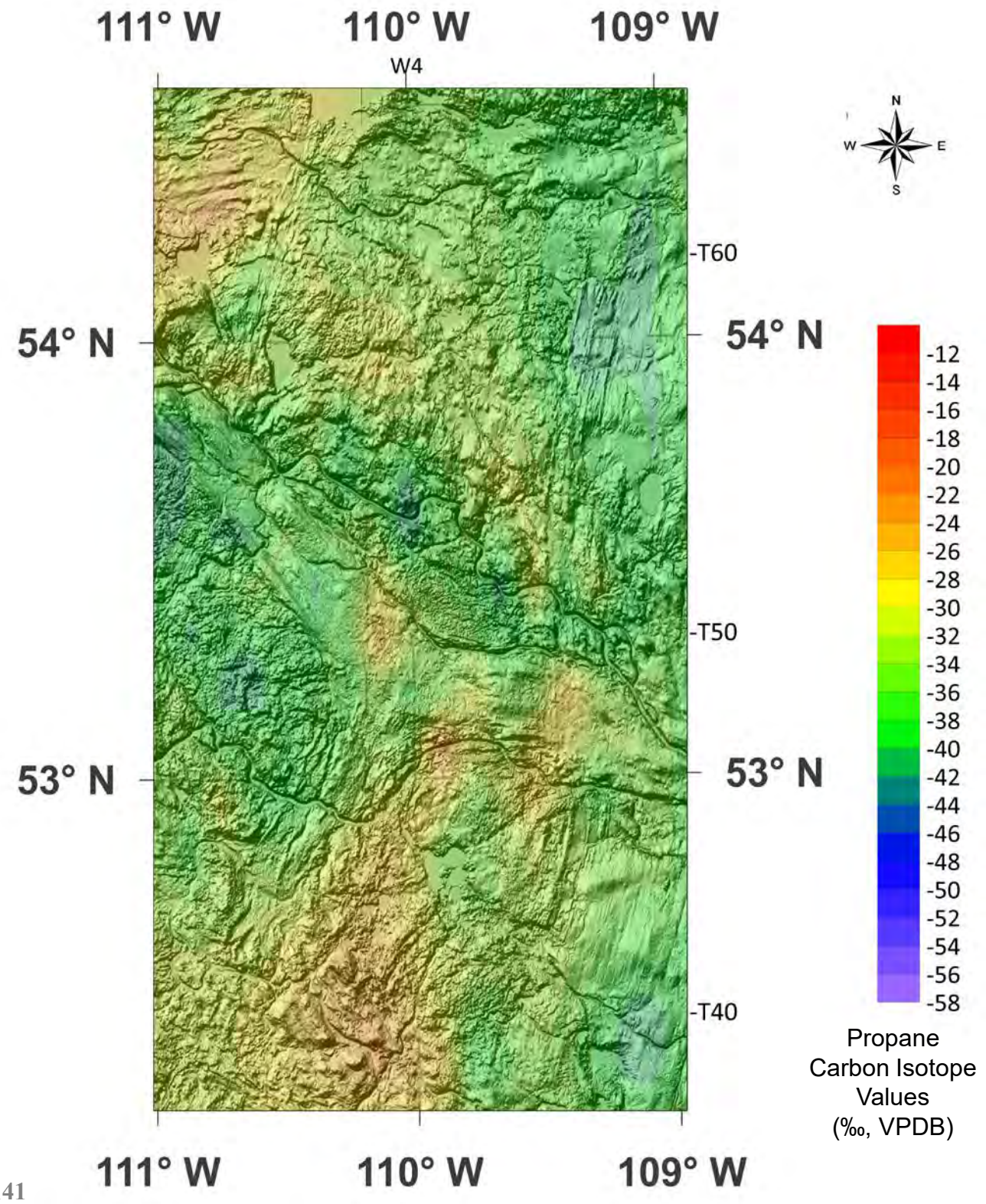

Fig. 24K. Contour Map of *n*-Butane Carbon Isotope Values of GM Lloydminster Zoom-in over Topographic Map

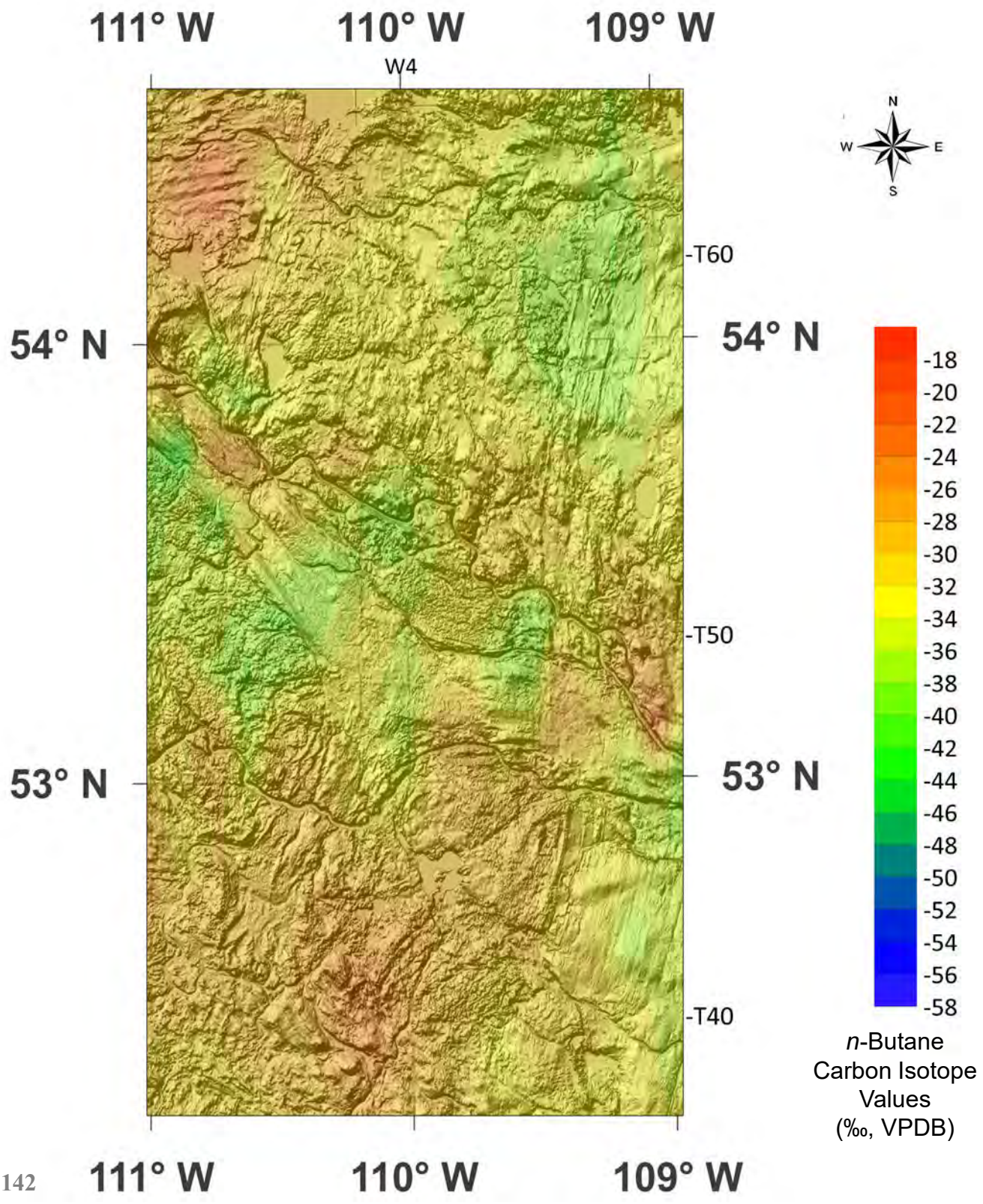

Fig. 24K. Contour Map of *i*-Butane Carbon Isotope Values of GM Lloydminster Zoom-in over Topographic Map

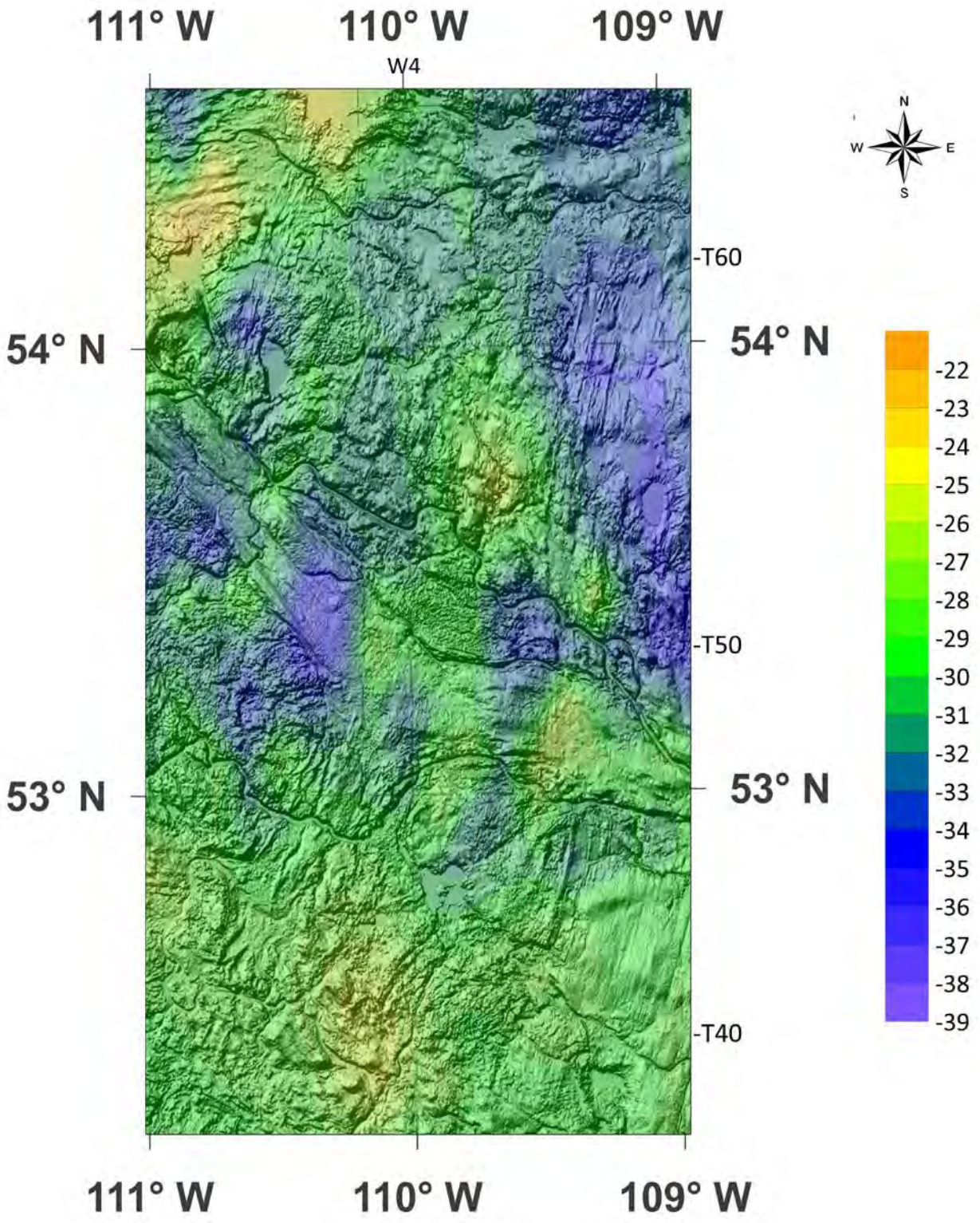

Fig. 24M. Contour Map of Carbon Dioxide Carbon Isotope Values of GM Lloydminster Zoom-in over Topographic Map

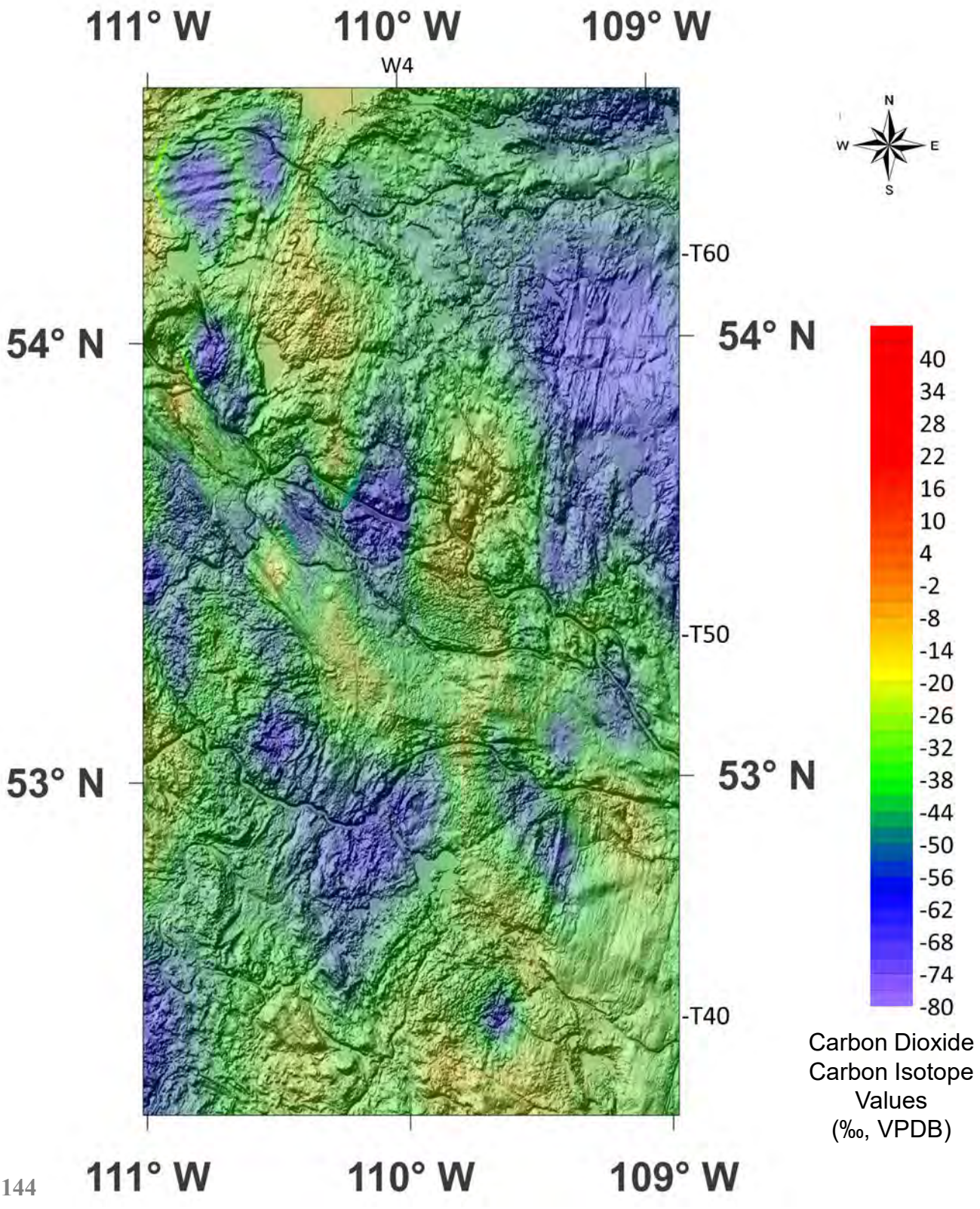

Fig. 25A. Map of Surface Casing Vent (SCV) Locations in the Lindbergh Zoom-in

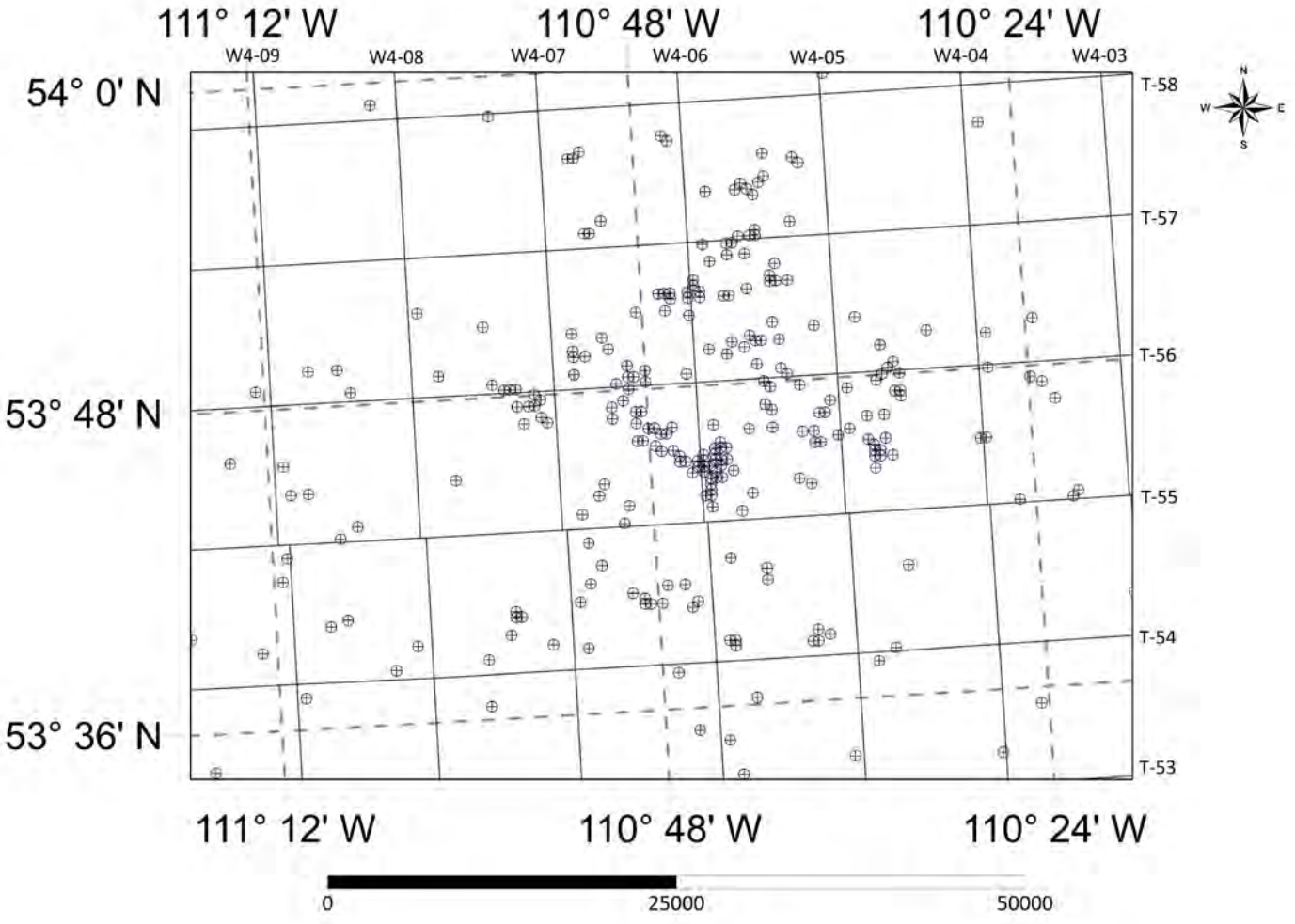

Fig. 25B. Contour Map of Methane Carbon Isotope Values of SCV Lindbergh Zoom-in

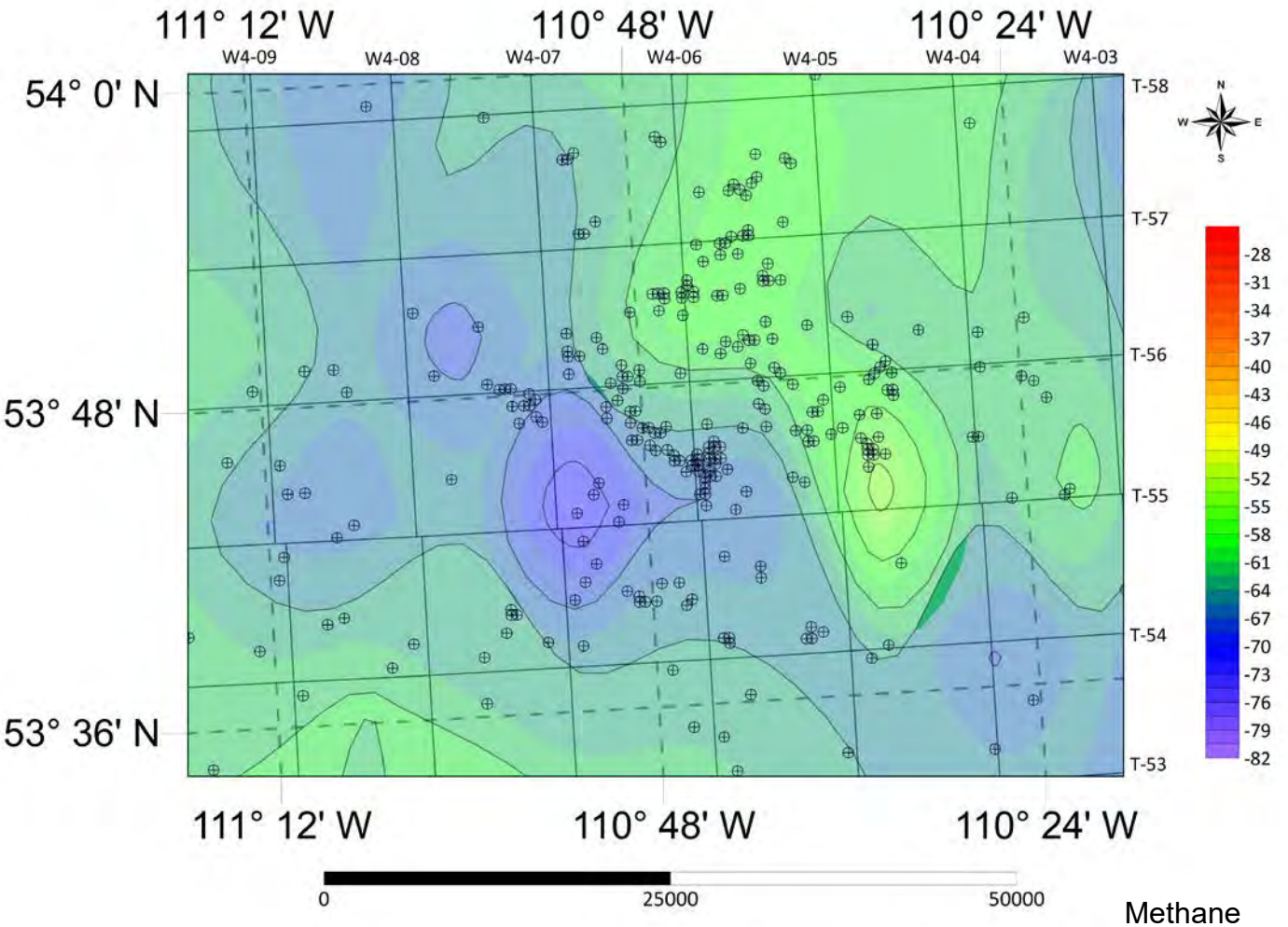

Fig. 25C. Contour Map of Ethane Carbon Isotope Values of SCV Lindbergh Zoom-in

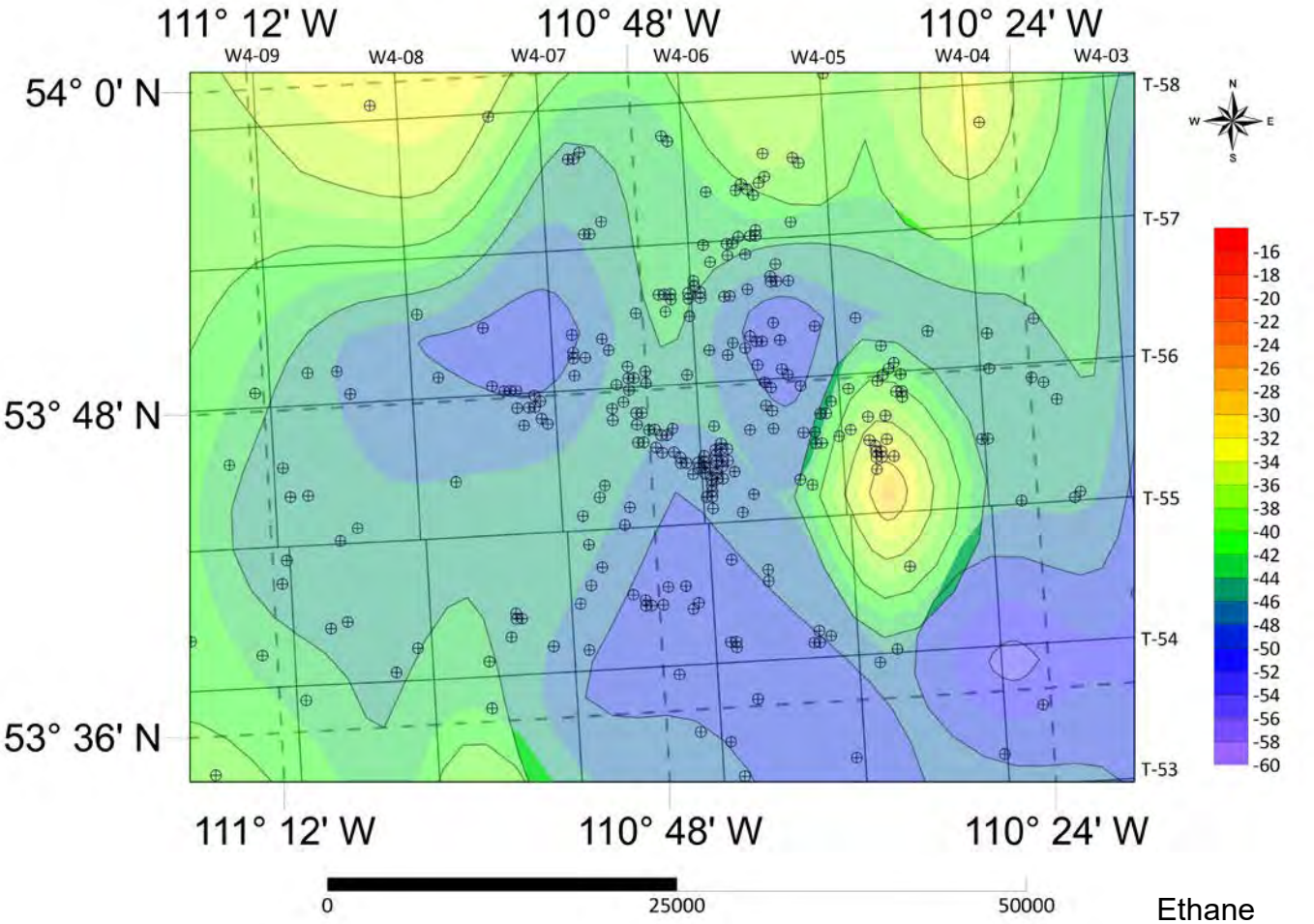

Ethane Carbon Isotope Values (‰, VPDB)

Fig. 25D. Contour Map of Propane Carbon Isotope Values of SCV Lindbergh Zoom-in

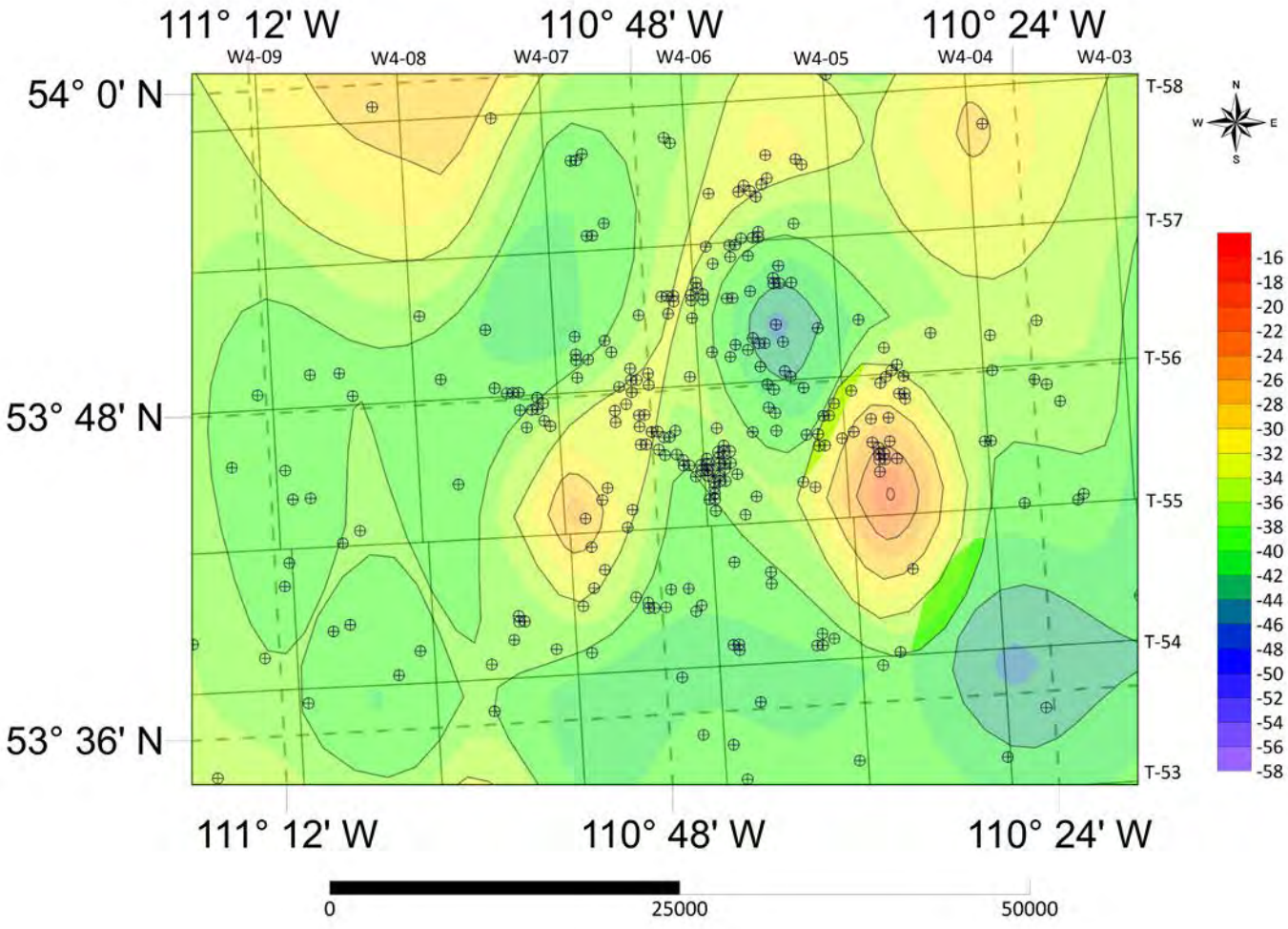

Propane Carbon Isotope Values (‰, VPDB)

Fig. 25E. Contour Map of *n*-Butane Carbon Isotope Values of SCV Lindbergh Zoom-in

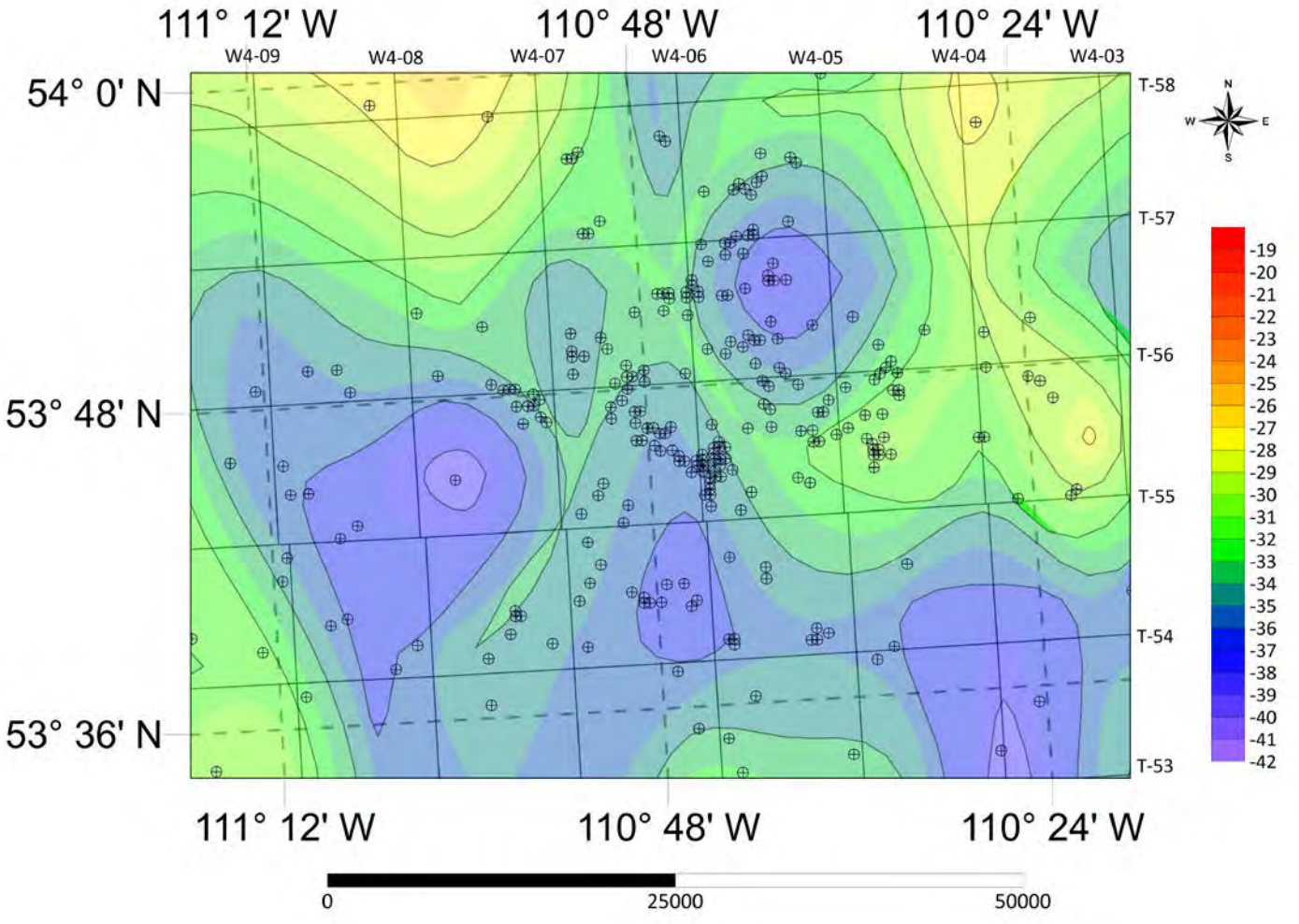

Carbon Isotope Values (‰, VPDB)

Fig. 25F. Contour Map of *i*-Butane Carbon Isotope Values of SCV Lindbergh Zoom-in

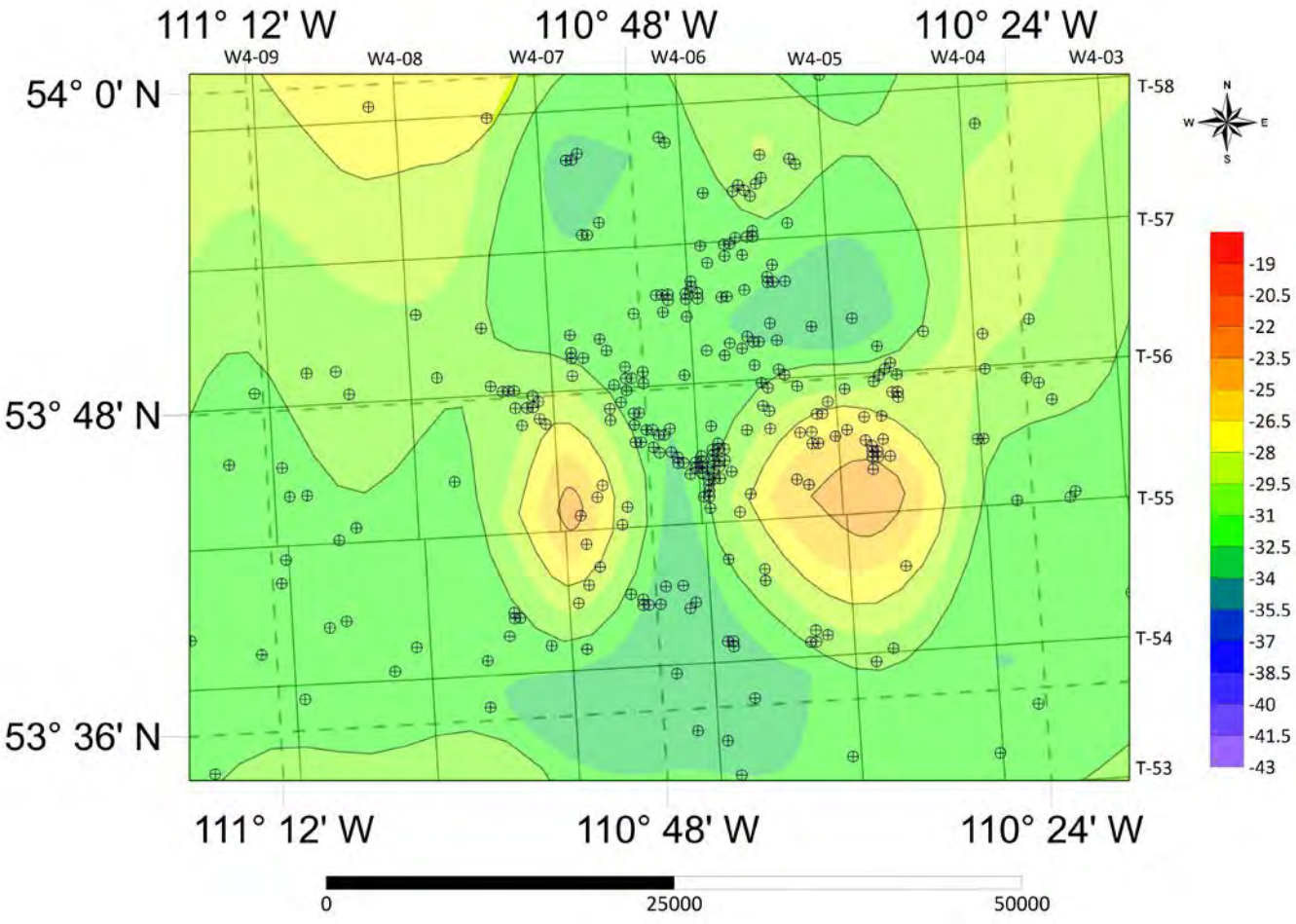

i-Butane Carbon Isotope Values (‰, VPDB)

Fig. 25G. Contour Map of Carbon Dioxide Carbon Isotope Values of SCV Lindbergh Zoom-in

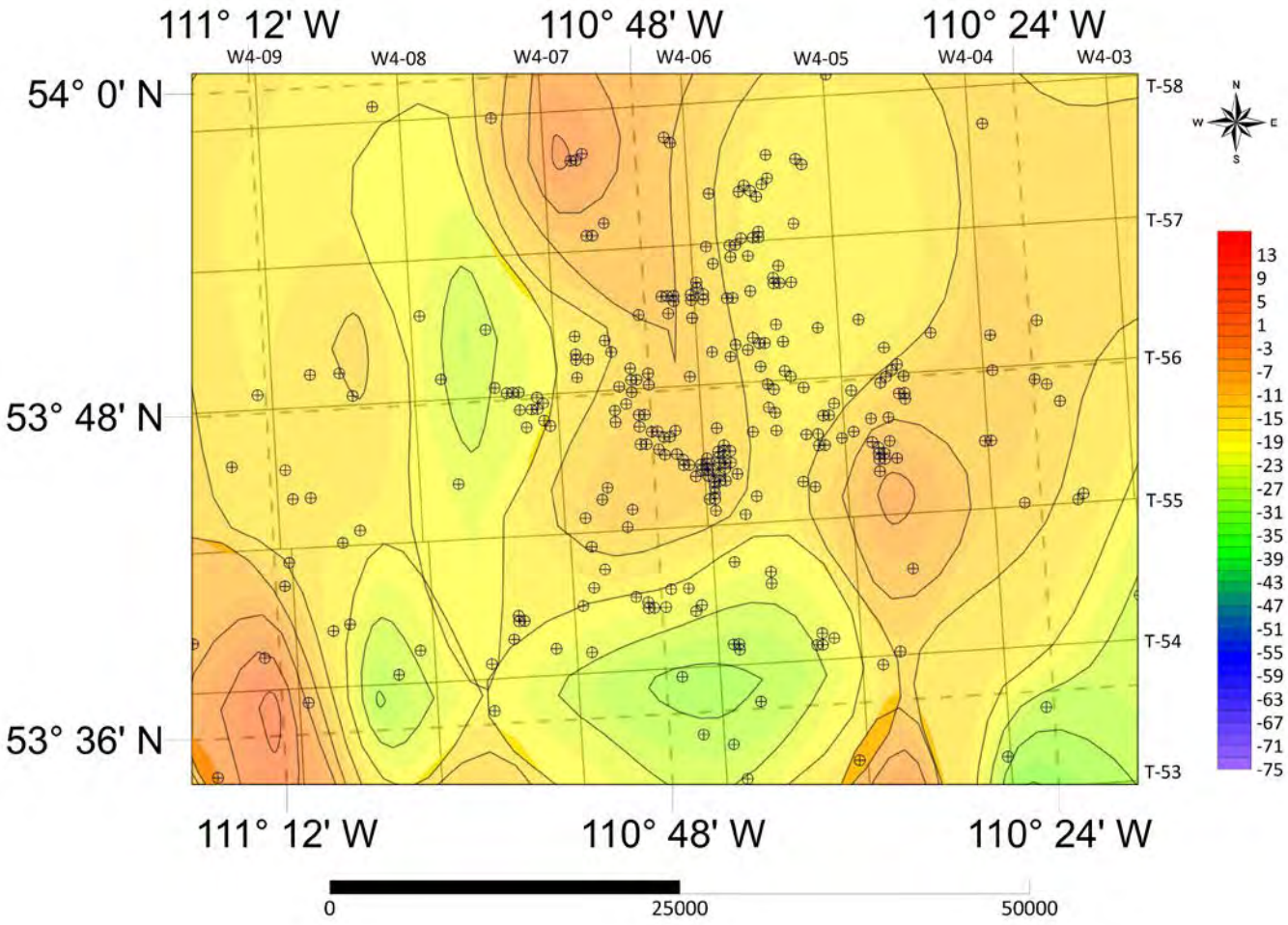

Carbon Dioxide Carbon Isotope Values (‰, VPDB)

Fig. 25H. Contour Map of Methane Carbon Isotope Values of SCV Lindbergh Zoom-in over Topographic Map

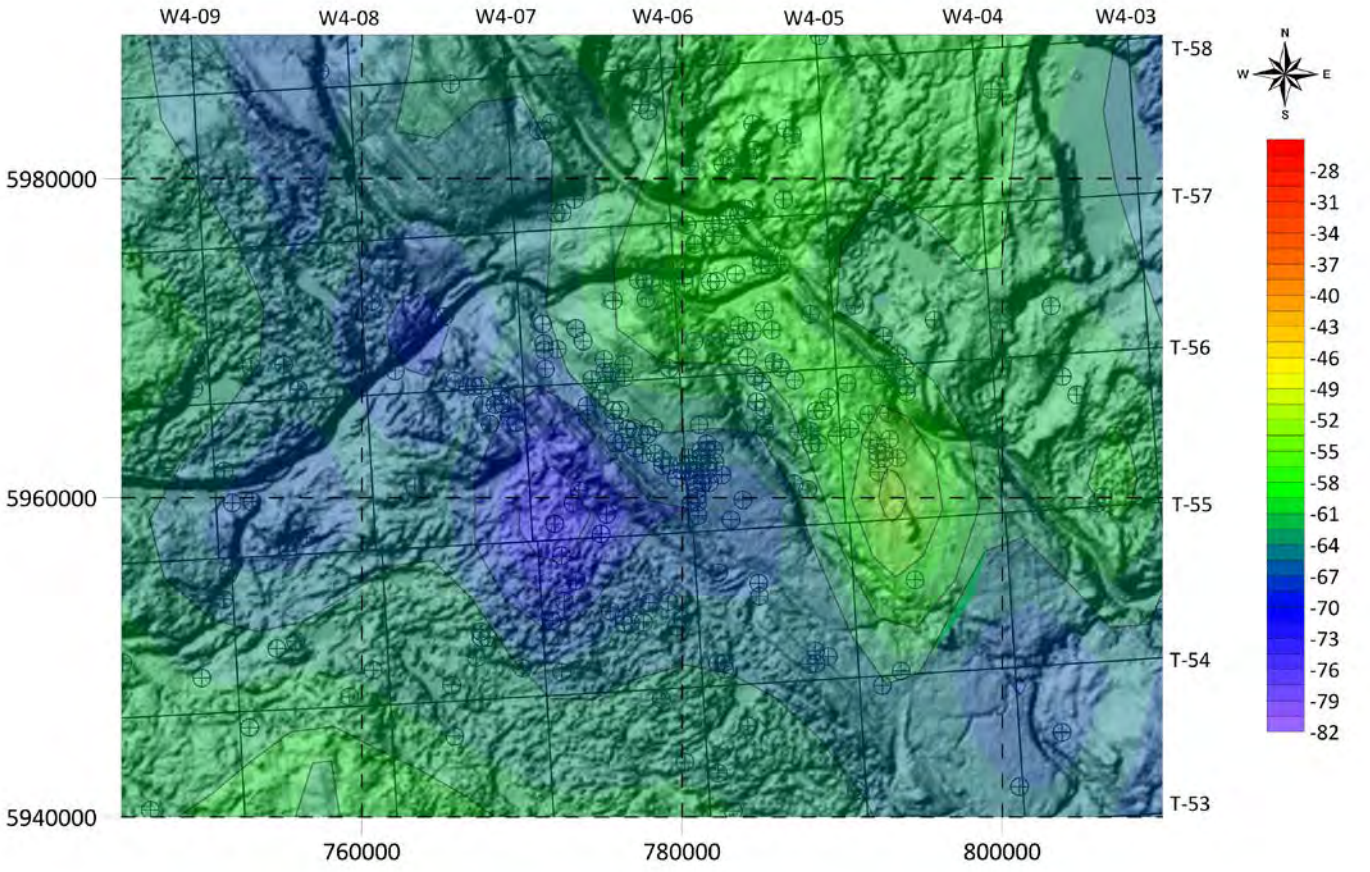

Methane Carbon Isotope Values (‰, VPDB)

Fig. 25I. Contour Map of Ethane Carbon Isotope Values of SCV Lindbergh Zoom-in over Topographic Map

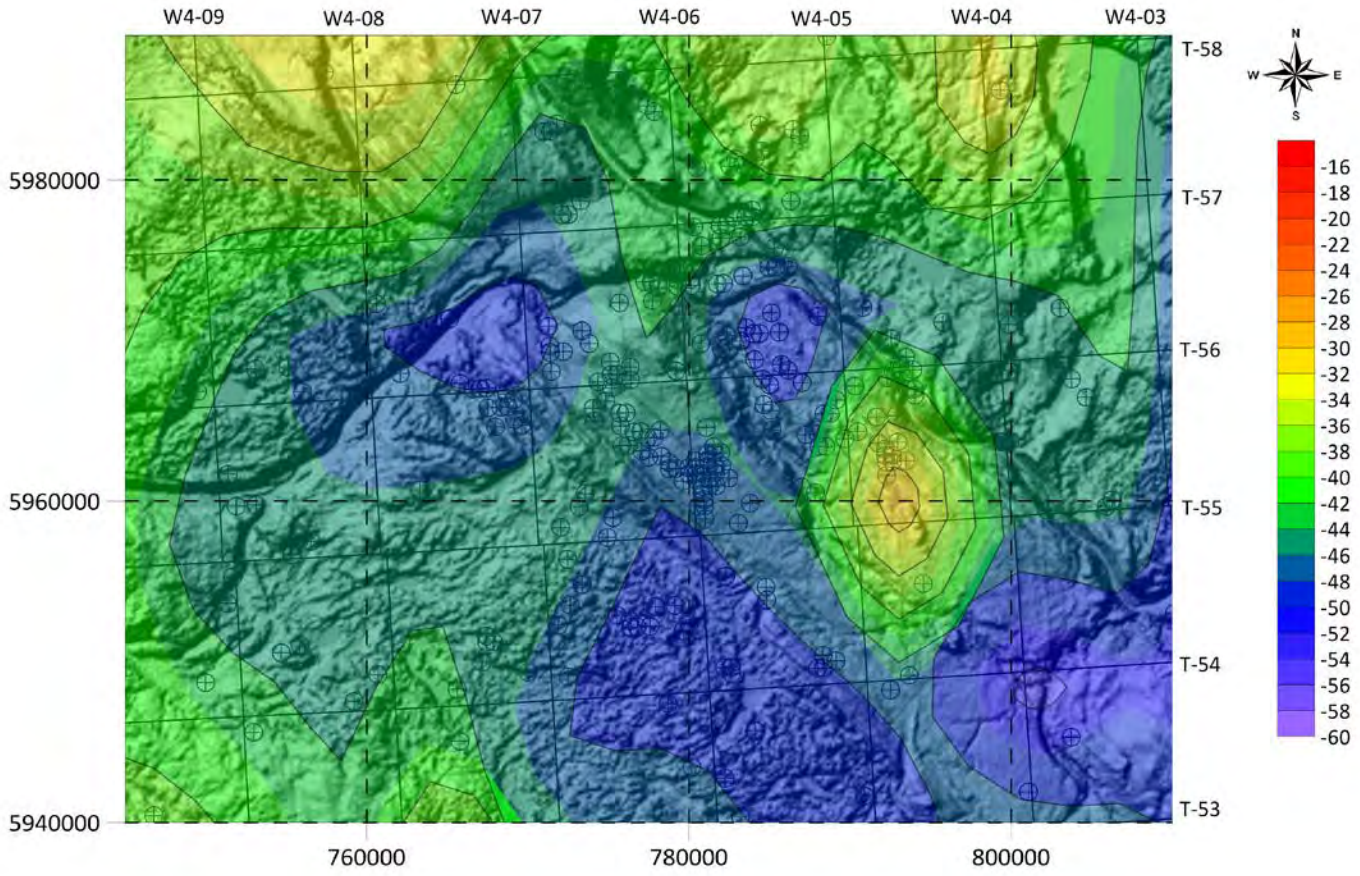

Ethane Carbon Isotope Values (‰, VPDB)

Fig. 25J. Contour Map of Propane Carbon Isotope Values of SCV Lindbergh Zoom-in over Topographic Map

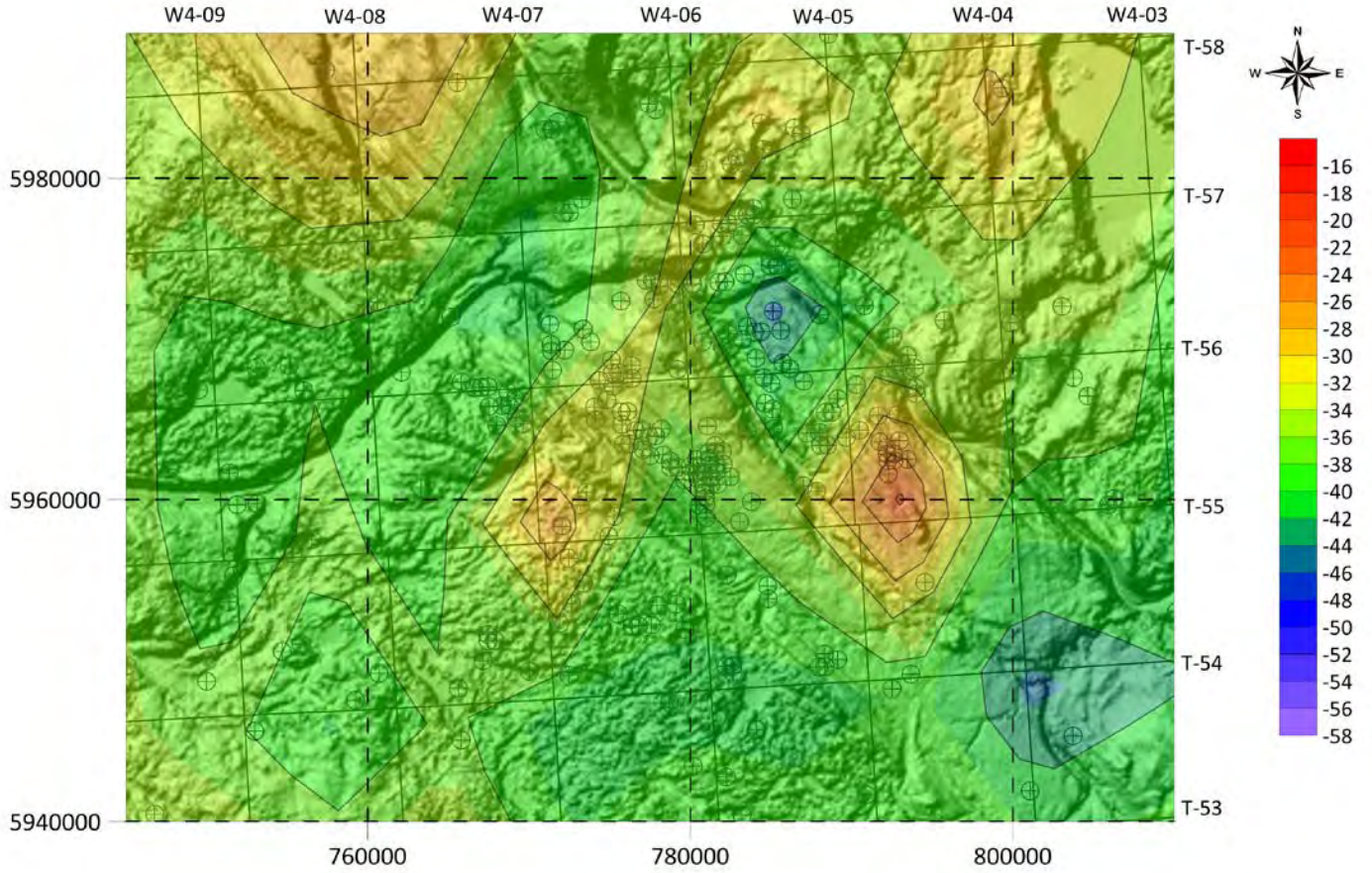

Propane Carbon Isotope Values (‰, VPDB)

Fig. 25K. Contour Map of *n*-Butane Carbon Isotope Values of SCV Lindbergh Zoom-in over Topographic Map

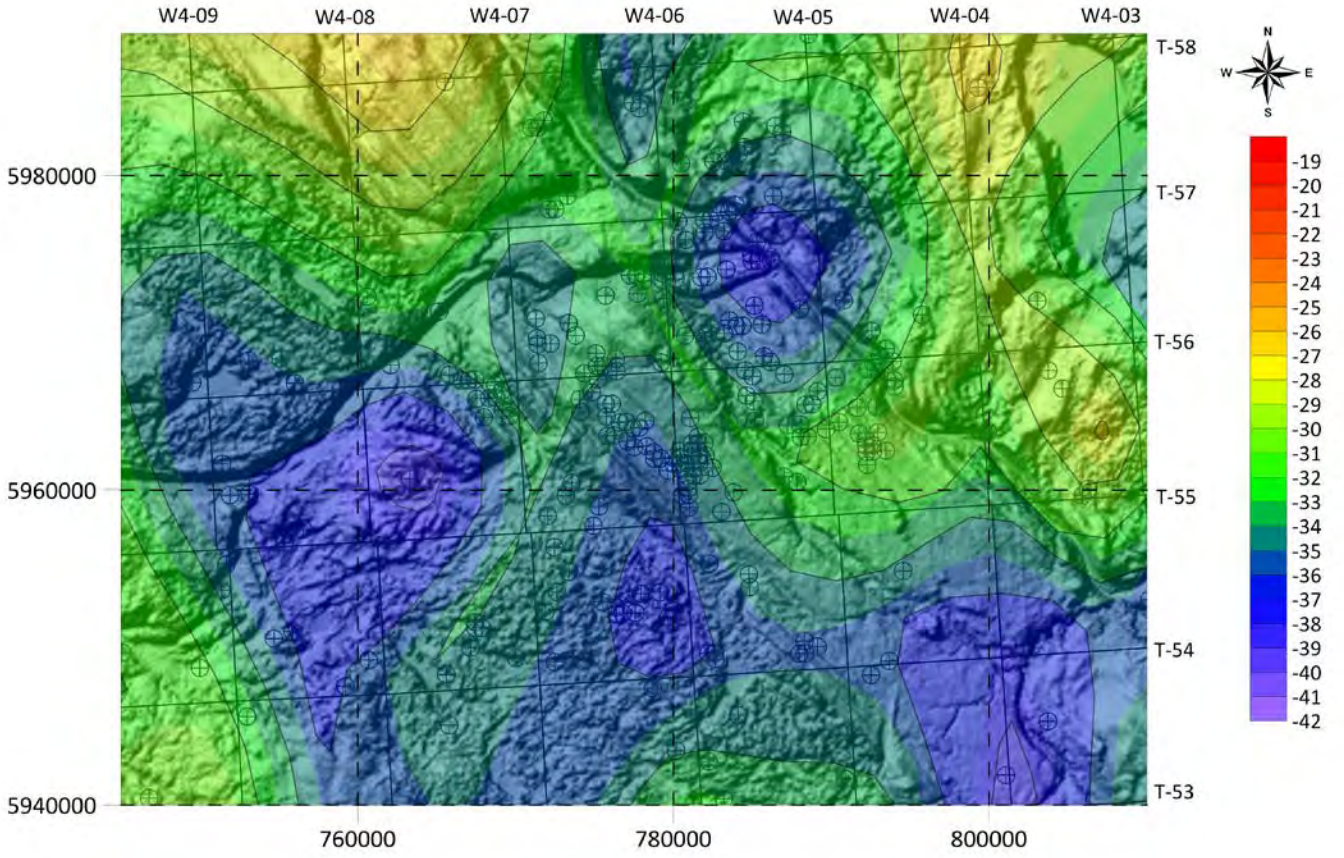

n-Butane Carbon Isotope Values (‰, VPDB)

Fig. 25L. Contour Map of *i*-Butane Carbon Isotope Values of SCV Lindbergh Zoom-in over Topographic Map

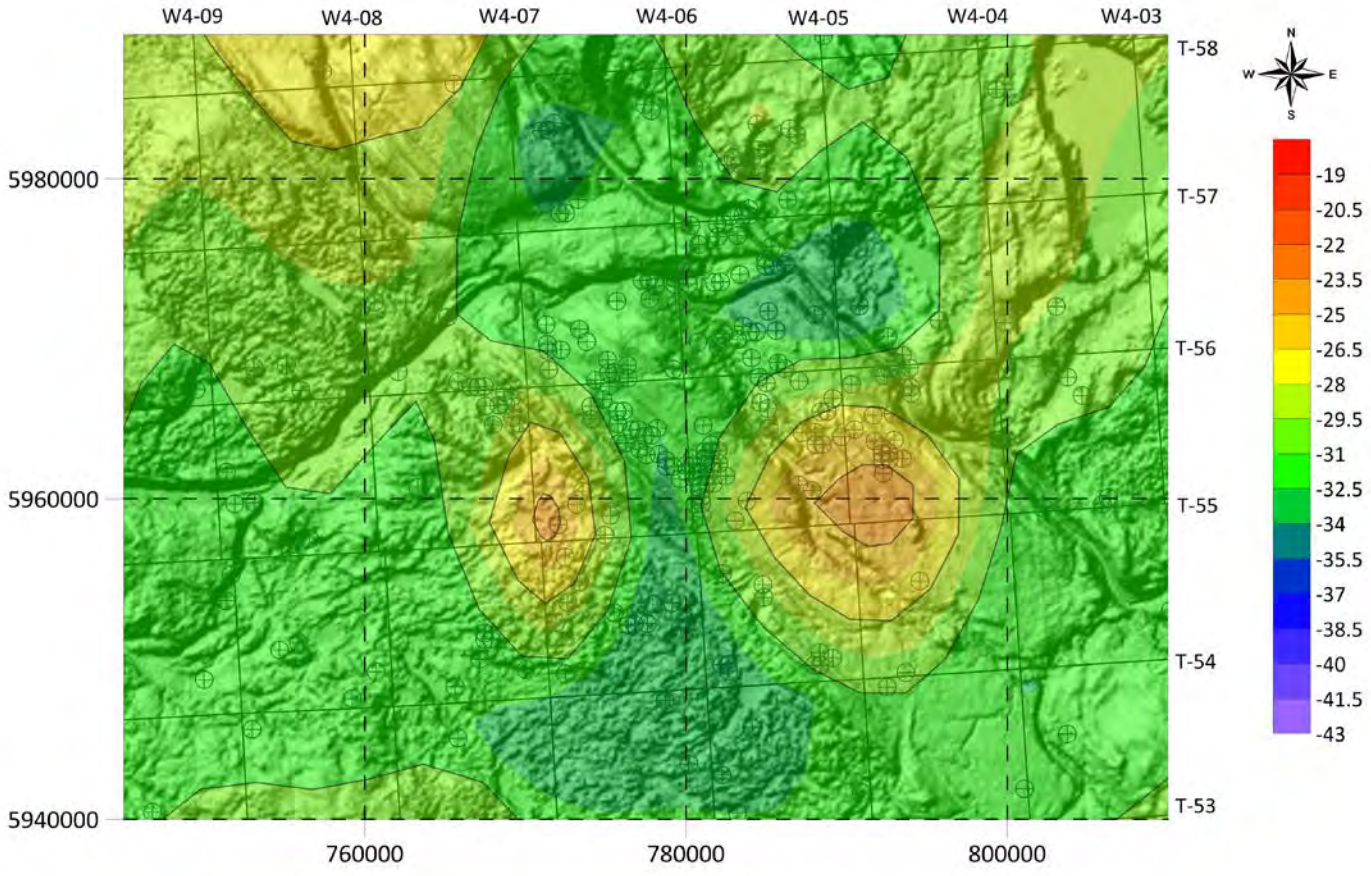

i-Butane Carbon Isotope Values (‰, VPDB)

Fig. 25M. Contour Map of Carbon Dioxide Carbon Isotope Values of SCV Lindbergh Zoom-in over Topographic Map

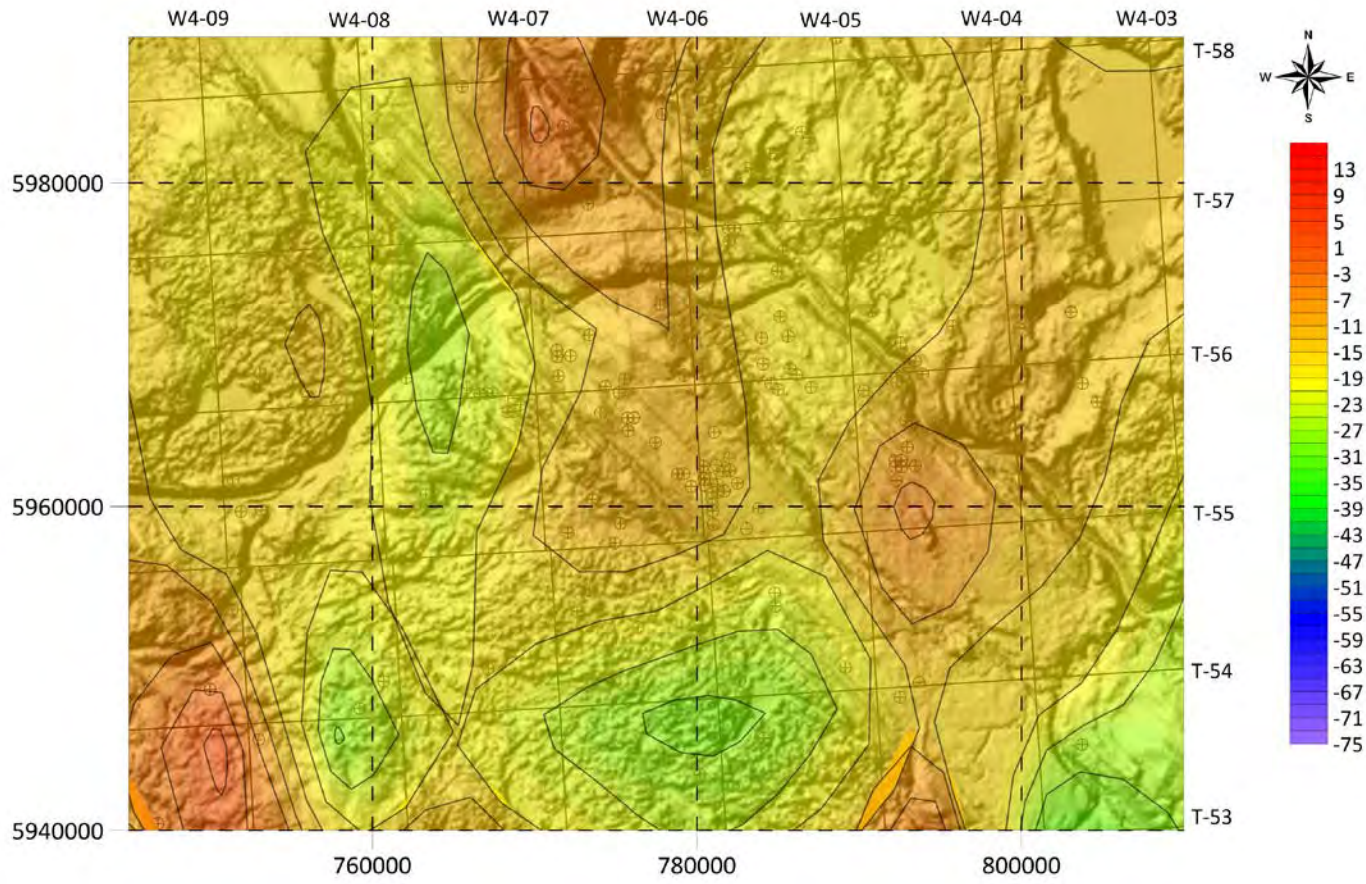

Carbon Dioxide Carbon Isotope Values (‰, VPDB)

Fig. 26A. Map of Ground Migration (GM) Locations in the Lindbergh Zoom-in

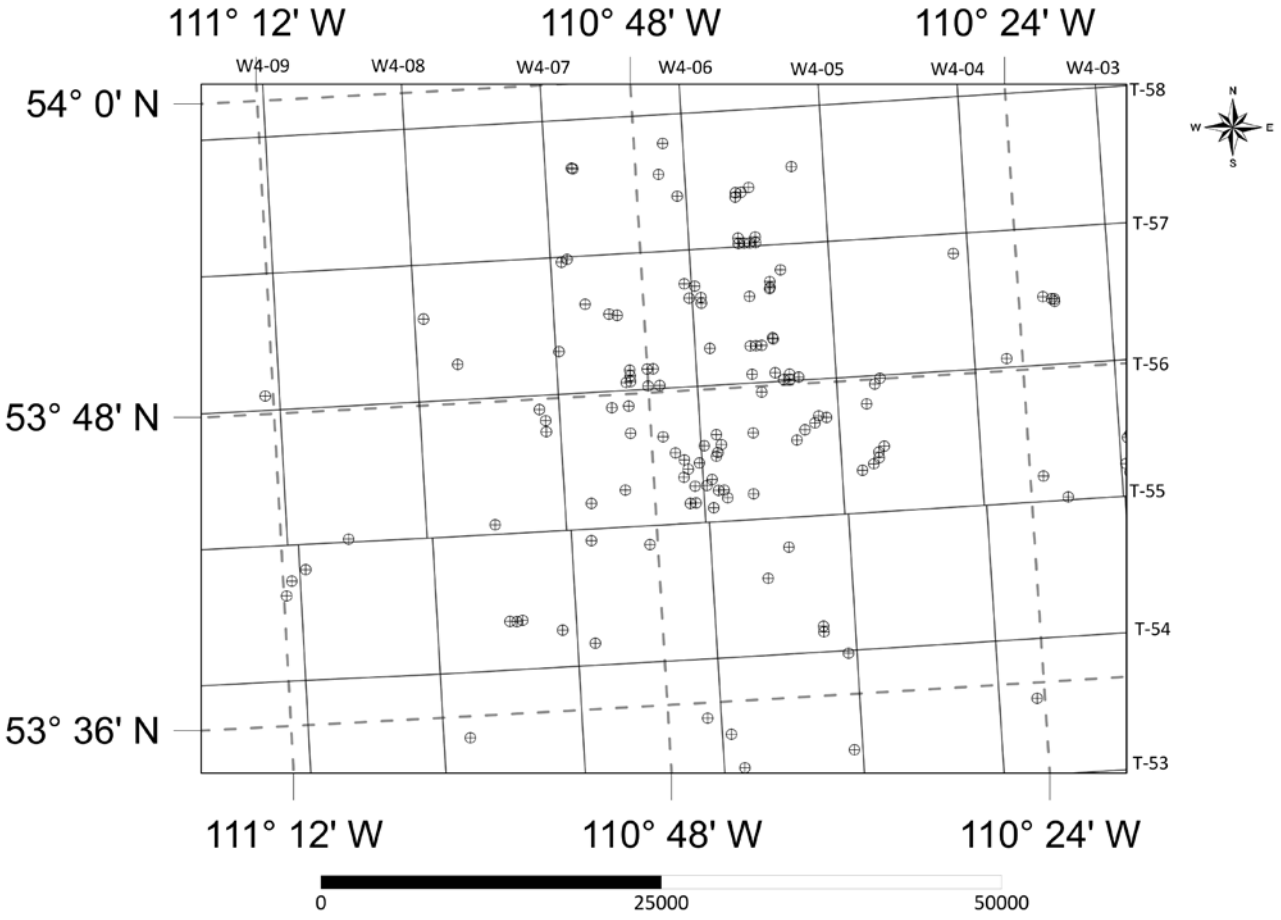

Fig. 26B. Contour Map of Methane Carbon Isotope Values of GM Lindbergh Zoom-in

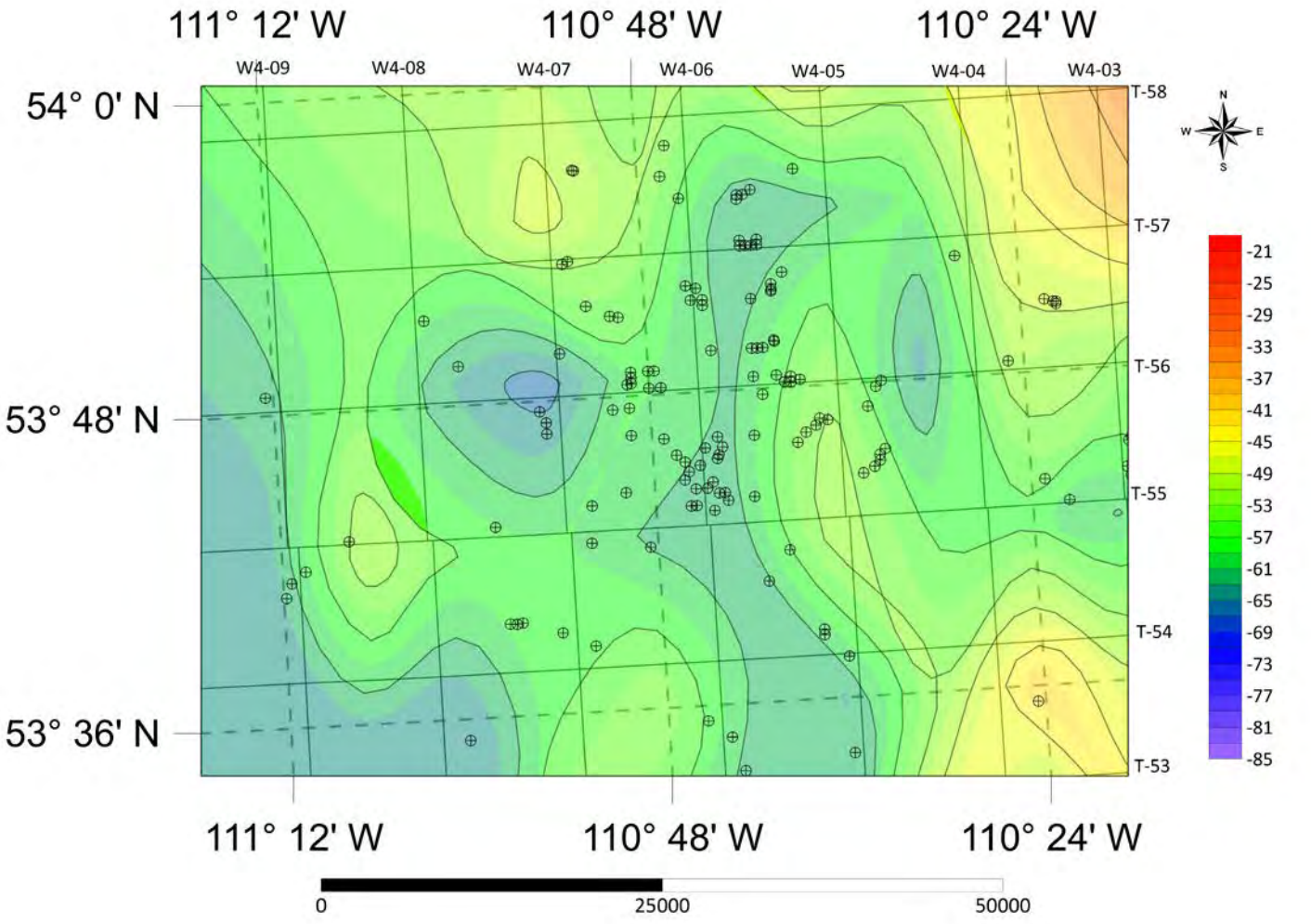

Methane Carbon Isotope Values (‰, VPDB)

Fig. 26C. Contour Map of Ethane Carbon Isotope Values of GM Lindbergh Zoom-in

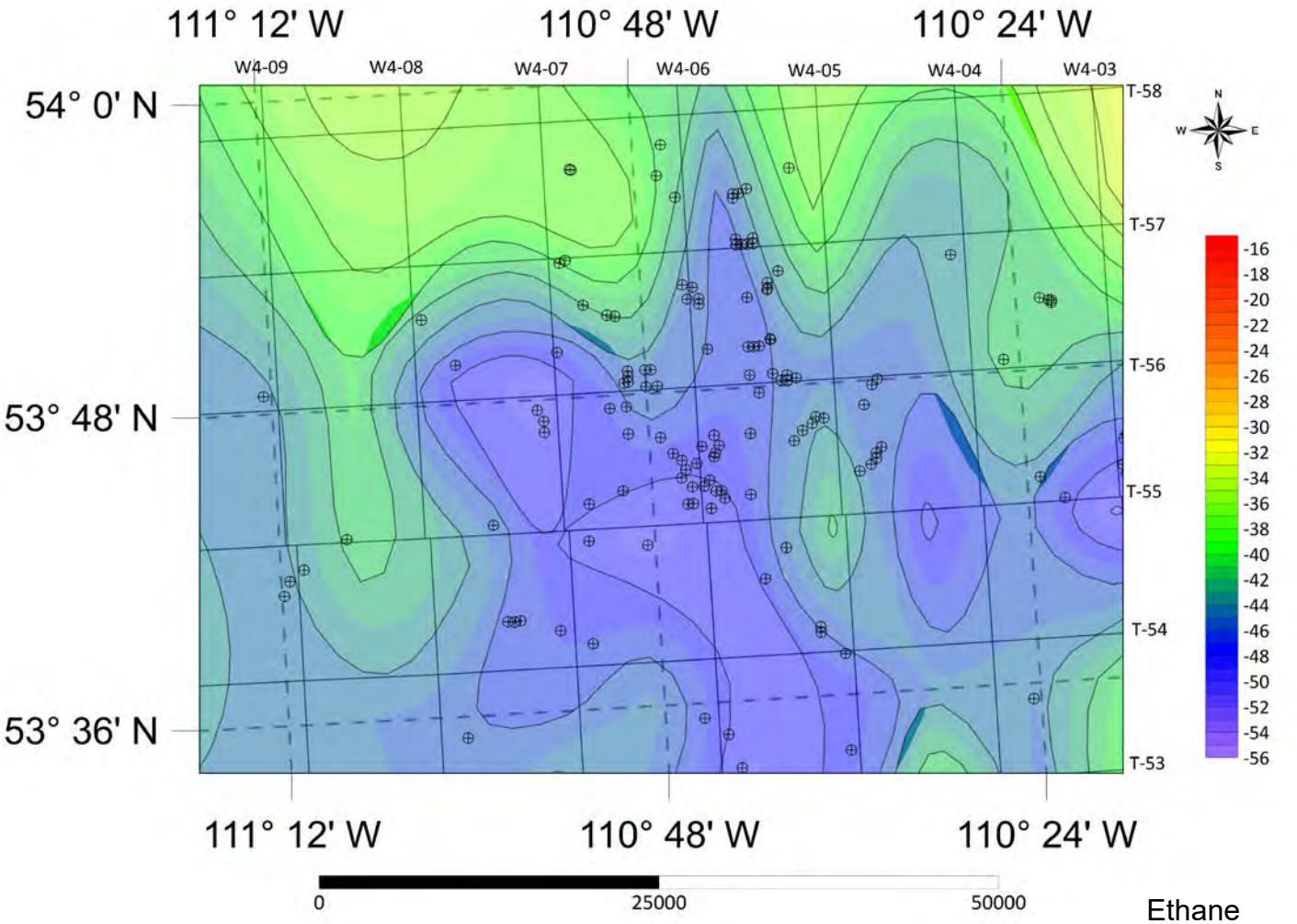

Fig. 26D. Contour Map of Propane Carbon Isotope Values of GM Lindbergh Zoom-in

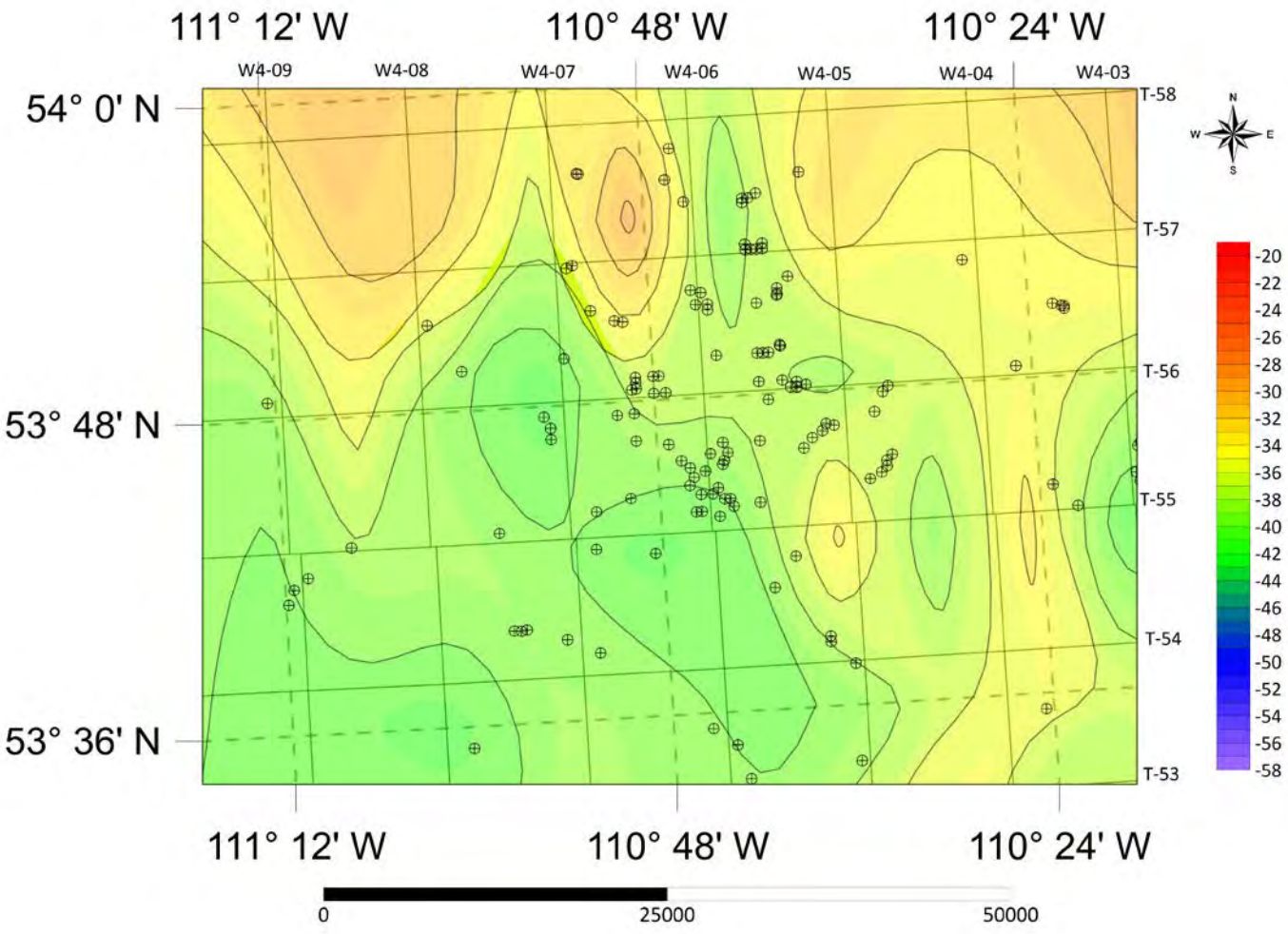

Propane Carbon Isotope Values (‰, VPDB)

Fig. 26E. Contour Map of *n*-Butane Carbon Isotope Values of GM Lindbergh Zoom-in

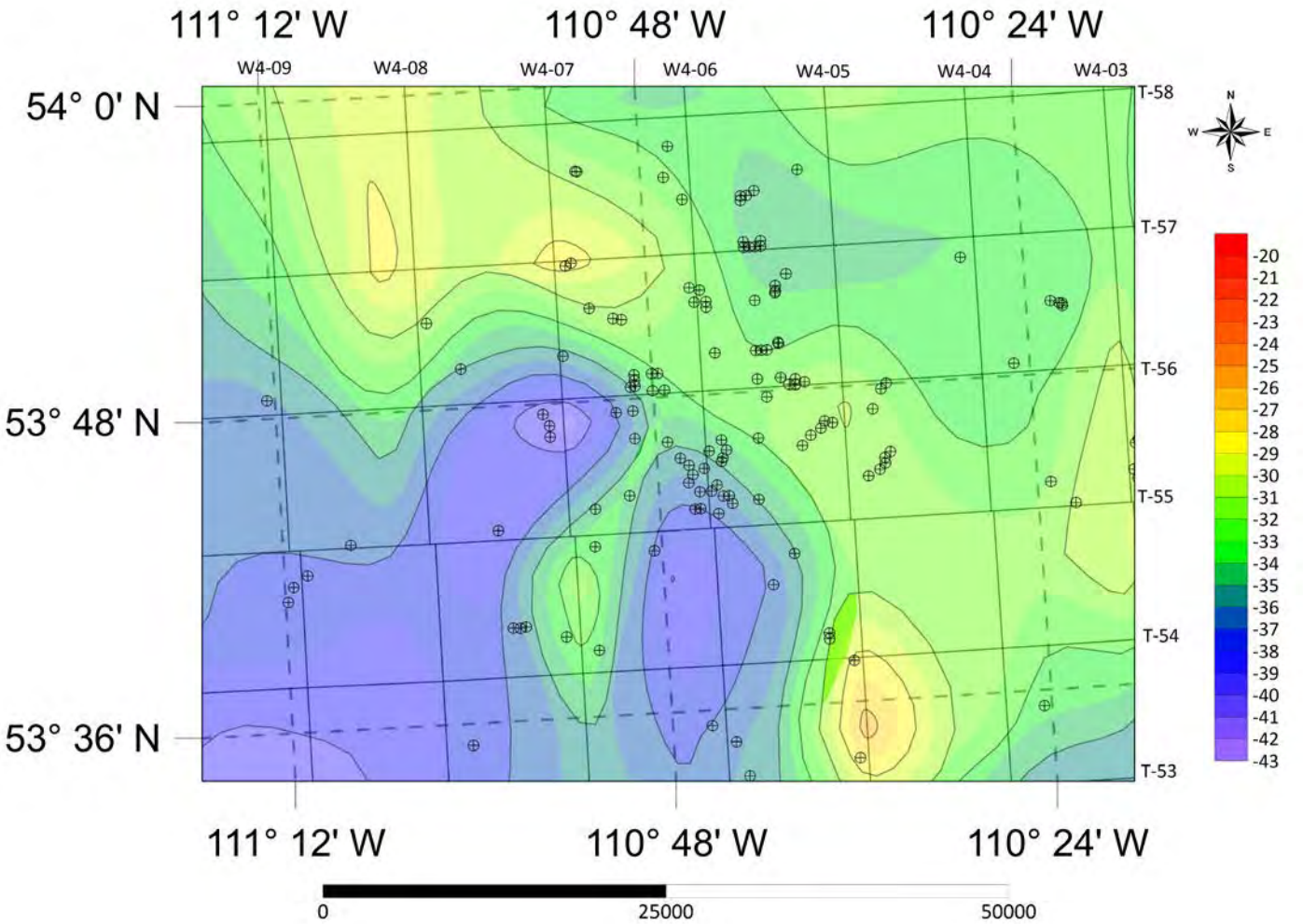

n-Butane Carbon Isotope Values (‰, VPDB)

Fig. 26F. Contour Map of *i*-Butane Carbon Isotope Values of GM Lindbergh Zoom-in

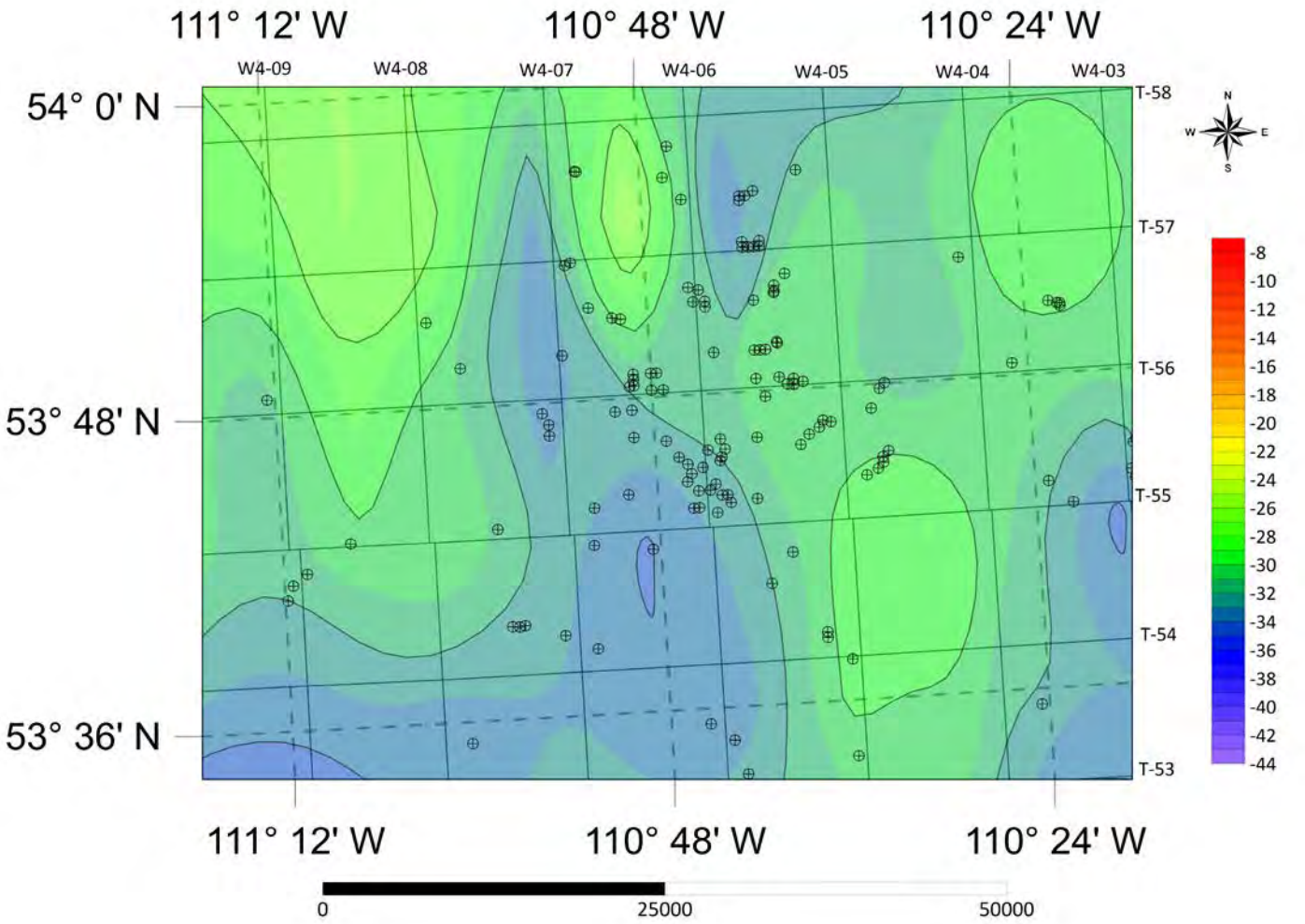

i-Butane Carbon Isotope Values (‰, VPDB)

Fig. 26G. Contour Map of Carbon Dioxide Carbon Isotope Values of GM Lindbergh Zoom-in

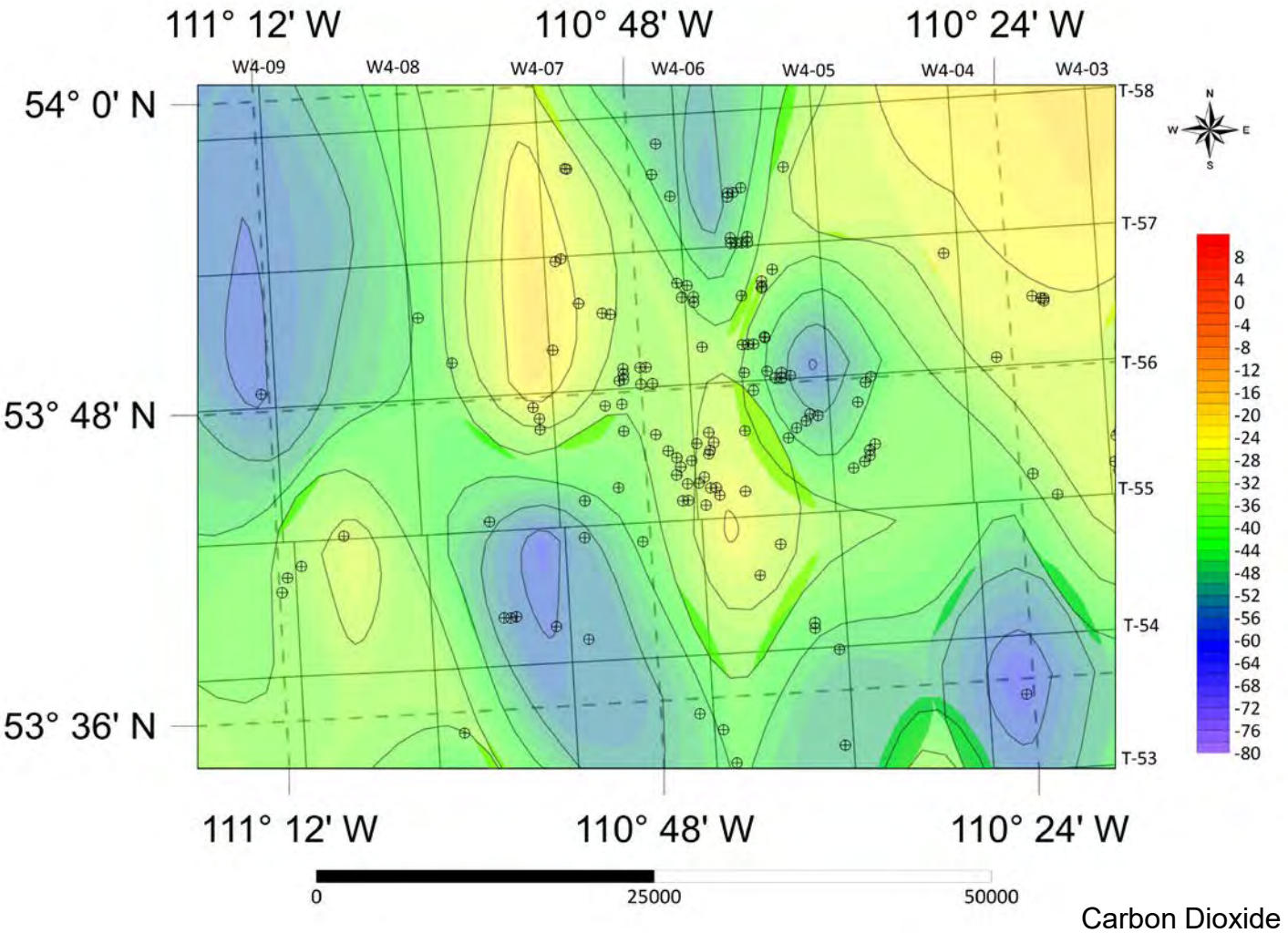

Carbon Dioxide Carbon Isotope Values (‰, VPDB)

Fig. 26H. Contour Map of Methane Carbon Isotope Values of GM Lindbergh Zoom-in over Topographic Map

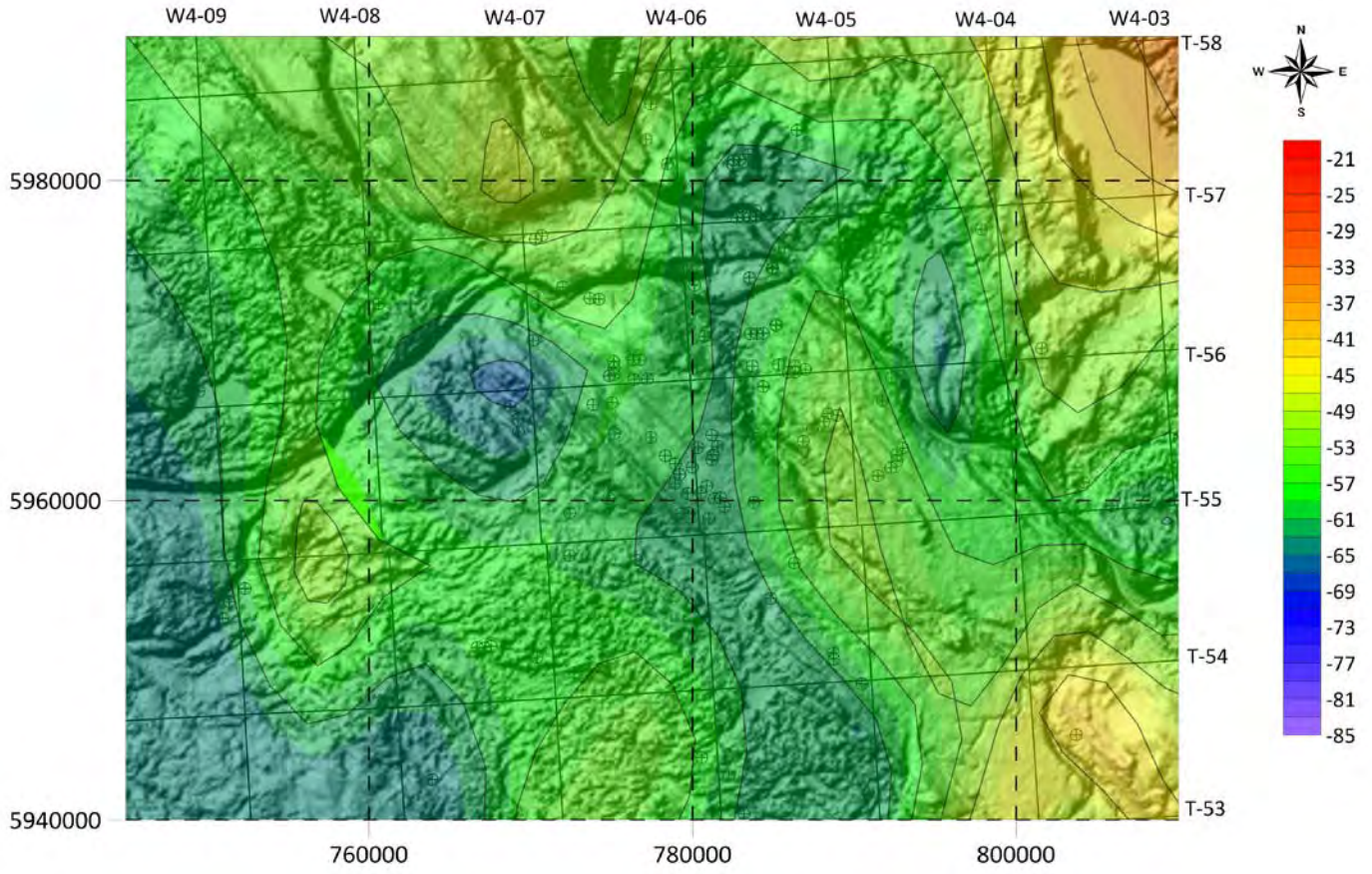

Methane Carbon Isotope Values (‰, VPDB)

Fig. 26I. Contour Map of Ethane Carbon Isotope Values of GM Lindbergh Zoom-in over Topographic Map

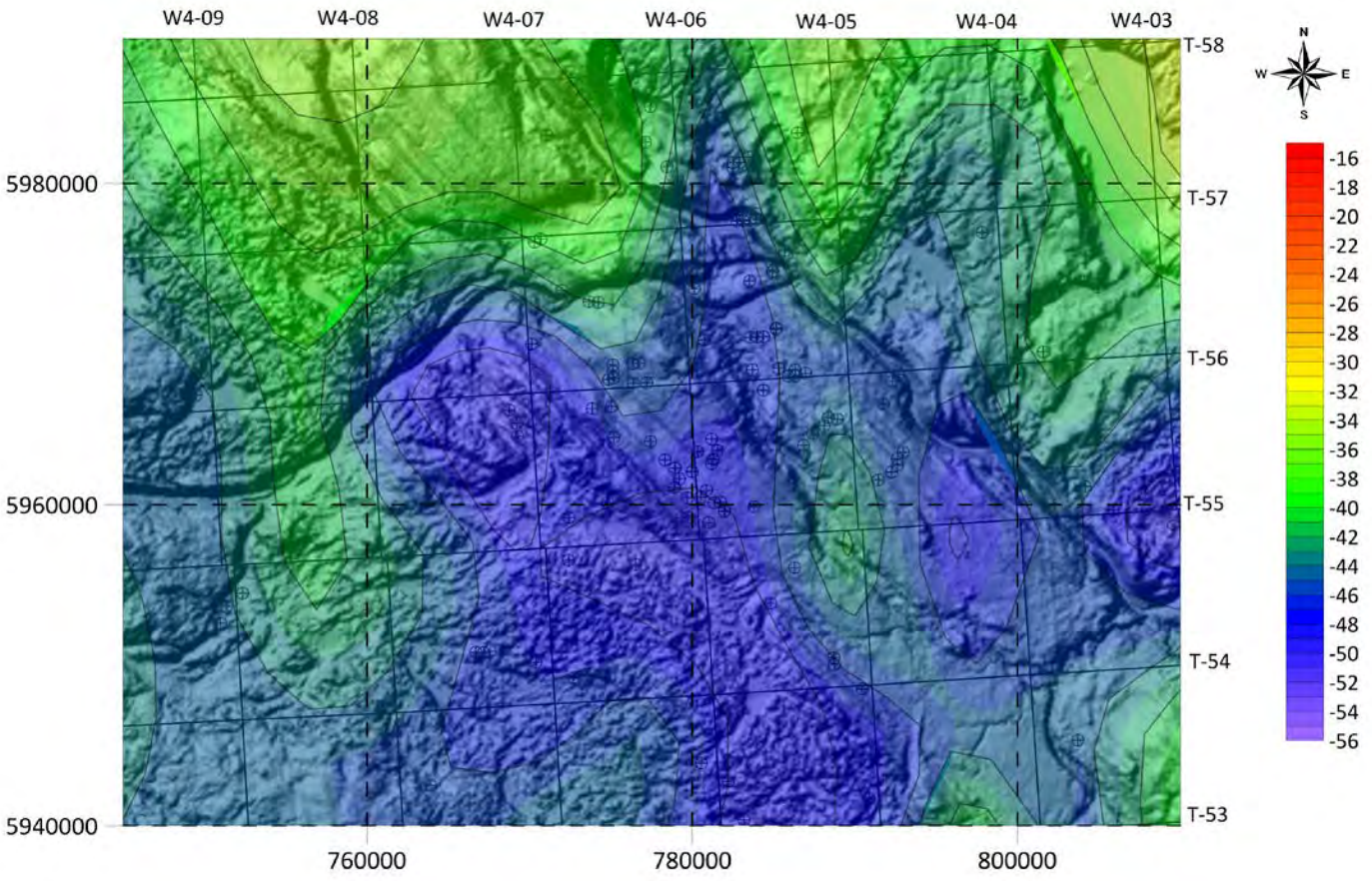

Ethane Carbon Isotope Values (‰, VPDB)

Fig. 26J. Contour Map of Propane Carbon Isotope Values of GM Lindbergh Zoom-in over Topographic Map

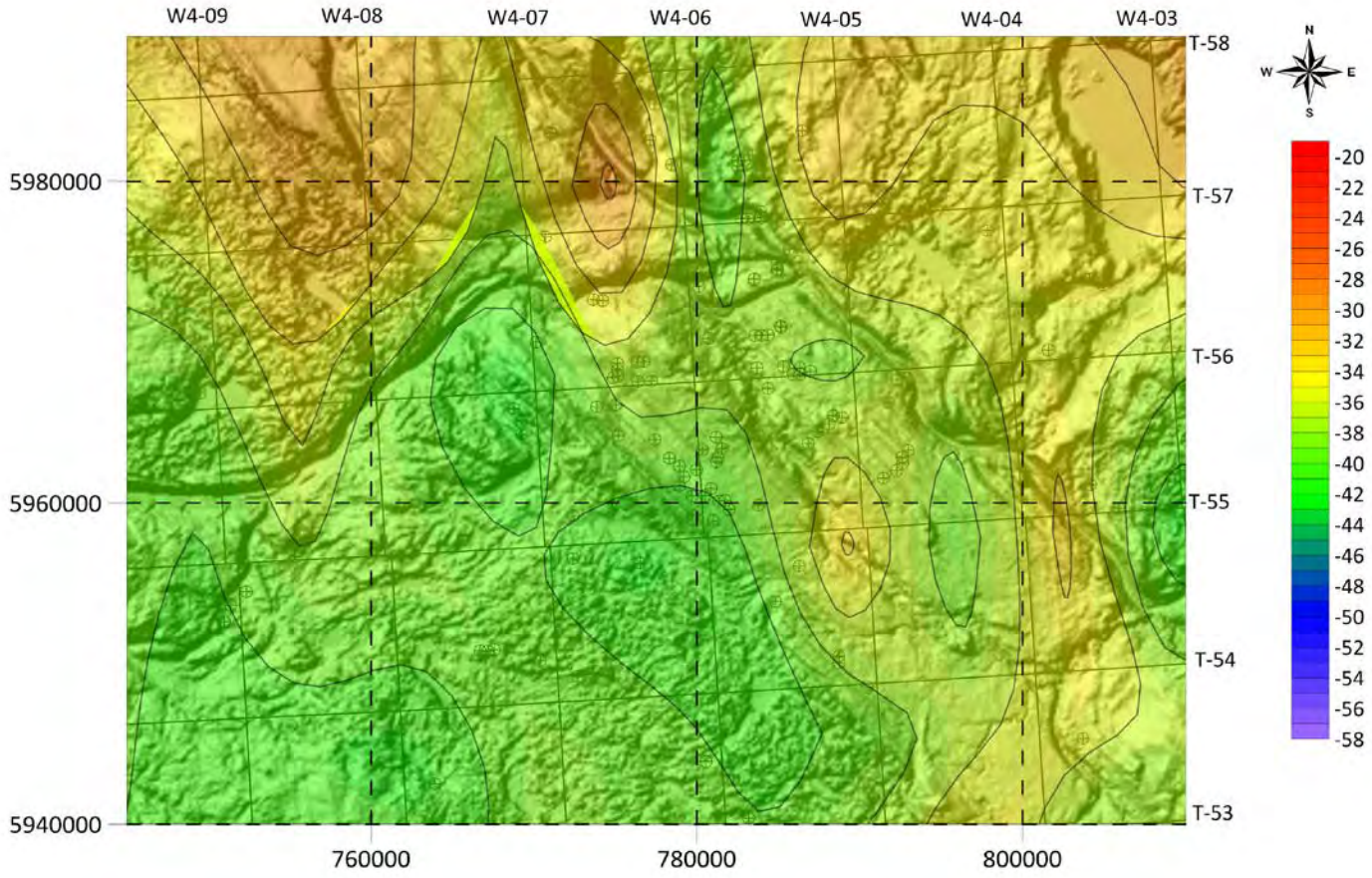

Propane Carbon Isotope Values (‰, VPDB)

Fig. 26K. Contour Map of *n*-Butane Carbon Isotope Values of GM Lindbergh Zoom-in over Topographic Map

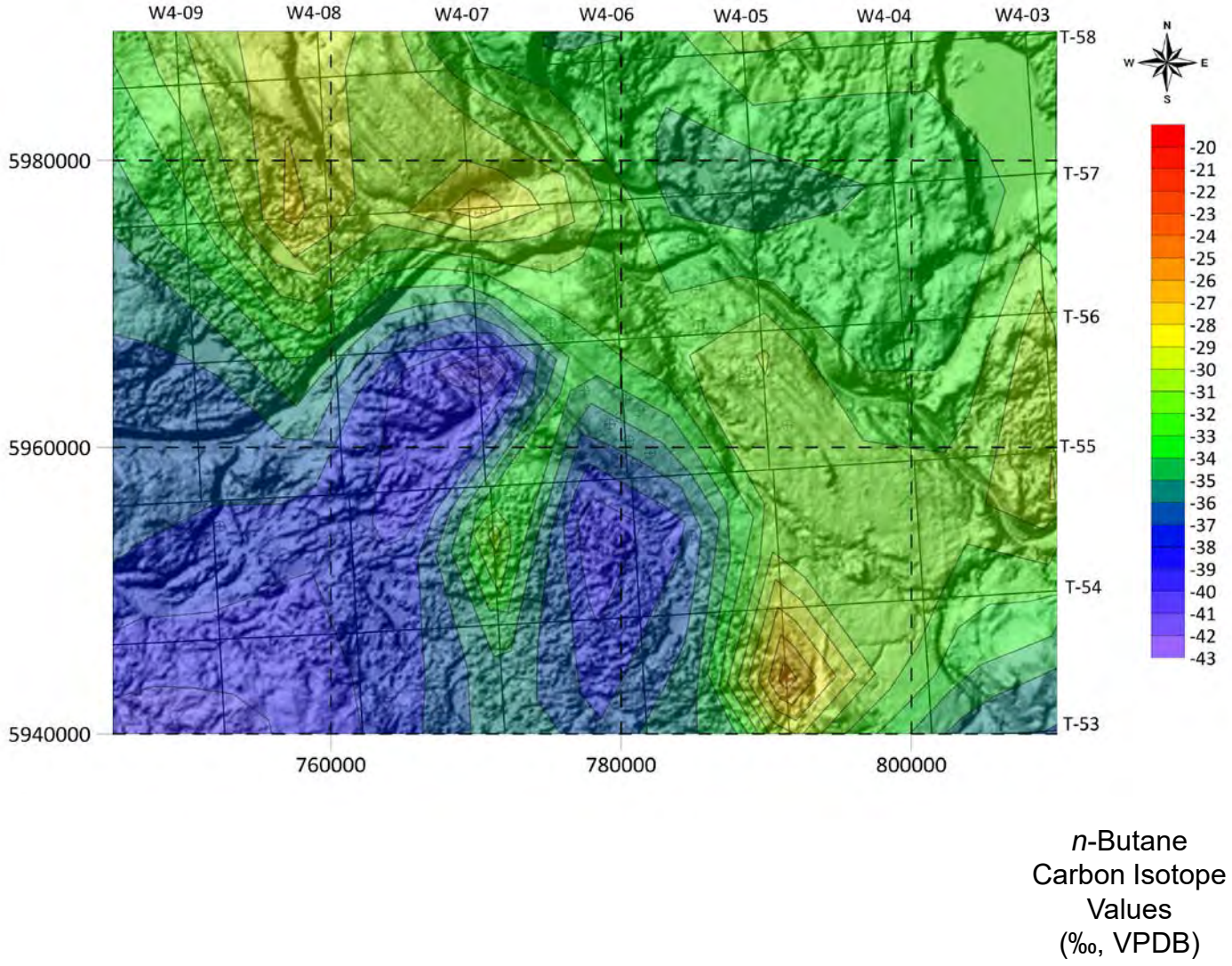

n-Butane Carbon Isotope Values (‰, VPDB)

Fig. 26L. Contour Map of *i*-Butane Carbon Isotope Values of GM Lindbergh Zoom-in over Topographic Map

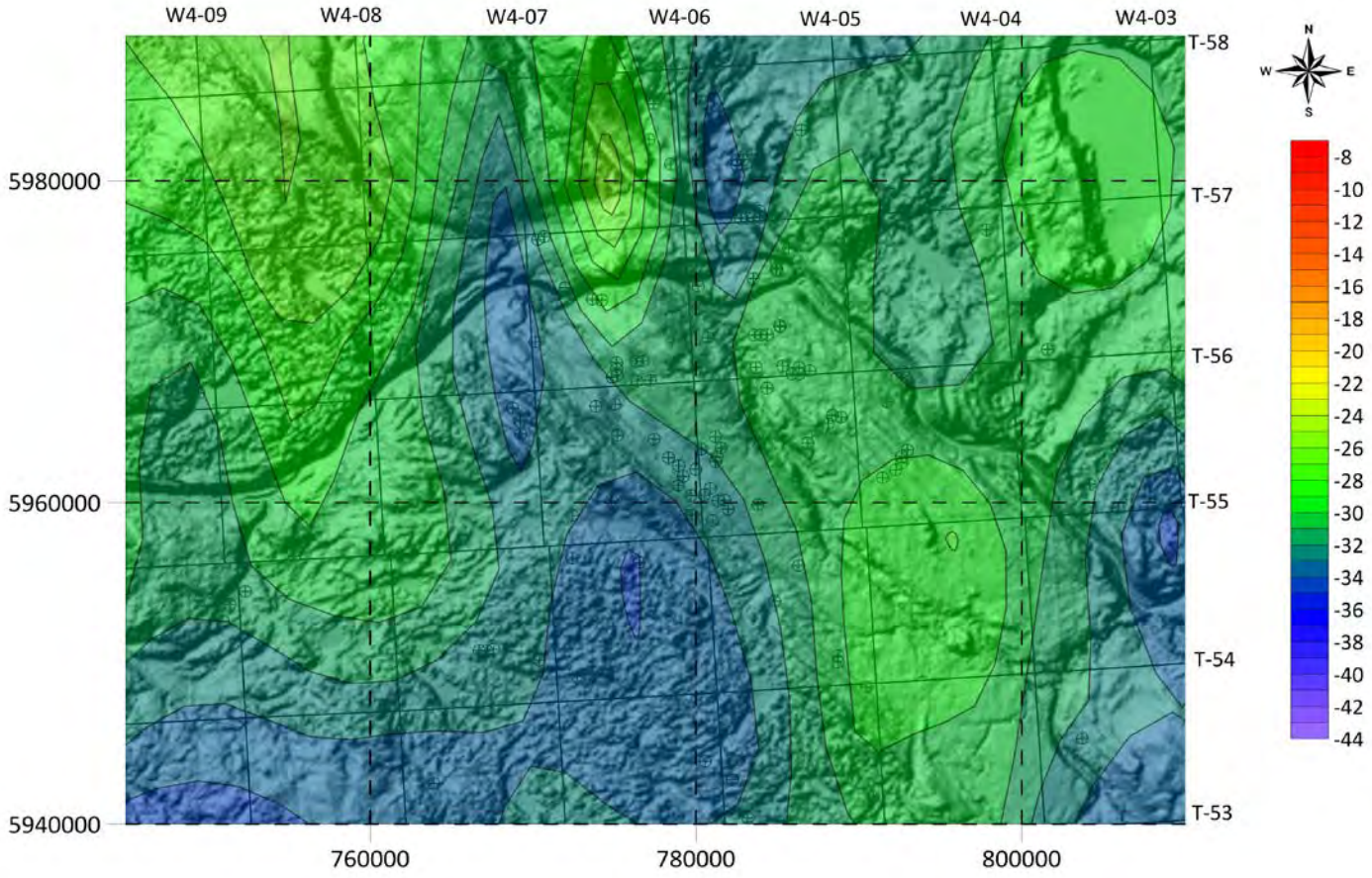

i-Butane Carbon Isotope Values (‰, VPDB)

Fig. 26M. Contour Map of Carbon Dioxide Carbon Isotope Values of GM Lindbergh Zoom-in over Topographic Map

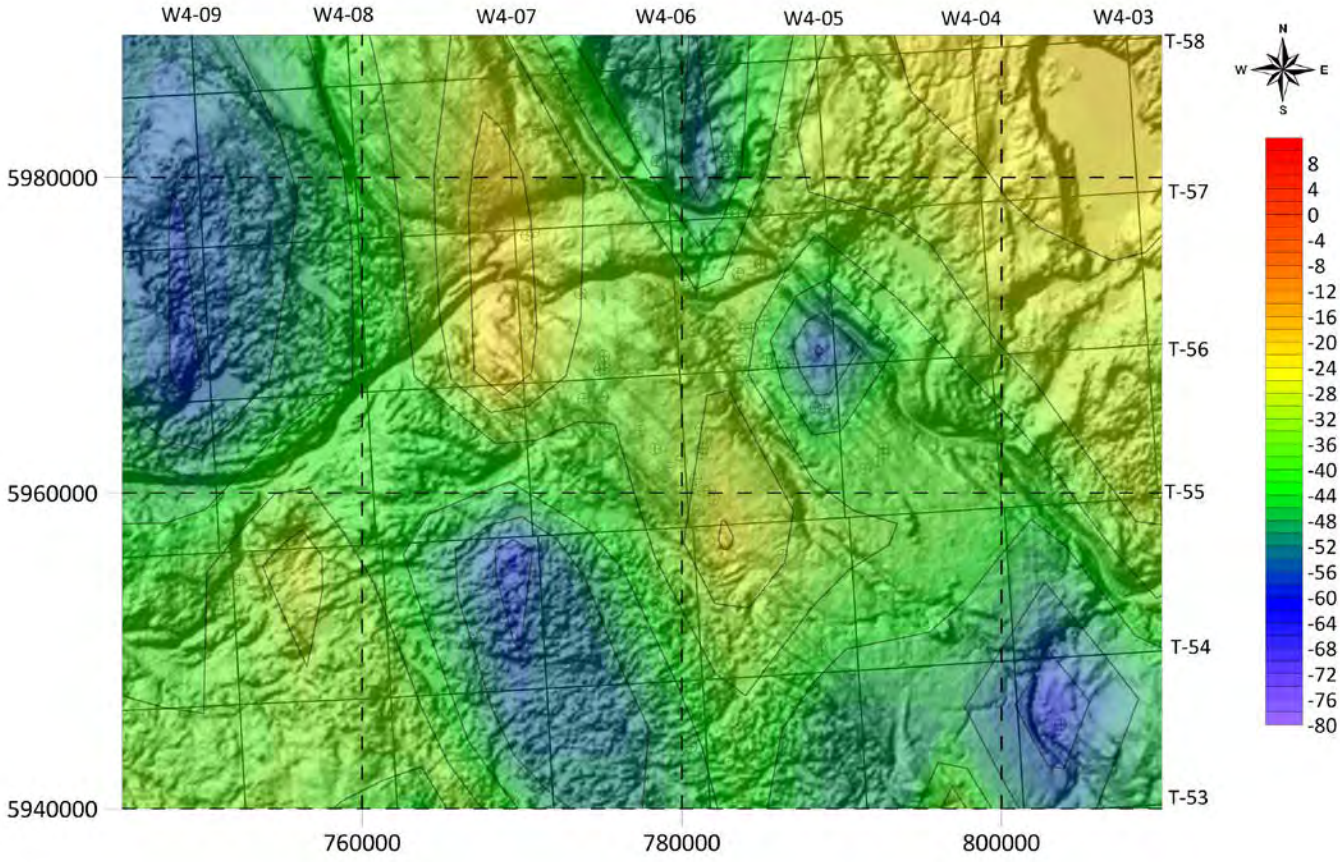

Carbon Dioxide Carbon Isotope Values (‰, VPDB)

Fig. 27A. Map of surface casing vent (SCV) Locations in the Wildmere Zoom-in

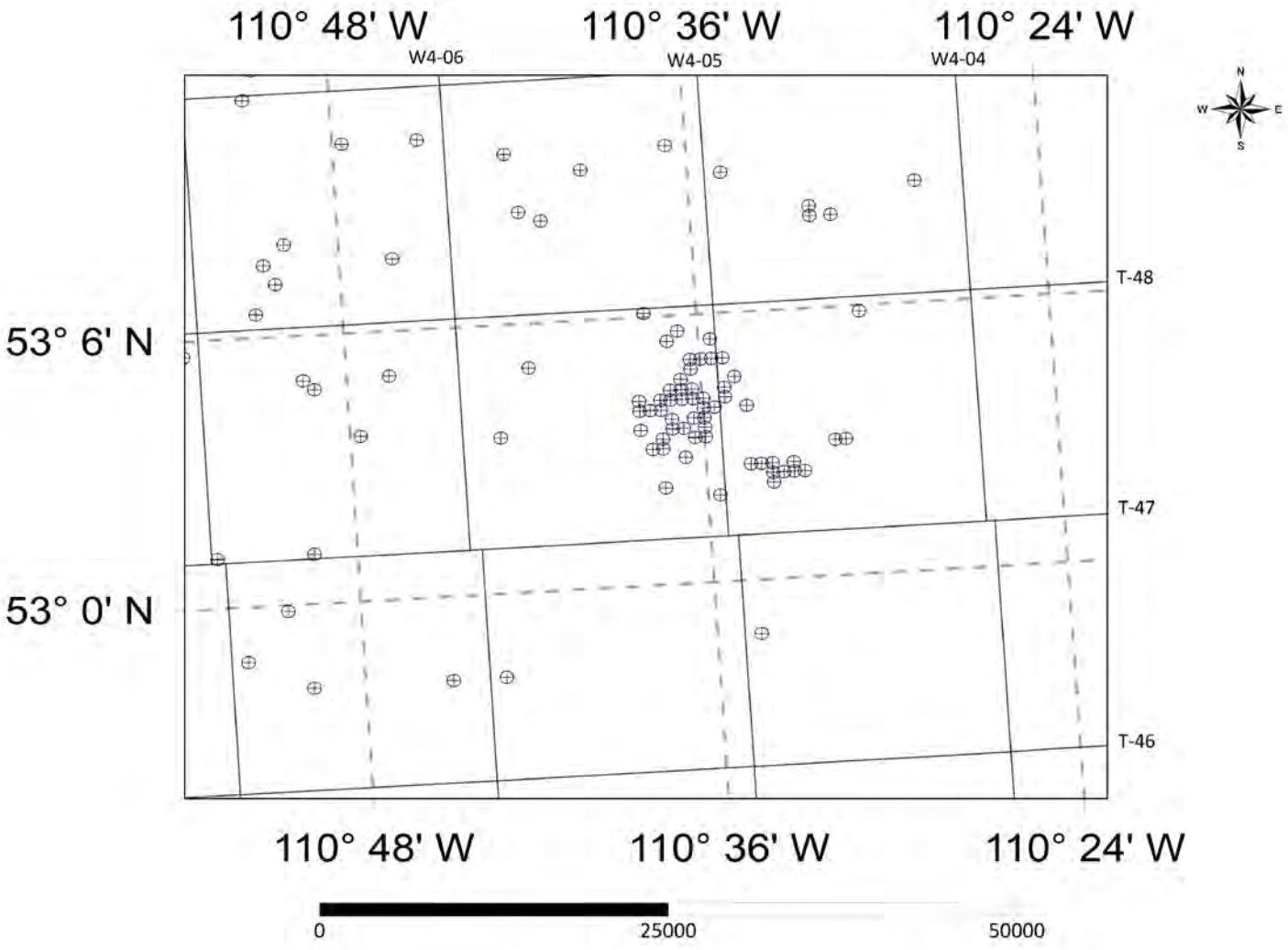

Fig. 27B. Contour Map of Methane Carbon Isotope Values of SCV Wildmere Zoom-in

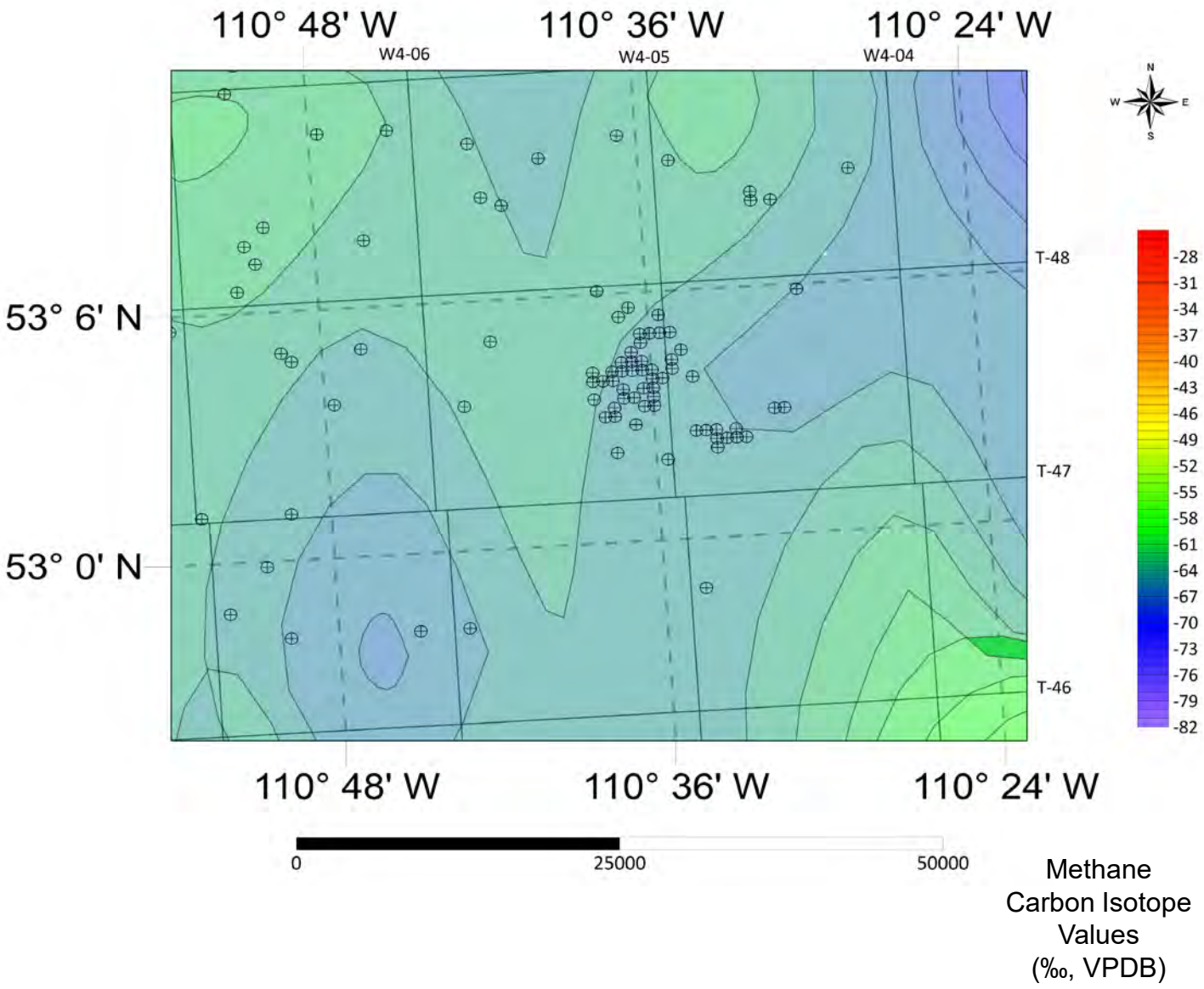

Fig. 27C. Contour Map of Ethane Carbon Isotope Values of SCV Wildmere Zoom-in

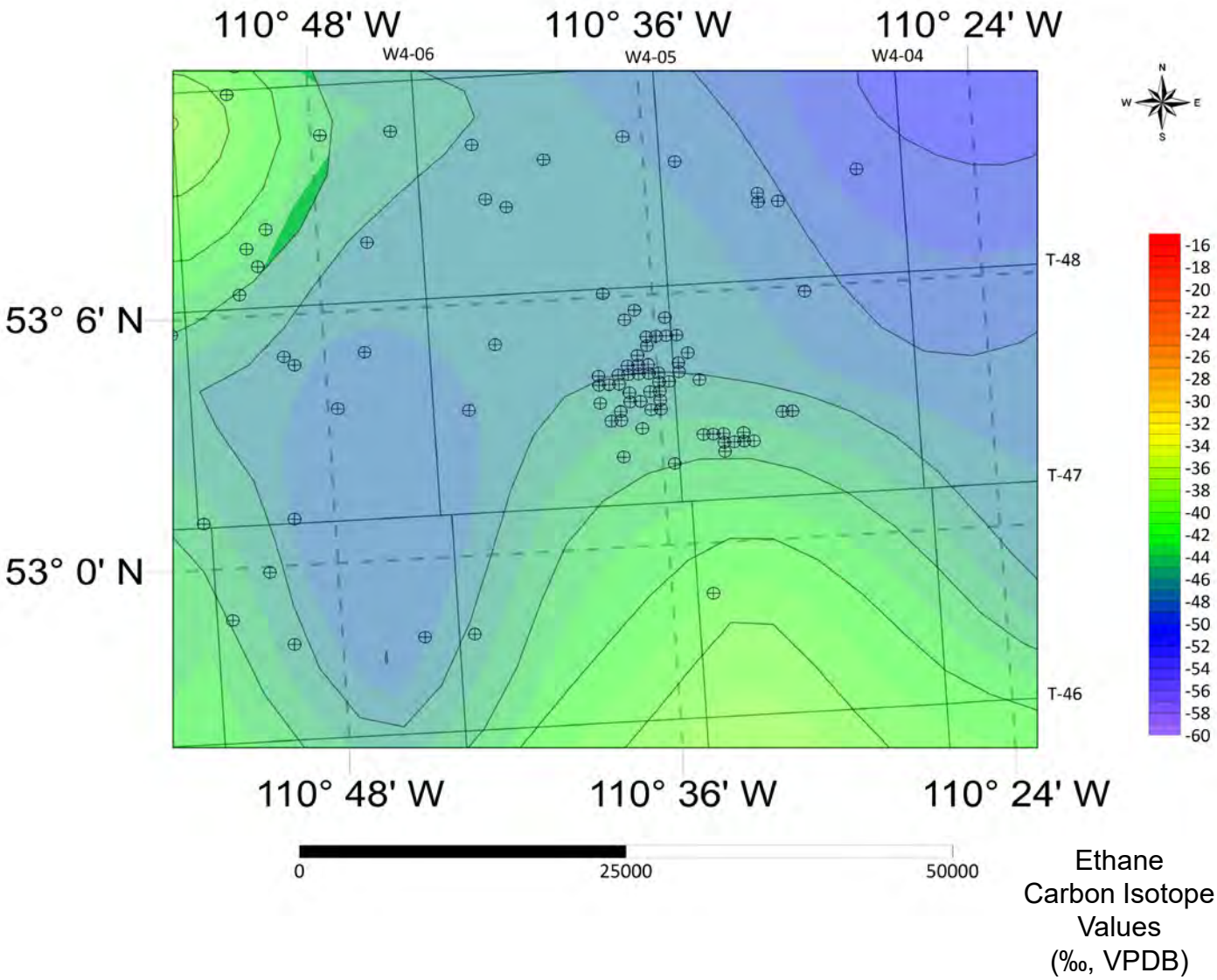

Fig. 27D. Contour Map of Propane Carbon Isotope Values of SCV Wildmere Zoom-in

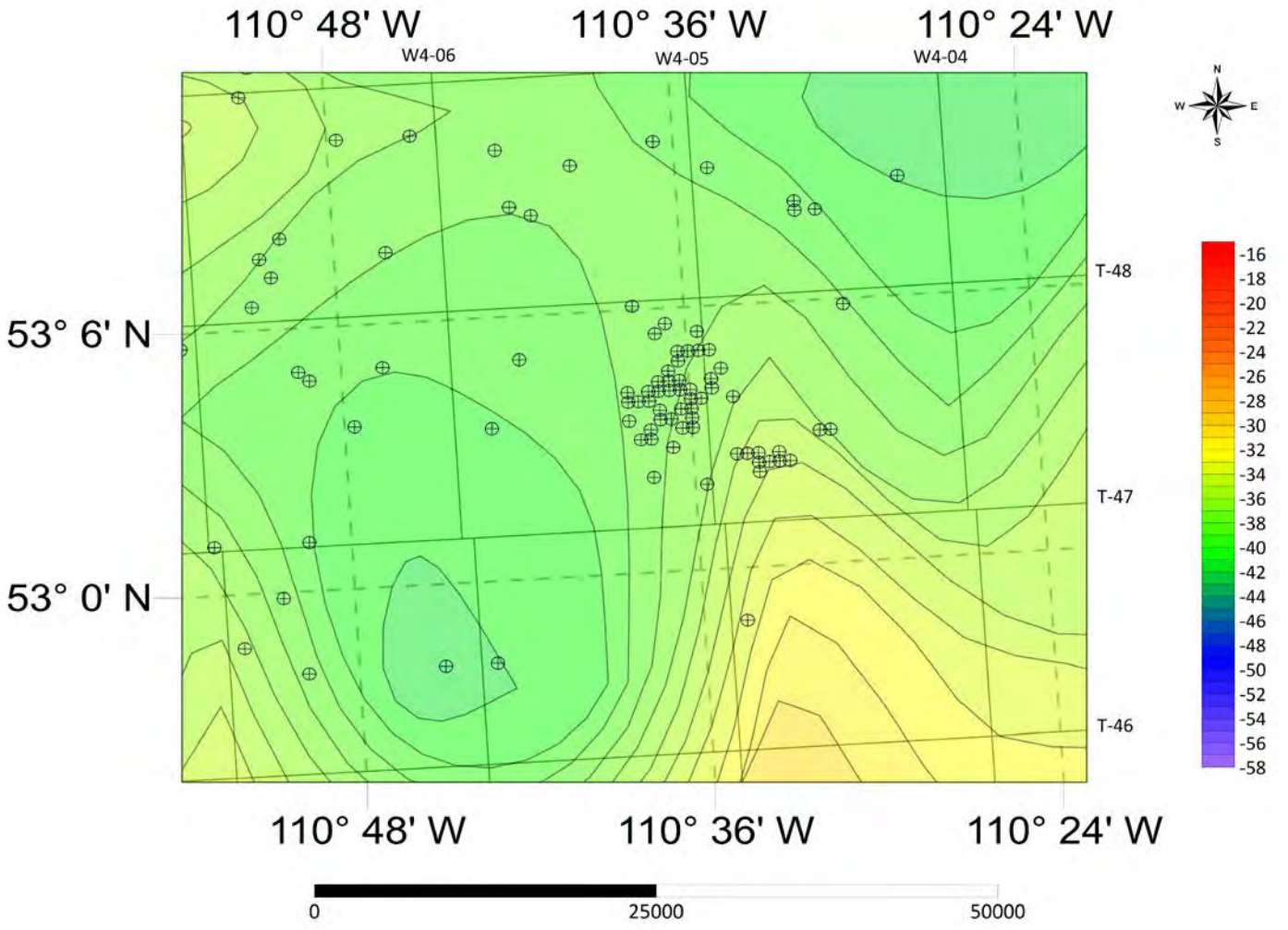

Propane Carbon Isotope Values (‰, VPDB)

Fig. 27E. Contour Map of *n*-Butane Carbon Isotope Values of SCV Wildmere Zoom-in

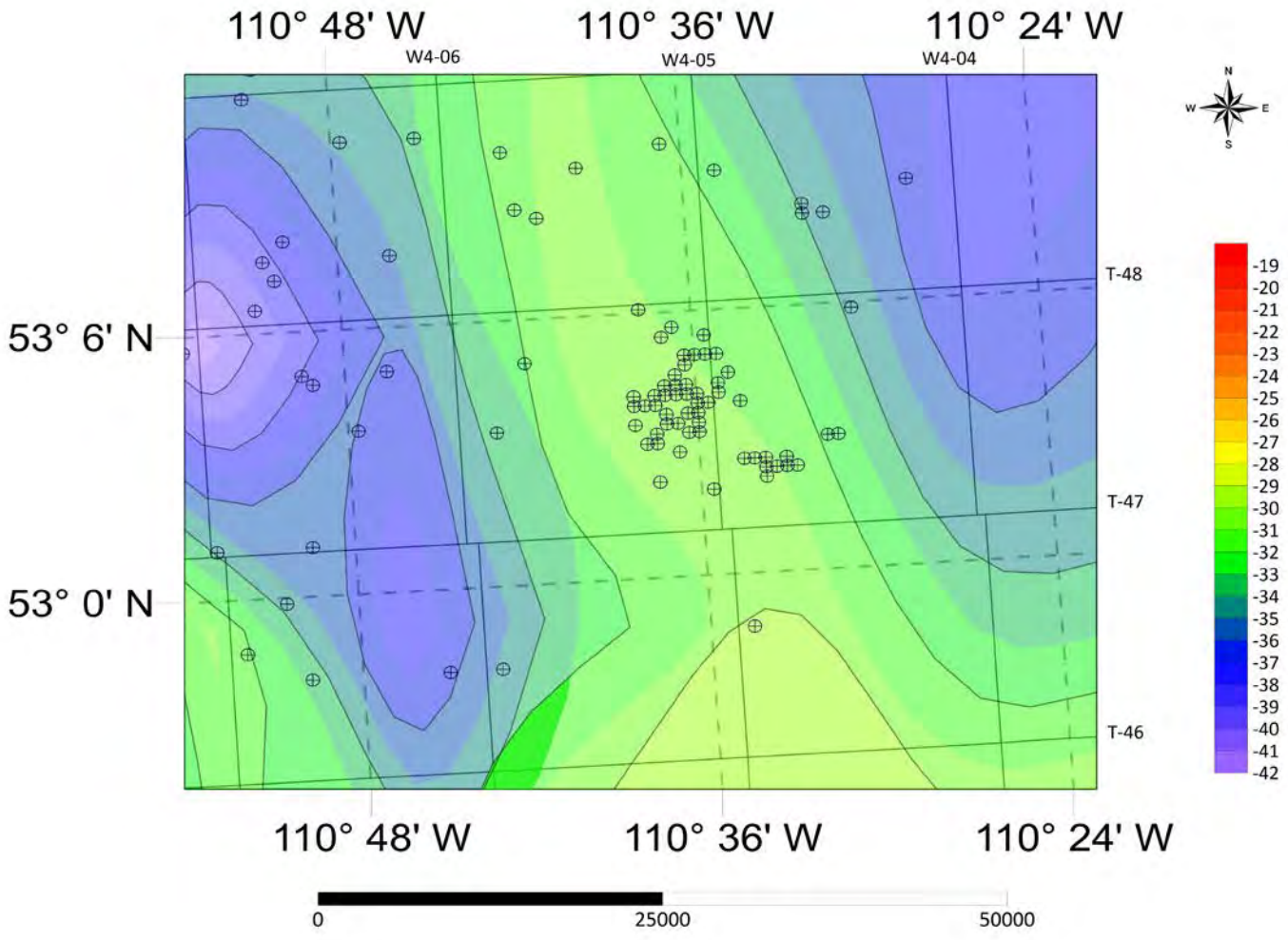

Carbon Isotope Values (‰, VPDB)

Fig. 27F. Contour Map of *i*-Butane Carbon Isotope Values of SCV Wildmere Zoom-in

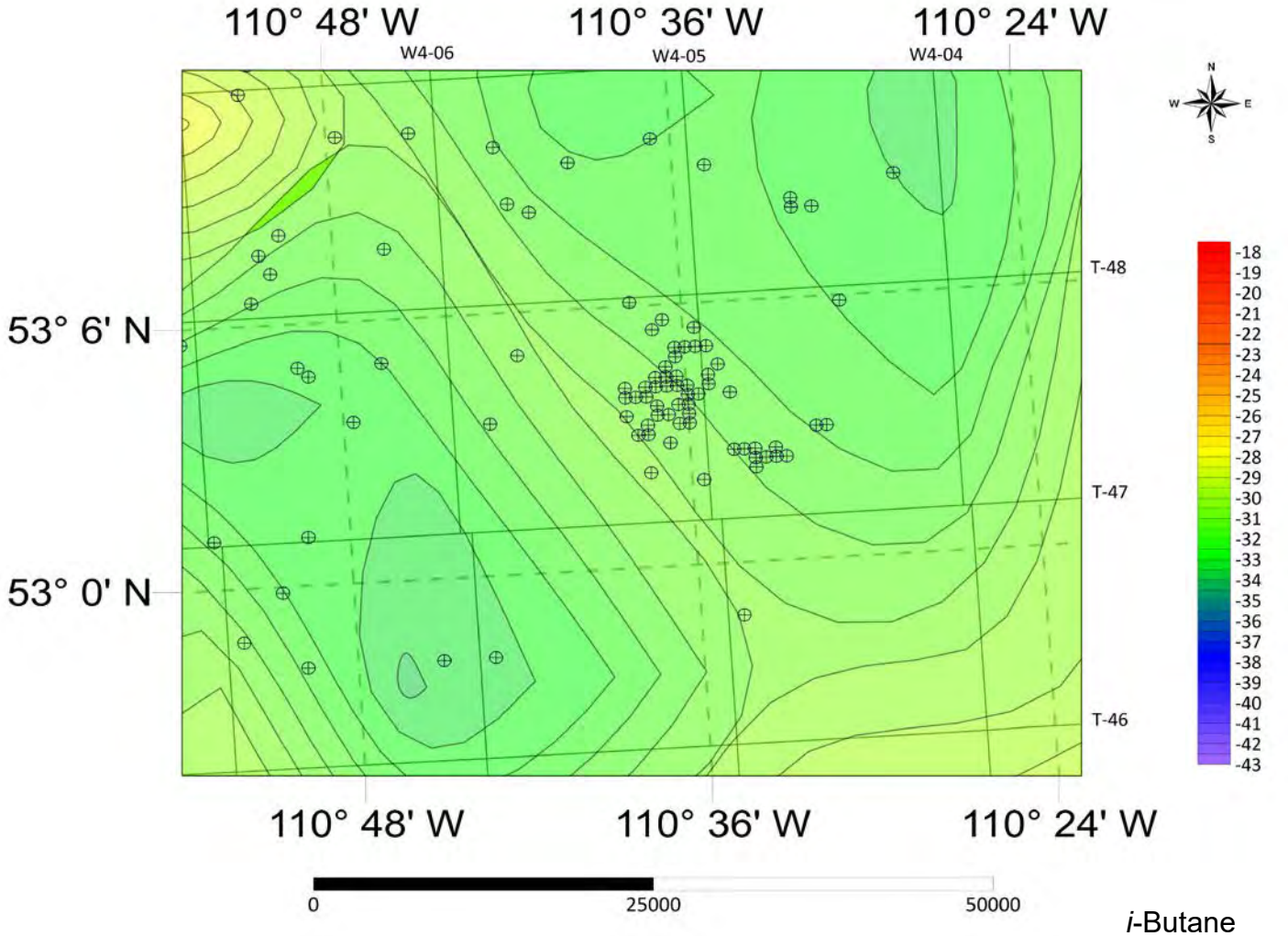

i-Butane Carbon Isotope Values (‰, VPDB)

Fig. 27G. Contour Map of Carbon Dioxide Carbon Isotope Values of GM Wildmere Zoom-in

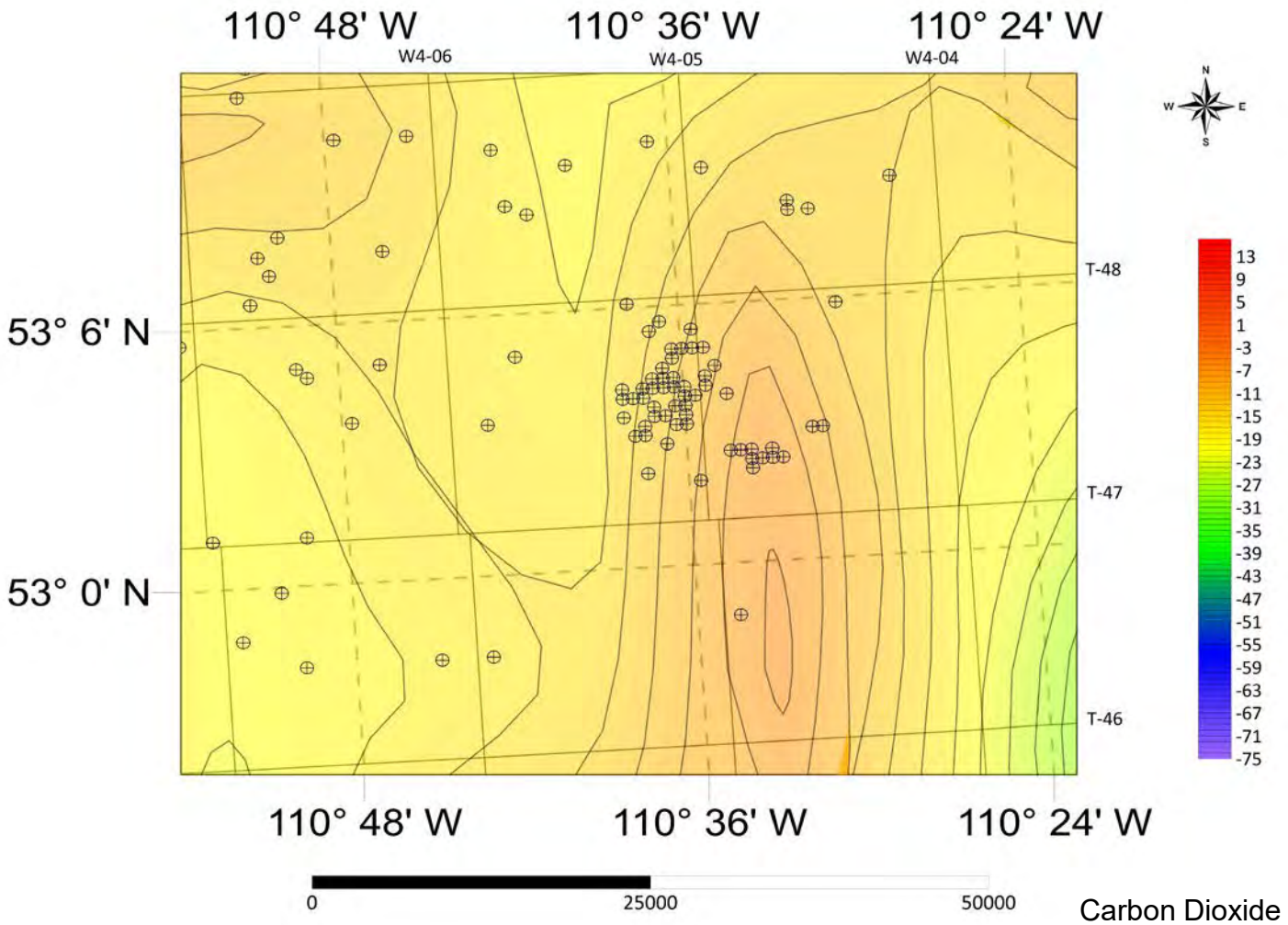

Fig. 27H. Contour Map of Methane Carbon Isotope Values of SCV Wildmere Zoom-in over Topographic Map

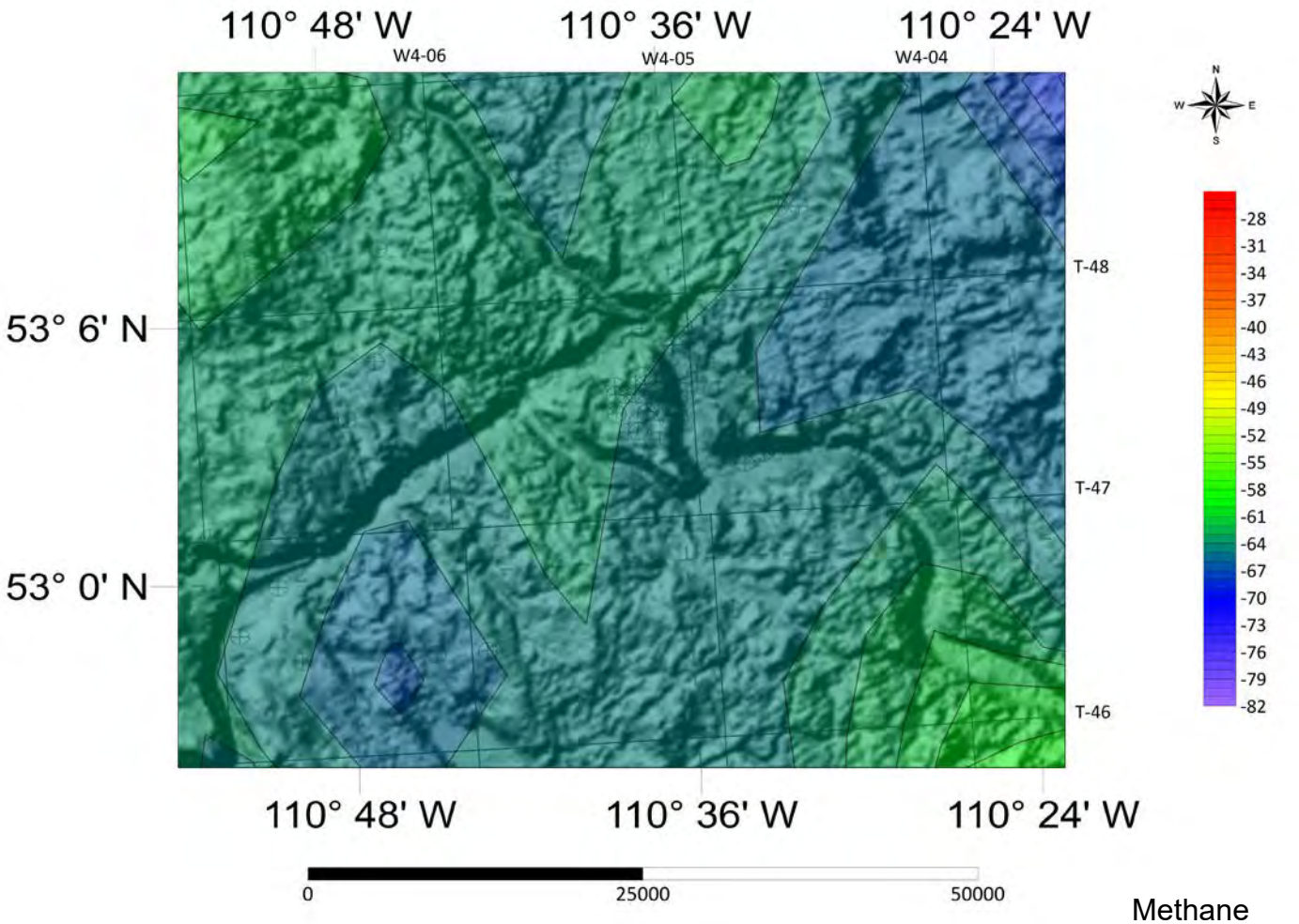

Methane Carbon Isotope Values (‰, VPDB)

Fig. 27l. Contour Map of Ethane Carbon Isotope Values of SCV Wildmere Zoom-in over Topographic Map

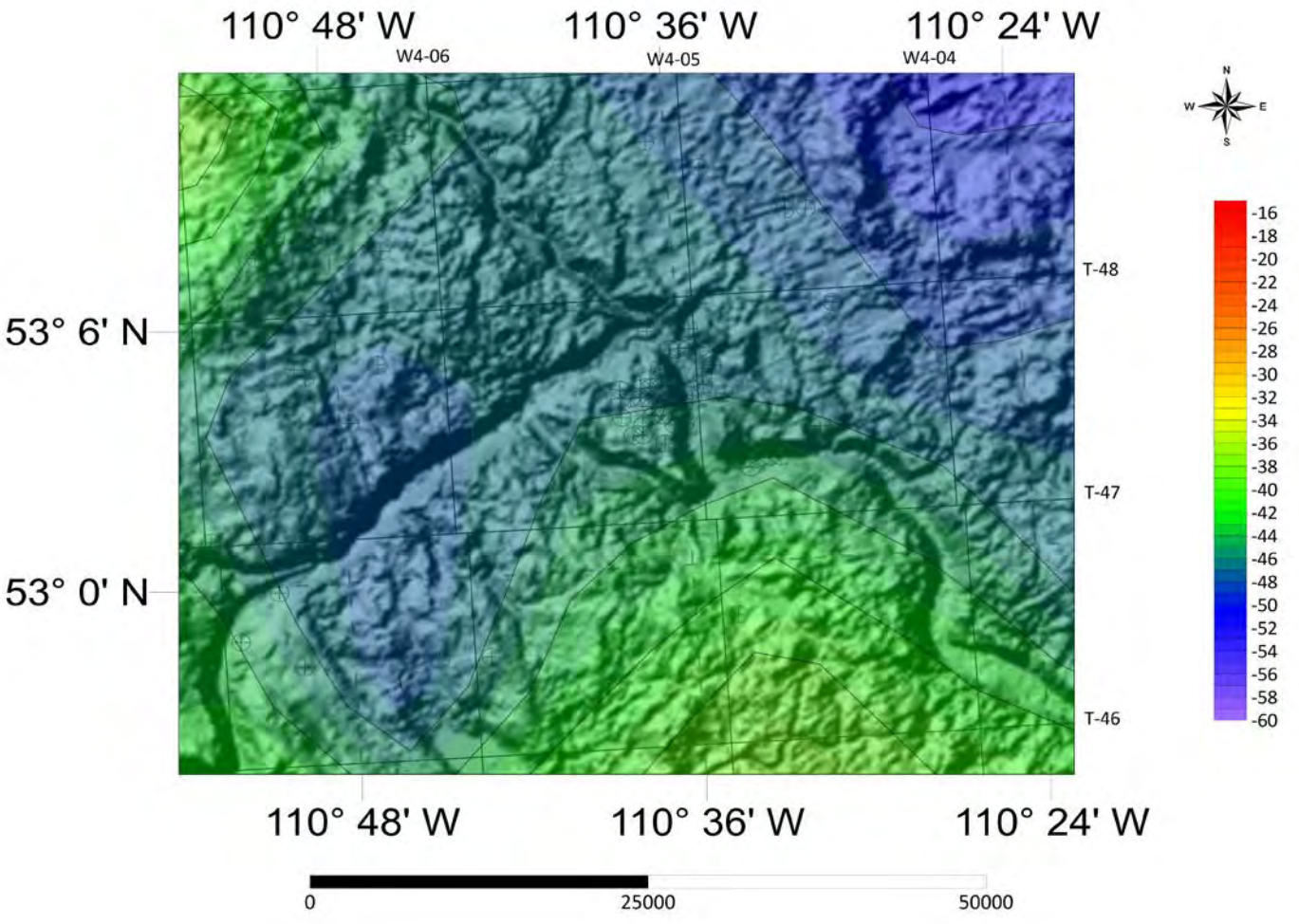

Ethane Carbon Isotope Values (‰, VPDB)

Fig. 27J. Contour Map of Propane Carbon Isotope Values of SCV Wildmere Zoom-in over Topographic Map

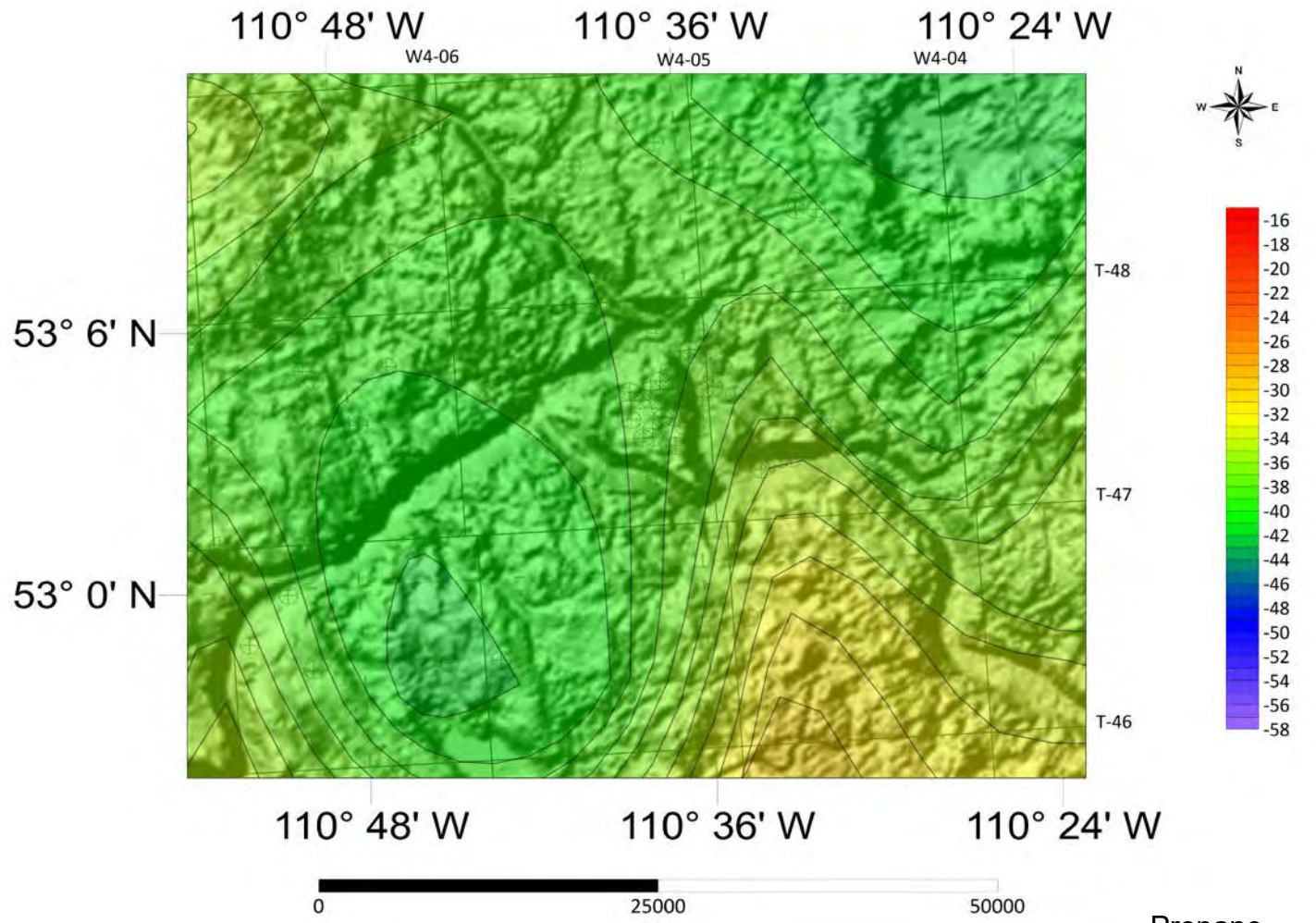

Propane Carbon Isotope Values (‰, VPDB)

Fig. 27K. Contour Map of *n*-Butane Carbon Isotope Values of SCV Wildmere Zoom-in over Topographic Map

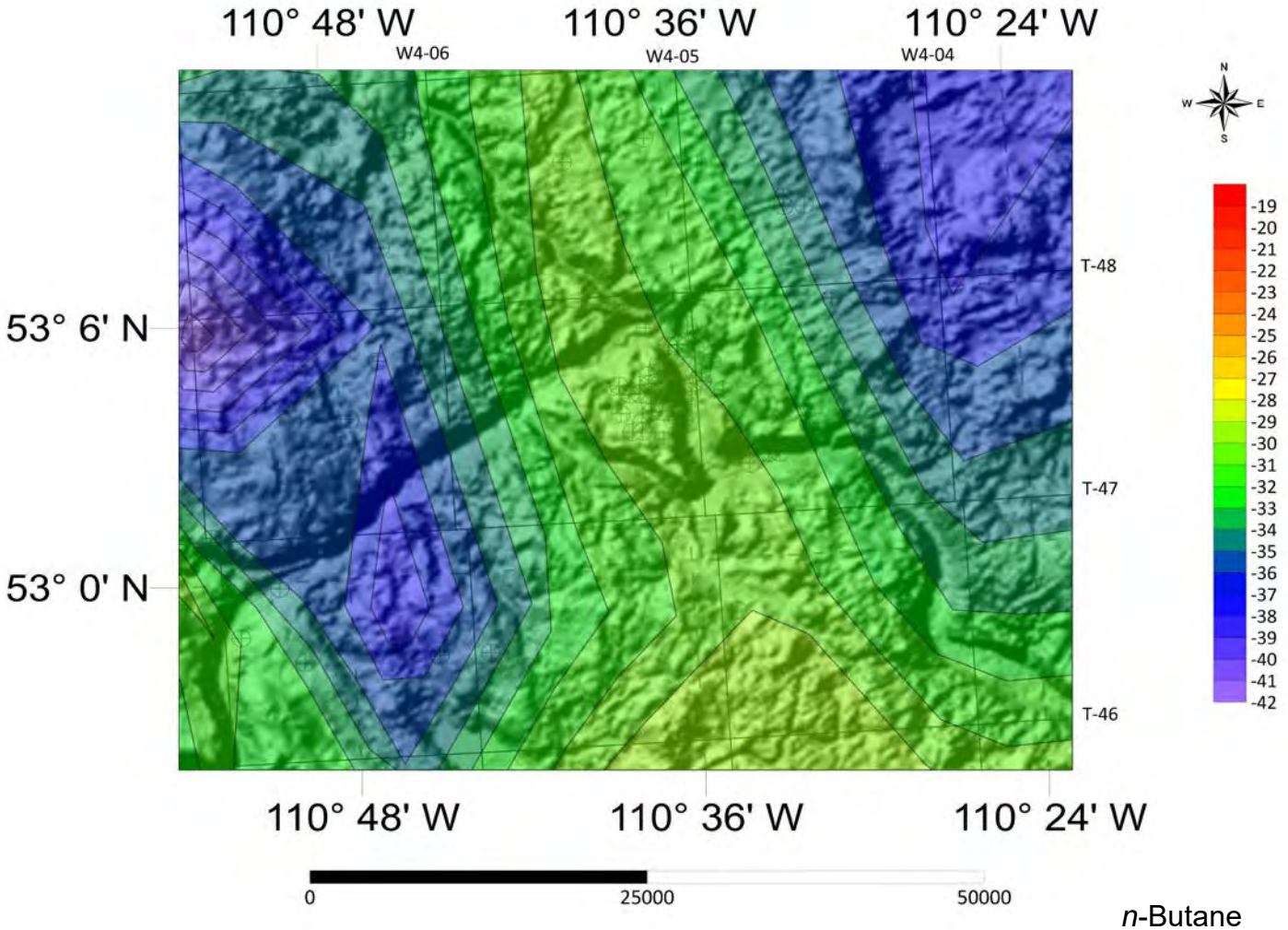

n-Butane Carbon Isotope Values (‰, VPDB)

Fig. 27L. Contour Map of *i*-Butane Carbon Isotope Values of SCV Wildmere Zoom-in over Topographic Map

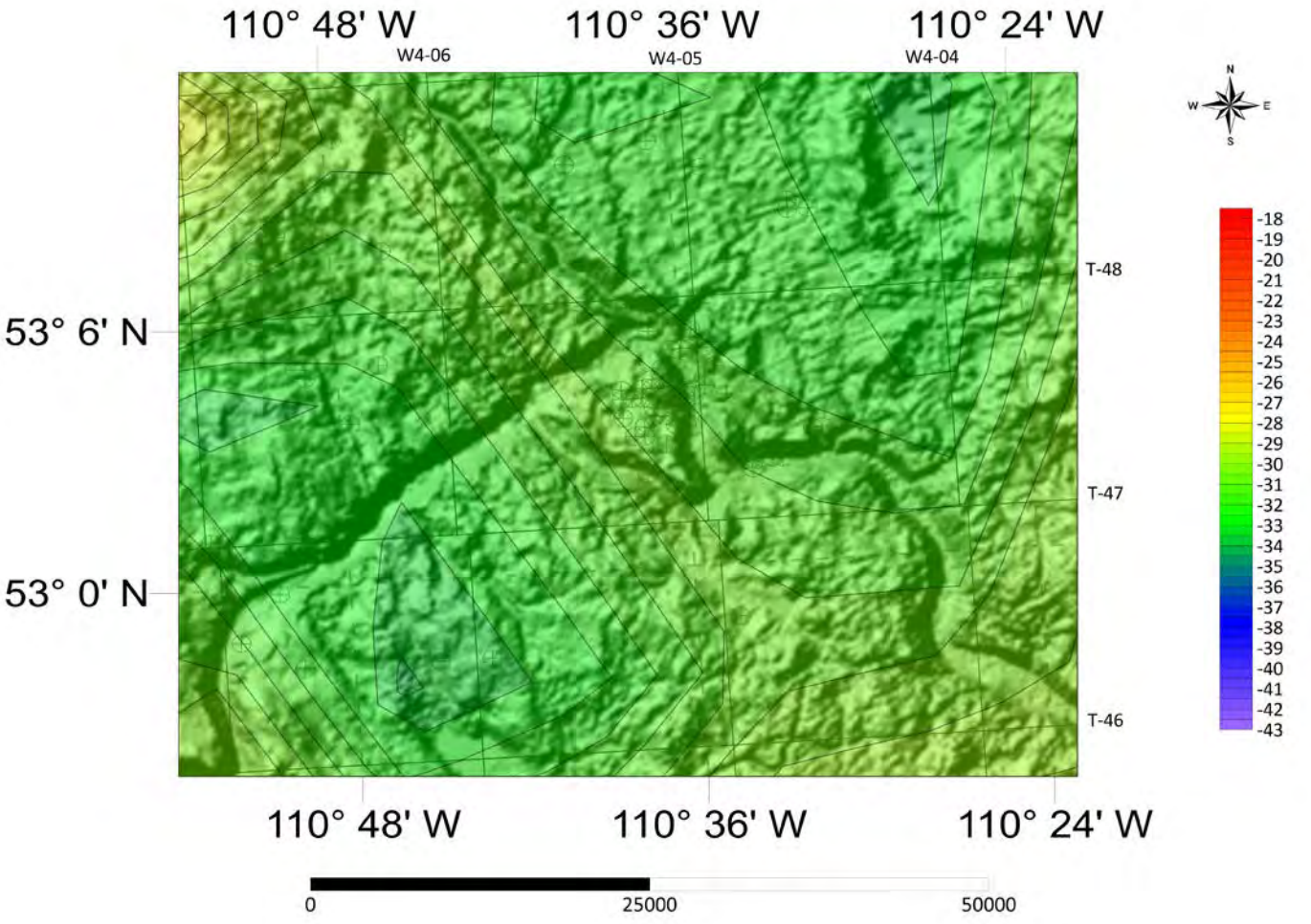

i-Butane Carbon Isotope Values (‰, VPDB)

Fig. 27M. Contour Map of Carbon Dioxide Carbon Isotope Values of SCV Wildmere Zoom-in over Topographic Map

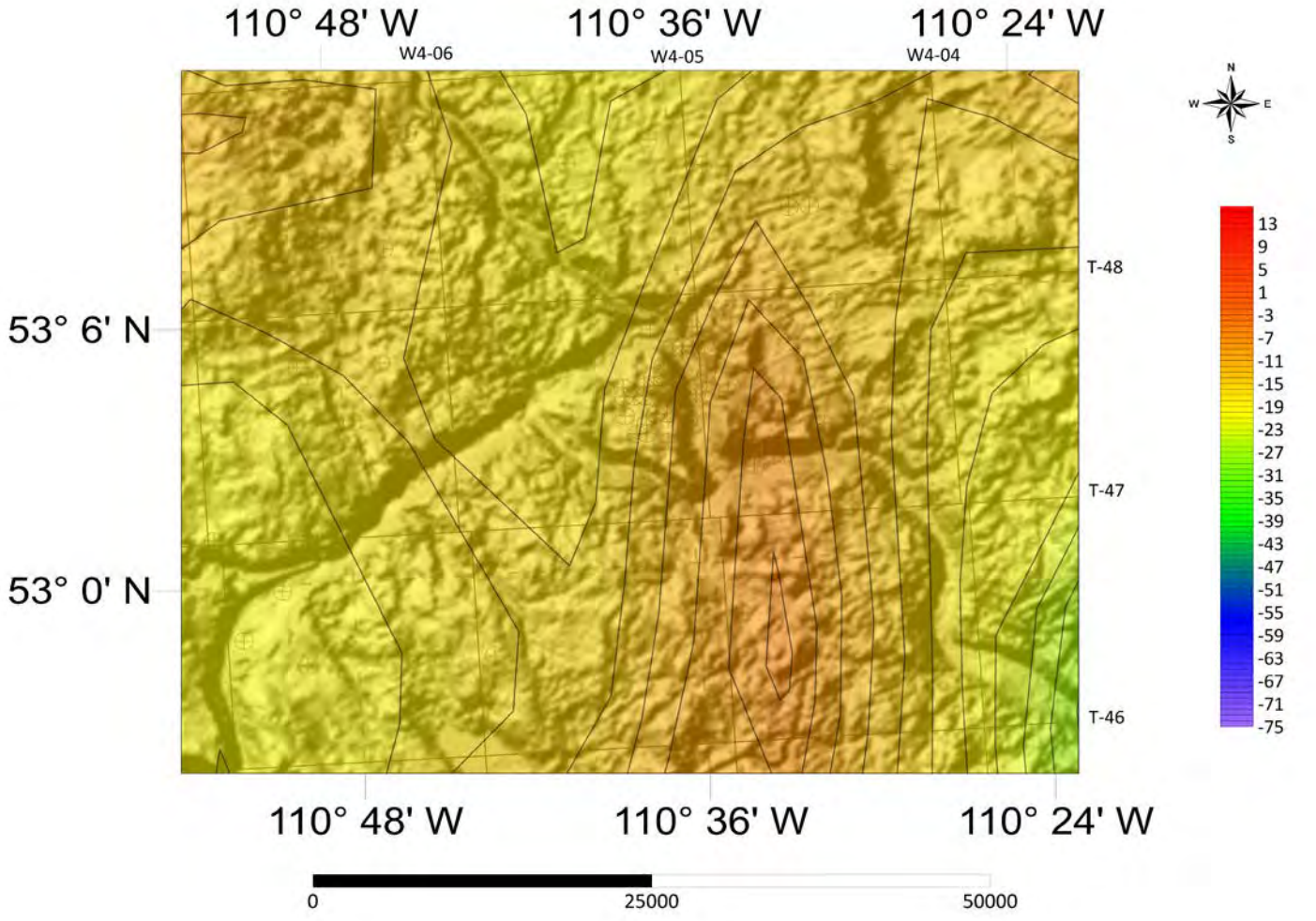

Carbon Dioxide Carbon Isotope Values (‰, VPDB)

Fig. 28A. Map of Ground Migration (GM) Locations in the Wildmere Zoom-in

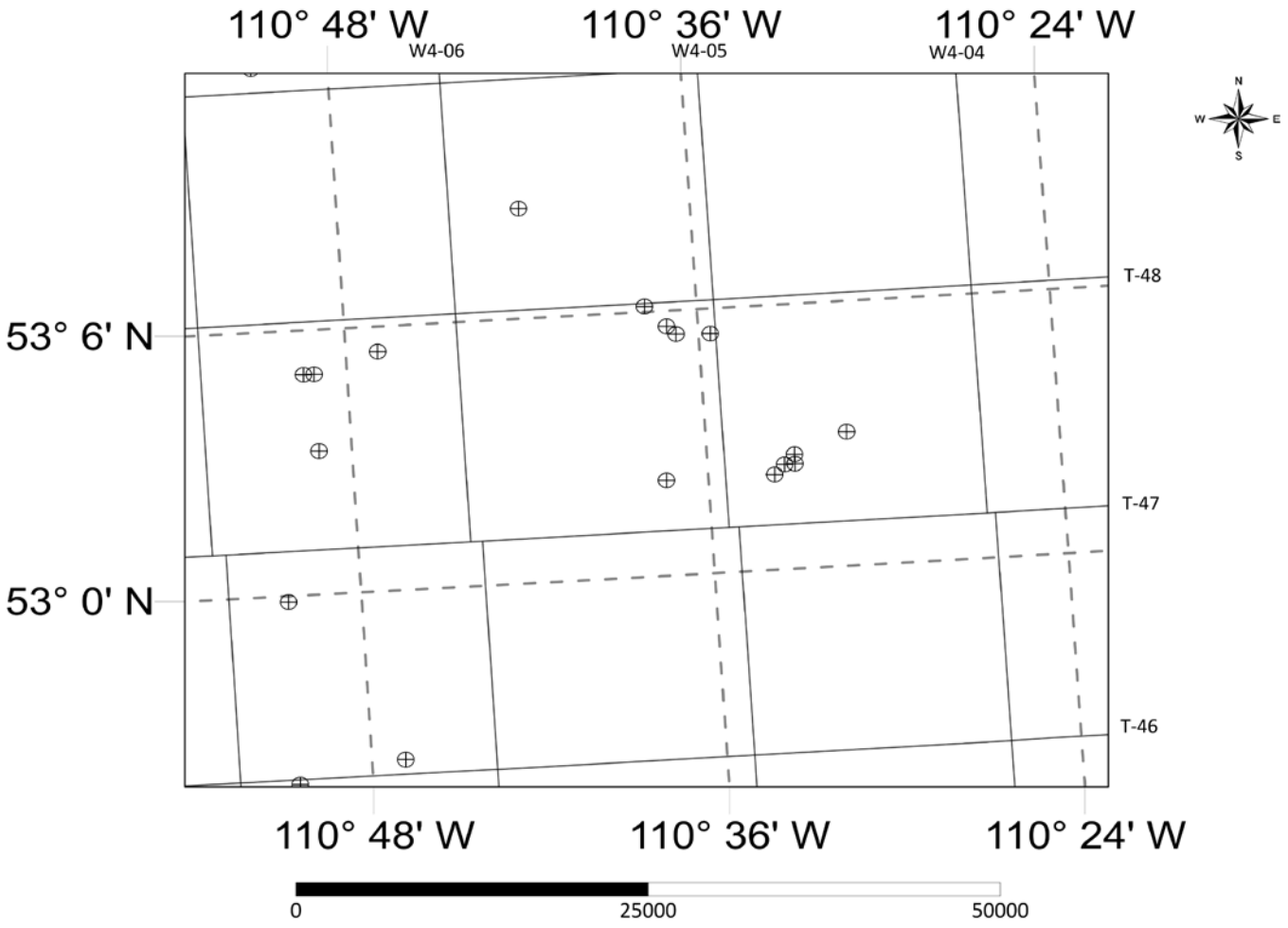

Fig. 28B. Contour Map of Methane Carbon Isotope Values of GM Wildmere Zoom-in

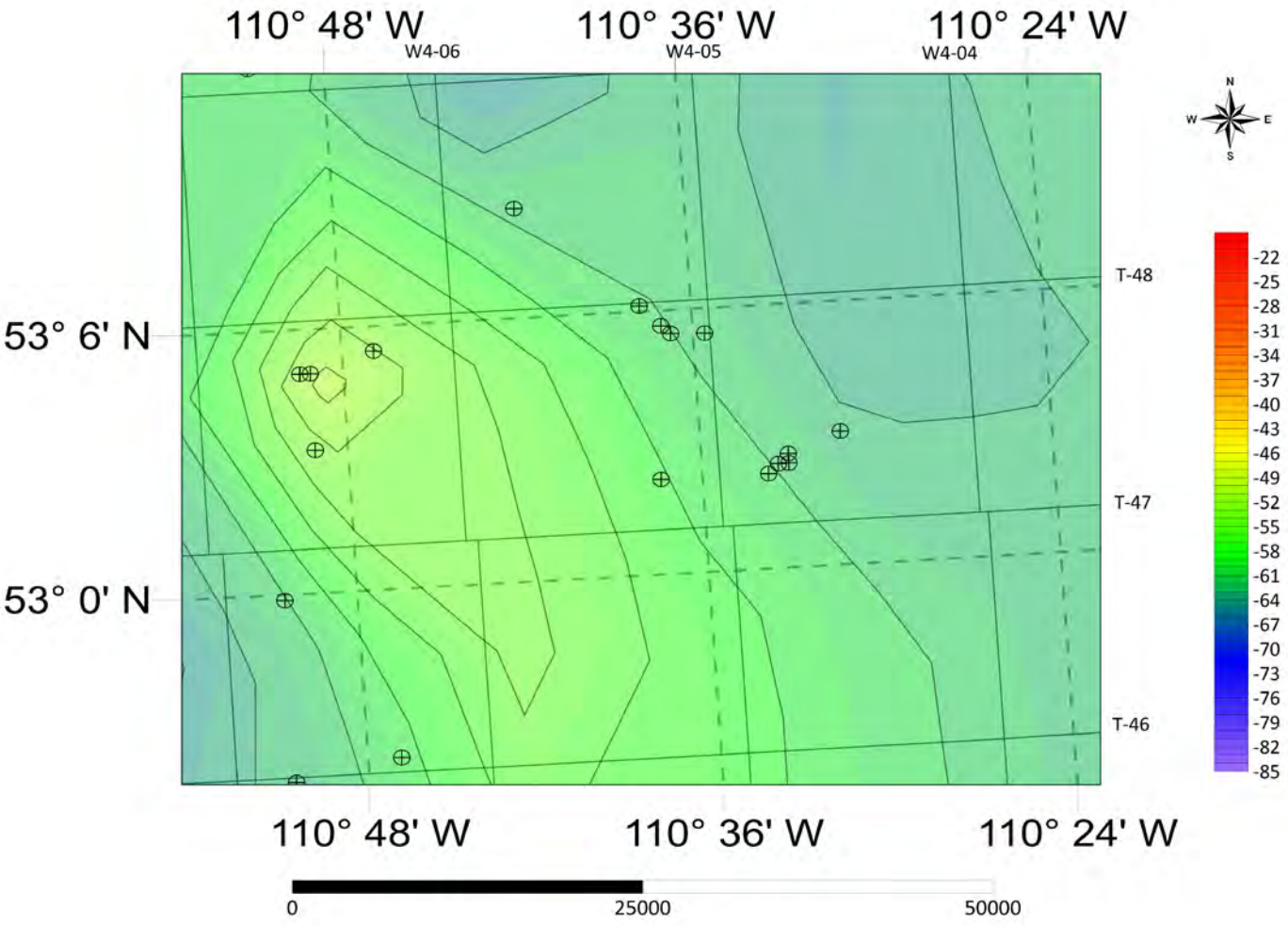

Methane Carbon Isotope Values (‰, VPDB)

Fig. 28C. Contour Map of Ethane Carbon Isotope Values of GM Wildmere Zoom-in

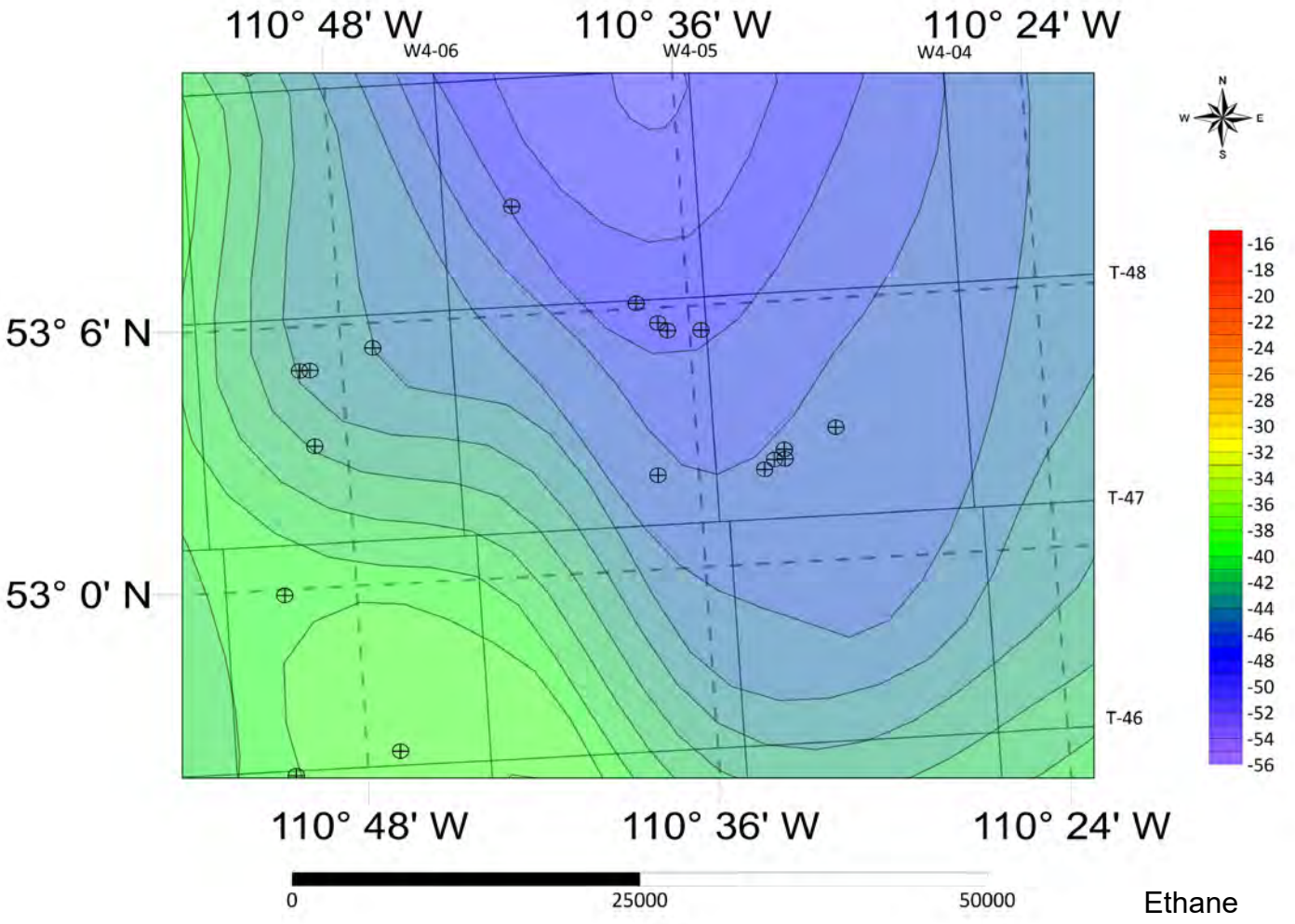

Fig. 28D. Contour Map of Propane Carbon Isotope Values of GM Wildmere Zoom-in

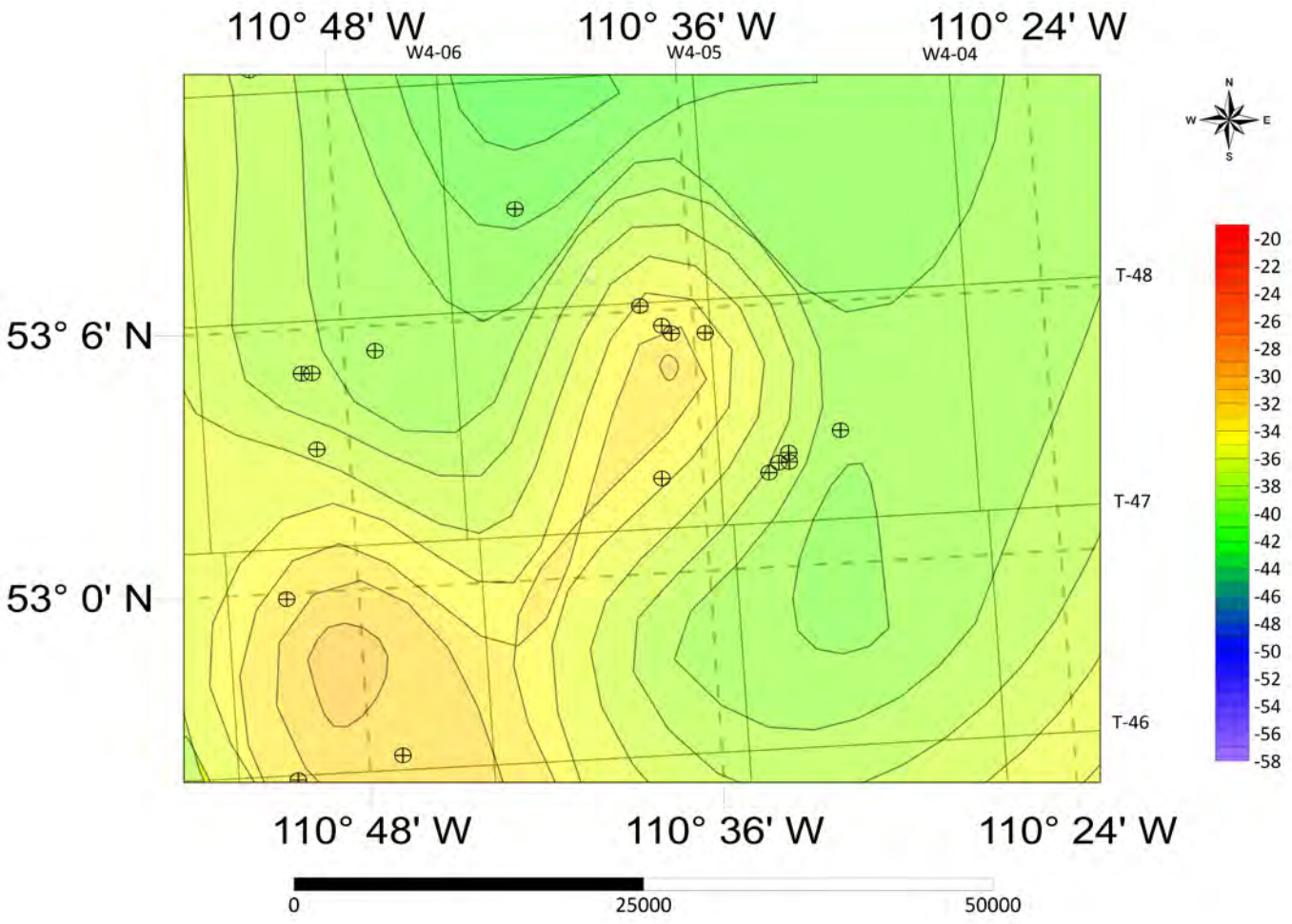

Propane Carbon Isotope Values (‰, VPDB)

Fig. 28E. Contour Map of *n*-Butane Carbon Isotope Values of GM Wildmere Zoom-in

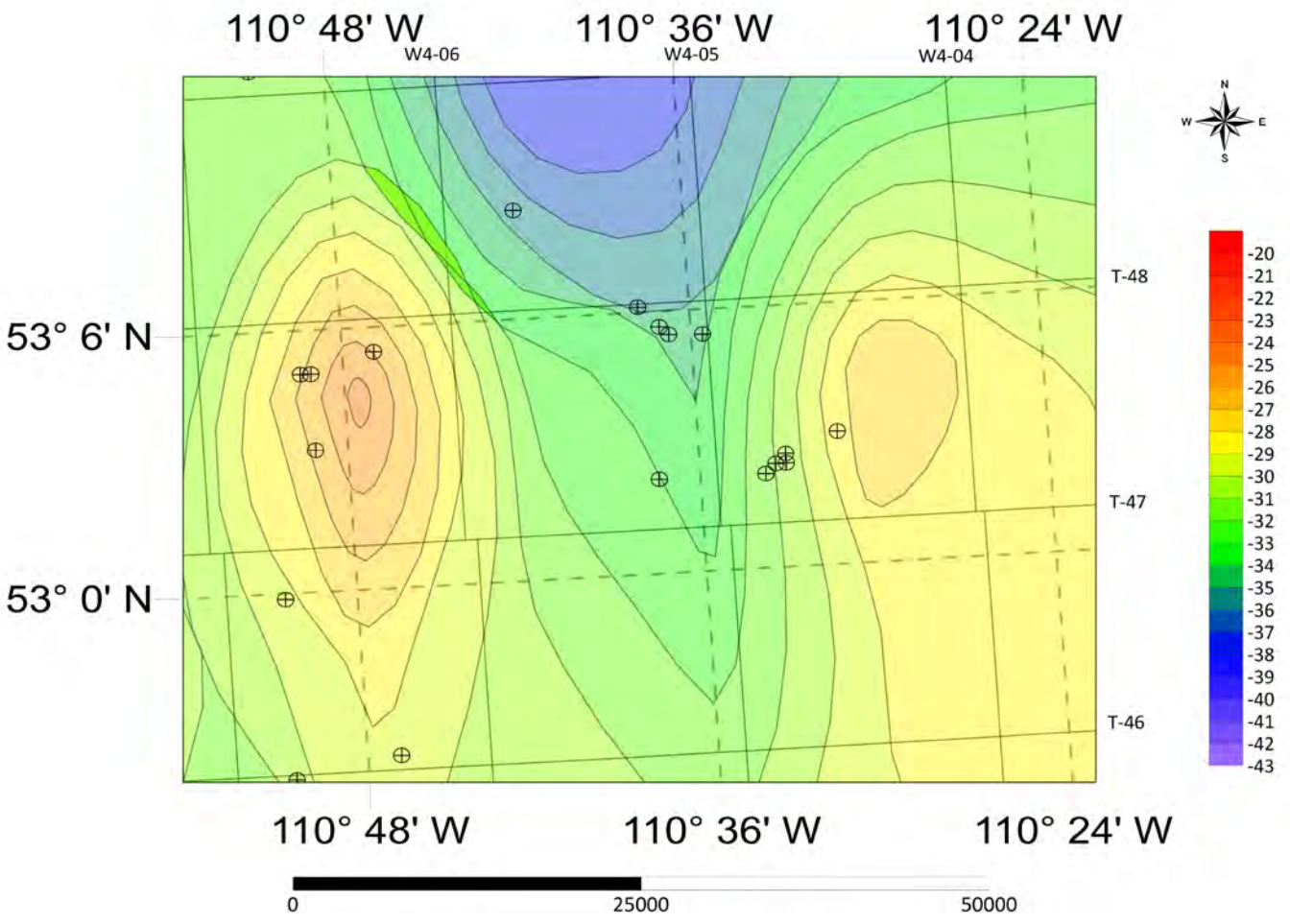

n-Butane Carbon Isotope Values (‰, VPDB)

Fig. 28F. Contour Map of *i*-Butane Carbon Isotope Values of GM Wildmere Zoom-in

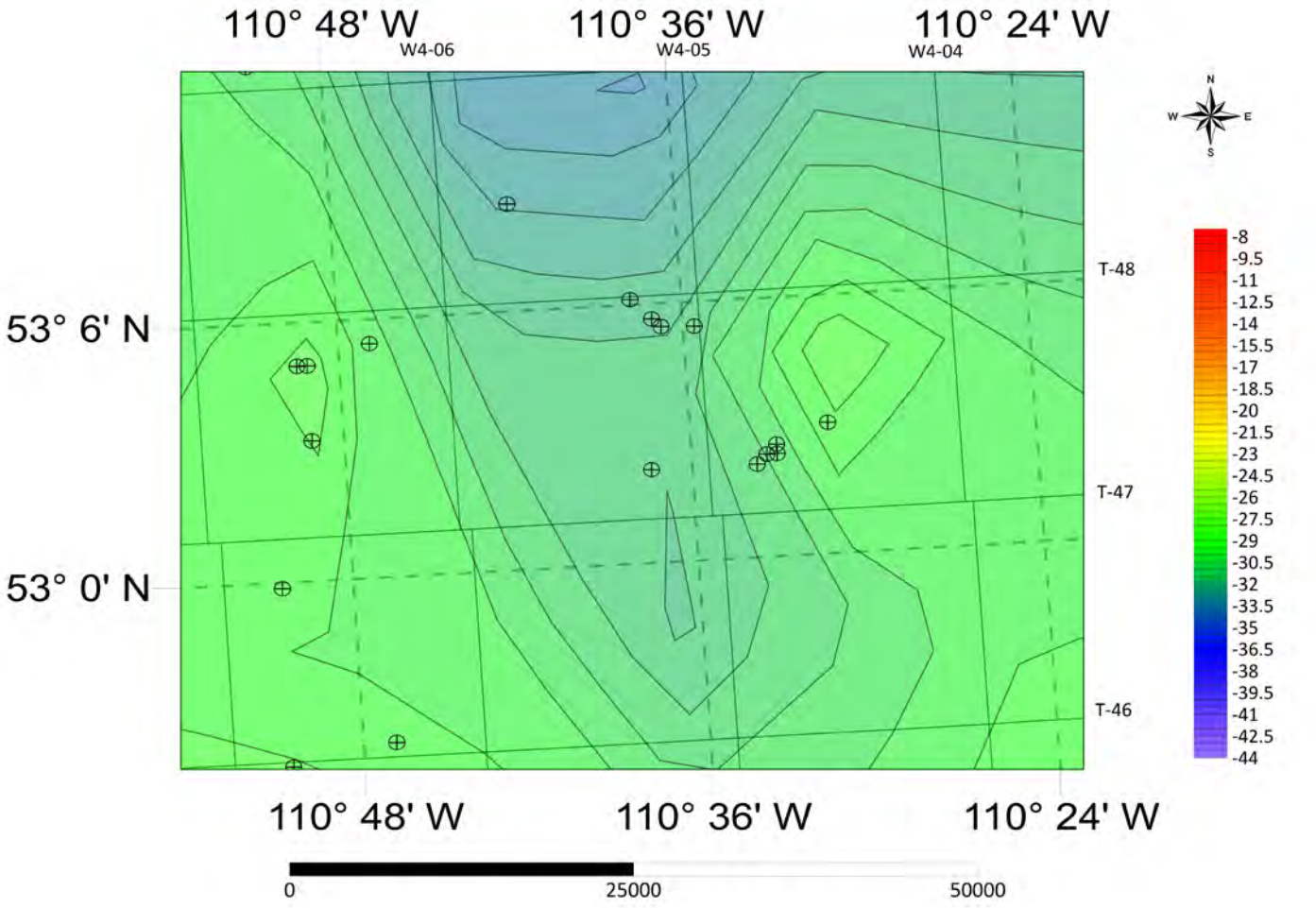

i-Butane Carbon Isotope Values (‰, VPDB)

Fig. 28G. Contour Map of Carbon Dioxide Carbon Isotope Values of GM Wildmere Zoom-in

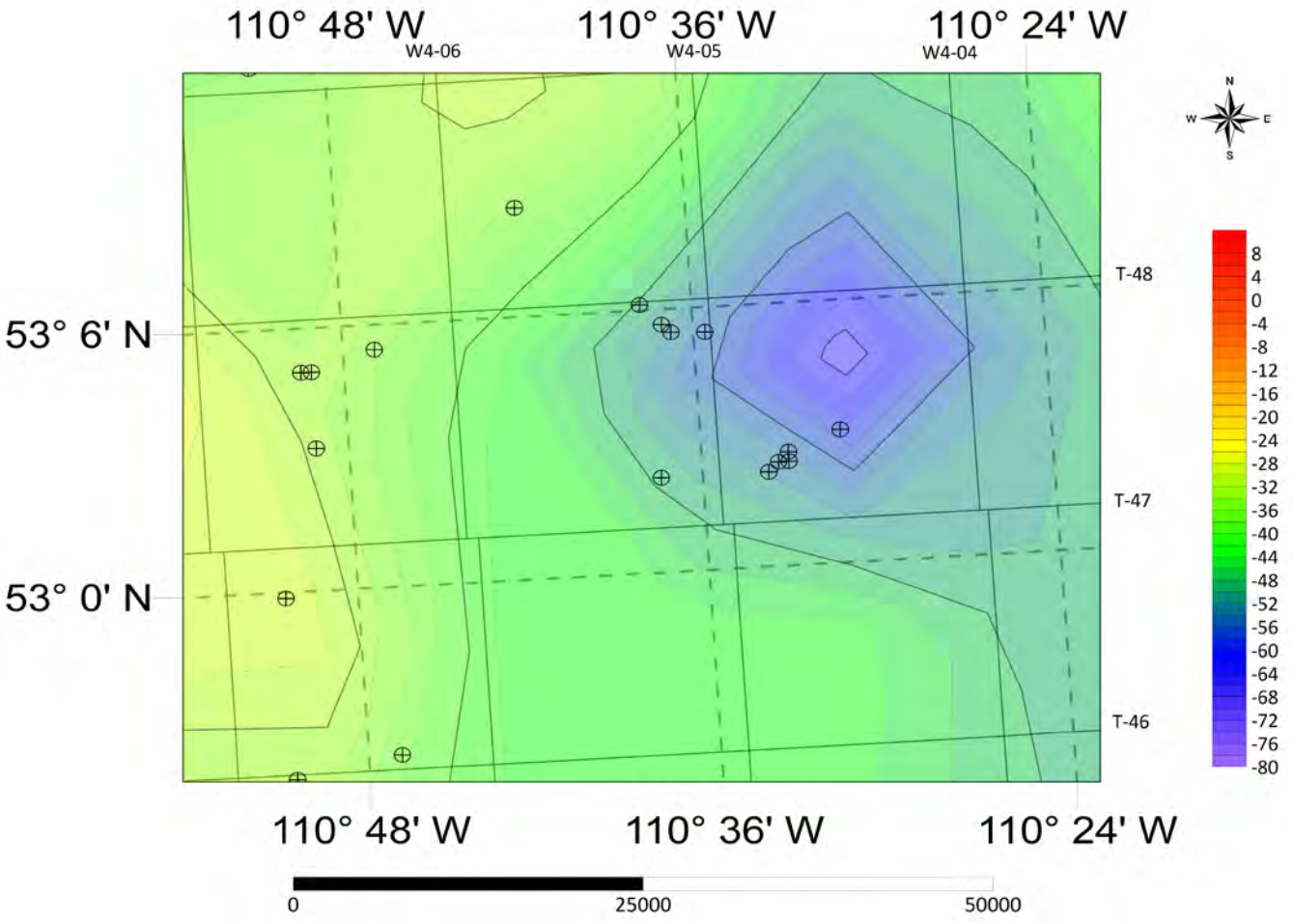

Carbon Dioxide Carbon Isotope Values (‰, VPDB)

Fig. 28H. Contour Map of Methane Carbon Isotope Values of GM Wildmere Zoom-in over Topographic Map

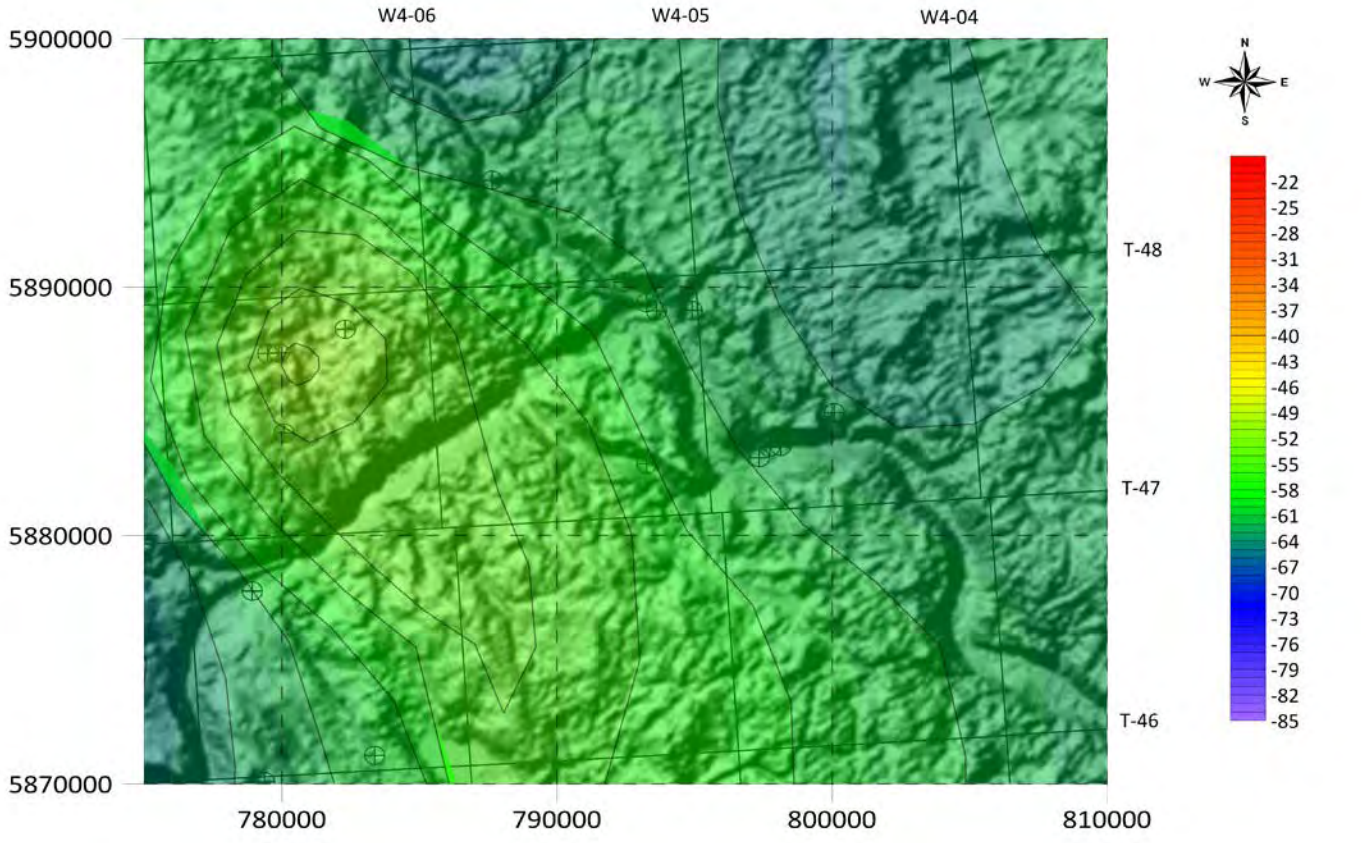

Methane Carbon Isotope Values (‰, VPDB)

Fig. 28I. Contour Map of Ethane Carbon Isotope Values of GM Wildmere Zoom-in over Topographic Map

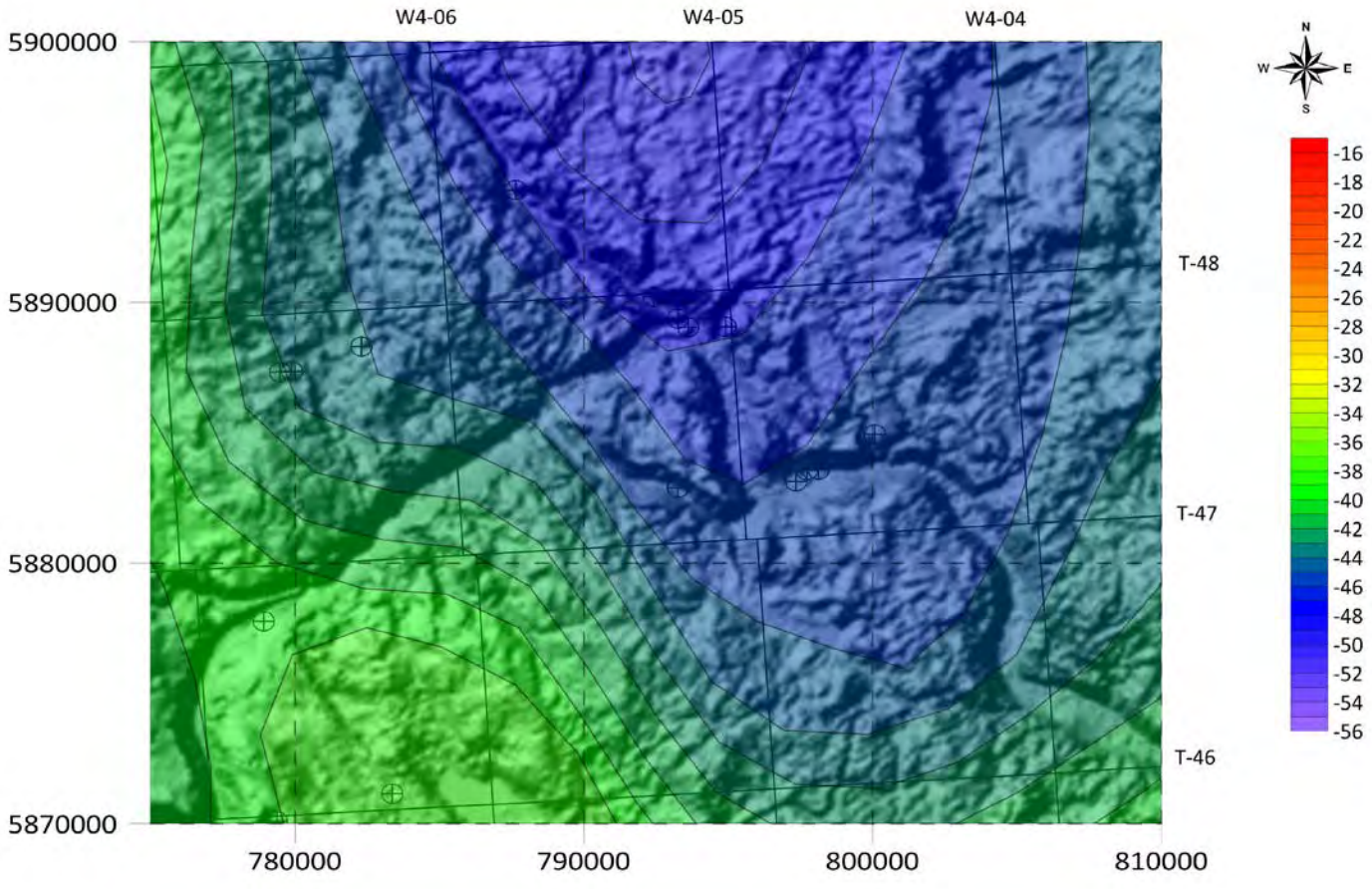

Ethane Carbon Isotope Values (‰, VPDB)

Fig. 28J. Contour Map of Propane Carbon Isotope Values of GM Wildmere Zoom-in over Topographic Map

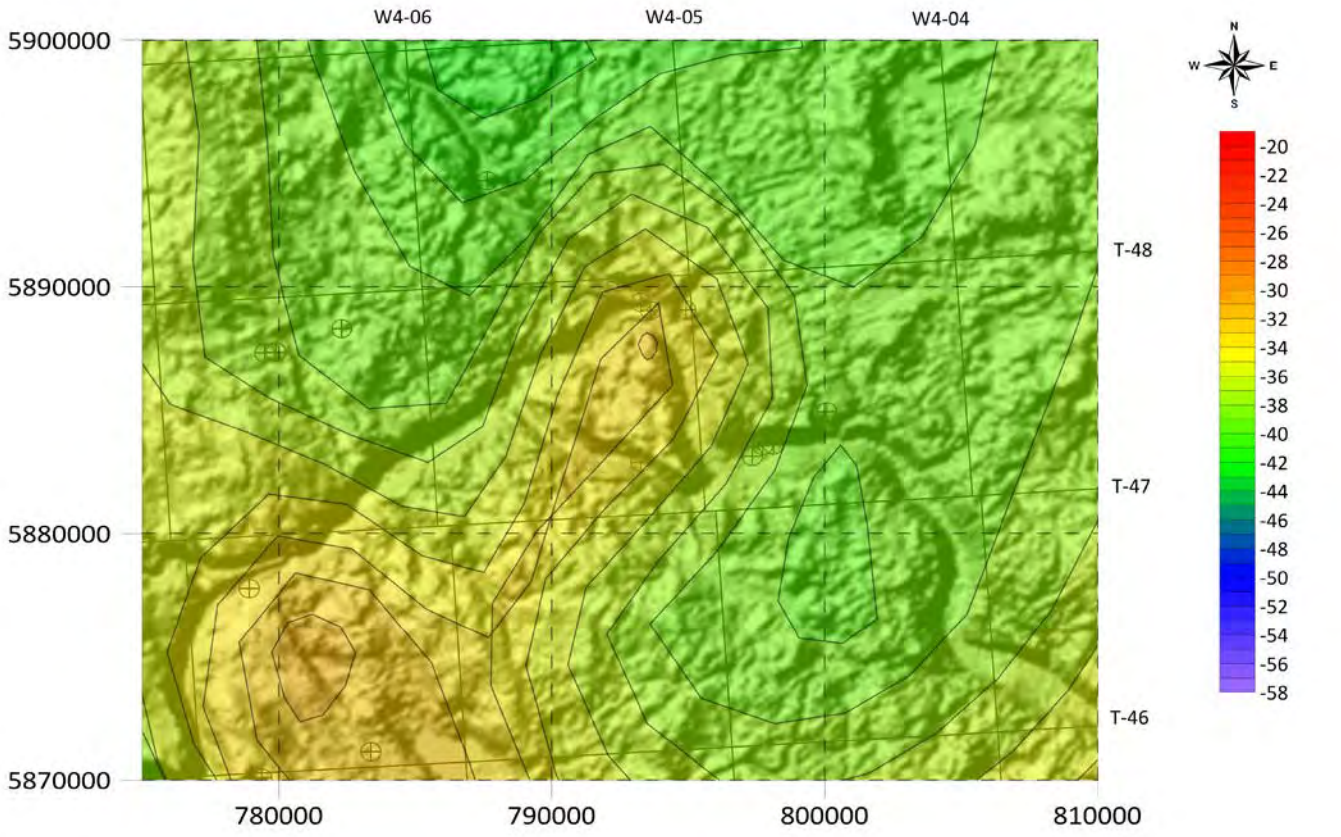

Propane Carbon Isotope Values (‰, VPDB)

Fig. 28K. Contour Map of *n*-Butane Carbon Isotope Values of GM Wildmere Zoom-in over Topographic Map

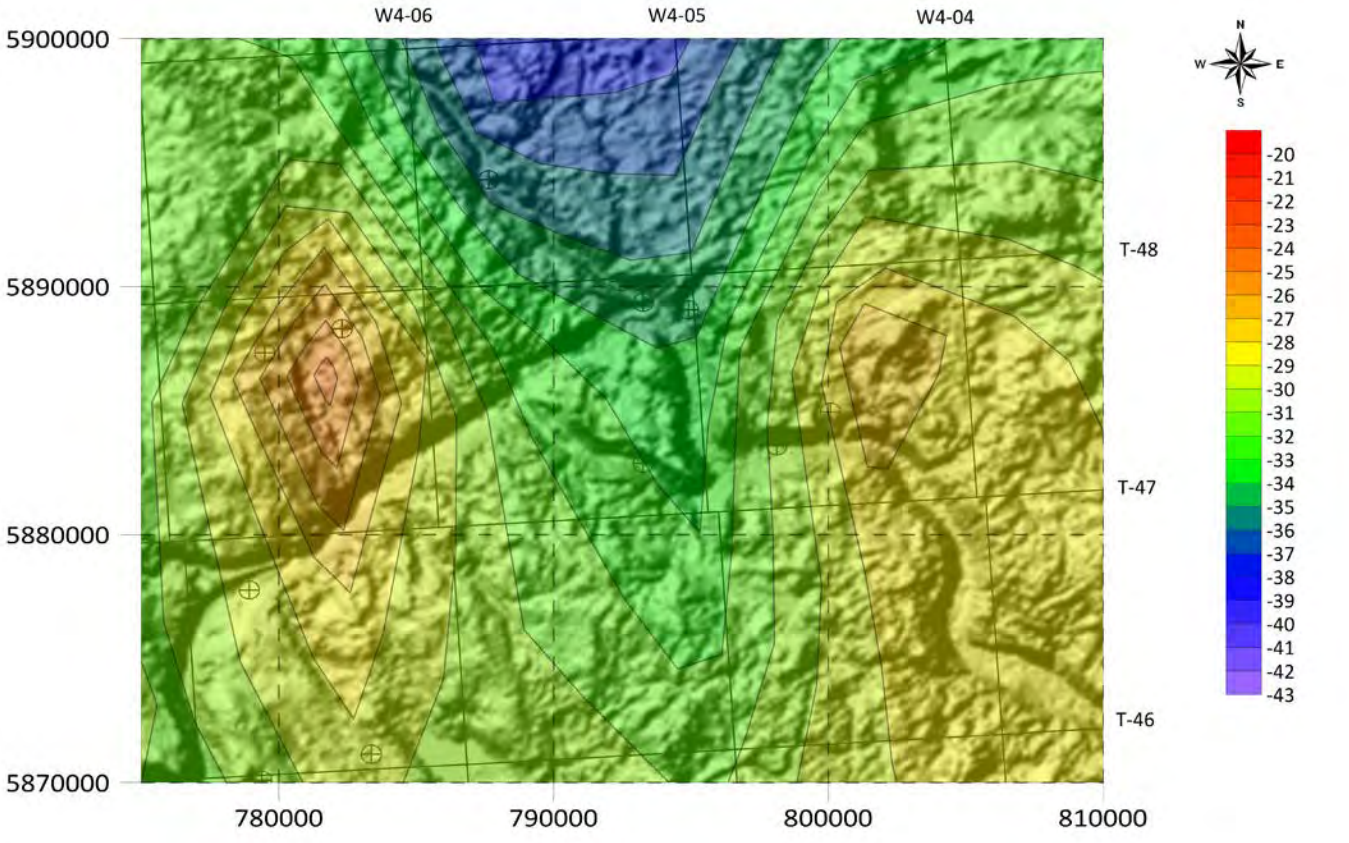

n-Butane Carbon Isotope Values (‰, VPDB)

Fig. 28L. Contour Map of *i*-Butane Carbon Isotope Values of GM Wildmere Zoom-in over Topographic Map

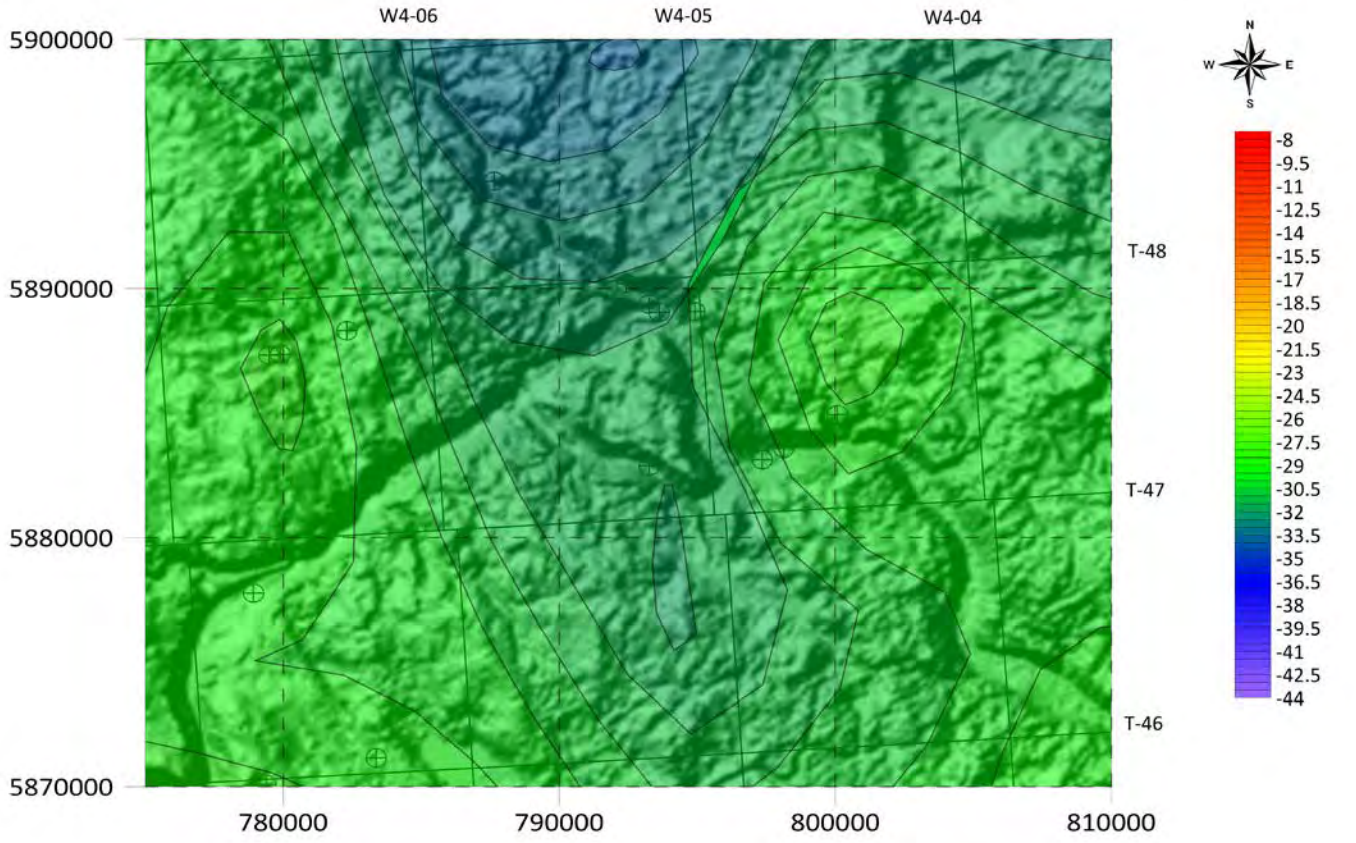

i-Butane Carbon Isotope Values (‰, VPDB)

Fig. 28M. Contour Map of Carbon Dioxide Carbon Isotope Values of GM Wildmere Zoom-in over Topographic Map

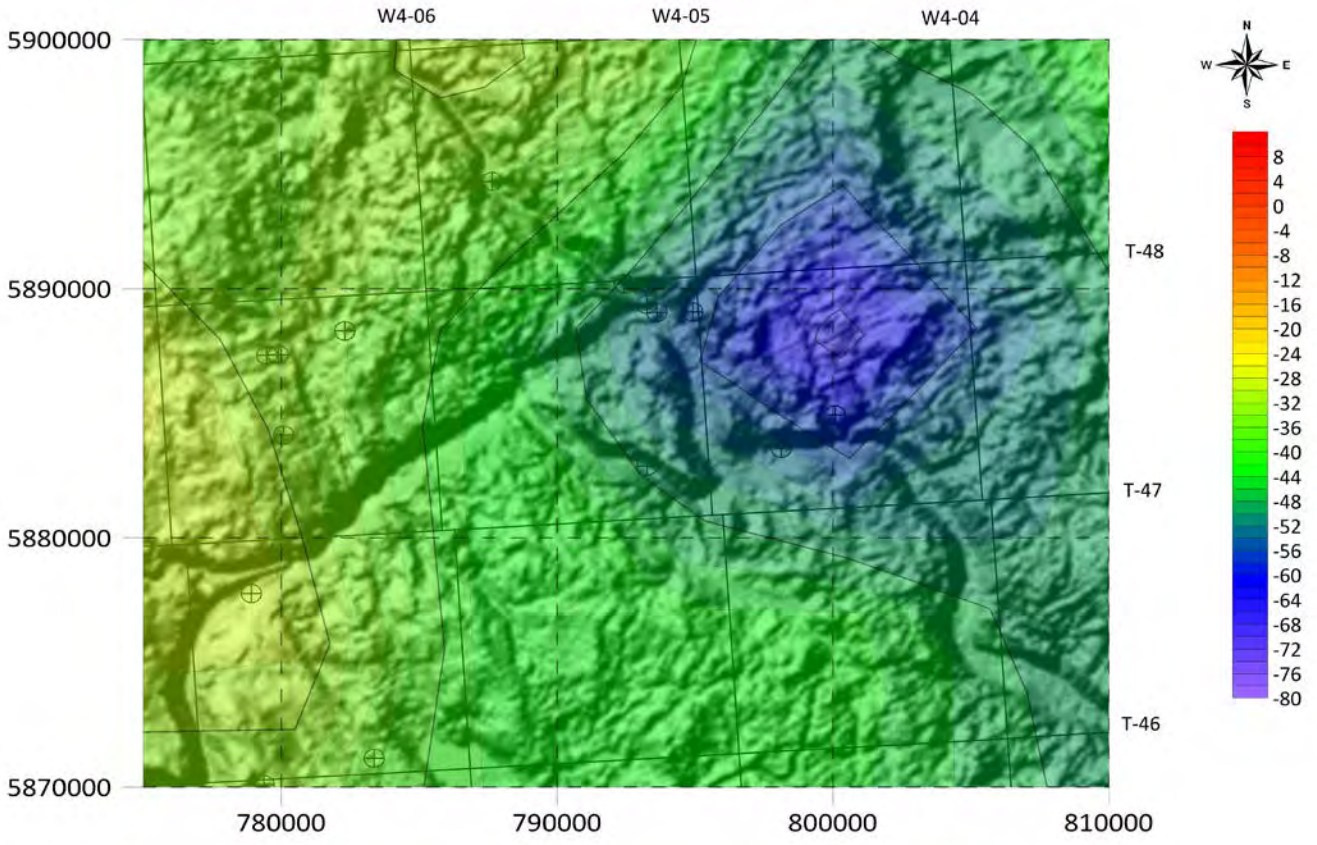

Carbon Dioxide Carbon Isotope Values (‰, VPDB)

Fig. 29A. Map of Surface Casing Vent (SCV) Locations in the Beaver Dam Zoom-in

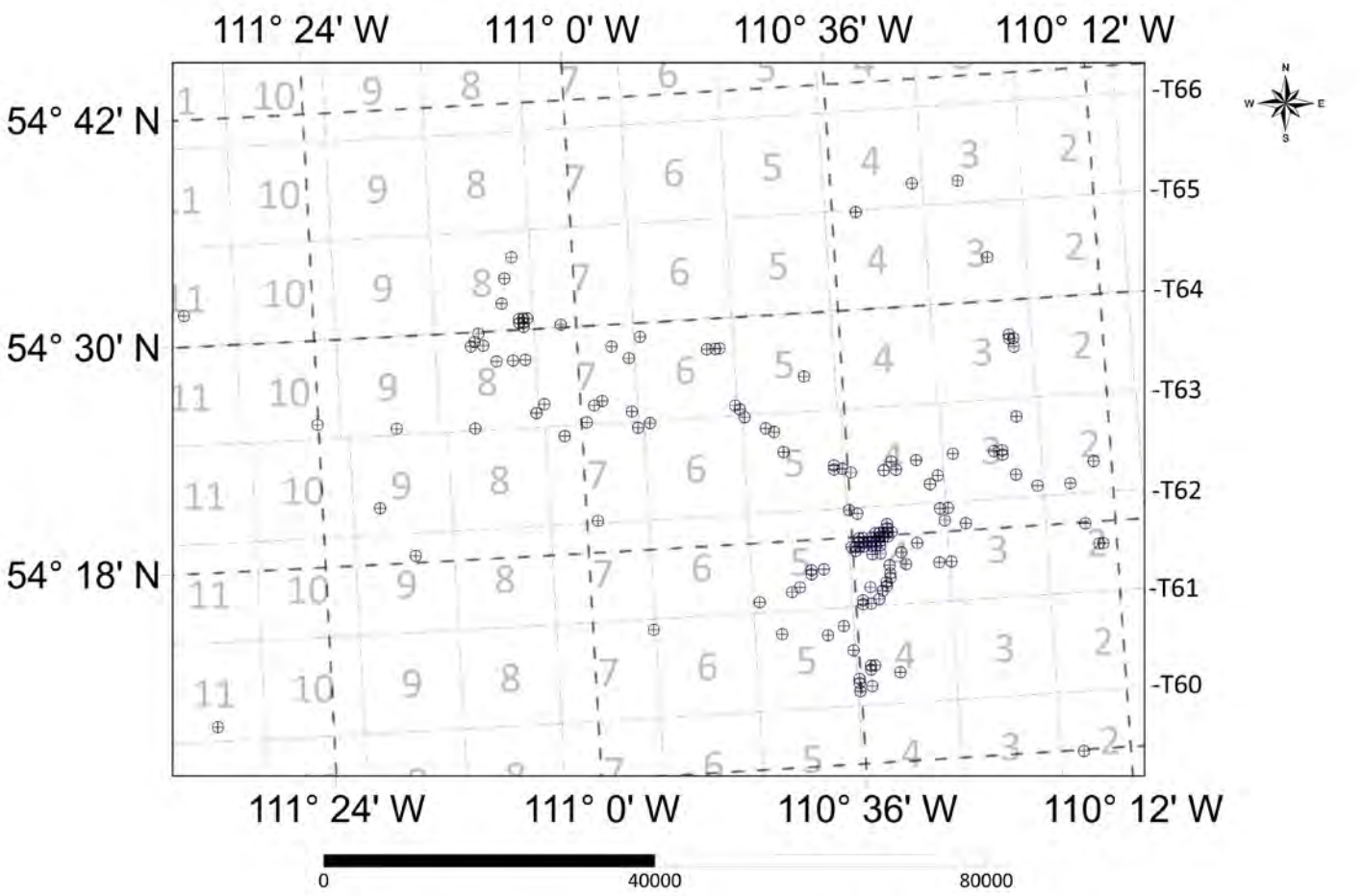

Fig. 29B. Contour Map of Methane Carbon Isotope Values of SCV Beaver Dam Zoom-in

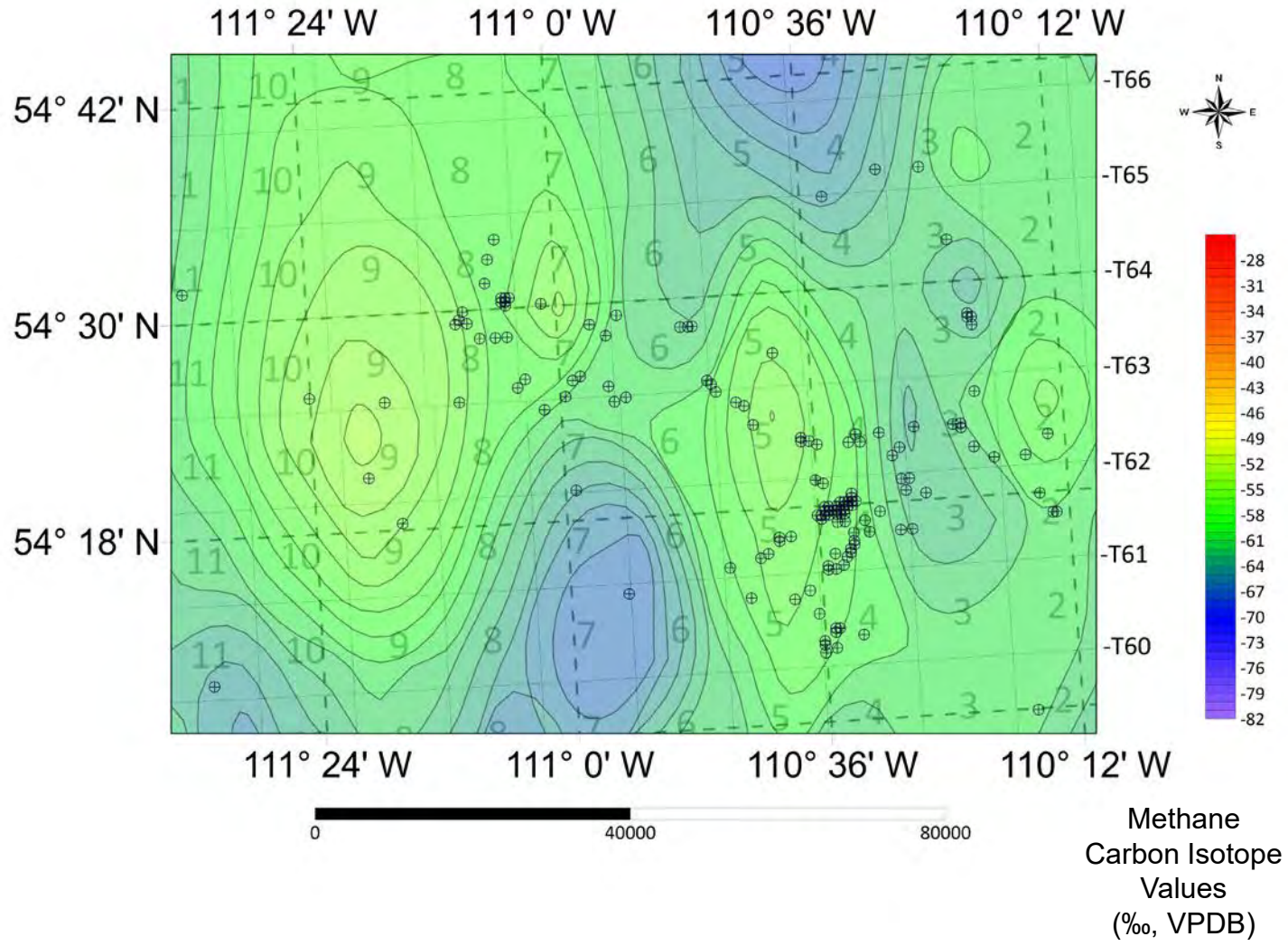

Fig. 29C. Contour Map of Ethane Carbon Isotope Values of SCV Beaver Dam Zoom-in

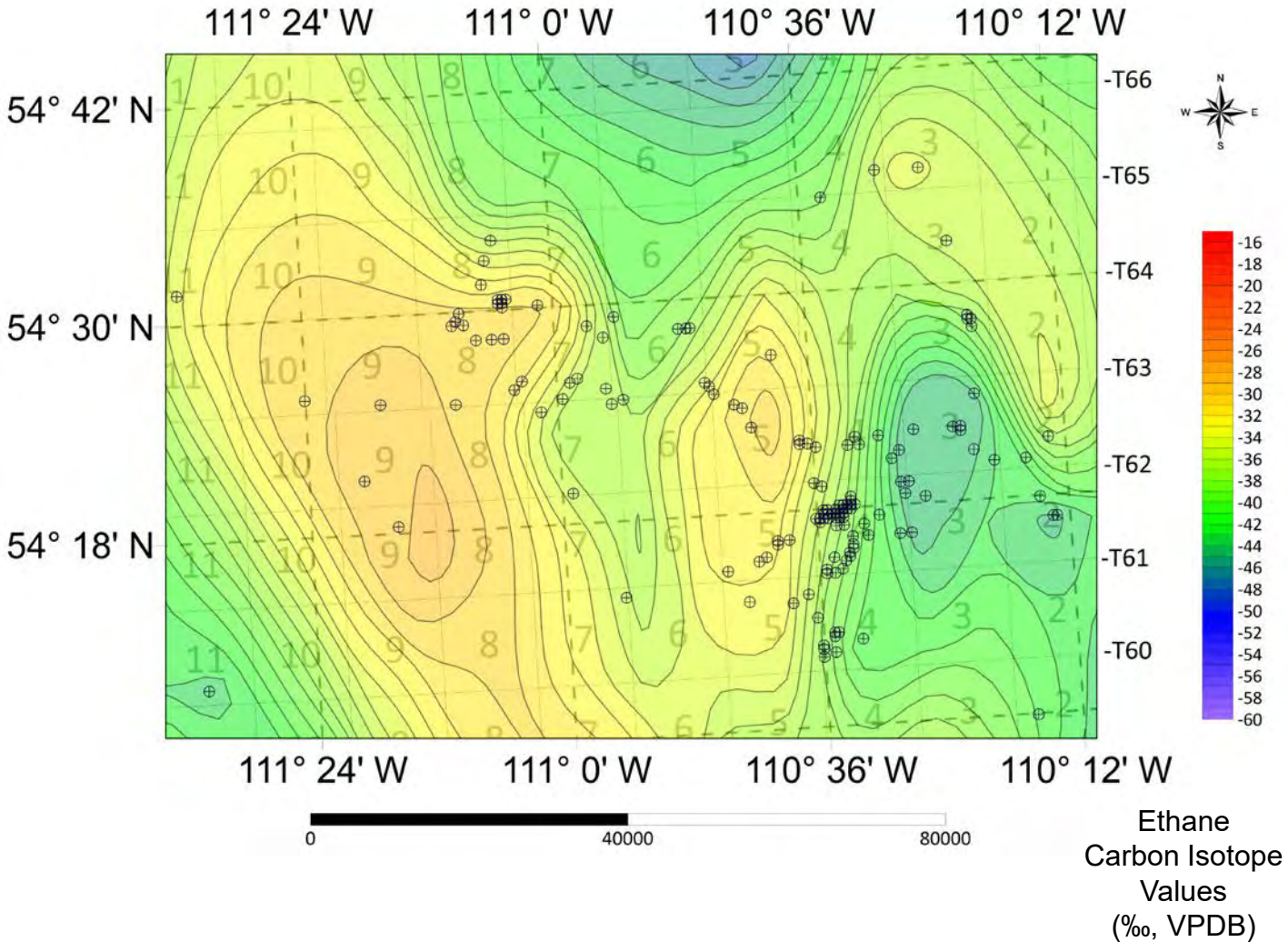

Fig. 29D. Contour Map of Propane Carbon Isotope Values of SCV Beaver Dam Zoom-in

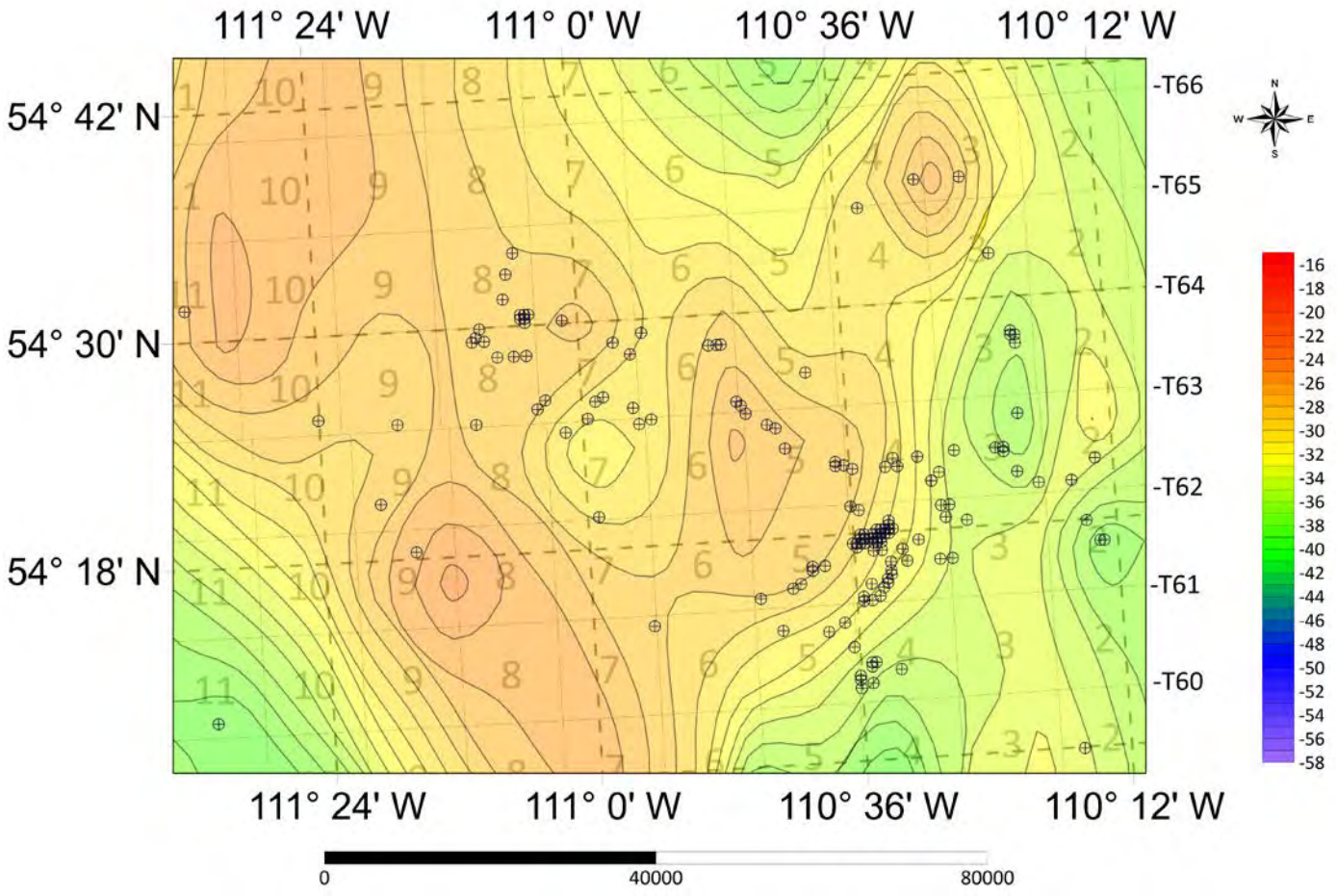

Propane Carbon Isotope Values (‰, VPDB)

Fig. 29E. Contour Map of *n*-Butane Carbon Isotope Values of SCV Beaver Dam Zoom-in

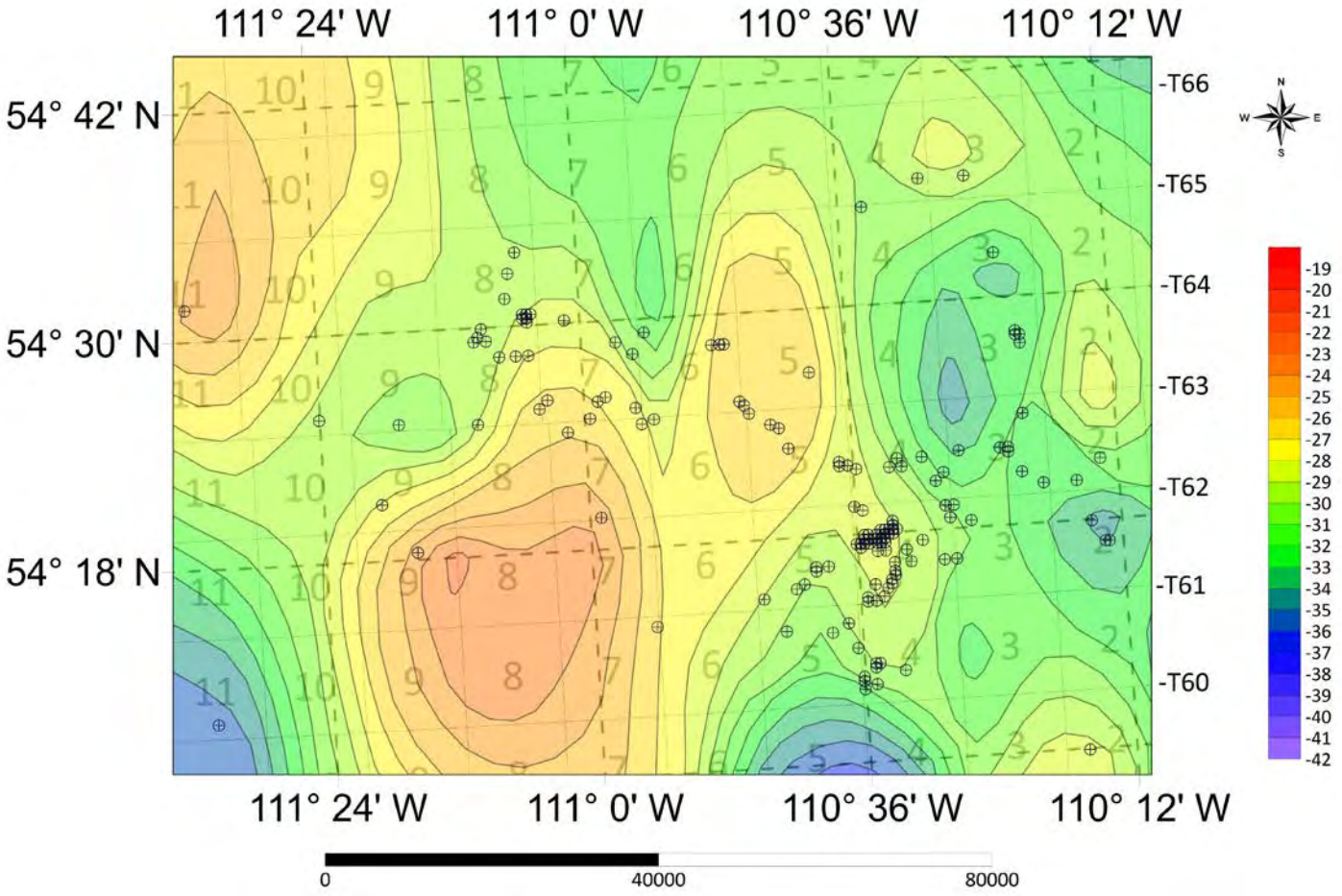

n-Butane Carbon Isotope Values (‰, VPDB)

Fig. 29F. Contour Map of *i*-Butane Carbon Isotope Values of SCV Beaver Dam Zoom-in

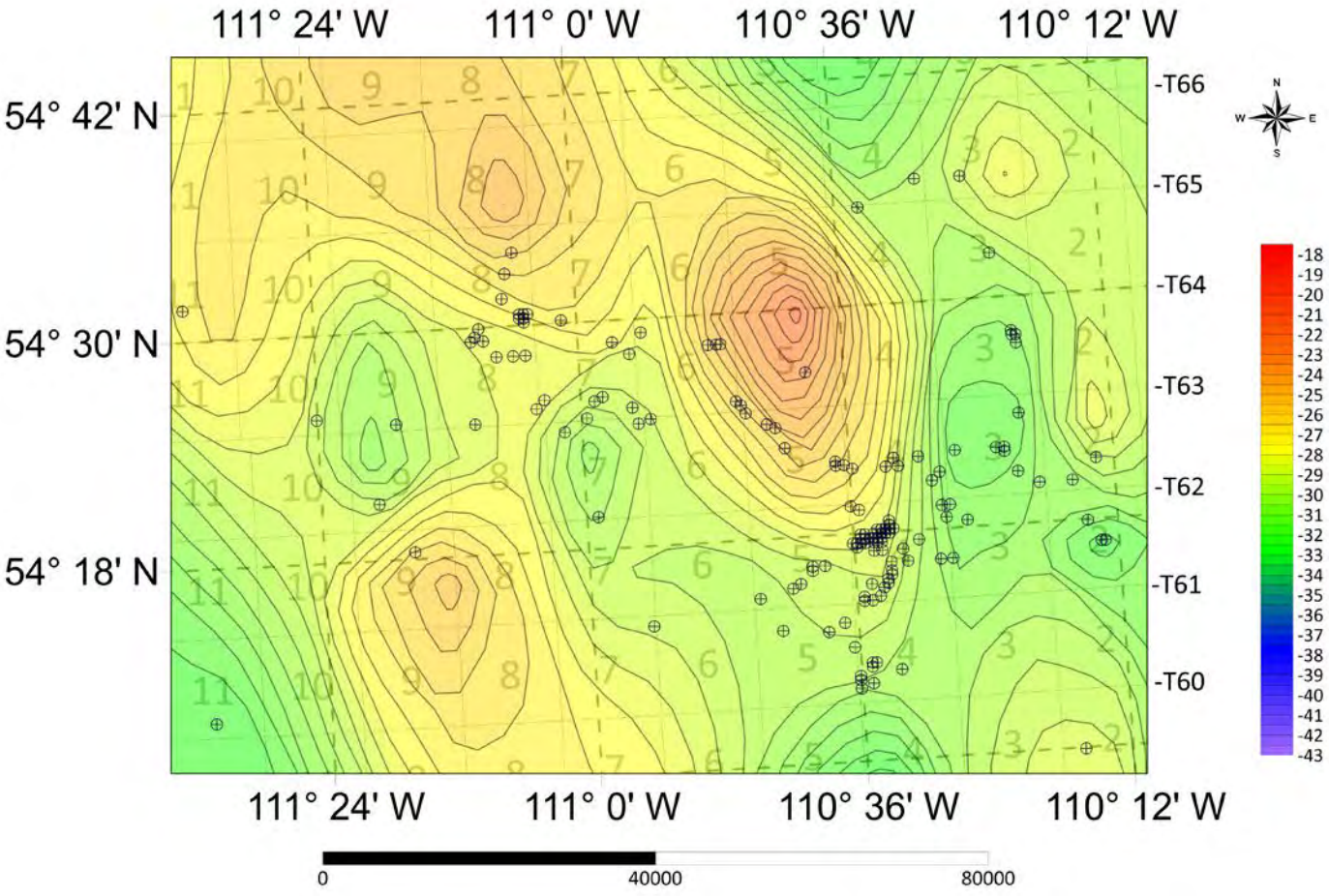

i-Butane Carbon Isotope Values (‰, VPDB)

Fig. 29G. Contour Map of Carbon Dioxide Carbon Isotope Values of SCV Beaver Dam Zoom-in

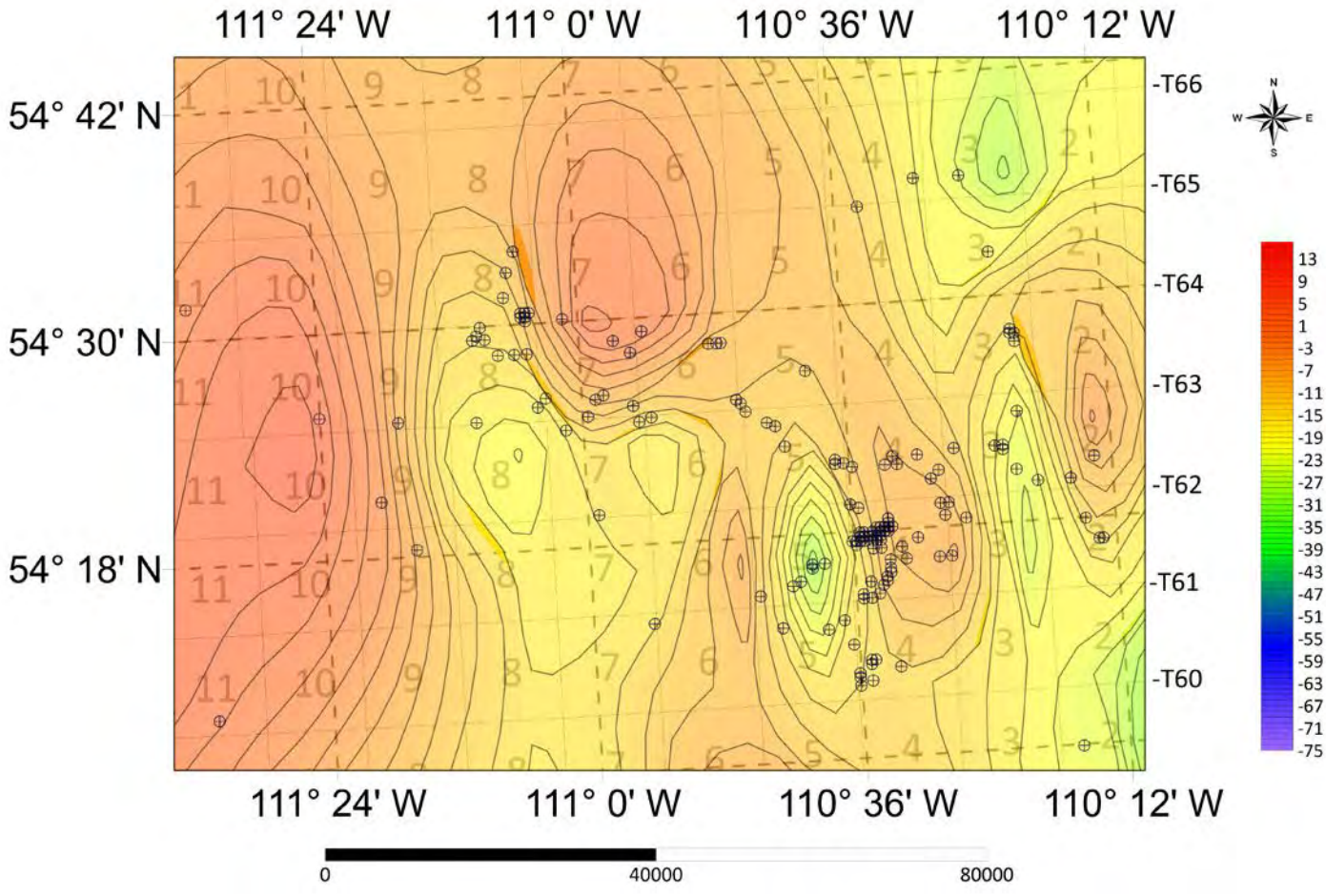

Carbon Dioxide Carbon Isotope Values (‰, VPDB)

Fig. 29H. Contour Map of Methane Carbon Isotope Values of SCV Beaver Dam Zoom-in over Topographic Map

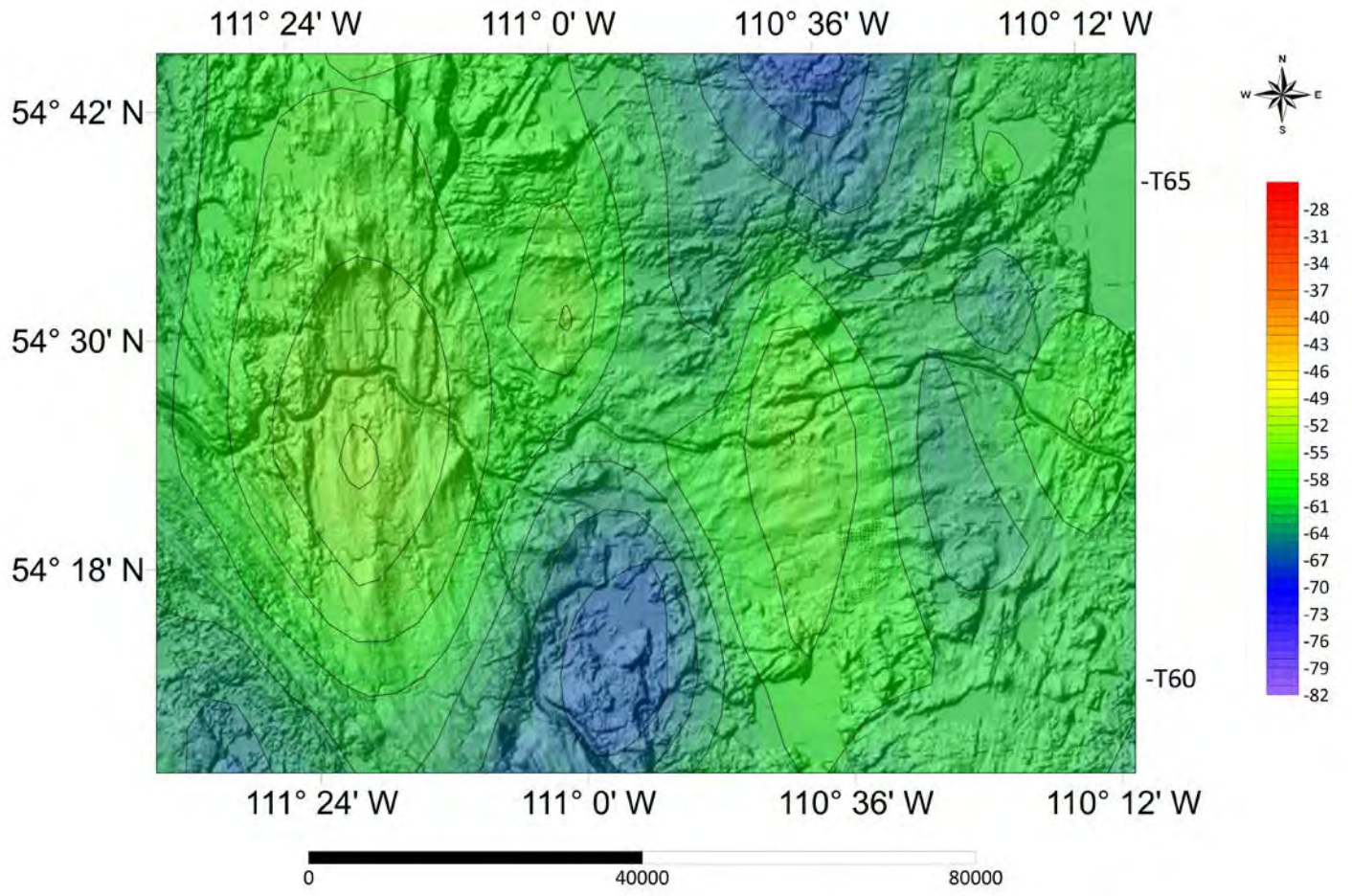

Methane Carbon Isotope Values (‰, VPDB)

Fig. 9I. Contour Map of Ethane Carbon Isotope Values of SCV Beaver Dam Zoom-in over Topographic Map

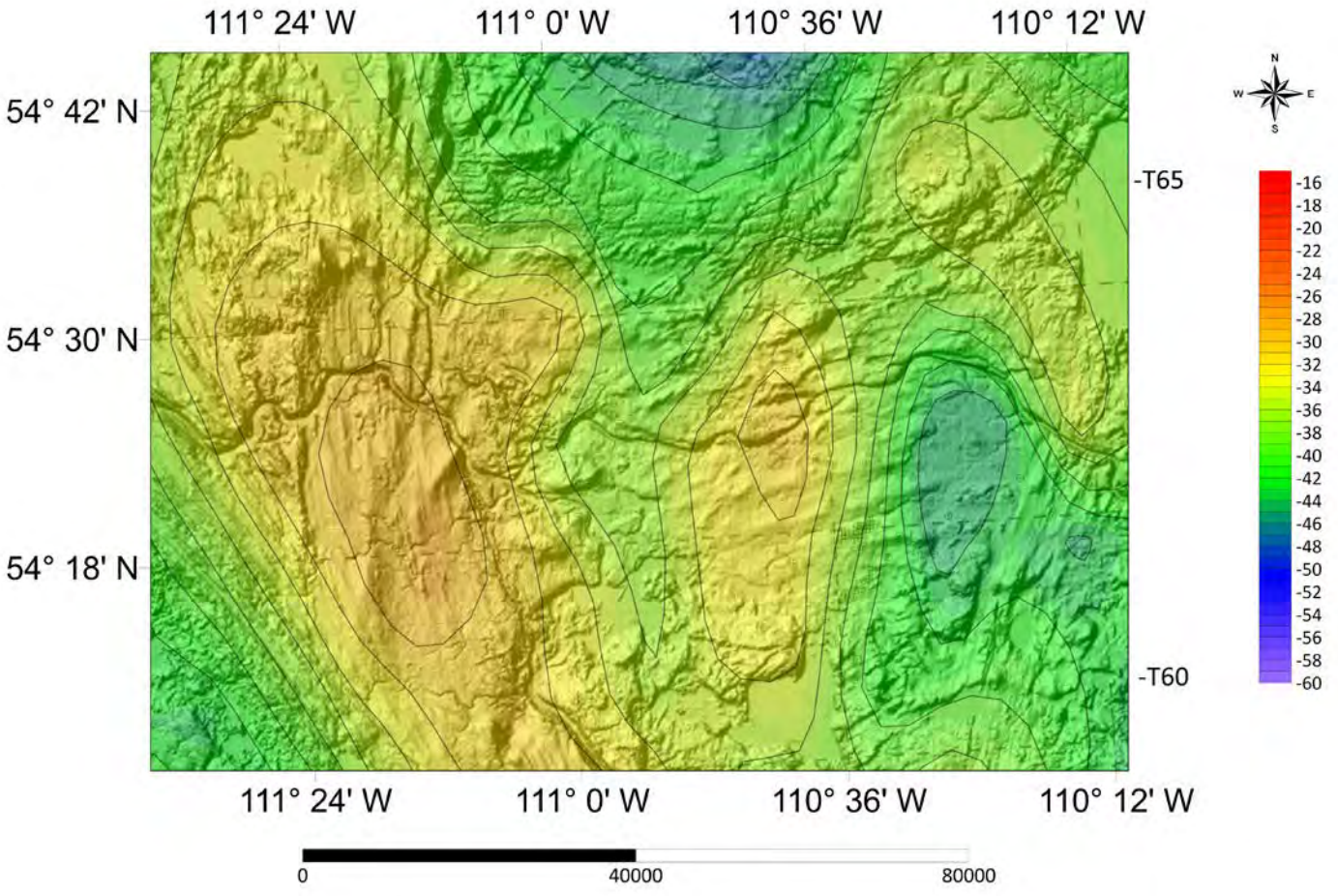

Ethane Carbon Isotope Values (‰, VPDB)

Fig. 9J. Contour Map of Propane Carbon Isotope Values of SCV Beaver Dam Zoom-in over Topographic Map

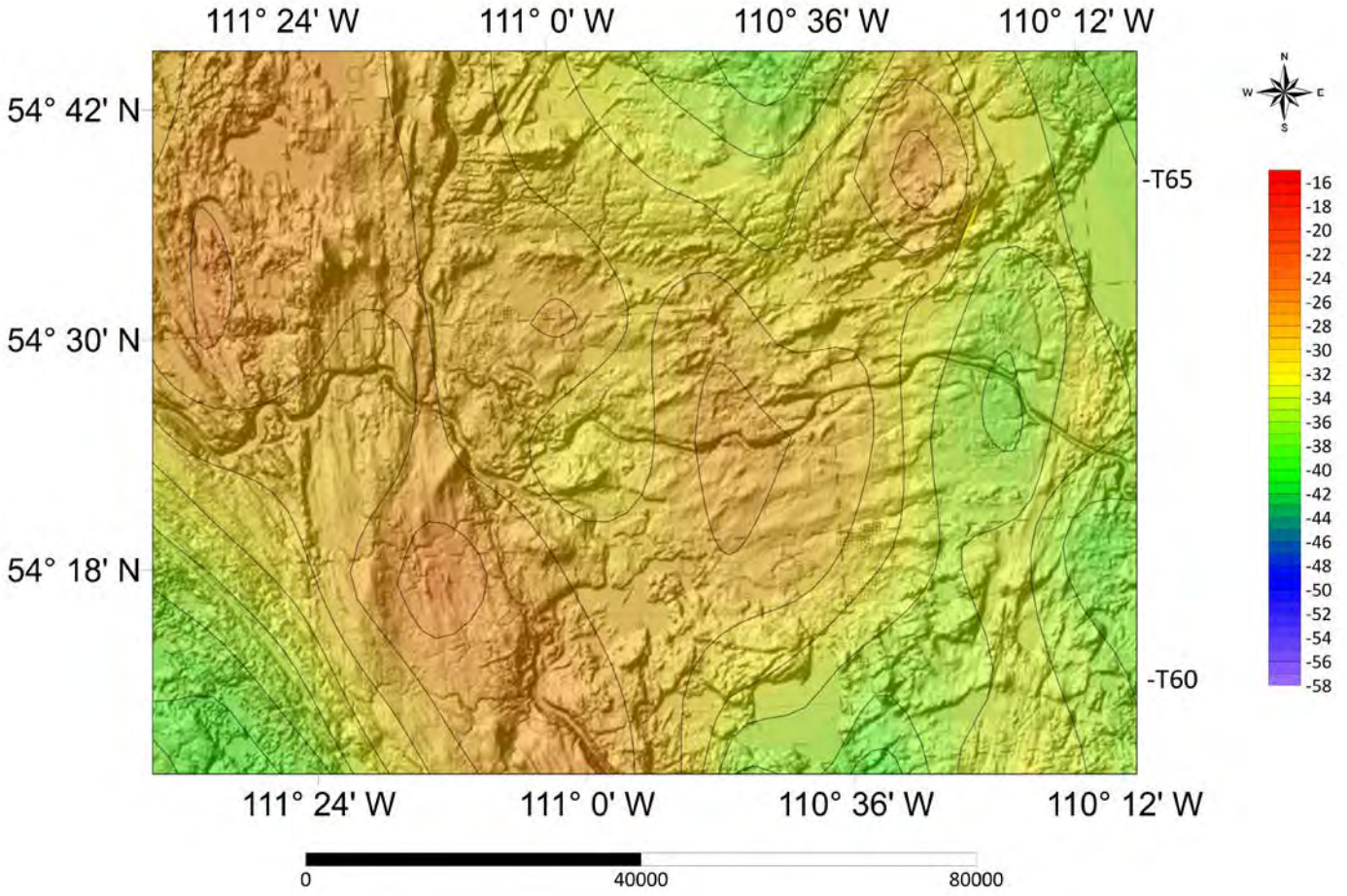

Propane Carbon Isotope Values (‰, VPDB)

Fig. 9K. Contour Map of *n*-Butane Carbon Isotope Values of SCV Beaver Dam Zoom-in over Topographic Map

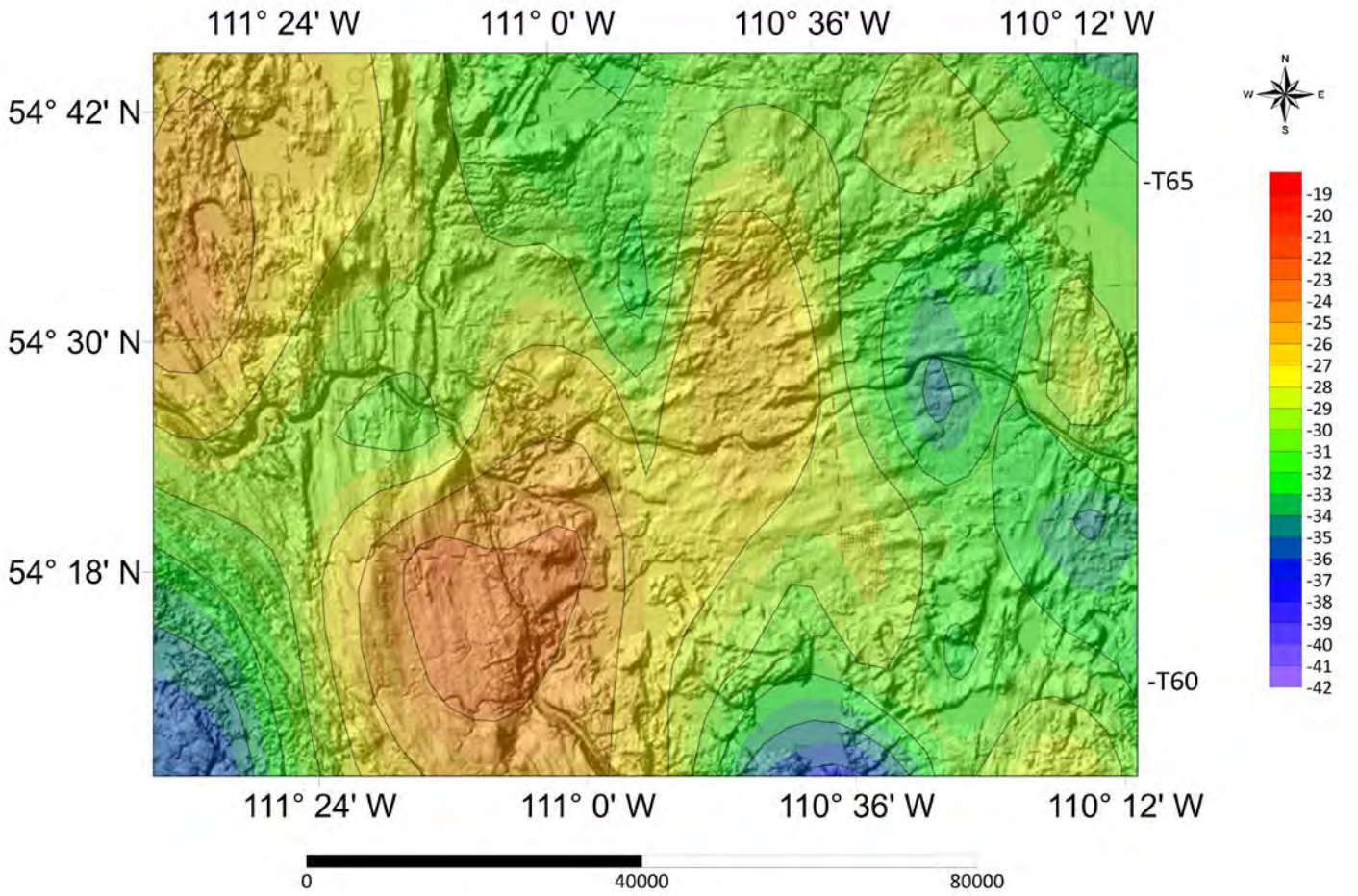

n-Butane Carbon Isotope Values (‰, VPDB)

Fig. 9M. Contour Map of *i*-Butane Carbon Isotope Values of SCV Beaver Dam Zoom-in over Topographic Map

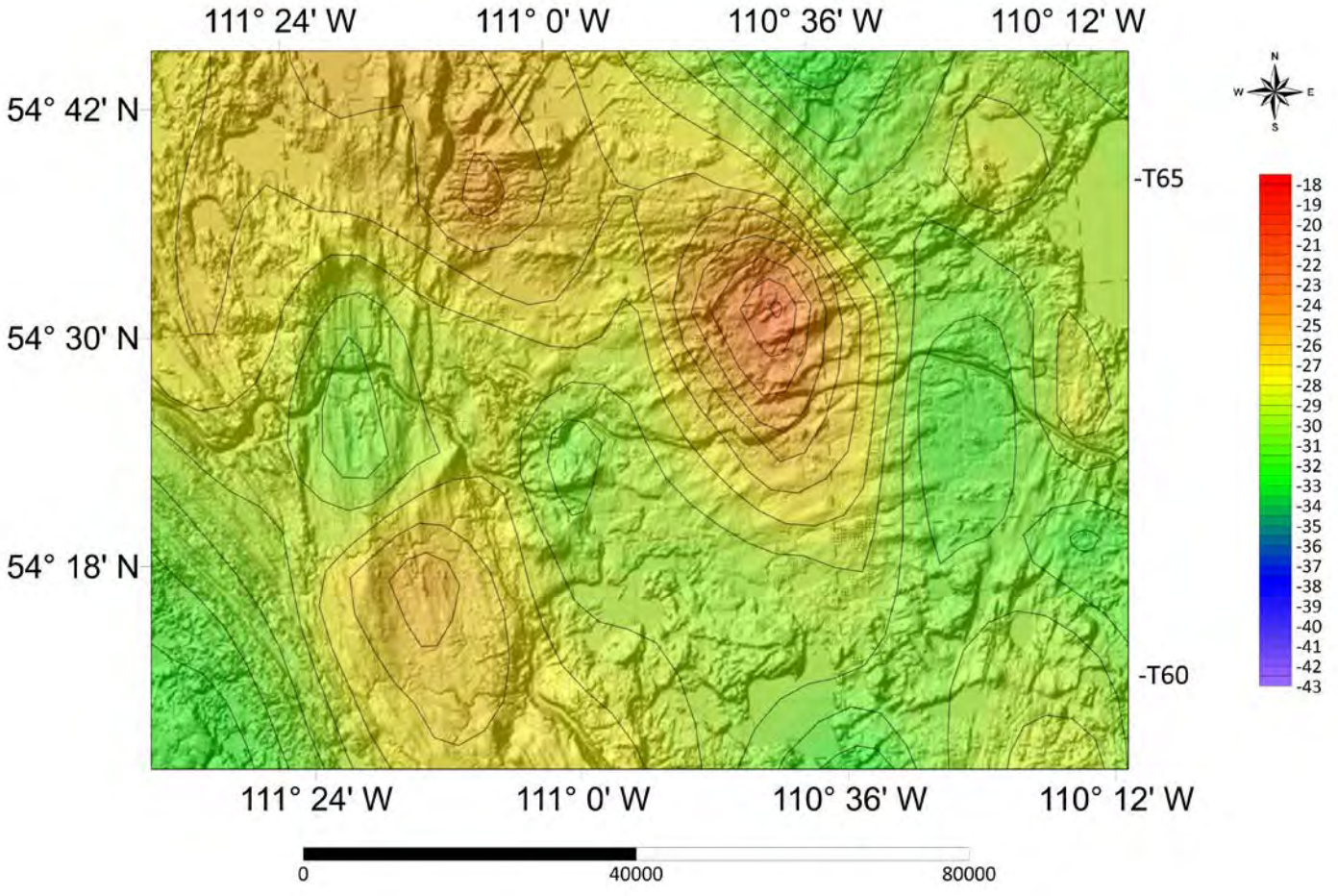

i-Butane Carbon Isotope Values (‰, VPDB)

Fig. 9N. Contour Map of Carbon Dioxide Carbon Isotope Values of SCV Beaver Dam Zoom-in over Topographic Map

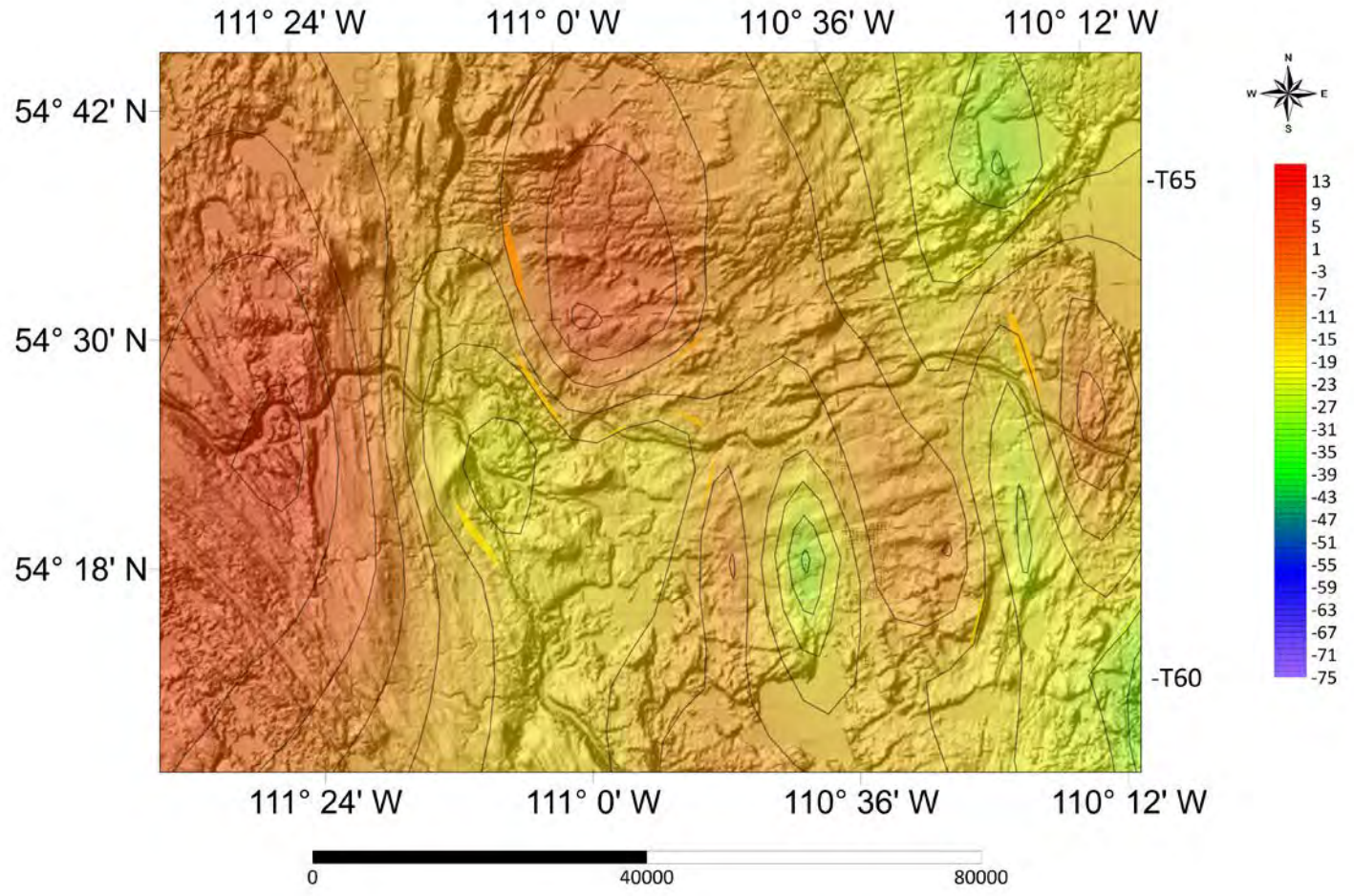

Carbon Dioxide Carbon Isotope Values (‰, VPDB)

Fig. 30A. Map of Ground Migration (GM) Locations in the Beaver Dam Zoom-in

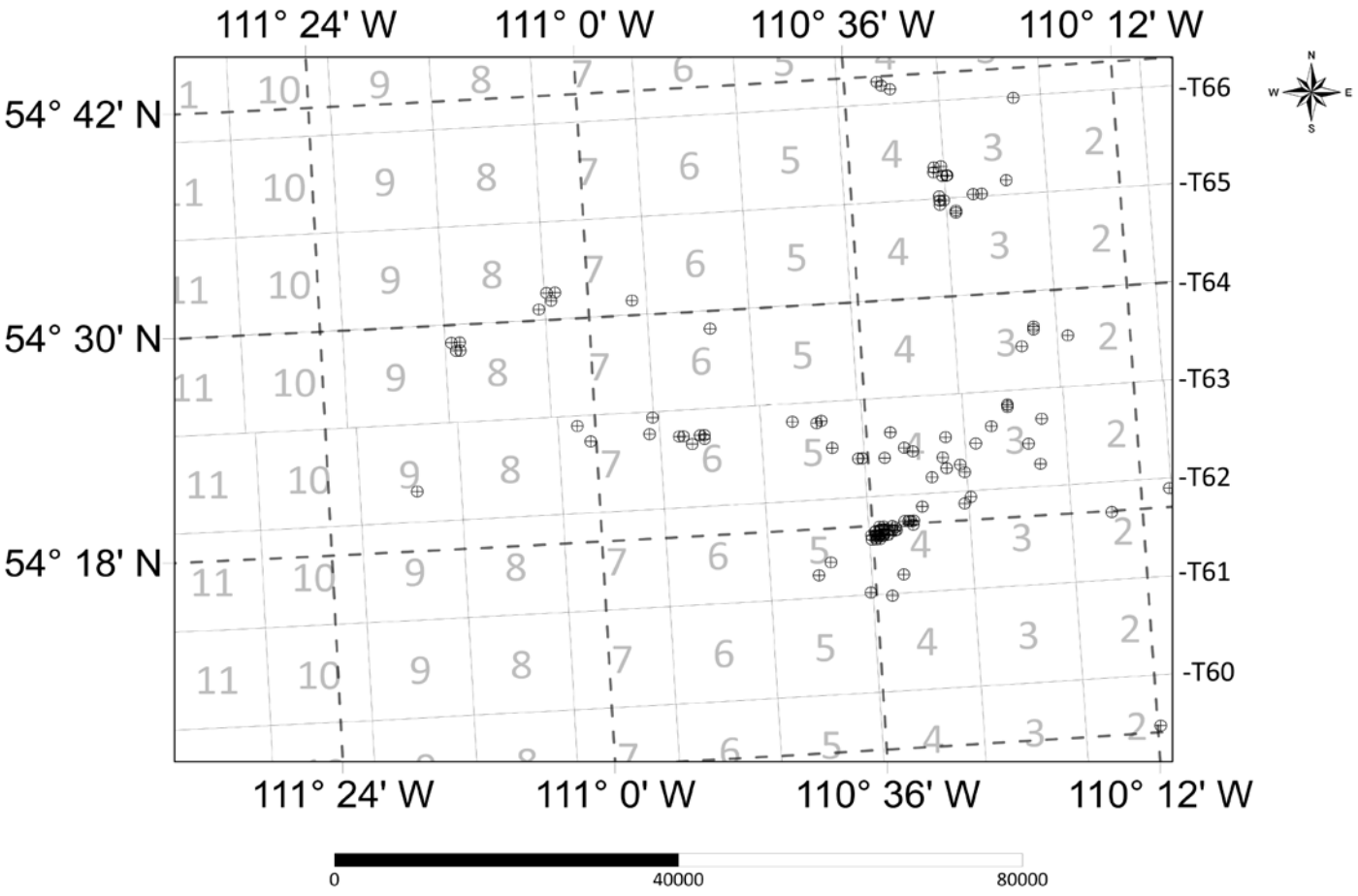

Fig. 30B. Contour Map of Methane Carbon Isotope Values of GM Beaver Dam Zoom-in

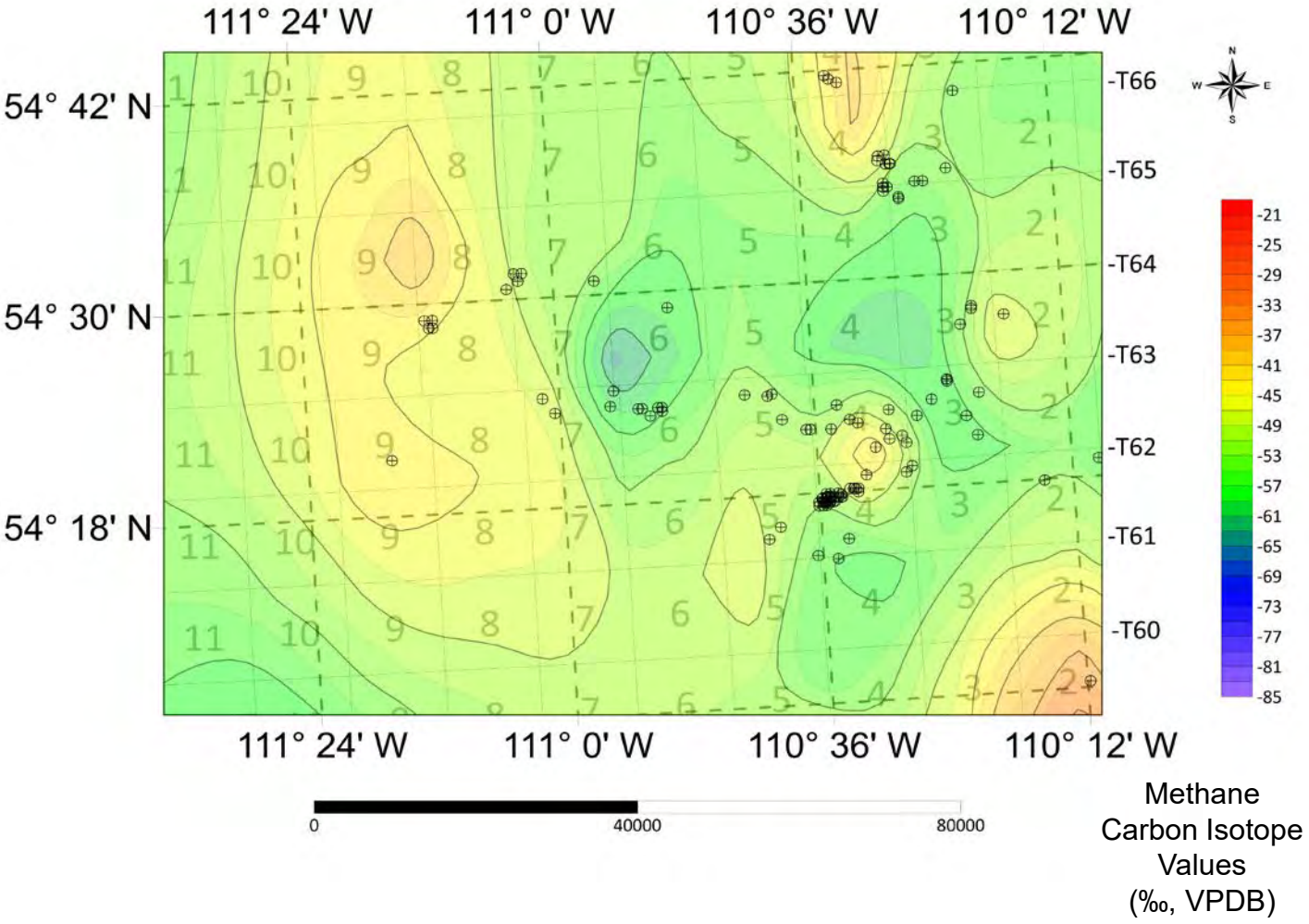

Fig. 30C. Contour Map of Ethane Carbon Isotope Values of GM Beaver Dam Zoom-in

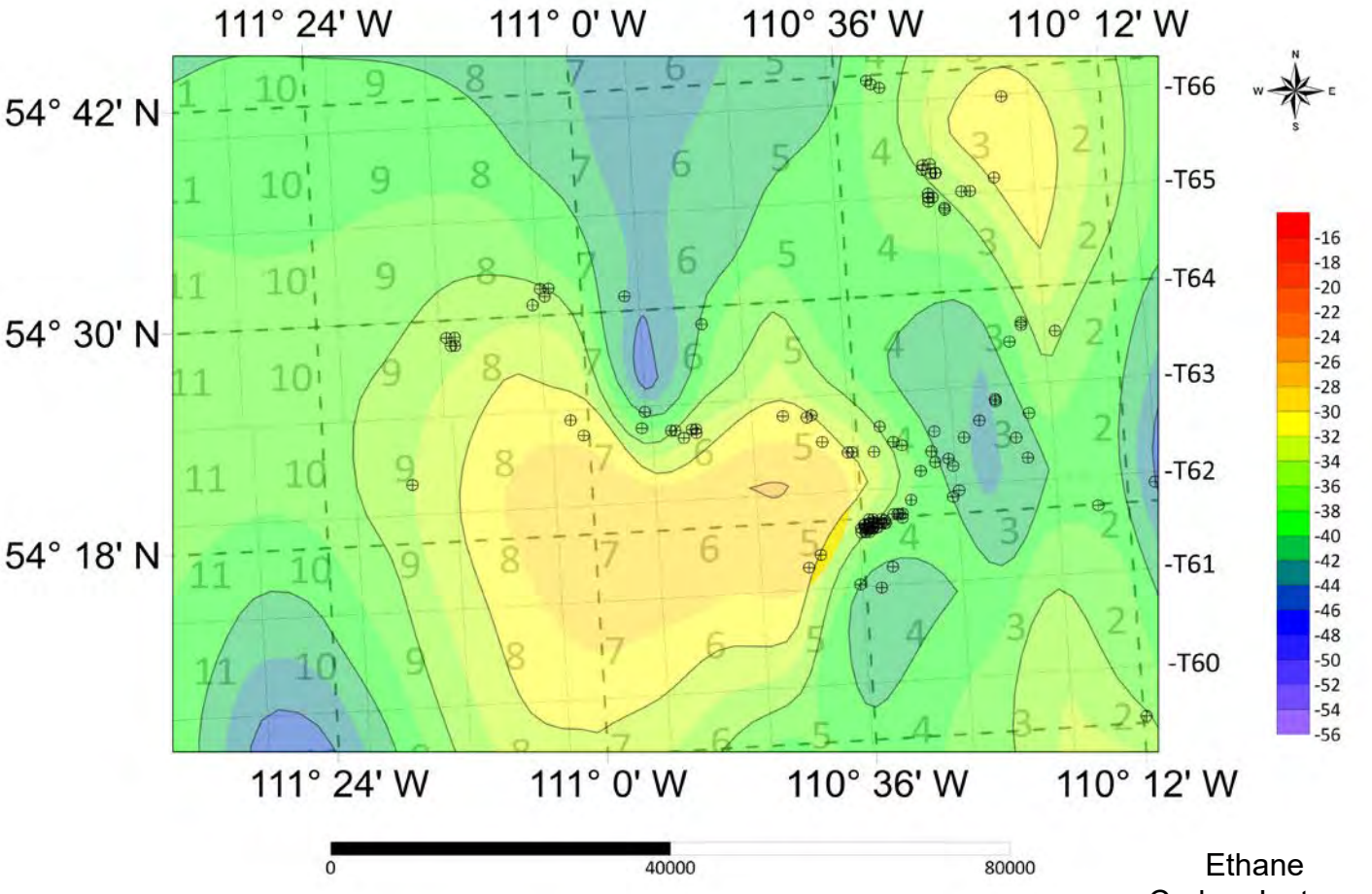

Ethane Carbon Isotope Values (‰, VPDB)

Fig. 30D. Contour Map of Propane Carbon Isotope Values of GM Beaver Dam Zoom-in

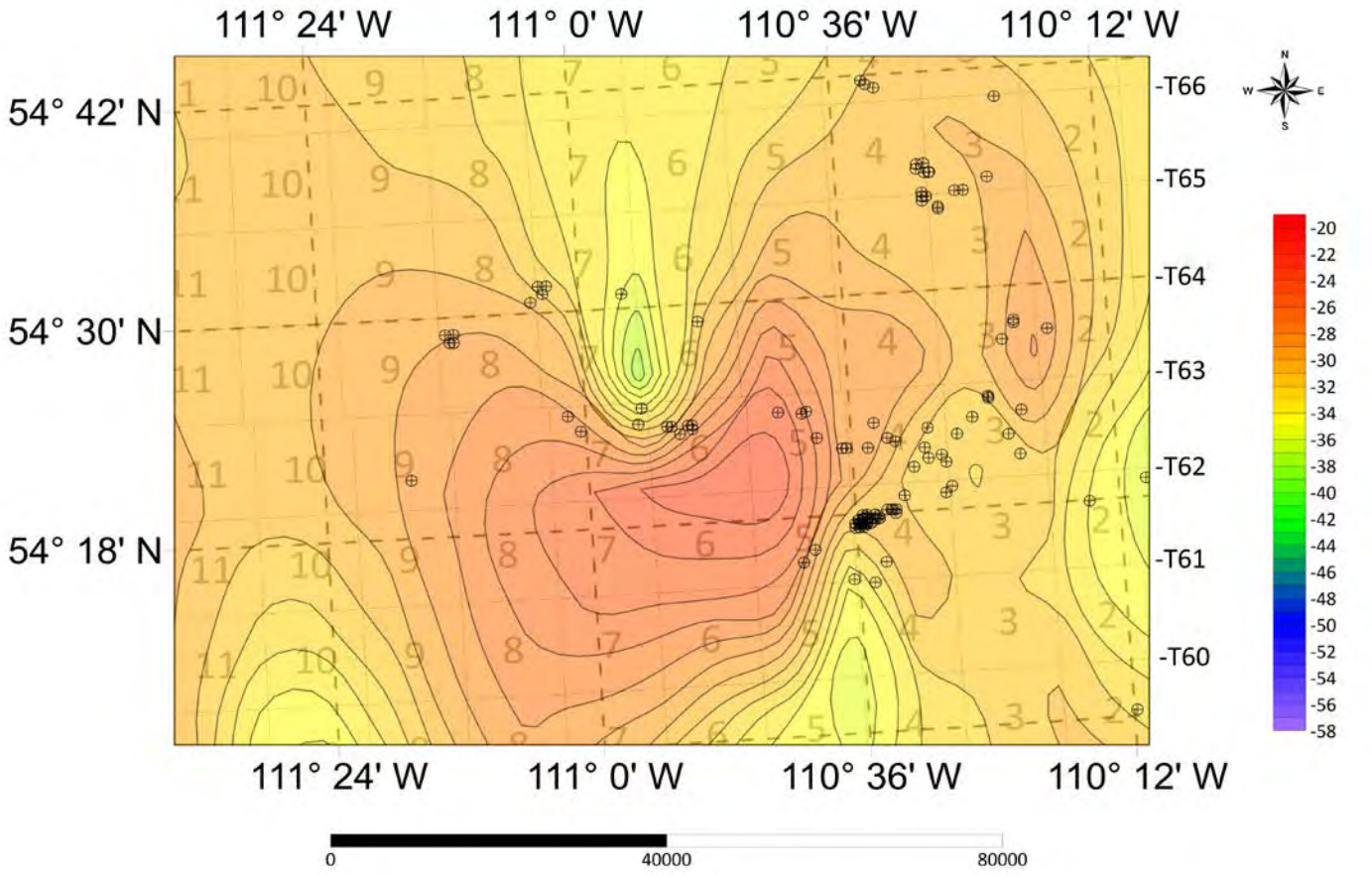

Propane Carbon Isotope Values (‰, VPDB)

Fig. 30E. Contour Map of *n*-Butane Carbon Isotope Values of GM Beaver Dam Zoom-in

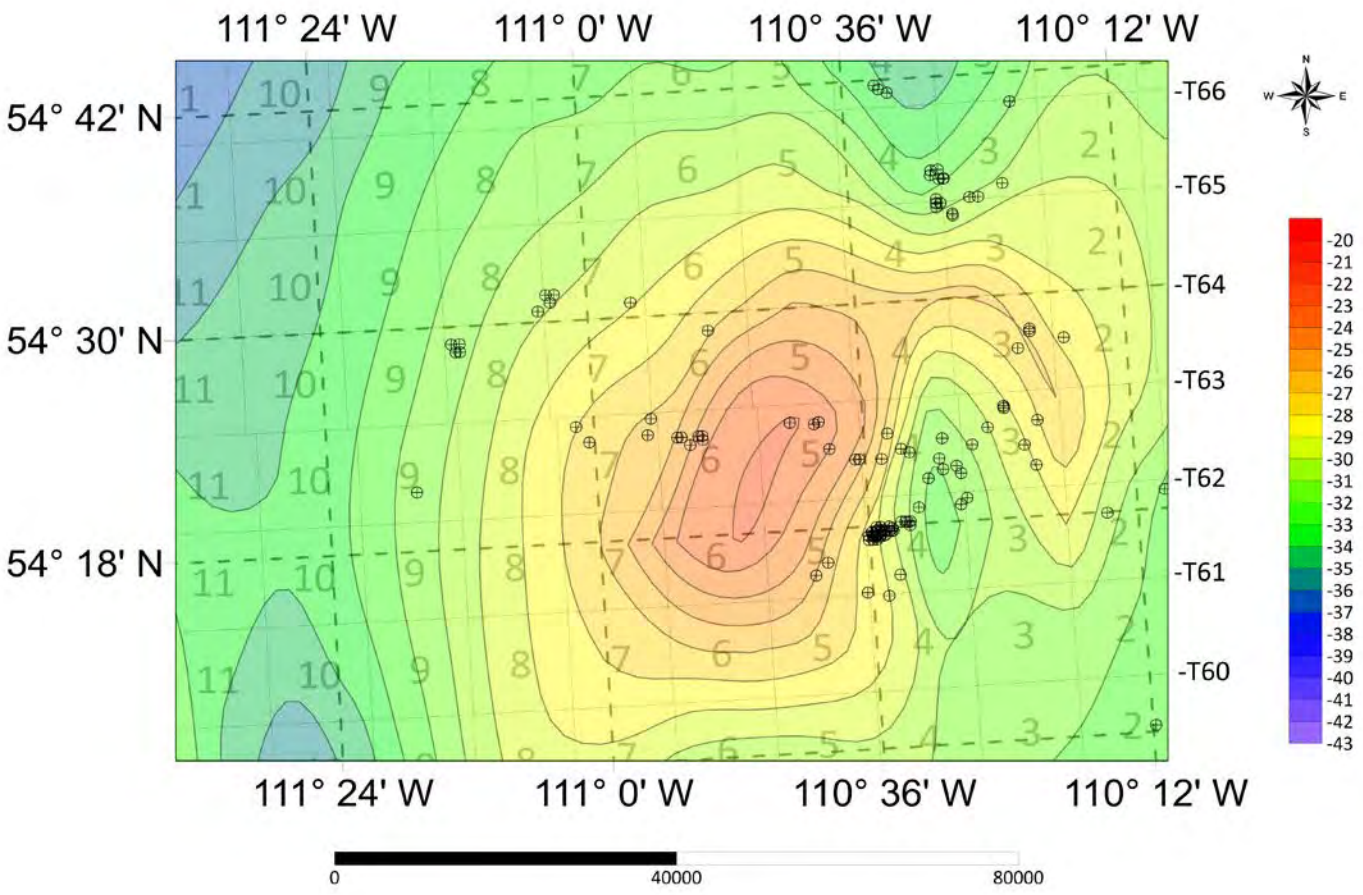

n-Butane Carbon Isotope Values (‰, VPDB)

Fig. 30F. Contour Map of *i*-Butane Carbon Isotope Values of GM Beaver Dam Zoom-in

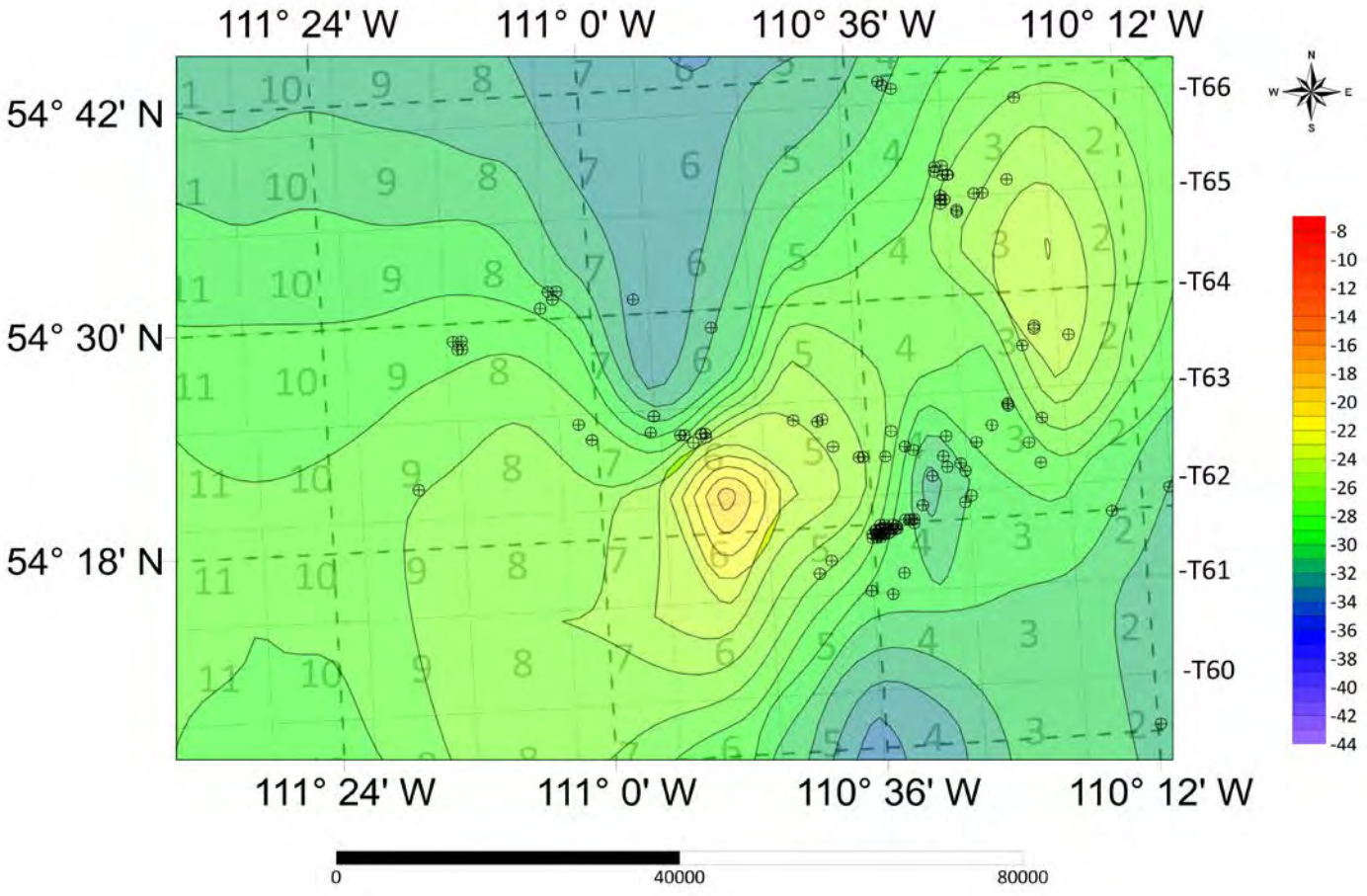

i-Butane Carbon Isotope Values (‰, VPDB)

Fig. 30G. Contour Map of Carbon Dioxide Carbon Isotope Values of GM Beaver Dam Zoom-in

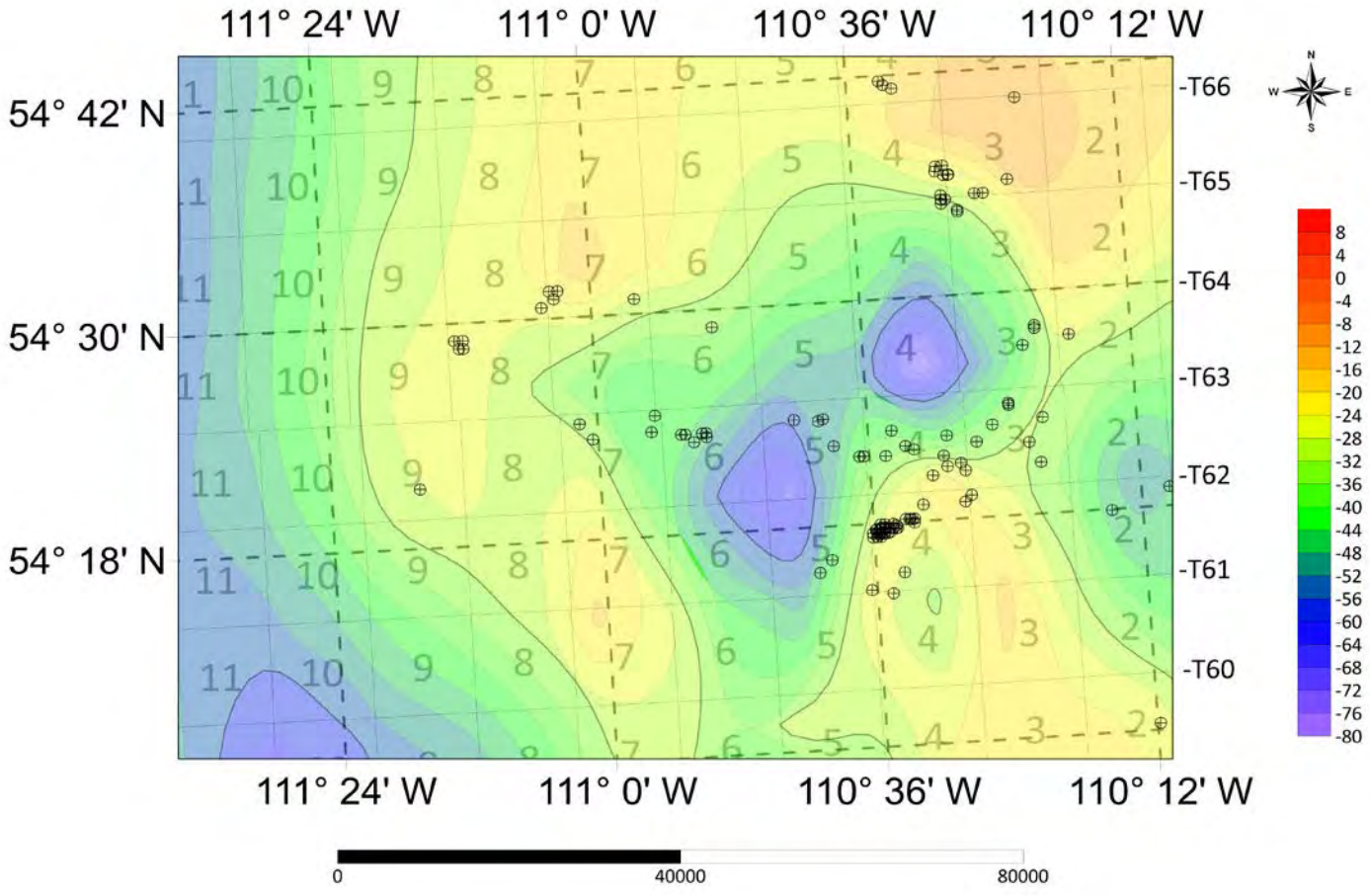

Carbon Dioxide Carbon Isotope Values (‰, VPDB)

Fig. 30H. Contour Map of Methane Carbon Isotope Values of GM Beaver Dam Zoom-in over Topographic Map

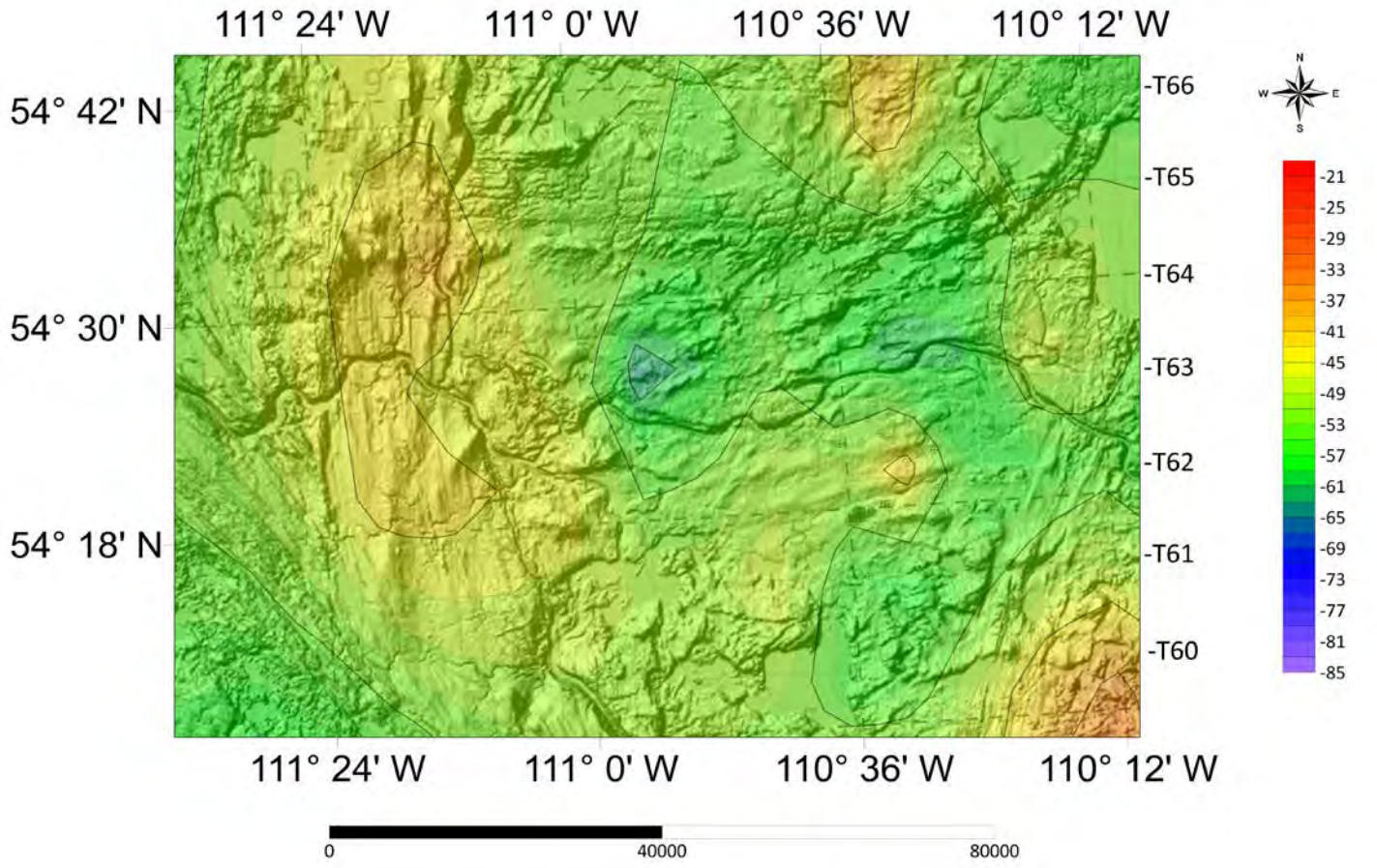

Methane Carbon Isotope Values (‰, VPDB)

Fig. 30I. Contour Map of Ethane Carbon Isotope Values of GM Beaver Dam Zoom-in over Topographic Map

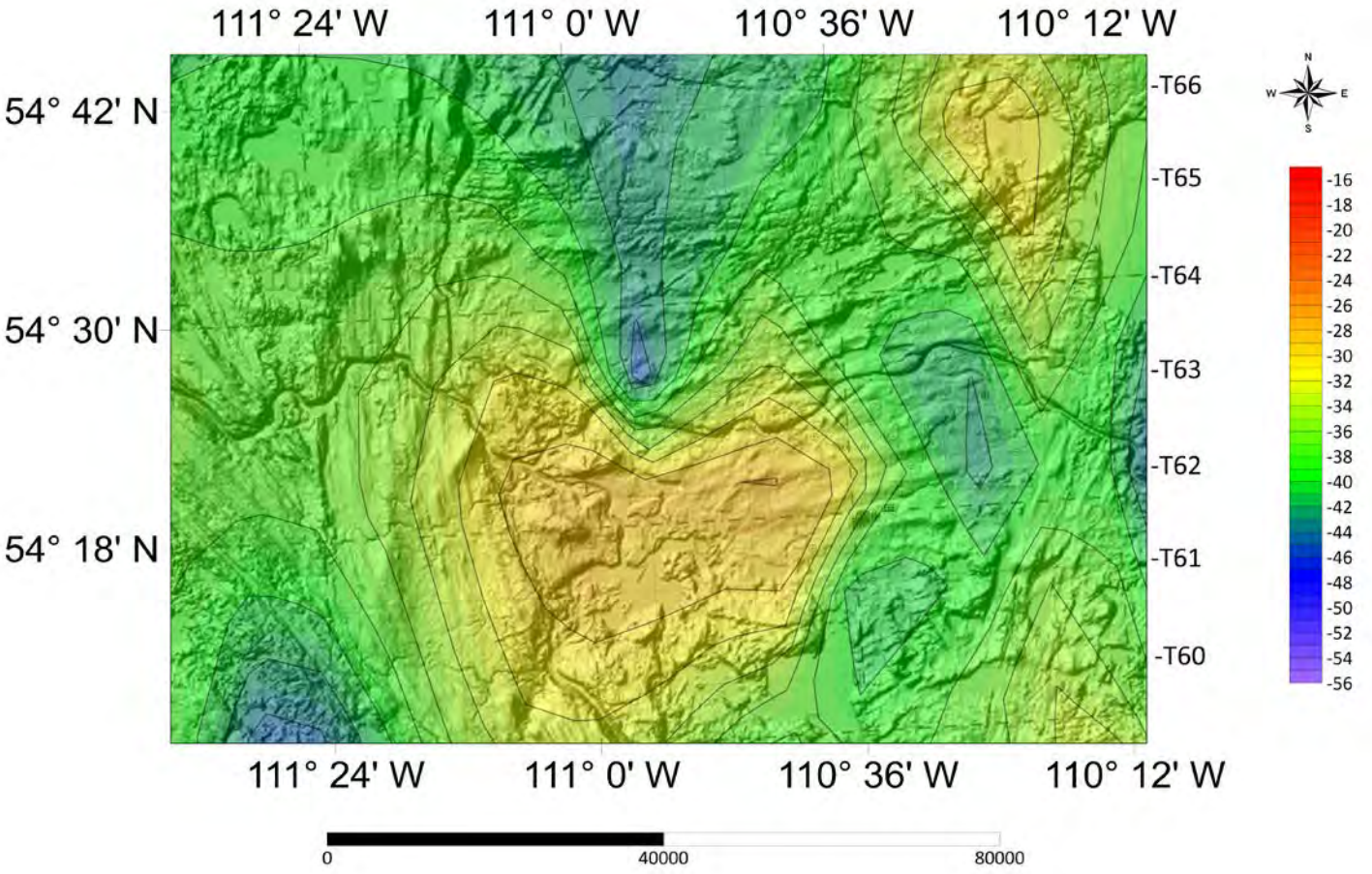

Ethane Carbon Isotope Values (‰, VPDB)

Fig. 30J. Contour Map of Propane Carbon Isotope Values of GM Beaver Dam Zoom-in over Topographic Map

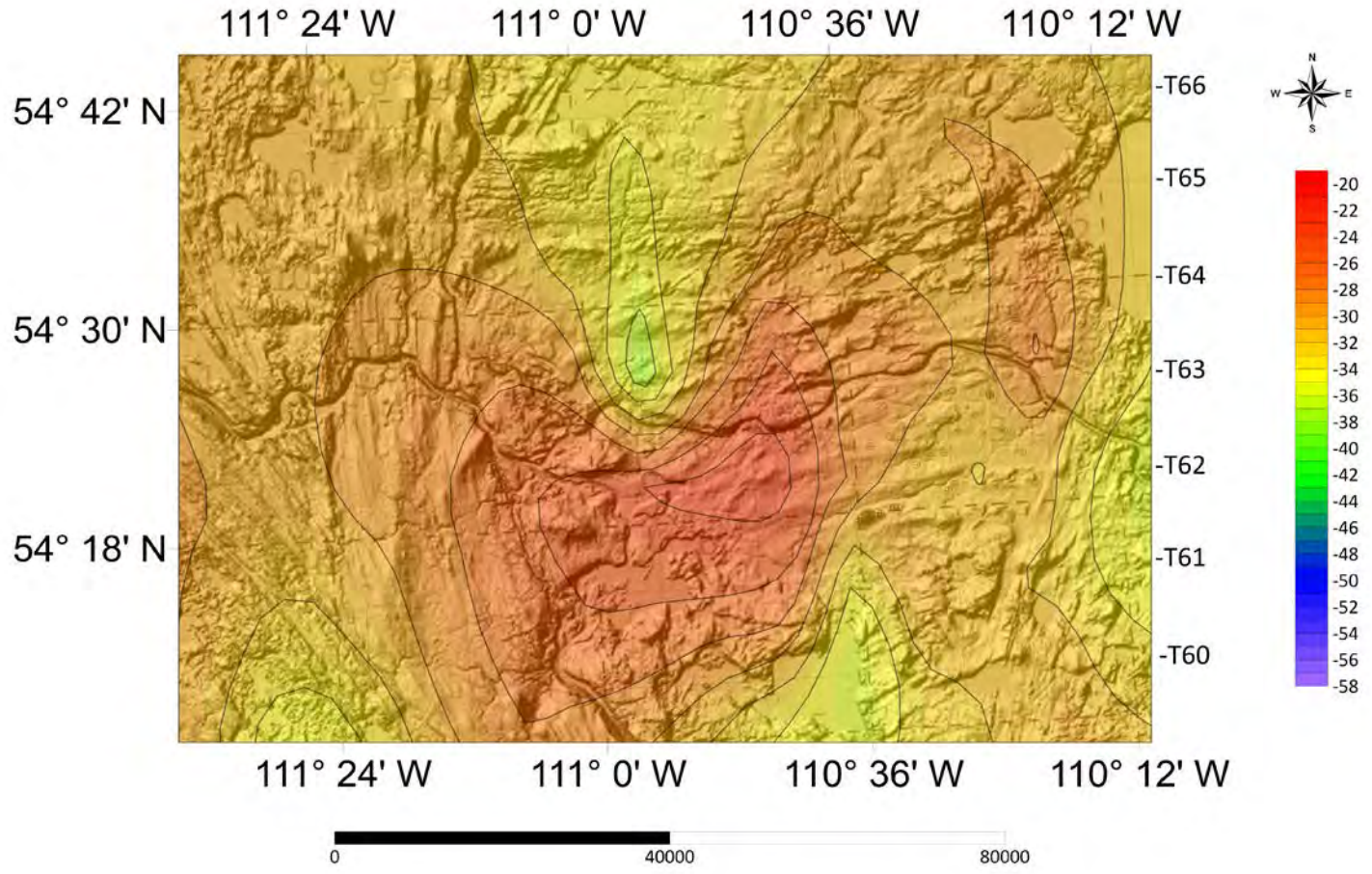

Propane Carbon Isotope Values (‰, VPDB)

Fig. 30K. Contour Map of *n*-Butane Carbon Isotope Values of GM Beaver Dam Zoom-in over Topographic Map

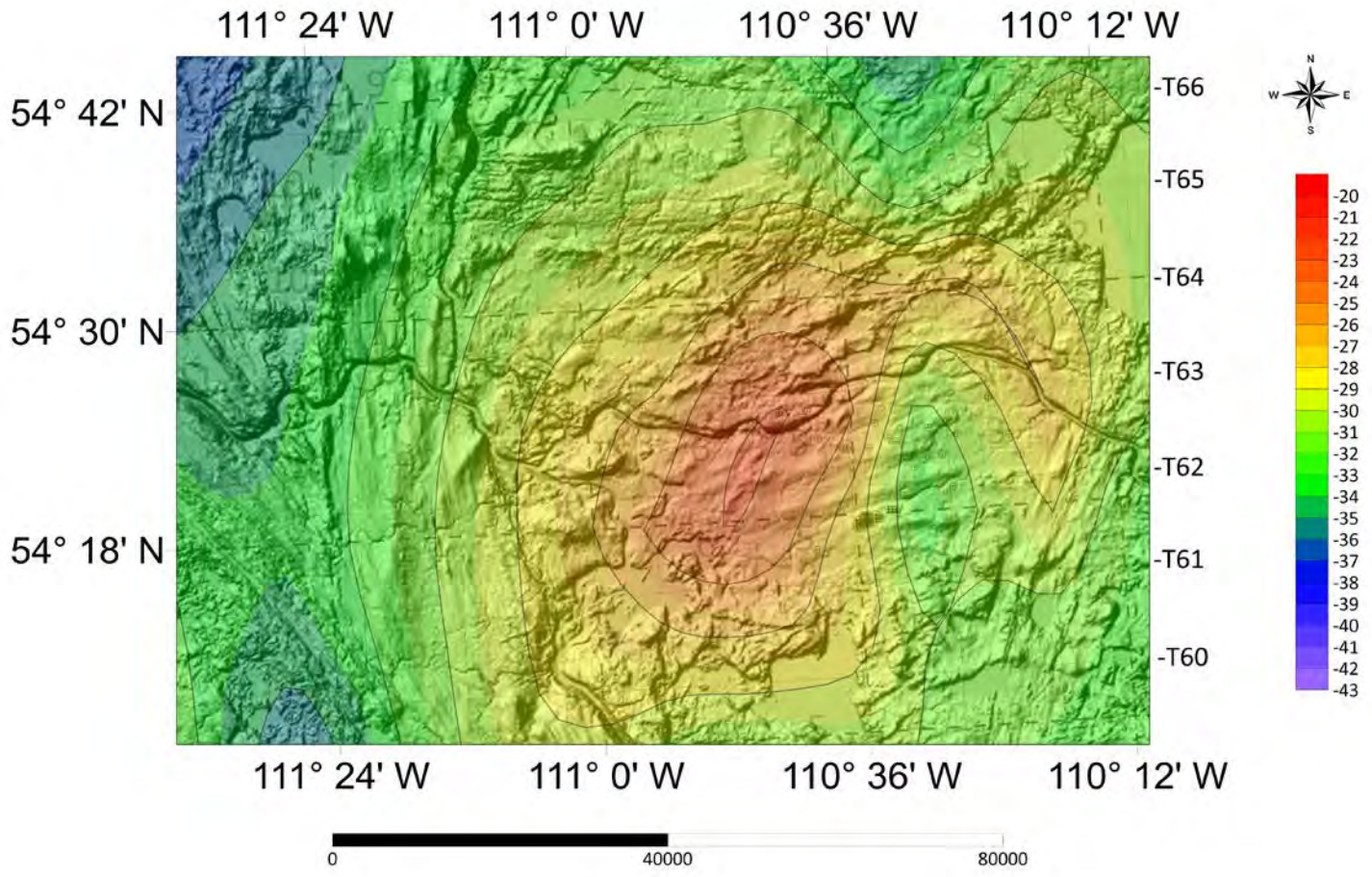

n-Butane Carbon Isotope Values (‰, VPDB)

Fig. 30L. Contour Map of *i*-Butane Carbon Isotope Values of GM Beaver Dam Zoom-in over Topographic Map

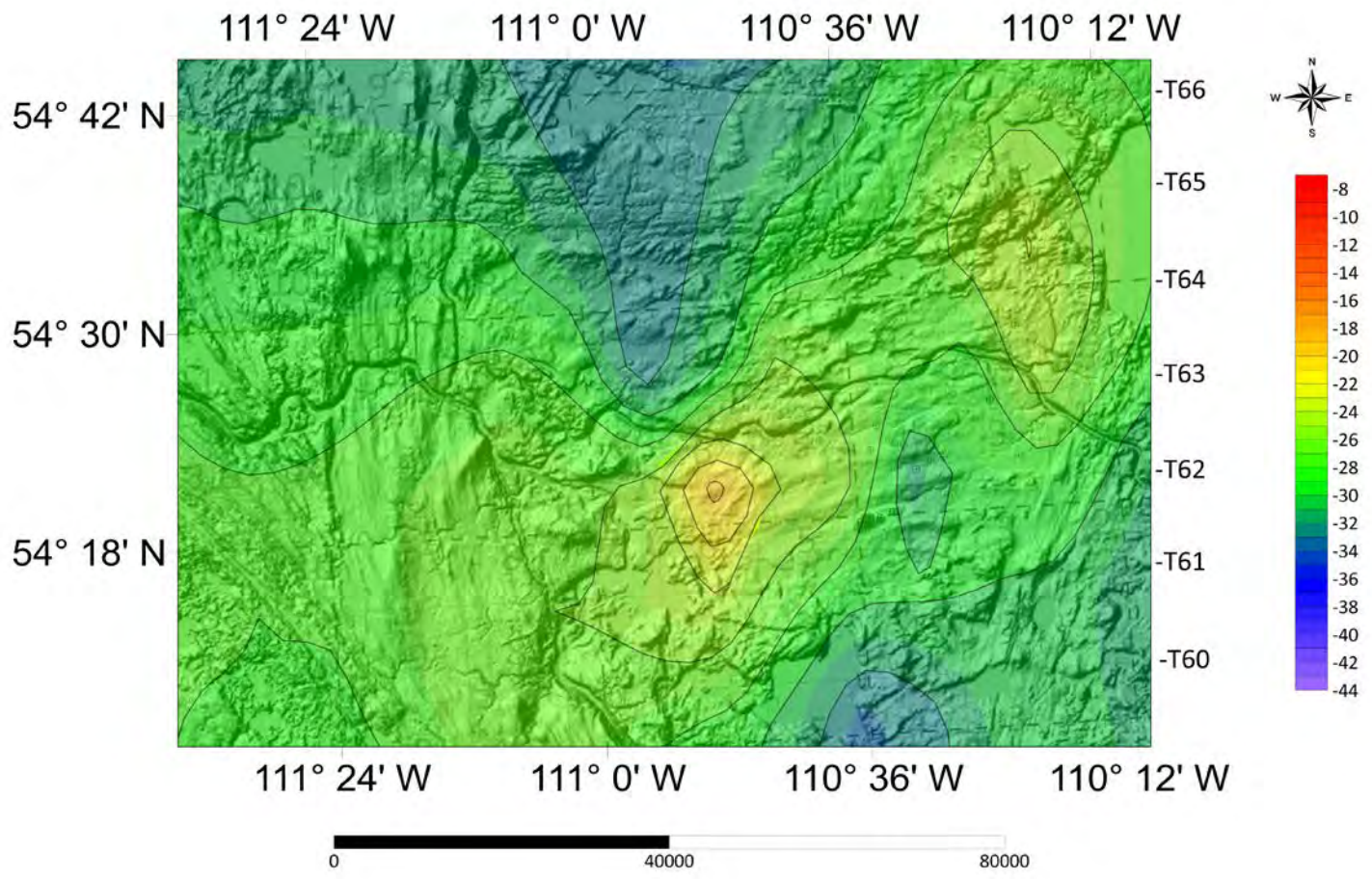

i-Butane Carbon Isotope Values (‰, VPDB)

Fig. 30M. Contour Map of Carbon Dioxide Carbon Isotope Values of GM Beaver Dam Zoom-in over Topographic Map

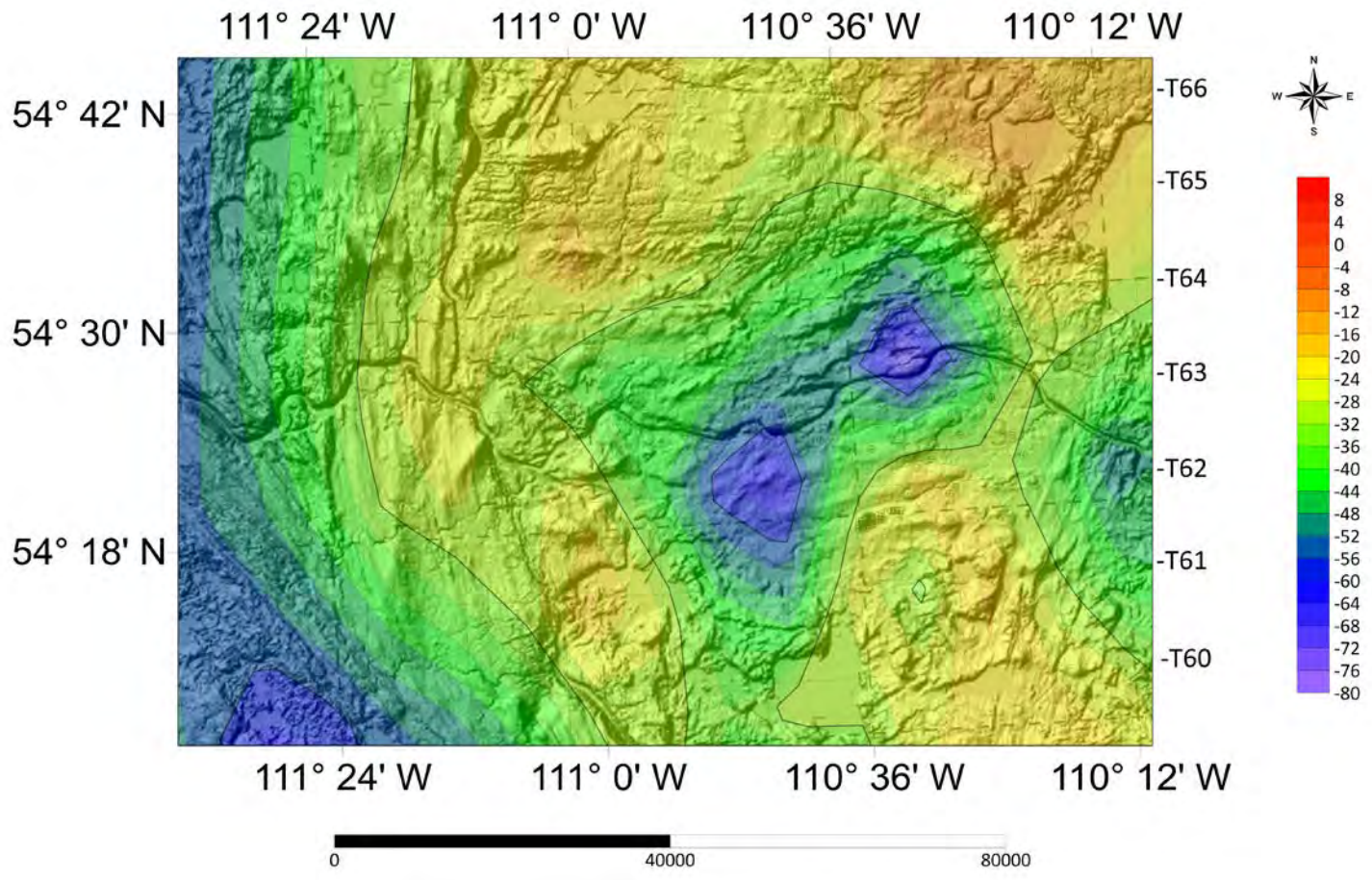

Carbon Dioxide Carbon Isotope Values (‰, VPDB)

Fig. 31A. Map of Surface Casing Vent (SCV) Locations in the Pembina Zoom-in

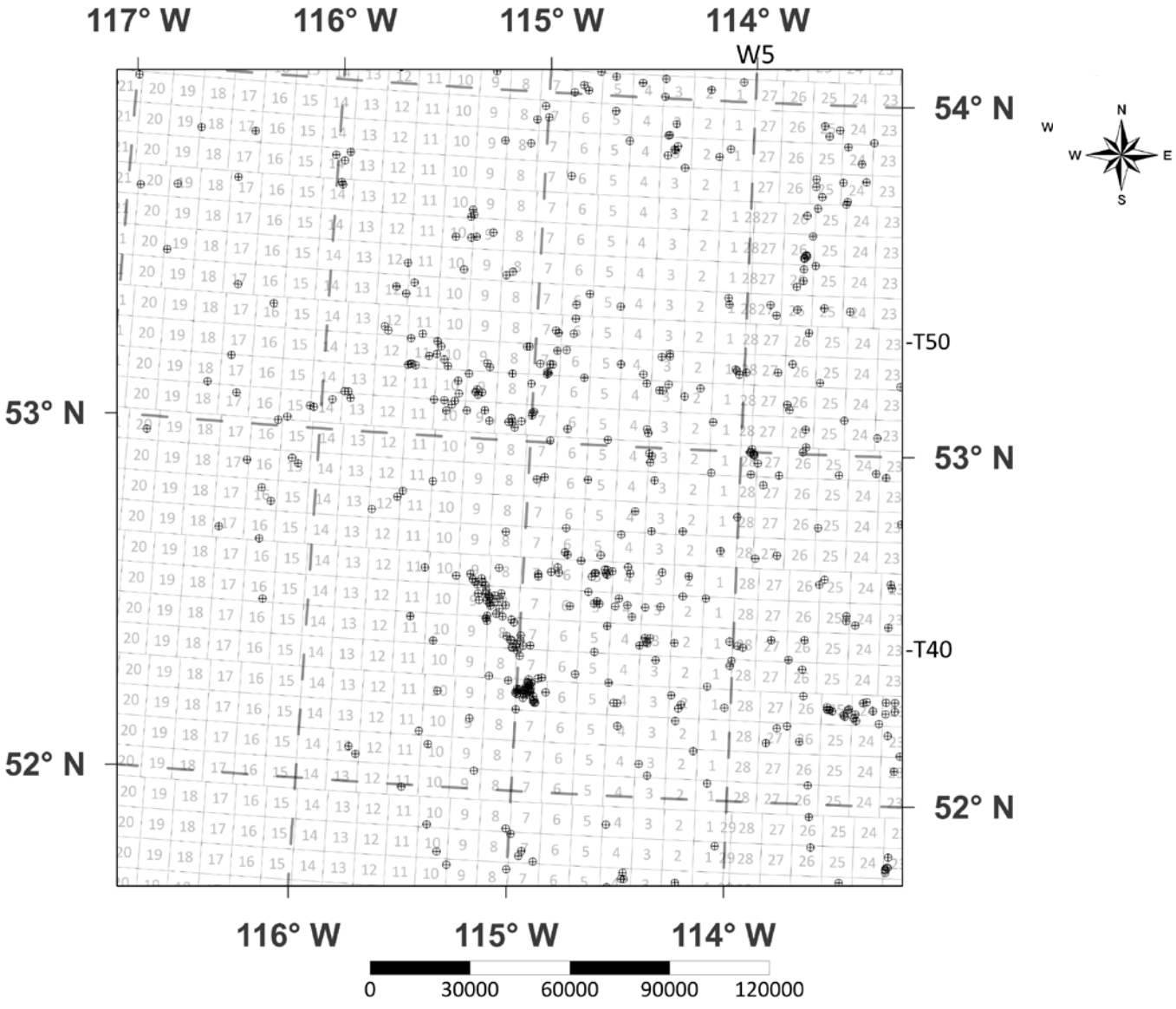

Fig. 31B. Contour Map of Methane Carbon Isotope Values of SCV Pembina Zoom-in

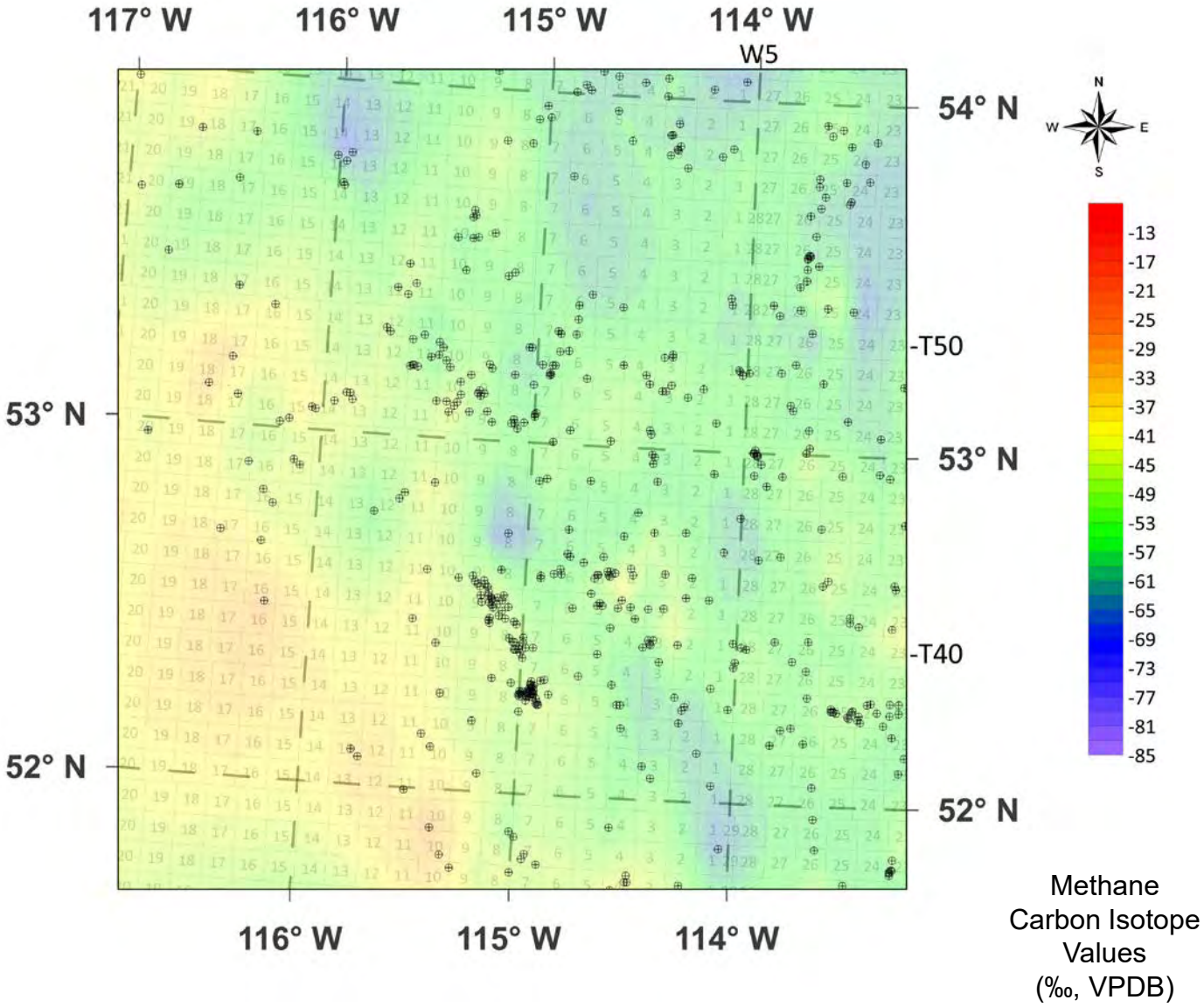

Fig. 31C. Contour Map of Ethane Carbon Isotope Values of SCV Pembina Zoom-in

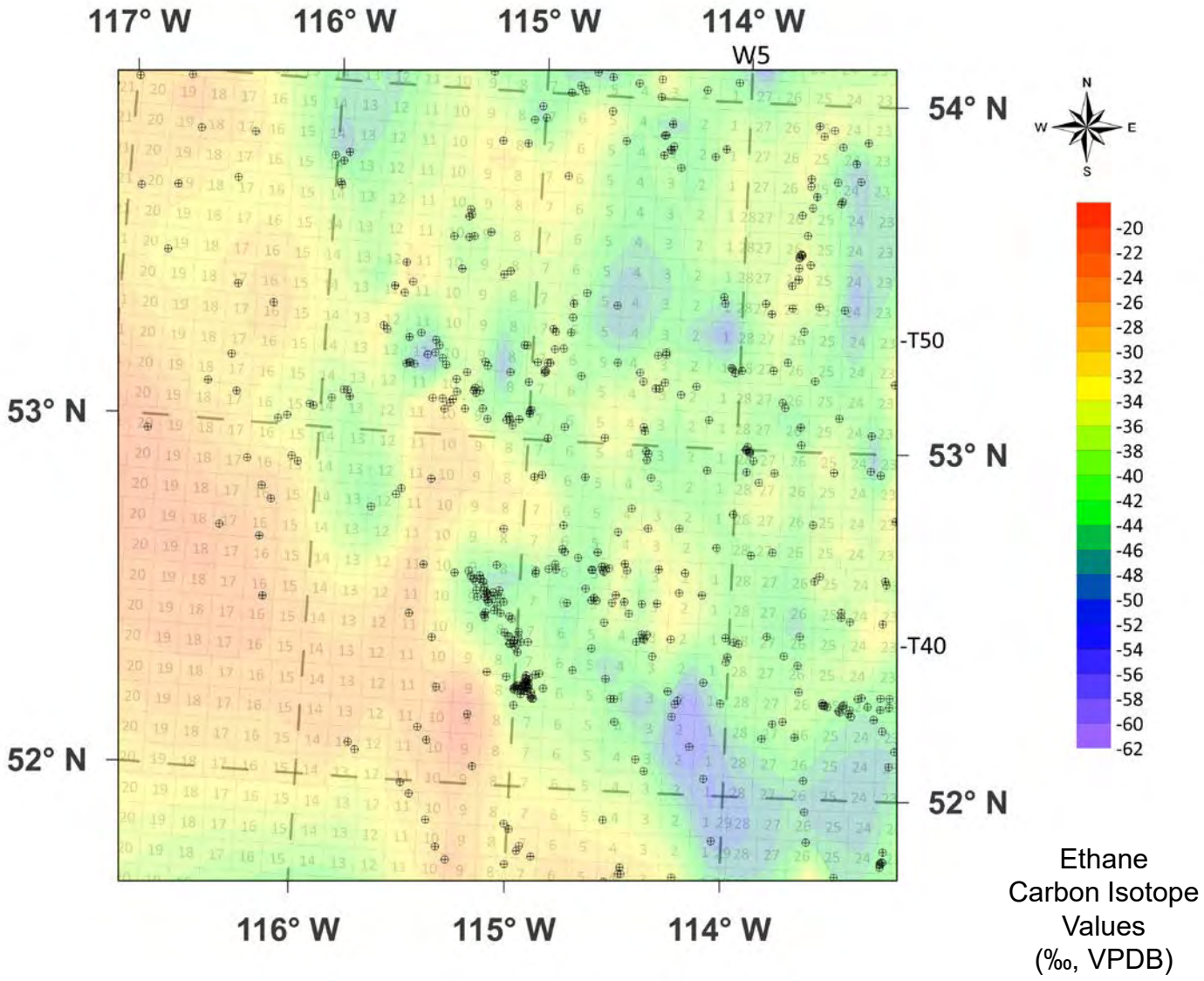

Fig. 31D. Contour Map of Propane Carbon Isotope Values of SCV Pembina Zoom-in

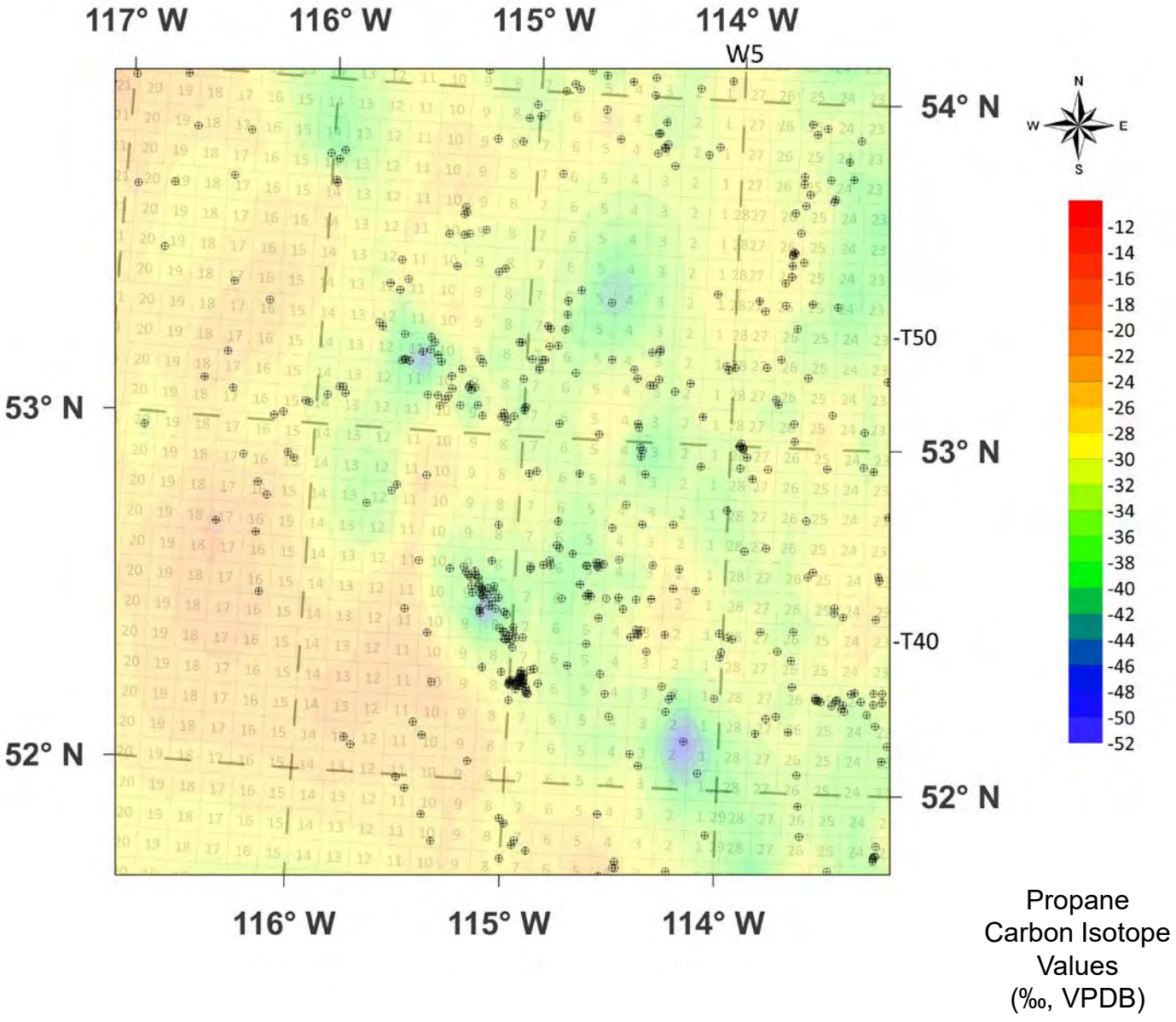

Fig. 31E. Contour Map of *n*-Butane Carbon Isotope Values of SCV Pembina Zoom-in

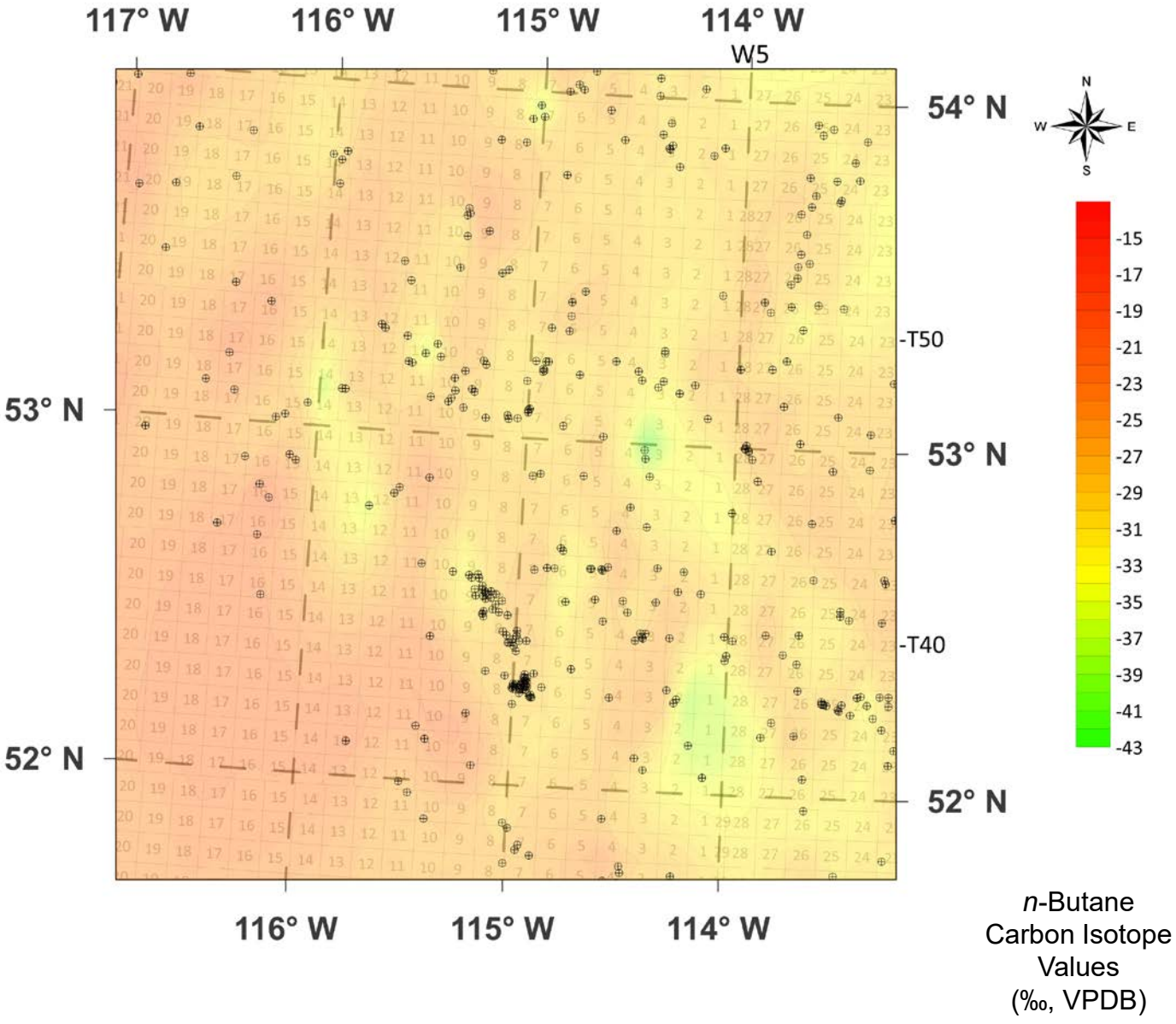

Fig. 31F. Contour Map of *i*-Butane Carbon Isotope Values of SCV Lloydminster Zoom-in

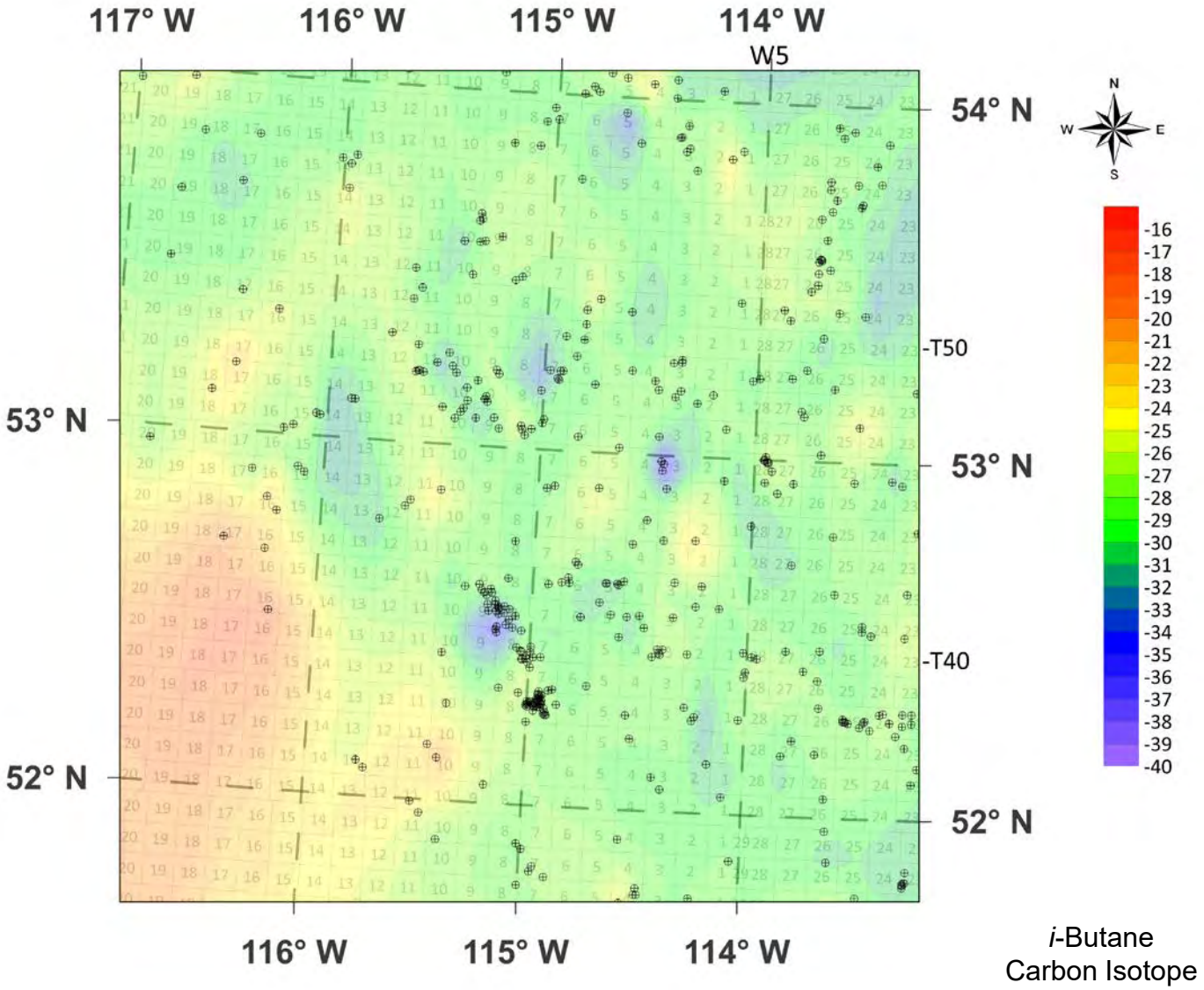

Fig. 31G. Contour Map of Carbon Dioxide Carbon Isotope Values of SCV Pembina Zoom-in

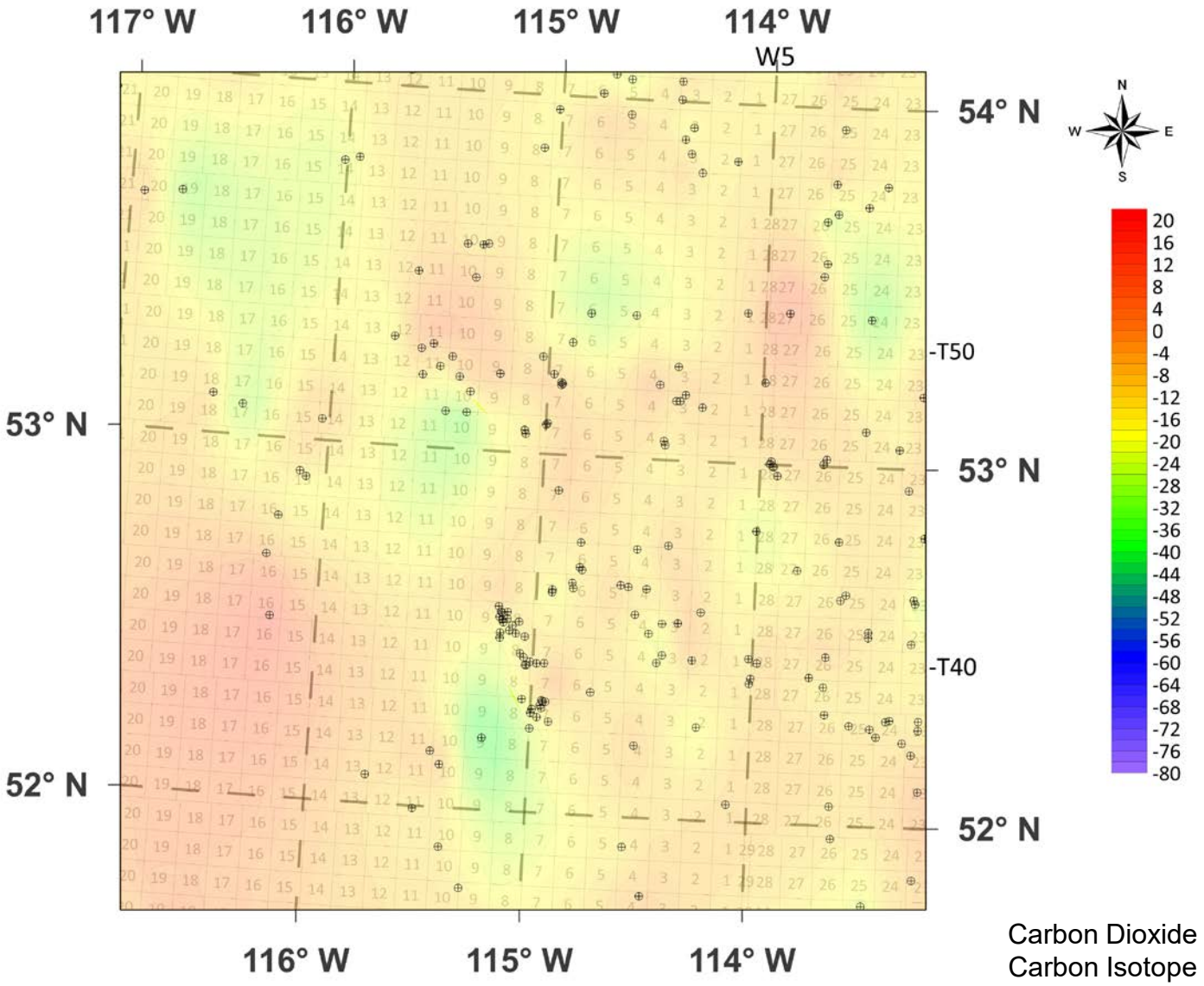

Fig. 31H. Contour Map of Methane Carbon Isotope Values of SCV Pembina Zoom-in over Topographic Map

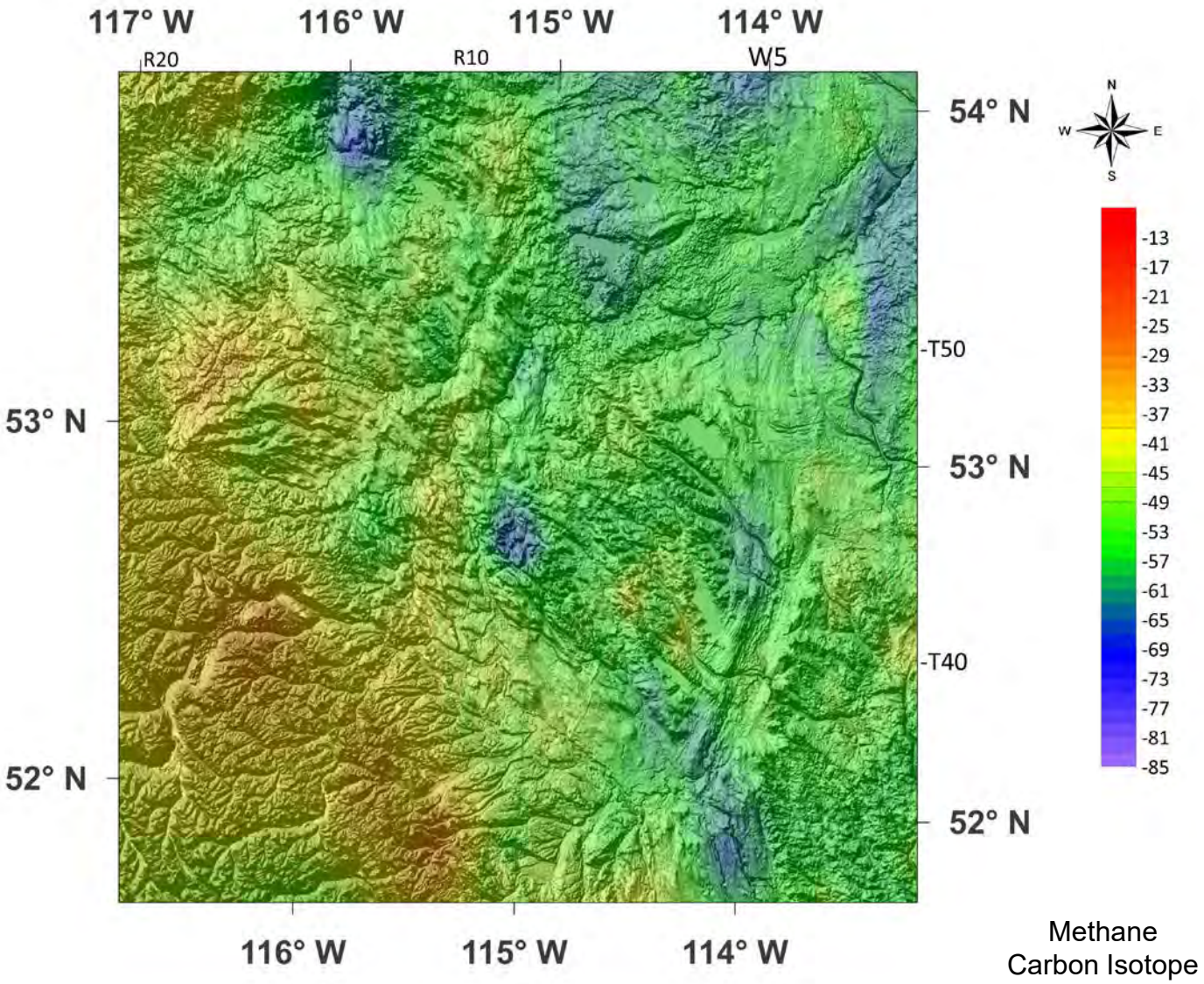

Fig. 31I. Contour Map of Ethane Carbon Isotope Values of SCV Pembina Zoom-in over Topographic Map

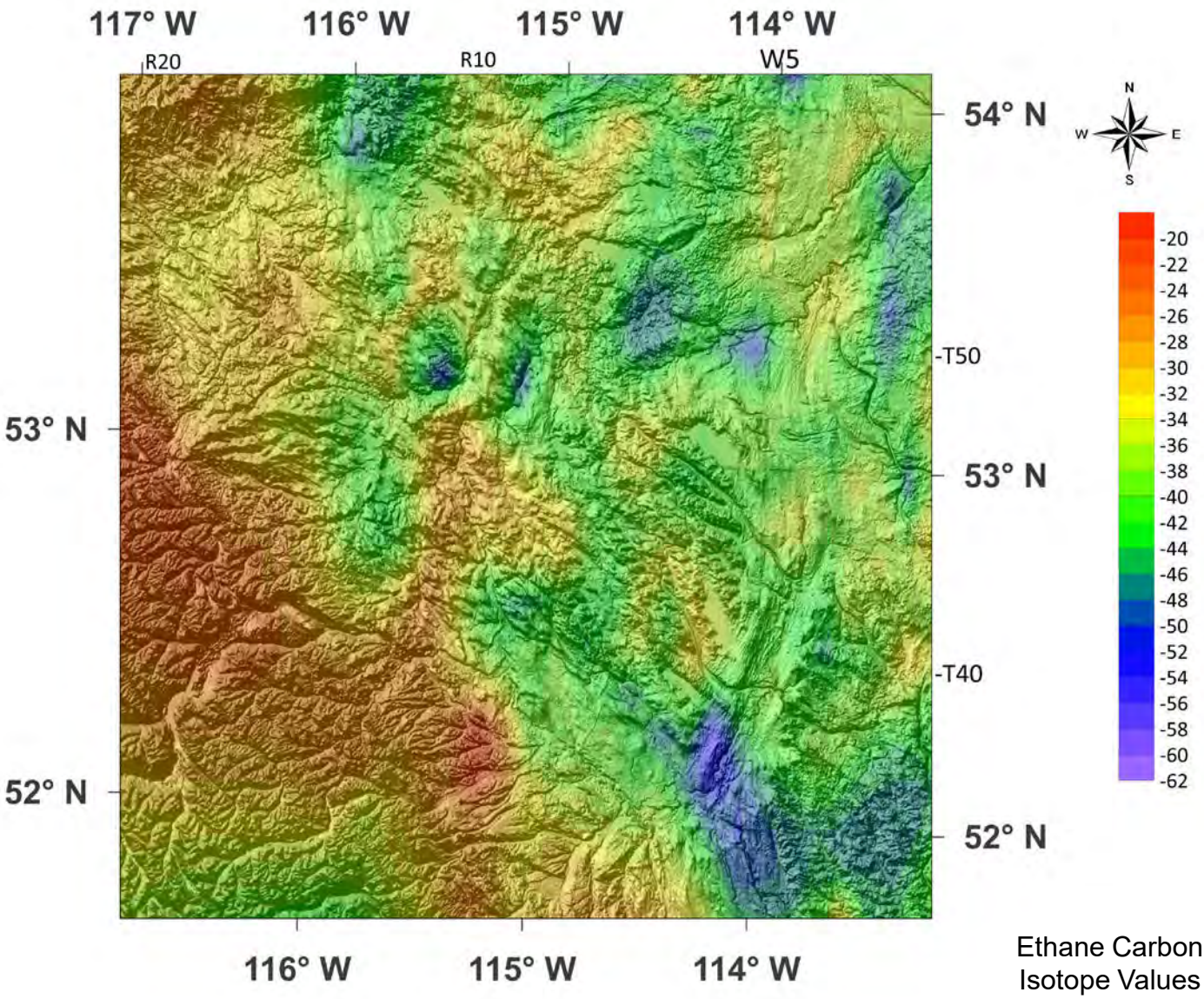

Fig. 31J. Contour Map of Propane Carbon Isotope Values of SCV Pembina Zoom-in over Topographic Map

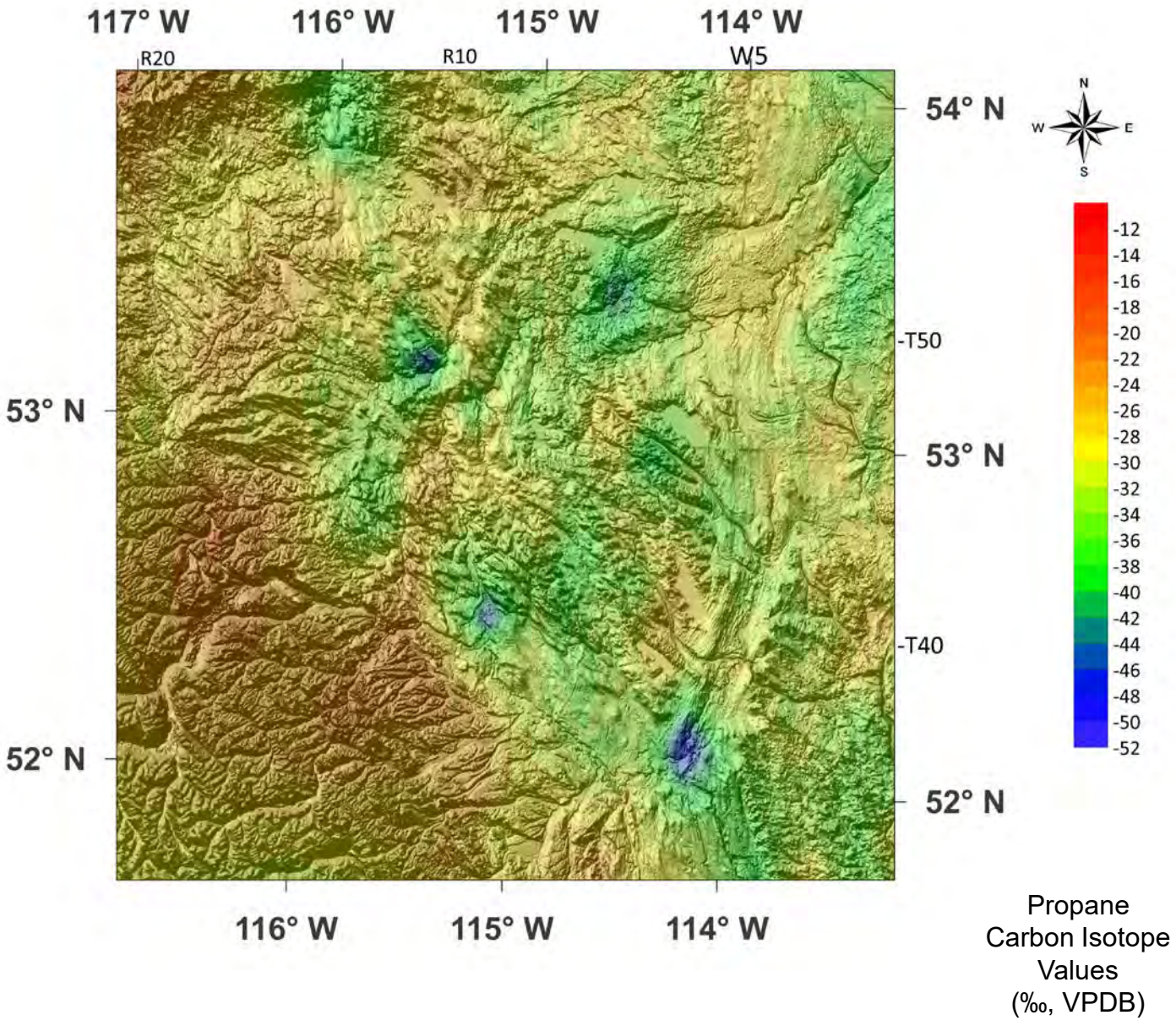

Fig. 31K. Contour Map of *n*-Butane Carbon Isotope Values of SCV Pembina Zoom-in over Topographic Map

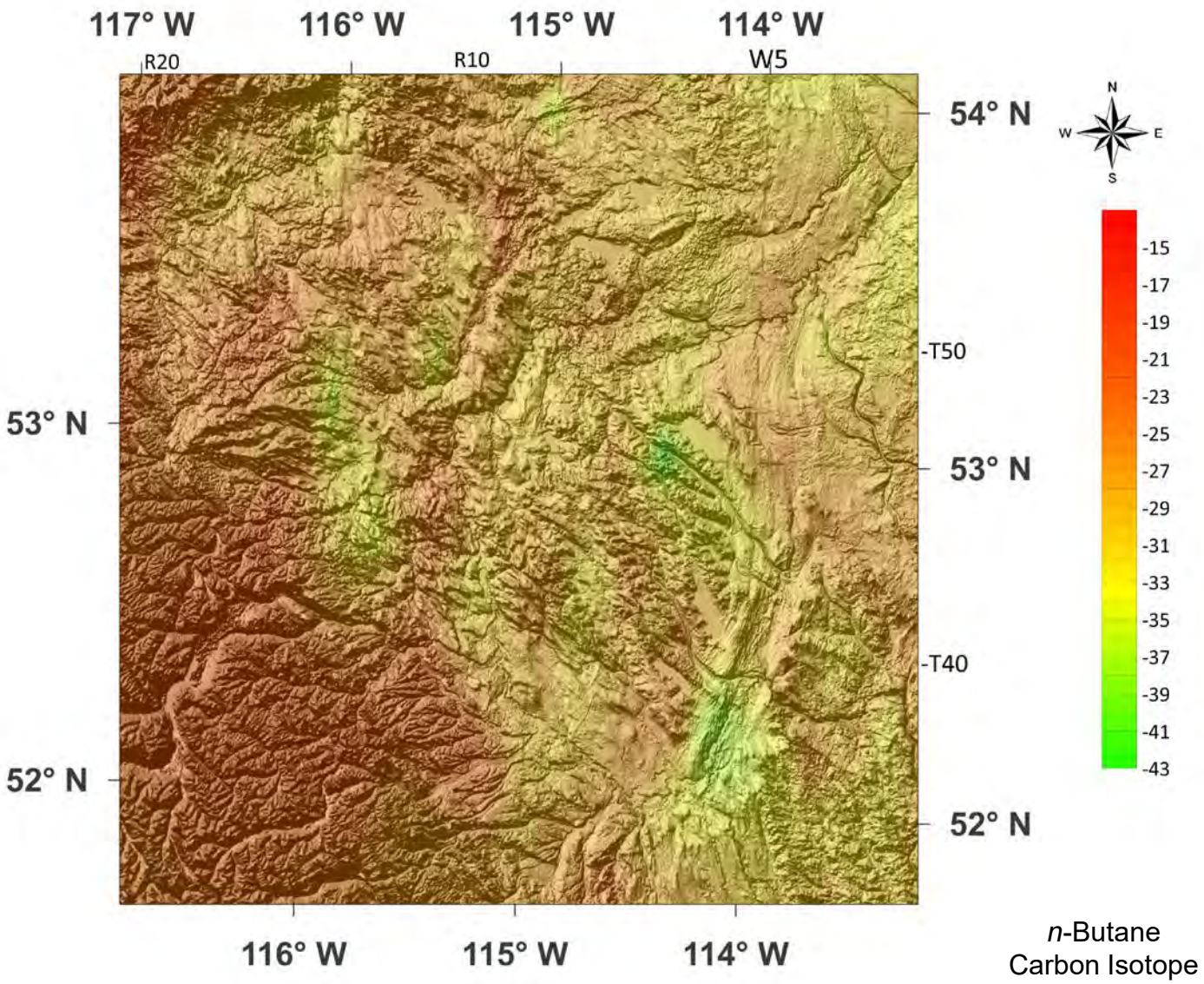

Fig. 31L. Contour Map of *i*-Butane Carbon Isotope Values of SCV Pembina Zoom-in over Topographic Map

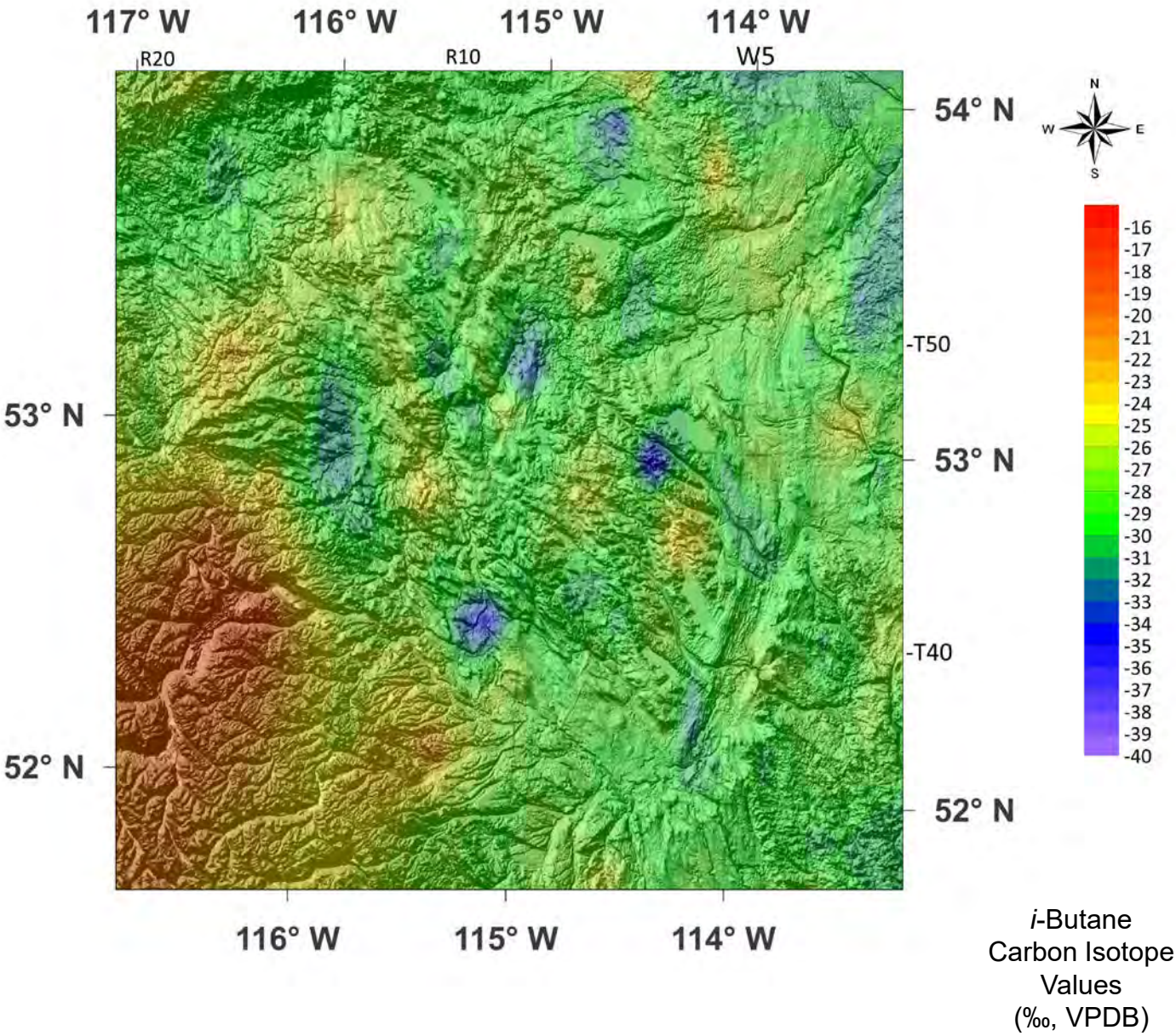

Fig. 31M. Contour Map of Carbon Dioxide Carbon Isotope Values of SCV Pembina Zoom-in over Topographic Map

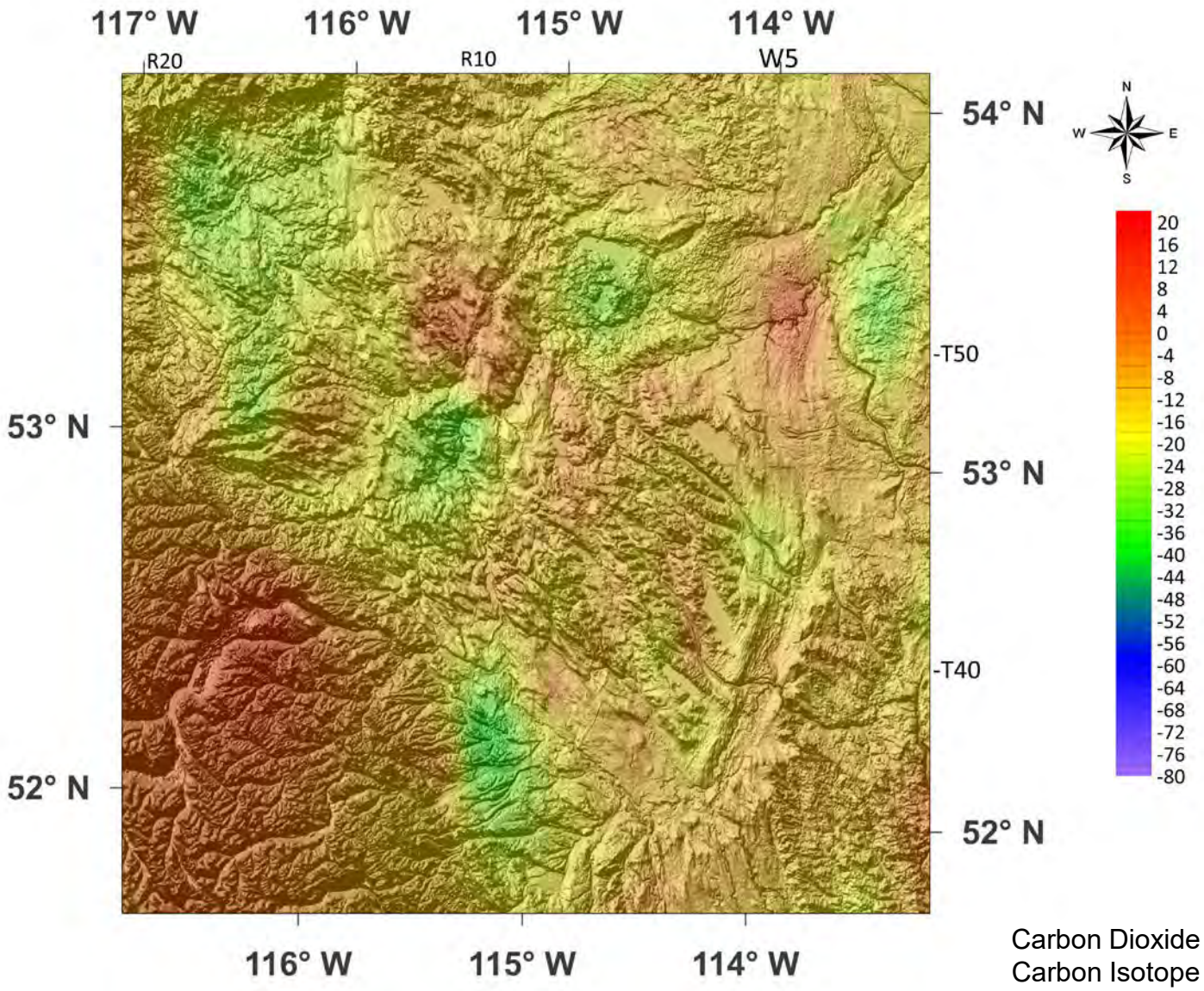

Fig. 32A. Map of Ground Migration (GM) Locations in the Pembina Zoom-in

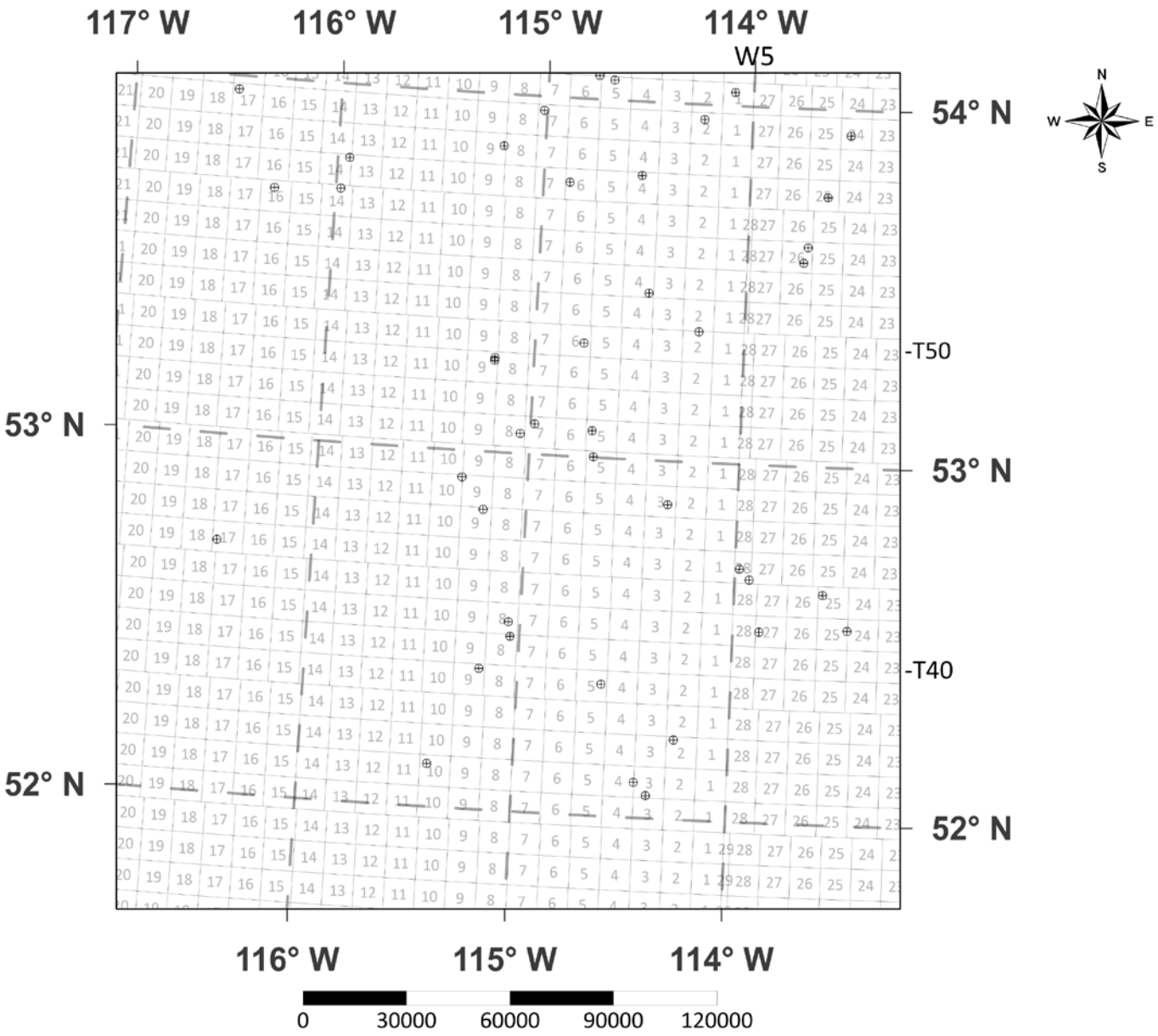

Fig. 32B. Contour Map of Methane Carbon Isotope Values of GM Pembina Zoom-in

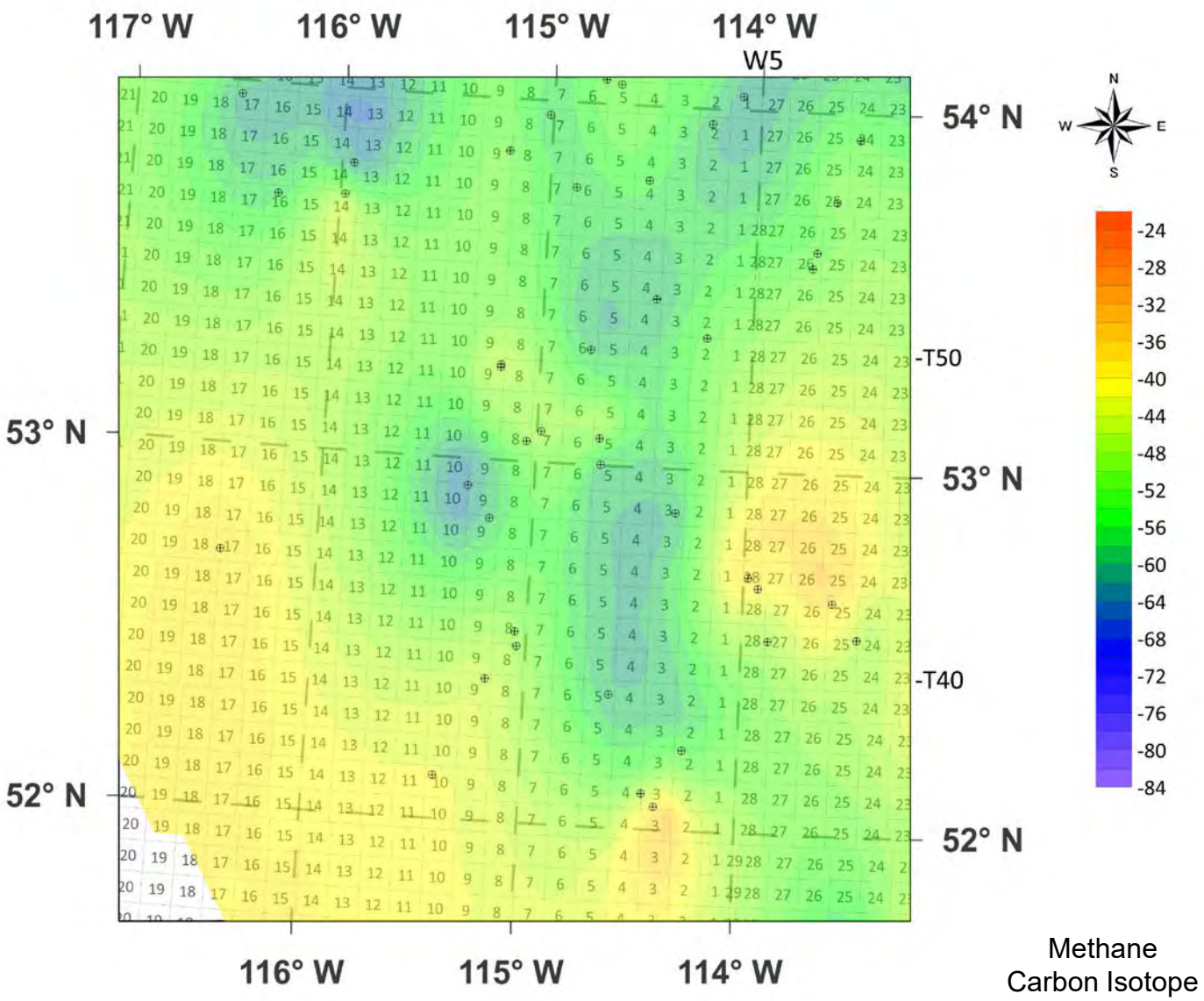

Fig. 32C. Contour Map of Ethane Carbon Isotope Values of GM Pembina Zoom-in

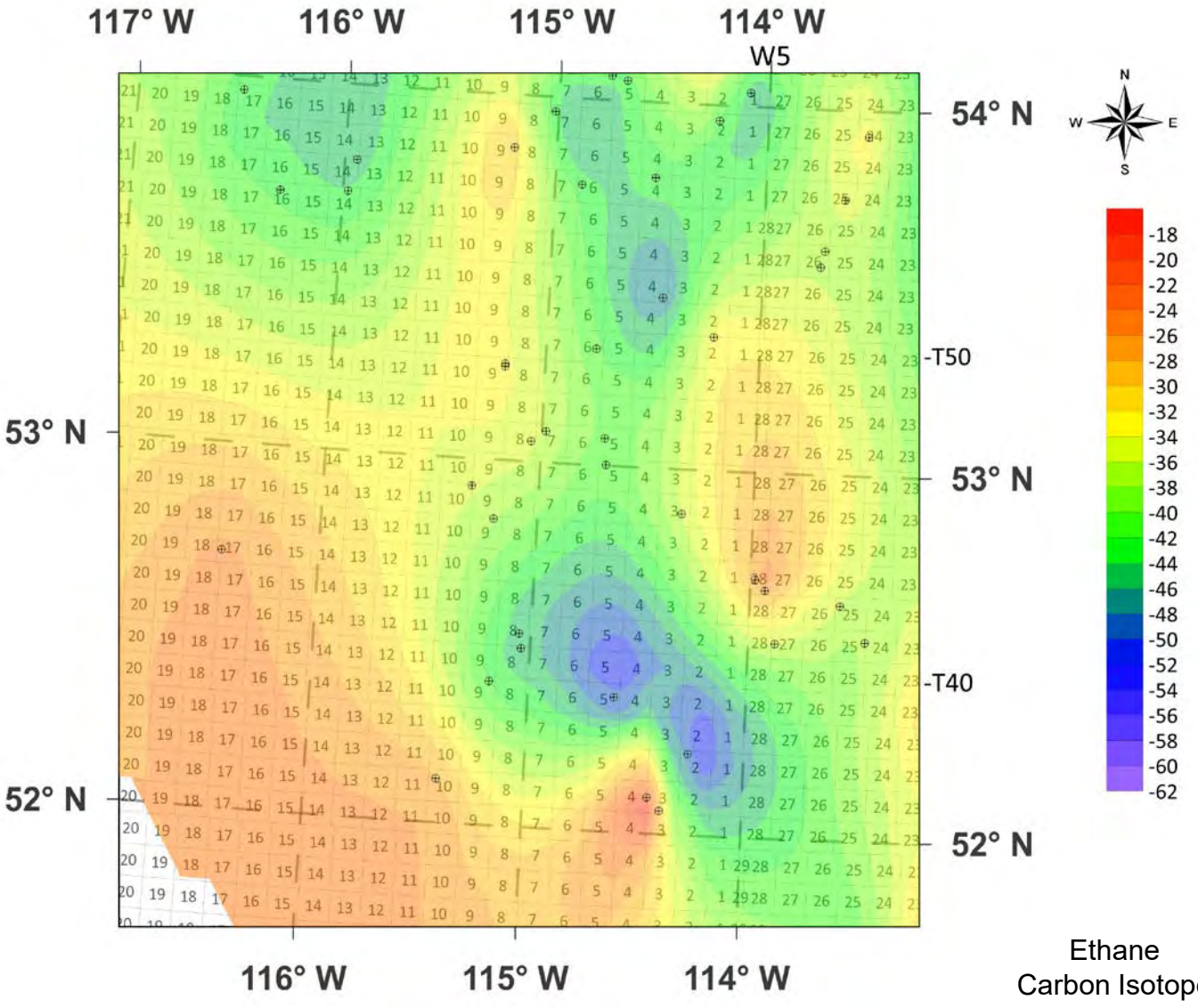

Fig. 32D. Contour Map of Propane Carbon Isotope Values of GM Pembina Zoom-in

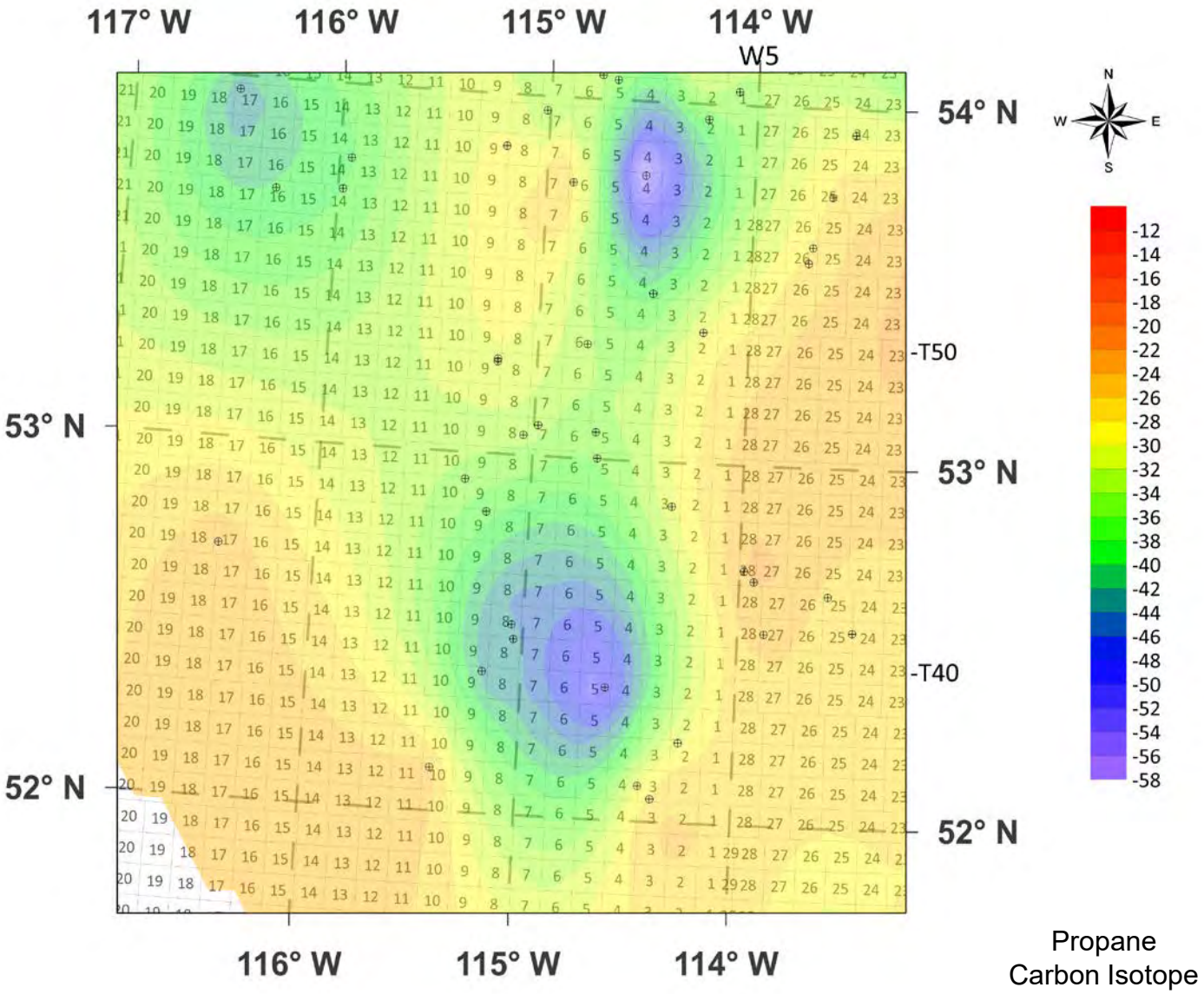

Fig. 32E. Contour Map of *n*-Butane Carbon Isotope Values of GM Pembina Zoom-in

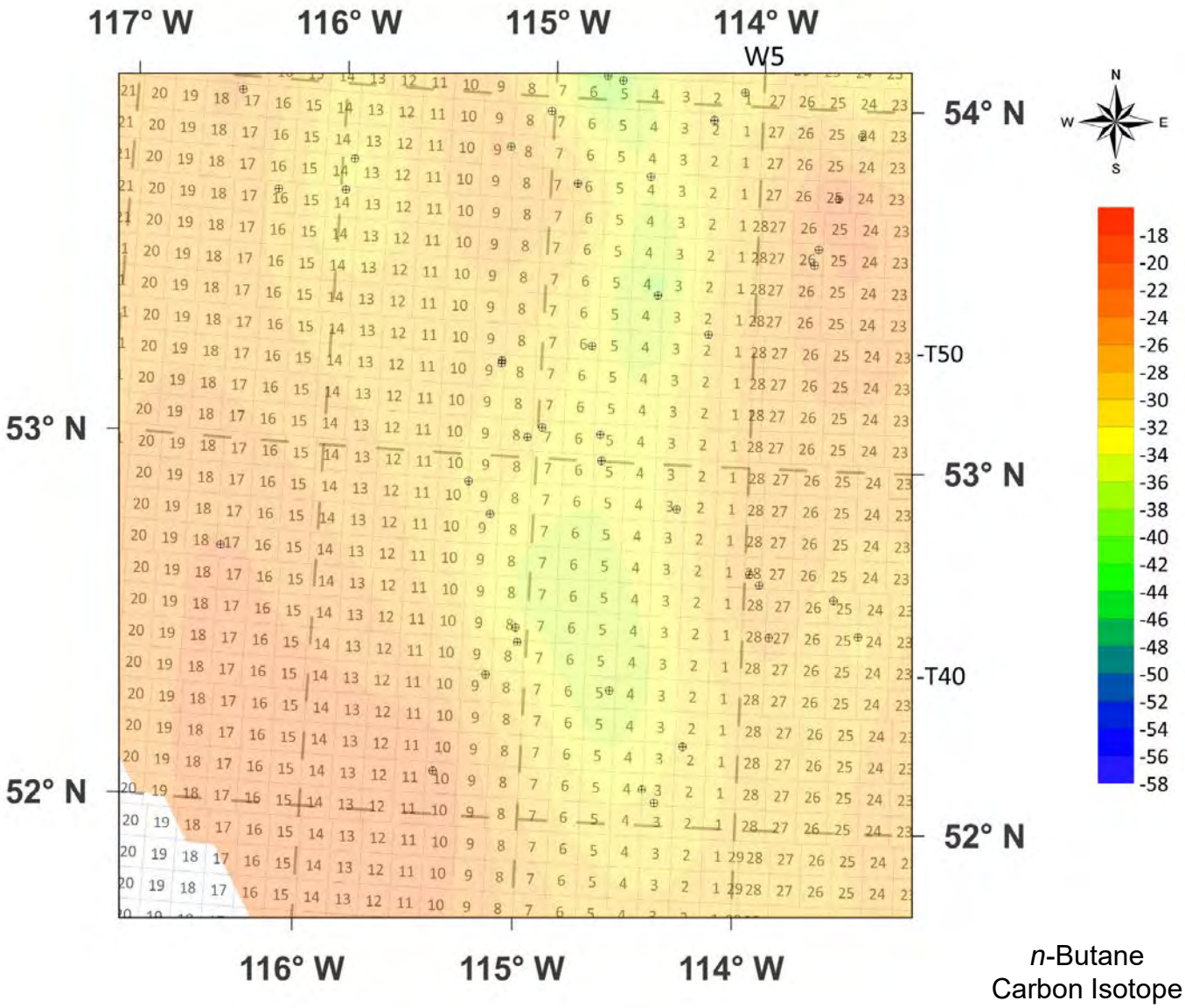

Fig. 32F. Contour Map of *i*-Butane Carbon Isotope Values of GM Pembina Zoom-in

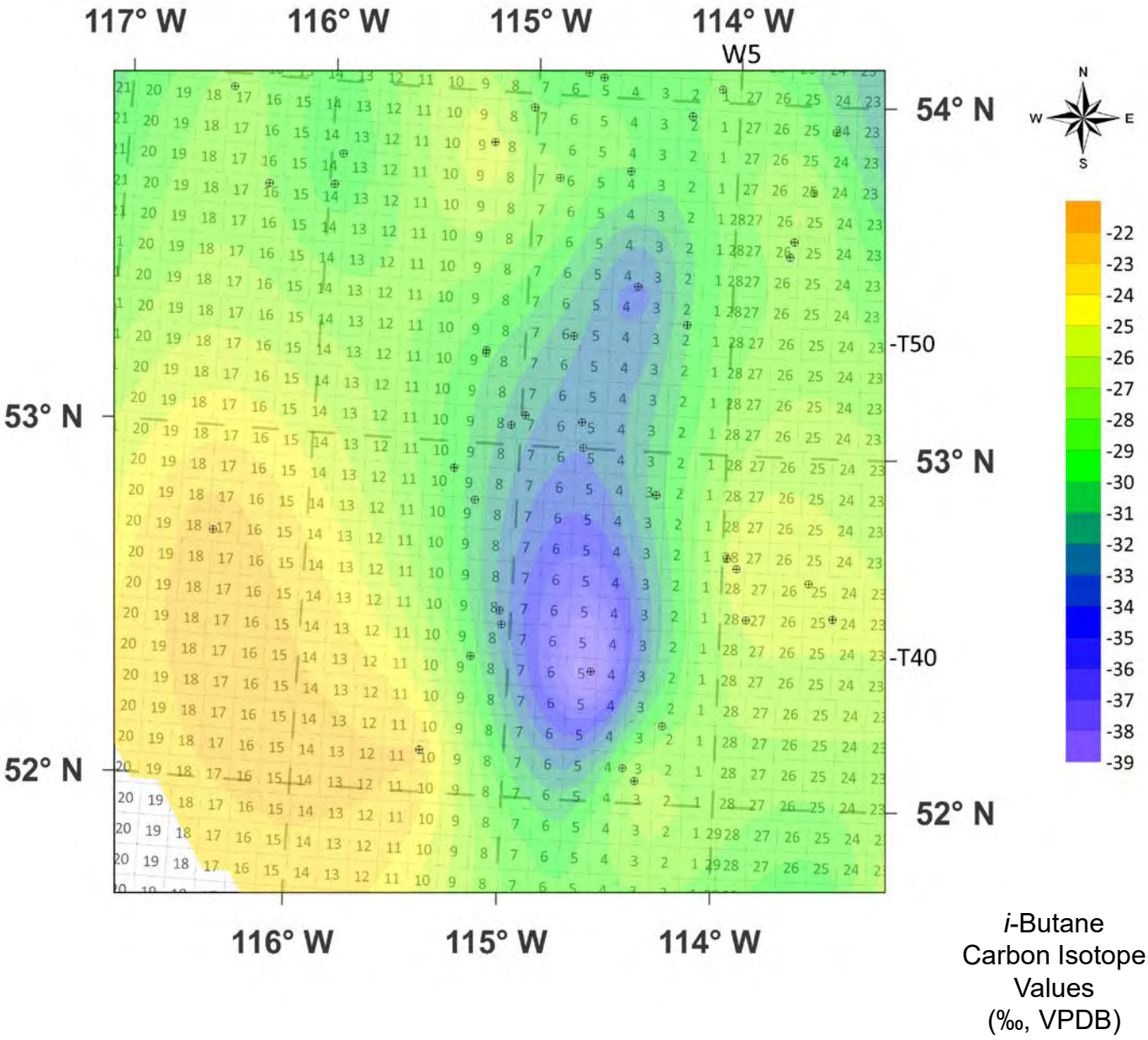

Fig. 32G. Contour Map of Carbon Dioxide Carbon Isotope Values of GM Pembina Zoom-in

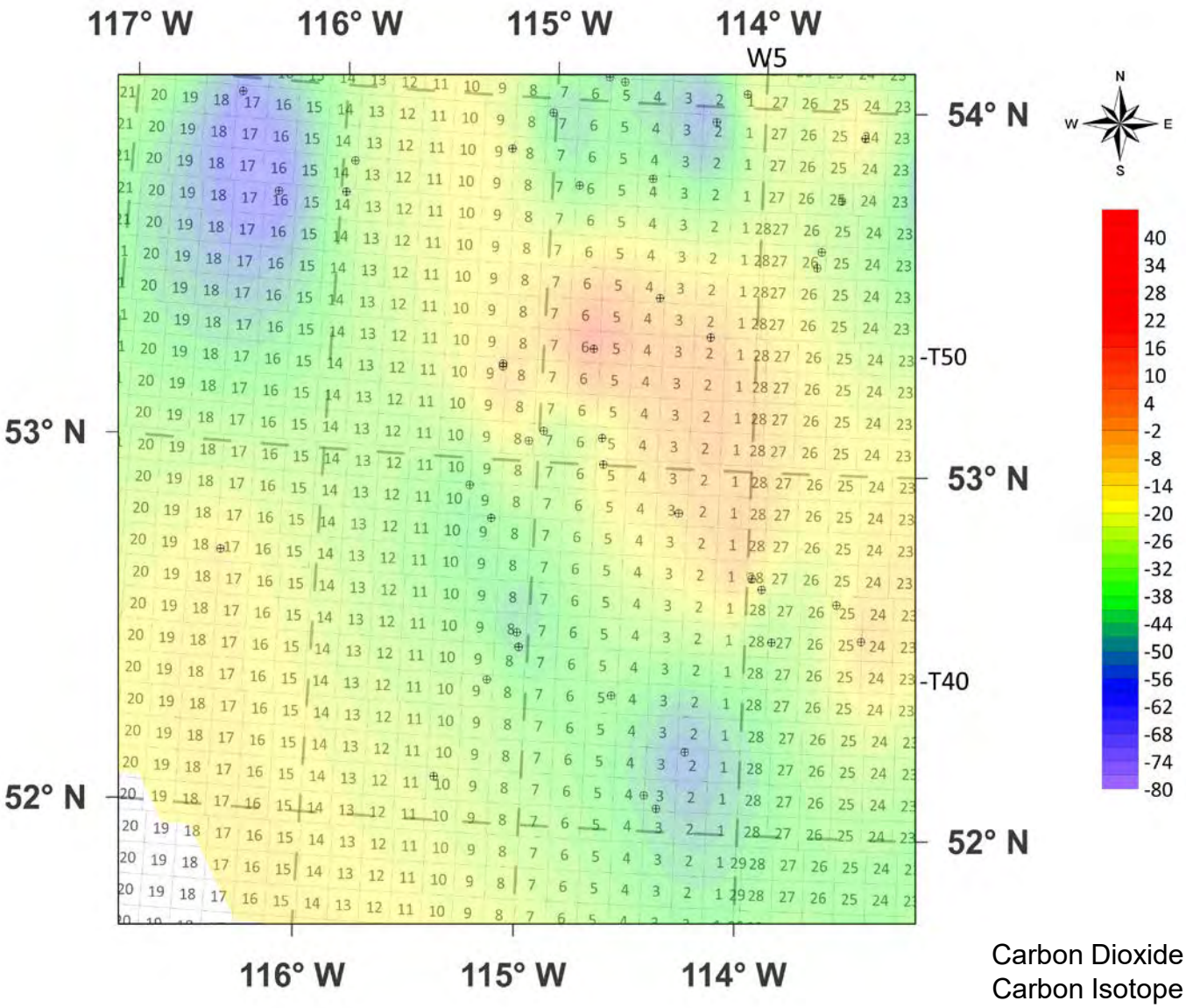

Fig. 32H. Contour Map of Methane Carbon Isotope Values of GM Pembina Zoom-in over Topographic Map

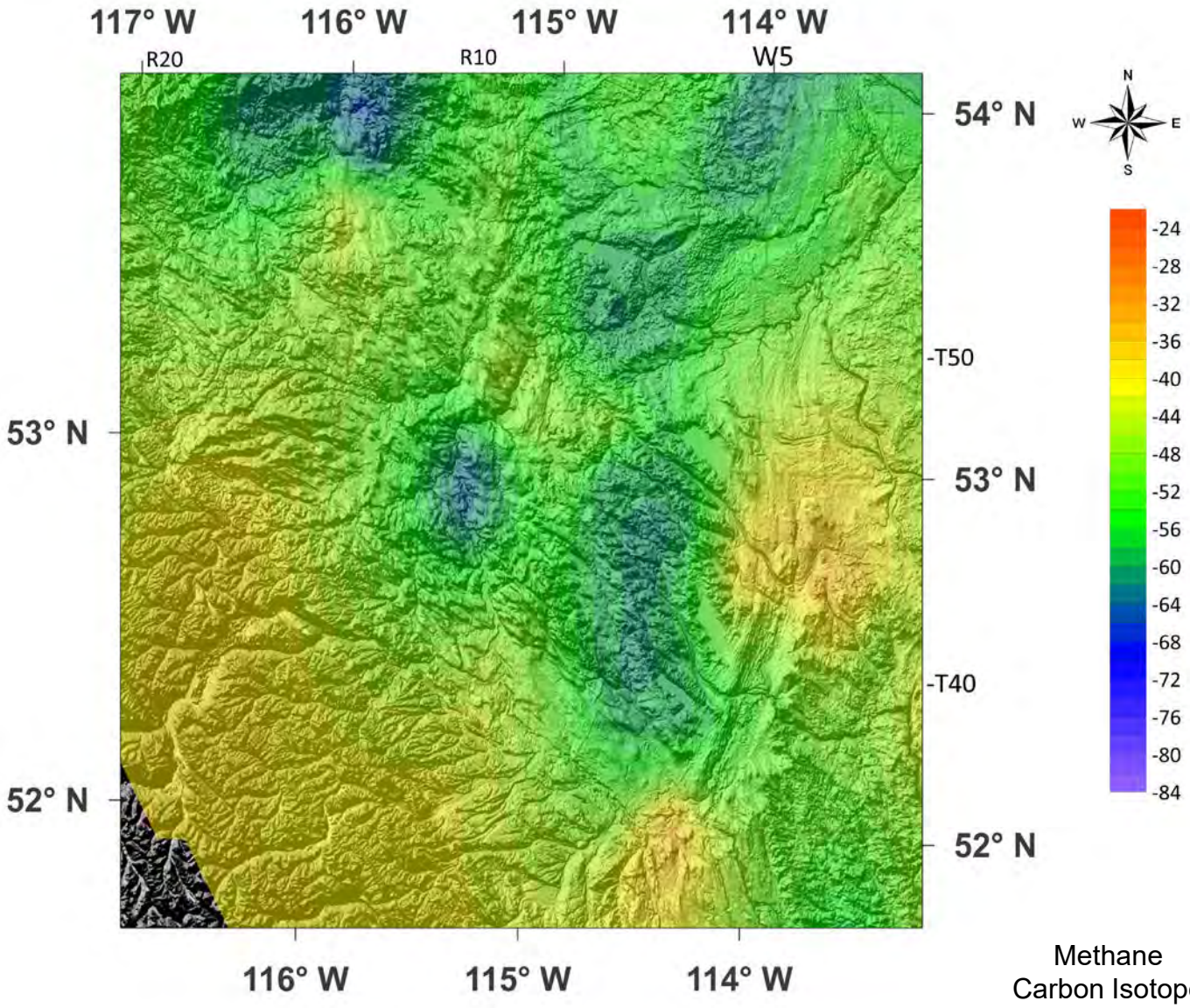

Fig. 32l. Contour Map of Ethane Carbon Isotope Values of GM Pembina Zoom-in over Topographic Map

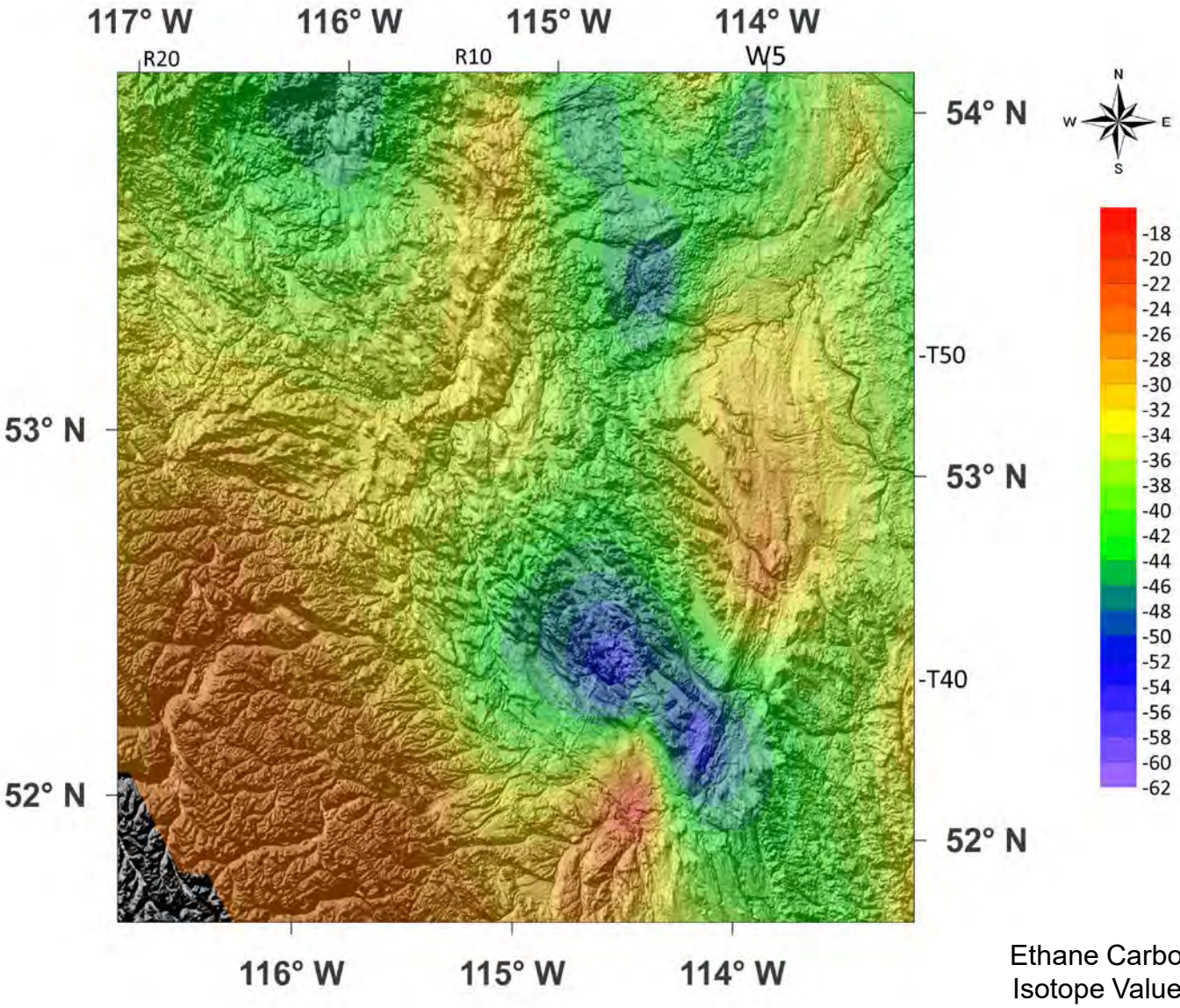

Fig. 32J. Contour Map of Propane Carbon Isotope Values of GM Pembina Zoom-in over Topographic Map

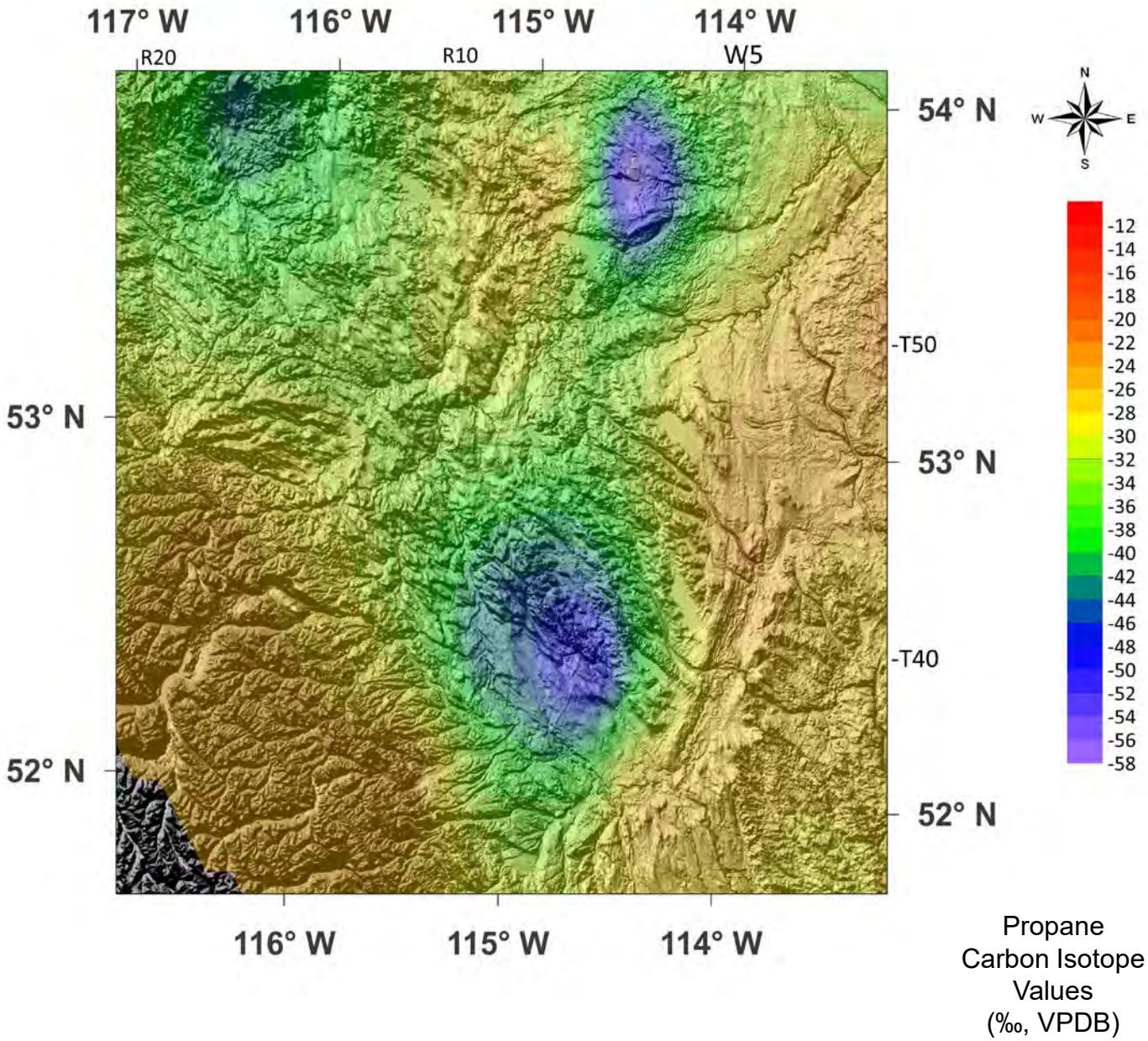

Fig. 32K. Contour Map of *n*-Butane Carbon Isotope Values of GM Pembina Zoom-in over Topographic Map

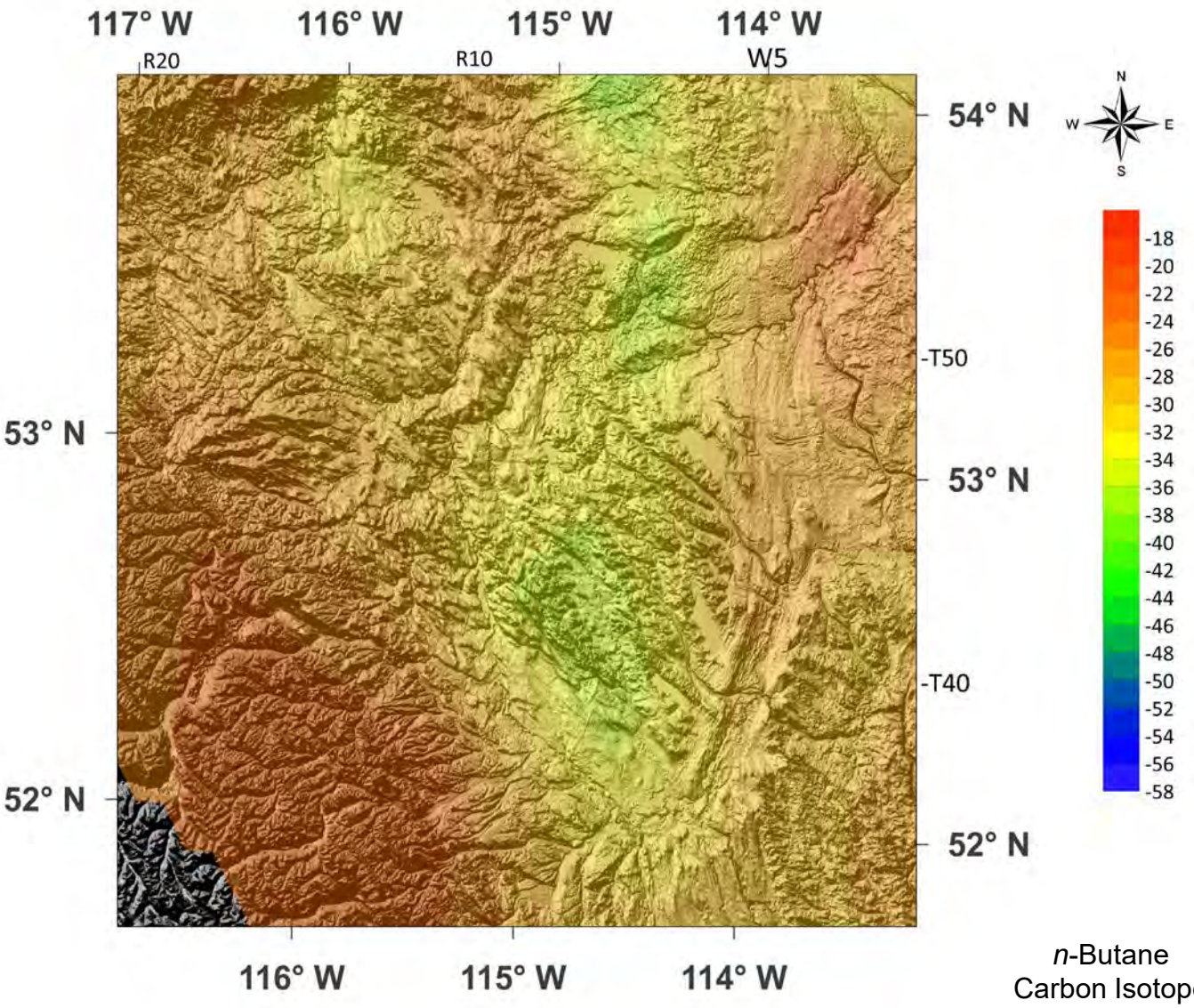

Fig. 32L. Contour Map of *i*-Butane Carbon Isotope Values of GM Pembina Zoom-in over Topographic Map

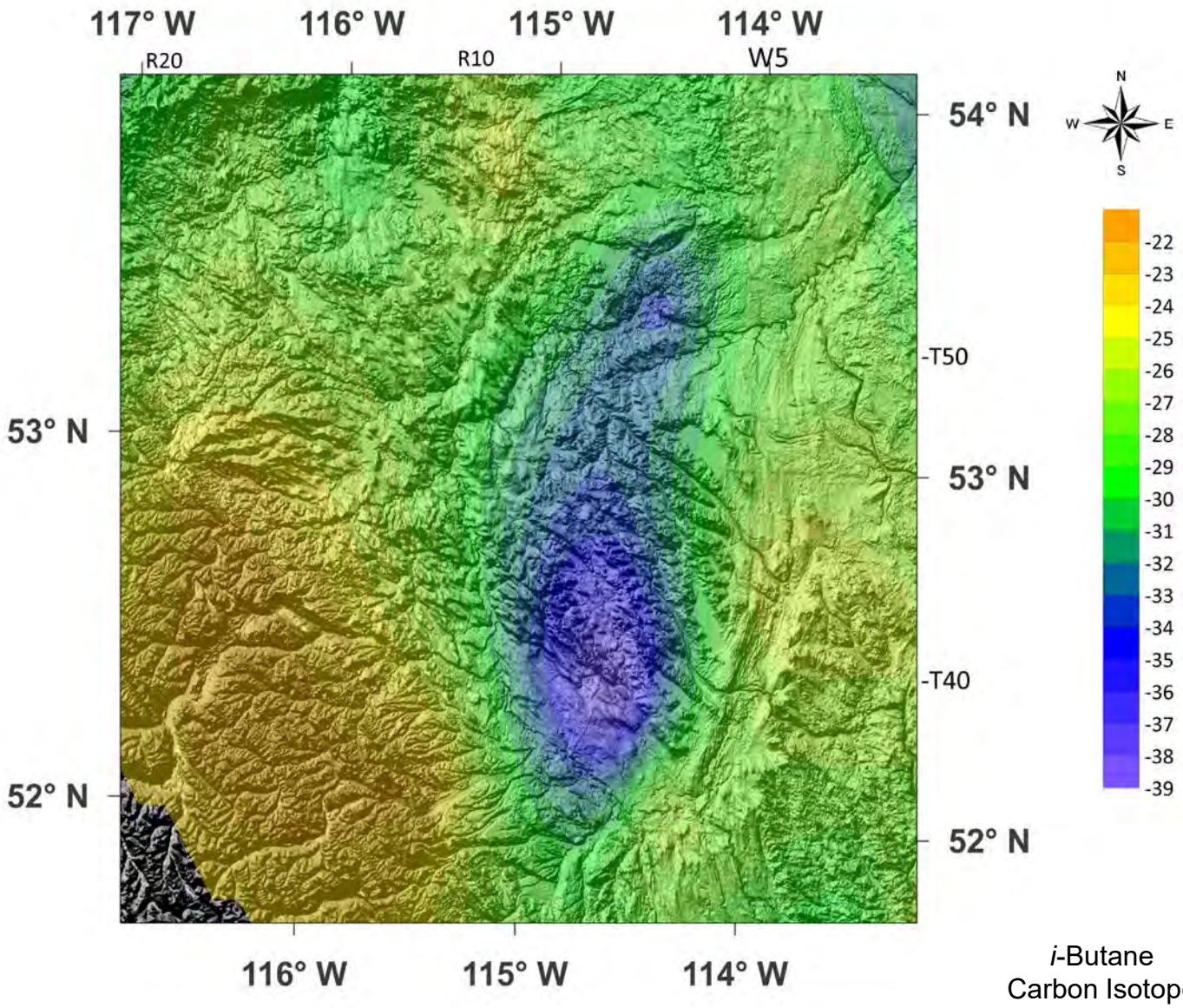

Fig. 32M. Contour Map of Carbon Dioxide Carbon Isotope Values of GM Pembina Zoom-in over Topographic Map

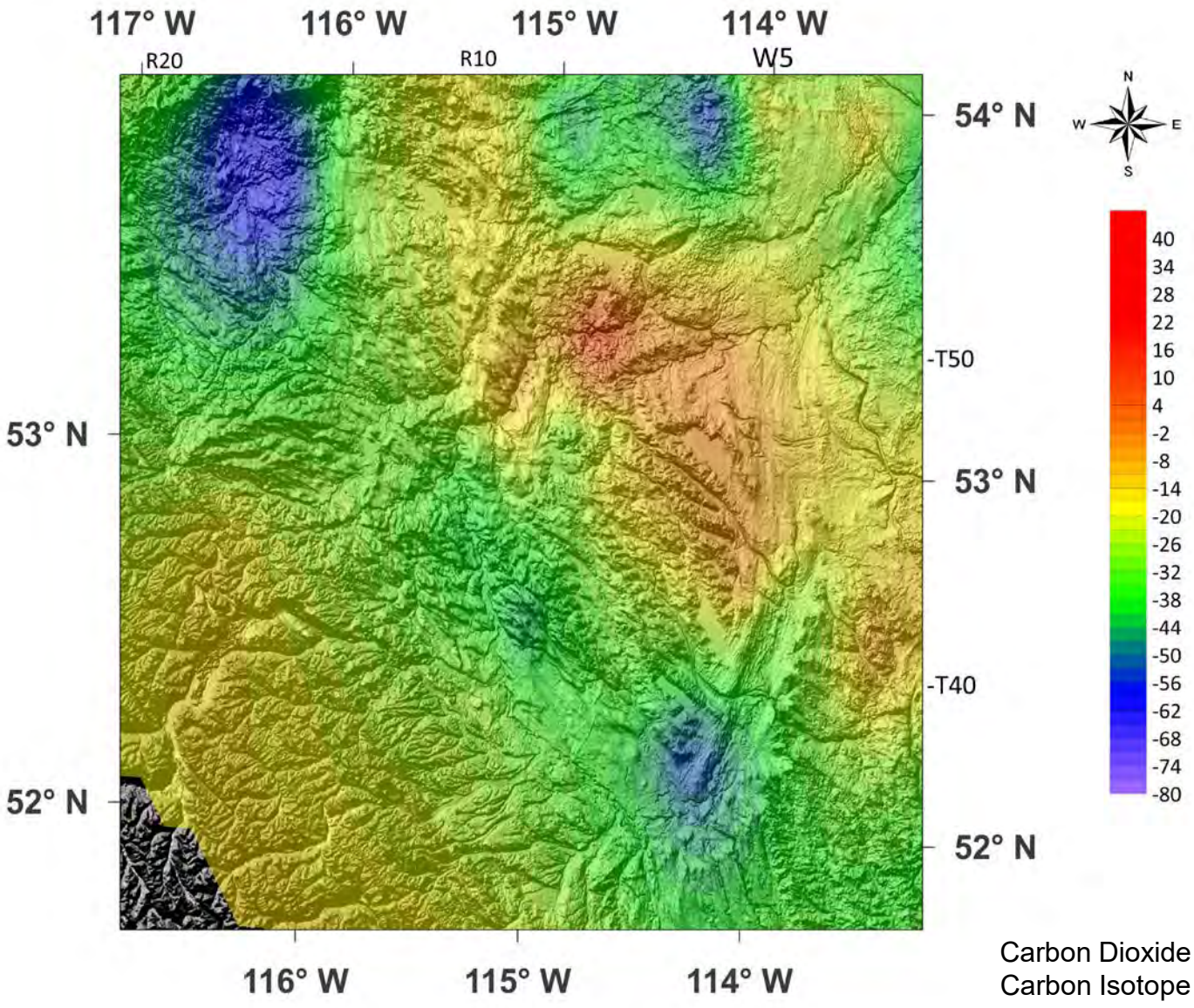

Fig. 33A. Contour Map of Methane Carbon Isotope Values of SCV

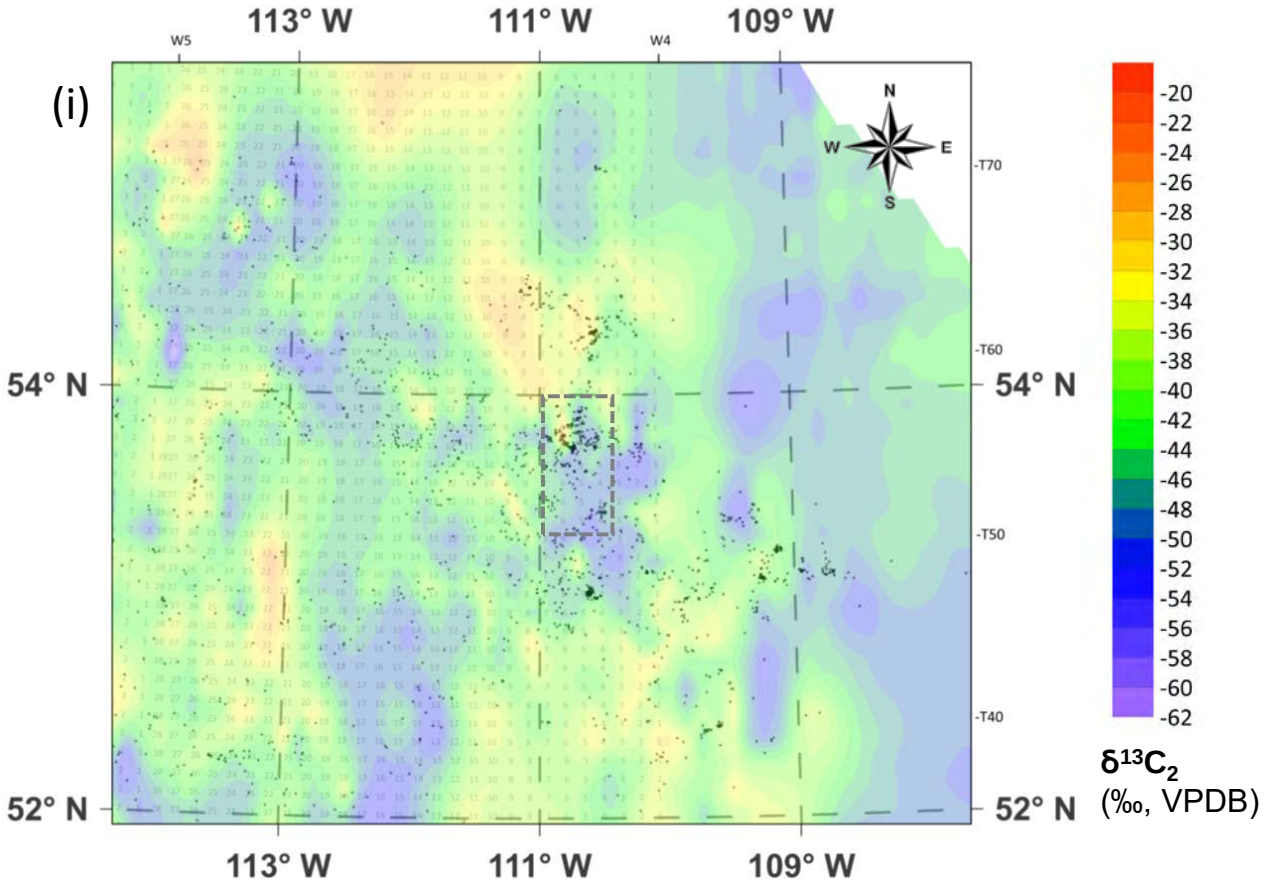

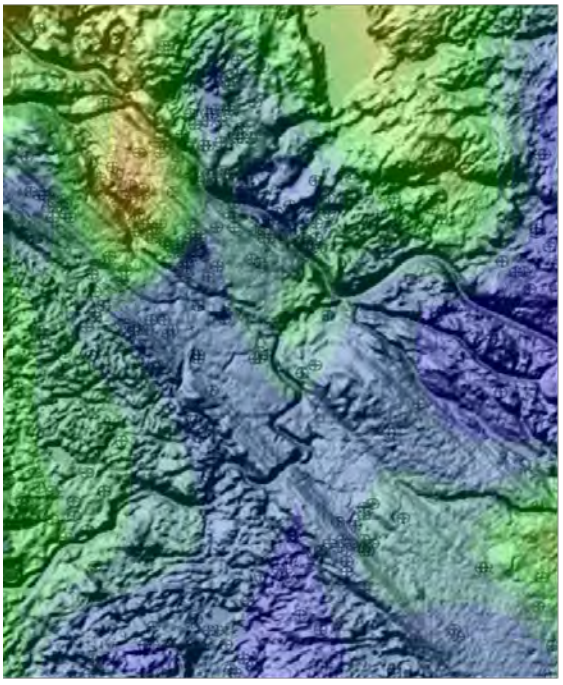

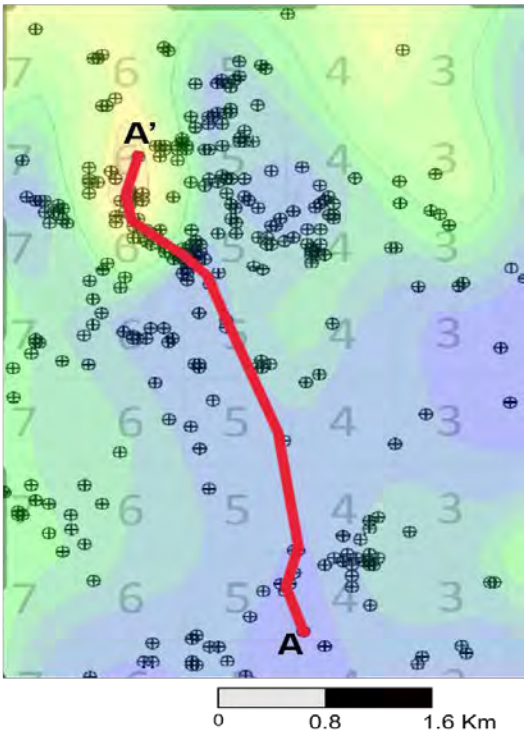

Fig. 33B. Cross Section A-A' Topography and *n*-alkanes Isotopic Response

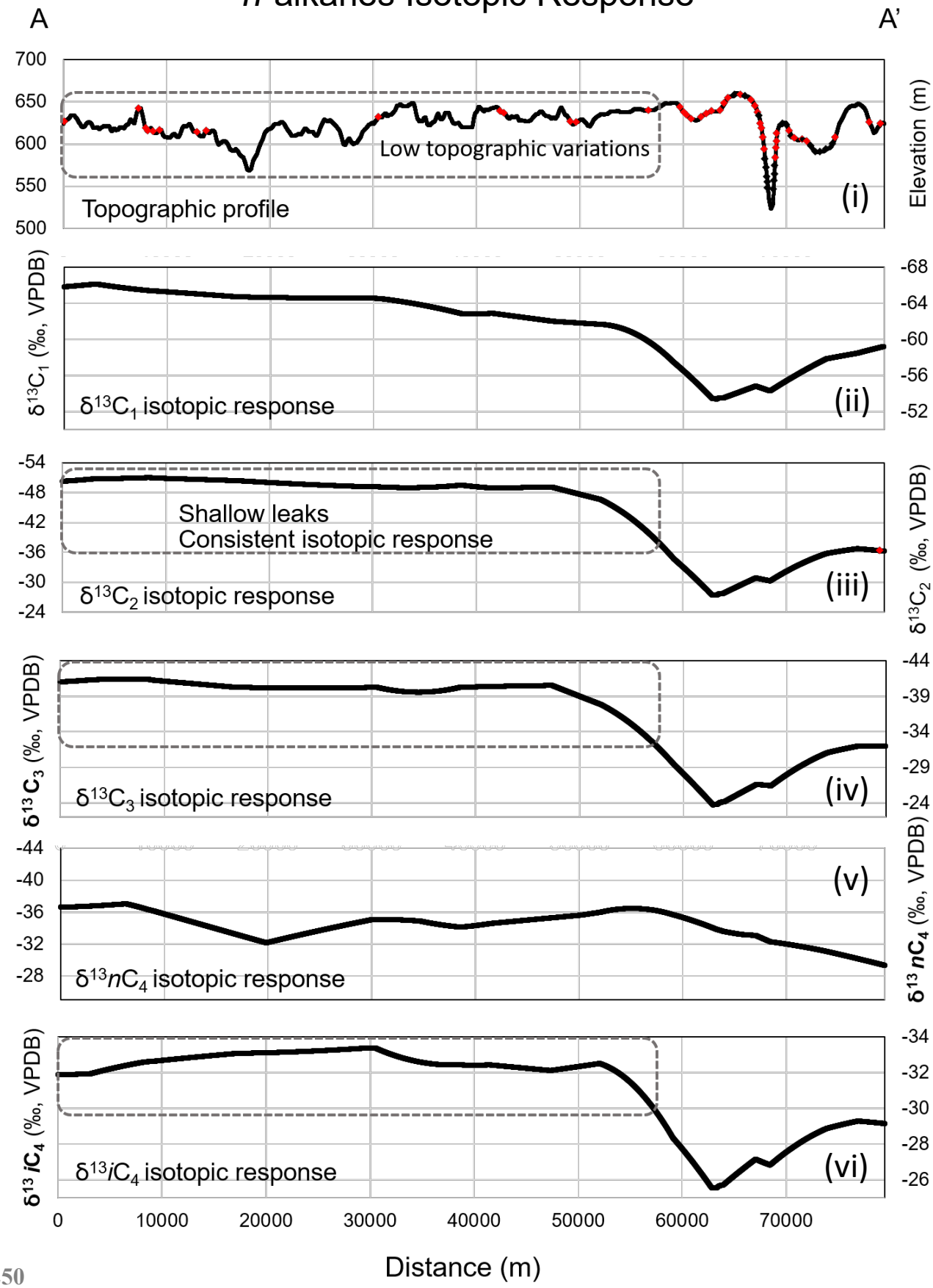

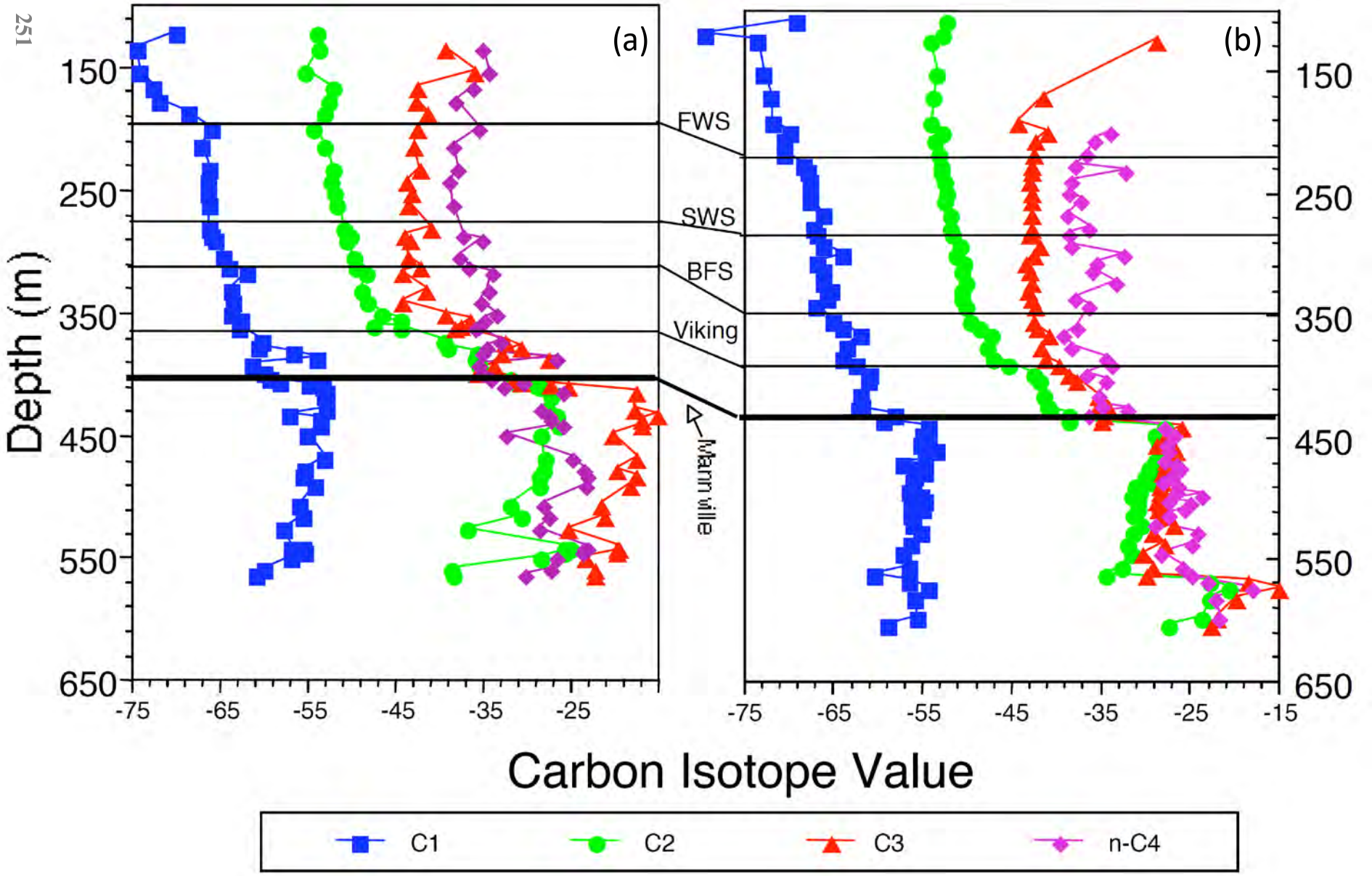

Fig. 34. Correlation of Isotope Mud-logs of Two Wells from the Lindberg Heavy Oil Field

Fig. 35A. Cross-plot of n-alkane production gases isotopic composition from W3

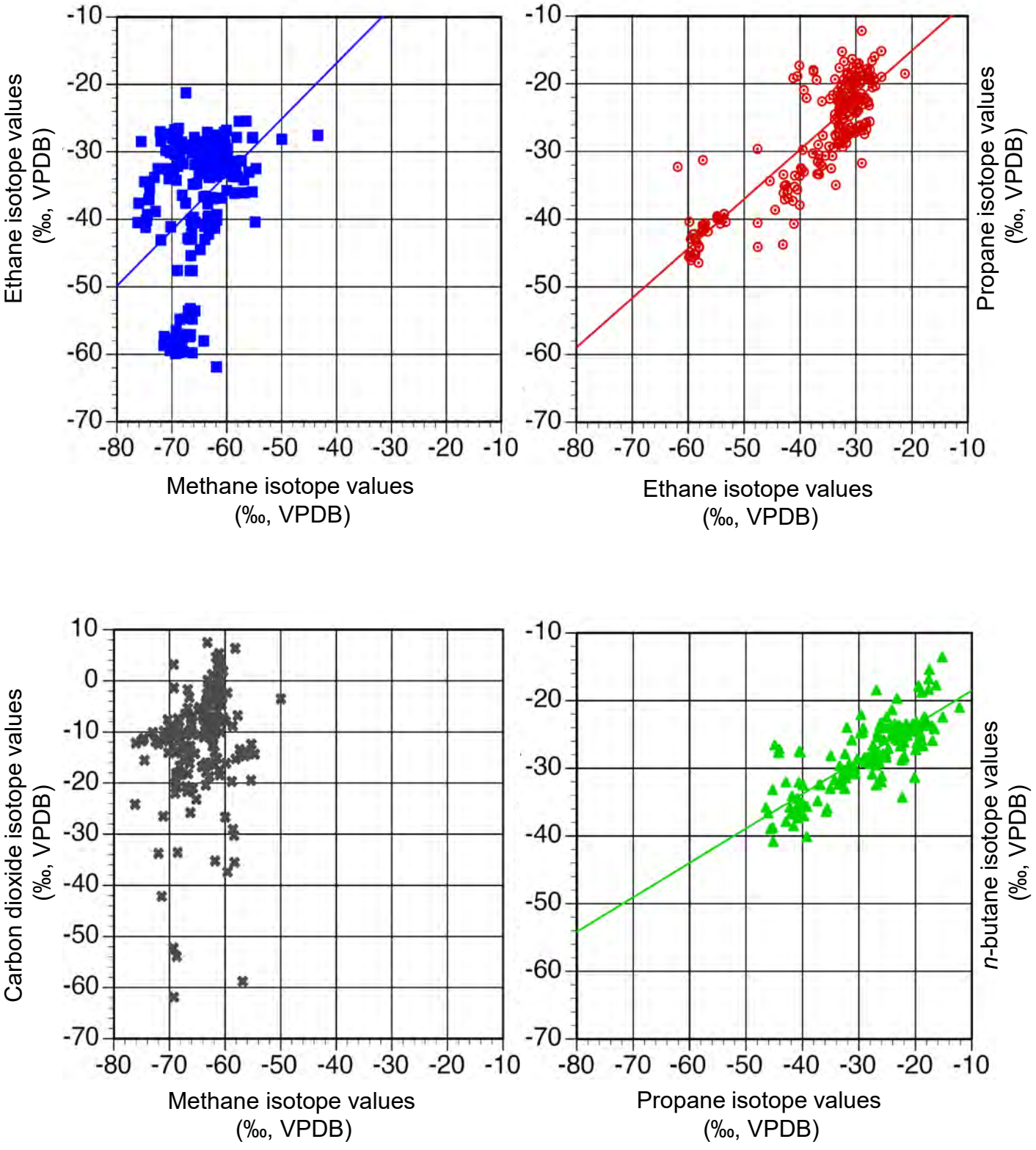

Fig. 35B. Cross-plot of n-alkane production gases isotopic composition from W4

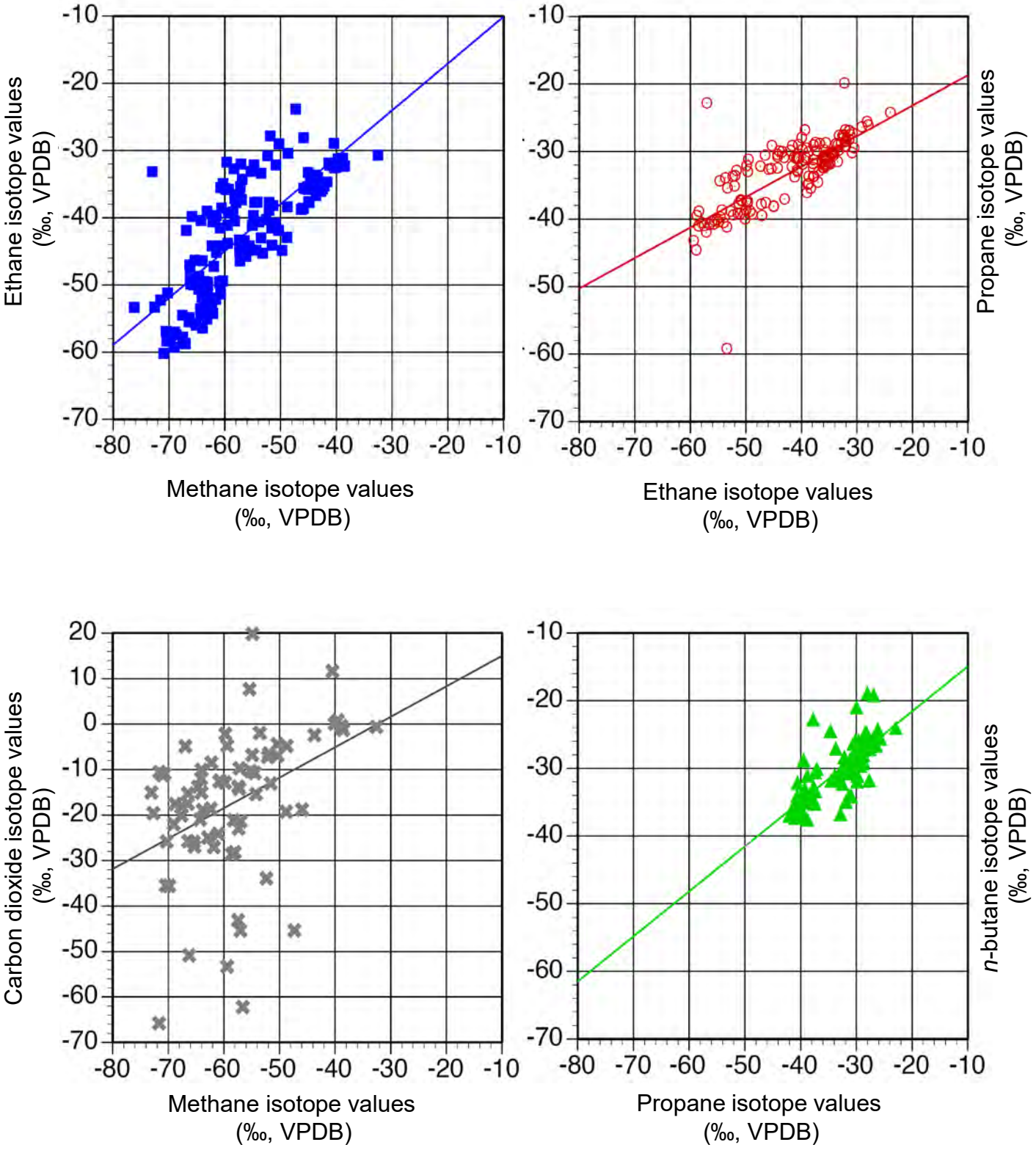

Fig. 35C. Cross-plot of n-alkane production gases isotopic composition from W5

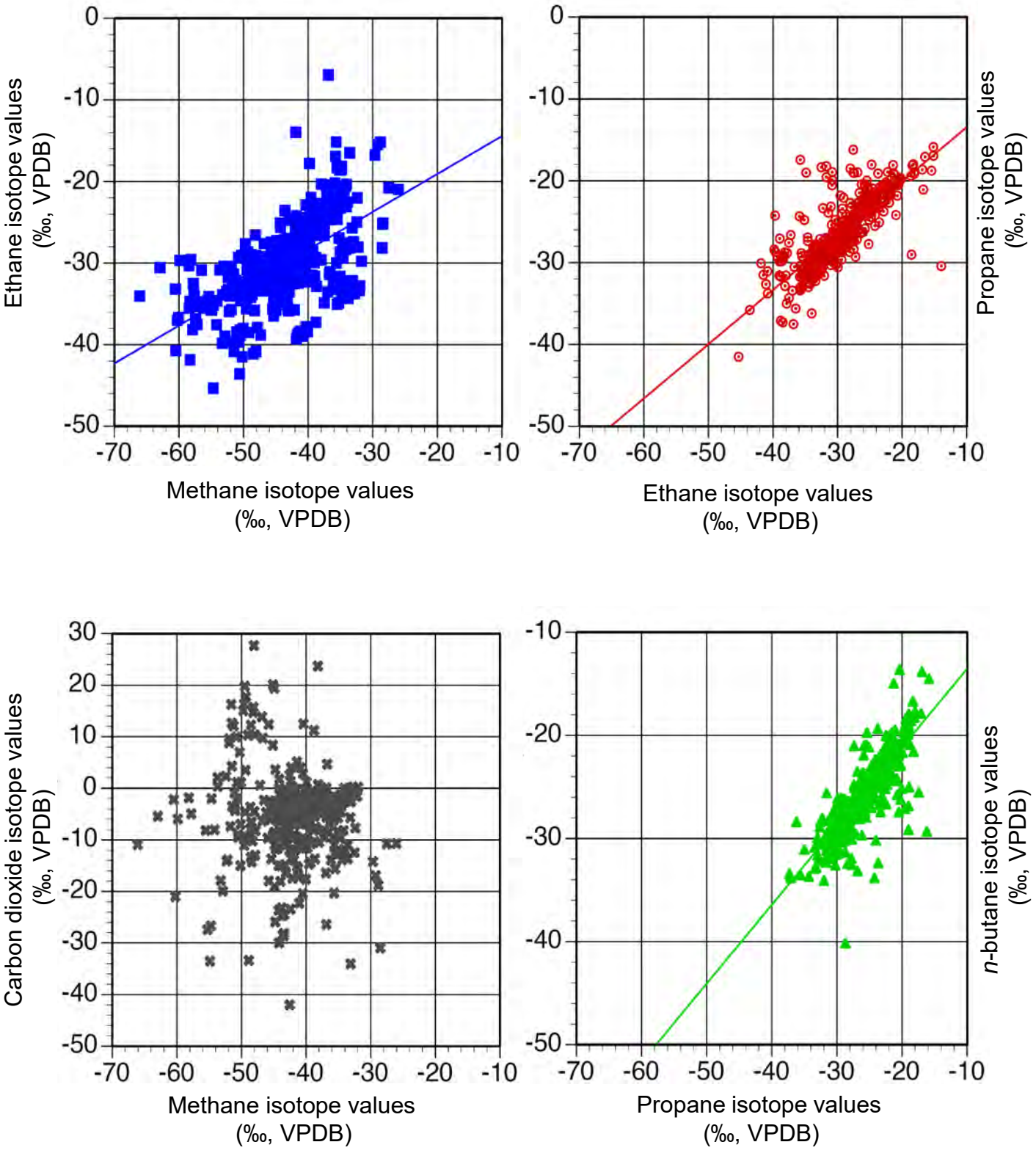

Fig. 35E. Cross-plot of n-alkane production gases isotopic composition from W6

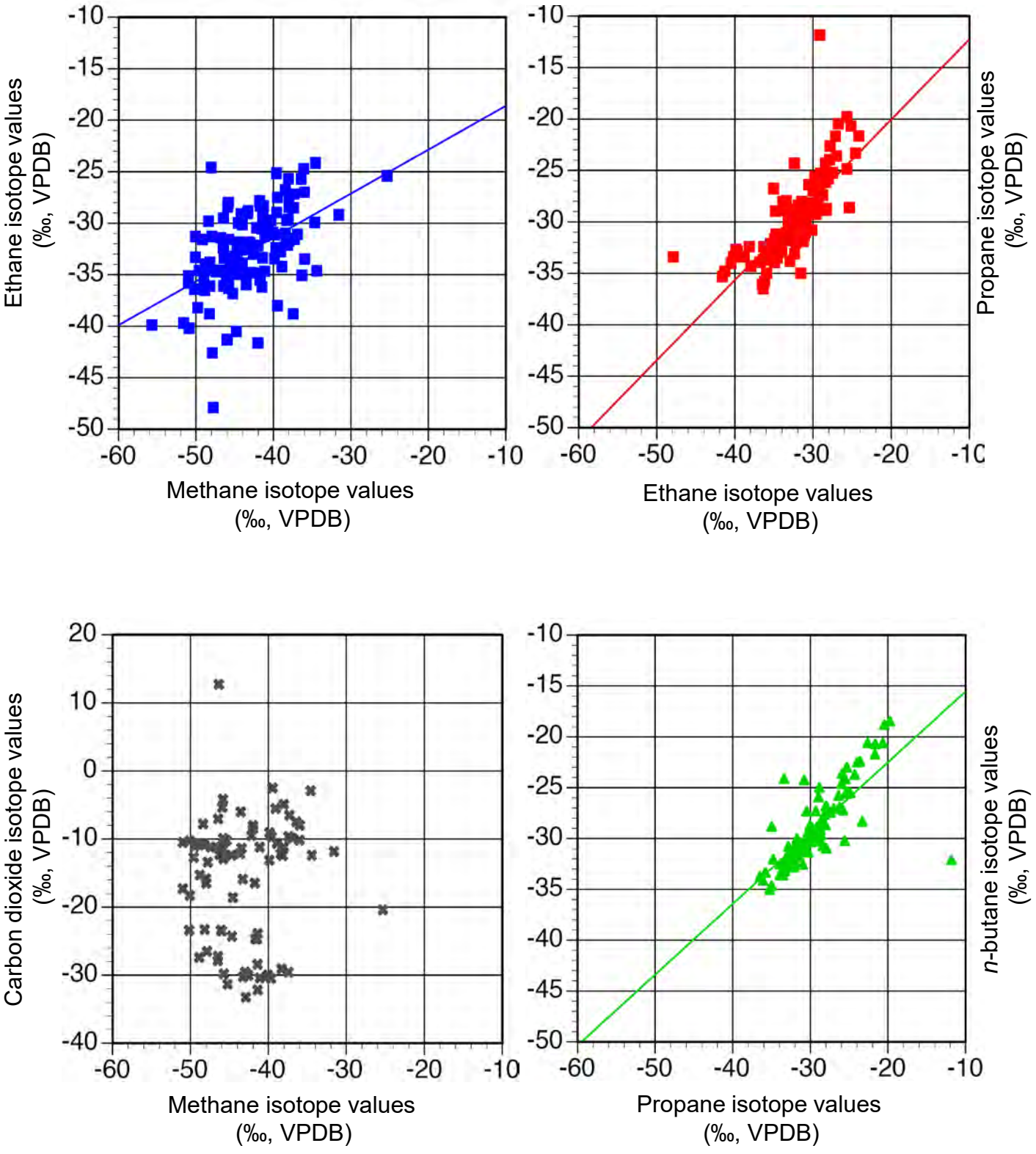

Fig. 35E. Cross-plot of n-alkane production gases isotopic composition from British Columbia